SHEAR STRENGTH OF REINFORCED CONCRETE MEMBERS SUBJECTED TO MONOTONIC AND CYCLIC LOADS

By

Malte von Ramin

Adolfo B. Matamoros

A Report on Research Sponsored by
THE UNIVERSITY OF KANSAS
DEPARTMENT OF CIVIL, ENVIRONMENTAL & ARCHITECTURAL ENGINEERING

Structural Engineering and Engineering Materials
SM Report No. 72

UNIVERSITY OF KANSAS CENTER FOR RESEARCH, INC.

Abstract

Shear Strength of Reinforced Concrete Members

Subjected to Monotonic and Cyclic Loads

The shear capacity of reinforced concrete members subjected to monotonic loads was investigated and used as the basis to formulate an expression to calculate the strength of members subjected to load reversals.

The monotonic shear capacity of slender beams, deep beams, walls, and columns was calculated by superposition of components related to arch-action, truss-action, friction, and from a contribution of the uncracked compression zone, which is related to the tensile strength of concrete. A procedure to calculate the shear strength of members in the transition phase from deep to slender members was formulated, so that the proposed expression can be used for all geometries considered. The shear strength of members with and without web reinforcement was analyzed. The proposed model was calibrated using an extensive database of test results, and was found to give good results compared to other analysis models in an *n*-fold cross validation.

The resistance to lateral load reversals was investigated for two failure modes: failure due to degradation of the flexural strength, and failure due to degradation of the shear strength. The degradation of flexural strength is expressed in terms of a linear slope derived from the displacement and load at yielding of the tensile reinforcement to the displacement at 80 percent of the yield load. Shear failure was defined by yielding of the transverse reinforcement. The degradation of shear strength was found to be non-linear with respect to the limiting displacement, and is formulated as a reduction factor for the initial shear strength. Degradation functions for the decrease in strength of the contributing arch and compression zone components, and for the truss mechanism are presented.

The following key conclusions were drawn from this study:

1. The monotonic shear capacity can be modeled by the proposed superposition of contributing components for member geometries ranging from squat to deep members. Simply superimposing the individual components, however, does not reflect the actual member behavior. Functions transitioning between squat and slender members, as well as between reinforced members and members without web reinforcement, are necessary to model the member behavior accurately.

2. In the proposed model, the friction component is used to control the so-called "size effect." It was found that the "size effect" is not only an effect of the section depth, but is also influenced by the compressive strength of concrete, the tensile reinforcement ratio, and the average shear stress.

3. The shear strength degradation under cyclic lateral loads was found to be due to a reduction of the components related to friction and the compression zone, and to a reduction of the truss mechanism.

4. The shear analysis according to the proposed model gave more accurate results than the other models considered in the study at hand. Moreover, with the exception of the approach proposed by Watanabe, compared to other methods, it was the only model applicable to a wide range of member configurations.

Keywords: shear analysis, reinforced concrete, strut-and-tie, truss model, friction, size effect, walls, seismic load

Acknowledgements

The report is based on a thesis prepared by Malte von Ramin in partial fulfillment of the requirements of the Ph.D. degree. During the work on this thesis, Malte von Ramin was supported by a Graduate Teaching Assistant appointment at the Department of Civil, Environmental, and Architectural Engineering at the University of Kansas.

Table of contents

List of Tables

List of Figures

List of Abbreviations

Geometry

a	=	shear span
b	=	width of the member
c	=	depth of the neutral axis
c_R	=	clear cover of the tensile reinforcement
d	=	effective depth
h	=	height of the member
h_a	=	embedment depth of the tensile reinforcement
h_f	=	depth of boundary element
jd	=	internal lever arm from linear flexural analysis
kd	=	depth of the neutral axis from linear flexural analysis
l	=	length of the member
l_b	=	dimension of the loading plate in axial direction
r	=	maximum depth of the strut along the column axis
s_{cr}	=	critical crack spacing
w	=	strut width
z_c	=	distance from centroid to center of the compression zone
A	=	area
A_g	=	gross area
A_w	=	area of the transverse reinforcement
L	=	length of the member, for shear degradation taken as shear span of the member
δ	=	drift ratio
ϕ	=	crack inclination, used for truss mechanism and friction component
φ	=	curvature
ψ	=	inclination of compression field related to horizontal truss
θ	=	strut inclination for arch-action
Δ	=	displacement
Δw	=	crack width perpendicular to crack surface
Δu	=	crack opening in axial direction at mid-depth of the crack
Δv	=	vertical displacement
Δs	=	slip parallel to crack surface

Material properties

f'_c = compressive cylinder strength of concrete
f_{ct} = tensile strength of concrete
f_s = stress in the steel
f_t = stress in the inclined compression field of truss mechanism
f_{wy} = yield stress of steel in the web
f_y = yield stress of steel
E_c = elastic modulus of concrete
E_s = elastic modulus of steel

β_n = nodal strength reduction factor
ε_w = strain in the web reinforcement
ε_s = strain in the tensile reinforcement
ρ_{be} = tensile reinforcement ratio in the boundary elements of walls
ρ_s = tensile reinforcement ratio
ρ_w = web reinforcement
τ = shear stress
τ_{fu} = critical shear stress related to friction

Loads

D = internal diagonal force
M = moment
N = internal axial load
P = external axial load
V = shear load

Strength values

k_c = function for the transition from deep to slender members for concrete related capacities
k_s = function for the transition from deep to slender members for struts
m = flexural strength degradation function

R_a = resistance fraction of the arch mechanism
R_h = resistance fraction of horizontal truss mechanism
R_v = resistance fraction of vertical truss mechanism
V_a = shear capacity of arch mechanism
V_{cz} = shear capacity from uncracked compression zone
V_f = shear capacity from friction
V_t = shear capacity of truss mechanism
V_u = ultimate shear capacity
V_{yt} = shear load at yielding of the transverse reinforcement

η = factor for strength degradation of concrete contributions
χ = factor for strength degradation of truss contributions

Subscripts

c = concrete
cr = critical
f = flexure, if related to failure mode
f = friction
h = horizontal
s = shear, if related to failure mode
s = tensile reinforcement
t = transverse reinforcement
u = ultimate state
v = vertical
w = wall, if related to wall analysis
w = web, if related to transverse reinforcement
y = related to yielding

1 Introduction

The design of reinforced concrete (RC) members for shear in most design codes is currently carried out through the use of empirically derived equations (ACI-318 2002). Furthermore, the effects of several important parameters such as shear span-to-depth ratio, axial load, member depth, and strength decay caused by cyclic loading are either not represented at all, or included using empirically derived correction factors that are applied to the main design equations. These correction factors are generally not related to contributing parameters that have an influence on strength degradation.

The use of empirical relationships has the disadvantage that it is limited to the range of the data used in their calibration. Results that are much more reliable may be obtained by using design procedures based on models for the physical behavior of the considered member, which were then calibrated using databases that cover a wide range of material properties and member geometries.

The provisions for calculating the shear strength of members with monotonic loading in Chapter 11 of the ACI code (ACI-318 2002) include an empirically derived term for the concrete contribution V_c. An improved statistical fit serves as the basis for the "more detailed" equations (11-5) through (11-7) for slender members, and (11-29) and (11-30) in the special provisions for walls. Recent studies have shown that the strength of members without transverse reinforcement decreases with increasing effective depth. This effect is not considered in the design equations put forward in the current ACI-318 2002 code and in other proposals as well. According to the ACI code, the load carrying capacity afforded by the transverse reinforcement is calculated using a truss model, in which a crack inclination angle of 45° is conservatively assumed. The truss model currently adopted by the ACI code (ACI-318 2002) does not account for the effects of axial and cyclic loading on shear strength.

Another significant shortcoming of the ACI provisions is the lack of a relationship between the provisions in chapter 11 of the ACI code and Chapter 21, "Special Provisions for Seismic Design." For most practical cases, the design provisions for beams in Chapter 21 neglect any direct contribution of the concrete to shear strength, and rely on spacing limits for transverse reinforcement to avoid a significant reduction in the capacity of the truss model under cyclic loading, and to prevent buckling of the longitudinal reinforcement. Additional limits are set to the amount of reinforcement, depending on the type of structure. Therefore, by relying on the truss mechanism, the ACI code considers indirectly the concrete strength, because the truss mechanism depends on the concrete compression field. None of the equations in Chapter 21 accounts for the effect of axial load on shear strength, the contribution of the uncracked concrete, or the reduction in shear strength with increased deformation under cyclic loading.

A model originally put forward by F. Watanabe and T. Ichinose (Aoyama 1993; Watanabe and Ichinose 1991) does consider the effects of the shear-span-to-depth ratio and cyclic shear loading. The original model has been adopted by the Architectural Institute of Japan guidelines (AIJ 1988). It consists of an arch contribution to describe the behavior of deep members, and a truss contribution to calculate the strength of slender members. Recent research focused on a modification of the AIJ guidelines to include effects of axial load and high-strength concrete (Kabeyasawa and Hiraishi 1998; Watanabe and Kabeyasawa 1998). However, several assumptions of this model seem to be flawed, and the modifications are not based on physical conditions within the member.

The goal of this study is to find a model based on physical and geometric considerations within an RC member, which can be used to estimate with accuracy the shear strength of RC members under various loading conditions, including axial and cyclic shear load. The proposed model is intended to represent the various mechanisms that contribute to shear strength, such as arch-action, truss-action, and contributions from the uncracked compression zone in the member and from friction between crack surfaces. The fact that the model is based on the superposition of the different load carrying mechanisms makes it easily applicable to several member configurations, such as slender and deep beams, walls, and columns. Various loading conditions, i.e. static shear load and strength degradation due to reversed lateral load, are considered.

The proposed model is developed for members with a single shear span as cantilever columns or simply supported beams subjected to a point load applied at the center of the span. The development of a model for RC members subjected to distributed loads or support conditions resulting in non-linear moment distributions is not in the scope of the work at hand.

An overview of existing shear-design approaches is presented in Chapter 3 in the work at hand. This overview focuses on behavior models that are directly applicable, i.e. on methods that do not rely on iterations or that are computer-based. The following Chapter 4 presents an evaluation of the approaches described in Chapter 3, and shows the ranges of applicability of the respective proposals.

The model proposed by the author is developed in Chapter 5, with a summary of the shear resisting components in Section 5.3. Chapter 6 shows the influence of the effective section depth on the average shear stress, and how the proposed model considers the so-called "size effect". The calibration of the model introduced in Chapter 5 is described in Chapter 7 of the work at hand. Chapter 7 describes the interaction of the previously defined load-carrying components and outlines the applicability of the components to the respective member configurations. A summary and evaluation of the calibrated model for the monotonic load case is provided in Section 7.4.

The degradation of flexural strength and shear strength due to cyclic loading is developed in Chapter 8. Section 8.1 describes the flexural strength degradation; Section 8.2 shows the strength degradation in shear-controlled members. The application of the developed strength reduction is demonstrated on a sample set of walls described in Section 8.3.

2 Objectives

The main objective of this thesis is to derive a model to calculate the shear strength of RC members that can be applied to members of various geometries, and members that are axially loaded. The capacity of the members for the basic case of monotonic shear load is used as the foundation to describe the strength degradation under cyclic shear, ultimately leading to flexural or shear failure. The proposed model is intended to be applicable to slender members as beams and columns, as well as to deep beams and walls. Member configurations with and without transverse reinforcement are examined.

3 Literature review

3.1 Current approaches

The modeling and analysis of reinforced concrete (RC) members under axial compression and variable horizontal loads as considered in the study at hand has been examined by various researchers. Five approaches to different aspects of shear design of RC members are discussed in the following sections.

The approach described first, based on work done by Watanabe et al. (Aoyama 1993; Watanabe and Ichinose 1991) represents a strut-and-tie approach that combines the common truss analogy with an arch model. This model is outlined in Section 3.2. Since the approach taken by Watanabe is one of the approaches the proposed model is based on, it is discussed in more detail than some other models.

Shear design of RC members without web-reinforcement by modeling the effects of the uncracked compression zone, friction between crack surfaces in the tension zone, and dowel action of the longitudinal reinforcement is described in Section 3.3. This method was proposed by Reineck (Reineck 1990, 1991b). The approach taken by Reineck is considered as another foundation for the proposed model, and is therefore discussed in more detail.

Section 3.4 describes a shear design method based on the drift limit of RC columns, which was developed by Pujol et al. (Pujol 2000). The approach taken by Pujol provides a recommendation for a definite configuration of transverse reinforcement depending on the ductility demand on the considered member. Therefore, it is not applicable to RC members without web reinforcement.

The analysis model described in Section 3.5 was developed by Priestley et al. (Priestley 1994), introducing a shear design method based on the expected ductility demand of the considered RC member. This approach models the shear strength of an RC member by superposition of concrete and steel components with an arch contribution that is solely relying on axial compression.

Section 3.6 discusses the shear-friction-truss model as proposed by Chen and MacGregor, which is based on the dry-friction law (Chen and MacGregor 1993).

The effect of the section depth on the average shear stresses was investigated by Bažant (Bažant 1997; Bažant and Kim 1984). The fracture mechanics approach taken by Bažant to describe "size effect", i.e. the reduction of the nominal shear stresses with increasing beam depth, is described in Section 3.7.

3.2 Analysis based on a combined truss and arch model

A model of combined truss- and arch-action, as it also has been adopted as a basic design philosophy for the current Architectural Institute of Japan (AIJ) Design Guideline (AIJ 1988), is based on work by Watanabe and Ichinose (Watanabe and Ichinose 1991). As stated by Watanabe and Ichinose, the method follows the capacity design method for RC ductile frames as it was developed by Paulay. The primary goal of the capacity design method is to define the desired failure mechanism, and to provide the corresponding member strength at all considered member locations. This is achieved by providing plastic hinges at the intended deflection points. After determining the desirable locations for plastic hinges, reinforcement for these areas is calculated, and the remaining elements are designed to fail after the plastic hinge mechanism has developed (Bachmann 1995, 2000; Paulay 1990).

The shear design approach of a combined model of truss- and arch-action as proposed by Watanabe et al. (Watanabe and Ichinose 1991) is based on constitutive laws for concrete and steel; and a simplified two dimensional stress distribution. The same approach has also been described later by Aoyama (Aoyama 1993). Further research is being conducted on the model, with an adjustment by Watanabe and Kabeyasawa for high-strength concrete and axial load (Watanabe and Kabeyasawa 1998); and an adjustment by Kabeyasawa and Hiraishi for deep members (Kabeyasawa and Hiraishi 1998). The basis for the subsequent research is outlined here. The improvements for the basic model are described and used in the evaluation of Watanabe's model in Chapter 4.2.

The load carried by the truss mechanism depends on the amount of web reinforcement; and the load carried by the arch and the compression members of the truss is limited by the strength of the concrete. The strength of the arch mechanism depends not directly on the amount of transverse reinforcement; it is limited by the stresses in the truss. The fundamental design equation for the combined approach is expressed as

$$V_n \leq V_u = V_t + V_s \tag{3.1}$$

Where V_n = nominal shear force,

V_u = ultimate shear strength,

V_t = shear strength ascribed to truss action,

V_s = shear strength ascribed to arch action.

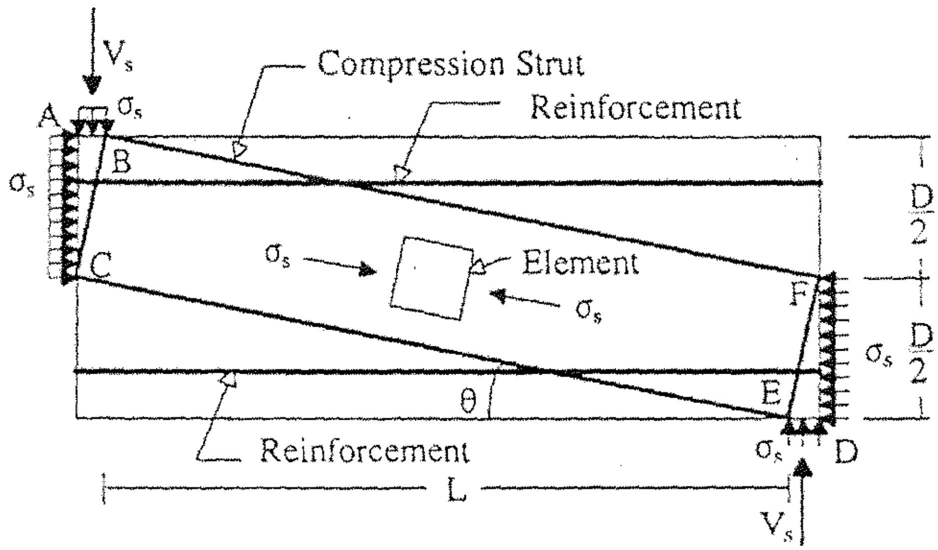

Figure 3-1 Stress conditions and geometry of assumed strut model (Watanabe and Ichinose 1991)

3.2.1 Arch-action

The contribution of the arch, depicted in Figure 3-1, is given as the bearing strength limit on the nodal zone by

$$V_s = \frac{1}{2} b \cdot D \cdot \sigma_s \tan\theta \tag{3.2}$$

Where b = width of the section [mm],

D = total depth of the section [mm],

σ_s = average stress in the compression strut [MPa],

θ = inclination of the arch.

For simplicity, it is assumed that the arch is linear, not bent, and has a depth of $D/2$. According to this assumption the angle is given by the geometry of the member as

$$\tan\theta = \frac{\sqrt{L^2 + D^2} - L}{D} = \sqrt{\left(\frac{L}{D}\right)^2 + 1} - \frac{L}{D} \tag{3.3}$$

With L = member length [mm].

Watanabe et al. assume that (a) the yield strength of the axial reinforcement is infinitely large, meaning the proposed model assumes design for shear failure at a load exceeding the flexural strength (Aoyama 1993), and (b) the shear carrying strength is maximized to act along a height of $D/2$ following the lower bound theorem of the theory of plasticity. The lower bound theorem of the theory of plasticity was formulated by Nielsen (Nielsen 1999) based on virtual work principles. The theory of plasticity assumes that in a rigid-plastic material stressed to the yield point, arbitrarily large deformations, i.e. strains, are possible and permissible without changing the magnitude of the stresses. The lower bound theorem describes the conditions that allow for a load that causes these stresses at the yield point, while satisfying equilibrium and compatibility conditions within the member. If these loads at the yield point are not exceeded, the member does not collapse according to the lower bound theorem of plasticity. Applied to a member as depicted in Figure 3-1, the maximum load is applied to the stress field inscribed by A-B-C, if the distance A-B is largest. The stress field is assumed to be in a hydrostatic state of stresses with a magnitude of the uniaxial stress in the strut (Nielsen 1999). Eq. (3.2) results from the geometry of the assumed arch following the conditions depicted in Figure 3-1. The average stress in the compression strut, σ_s, is defined by the reduced concrete strength and the relation of the inclined stress in the truss to the reduced concrete strength as described later in Sections 3.2.3 and 3.2.4.

The previously outlined arch-model as used by Watanabe et al. is based on a model to describe the behavior of RC members earlier proposed by M. P. Nielsen (Nielsen 1999). This model assumes a hydrostatic state of stresses, in which the stress within the strut as well as on sections A-B and A-C in Figure 3-1 (D-E and D-F on the opposite side, respectively) is equal to the effective concrete strength. The model proposed by Nielsen assumes that the angle spanning open section A-B is the same angle that forms the strut inclination. This does not necessarily need to be true, because it will depend on the stress distribution along the loading points, if the same angle can be assumed. Besides the problem of how to distribute the applied loads over large sections A-B and A-C, an extensively long section A – C = $D/2$ in a more squat member would make the strut unreasonably wide. Setting the projected strut width equal to half of the member depth does not consider possible cracks. A compression strut cannot develop across cracked sections of the member. As tests have shown, shear cracks in a squat member certainly also will develop in the interior of the member area (ASCE-ACI Committee 445 1998). A wide strut as it would result from using the model developed by Nielsen would have to cross these cracks. Furthermore, it does not seem appropriate to employ the tensile component in the axial reinforcement over such a long distance with the load acting out of center of section A-C.

3.2.2 Truss-action

The truss mechanism as shown in Figure 3-2 is modeled using the distance between the centroids of the upper and lower reinforcement for determining the height of the truss. It is assumed that the inclined truss force is uniformly distributed by the (uniform) web reinforcement. The shear force attributed to truss action is given by equilibrium of forces in a free body diagram of the truss model as shown in Figure 3-2 a):

$$V_t = b \cdot j_t \cdot \rho_w f_{wy} \cot \phi \tag{3.4}$$

The average inclined stress in compression can be calculated from equilibrium of stresses in an infinitesimal stringer element following Figure 3-2 b) as

$$\sigma_t = \rho_w f_{wy} (1 + \cot^2 \phi) \tag{3.5}$$

Where σ_t = average diagonal stress in compression [MPa],

ρ_w = web reinforcement ratio,

f_{wy} = yield strength of the web reinforcement [MPa] with $f_{wy} \leq 25f'_c$,

f'_c = concrete cylinder strength [MPa],

ϕ = inclination of compressive stress in the concrete to member axis,

j_t = distance between upper and lower stringer [mm].

The total shear is calculated by eq. (3.1) as the superposition of arch- and truss contributions, with the truss angle ϕ and the arch stress σ_s being the variables. These variables depend on the considered location, that is, whether the desired behavior at the respective location is non-ductile or ductile.

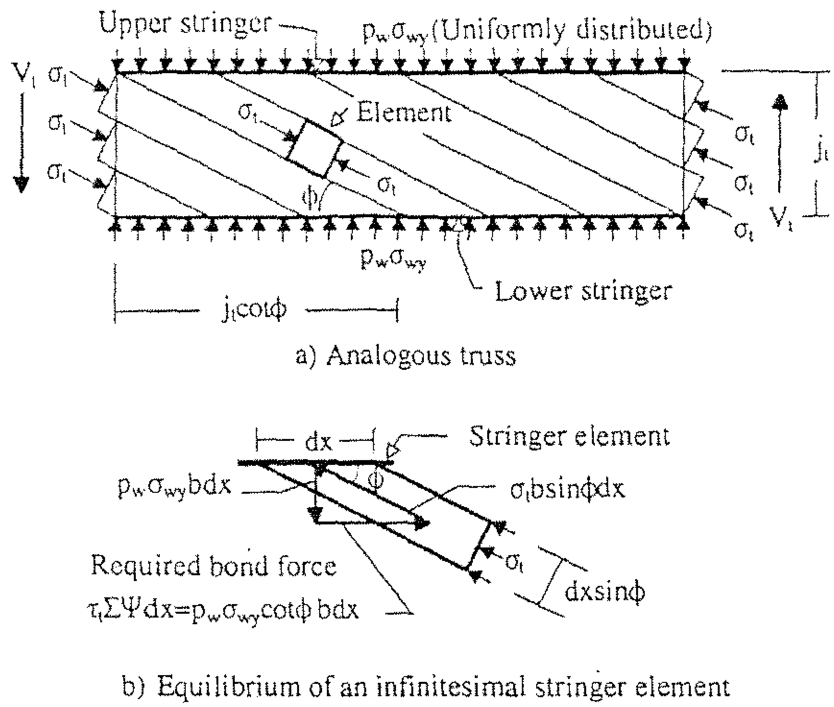

Figure 3-2 Assumed analogous truss model (Watanabe and Ichinose 1991)

3.2.3 *Non-ductile members*

For the limiting shear capacity, the web reinforcement is assumed to have reached the yield-point. Using a reduction factor, v_o, which has been proposed by Nielsen (Nielsen 1999) as

$$v_0 = 0.7 - \frac{f'_c}{200} \tag{3.6),}$$

and the condition that combined compressive stresses from strut and arch action cannot be higher than the reduced concrete cylinder strength

$$\sigma_t + \sigma_s = v_0 f'_c \tag{3.7),}$$

the ultimate shear strength for a non-ductile section of the RC member can be calculated from eqs. (3.1), (3.2), and (3.4) as

$$V_u = V_t + V_s = b \cdot j_t \cdot \rho_w f_{wy} \cot\phi + b\frac{D}{2}(1-\beta)v_0 f'_c \tan\theta \tag{3.8}$$

with $$\sigma_s = (1-\beta)v_0 f'_c \tag{3.9}$$

As a simplification, equation (3.7) assumes that the stresses under arch action, σ_s, and truss action, σ_t, act at the same angle. Based on this assumption, eq. (3.8) can be calculated as the superposition of arch and truss action, which is influenced by the factors described in the following.

The dimensionless factor β is the relation of the average inclined stress in compression to the reduced concrete strength

$$\beta = \frac{\sigma_t}{\nu_0 f'_c} = \frac{\rho_w f_{wy}(1+\cot^2\phi)}{\nu_0 f'_c} \tag{3.10}$$

Evaluating equation (3.9), the contribution of arch action is limited by the fraction of concrete strength, which exceeds the stresses induced by the truss mechanism. Resubstituting eq. (3.10) into the strut contribution, eq. (3.9) can be rewritten as a different form of equation (3.7):

$$\sigma_s = \nu_0 f'_c - \sigma_t \tag{3.11}$$

Equation (3.8) is quadratic in cot ϕ since β is quadratic in cot ϕ. The total shear capacity V_u increases with the increase of cot ϕ in a range of

$$\cot\phi \leq \frac{j_t}{D \cdot \tan\theta} \tag{3.12}$$

Additional limits to cot ϕ are set by the condition that (a) the diagonal stress in compression can not be larger than the effective strength and (b) by a proposal by Thürlimann (Thürlimann 1979) to limit the possible truss angle. Condition (a) results from eq. (3.10) as

$$\cot\phi \leq \sqrt{\frac{\nu_0 f'_c}{\rho_w f_{wy}} - 1} \tag{3.13}$$

Condition (b) was proposed to prevent excessive transverse strains due to loss of aggregate interlock in small inclined trusses as

$$\cot\phi \leq 2 \tag{3.14}$$

Eq. (3.14) limits the strut inclination to values of $\phi > 26.5°$.

It is appropriate to choose the smallest cot ϕ within the constraints set by eqs. (3.12) through (3.14). If eq. (3.13) governs as the smallest value for cot ϕ, substituting eq. (3.13) into eq. (3.10) yields $\beta = 1$. This leads to the disappearance of the term related to arch-action in eq. (3.8). For a value of $\beta < 1$, the arch is contributing to the total shear capacity depending on the capacity of the truss. If the strength of the truss is not sufficient in terms of the reduced concrete strength, the remainder is attributed to the arch. The arch contribution of the total shear capacity, V_s, is dependent on the aspect ratio L/D. Figure 3-3 shows the influence of the shear-span-to-depth ratio L/D on the shear capacity for a hypothetical set of input values. For comparison, Figure 3-4 shows the direct influence of the aspect ratio on the inclination expressed as tan θ. As can be seen from Figure 3-3, for low aspect ratios the arch contribution is higher and decreases asymptotically with an increasing aspect ratio according to eq. (3.3). Watanabe et al. do not set a limit for the inclination of the strut angle θ depending on the slenderness of the member. However, with an increasing slenderness, tan θ becomes very small and the arch contribution to the total shear capacity becomes negligible.

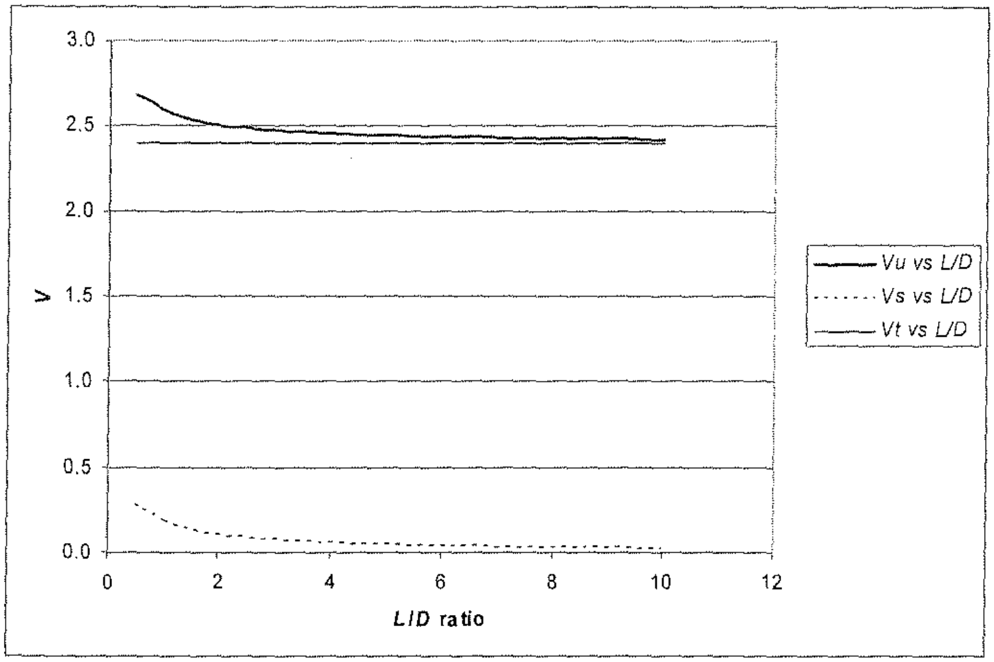

Figure 3-3 Influence of aspect ratio on shear capacity, hypothetical V_t contribution

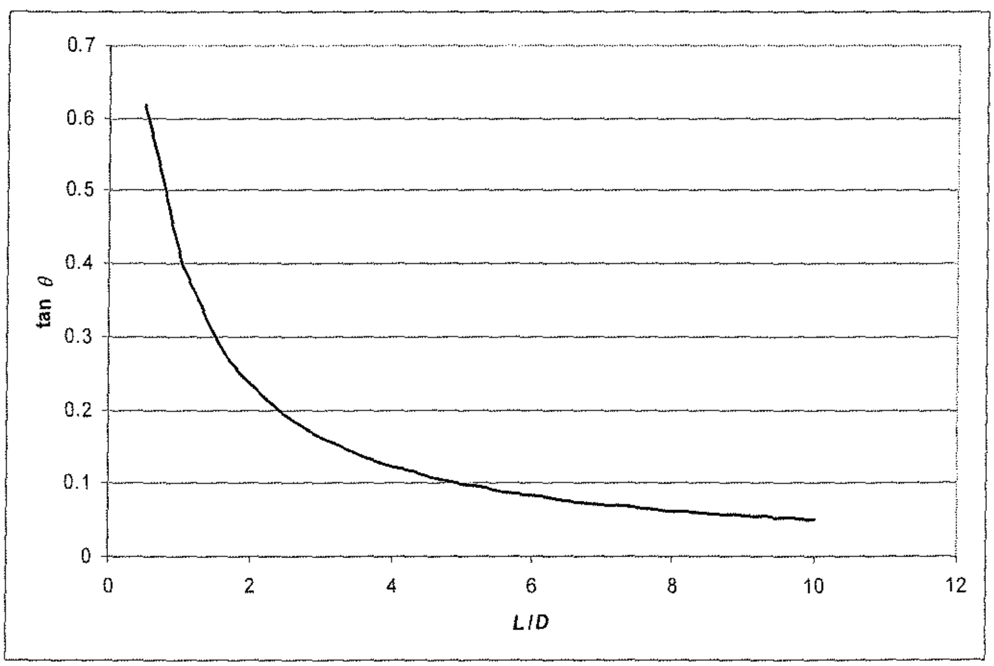

Figure 3-4 Influence of aspect ratio on tan θ

A relationship between V_u and the uniform stress in the web reinforcement, $\rho_w f_{wy}$, is shown in Figure 3-5. The figure illustrates the varying influences of strut and truss action on the shear strength changing with the amount of shear reinforcement in terms of reduced concrete strength.

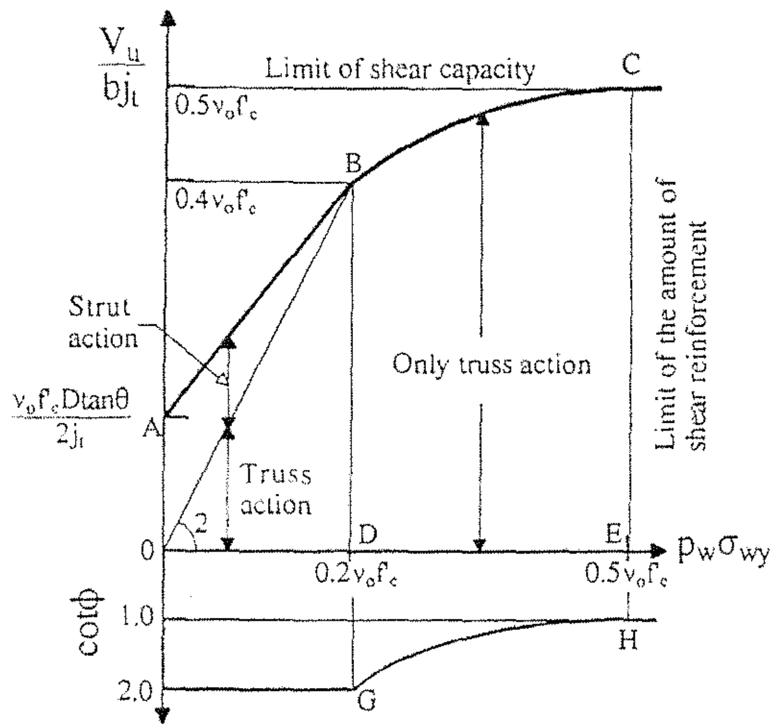

Figure 3-5 Relationship between V_u and $\rho_w \sigma_{wy}$ (Watanabe and Ichinose 1991)

Figure 3-5 also shows the relation of the inclination of the struts to the arch-component. As long as an arch component is contributing to the total shear strength, the inclination is limited to a value of cot ϕ = 2. As stated by Watanabe et al. (Watanabe and Ichinose 1991), the relationship of eq. (3.12) is ignored in the graph for simplicity. If, however, cot ϕ is also limited to values in which the total shear capacity increases, eq. (3.12) needs to be applied.

3.2.4 Ductile members

For member sections with required ductile behavior, the effective concrete strength is lowered to take into account the intersecting set of inclined cracks in the plastic hinge zone. Depending on the expected maximum rotation angle, which for small rotations is approximately the drift ratio, the effective strength of the web concrete is calculated by eqs. (3.15) and (3.16):

$$\nu = (1 - 15R_p)\nu_0 \text{ for } R_p \leq 0.05 \tag{3.15}$$

$$\nu = \frac{\nu_0}{4} \text{ for } R_p > 0.05 \tag{3.16}$$

with ν = strength reduction factor for the web-concrete of a ductile member,

R_p = expected maximum hinge rotation angle [rad].

Additionally, the upper limit of cot ϕ in the hinge region is reduced depending on the expected hinge rotation angle, R_p:

$$\cot \phi_h \leq \lambda \tag{3.17}$$

$$\text{with } \lambda = 2\text{-}50R_p \text{ for } R_p \leq 0.02 \tag{3.18}$$

$$\lambda = 1 \text{ for } R_p > 0.02 \tag{3.19}$$

For members with uniformly distributed shear reinforcement, the ultimate shear strength of a ductile member can be obtained by replacing the effective concrete strength $\nu_0 \cdot f'_c$ by $\nu \cdot f'_c$. In addition, the relationship (3.14) is substituted by (3.15) or (3.16), respectively, to account for the changed conditions along the plastic hinge.

The shear design approach described above is conceptually sensible. However, the model has some shortcomings. It does not take into account a possible axial load on the member, because it has been developed primarily for flexural members. This shortcoming was overcome by the "New RC proposal" by Watanabe and Kabeyasawa (Watanabe and Kabeyasawa 1998), which has been considered in the evaluation in the following chapter.

Because the strut width is taken as a fixed value, it is not possible to adjust to a larger strut width. Connecting the strut width to the depth of the compression zone, which increases with an applied axial load, appears to reflect the conditions in a member more accurately. Furthermore, the assumption that the stresses from both mechanisms act at the same angle simplifies the basic equation (3.7) significantly. It seems questionable to make this assumption first, and when determining the separate contributions treating the respective angles separately as well.

Additional limits of Watanabe's model are set by the concrete reduction factor v_0, which was empirically developed for concrete cylinder strengths from 18 to 60 MPa. For higher strength concrete $v_0 \cdot f'_c$ reaches a maximum value of 24.5 MPa at f'_c = 70 MPa, with decreasing values for higher strength concrete. Also this shortcoming has been addressed in (Watanabe and Kabeyasawa 1998), and is considered in the analytical evaluation of the method as described in Section 4.2.

A truss as depicted in Figure 3-2 can not work in squat members, i.e. in "disturbed" regions ("D-regions" (Schlaich et al. 1987)). Assuming that tensile stresses are taken by the strength of the stirrups, the inclined compression field needs to tie back to an adjacent tensile member over its entire length. This is not provided in a deep member if the transverse reinforcement is assumed uniformly distributed along the entire span. It seems more appropriate to assume the tensile forces lumped in the center of the D-region, with the compression field spanning between supports and stirrup.

The model as described by Watanabe et al. is evaluated on different databases in Section 4.2. The cases considered are slender beams without transverse reinforcement, web-reinforced slender RC beams, and RC members under axial and cyclic shear load. Kabeyasawa proposed a different load reduction factor to account for higher strength concrete in the context of walls (Kabeyasawa and Hiraishi 1998). The application of the model to RC walls and deep beams with and without transverse reinforcement is also evaluated in Section 4.2.

3.3 Shear strength of beams without transverse reinforcement

A model to describe physically the shear strength of slender members without transverse reinforcement has been developed by Reineck (Reineck 1990), and was summarized in (Reineck 1991b). Reineck uses equilibrium conditions in a free-body diagram of an RC member as shown in Figure 3-6.

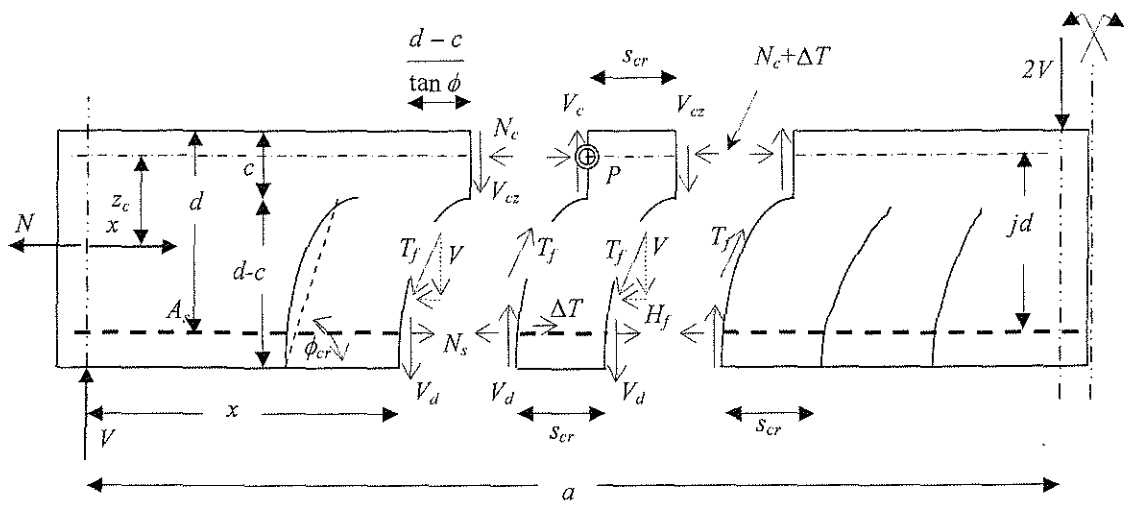

Figure 3-6 RC member with tooth element and its forces in B-region, adapted from (Reineck 1991b)

The shear-carrying mechanism of the beam is considered to have three different contributions:

V_{cz} = a contribution of the uncracked compression zone

V_f = a contribution related to friction between crack surfaces

V_d = a contribution from dowel-action in the longitudinal reinforcement

As stated by Reineck, an additional contribution from cantilevering action of the tooth from the compression zone is negligible (Reineck 1990, 1991b).

The tooth in Figure 3-6 is subjected to a constant part of the flexural moment within the element length. To avoid possible side-effects from a *D*-region, Reineck's proposed method is sought to be valid if the load is applied at a distance $2h$ from the support (Reineck 1990, 1991b). This requirement is equivalent to a condition that the aspect ratio a/d of the member should be larger than a value of two to ensure the analysis is carried out in a *B*-region of the member. In other words, this method is not valid for deep beams and walls.

The failure criterion formulated by Reineck is that a crack propagates further into the compression zone, breaking away the tooth from the compression zone. This is related to a rotation of the tooth element related to a critical slip at mid-depth of the crack (Reineck 1990). Since the model relies on the conditions within the crack, a characterizing crack has to be explicitly modeled. The spacing between cracks was derived in (Reineck 1990) as

$$s_{cr} = 0.7 \cdot (d - c) \tag{3.20}$$

wherein d = effective depth of the member

c = depth of the compression zone

According to the author, the cracks are assumed straight cracks with a critical inclination of $\beta_{cr} = 60^\circ$.

From equilibrium in the free-body diagram of Figure 3-6, it is found that the applied shear force has to equal the sum of the different contributions named above

$$V = V_{cz} + V_f + V_d \tag{3.21}$$

Moment equilibrium in the tooth element yields

$$\begin{aligned} & V \cdot s_{cr} = \Delta T \cdot jd \\ \Leftrightarrow & \frac{\Delta T}{b_w \cdot s_{cr}} = \frac{V}{b_w \cdot jd} = v_n \end{aligned} \tag{3.22}$$

Equation (3.22) constitutes the basic equation for the nominal shear stress as the resultant from a change in the force within the longitudinal reinforcement, ΔT. This force is equivalent to the bond-force of the longitudinal reinforcement, which is dependent on the change in the bending moment.

If the axial stresses in the compression zone are assumed linearly distributed as depicted in Figure 3-7, the contribution of the compression chord to the shear-capacity is found by integrating the stress over the uncracked area:

$$\begin{aligned} & V_c = \frac{2}{3} c \cdot b_w \cdot v_n = \frac{2}{3} \frac{c}{jd} V \\ & \text{with } jd = d - \frac{c}{3} \end{aligned} \tag{3.23}$$

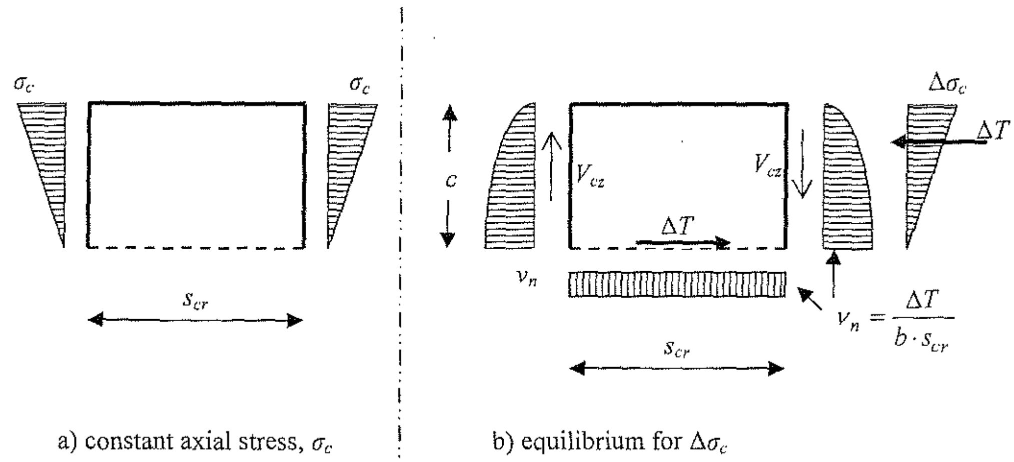

Figure 3-7 Equilibrium of stresses in the compression zone of a tooth element, adapted from (Reineck 1991b).

As stated by Reineck, a linear distribution of axial stresses within the tooth element can be assumed, because the element itself is uncracked. Consequently, also the depth of the compression zone can be calculated from linear elastic bending theory as $c = kd$. The contribution of the compression chord is eliminated from eq. (3.21) by substituting eq. (3.23) into (3.21):

$$V = \frac{jd}{d-c}\left(V_f + V_d\right) \tag{3.24}$$

To describe the conditions within the cracks, Reineck derives the strain in the longitudinal reinforcement. The strain will be used later to calculate the crack width at mid-depth of the crack. From moment equilibrium in Figure 3-6, the strain is calculated as

$$\varepsilon_s = \frac{1}{E_s A_s jd}\left[V\left(x + \Delta x\right) + N \cdot z_c - V_d \frac{jd}{\tan \beta_{cr}}\right] \tag{3.25}$$

with $\Delta x = \dfrac{d-c}{\tan\beta_{cr}}\left(1+\dfrac{2}{3}\dfrac{c}{jd}\right)$

Assuming a constant distribution of shear stresses related to friction, and a parabolic distribution of shear stresses related to dowel action, Reineck derives the shear capacity of the member as a function of frictional shear stresses, τ_f, and dowel action, V_d (Reineck 1991b):

$$V = b_w \cdot jd \cdot \tau_f + \frac{3}{4}\frac{jd}{d-c}V_d \tag{3.26}$$

The stress field in the tooth element is explained by a truss model developed for principal compression and tension stresses in the concrete, inclined at an angle $\beta_{cr}/2$.

The strength resulting from dowel action was derived by Reineck (Reineck 1990), and is given in (Reineck 1991b) as

$$V_{du} = 1.4\frac{\rho^{8/9}}{f_c^{2/3}\cdot d^{1/3}}b_w \cdot d \cdot f_c \tag{3.27}$$

With the concrete compressive strength taken as $f_c = 0.95f'_c$ [MPa], and the effective member depth d in [m].

Reineck (Reineck 1991b) proposes the constitutive equation for the ultimate frictional shear stress along the crack surfaces based on earlier work on friction transfer at constant crack widths by Walraven (Walraven 1980, 1981a) as:

$$\tau_{fu} = 0.45 \cdot f_{ct}\left(1-\frac{\Delta n}{\Delta n_u}\right) \tag{3.28}$$

with $f_{ct} = 0.246 \cdot f_c^{2/3}$ = tensile strength of concrete

$\Delta n_u = 0.9$ mm = critical crack width

Δn = calculated crack width

According to Reineck, the loss of shear stresses, and therefore the failure of the member, is related to a critical slip at mid-depth of the crack. This critical slip is given as a function of the crack width Δn by

$$\Delta s_u = 0.336 \cdot \Delta n + 0.01 \text{ [mm]} \tag{3.29}$$

From geometrical examination within the crack (Figure 3-8), the in-situ crack width can be calculated from the horizontal displacement, Δu, and the critical slip, Δs_u. In (Reineck 1990) it was shown that the horizontal displacement at mid-depth of the crack is approximately half of the horizontal displacement at the longitudinal reinforcement, which is known from the strain in the reinforcement.

$$\begin{aligned} \Delta u &= 0.5 \Delta u_L = 0.5 \cdot \varepsilon_{sm} \cdot s_{cr} \\ &= 0.5\left(\varepsilon_s - \Delta \varepsilon_s\right) \cdot s_{cr} \end{aligned} \tag{3.30}$$

in which $\Delta \varepsilon_s$ = strain in the longitudinal reinforcement from (3.25),

$\Delta \varepsilon_s$ = strain that considers a tension stiffening effect of the concrete between the cracks. As stated in (Reineck 1991b), the value for $\Delta \varepsilon_s$ is negligible in the calculation of the ultimate shear force.

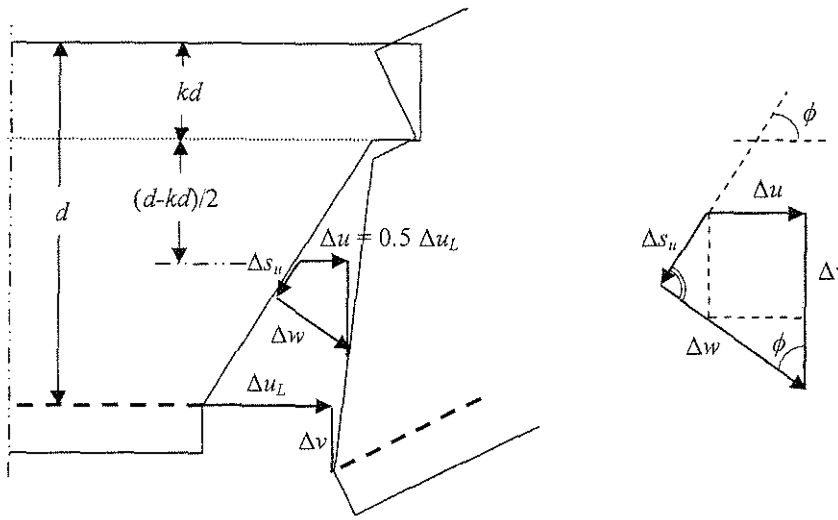

Figure 3-8 Geometry within the crack, adapted from (Reineck 1991b).

Following a derivation in (Reineck 1991b), and using a critical crack inclination of $\beta_{cr} = 60^{\circ}$, the crack width as a function of the strain in the longitudinal reinforcement and the critical crack spacing is given as

$$\Delta n = 0.71 \cdot \varepsilon_s \cdot s_{cr} \tag{3.31}$$

Using equations (3.25) through (3.31) the shear capacity of an RC member can then be calculated from equation (3.26).

The ultimate shear capacity, including all contributions, results in:

$$\begin{aligned} V_u = {} & 0.45 \cdot f_{ct} \cdot b_w \cdot jd\left(1 + 0.5\frac{d-c}{\Delta n_u}\Delta\varepsilon_s\right) - 0.224\left(1 - \frac{c}{d}\right)\frac{z_c}{d} \cdot \frac{f_{ct}}{f_c} \cdot \lambda \cdot N \\ & + V_d \cdot \frac{\left(\frac{3}{4}\frac{jd}{d-c} + 0.224\left(1-\frac{c}{d}\right)\frac{jd}{d \cdot \tan\beta_{cr}} \cdot \frac{f_{ct}}{f_c} \cdot \lambda\right)}{\left(1 + 0.224\left(1-\frac{c}{d}\right) \cdot \frac{f_{ct}}{f_c} \cdot \lambda \cdot \frac{x + \Delta x}{d}\right)} \end{aligned} \tag{3.32}$$

with $\lambda = \dfrac{\varepsilon_{sy} \cdot d}{\omega \cdot \Delta n_u}$

$$\omega = \frac{\rho_s f_y}{f_c}$$

$$\varepsilon_{sy} = \frac{f_y}{E_s}$$

Since expression (3.32) is rather cumbersome to determine, Reineck suggests the following simplification, "ignoring small terms", and the axial force N. The internal lever arm jd is taken as $jd = 0.9d$, and $\Delta x = 0.5d$ (Reineck 1991b):

$$V_u = \frac{b_w \cdot d \cdot 0.4 \cdot f_{ct} + V_{du}}{\left[1 + 0.16 \dfrac{f_{ct}}{f_c} \lambda \left(\dfrac{a}{d} - 1\right)\right]} \tag{3.33}$$

It should be noted that the previous model can be extended to RC members with transverse reinforcement (Reineck 1991a).

Reineck's model as previously described is physically explainable and considers important factors as shear-span-to-depth ratio, and axial forces. Furthermore, it delivers a physical explanation for the contribution of the uncracked compression zone, and friction in the tensile zone of the member.

An evaluation of the model follows in Chapter 4.3. In the evaluation, equation (3.33) was applied to a database of 395 slender RC members without web reinforcement that failed in monotonic shear.

Since the model as previously derived is rather cumbersome and hard to use as a design tool, a simplification is proposed in Chapter 5.2.3. This simplification represents one of three contributing shear-resisting mechanisms in the proposed model.

3.4 Analysis based on drift capacity

The shear capacity of columns under axial and variable horizontal loads as a function of maximum axial and shear unit stresses, maximum drift ratio, and the properties of the column has been examined by S. Pujol, M. Sözen, and J. Ramírez (Pujol 2000) based on the observation that "the main function of transverse reinforcement is to confine the core subjected to a complex state of stress rather than simply resist shear or improve deformability under axial compression." (Pujol 2000) This research is based on earlier work by S. Pujol (Pujol 1997).

According to this study, the yielding of the transverse reinforcement is the "defining event" in the specimen behavior: Before yielding, the column is able to keep its strength; after yielding very fast strength-decay sets in, ultimately leading to failure. The constant axial load reduces the ductility of the column, and thus accelerates the stiffness and strength degradation. It is concluded that the amount of reinforcement, and therefore the column shear capacity, has to be determined as a direct combination of normal and shear stresses. This is done using the Coulomb criterion (Figure 3-9).

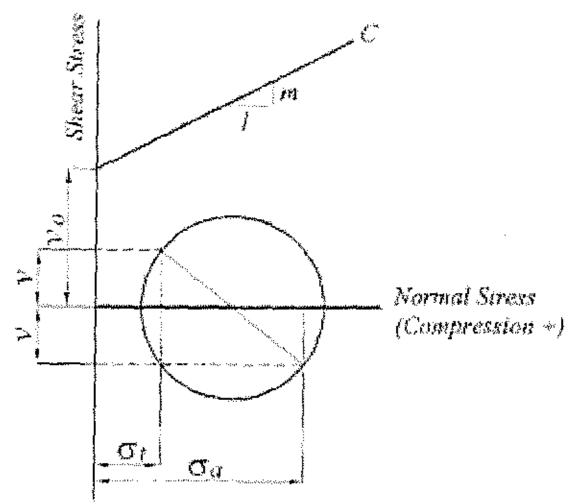

Figure 3-9 Coulomb's criterion (Pujol 2000)

The Coulomb criterion consists of a "failure line", *C*, and a Mohr's circle representing a particular combination of axial and shear stresses. Line *C* is depending on the unit stress acting perpendicular to the potential failure plane and is defined by

$$v_u = v_0 + m\sigma \tag{3.34}$$

where v_u = unit shear strength

v_0 = ordinate of line representing Coulomb's criterion at $\sigma = 0$

m = slope of line representing Coulomb's criterion

σ = unit stress acting perpendicular to the potential failure plane.

Failure of the specimen is defined as the particular combination of axial and shear stresses, which results in a Mohr's circle transgressing the line *C*.

Since it is difficult to make a clear statement concerning the equilibrium that defines Mohr's circle at the specific location of the failure plane in the column, forces instead of unit local stresses are used to construct Mohr's circle at the limiting stage of loading under shear reversals. The forces are normalized by the core area of the column and are given as (Pujol 2000):

$$\sigma_a = \frac{P+T}{h_c \cdot b_c} \qquad = \text{axial stress} \qquad (3.35),$$

$$v = \frac{V}{h_c \cdot b_c} \qquad = \text{mean shear stress} \qquad (3.36),$$

$$\sigma_t = \frac{A_w \cdot f_{yw}}{s \cdot b_c} \qquad = \text{tensile stress normal to the column axis in the}$$

plane of shear with transverse reinforcement at yielding (3.37)

where P = applied axial load,

T = force in the tensile reinforcement, taken as $T = 0.5A_s f_y$,

V = shear force,

A_s = area of longitudinal reinforcement,

A_w = area of hoop bars in planes parallel to the shear plane,

f_y = yield stress of longitudinal reinforcement,

f_{yw} = yield stress of transverse reinforcement,

h_c = depth of core (taken as center-to-center from peripheral hoops),

b_c = width of core (taken as center-to-center from peripheral hoops),

s = spacing of transverse reinforcement.

Following an approach by Richart et al. (Richart 1929), which relates the Coulomb criterion to the strength of concrete as

$$v_u = k_1 f'_c + k_2 \sigma \qquad (3.38),$$

Pujol et al. define the factor k_1 as a variable depending on the drift ratio γ. This is based on the hypothesis that k_1 as the only variable is representing the decay of concrete strength due to cumulative effects of micro-cracks resulting from an interaction of the number, N, and extent, γ, of the loading cycles. Each subsequent loading in the same direction will result in further damage of the concrete and therefore weaken the concrete strength. Due to a lack of experimental data to define the constants for equation (3.34), the equation is presented in relation to the displacement only; the number of loading cycles is not considered. In a preceding study, the "parameter γ/λ was found to be suitable for normalizing the drift capacity data from RC members subjected to cyclic shear" (Pujol 1997). The factor λ represents the ratio of the shear span to the effective depth, a/d. Following an evaluation of the results of 29 tested RC columns; the lower bound of k_1 depending on γ/λ is presented as

$$k_1 = \frac{1}{7}\left(1 - \frac{100}{3} \cdot \frac{\gamma}{\lambda}\right) \geq 0 \qquad (3.39)$$

Geometric examination of the failure condition for the Coulomb criterion, the criterion in terms of axial and tensile stresses in the failure surface is expressed as

$$\frac{\sigma_t}{\sigma_a} = \frac{3}{8} \cdot \alpha + 1 - \frac{5}{8}\sqrt{\alpha^2 - \beta^2} \tag{3.40}$$

Factors α and β are given in (Pujol 2000) as:

$$\alpha = 4\frac{k_1 \cdot f'_c}{\sigma_a} + 3$$

$$\beta = 4\frac{v}{\sigma_a}$$

Substituting equation (3.37) into (3.40) results in the required transverse reinforcement ratio:

$$\rho_w = \frac{A_w}{s \cdot b_c} = \left[\frac{3}{8} \cdot \alpha + 1 - \frac{5}{8}\sqrt{\alpha^2 - \beta^2}\right] \cdot \frac{\sigma_a}{f_{yw}} \tag{3.41}$$

Equation (3.41) gives a design recommendation for transverse reinforcement based on the assumed conditions in the member. However, it is not possible to evaluate this approach on a set of tested beams that have not been built according to equation (3.41), since the equation allows only for one specific web reinforcement configuration. Nevertheless, equation (3.41) was solved by the author for an ultimate shear capacity V_u as follows to allow for a comparison with other analysis models.

The ultimate shear strength of a RC column can be derived by solving eq. (3.41) for the shear strength V_u with the designations as previously listed:

$$V_u = \frac{2}{5}\left(\frac{\rho_w f_{yw}}{\sigma_a} + \frac{1}{4}\alpha - 1\right)(P + T) \tag{3.42}$$

Pujol et al. assume that the initial shear strength of the column under static shear meets the requirements of the ACI 318 (2002) shear equation:

$$V_u = V_c + V_s \tag{3.43}$$

Wherein the "steel" contribution is calculated as

$$V_s = \frac{A_v f_y d}{s} \tag{3.44}$$

The "concrete" contribution V_c is determined using eqs. (3.45):

$$V_c = 0.17 \cdot \left(1 + \frac{\sigma_a \cdot A_c - T}{13.8 \cdot A_g}\right) \cdot \sqrt{f'_c} \cdot (0.8A_g) \quad \text{(SI units)} \tag{3.45}$$

$$V_c = 2 \cdot \left(1 + \frac{\sigma_a \cdot A_c - T}{2000 \cdot A_g}\right) \cdot \sqrt{f'_c} \cdot (0.8A_g) \quad \text{(British units)}$$

The described approach was derived using experimental results from tested RC columns with a slenderness ratio λ from 1.9 to 3.5 and a nominal unit shear stress range from 0.5 to $1.1\sqrt{f'_c}$ MPa. The applied compressive load was in the range from 7 to 35 percent of the nominal axial compression capacity. The examined columns had rectangular cross-sections and confined cores. As is stated by Pujol, the proposed model is applicable to columns having an axial stress of $\sigma_a \leq 0.35f'_c$ and a nominal unit shear stress range from 0.5 to $0.7\sqrt{f'_c}$ MPa (Pujol 2000).

An analytical evaluation of equation (3.42) is described in Chapter 4.4 using the amount of reinforcement provided in the considered database.

3.5 *Shear strength as a function of required displacement ductility*

Research carried out at the University of California at San Diego (UCSD) establishes an interaction between the flexural ductility and the shear strength for circular and rectangular columns. The main body of the work is described by M.J.N. Priestley et al. (Priestley 1994). It is based on previous research by Ang et al. (Ang et al. 1989) and Wong et al. (Wong 1993). Similar to (Watanabe and Ichinose 1991), the shear capacity of RC columns is treated separately comprising an arch component and a truss component. The strength enhancement through axial load is treated in the arch model, the "concrete component" of the shear strength is considered in the truss model, complemented by the contribution from transverse shear reinforcement. Based on the work by Ang et al. and Wong et al., Priestley's work tries to compensate for an apparent underestimation of the influence of axial load on the shear capacity of RC columns in the preceding research (Priestley 1994). Ang and Wong examined circular columns subjected to multidirectional load paths. A shear design method was proposed, which was taking the ductility of the columns into account, and which changed the inclination of the compression struts depending on the transverse reinforcement.

Priestley et al. propose to describe the shear strength of RC columns with three components: a concrete component V_c, of which the magnitude depends on the level of required ductility, an axial load component V_p that depends on the column aspect ratio, and a truss component V_s, which is considering the transverse reinforcement. The nominal shear capacity is given as the superposition of these three components as

$$V_n = V_c + V_p + V_s \tag{3.46}$$

The concrete component is described in a form of

$$V_c = k\sqrt{f'_c}A_e \tag{3.47}$$

in which $A_e = 0.8A_g$ = effective area,

k = a reduction factor depending on the required displacement ductility level.

Depending on the required displacement ductility level, μ, Priestley presents a graph for the factor k that can also be expressed as (Priestley 1994)

$$k = \begin{cases} 0.29 & \mu \le 2 \\ \left(0.48 - 0.19 \cdot \dfrac{\mu}{2}\right) & 2 \le \mu \le 4 \\ 0.1 & 4 \ge \mu \end{cases} \tag{3.48}$$

with $\mu = \dfrac{\Delta_{\max}}{\Delta_y}$ = displacement ductility (3.49)

where Δ_{max} = maximum displacement,

Δ_y = displacement at yielding of longitudinal reinforcement.

The axial load component is provided by the projection of the axial load on the shear plane:

$$V_p = P \cdot \tan\alpha = P \cdot \frac{D-c}{2a} \tag{3.50}$$

where P = axial load,

α = inclination of the strut,

D = total section depth,

c = depth of the compression zone,

a = effective length of the column, taken as L for a cantilever column and $L/2$ for a column in reversed bending.

Equation (3.50) represents a straight, linear arch as in the Watanabe approach. Unlike the arch model proposed by Watanabe et al. it is depending solely on the axial load. The concrete strength does not influence the arch capacity. Its depth is determined by the depth of the compression zone, c, under design loads. As the axial load and/or the applied moment increases, the effective fraction of V_p to the overall shear strength decreases, since the depth of the compression zone is increasing. V_p is not degraded by increasing ductility. The compression zone depth is calculated from equilibrium conditions of internal forces in the column under the considered load case. Though it is desirable to include the effects of axial loads on the shear capacity, it is not clear why the axial load should contribute as an inclined resistance to the overall shear capacity. Instead of a direct contribution on the shear capacity, a possible axial load will rather affect the shear resisting mechanisms as aggregate interlock, or, as realized by Priestley et al., it will increase the depth of the compression zone. An increasing depth of the compression zone will increase the shear resistance contributed by the uncracked compression zone. The arch as a shear resisting mechanism, however, should be related to the compressive strength of the concrete and the possible stress distribution for stresses related to arch action within the member.

The truss mechanism component, V_s, proposed by Priestley et al. implies a 30° crack inclination angle, or a corner-to-corner inclination, whichever is larger. For circular and rectangular columns, respectively, Priestley (Priestley 1994) proposes the following equations:

$$V_s = \frac{\pi}{2} \frac{A_{sh} f_{yh} D'}{S} \cot 30° \tag{3.51}$$

$$V_s = \frac{A_v f_{yh} D'}{S} \cot 30° \tag{3.52}$$

with D' = distance between centers of the peripheral hoop or spiral,

S = spacing of transverse reinforcement,

A_{sh}, A_v = area of peripheral spirals or ties,

f_{yh} = yield stress of peripheral hoops.

As stated in Priestley's proposal (Priestley 1994), using D' provides a larger effective depth for rectangular columns than usually taken. The approach for equations (3.51) and (3.52) has been adopted from the proposals by Ang (Ang et al. 1989) and Wong (Wong 1993).

The examination of different multi-directional load paths as conducted by Wong et al.(Wong 1993) did not yield a considerable change in specimen behavior depending on the displacement pattern. The consideration of a simple "b-type" displacement pattern, i.e. a full displacement cycle in each consecutive direction, yielded similar results as the use of more complex displacement patterns. Under biaxial displacement patterns, the concrete shear capacity decreased for the second displacement path in the same load cycle. "However, the reduction of initial shear strength, and ductility capacity of squat columns, subjected to biaxial displacement history was not very significant" (Wong 1993).

A numeric evaluation of the shear design method as proposed by Priestley et al. is described in Section 4.5.

3.6 Analysis based on shear-friction

An approach to describe the shear strength of an RC member by modeling a shear-friction mechanism has been developed by Chen and MacGregor (Chen and MacGregor 1993). In addition to the truss mechanism as described by Collins et al. (Collins 1991), a shear-friction mechanism between crack surfaces in the inclined compression field is described to contribute to the shear resistance of an RC member. According to Chen, shear-friction will form an additional part to the truss model, as it will increase the shear capacity of the member by relating the axial force to the resisting stresses in the inclined compression field (Chen and MacGregor 1993). This is done through shear-friction along the cracks. Therefore, the inclination ϕ of the cracks defines the inclination of the shear-friction component V_{sf}. The friction forces will be mostly dependent on the axial compression force of the truss mechanism, N_t. Consequently, the effect of shear-friction is closely tied to the truss mechanism.

According to Chen, the shear transfer along two cracked surfaces can be calculated by the dry friction law:

> "The limiting static friction force is directly proportional to the magnitude of the normal force N, and is independent on the area in contact." (Chen and MacGregor 1993)

Following this, Chen proposes that the shear force V transferred across two cracked surfaces is expressed in terms of an axial force N acting normal to the interface by a coefficient for static friction, μ_s:

$$V = \mu_s N \tag{3.53}$$

As described by Chen, if the shear force V has to be transferred along an inclined crack as shown in Figure 3-10, the forces can be expressed by their respective components, V_ϕ and N_ϕ:

$$V_\phi = V \cdot \sin\phi + N \cdot \cos\phi \tag{3.54}$$

$$N_\phi = V \cdot \cos\phi - N \cdot \sin\phi \tag{3.55}$$

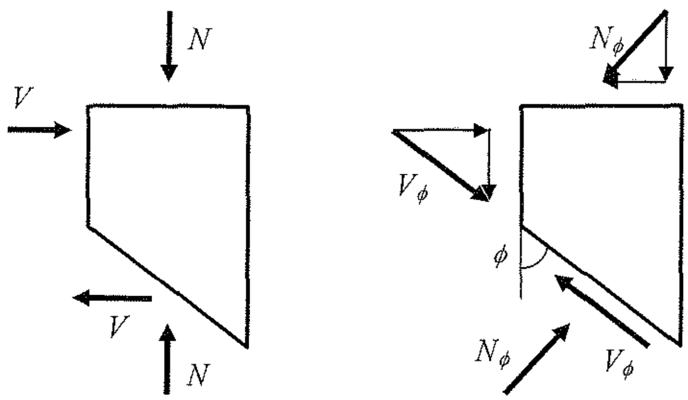

Figure 3-10 Rotation of forces (Adapted from (Chen and MacGregor 1993))

Since V_ϕ and N_ϕ are perpendicular, eq. (3.53) holds true and becomes:

$$V_\phi = \mu_s N_\phi \tag{3.56}$$

Substituting eqs (3.54) and (3.55) into eq. (3.56) yields

$$\begin{aligned} &V\sin\phi + N\cos\phi = \mu_s\left(N\sin\phi - V\cos\phi\right) \\ &\Leftrightarrow V + N\cot\phi = \mu_s\left(N - V\cot\phi\right) \\ &\Leftrightarrow V + \mu_s V\cot\phi = \mu_s N - N\cot\phi \end{aligned}$$

This can be expressed in a form similar to eq. (3.53) as

$$V = \frac{\mu_s - \cot\phi}{1 + \mu_s \cot\phi} N \tag{3.57}$$

The coefficient for inclined friction under V and N thus becomes according to Chen:

$$\frac{\mu_s - \cot\phi}{1 + \mu_s \cot\phi} = \mu_\phi \tag{3.58}$$

Using the expression in (3.58), equation (3.57) can be rewritten as

$$V = \mu_\phi N \tag{3.59}$$

With equation (3.59), the friction between two inclined cracked surfaces is described by Chen and MacGregor (Chen and MacGregor 1993) as a function of the crack-angle ϕ, if the coefficient for static friction under normal forces, μ_s, is known. The force N is the longitudinal compression force in the concrete.

The contribution of the shear-friction mechanism to the overall shear resistance of the member will increase with an increasing axial force N acting on the cracked surfaces. With an increase of the axial force N, the area of the compression zone will increase. Therefore, the shear transferred by the uncracked compression zone will increase. Additionally, the coefficient for inclined friction according to eq. (3.58) will increase with an increasing angle ϕ. This will also result in an increase of the contribution of the shear-friction mechanism.

It follows that the longitudinal compression force in the concrete, N, can be related to the shear-friction mechanism by assuming that the shear contribution of the forces in the concrete is directly proportional to the magnitude of the longitudinal compression force in the concrete. According to Chen, the shear contribution of the concrete is given by the sum of the transverse components of the frictional forces, F_{dy}, the shear carried by the uncracked compression zone, F_{cy}, and dowel action of the tensile reinforcement, V_d (Chen and MacGregor 1993).

$$V_{sf} = F_{dy} + F_{cy} + V_d \tag{3.60}$$

The internal forces in a cracked beam following Chen's approach are shown in Figure 3-11. Figure 3-11 a) shows the state of stresses in the member, wherein f_c is the compressive stress in the uncracked concrete, and f_d is the compressive stress due to friction along the crack plane. The forces V_s and V_d represent the tensile force in the transverse reinforcement and the resisting force from dowel action of the longitudinal reinforcement, respectively. The stresses from friction in the crack plane are caused by the relative movement between the two surfaces. Since this relative movement changes along the crack, magnitude and direction of the stresses induced by friction gradually change from axial direction and a relatively high amount towards the direction of the crack and zero amount of stress. Figure 3-11 b) shows the resulting forces of the stresses in Figure 3-11 a), and Figure 3-11 c) shows the longitudinal and transverse components of theses forces. Chen assumes that the resultant of the lateral components, V_{sf}, is acting at the center of the crack, located at the same point as the tensile force in the stirrups, V_s, as shown in Figure 3-11 d) (Chen and MacGregor 1993). The resultant C of the compression forces F_{dx} and F_{cx} in longitudinal direction is assumed to act in the compression zone.

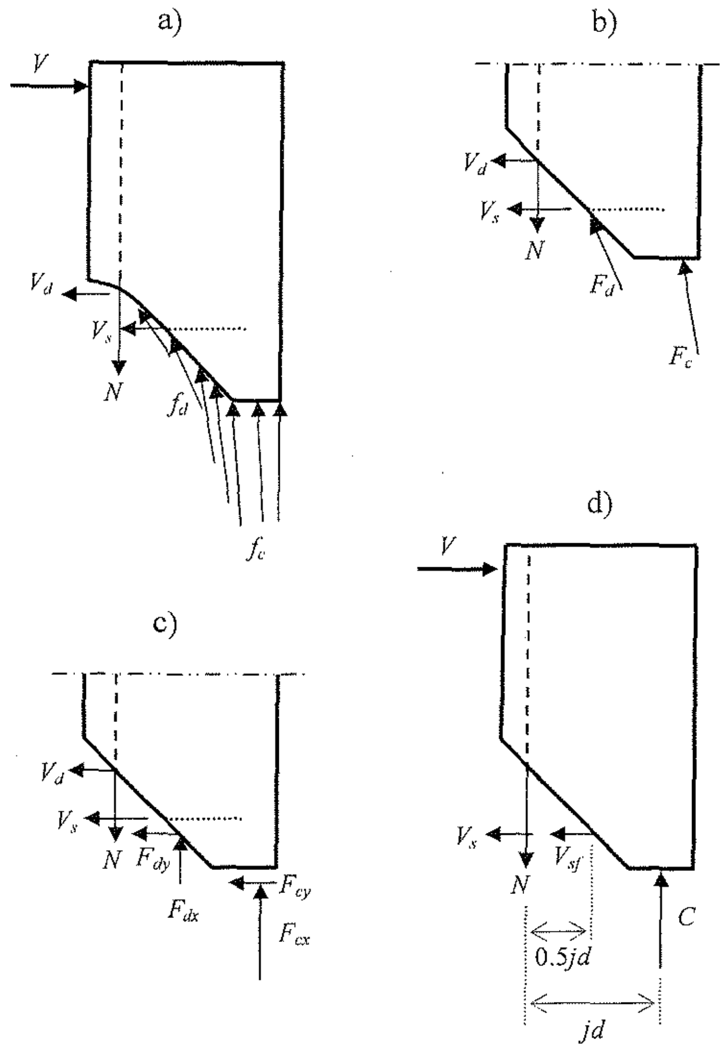

Figure 3-11 Internal forces for the shear-friction mechanism (Adapted from (Chen and MacGregor 1993))

Figure 3-12 shows the shear-friction model as proposed by Chen and MacGregor applied to the variable angle truss model developed by Collins (Collins 1991). The figure displays equilibrium of forces in the crack plane and the adjacent section. Additional to the shear resisted by truss-action, V_t, the shear-friction component V_{sf} is acting on the crack plane. Therefore, the shear resisted by truss-action is extended by the shear-friction component to

$$V = V_t + V_{sf} \tag{3.61}$$

For a combination of the traditional truss model with the shear-friction model, the force V_s in Figure 3-11 is replaced by V_t, the component from truss-action.

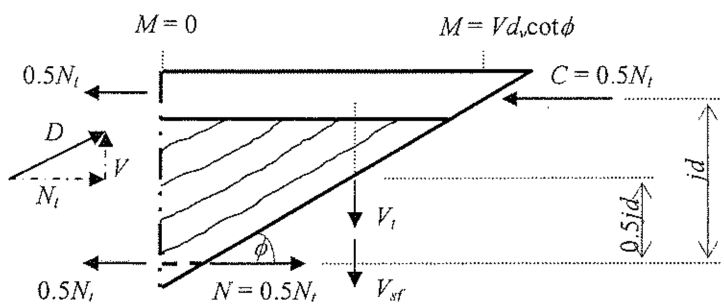

Figure 3-12 Equilibrium of forces in the combined truss and shear-friction model (Adapted from (Chen and MacGregor 1993))

Following Chen, the shear carried by the shear-friction mechanism can be formulated similar to eq. (3.59) with the inclusion of an efficiency factor ν as:

$$V_{sf} = \nu N \tag{3.62}$$

The efficiency factor ν is of a form similar to the coefficient for inclined friction, μ_ϕ:

$$\nu = \frac{\nu_0 - \cot\phi}{1 + \nu_0 \cot\phi} \tag{3.63}$$

Substituting ν into equation (3.62) yields

$$V_{sf} = \frac{\nu_0 - \cot\phi}{1+\nu_0 \cot\phi} N \tag{3.64}$$

Independent of the efficiency factor ν, in terms of the crack inclination ϕ, the shear-friction component behaves different than the truss mechanism. While the capacity of the truss mechanism decreases with an increasing value ϕ, the contribution of the shear-friction mechanism increases with steeper cracks due to an increasing shear-friction coefficient (eq.(3.64)). As stated by Chen, the function of the total shear resulting from truss-action and shear-friction, defined by the sum $V_t + V_{sf}$ has a vertex with a minimum value (Chen and MacGregor 1993). Shear failure will occur at this vertex value at an inclination found by setting the derivative of V with respect to ϕ to zero:

$$\frac{\partial\left(V_t + V_{sf}\right)}{\partial\phi} = 0 \tag{3.65}$$

If the compressive force in the concrete, N, in eq. (3.64) is assumed mainly to be a function of the bending moment, rather than a function of the crack inclination, equation (3.65) yields

$$\tan\phi = \frac{\nu_0}{\sqrt{\left(1+\nu_0^{\,2}\right)\dfrac{N}{A_w f_{wy} jd/s} - 1}} \tag{3.66}$$

The expression in eq. (3.66) relates the inclination at shear failure to the efficiency factor ν and the longitudinal force N. Since neither the inclination nor the longitudinal force at shear failure is known, one of the unknowns has to be assumed in order to calculate the shear capacity of the member. Chen proposes to assume the critical crack inclination ϕ for design (Chen and MacGregor 1993).

To evaluate Chen's proposed method, Figure 3-13 shows the contribution of the shear-friction component V_{sf} in variation with the angle ϕ and the efficiency factor ν. Values for ν have been experimentally derived in (Chen and MacGregor 1993) within a range of $3 \le \nu \le 8$. For the evaluation, eq. (3.66) is solved for the axial load N, and inserted into the basic equation for friction, eq. (3.64). The contribution of the stirrups, $A_w f_{wy} jd/s$, resulting from the derivative of the equation for the total capacity of the combined shear-friction / truss model, is assumed for evaluation purposes to be a value of 250. This value merely represents a scaling factor for the comparison of different efficiency factors. It can be seen that for very small efficiency factors $0 \le \nu_0 \le 1$, the contribution of shear-friction would be negative. It can be argued that considering the scaling factor of 250, the contribution is effectively zero. However, for larger efficiency factors and larger crack inclination, the resisting force from shear-friction and truss model becomes smaller than the value from truss action alone. This would mean that the shear-friction mechanism acts against the truss mechanism. For $2 \le \nu_0 \le 4$, V_{sf} increases slightly with an increasing assumed crack inclination, before it decreases with relatively large values for ϕ. This effect becomes more distinct, the higher the efficiency factor is. For $\nu_0 = 5$, V_{sf} decreases almost linearly with an increasing angle.

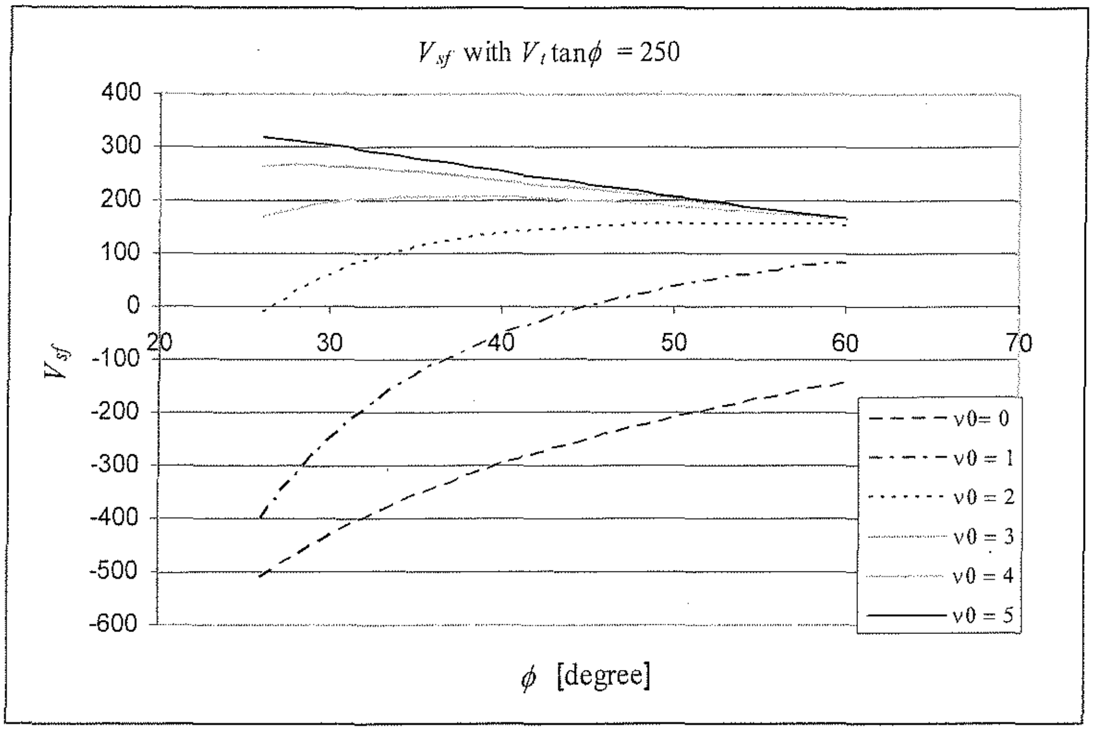

Figure 3-13 Relation of V_{sf}, assumed crack inclination, and efficiency factor

Conceptually, this means that the contribution of the shear-friction mechanism to the total strength of the truss decreases, even if the efficiency factor ν according to eq. (3.63) increases with a steeper crack inclination. This is clearly a contradiction in the model proposed by Chen and MacGregor. For a constant axial load N, the contribution from shear-friction should be higher for larger crack inclinations following the dry-friction law as stated before. Since the shear-friction contribution should be higher, also the overall resistance should be higher than from truss action alone.

In addition to these conceptual shortcomings, the model is not able to represent effects of the size of the member, or a direct contribution of the uncracked compression zone. The function represented by the differential equation (3.65) has no optimum regarding the two variables, crack inclination ϕ, and axial force N. Assuming the crack inclination and solving the equation for N yields several values for the axial force, depending also on the efficiency factor. However, in turn, the efficiency factor describes the relationship of the axial force to the shear resistance. This makes it impossible to determine the actual contribution of the normal force in the concrete to shear resistance.

3.7 Fracture mechanics approach to "size effect"

It is commonly acknowledged that an increase in the effective depth of an RC beam decreases the average shear stress (ASCE-ACI Committee 445 1998; Bažant 1997; Bažant and Kim 1984; Collins 1991; Kotsovos and Pavlovic 2004; Tompos and Frosch 2002). This so-called "size effect" was investigated from a fracture mechanics point of view by Bažant (Bažant and Kim 1984). According to Bažant, the nominal shear stress v_u can be calculated from a statistical fit to considerations describing the energy release rate at microcracks in a "fracture process zone" eventually forming the shear crack at failure. Bažant uses a non-linear approach to fracture mechanics, because a linear approach (linear in terms of the logarithm of d) would yield too large nominal shear stresses (Bažant and Kim 1984). Based on earlier work (Bažant 1984), Bažant describes the nominal stress at failure as a function of the tensile strength of concrete, the section depth, and the aggregate size.

$$\sigma_N = f'_t \, \phi(\lambda) \tag{3.67}$$

with

$$\phi(\lambda) = \frac{1}{\sqrt{1 + \lambda / \lambda_0}} \quad \text{in which } \lambda = \frac{d}{d_a} \tag{3.68}$$

where σ_N = nominal stress at failure

f'_t = direct tensile strength of concrete

d_a = aggregate size

λ_0 = constant

According to Bažant, the function ϕ describes the effect of the section depth. If the effective section depth is small compared to the aggregate size, the factor 1 in the square root in equation (3.68) controls, and size effect is not of concern. For relatively large values of d, the factor λ/λ_0 controls. As stated by Bažant, the function ϕ therefore defines a gradual transition from an influence of size effect for large values of λ to no size effect for small section depth, that is $\lambda < \lambda_0$ (Bažant and Kim 1984).

To illustrate the effect of the section depth in relation to shear-carrying components, Bažant describes the shear force as a sum of two components resulting from taking the shear force as the derivative of the applied moment (Bažant and Kim 1984).

$$V = \frac{dM}{dx} \tag{3.69}$$

with $M = T \cdot jd$:

$$V = \frac{d(T \cdot jd)}{dx} = \frac{dT}{dx} jd + \frac{dj}{dx} T \cdot d = V_1 + V_2 \tag{3.70}$$

where T = tensile force in the longitudinal reinforcement

$j = j(x)$ = variable coefficient describing the internal lever arm

The two components V_1 and V_2 in equation (3.70) represent components of the shear capacity due to a change in bond stress, and arch-action, respectively. The variable coefficient $j(x)$ is chosen as a function depending on the shear span, a, and the longitudinal reinforcement ratio, ρ, as

$$j = k\rho^{-m}\left(\frac{x}{a}\right)^{r} \tag{3.71}$$

in which k, m, r are constants

Following Bažant, the component related to bond stress, V_1, is chosen as a function of the form

$$V_1 = k_1\rho^{1/2\cdot m} f'^{q}_{c}\, bd \tag{3.72}$$

with k_1, m, q = constants

Equation (3.72) relates the shear contribution from bond stress in the longitudinal reinforcement to the longitudinal reinforcement ratio and the compressive strength of concrete.

Taking the force in the longitudinal reinforcement as $T = \sigma_s \rho bd$, the contribution from arch-action at a location $x = d$, according to Bažant, is assumed to be of a form shown in equation (3.73)

$$V_2 = c_2 \frac{\rho^{1-m}}{(a/d)^r} bd \tag{3.73}$$

in which c_2 = constant

Calculating the average shear stress, v, as $v = V/bd$, the shear stress from equations (3.72) and (3.73) results in

$$v = k_1 \rho^p \left(f'^q_c + k_2 \frac{\sqrt{\rho}}{(a/d)^r} \right) \tag{3.74}$$

with $k_2 = c_2/k_1$

k_1, k_2, p, q, r = constants to be determined by the statistical fit

The average shear stress from equation (3.74) does not consider the effect of the section depth on the average shear stress. Therefore, equation (3.74) is multiplied by a modified version of the function $\phi(\lambda)$ (eq. (3.68)) used by Bažant to describe the size effect.

$$v = k_1 \rho^p \left(f'^q_c + k_2 \frac{\sqrt{\rho}}{(a/d)^r} \right) \left(1 + \frac{d}{\lambda_0 d_a} \right)^{-1/2} \tag{3.75}$$

The statistical fit of equation (3.75) to a database comprising 296 beams (Bažant and Kim 1984) yielded

$$v_u = \frac{10\sqrt[3]{\rho_s}}{\sqrt{1 + d/25d_a}} \left[\sqrt{f'_c} + 3000\sqrt{\rho_s/(a/d)^5} \right] \quad \text{[psi]} \tag{3.76}$$

Equation (3.76) represents an empirical fit of various parameters related to shear strength and size effect. In fact, most of the parameters used in equation (3.76) are related to friction, such as the longitudinal reinforcement ratio, concrete strength, and aggregate size. However, equation (3.76) does not describe the mechanisms controlling the effect of the section depth. It appears to be more appropriate to express the effect of the section depth on the average shear stress by a model explaining the mechanics related to friction as the model proposed by Reineck (Reineck 1990, 1991b), outlined in Section 3.3. By relating frictional stresses to the displacements due to a rotation of the crack surfaces, Reineck formulates a mechanism that explains the reduction of shear stresses with increasing section depth. As the section depth increases, and/or the longitudinal reinforcement ratio decreases, the friction-related stresses along the crack surfaces become smaller, decreasing also the average shear stress (Reineck 1990, 1991b). In a paper published 13 years after the proposal of equation (3.76) (Bažant 1997), Bažant develops a fracture mechanics concept that supports equation (3.76) as an approach to shear design taking into account the effect of the section depth. This approach describes the failure process in terms of the energy release in a fractured section of a compression strut in a strut-and-tie model. The failure state is defined by a limiting depth of the fracture zone. Though the explanation for the development of the fracture zone is different, this model is similar to defining a critical slip between crack surfaces as employed by Reineck (Reineck 1990), based on work by Walraven (Walraven 1981a, b).

The performance of equation (3.76) on test series by Shioya, by Podgorniak and Stanik, and by Yoshida is compared to the method proposed in this work in Chapter 6. It is shown that while the approach proposed by Bažant generally reflects the size effect well, it reveals a different behavior for each of the two considered test series. This is attributed to a the term outside the brackets in equation (3.76).

3.8 Additional research

Numerous approaches to shear design of RC members have been published in the open literature. However, these works do not primarily propose shear design methods, but merely supply to the general knowledge base on shear behavior of RC members under axial and variable horizontal loads. In other cases, iterative solutions are proposed, which require programming the iteration algorithm for each member to be designed. This might give a very good estimate of the shear capacity of the examined member, but it does not provide a tool for a design "by hand".

In works following the findings of Watanabe (Watanabe and Ichinose 1991) and Aoyama (Aoyama 1993), F. Watanabe et al. developed shear design methods for beams, which are iterative methods suitable for computer-analysis of RC beams (Lee 1996; Nielsen 1999). These empirically developed models are very sensitive concerning the input data for the iterations. Axial load was not considered in the development of these approaches. A view on the open literature reveals there are several factors contributing to the shear capacity of squat columns under axial load, which are not considered in the models developed for RC beams that it does not appear to be appropriate to apply approaches as in (Lee 1996) or (Watanabe and Lee 1998) to RC columns. An adjustment to consider axial loads would be necessary.

Work done by Collins and Vecchio et al. (Collins et al. 1996; Selby et al. 1996) is based on the modified compression field theory (Collins 1991). The first work (Collins et al. 1996) proposes a shear design method developed for flexural members, which was established using an experimental data base of beams under bending load. The subsequent paper (Selby et al. 1996) is concerned about the ability of finite element analyses to accurately describe the behavior of concrete elements subjected to shear and axial compression. However, the scope of these proposals lies not in the range of members examined in the work at hand, and computer based methods as in (Selby et al. 1996) are not considered in the scope of this work.

After reviewing the evaluation of the methods described above (Chapter 4), there seems to be an apparent discrepancy between the different models as they have been empirically developed using different databases. Furthermore, the degradation of shear strength under cyclic load is not directly addressed. The respective models are limited to the range of input data from the examined specimens. A more phenomenological based mechanical model as demanded by Aschheim (Aschheim 2000) seems to be more appropriate due to its generality and applicability to a full range of squat RC columns. Aschheim uses, similar to (Pujol 2000), the Mohr-Coulomb failure criterion to describe shear strength degradation in terms of cohesion. The "steel" component of the shear capacity is only considered within the confined compression zone. It is contributing to the flexural strength of the cross-section. However, the approach proposed by Aschheim does not take the effects of axial load into account, even though he mentions that "other assumptions would be more relevant to columns having externally imposed axial loads" (Aschheim 2000). It is an iterative method not directly suitable for design purposes.

4 Evaluation of current methods

4.1 Scope of the evaluation

Four of the previously described methods were evaluated according to their respective derivations on several databases from the open literature (Berry et al. 2003; Brachmann 2002; Chen and MacGregor 1993; Kabeyasawa and Hiraishi 1998; Matamoros and Wong 2003; Reineck et al. 2003; Wood 1990; Zararis 2003). The approaches as described by Watanabe, Reineck, Pujol, and Priestley were evaluated. They are the only models of the previously described that are possible to apply to the existing databases.

A database provided by the University of Washington (UW) comprises 252 rectangular RC columns with confined cores under variable lateral load and axial load as tested by various researchers between 1984 and 2002 (Berry et al. 2003). This database was modified and extended by Brachmann (Brachmann 2002), resulting in 139 considered members that meet the scope of the work at hand. The modified database comprises 116 RC members under cyclic shear load and axial compression that reportedly developed a flexural mode of failure. Only 30 members reportedly failed in shear or due to buckling of the tensile reinforcement after yielding of the transverse reinforcement. The shear subset was extended by the author with test results of eight members reported by Ichinose (Ichinose et al. 2001). All considered columns were exposed to axial compression and cyclic lateral load. The models proposed by Priestley, Pujol, and Watanabe will be evaluated on this database.

A database comprised by Reineck, Kuchma et al. (Reineck et al. 2003) consists of 395 beams without transverse reinforcement that failed under static shear load. This database was suggested by Reineck, Kuchma et al. as a comprehensive database for the examination of shear behavior of RC beams without web reinforcement. The combined arch / truss model for non-ductile members as proposed by Watanabe et al., and the model proposed by Reineck for RC beams without web reinforcement will be evaluated using this database for monotonic shear load on RC members without transverse reinforcement.

The database of slender RC members with web reinforcement consists of 168 RC beams that failed under monotonic shear load. This database was comprised by the author from the open literature (Chen and MacGregor 1993; Zararis 2003). It was used for an evaluation of the proposal by Watanabe on members with transverse reinforcement.

Watanabe's model and its proposed modifications have also been evaluated on databases for deep beams and for walls. The database for deep beams comprises 50 deep beams without web reinforcement and 146 deep beams that were reinforced. The deep beam database was collected by Matamoros et al. (Matamoros and Wong 2003), and was extended by the author.

The database for walls was collected from publications by Wood and Kabeyasawa (Kabeyasawa and Hiraishi 1998; Wood 1990). It includes 146 RC walls with web reinforcement.

Properties and calculation results for all examined databases and models are provided in a file on the accompanying data CD and in the Appendix. The CD contains a Microsoft® Excel spreadsheet file, and an HTML file that can be opened with any application supporting file formats used for world-wide-web publications. Both files and the Appendix provide the same information. The respective databases are listed in separate worksheets on the CD. Comparisons of measured and calculated responses are provided in figures within this text.

4.1.1 Validation

To compare the approaches described in Chapter 3 to the model proposed in the subsequent chapters, the shear strength was computed and was related to the respective measured shear strength of the tested specimens. Since the model proposed in Chapter 5 was calibrated on the same databases, an objective method to validate and compare the different proposals was to carry out an n-fold cross validation. For the n-fold cross validation, the databases were divided into ten subsets $n = \{1, 2, \ldots 10\}$ comprised of randomly chosen 90 % of the complete set of data. Using the mean values $\mu_n = \left(V_{mes} / V_{cal}\right)_n$ of each sub-database, the average of the mean values and their standard deviation were calculated from equations (4.1) and (4.2):

$$\overline{\mu} = \frac{1}{n} \sum_{i=1}^{n} \mu_i \tag{4.1}$$

$$\sigma = \sqrt{\frac{1}{n-1} \sum_{i=1}^{n} \left(\mu_i - \overline{\mu}\right)^2} \tag{4.2}$$

The 95 % confidence interval for an unknown empirical value λ is given for this mean value and standard deviation as

$$P\left(\overline{\mu}-\sigma\cdot t_{r;0.975}/\sqrt{n}\leq\lambda\leq\overline{\mu}+\sigma\cdot t_{r;0.975}/\sqrt{n}\right)=0.95 \quad (4.3)$$

With a redundant $r = n\text{-}1 = 9$, it is $t_{r;\,0.975} = 2.26$ (Schneider 1998).

Using these values, an interval can be given in the form of eq. (4.4):

$$V_{mes}/V_{cal} = x \pm y\% \quad (4.4)$$

The interval shows the expected average value V_{mes}/V_{cal} with a confidence level of 95 %. If the considered set of data is very small, n becomes the number of tests considered and the value for $t_{r;0.975}$ is changed accordingly.

The standard deviation of the ratio of measured to calculated shear strength and the coefficient of variation will additionally be given for comparisons and evaluation purposes. According to (Schneider 1998), it is not sensible to calculate a confidence interval for the standard deviation for databases of the given size. Therefore, standard deviation and coefficient of variation will be calculated using complete databases with the average value $\overline{\mu} = V_{mes}/V_{cal}$.

4.2 Evaluation of the combined truss and arch model

The combined truss and arch model as proposed by Watanabe et al. (Watanabe and Ichinose 1991) and described by Aoyama (Aoyama 1993) was outlined in Section 3.2. Since this model is considered one of the conceptual foundations for the approach proposed by the author, it was evaluated as a frame of reference on all applicable data sets.

The model for non-ductile members was evaluated using the Reineck / Kuchma database (Reineck et al. 2003) for members without transverse reinforcement and the Chen / Zararis database for web-reinforced members (Chen and MacGregor 1993; Zararis 2003). The modification for ductile members was evaluated using the subset of 38 members with reported shear failures from the UW database (Berry et al. 2003). Adjustments proposed by Watanabe and Kabeyasawa (Watanabe and Kabeyasawa 1998) were considered and are described below. The model first proposed by Watanabe, included in the AIJ Guidelines (AIJ 1988), and modified for walls and high-strength concrete by Kabeyasawa (Kabeyasawa and Hiraishi 1998) was evaluated using the comprised wall database (Kabeyasawa and Hiraishi 1998; Wood 1990) and the databases for deep beams (Matamoros and Wong 2003).

4.2.1 Proposed adjustments for high-strength concrete and axial load

In ongoing research on the model proposed by Watanabe, the shortcomings of the model concerning high-strength concrete and axial load were addressed

(Watanabe and Kabeyasawa 1998). The proposed changes were used in the evaluation of the combined arch – truss approach.

To allow the applicability of the model for high-strength concrete and axial load, the strength reduction factor was changed to

$$\nu_0 f'_c = 1.7(1+2n) f'^{\,0.667}_c \tag{4.5}$$

with $n = P/(Af'_c)$ = axial load level

Additionally, the inclination of the truss was changed to account for possible axial load. The inclination of the truss was, according to Watanabe and Kabeyasawa, taken as the minimum value from equations (4.6), but not smaller than 1.0 (Watanabe and Kabeyasawa 1998).

$$\begin{aligned} \cot\phi &= \sqrt{\frac{\nu_0 f'_c}{\rho_w f_{wy}} - 1} \\ \cot\phi &= 2.0 - 3n \\ \cot\phi &= \frac{j_t}{\tan\theta \cdot D} \end{aligned} \tag{4.6}$$

Excessive stresses in the shear reinforcement were proposed as limited to

$$f_{wy} \le 125\sqrt{\nu_o f'_c} \tag{4.7}$$

Similar to the original approach as outlined in Chapter 3.2, the modified equation for shear capacity is given as

$$V_u = \gamma\left[b j_t \rho_w f_{wy} \cot\phi + (1-\beta) bh \cdot \nu_0 f'_c \cdot \tan\theta\right] \tag{4.8}$$

With $\tan\theta$ given by eq. (3.3), and β given by eq. (3.10):

$$\tan\theta = \sqrt{\left(\frac{L}{D}\right)^2 + 1} - \frac{L}{D} \qquad \text{((3.3) Repeated)}$$

$$\beta = \frac{\sigma_t}{\nu_0 f'_c} = \frac{\rho_w f_{wy}(1+\cot^2\phi)}{\nu_0 f'_c} \qquad \text{((3.10) Repeated)}$$

A new safety factor γ was introduced, taking the following values:

$$\begin{aligned} \gamma &= 0.91 \text{ for beams} \\ \gamma &= 0.95 \text{ for columns} \end{aligned} \qquad (4.9)$$

The values for γ are applicable if j_t is taken as the distance between centroids of the reinforcement under tension and compression (Watanabe and Kabeyasawa 1998).

4.2.2 Members without web reinforcement under static shear load

A total of 395 RC beams from the Reineck / Kuchma database were evaluated according to equations (4.8), neglecting the term related to transverse reinforcement. The properties and calculated capacities for all members are listed in the worksheet "Slender beams without web reinforcement" in Appendix A2 and on the supplementary CD. The respective figures are listed at the end of this section.

The plot of measured to calculated shear strength in Figure 4-1 at the end of this section shows that the model applied to RC beams without transverse reinforcement largely overestimated the shear capacity of the members. This is especially true for large measured shear strengths. The mean value of V_{mes}/V_{cal} was found to be 1.08 ± 0.42 %, within a 95 % confidence region. The coefficient of variation was 34.6 %

resulting from a standard deviation of 0.38. Marked with grey dots in Figure 4-1 and the subsequent figures are beams tested by Podgorniak / Stanik, and Yoshida et al. (Reineck et al. 2003). Besides their effective depth *d*, the properties of these beams were identically scaled and could be used to evaluate possible size effects related to the effective depth of the beam. As can be seen in Figure 4-1, their strength was generally overestimated. Furthermore, the model proposed by Watanabe also increasingly overestimated the shear strength of these members with an increasing effective depth. This is more noticeable in Figure 4-4, showing a plot of the effective depth *d* versus the ratio V_{mes}/V_{cal}.

Figure 4-2 shows the ratio of measured to calculated shear strength plotted against the shear-span-to-depth ratio, *a*/*d*. With an increasing aspect ratio, Watanabe's model becomes increasingly conservative. As previously shown in Chapter 3.2, this is directly related to equation (4.8), because the expression becomes small for small values of tan θ, which is related to the aspect ratio by equation (3.3).

The ratio of measured to calculated shear strength is plotted against the concrete compressive strength in Figure 4-3. A distinct unconservative trend with increasing concrete strength is discernible. Especially the strength of beams with a concrete strength larger than approximately 60 MPa was overestimated.

As mentioned before, Figure 4-4 shows a distinct trend with respect to the effective depth of the tested beams. This trend is reflected in the five marked specimens used to evaluate possible size effects. While the analysis for these members generally overestimated the shear strength, it is obvious that the model yielded increasingly unconservative results with an increasing effective depth.

The graph in Figure 4-5 shows the ratio of measured to calculated shear strength plotted against the tensile reinforcement ratio, ρ_s. With the scatter evenly distributed over the entire range, the trend line is considered to give a good estimate of the general trend with respect to the tensile reinforcement ratio. For low values of ρ_s, the model proposed by Watanabe overestimated the shear strength of the considered beams. Starting at approximately $\rho_s = 2$ %, the model gave improved results with the trend line becoming close to horizontal for larger values of ρ_s. The tensile reinforcement ratio influences the depth of the uncracked compression zone and the crack width in the tensile zone. Contributions related to both of these factors are not considered in the approach proposed by Watanabe.

4.2.3 Members with web reinforcement under static shear load

The model proposed by Watanabe for RC beams with web reinforcement was evaluated on a total of 168 beams of the combined Chen / Zararis databases (Chen and MacGregor 1993; Zararis 2003). The beams are listed in the worksheet "Slender beams with web reinforcement" on the added data CD and in Appendix A3. Results from an evaluation similar to the one in the previous section are provided for the application of equation (4.8), which is considered the improved approach for the model proposed by Watanabe as previously discussed.

The ratio of measured to calculated shear strength, plotted in Figure 4-6, was found as $V_{mes}/V_{cal} = 1.08 \pm 0.56\%$ within a 95 % confidence interval. The standard deviation was 0.26 resulting in a coefficient of variation of 24.36 percent. The plot shows a trend similar to the one visible in the evaluation of beams without transverse reinforcement (Figure 4-1). While in low load ranges the model gave a good estimate, it showed increasingly unconservative results in higher load ranges. The trend was not as distinct as in the model solely relying on arch action.

The plot of the ratio of measured to calculated shear strength versus aspect ratio in Figure 4-7 and the following figures confirm the trends that could be seen for the results for slender beams without web reinforcement. As is generally expected for members with transverse reinforcement, scatter was smaller.

Figure 4-8 shows the graph of V_{mes}/V_{cal} against the compressive strength of concrete. Similar to results seen in the evaluation of the database for beams without transverse reinforcement, a negative trend with respect to high-strength concrete beams is discernible with the scatter evenly spread out over the full set of data.

Increasingly unconservative estimates for larger effective depths are evident in Figure 4-9. This graph shows the ratio of V_{mes}/V_{cal} plotted against the effective depth d. A set of data to investigate solely the effect of member size comparable to the beams without web reinforcement tested by Podgorniak / Stanik and Yoshida et al. is not available. The fact that the tested data is evenly represented over the covered range of effective depths, however, shows that the trend was related to the effect of d.

The ratio of measured to calculated shear strength is plotted against the tensile reinforcement ratio in Figure 4-10. The distinct trend that was visible for slender beams without transverse reinforcement diminished slightly. For tensile reinforcement ranges between approximately 0.5 and 1.5 percent, the model gave unconservative results. The model yielded better results that correspond to the total average value of $V_{mes} / V_{cal} = 1.08 \pm 0.56\%$ for ρ_s larger than approximately 1.5 percent.

4.2.4 Columns under cyclic loading

A database comprised of 38 RC columns of the UW, Brachmann, and Ichinose databases (Berry et al. 2003; Brachmann 2002; Ichinose et al. 2001) that reportedly failed under cyclic shear was examined using equation (4.8), the modification of Watanabe's model. Column properties can be found in the "Seismic shear failure" worksheet on the accompanying CD and in Appendix A7.

While the original approach by Watanabe did include specific regulations for ductile members (Aoyama 1993; Watanabe and Ichinose 1991), the modification by Watanabe and Kabeyasawa does not explicitly include such provisions. Since Watanabe and Kabeyasawa do not address cyclically loaded columns (Watanabe and Kabeyasawa 1998), it was concluded that a further reduction depending on the drift ratio is appropriate and a safe assumption. In this evaluation, the reduction factor of equations (3.15) and (3.16) was used.

$$\nu = (1 - 15R_p)\nu_0 \qquad \text{for } R_p \leq 0.05 \qquad \text{((3.15) Repeated)}$$

$$v = \frac{v_0}{4} \qquad \text{for } R_p > 0.05 \qquad \text{((3.16) Repeated)}$$

Figure 4-11 shows a comparison of measured maximum shear strength to calculated shear strength. It is apparent that the proposed model underestimated the shear capacity of RC columns for a considerable portion of the examined columns. This confirms the trends discernible for static shear load. The mean value of measured to calculated shear strength was $V_{mes} / V_{cal} = 0.75 \pm 1.31\%$ within a 95 percent confidence interval. As can be expected, the scatter for V_{mes}/V_{cal} was considerable, but not excessively high for shear failures under cyclic lateral load. The standard deviation was found to be 0.30 with a coefficient of variation of 39.8 percent.

A plot of the ratio of measured to calculated shear strength against the aspect ratio is shown in Figure 4-12. This plot does not confirm the trend apparent for statically loaded members. Under lateral load reversals, a slight negative trend towards larger aspect ratios is visible. It should be noted, though, that the majority of examined columns had smaller shear-span-to-depth ratios than previously considered.

A slight negative trend with respect to the compressive strength of concrete can be observed in Figure 4-13, which agrees with similar findings for members under static load.

Figure 4-14 shows V_{mes}/V_{cal} plotted against the level of axial load. A slight negative trend can be seen, showing increasingly unconservative results for increasing axial loads. Still, axial loads exceeding approximately 30 percent of the axial strength of the member are largely underrepresented. The visible trend could thus also be the result of the specific test series by Zhou et al. with $P/(Af'_c) = 0.7$. It is stated in (Watanabe and Kabeyasawa 1998) that axial loads exceeding 60 % of the axial capacity were found to decrease shear strength. This was attributed to additional strain demand in the transverse reinforcement.

The ratio of measured to calculated shear strength is plotted versus drift ratio in Figure 4-15. Obviously, the model overestimated the effect of lateral drift, showing unconservative results mostly for small drifts. With increasing deflections, the model proposed by Watanabe became increasingly conservative, yielding relatively good results at a drift ratio of approximately five percent and larger.

4.2.5 Deep beams and walls

The capacity of deep beams and walls was calculated using the modification of Watanabe's model by Kabeyasawa and Hiraishi (Kabeyasawa and Hiraishi 1998). All walls and deep beams are listed in the "Walls database" and "Deep beams" worksheet included in the provided spreadsheet file and in the Appendix.

Kabeyasawa et al. propose to reduce the compressive strength of concrete by a factor

$$\nu = 1.7 f'_c{}^{-1/3} \tag{4.10}$$

Reducing the concrete strength f'_c by (4.10), is equivalent to reducing f'_c according to eq. (4.5) if no axial load is considered:

$$\nu f'_c = 1.7 f'^{-1/3}_c \cdot f'_c$$
$$= 1.7 f'^{2/3}_c \cong 1.7 f'^{0.667}_c$$

This is not surprising, because the modification for high strength concrete and walls by Kabeyasawa et al. was also proposed in the context of the "New RC proposal", and comes from the co-author of the previously described adjustment for high-strength concrete and axial loads (Kabeyasawa and Hiraishi 1998; Watanabe and Kabeyasawa 1998). The original proposal by Watanabe (Watanabe and Ichinose 1991) was modified by expression (4.10) to account for high-strength concrete according to Kabeyasawa (Kabeyasawa and Hiraishi 1998) to evaluate the shear strength of deep beams and walls.

4.2.5.1 Deep beams without web reinforcement

The model was evaluated on 50 deep beams without transverse reinforcement of the deep beam database comprised by (Matamoros and Wong 2003). The approach proposed by Watanabe relies on arch-action. It was expected to give good estimates of the shear strength of deep beams, because arch-action is considered the main load-carrying mechanism for deep members. Figure 4-16, though, shows that arch-action as considered in the proposed model greatly underestimated the shear strength of deep members. A reason for this could be that calculating the strut width from *D*/2 might overestimate the vertical dimension of the strut and additionally it does not fulfill basic equilibrium, but it also underestimates the horizontal dimension of the strut. The average value of measured to calculated shear strength for the examined data was found as $V_{mes} / V_{cal} = 1.52 \pm 0.94\%$ within a 95 percent confidence region. The three specimens of which the strength was overestimated are beams tested by Kong et al. (Kong et al. 1994) with very low aspect ratios of a/d = 0.46. Small shear-span-to-depth ratios increase the value of tan θ, therefore increasing the calculated strength.

The specimens tested by Kong are also visible in Figure 4-17, showing the ratio of measured to calculated strength plotted against the aspect ratio. The majority of tested beams had aspect ratios exceeding 1.0, and the scatter for these is evenly distributed. The three specimens tested by Kong are the only beams with such a small aspect ratio in the considered set of data.

Figure 4-18 shows a distinct trend towards increasingly unconservative values with an increasing concrete strength. The two specimens with the highest concrete strength, though, are the previously mentioned beams tested by Kong et al. It is therefore possible that the marked trend was amplified by other factors as the aspect ratio. The third of the mentioned Kong specimens had a concrete strength of approximately 40 MPa. It is marked by the lowest tick within this strength range.

Figure 4-19 and Figure 4-20 confirm earlier detected trends with respect to the effective depth and the tensile reinforcement ratio.

4.2.5.2 Deep beams with web reinforcement

The database used to examine deep beams (Matamoros and Wong 2003) includes 146 members with web reinforcement. Figure 4-21 through Figure 4-25 show the results from an evaluation following the model proposed by Watanabe (Watanabe and Ichinose 1991) and modified by Kabeyasawa (Kabeyasawa and Hiraishi 1998).

The plot of measured against calculated shear strength in Figure 4-21 reveals relatively small scatter and a negative trend that was mostly caused by significantly overestimating the strength of six beams. These beams are specimens with relatively high ratios of vertical reinforcement (ρ_w = 2.45 %) tested by Kong et al. (Kong et al. 1970). Additionally, these beams had very low aspect ratios. The model proposed by Watanabe does not limit the angle of the truss for deep members. As briefly discussed in Chapter 3.2, a truss as depicted in Figure 3-2 cannot develop in D-regions, because the inclined compression field cannot develop in the end regions of a member. Assuming an evenly distributed truss mechanism over the entire length of a deep beam might therefore overestimate the strength of this beam.

The average of measured to calculated shear strength was 1.04 ± 0.31 % within a 95 percent confidence region for the examined dataset. The standard deviation was 0.22, resulting in a coefficient of variation of 20.8 percent.

Figure 4-22, Figure 4-23, and Figure 4-24 display no visible trends related to aspect ratio, concrete strength, and effective depth, respectively. The model as proposed by Watanabe appeared to give good results with evenly spread out scatter over the entire respective ranges in deep beams with web reinforcement. This can be seen as an indication that conceptually a combination of truss and arch action is sensible for stocky members. The slight trend towards increasingly conservative results with an increasing tensile reinforcement appears diminished for deep beams with web reinforcement.

4.2.5.3 Walls

The modification of Watanabe's model by Kabeyasawa was originally proposed for the application on walls. It was evaluated on a database comprised by tests considered by Wood (Wood 1990) and Kabeyasawa (Kabeyasawa and Hiraishi 1998; Wallace 1998). The database includes 146 wall specimens with varying geometry of boundary elements. Barbell-type walls, flanged walls, and rectangular walls were considered. The load was applied monotonic, in alternating reversals, or repeatedly in the same direction. The model by Kabeyasawa was applied on the wall panels, without considering the boundary elements. Because the approach proposed by Watanabe and Kabeyasawa does not consider bi-directional web reinforcement, only the horizontal web reinforcement, i.e. in load direction, was considered. Any strength from vertical web reinforcement was neglected.

Figure 4-26 shows the plot of measured to calculated shear strength of the examined wall specimens. The same trend as for web reinforced deep beams can be seen: With increasing measured strength, the predicted strength became increasingly unconservative and scatter became larger. The two walls with the most unconservative estimates are specimens tested by Paulay (W1, W3) (Wood 1990). Their strength was greatly overestimated by the truss model; the arch component is zero. As was the case for the previously mentioned deep beams tested by Kong, specimens W1 and W3 have relatively low aspect ratios in combination with a relatively high horizontal web reinforcement ratio. The overall scatter in the ratio of measured to calculated shear strength was in a reasonable range. The standard deviation was 0.3, the coefficient of variation 32.4 percent. The average value of measured to calculated strength was found to be 0.93 ± 0.43 % within a 95 percent confidence interval.

Plots of the ratio measured to calculated shear strength against aspect ratio, concrete strength, wall panel length, and tensile reinforcement ratio are shown in Figure 4-27, Figure 4-28, Figure 4-29, and Figure 4-30, respectively. They confirm the slight trends that were visible for the model applied on other specimens, especially deep beams.

Figure 4-31 shows a plot of the ratio of measured to calculated shear strength against the axial load level, $P/(Af'_c)$. Axial loads on the wall specimens were mostly very low, between 0 and 0.3 percent. In combination with higher axial loads, a trend to be more conservative can be observed. However, if only axial loads between approximately 7 and 18 percent of the axial strength of the walls are considered, no bias with axial load is evident.

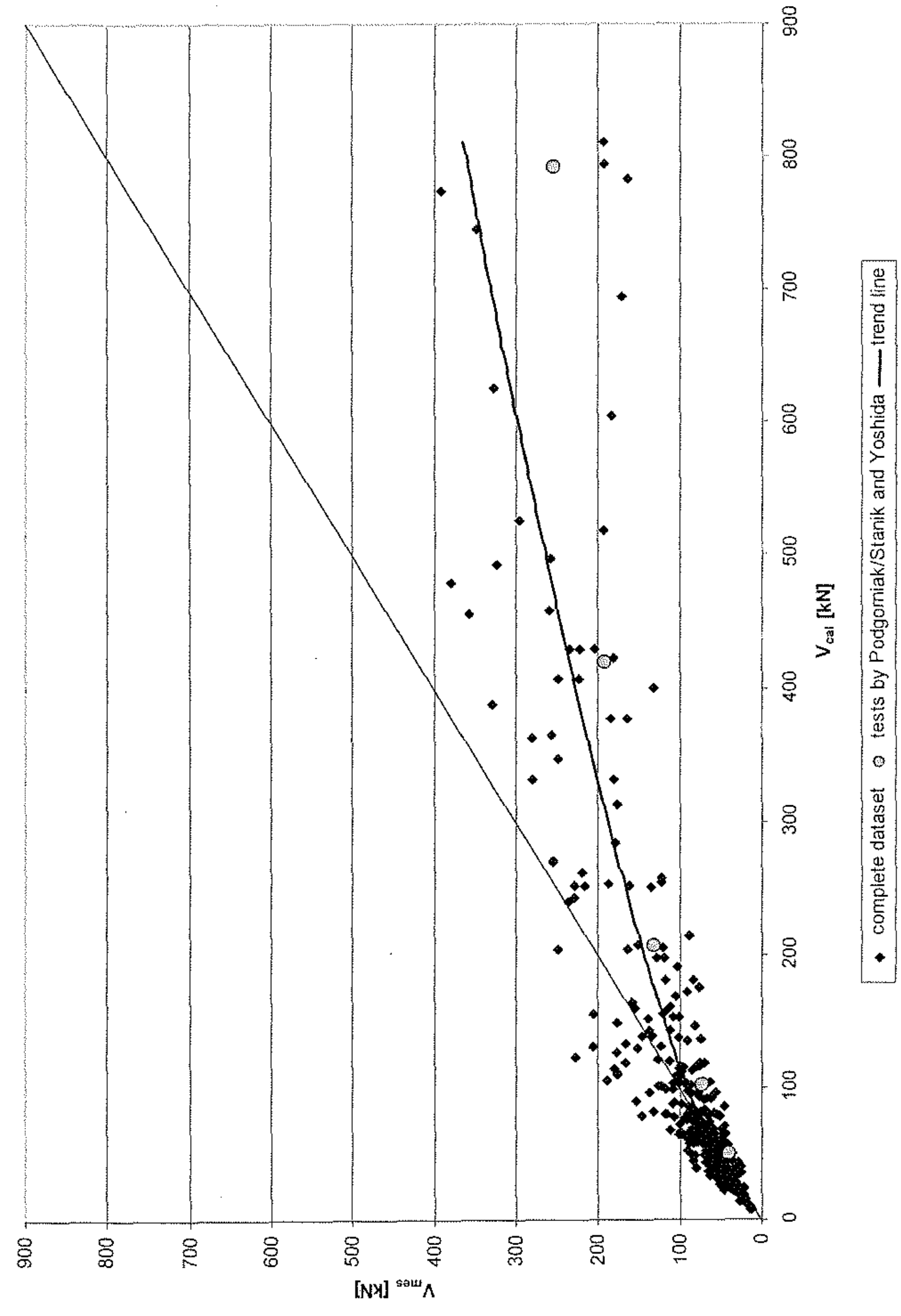

Figure 4-1 Measured versus calculated ultimate shear strength for slender beams without transverse reinforcement following Watanabe's approach

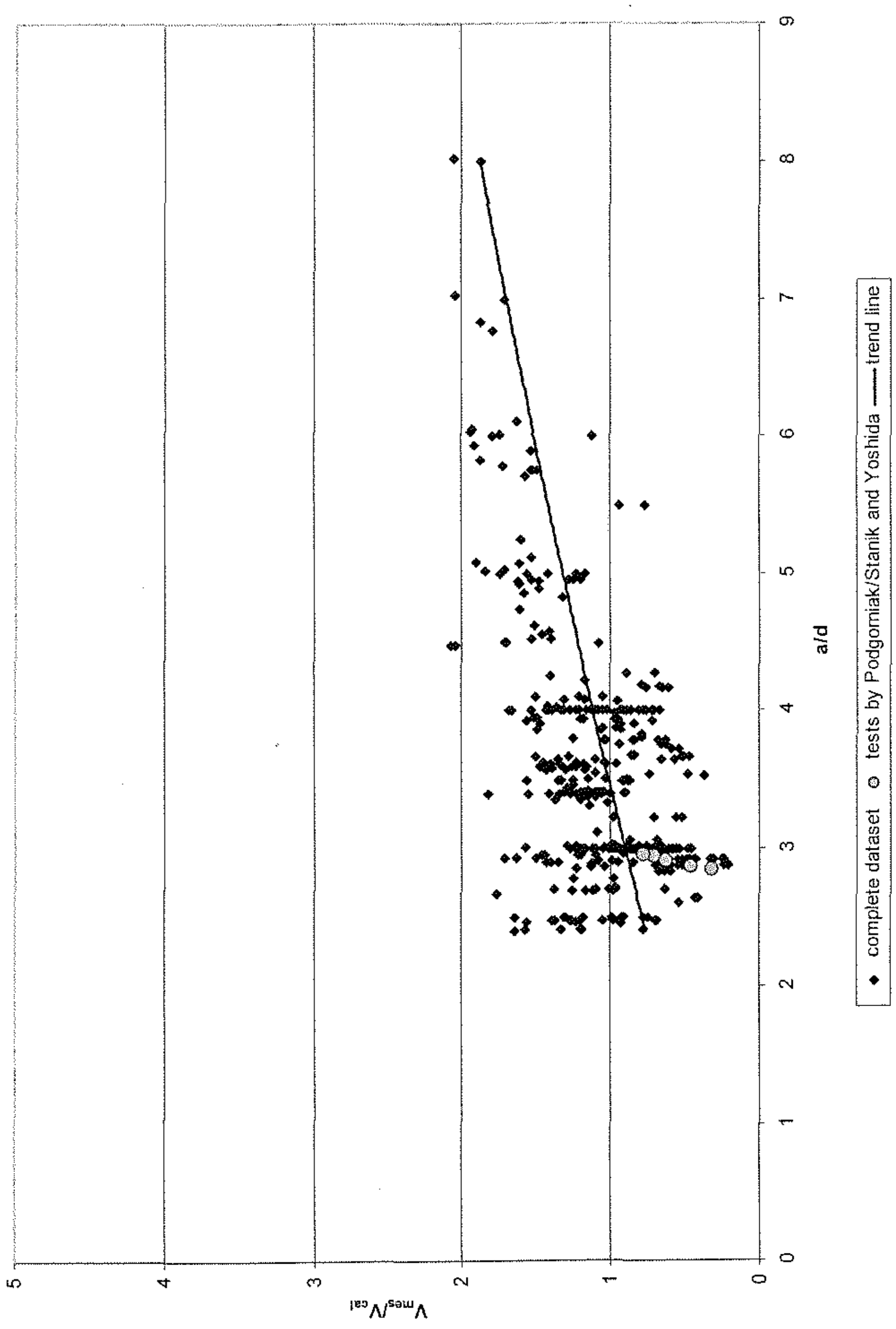

Figure 4-2 Ratio of measured to calculated shear strength versus aspect ratio following Watanabe's approach for slender RC beams without web reinforcement

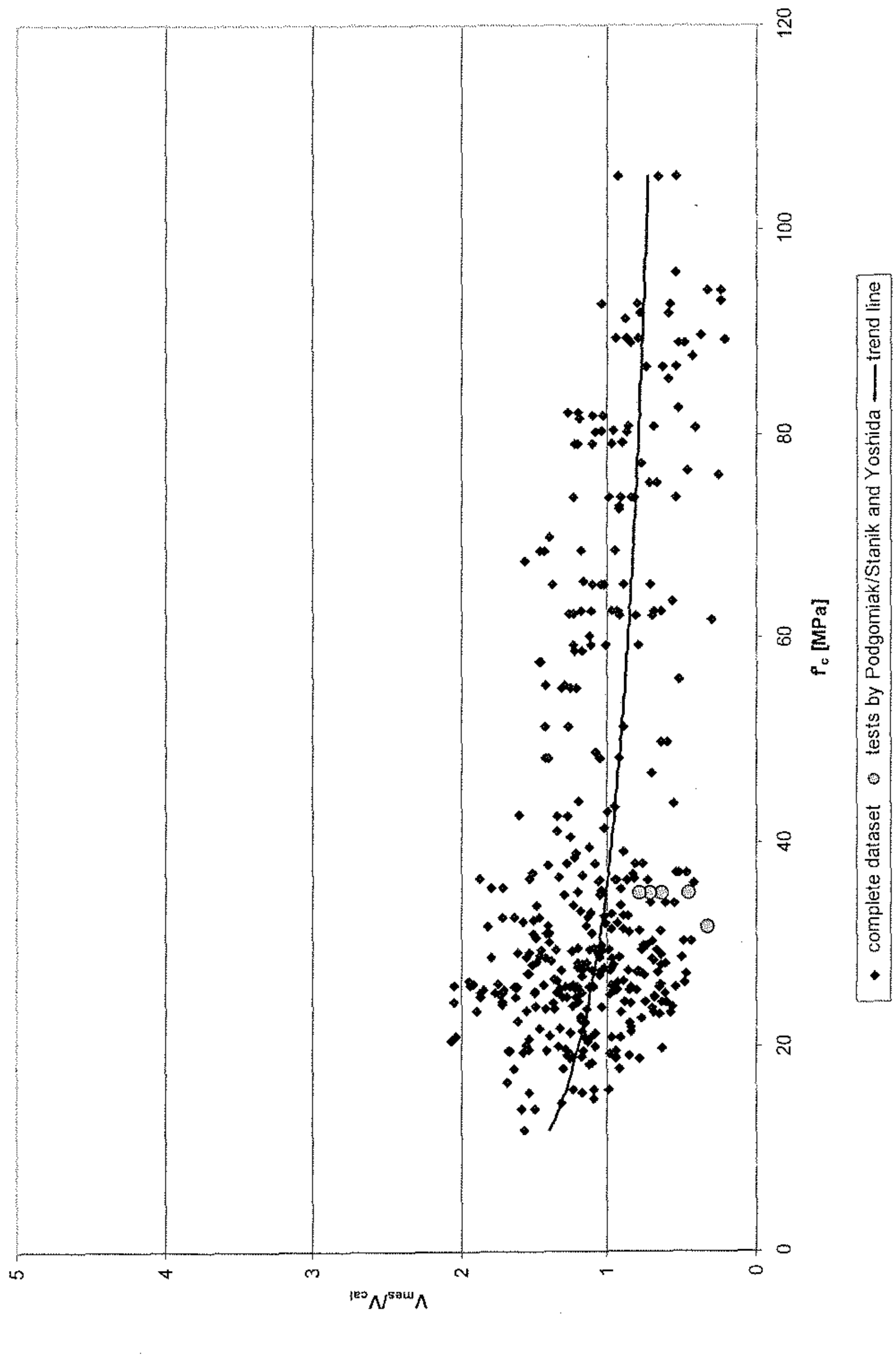

Figure 4-3 Ratio of measured to calculated shear strength versus compressive strength of concrete for slender RC beams without web reinforcement following Watanabe's approach

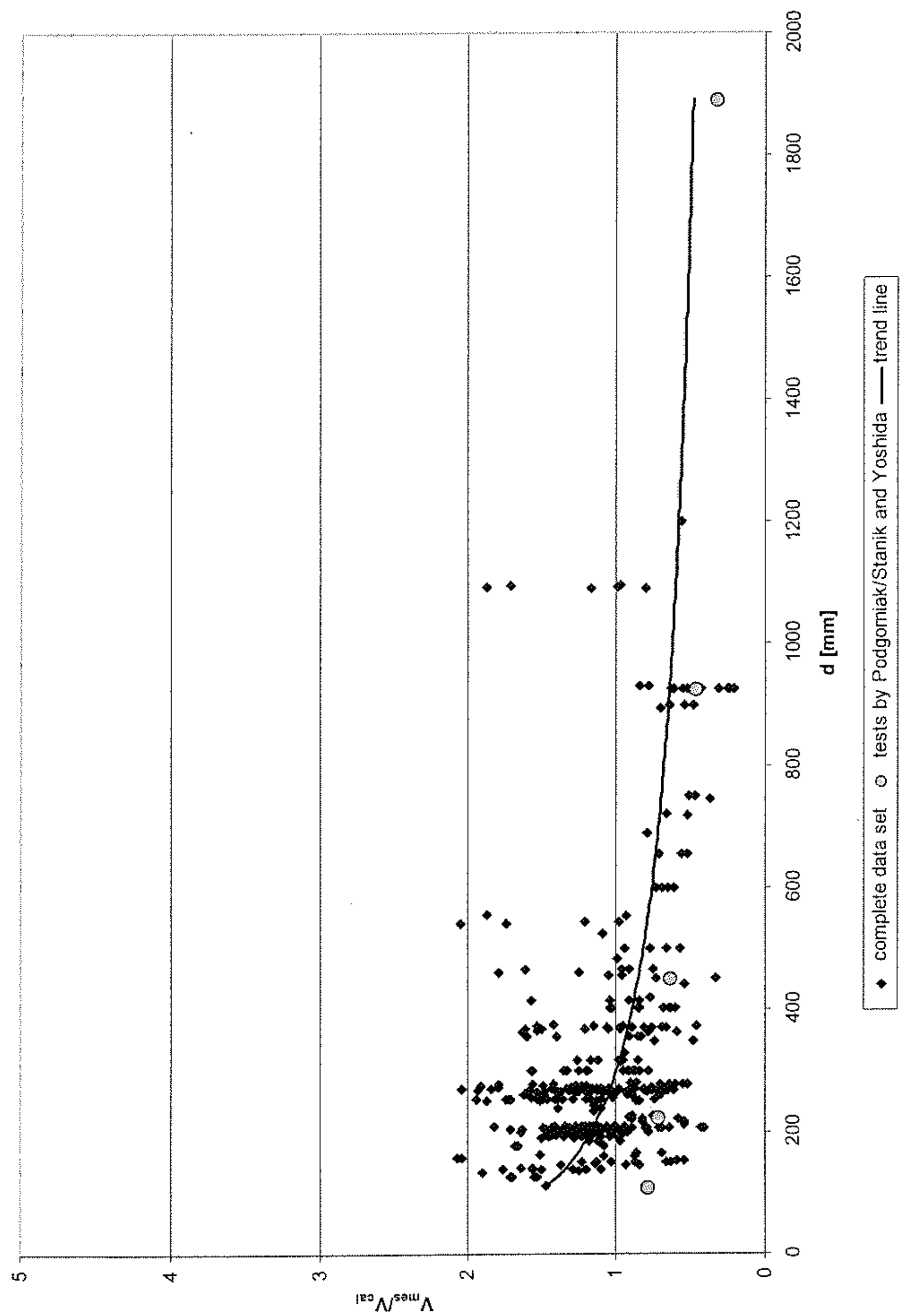

Figure 4-4 Ratio of measured to calculated shear strength versus effective depth for slender RC beams without web reinforcement following Watanabe's approach

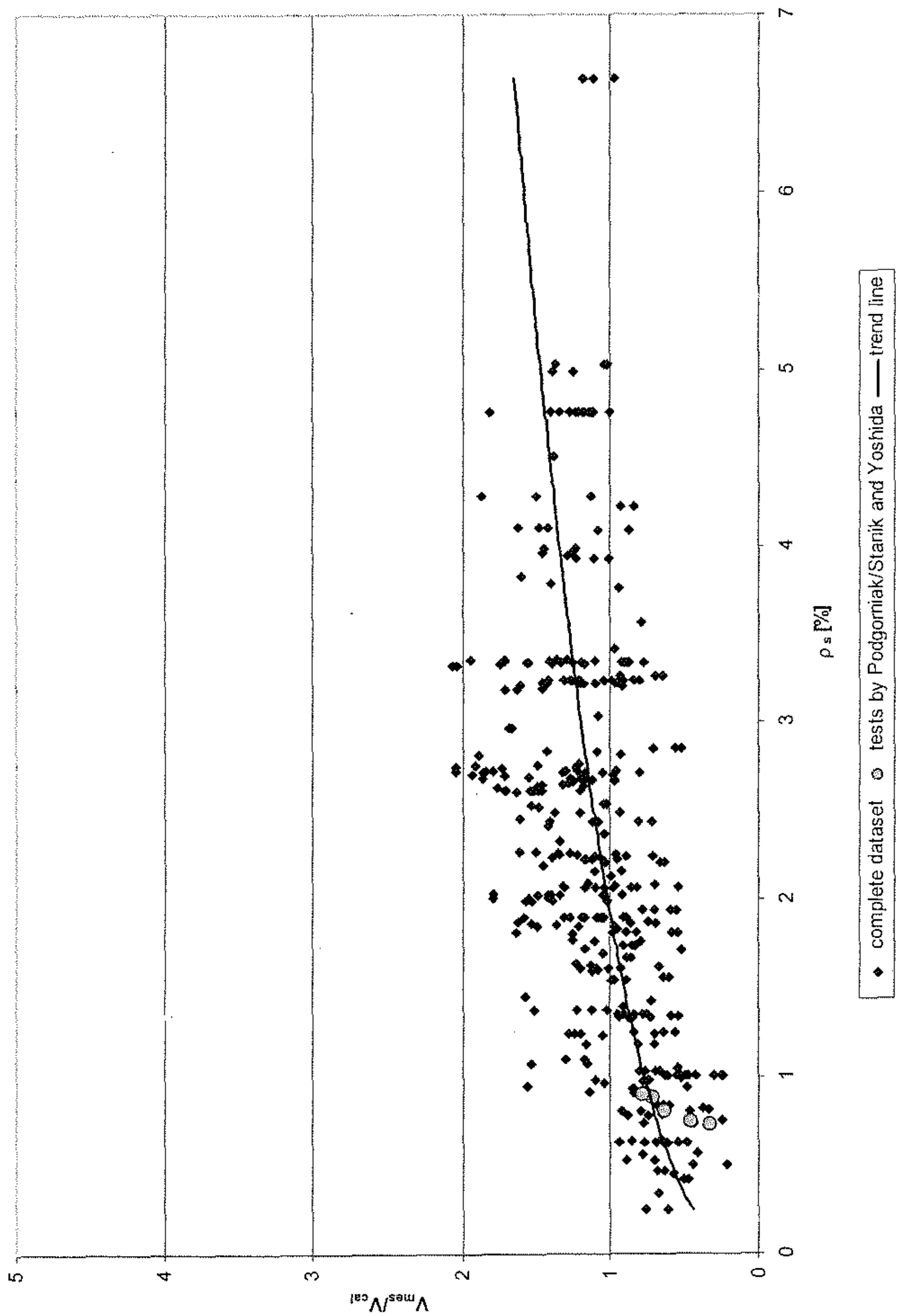

Figure 4-5 Ratio of measured to calculated shear strength versus tensile reinforcement ratio for slender RC beams without web reinforcement following Watanabe's approach

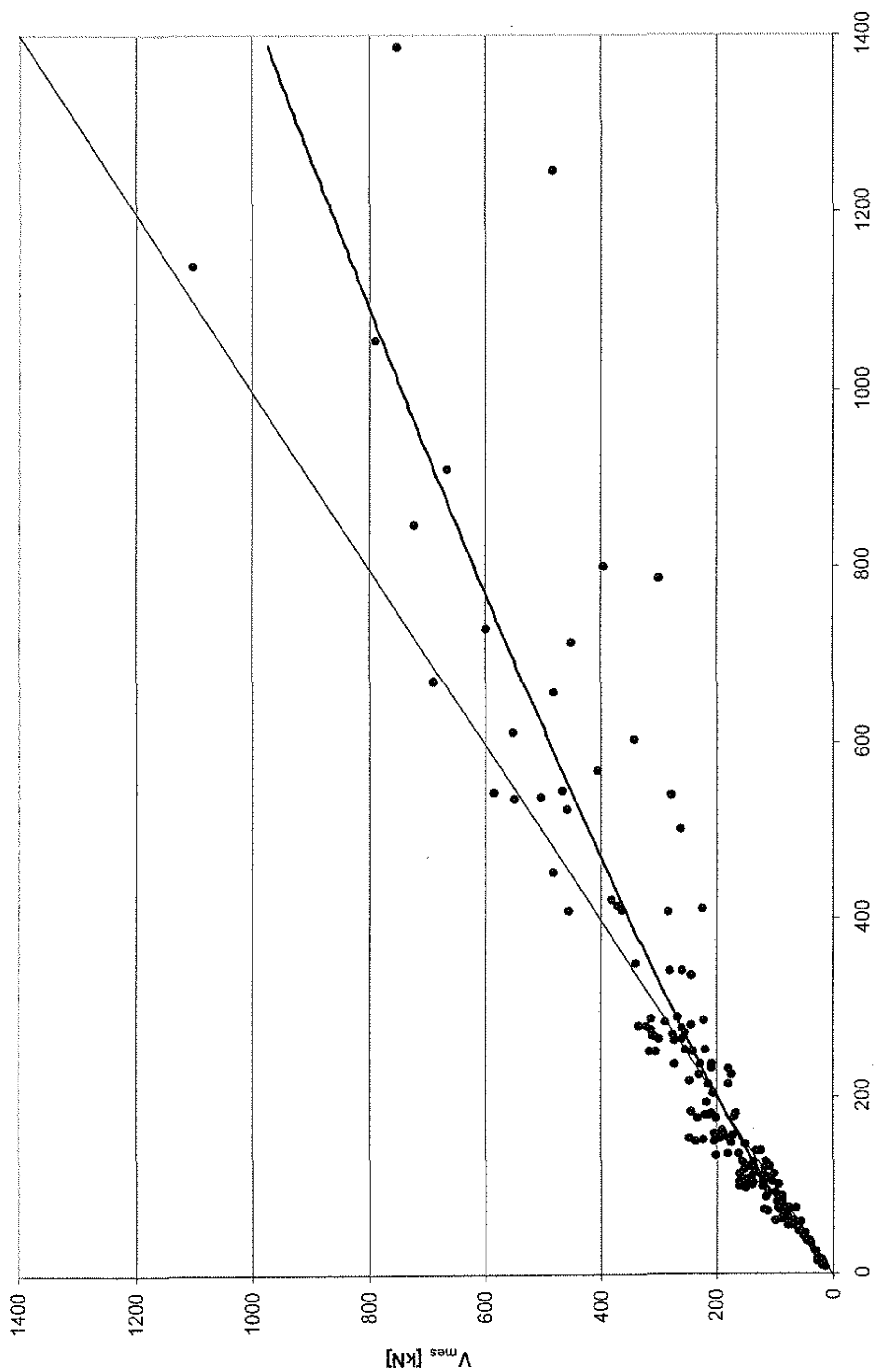

Figure 4-6 Measured versus calculated shear strength for slender beams with transverse reinforcement following Watanabe's approach

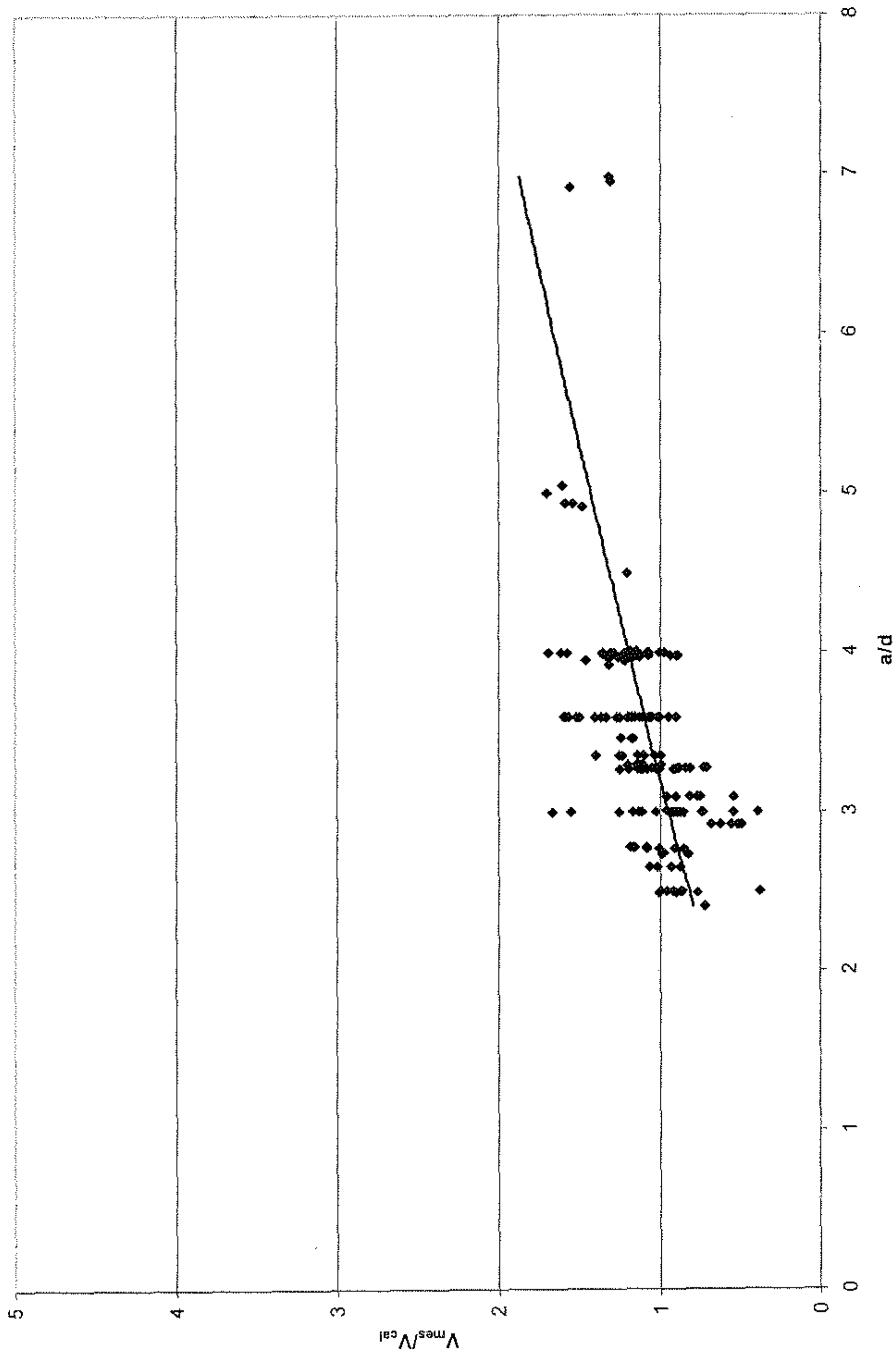

Figure 4-7 Ratio of measured to calculated shear strength versus aspect ratio following Watanabe's approach for slender RC beams with web reinforcement

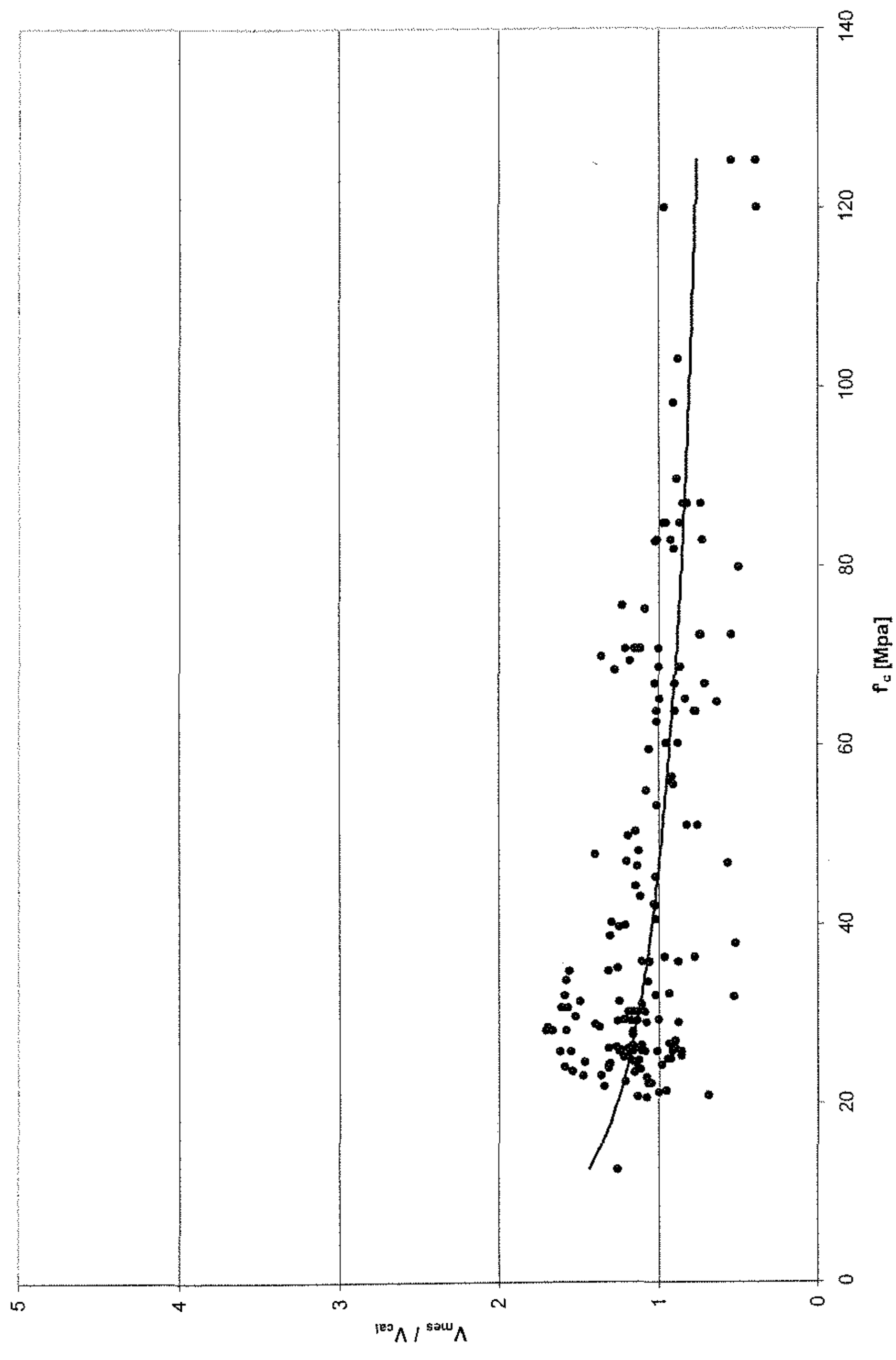

Figure 4-8 Ratio of measured to calculated shear strength versus compressive strength of concrete for slender RC beams with web reinforcement following Watanabe's approach

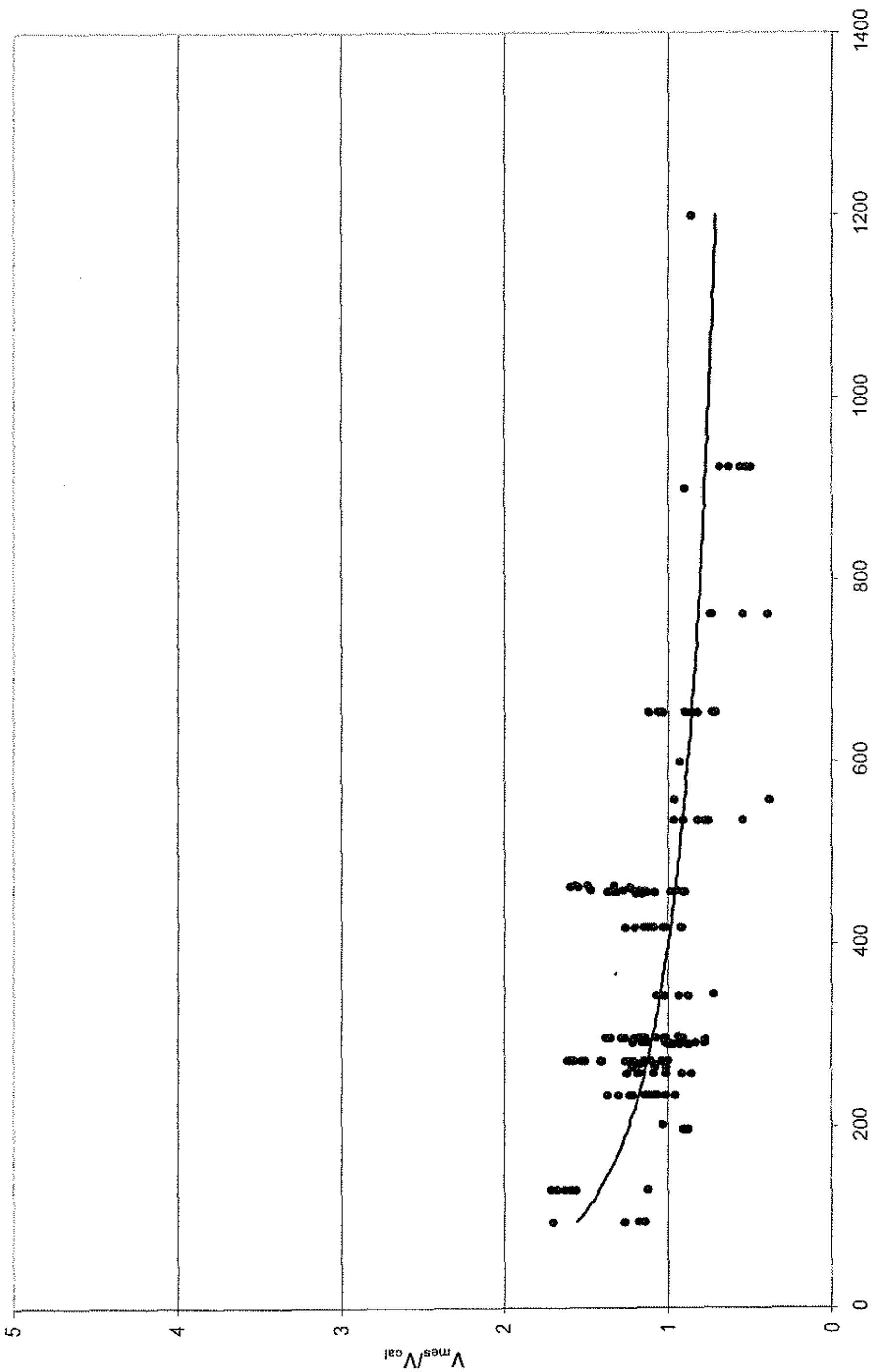

Figure 4-9 Ratio of measured to calculated shear strength versus effective depth for slender RC beams with web reinforcement following Watanabe's approach

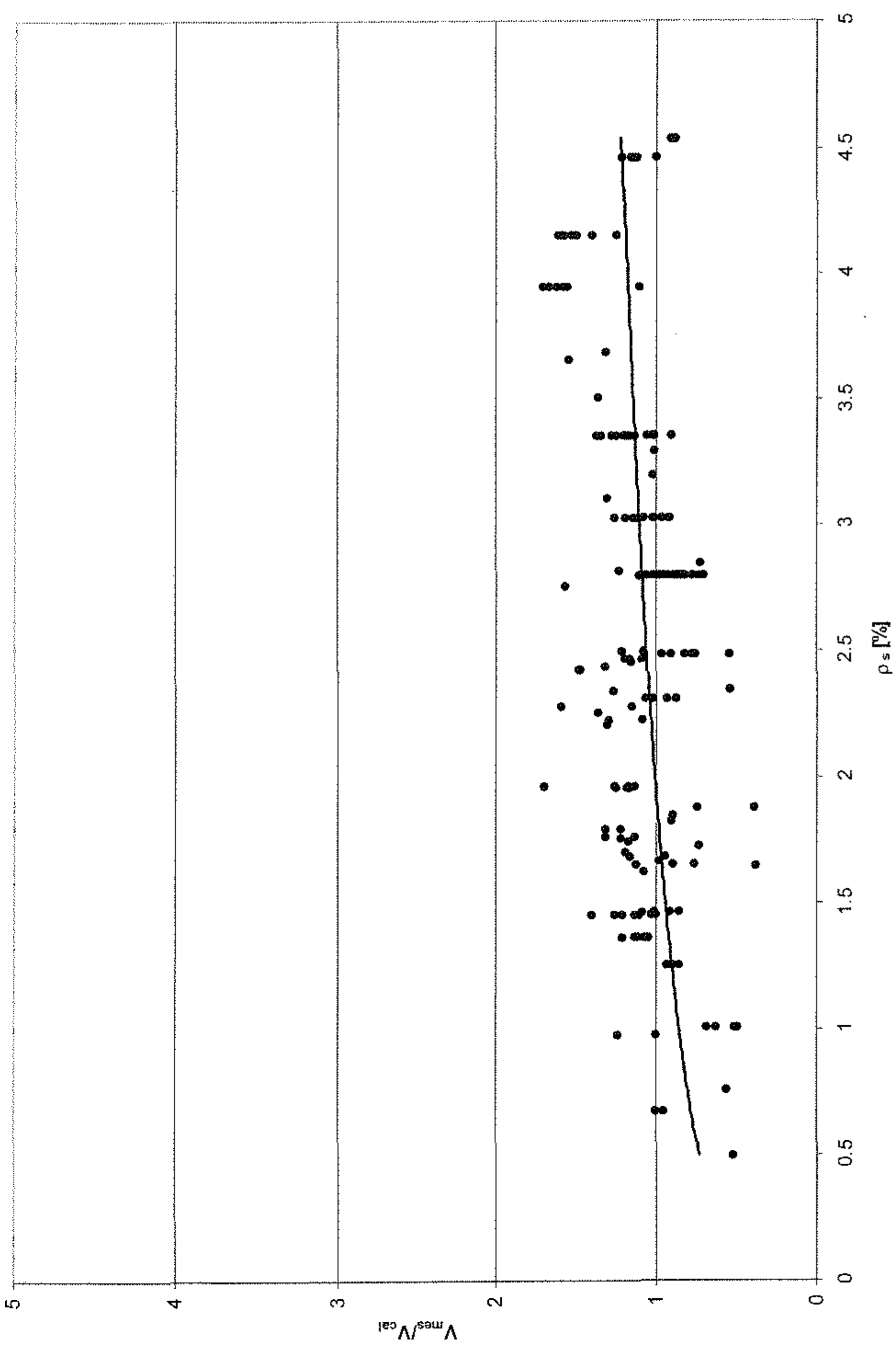

Figure 4-10 Ratio of measured to calculated shear strength versus tensile reinforcement ratio for slender RC beams with web reinforcement following Watanabe's approach

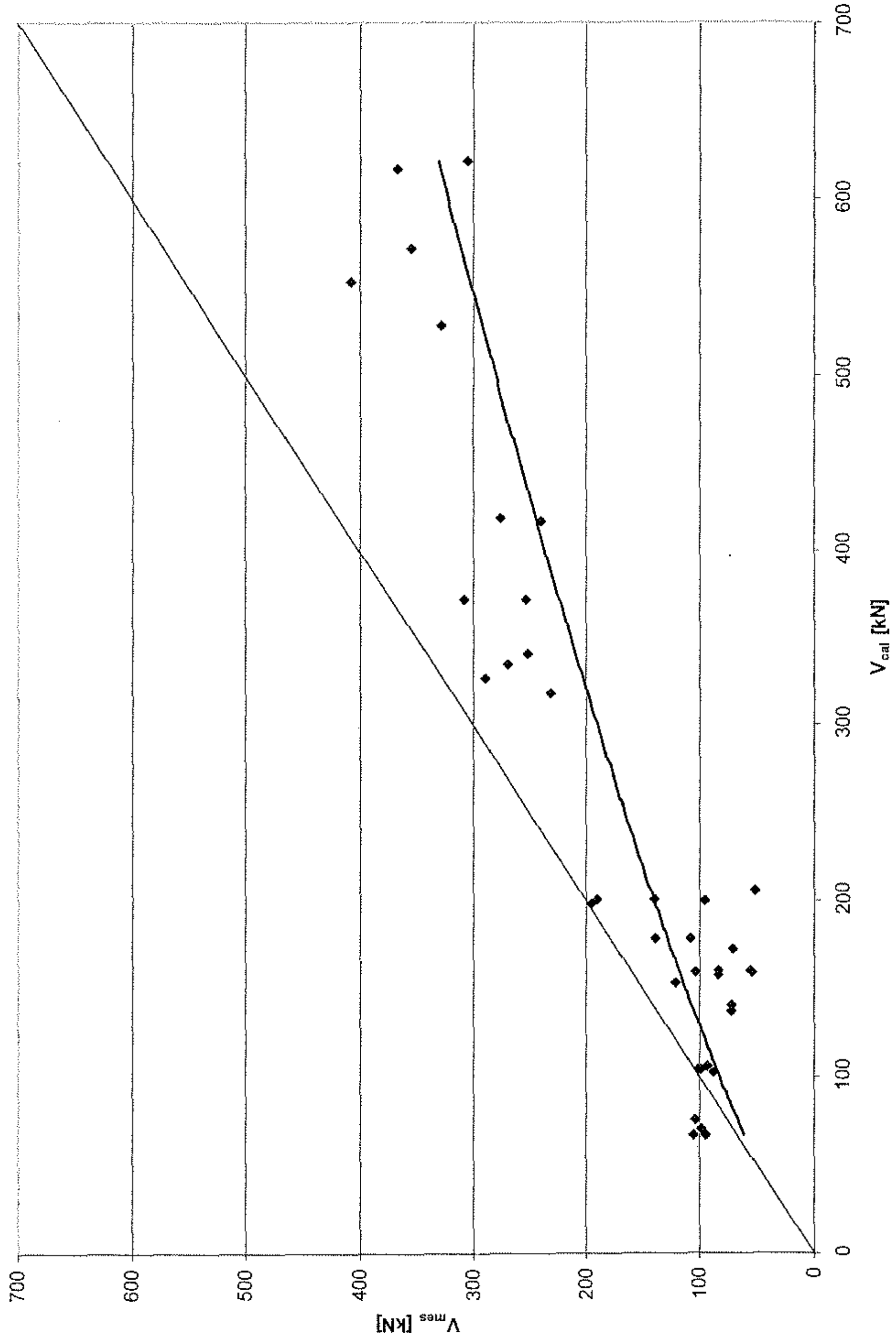

Figure 4-11 Measured versus calculated shear strength for RC columns under cyclic lateral load following Watanabe's approach

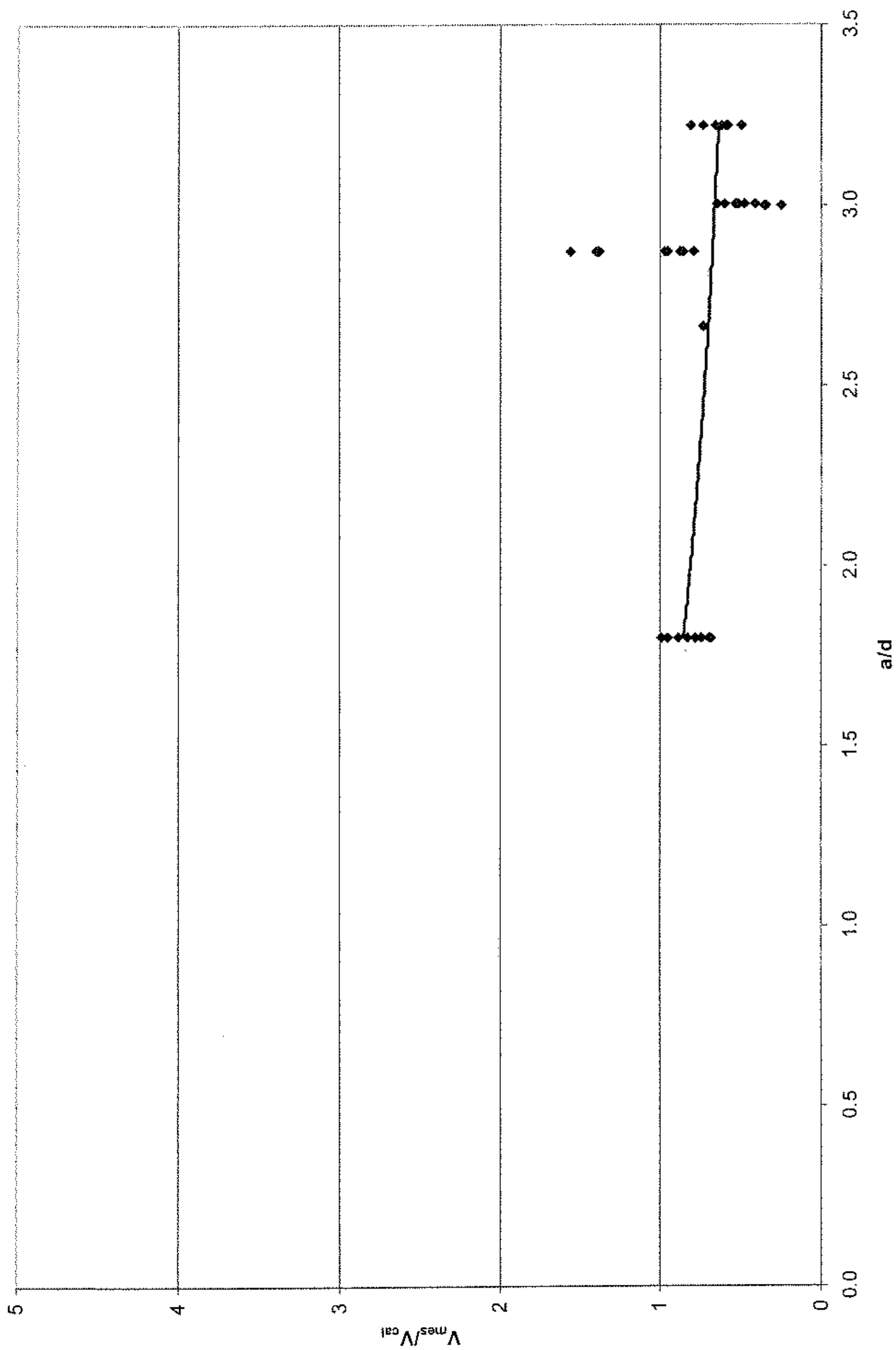

Figure 4-12 Ratio of measured to calculated shear strength versus aspect ratio for RC columns under cyclic lateral load following Watanabe's approach

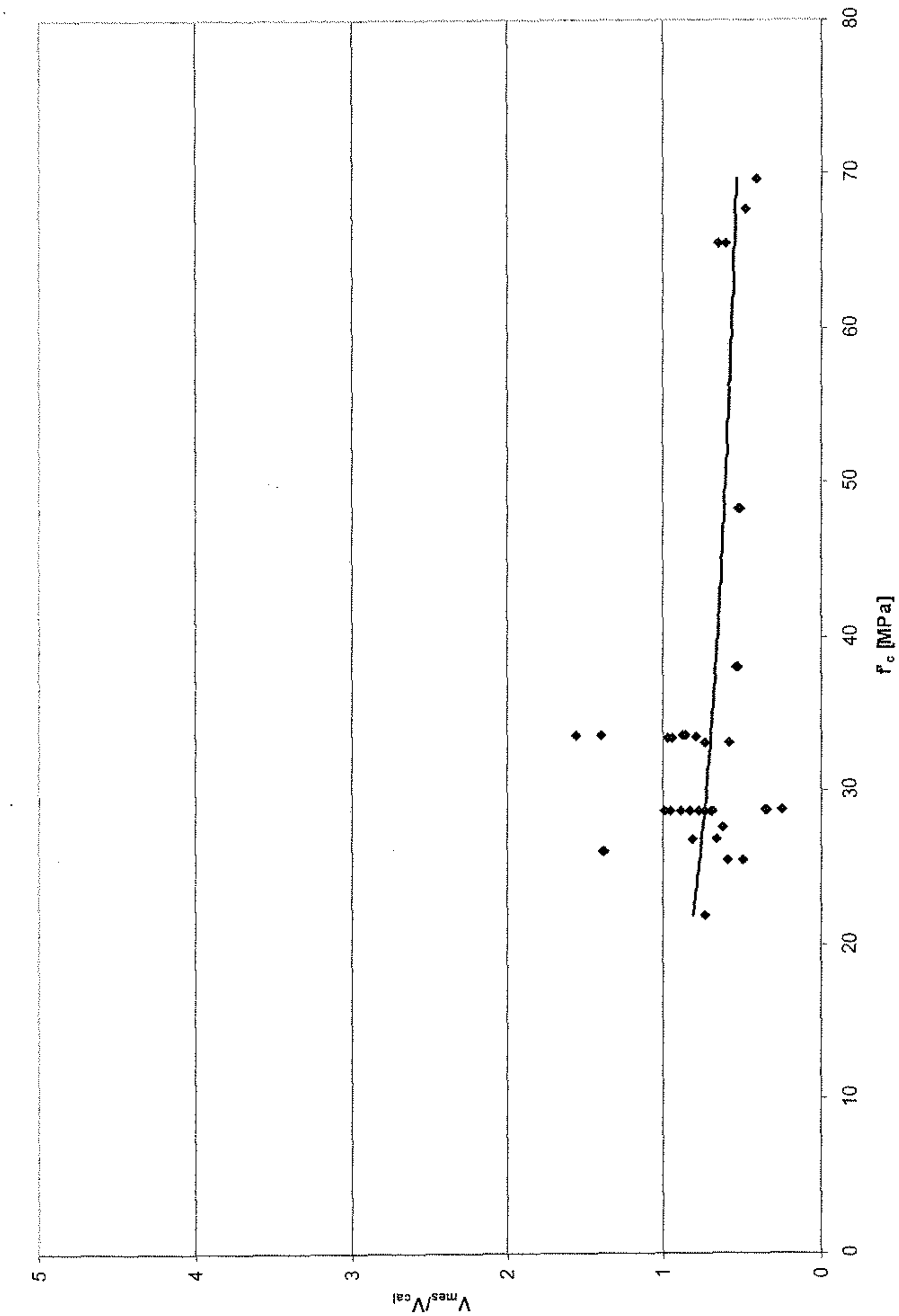

Figure 4-13 Ratio of measured to calculated shear strength versus compressive strength of concrete for RC columns under cyclic lateral load following Watanabe's approach

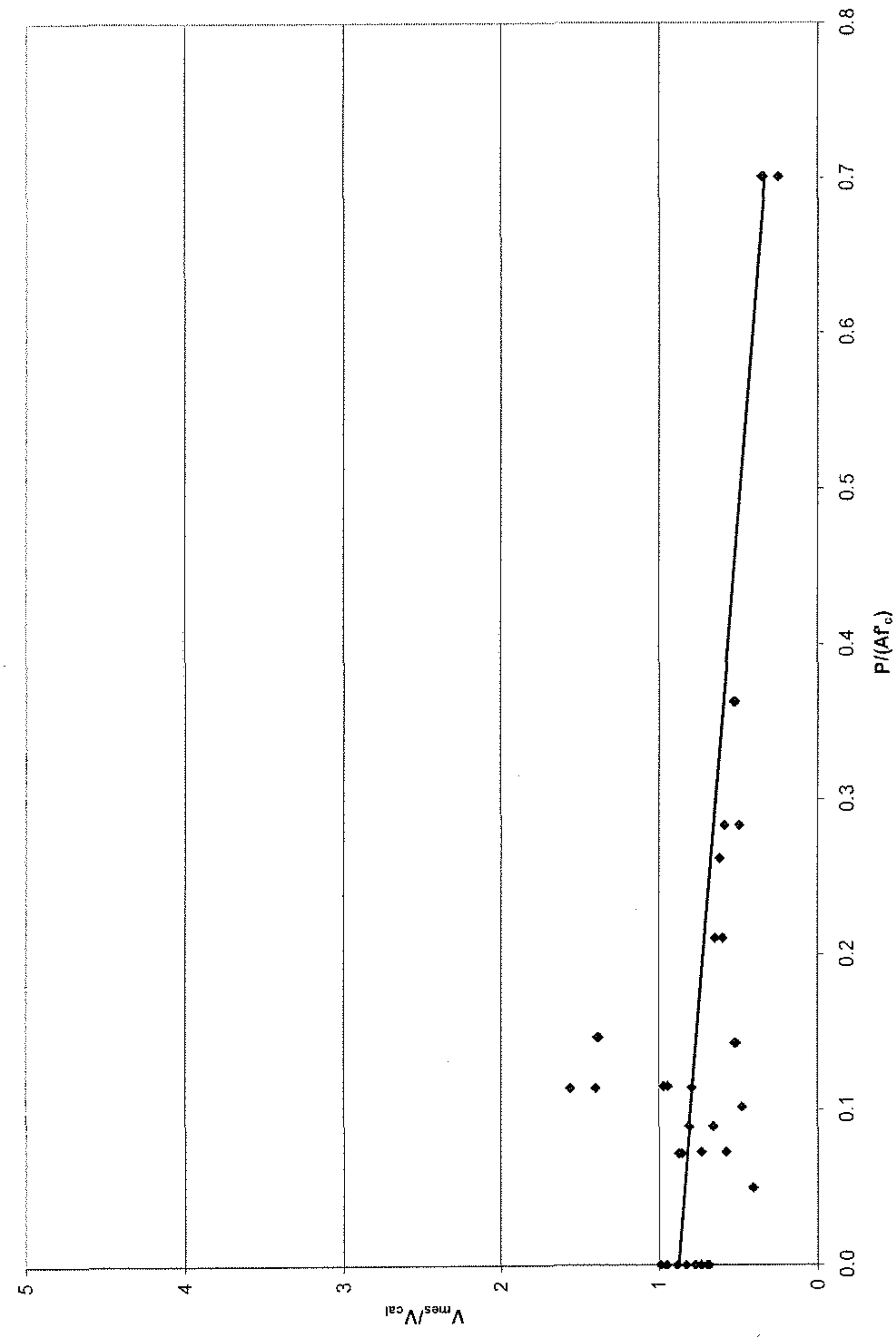

Figure 4-14 Ratio of measured to calculated shear strength versus axial load for RC columns under cyclic lateral load following Watanabe's approach

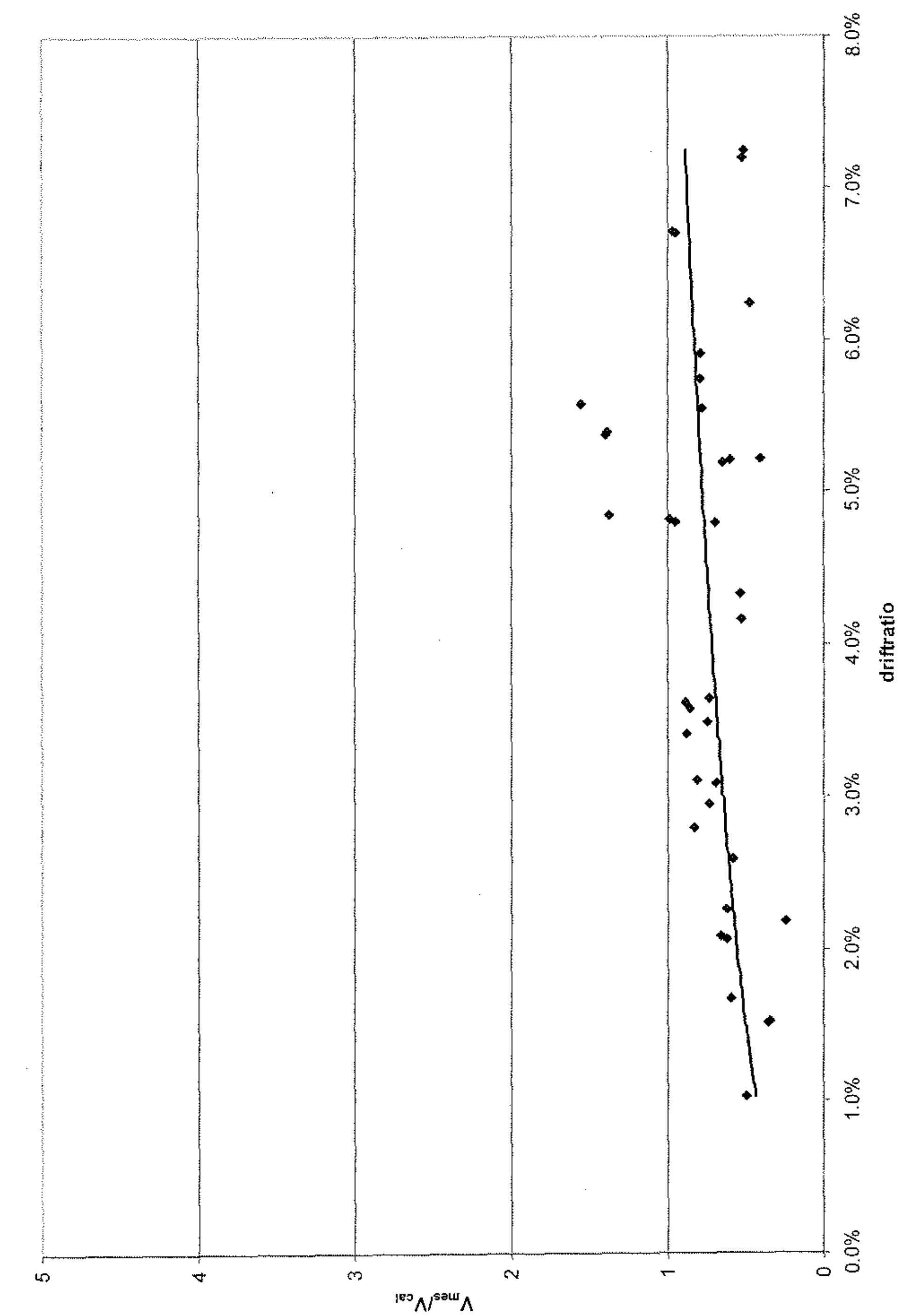

Figure 4-15 Ratio of measured to calculated shear strength versus drift ratio for RC columns under cyclic lateral load following Watanabe's approach

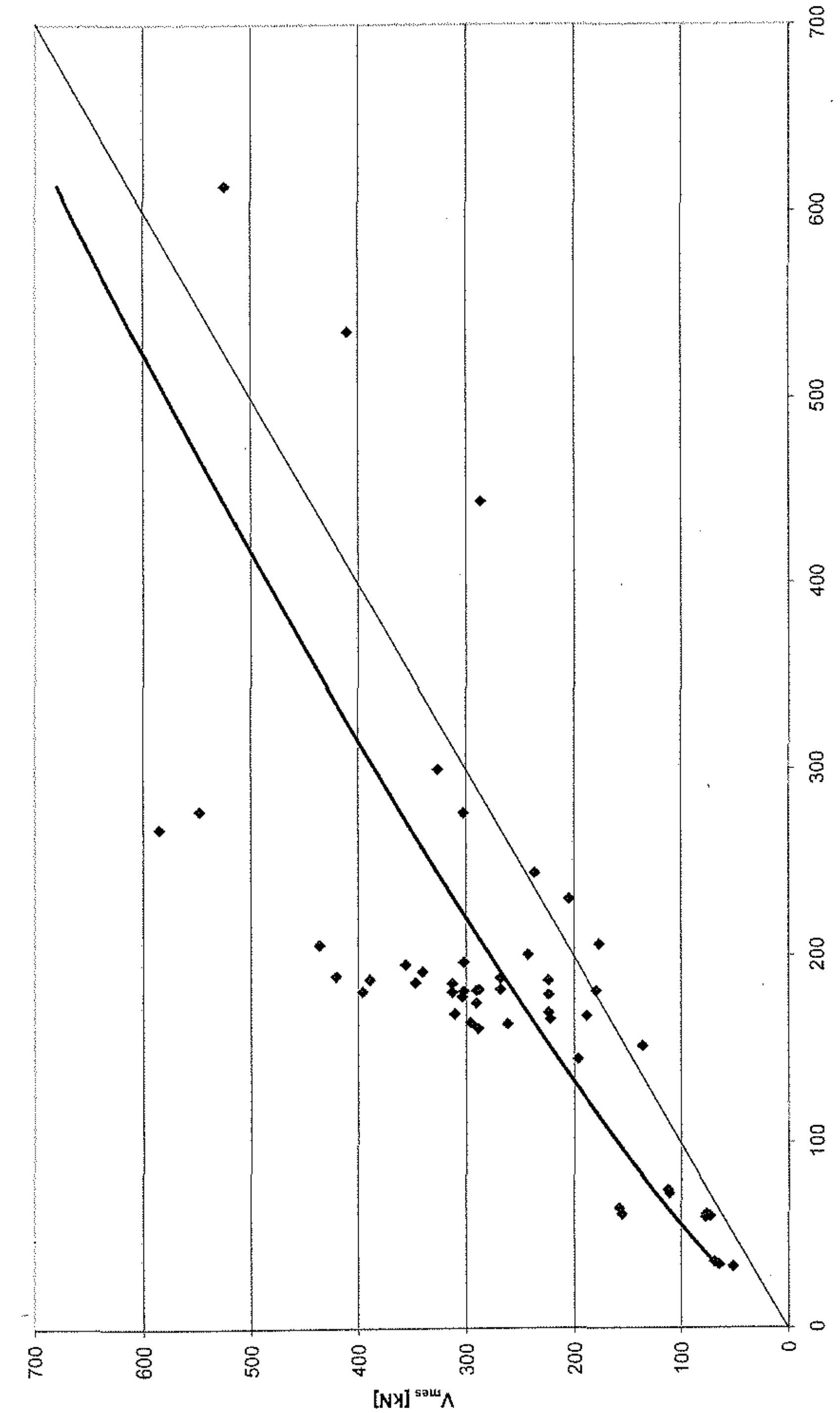

Figure 4-16 Measured versus calculated shear strength of deep beams without web reinforcement following Watanabe's approach

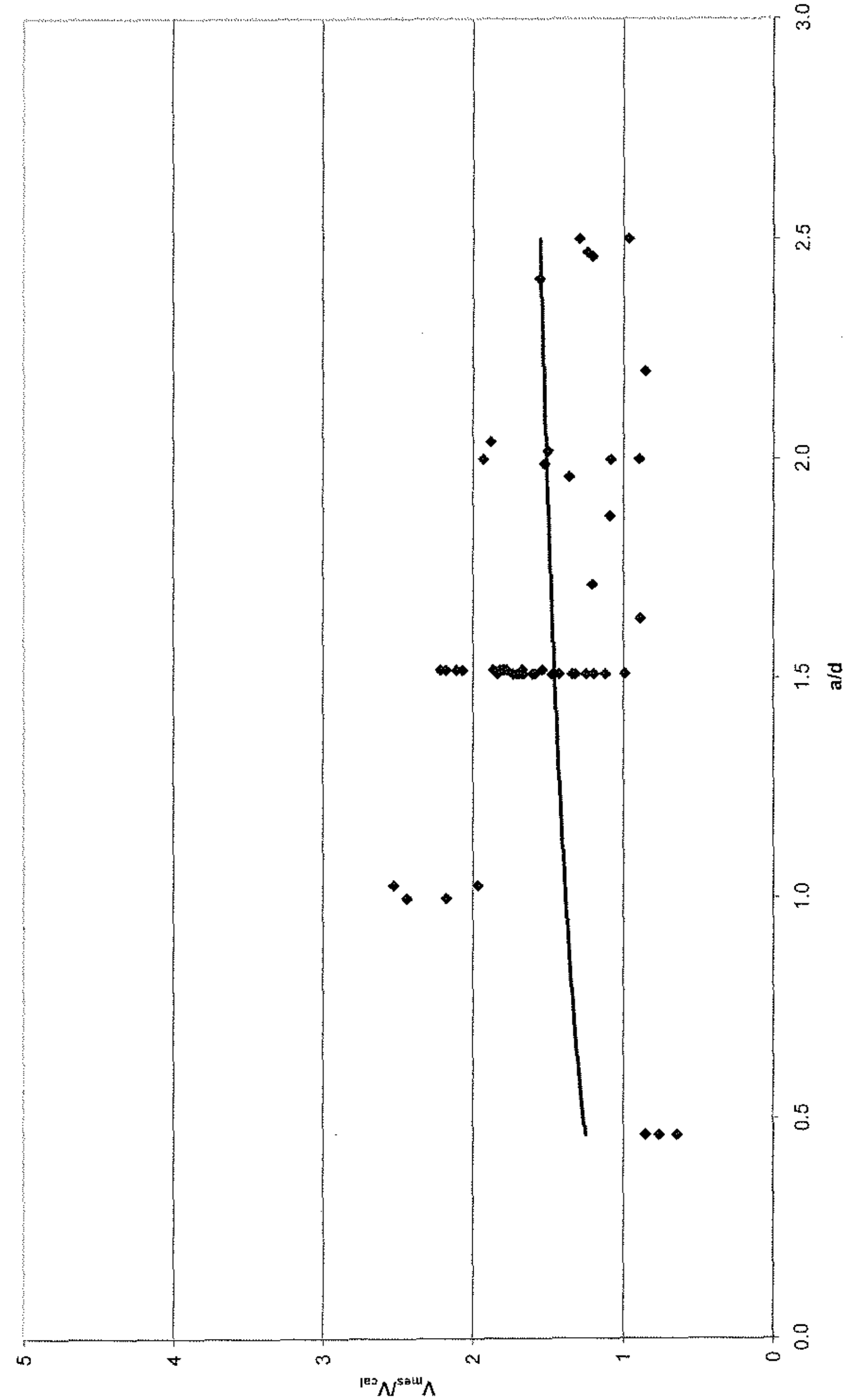

Figure 4-17 Ratio of measured to calculated shear strength versus aspect ratio of deep beams without web reinforcement following Watanabe's approach

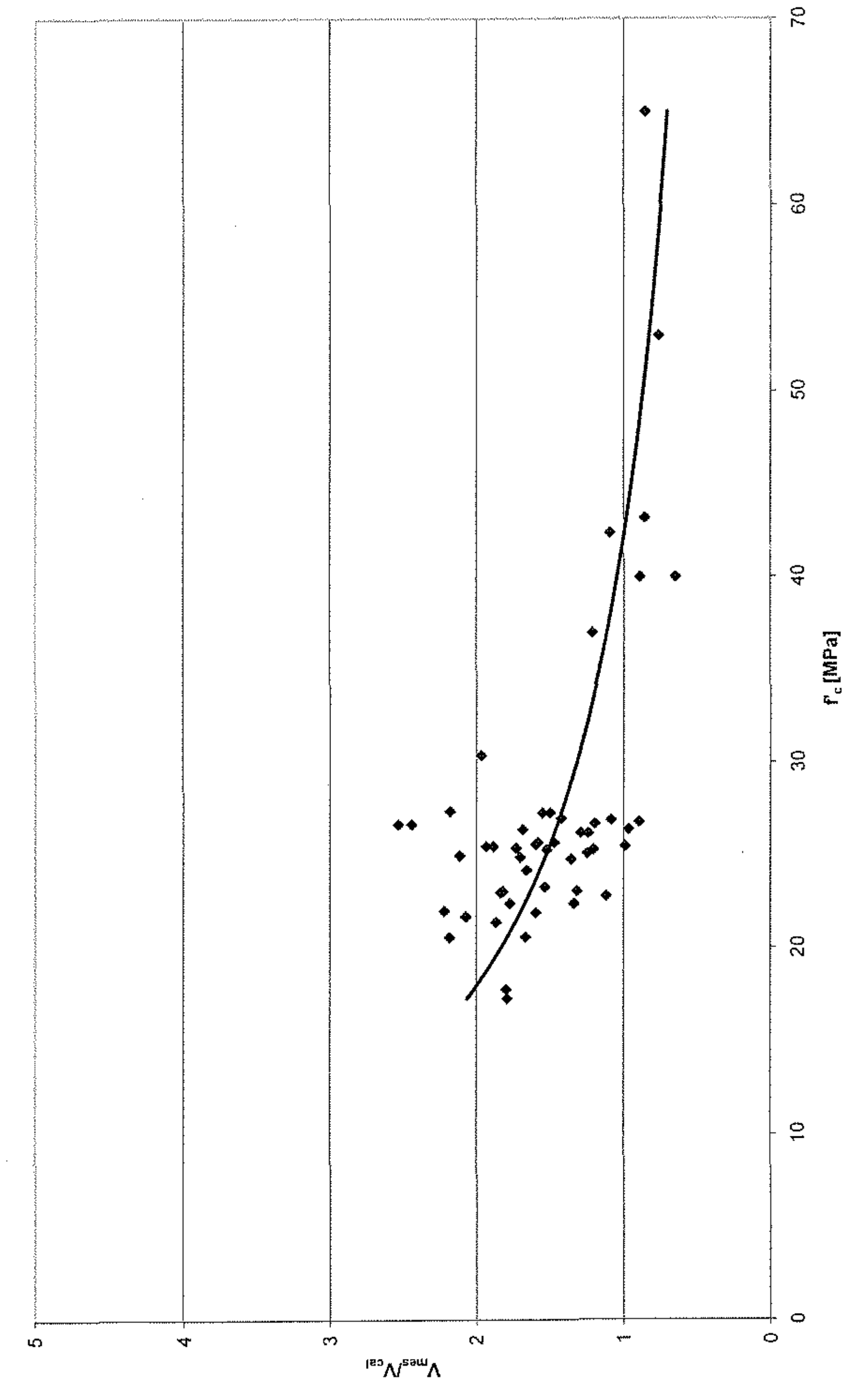

Figure 4-18 Ratio of measured of measured to calculated shear strength versus concrete strength of deep beams without web reinforcement following Watanabe's approach

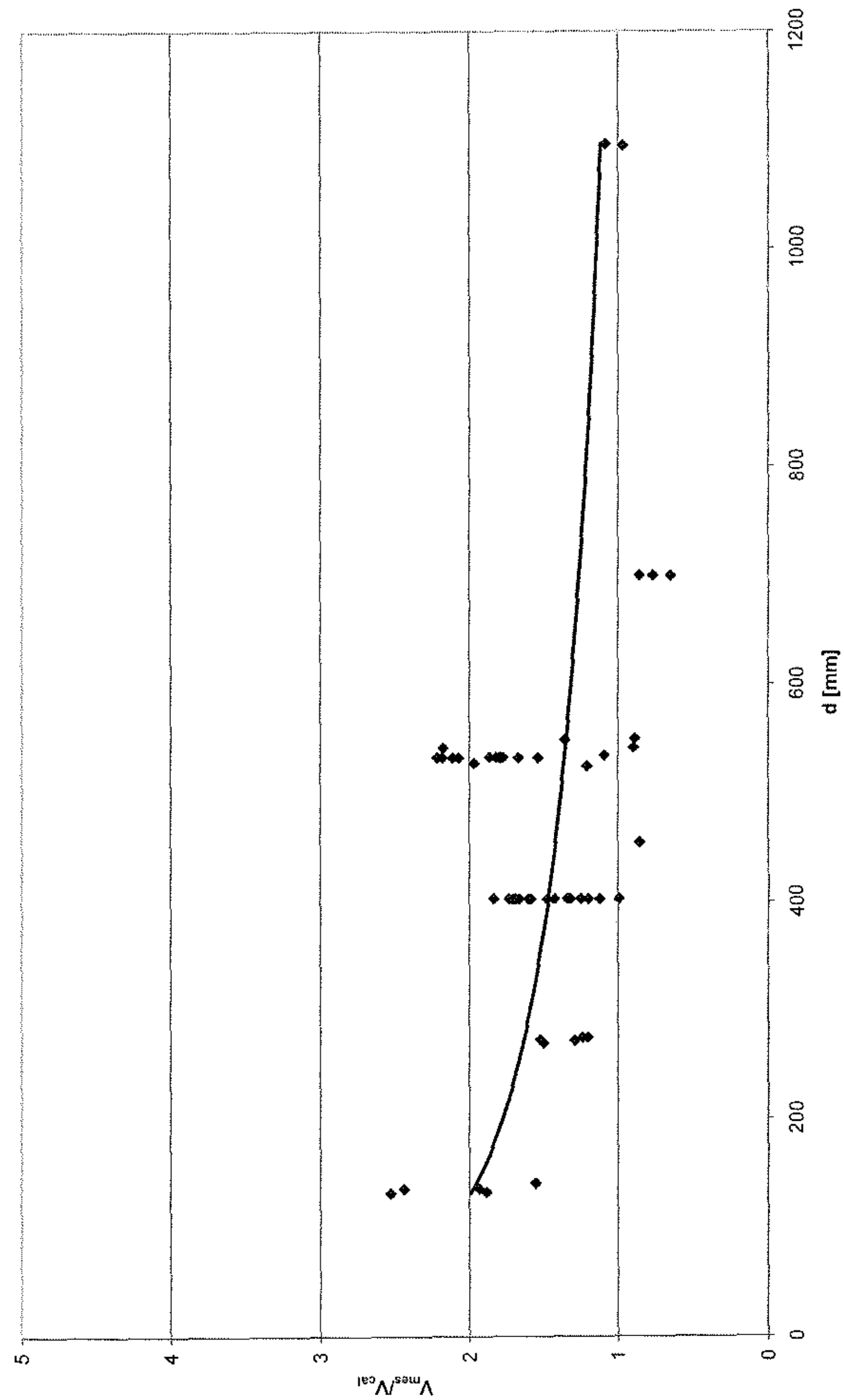

Figure 4-19 Ratio of measured to calculated shear strength versus effective depth of deep beams without web reinforcement following Watanabe's approach

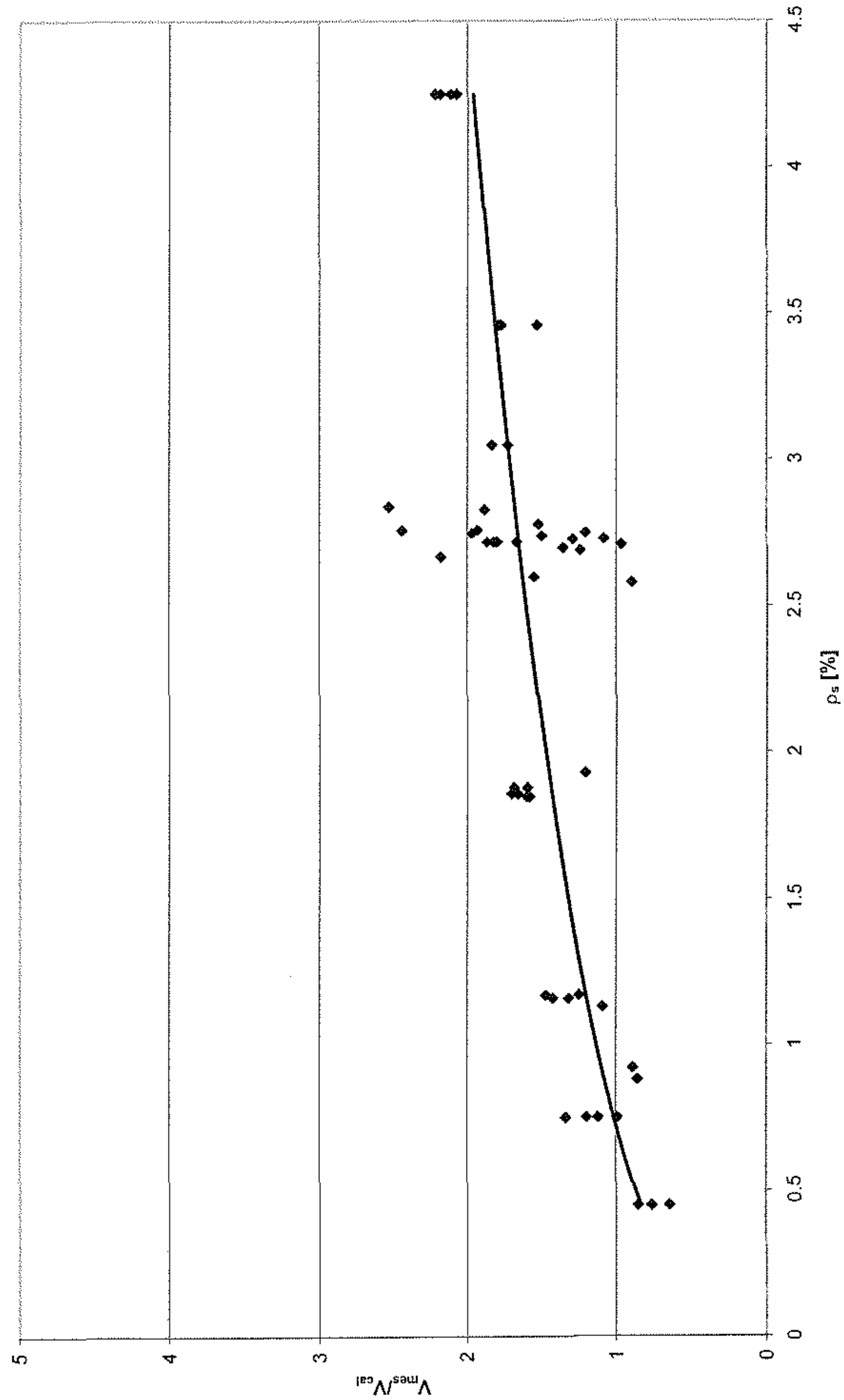

Figure 4-20 Ratio of measured to calculated shear strength versus tensile reinforcement ratio of deep beams without web reinforcement following Watanabe's approach

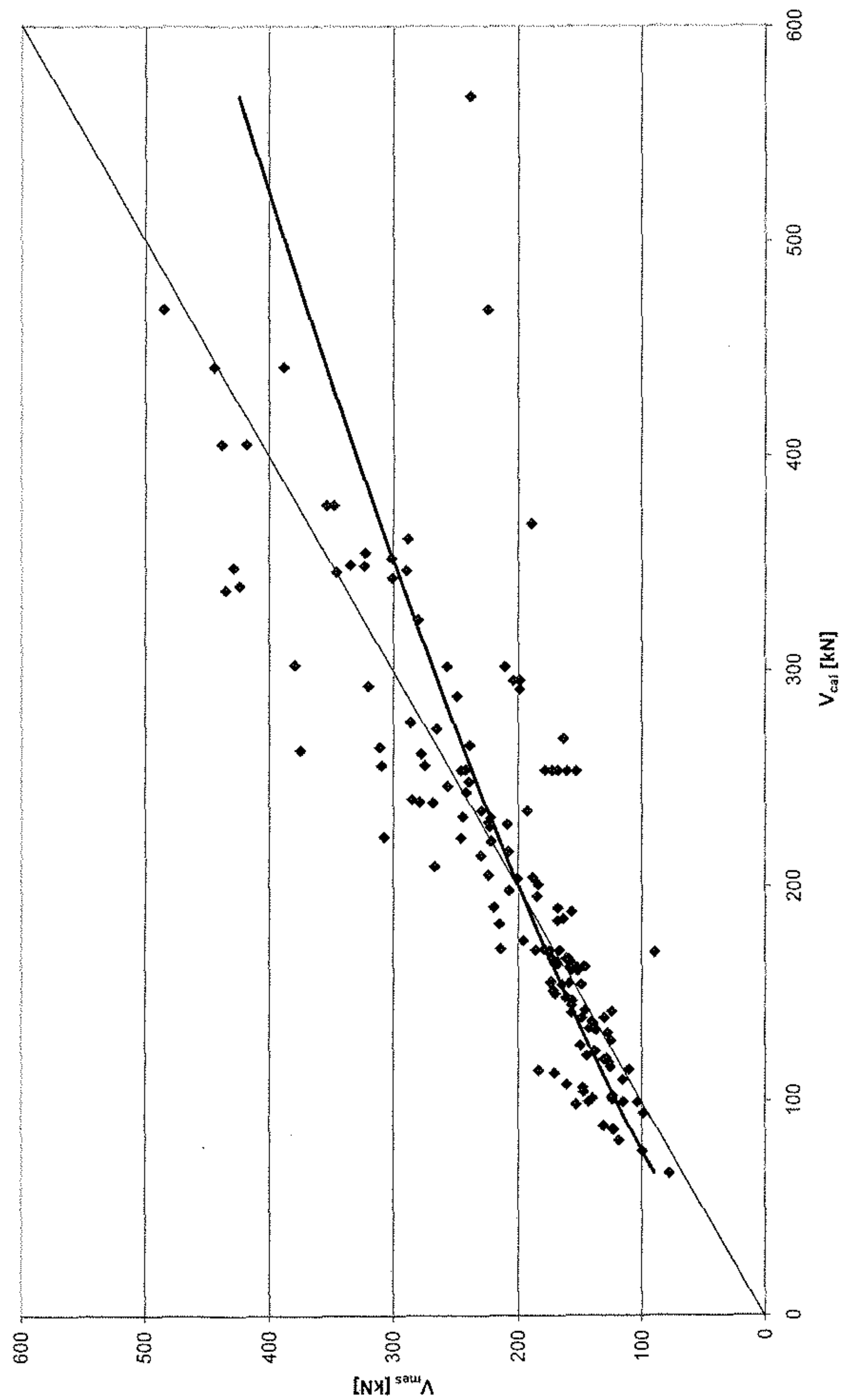

Figure 4-21 Measured to calculated shear strength of deep beams with web reinforcement following Watanabe's approach

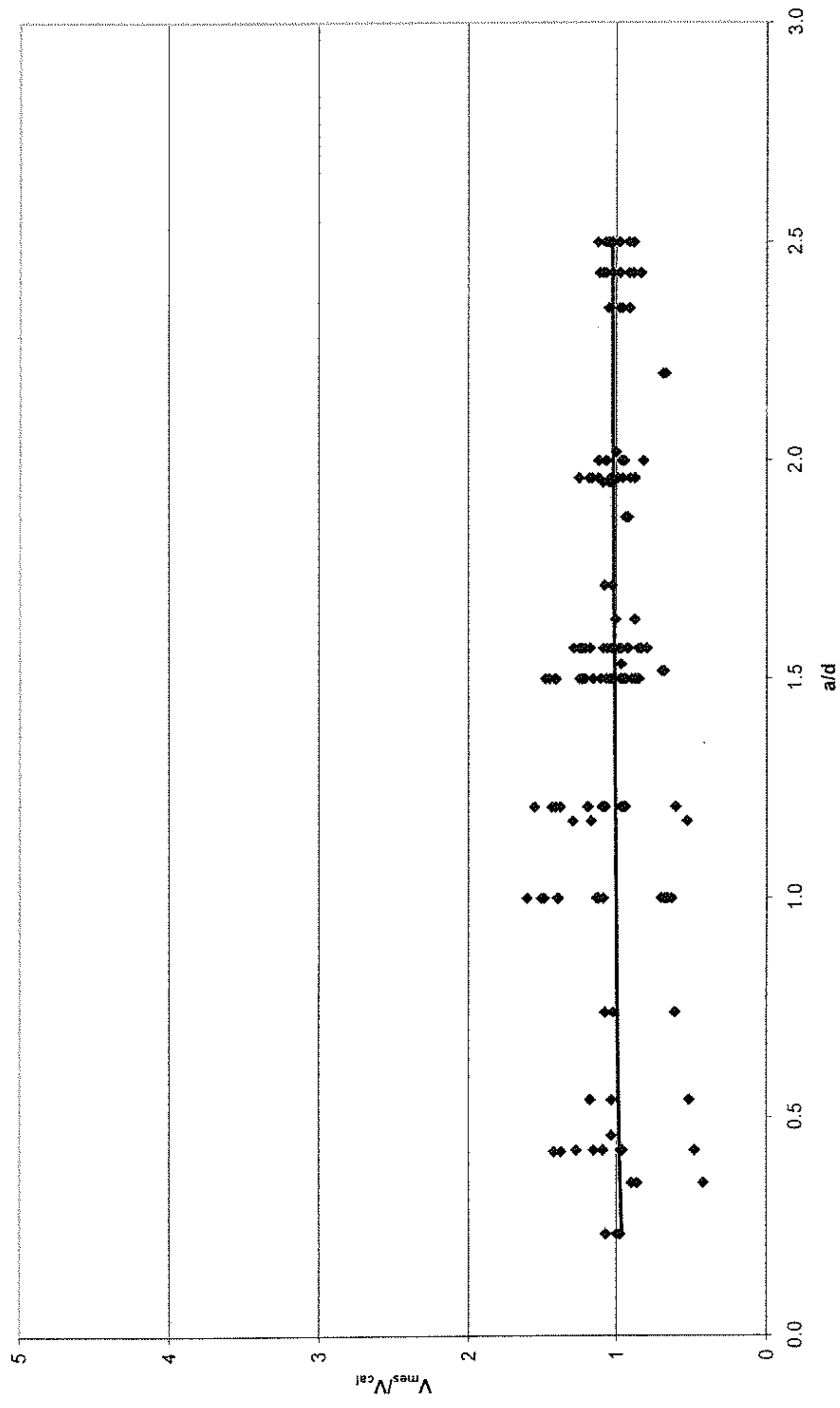

Figure 4-22 Ratio of measured to calculated shear strength versus aspect ratio for deep beams with web reinforcement following Watanabe's approach

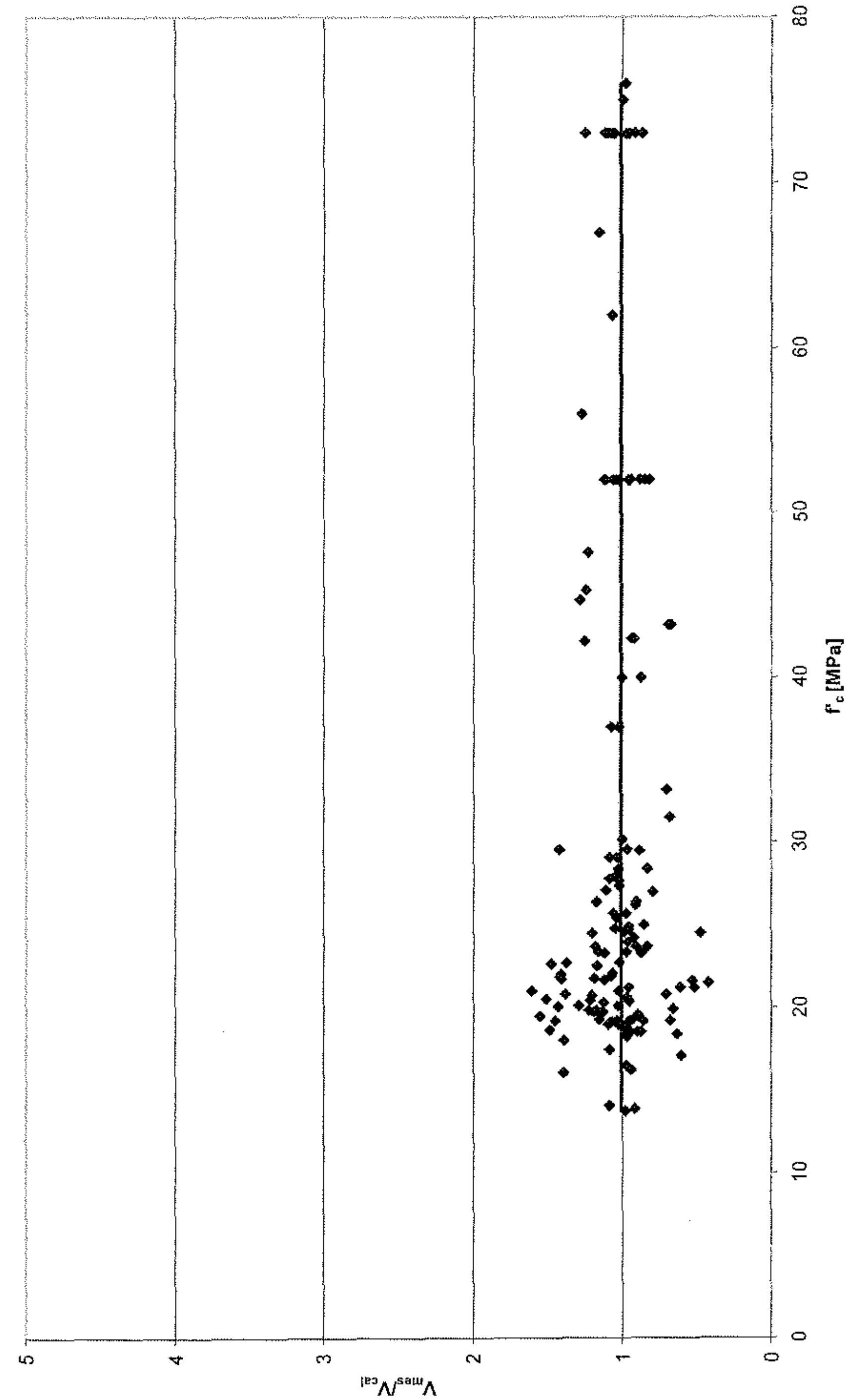

Figure 4-23 Ratio of measured to calculated shear strength versus concrete strength for deep beams with web reinforcement following Watanabe's approach

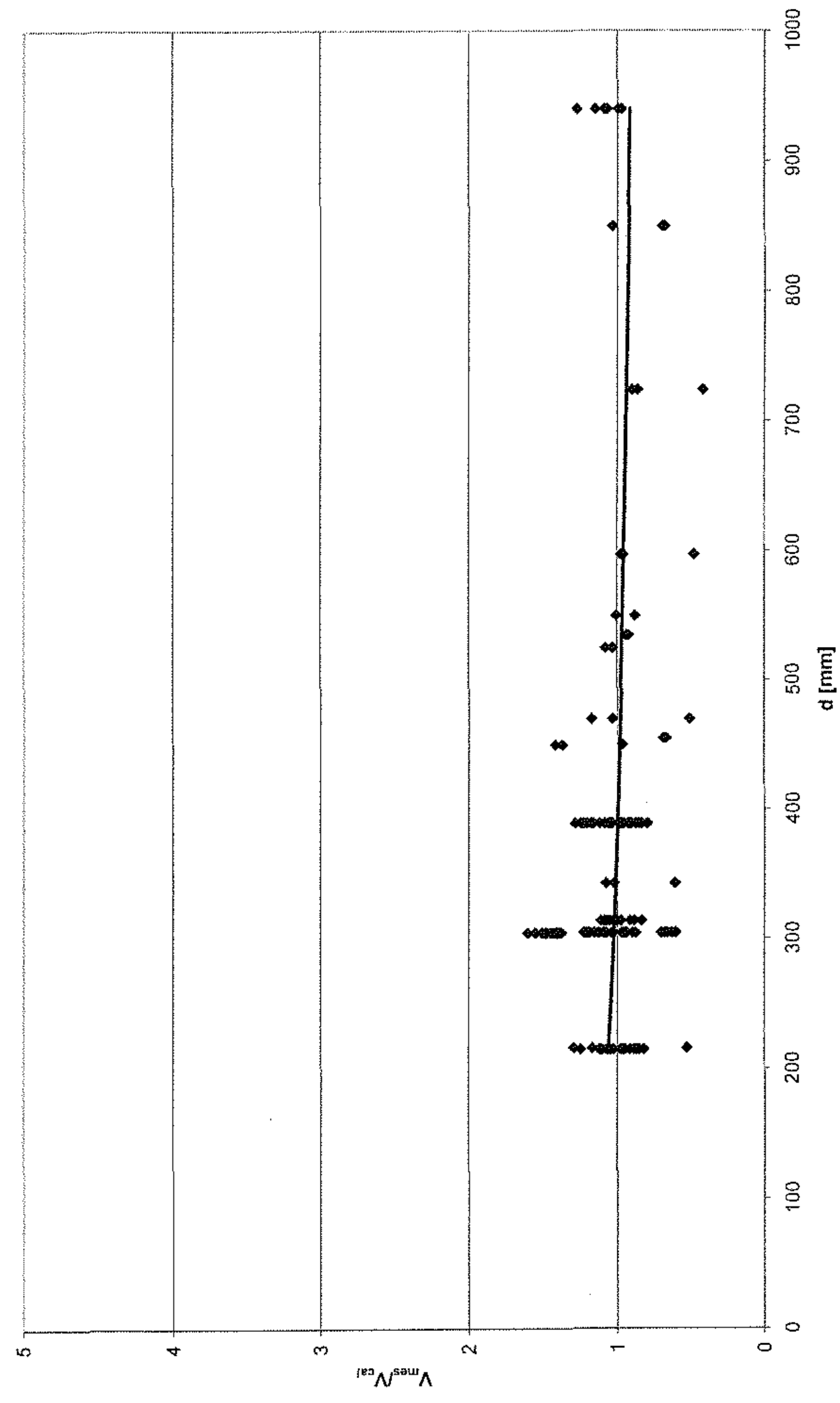

Figure 4-24 Ratio of measured to calculated shear strength versus effective depth of deep beams with web reinforcement following Watanabe's approach

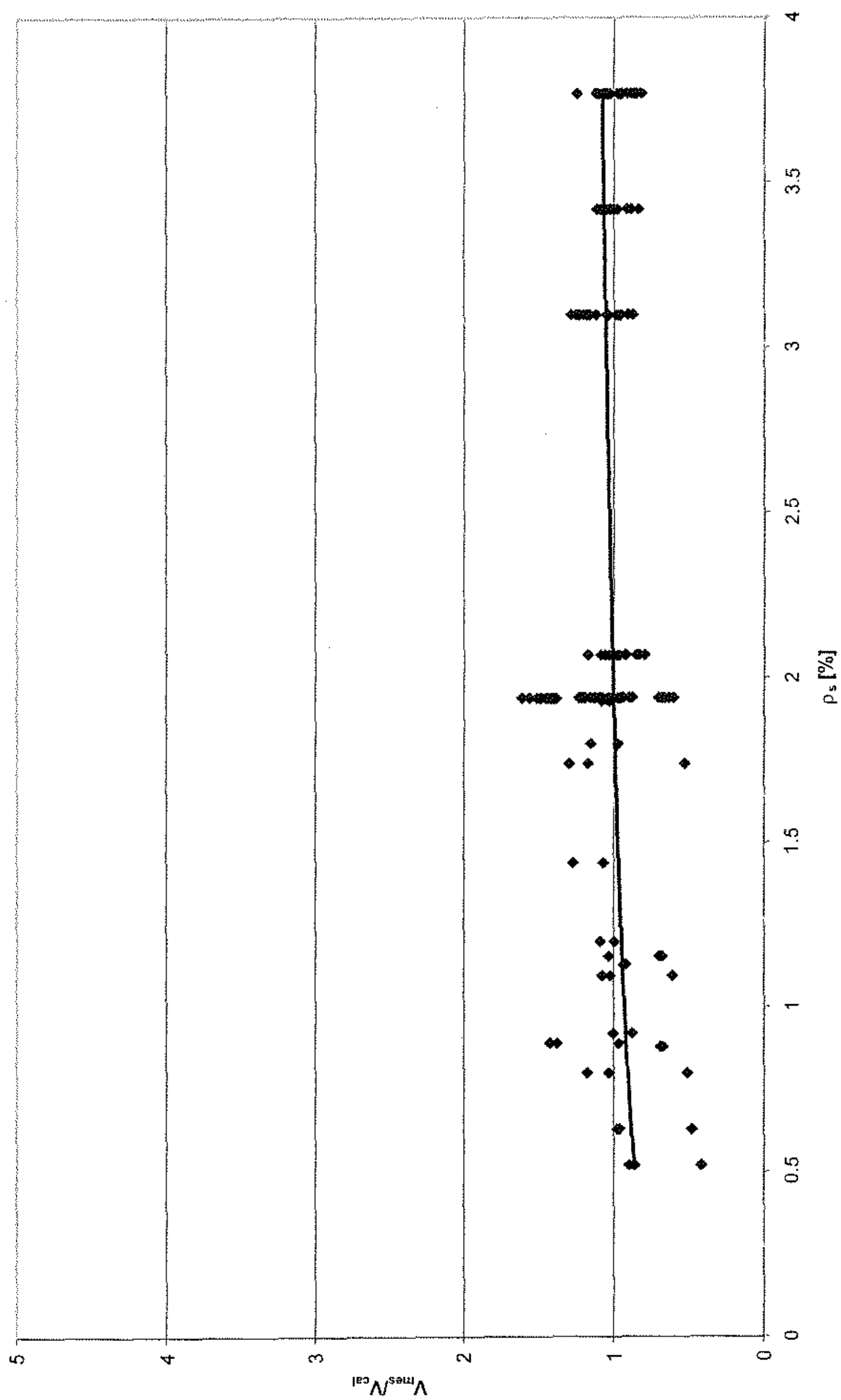

Figure 4-25 Ratio of measured to calculated shear strength versus tensile reinforcement ratio of deep beams with web reinforcement following Watanabe's approach

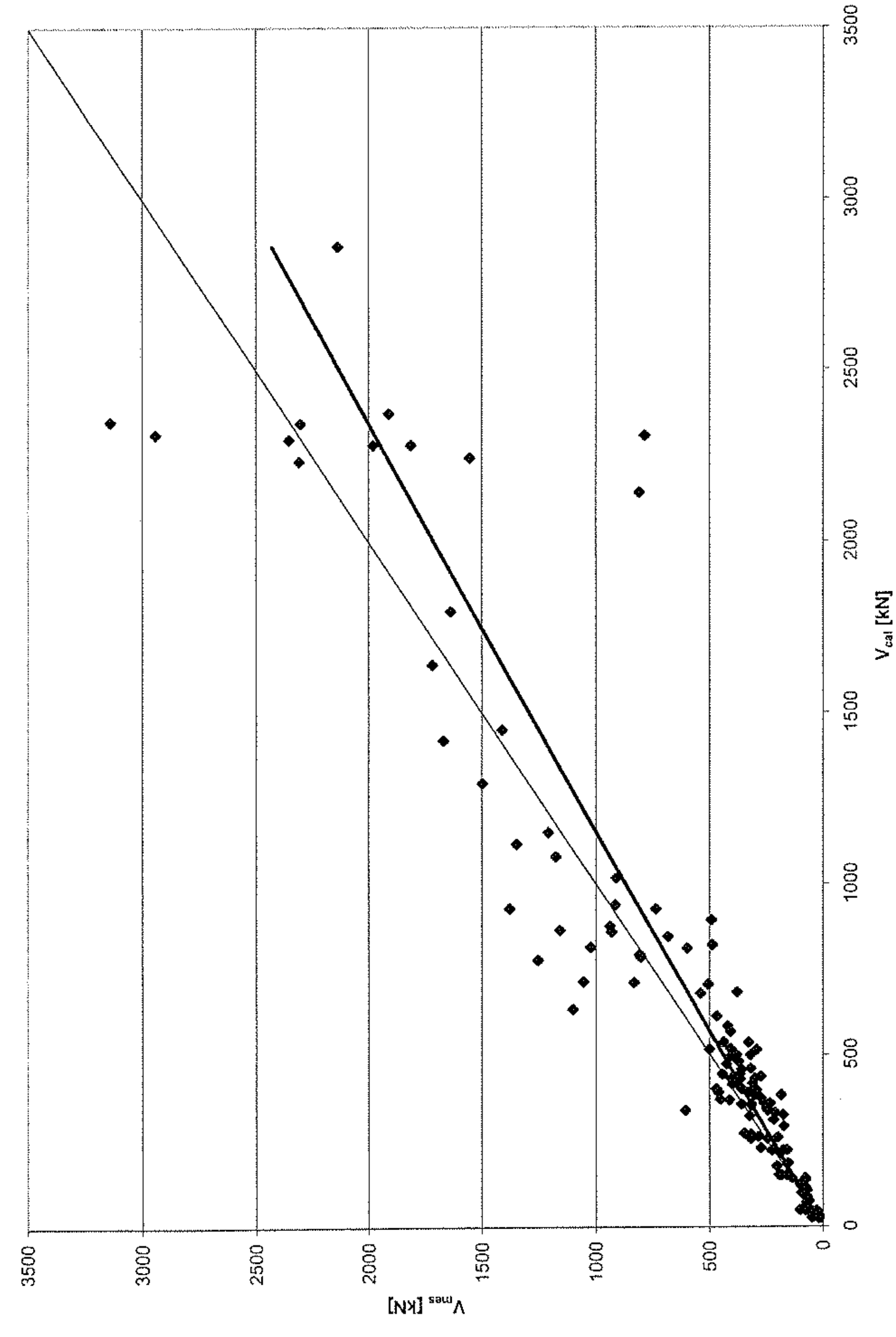

Figure 4-26 Measured to calculated shear strength of walls following Watanabe's approach

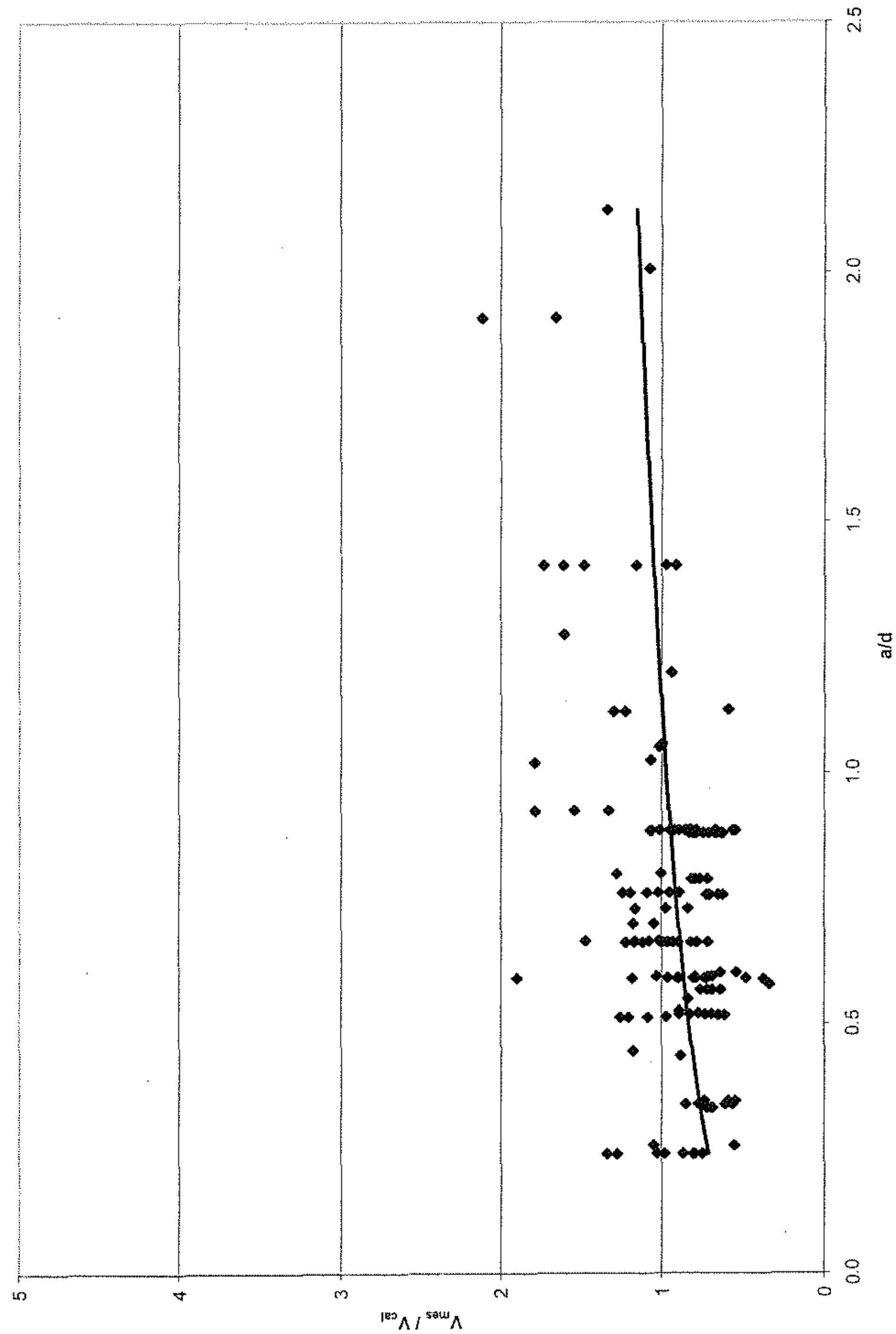

Figure 4-27 Ratio of measured to calculated shear strength versus aspect ratio of walls following Watanabe's approach

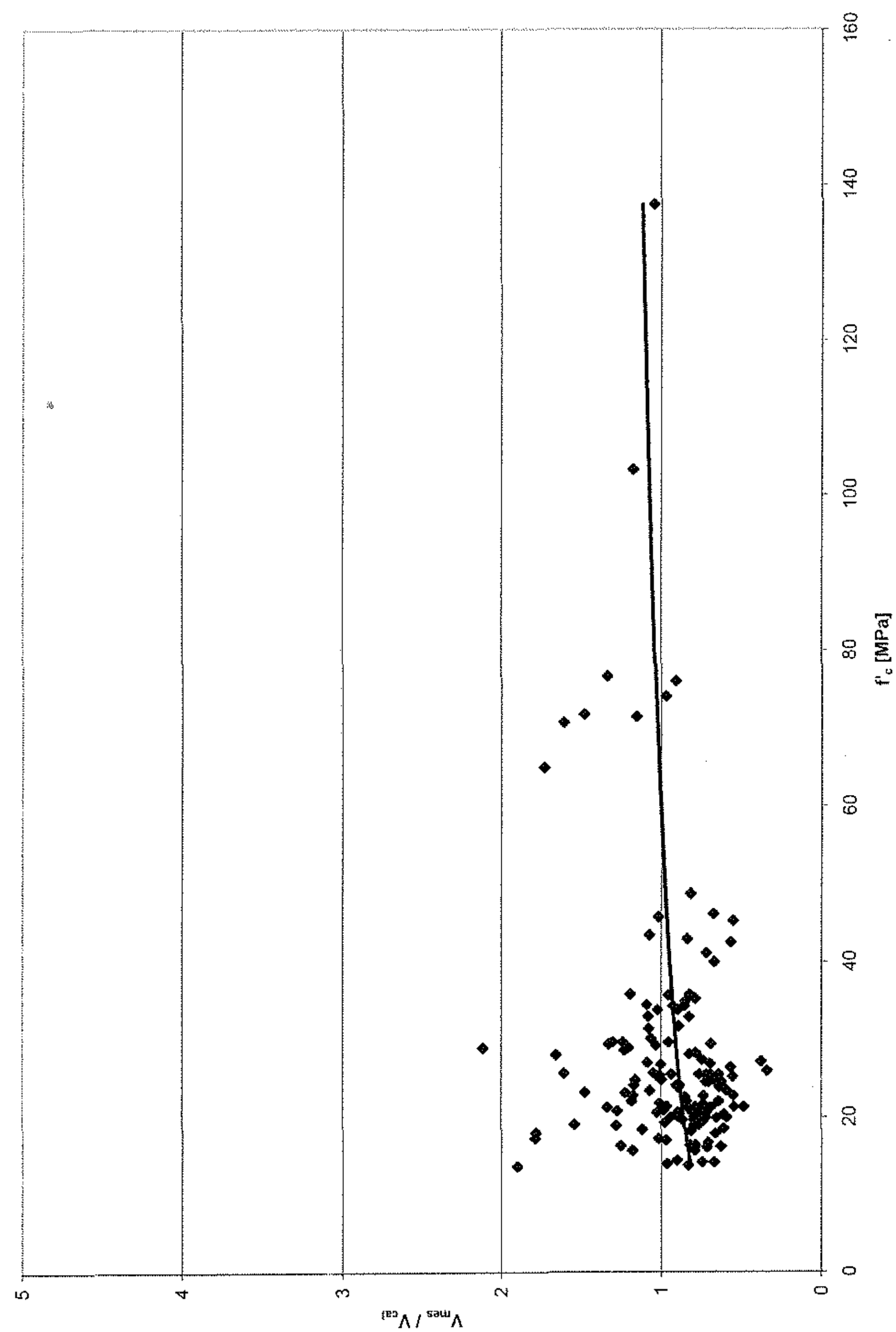

Figure 4-28 Ratio of measured to calculated shear strength versus concrete strength of walls following Watanabe's approach

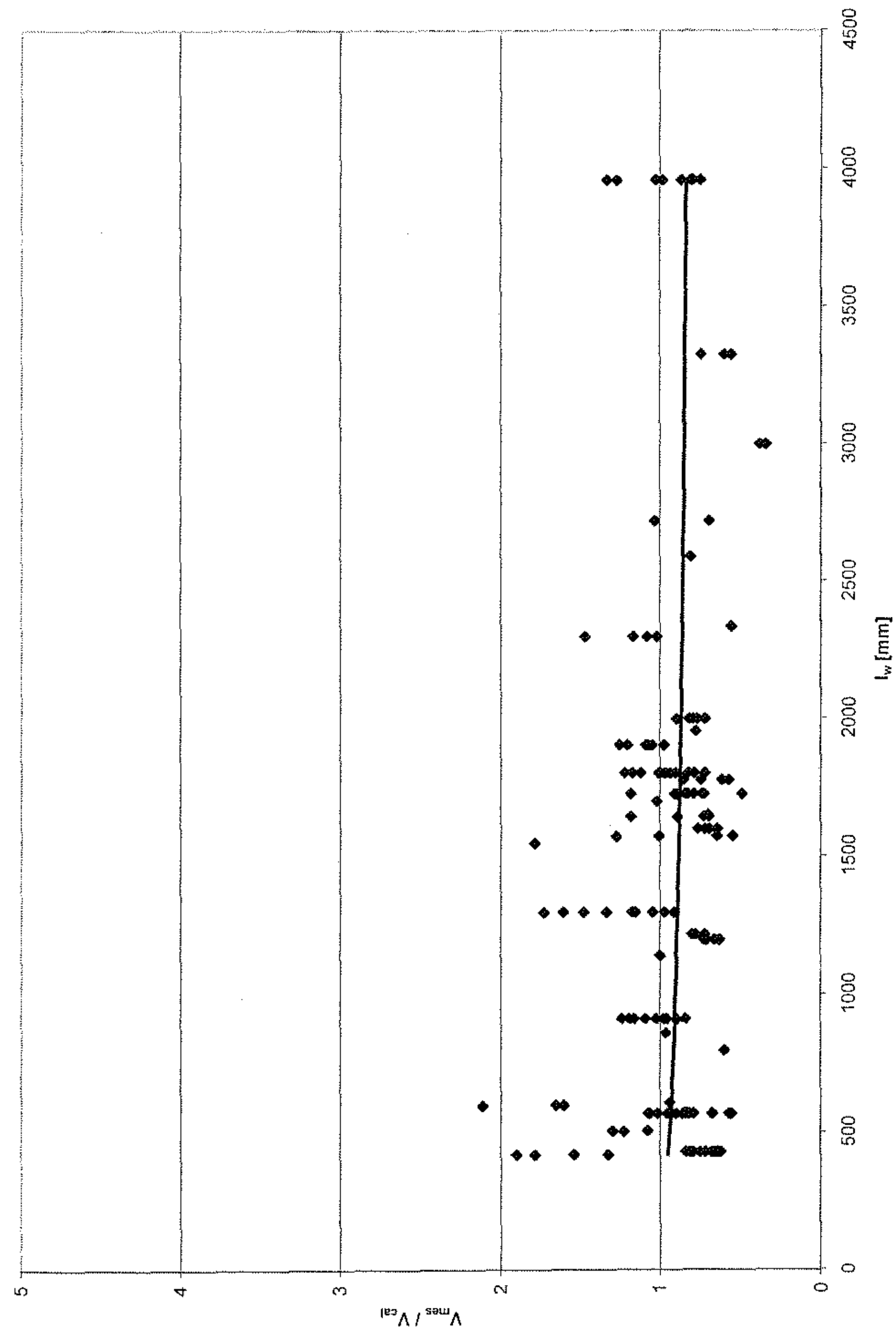

Figure 4-29 Ratio of measured to calculated shear strength versus wall panel length following Watanabe's approach

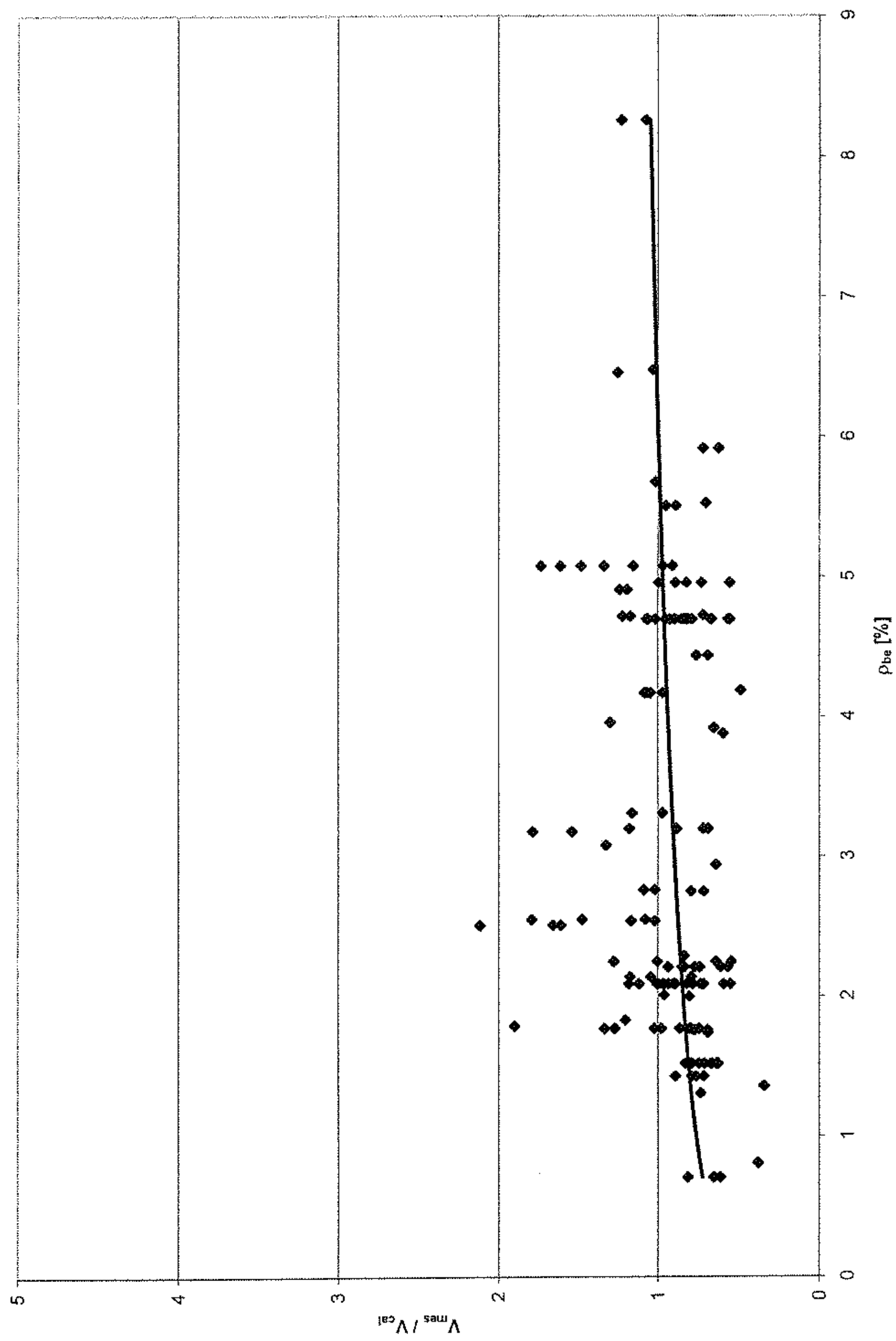

Figure 4-30 Ratio of measured to calculated shear strength versus tensile reinforcement ratio of walls following Watanabe's approach

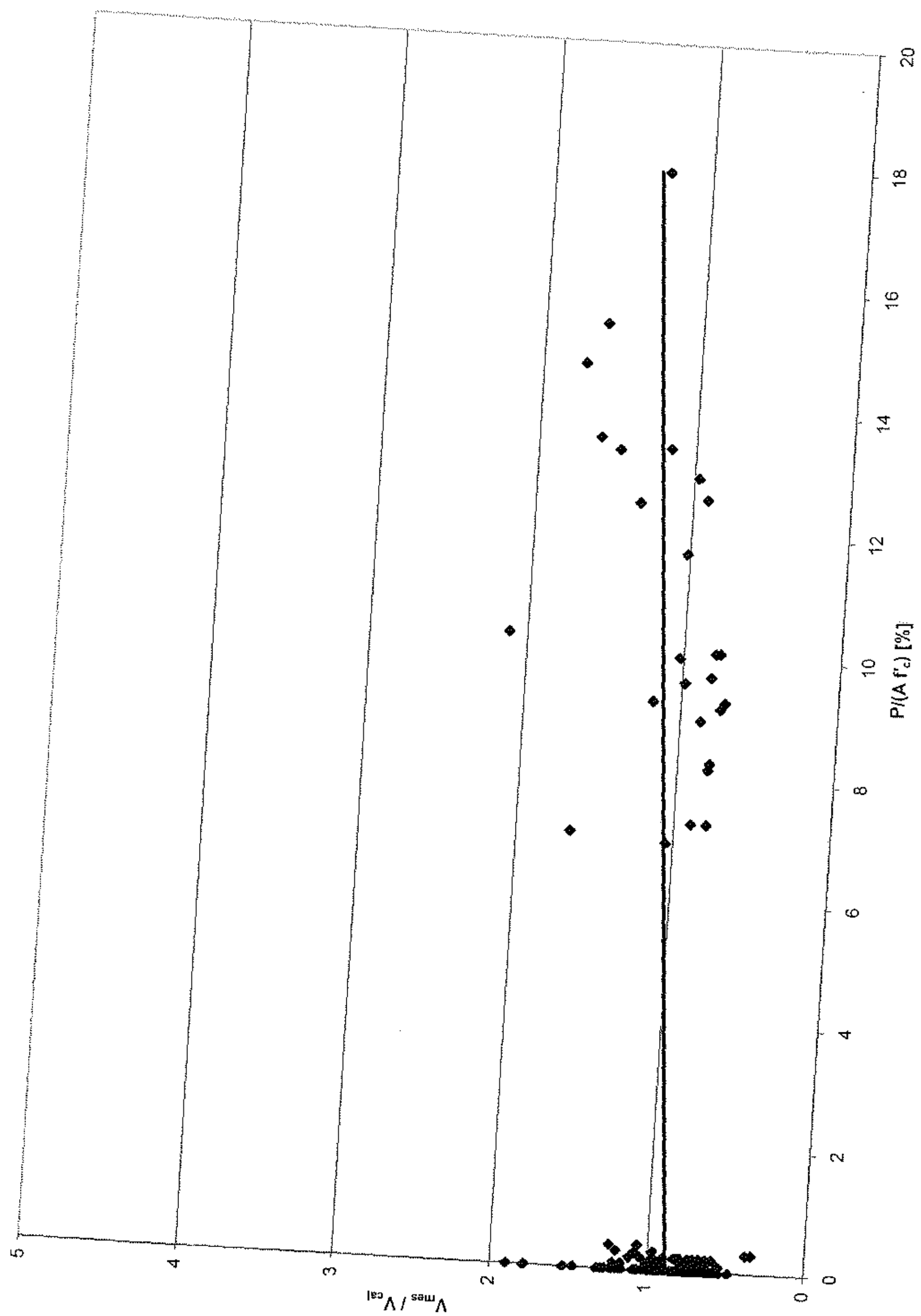

Figure 4-31 Ratio of measured to calculated shear strength versus axial load ratio of walls following Watanabe's approach

4.3 Shear strength of slender RC beams without transverse reinforcement

The calculation of the ultimate shear force following the proposal by Reineck as described in Section 3.3 (Reineck 1990, 1991b) was performed using equation (3.33) on a database of 395 slender RC members that failed in shear. This database was collected by Reineck and Kuchma as a comprehensive database for the evaluation of analytical models for the shear behavior of RC members without transverse reinforcement (Reineck et al. 2003). Beam properties are listed along with the ratios of measured to calculated shear strength on the "Slender beams without web reinforcement" worksheet on the accompanying CD and in Appendix A2. Abbreviations for the evaluation of equation (3.33) can be found in Chapter 3.3.

$$V_u = \frac{b_w \cdot d \cdot 0.4 \cdot f_{ct} + V_{du}}{\left[1 + 0.16 \frac{f_{ct}}{f_c} \lambda \left(\frac{a}{d} - 1\right)\right]} \qquad \text{((3.33) Repeated)}$$

The evaluation of the database yielded generally satisfactory, but slightly conservative, results. The mean value of the ratio of measured to calculated shear strength was 1.55 ± 0.46 % within a 95 % confidence region. The standard deviation was found to be 0.42, resulting in a coefficient of variation of 27.43 %. Figure 4-32 shows a plot of measured against calculated shear strength. Only a slight negative trend is apparent, which might also be the result of single test specimens. Indicated with grey marks are again the specimens scaled to verify the effect of the effective depth, *d*. These beams were previously described in the evaluation of the model proposed by Watanabe on RC beams without web reinforcement. Compared to the model proposed by Watanabe, bias with respect to the effective depth seems to be of less concern. Only a slight trend to increasingly unconservative estimates with increasing effective depths is to be seen, which is a trend that is confirmed by Figure 4-35, the plot of V_{mes}/V_{cal} against the effective depth, d.

The aspect ratio of the examined beams is plotted against the ratio of measured to calculated strength in Figure 4-33. The approach proposed by Reineck appears to be slightly biased for low aspect ratios between 2.5 and 3.5. A reason for this could be that this range of the aspect ratio is a transitional range, in which part of the shear is carried by arch-action, while the other part is carried by friction and the contribution of the compression zone. The model proposed by Reineck does not account for possible arch-action. A transition from arch-action to components relevant for slender members will be addressed in the development of the proposal by the author in Chapters 5 and 6.

Figure 4-34 displays bias of the model proposed by Reineck with respect to the compressive strength of concrete. The model tends to overestimate the shear strengths of members with high-strength concrete. Scatter is spread relatively even along the plotted trend line, indicating that the trend line is giving an appropriate estimate of member behavior.

A trend towards increasingly conservative values with increasing ratios of tensile reinforcement is discernible in Figure 4-36. Though the majority of tested beams had tensile reinforcement ratios in the range of approximately 0.3 % to 3.5 %, a trend towards larger values of ρ_s is obvious. This could be related to an underestimation of the contribution from the compression zone, which increases with an increasing depth of the neutral axis, again increasing with larger tensile reinforcement ratios.

Overall, the model proposed by Reineck seemed to give good results; it might not consider additional contributions accordingly, though. The trends with respect to the aspect ratio, and the tensile reinforcement ratio, could be lessened by considering a contribution from arch-action for small and intermediate shear-span-to-depth ratios. The tensile reinforcement ratio indirectly affects a possible arch contribution by increasing the neutral axis depth, and therefore the strut width of a possible arch.

A combination of arch-action with frictional and compression zone related components will be proposed by the author in the course of this study.

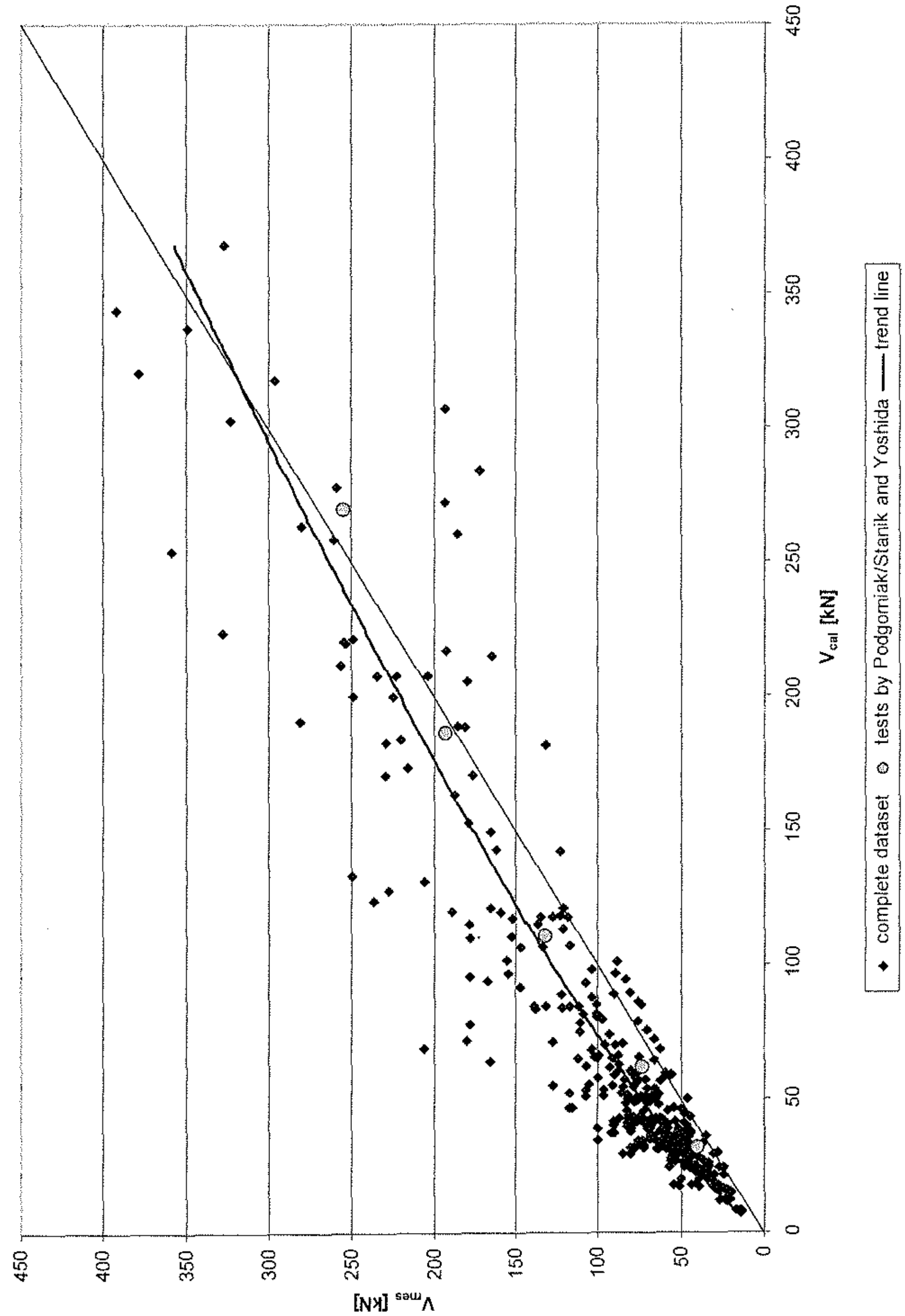

Figure 4-32 Measured versus calculated shear strength of slender RC beams without web reinforcement following Reineck's proposal

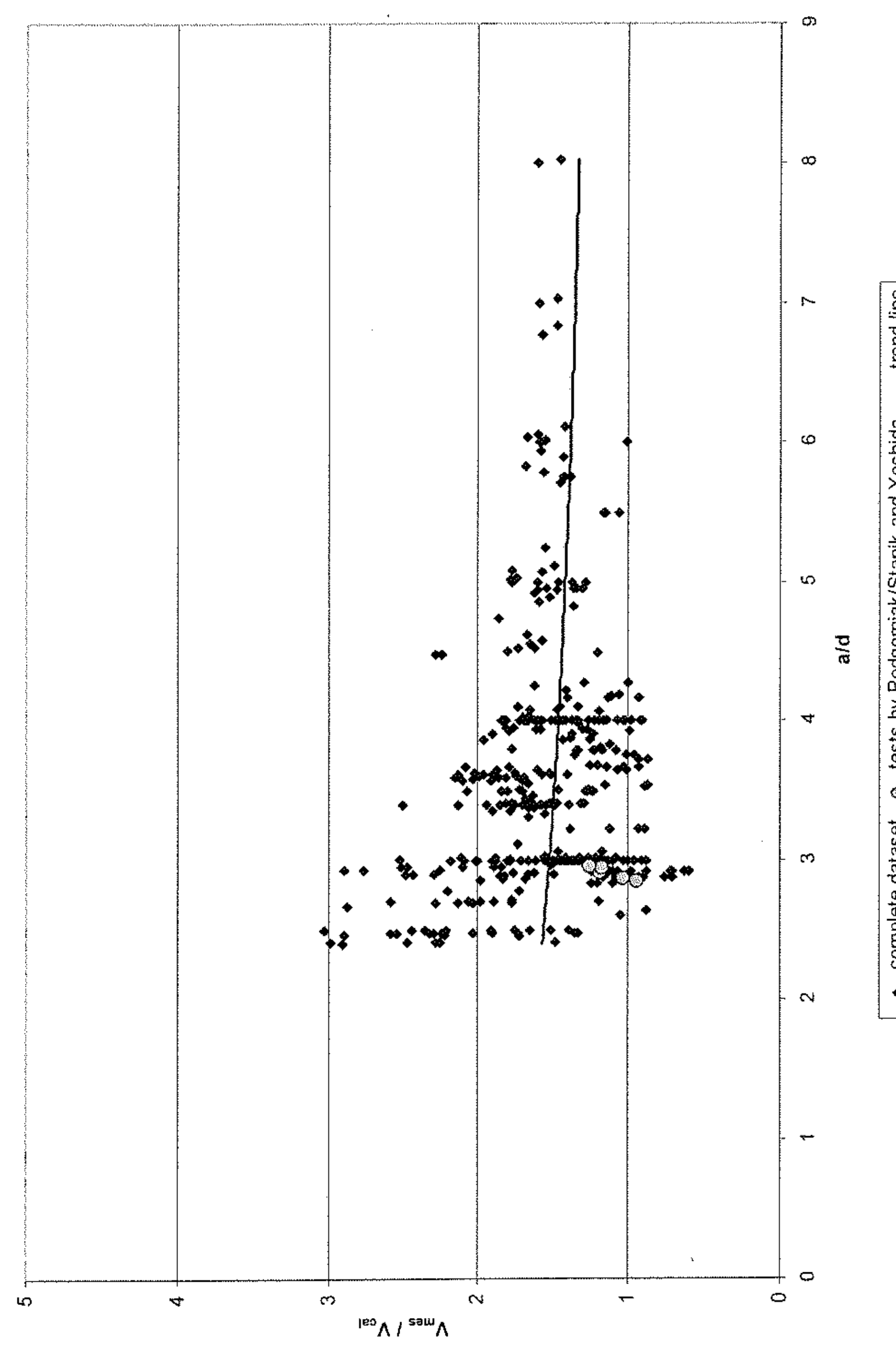

Figure 4-33 Ratio of measured to calculated shear strength versus aspect ratio of slender RC beams without web reinforcement following Reineck's proposal

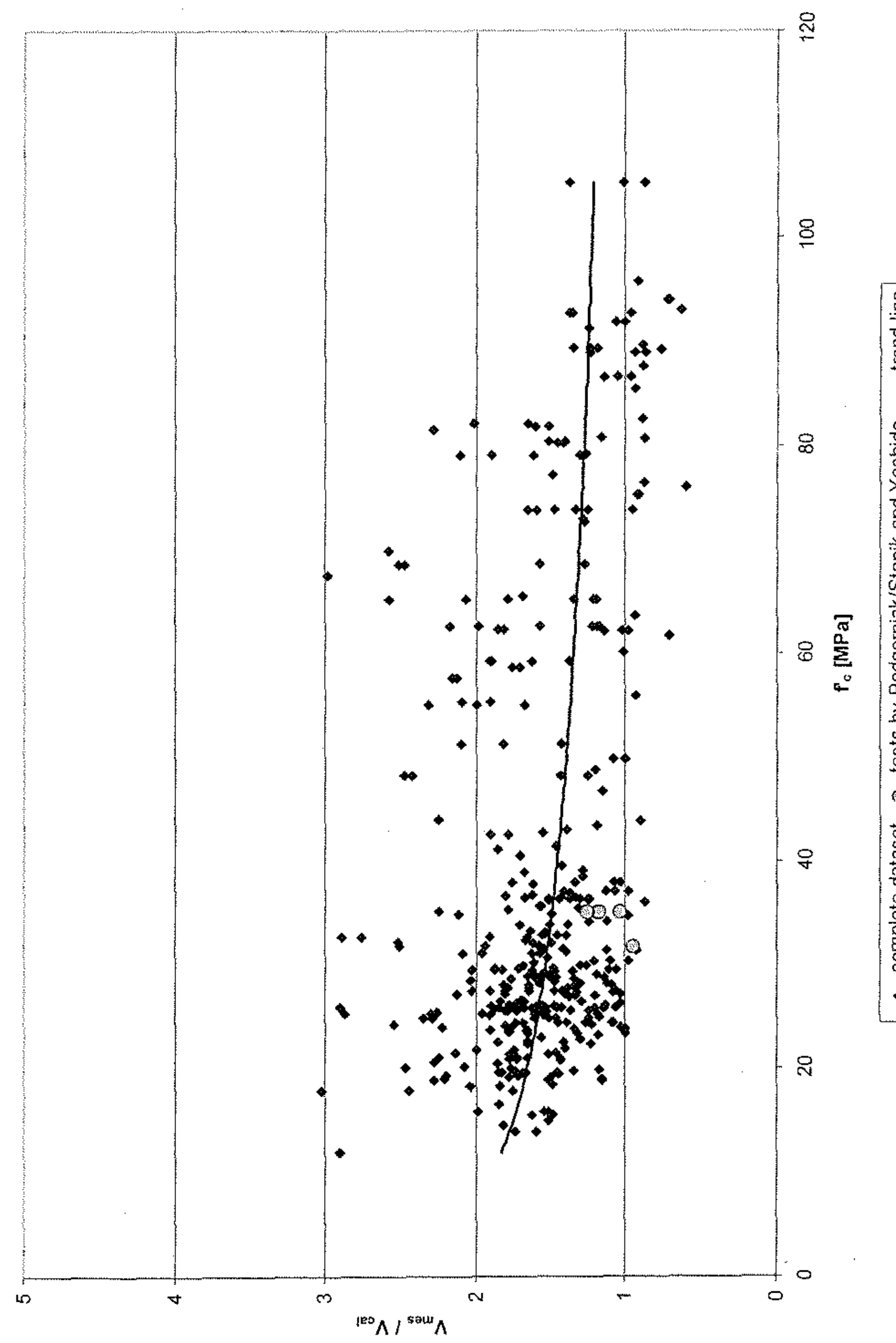

Figure 4-34 Ratio of measured to calculated shear strength versus concrete strength of slender RC beams without web reinforcement following Reineck's proposal

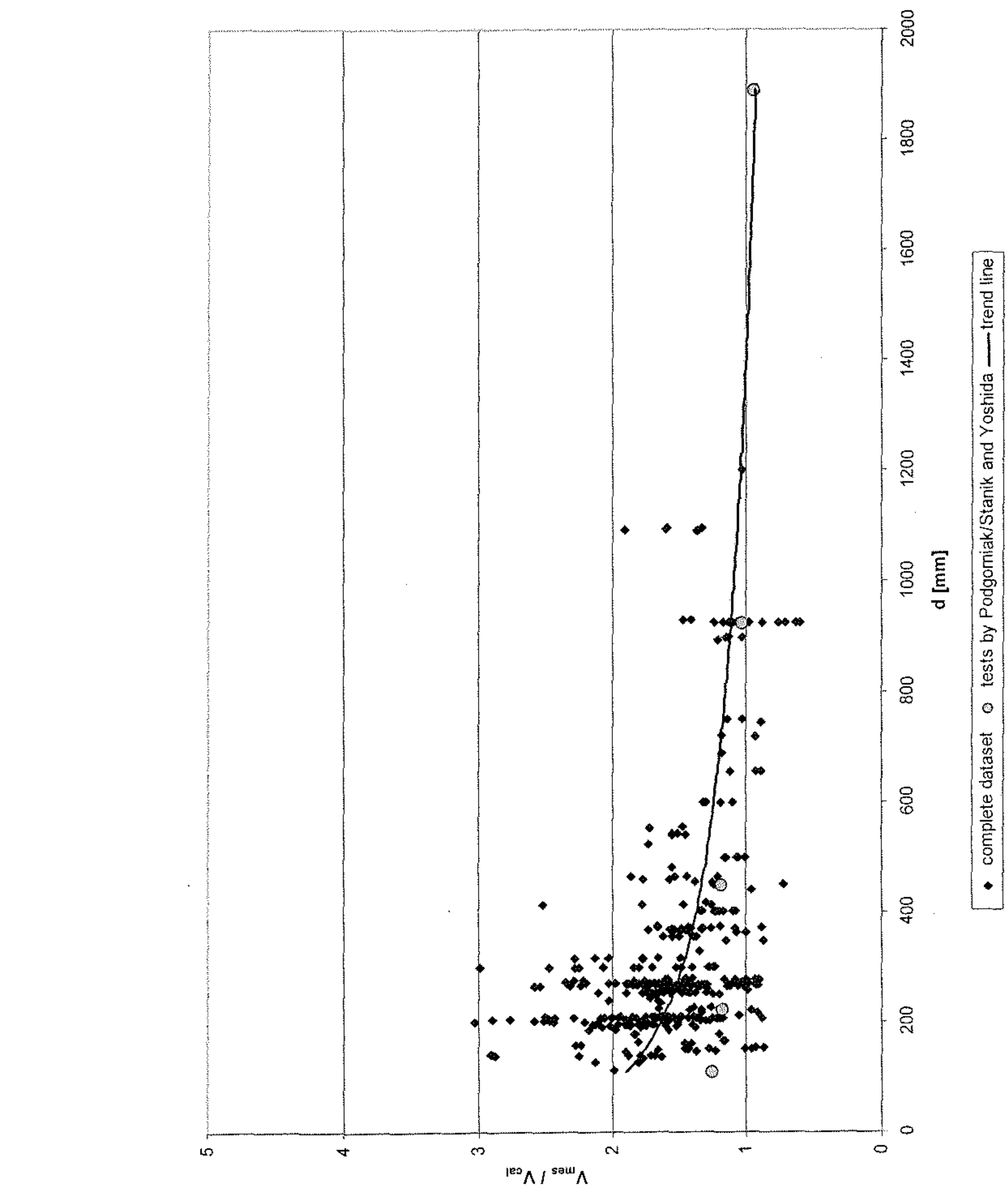

Figure 4-35 Ratio of measured to calculated shear strength versus effective depth of slender RC beams without web reinforcement following Reineck's proposal

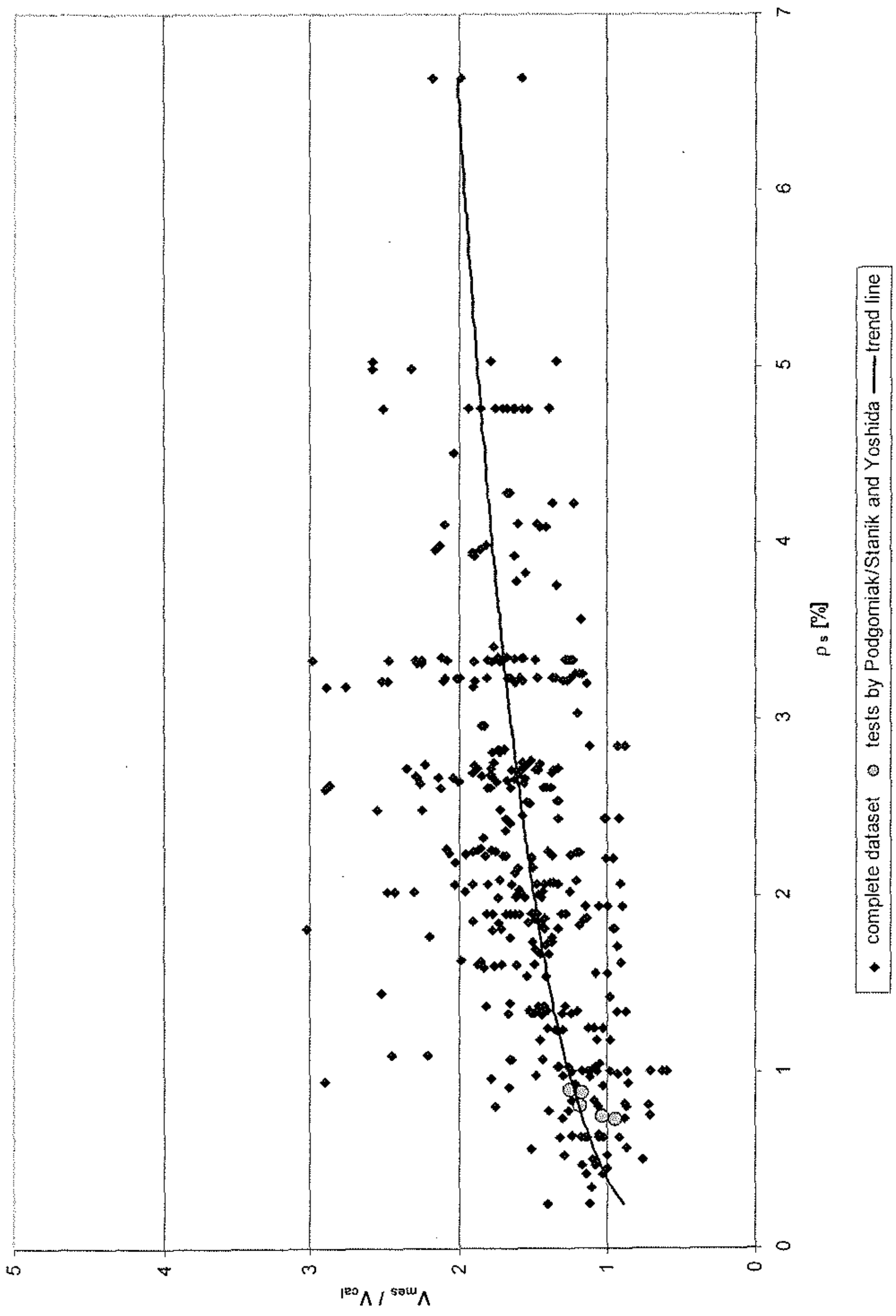

Figure 4-36 Ratio of measured to calculated shear strength versus tensile reinforcement ratio of slender RC beams without web reinforcement following Reineck's proposal

4.4 Drift capacity model

The analysis model based on drift capacity as proposed by Pujol et al. (Pujol 2000) was evaluated on the 38 columns of the combined UW / Brachmann / Ichinose database of columns under reversed cyclic load that failed in a shear related mode (Berry et al. 2003; Brachmann 2002; Ichinose et al. 2001). 17 of the available specimens meet the limits listed in Section 3.4, i.e. these 17 columns had an axial stress σ_a smaller or equal to $0.35f'_c$, and a nominal unit shear stress range from 0.5 to $1.1\sqrt{f'_c}$ MPa. Computational results and column properties are listed in Appendix A7 and in the "Seismic shear failure" worksheet on the supplementary CD.

It was expected that solving equation (3.41) for an ultimate shear capacity (equation (3.42)) would not yield reasonable results in its application on tested specimens, because the tested specimens were not built according to the proposed design equation. Formulation (3.41) allows for one specific transverse reinforcement ratio related to assumed conditions in the member.

$$\rho_w = \frac{A_w}{s \cdot b_c} = \left[\frac{3}{8} \cdot \alpha + 1 - \frac{5}{8}\sqrt{\alpha^2 - \beta^2}\right] \cdot \frac{\sigma_a}{f_{yw}} \qquad \text{((3.41) Repeated)}$$

$$V_u = \frac{2}{5}\left(\frac{\rho_w f_{yw}}{\sigma_a} + \frac{1}{4}\alpha - 1\right)(P + T) \qquad \text{((3.42) Repeated)}$$

Plotted in Figure 4-37 is the evaluation of the analysis of the 17 columns analyzed by equation (3.42). Even though the number of evaluated data is small, it is obvious that the shear capacity of these columns was greatly underestimated. The mean value of measured to calculated shear strength was 4.47 ± 3.12 % within a 95 % confidence interval. The standard deviation was 3.84, resulting in a coefficient of variation of 86.1 percent.

Because it is obviously not sensible to use the model proposed by Pujol et al. for the calculation of capacities of tested specimens, this approach was not investigated further.

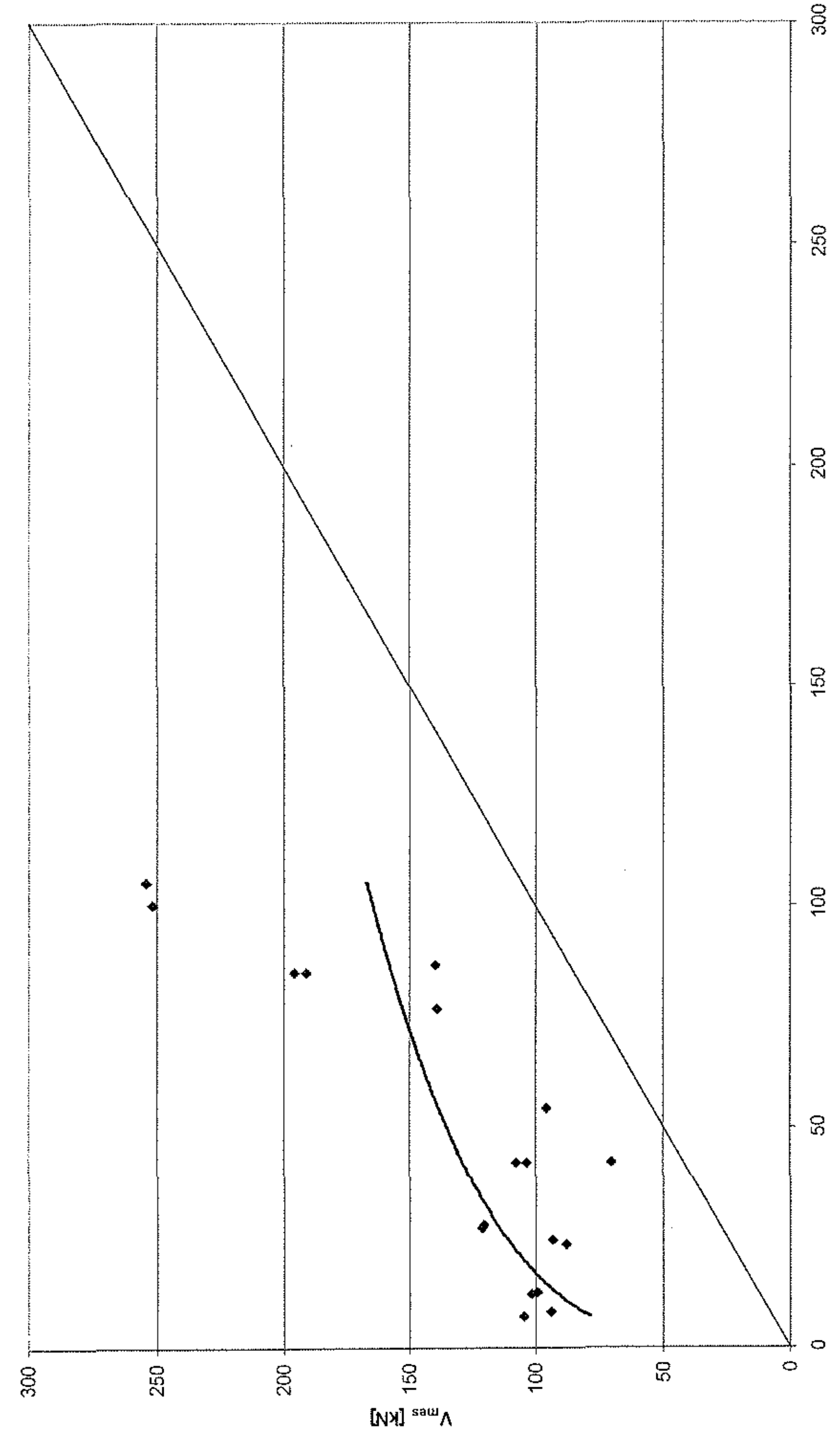

Figure 4-37 Measured to calculated shear strength of columns under cyclic shear following Pujol's approach

4.5 Influence of ductility demand on shear capacity

The calculation of the ultimate shear capacity based on displacement ductility was described in Chapter 3.5 as proposed by Priestley (Priestley 1994). The verification of this method was carried out on 38 RC columns of the combined UW / Brachmann / Ichinose database, which was previously used for the evaluation of the model proposed by Watanabe for seismically loaded columns (Berry et al. 2003; Brachmann 2002; Ichinose et al. 2001). The evaluation followed equations (3.46), (3.47), (3.50), and (3.52) for rectangular columns:

$$V_n = V_c + V_p + V_s \qquad \text{((3.46), repeated)}$$

$$V_c = k\sqrt{f'_c}A_g \qquad \text{((3.47), repeated)}$$

$$V_p = P \cdot \tan\alpha = P \cdot \frac{D-c}{2a} \qquad \text{((3.50), repeated)}$$

$$V_s = \frac{A_v f_{yh} D'}{S}\cot 30° \qquad \text{((3.52), repeated)}$$

Column properties and the ratio of V_{mes}/V_{cal} for the respective specimens are listed in Appendix A7 and on the "Seismic shear failure" worksheet on the added CD.

Figure 4-38 shows that the method as described by Priestley (Priestley 1994) considerably overestimated the shear capacity of the examined columns. The evidently large scatter was considered acceptable for this mode of failure. However, a mean value of $V_{mes}/V_{cal} = 0.55 \pm 1.67\%$ within a 95 percent confidence region with a negative trend towards increasing shear loads is very unconservative. The shear strength of only one column was safely predicted. The standard deviation for the considered database was 0.21, the coefficient of variation 38.12 percent.

The fact that no considerably distinct negative trends are visible in the following plots indicates that the model proposed by Priestley generally overestimated the shear capacity of cyclically loaded members. One reason can be that the "concrete" component is reduced with respect to the drift, but not the truss component. Several researchers have pointed out that under seismic loads the strength of concrete related components and the truss component degrades (Ichinose et al. 2001; Kinugasa 2001; Watanabe and Ichinose 1991).

The model proposed by Priestley showed no bias with respect to the aspect ratio for the specimens considered. The ratio of measured to calculated shear strength is plotted against the shear-span-to-depth ratio in Figure 4-39.

A slight trend can be seen with respect to the compressive strength of concrete. Figure 4-40 shows very unconservative estimates of the shear strength of high-strength concrete columns. However, in view of the small amount of available data in this range, no exact statement can be made.

The same holds true for the effect of axial load. It appears that large axial demands caused the model to overestimate greatly the shear strength (Figure 4-41). This could be due to the direct relation between axial load and shear capacity by equation (3.50). Nevertheless, only limited data was available in the load range of 70 percent of the axial strength, and no data was available between load levels of approximately 35 % and 70 %. Therefore, the trend could also be the result of single test specimens.

A slight negative trend with respect to drift is apparent in Figure 4-42. The ratio of measured to calculated shear strength is plotted against displacement ductility instead of drift ratio, because the "concrete component" in Priestley's model is reduced with respect to displacement ductility. As can be concluded from the evenly spread out range of ductilities considered, a negative trend is apparent for increasing ductility demand.

From this evaluation, it can be concluded that the approach proposed by Priestley did not only overestimate seismic shear strength of RC columns because it neglects strength degradation of the truss component, but the model also underestimated other effects. The direct relation of axial load to shear strength led to increasingly large overestimations of the shear strength with increasing axial load. The capacity of high-strength columns appeared to be overestimated by equation (3.47).

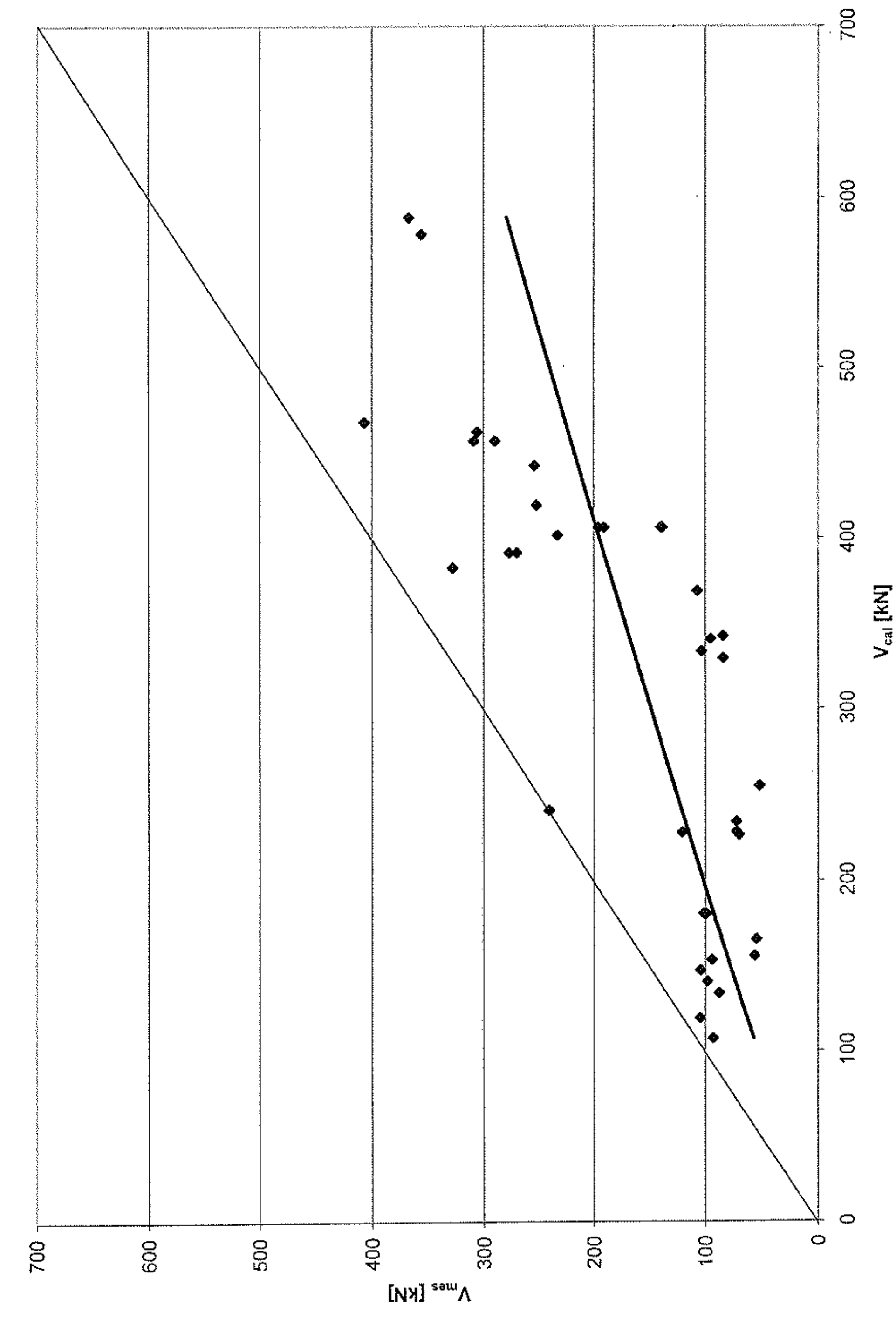

Figure 4-38 Measured to calculated shear strength of RC columns under cyclic lateral load following Priestley's approach

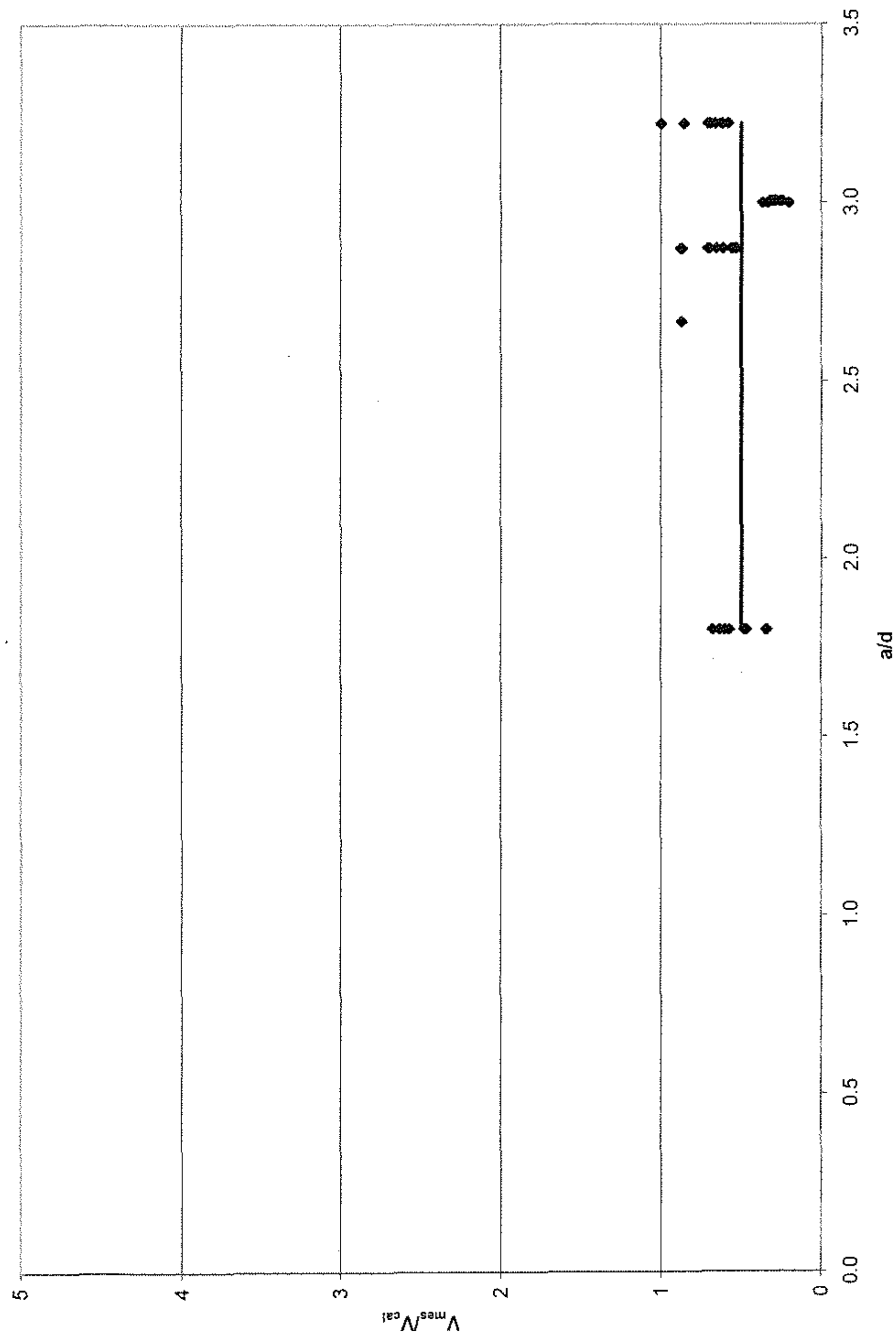

Figure 4-39 Ratio of measured to calculated shear strength versus aspect ratio for RC columns under cyclic load following Priestley's approach

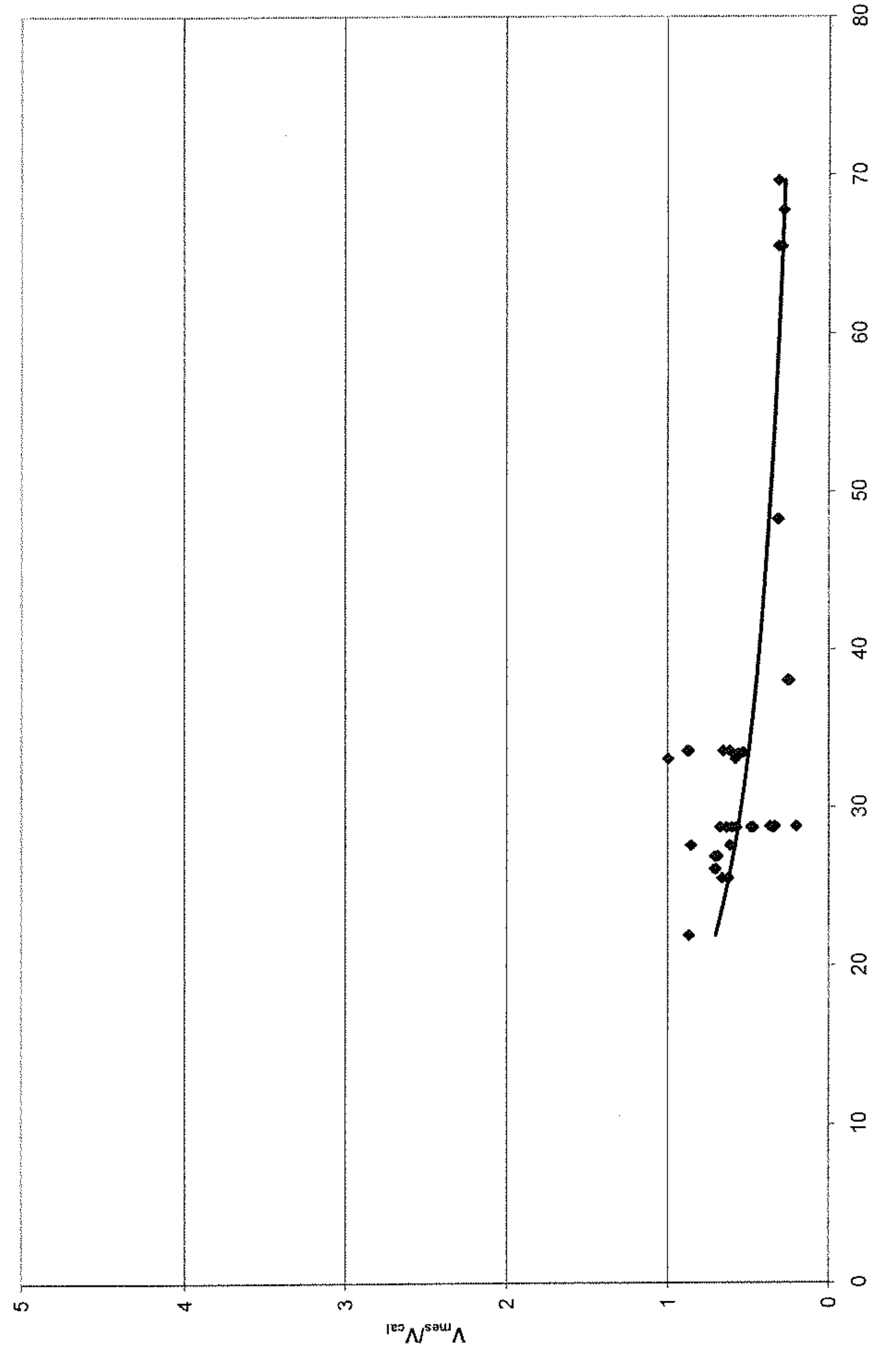

Figure 4-40 Ratio of measured to calculated shear strength versus concrete strength for RC columns under cyclic load following Priestley's approach

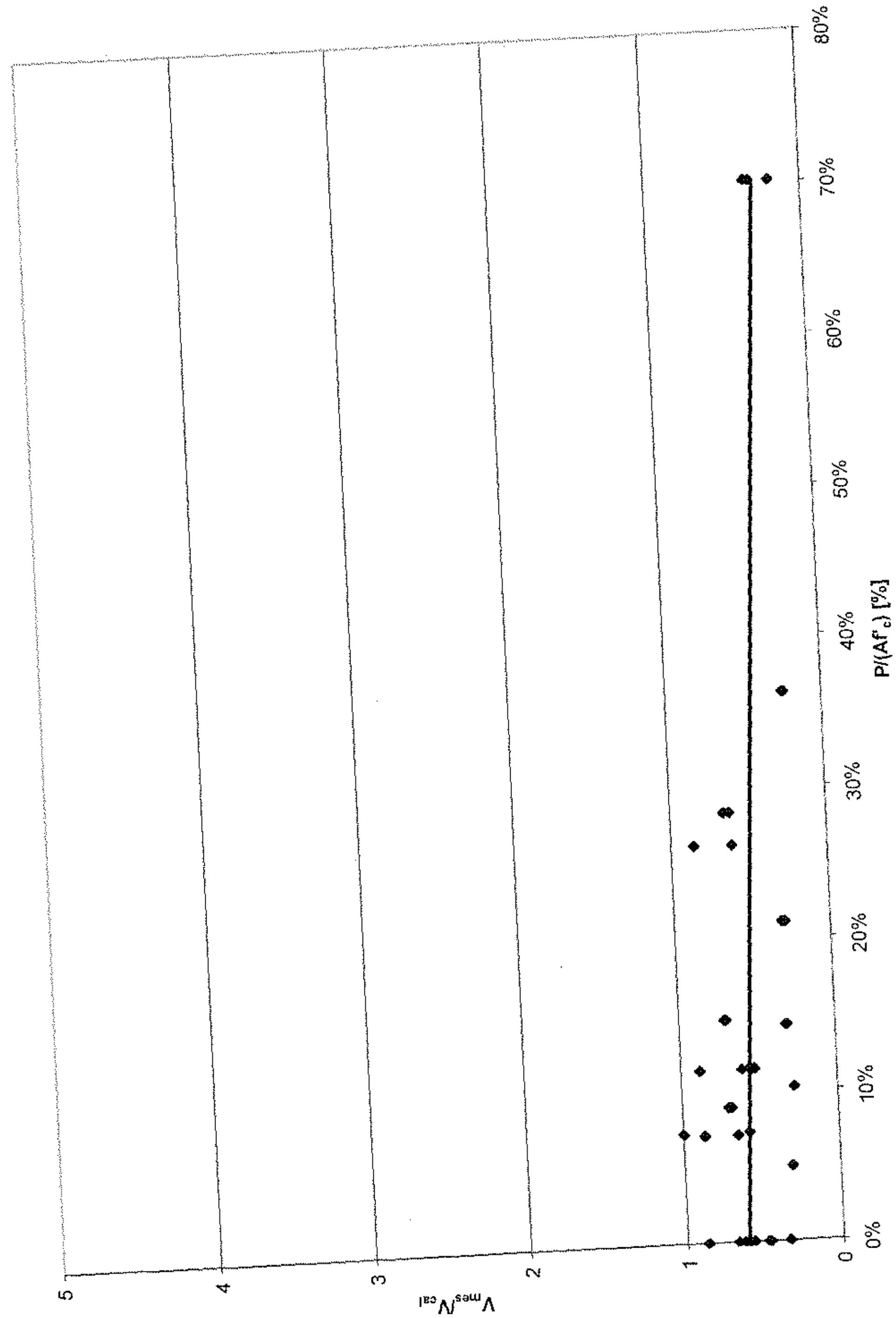

Figure 4-41 Ratio of measured to calculated shear strength versus axial load level of RC columns under cyclic load following Priestley's approach

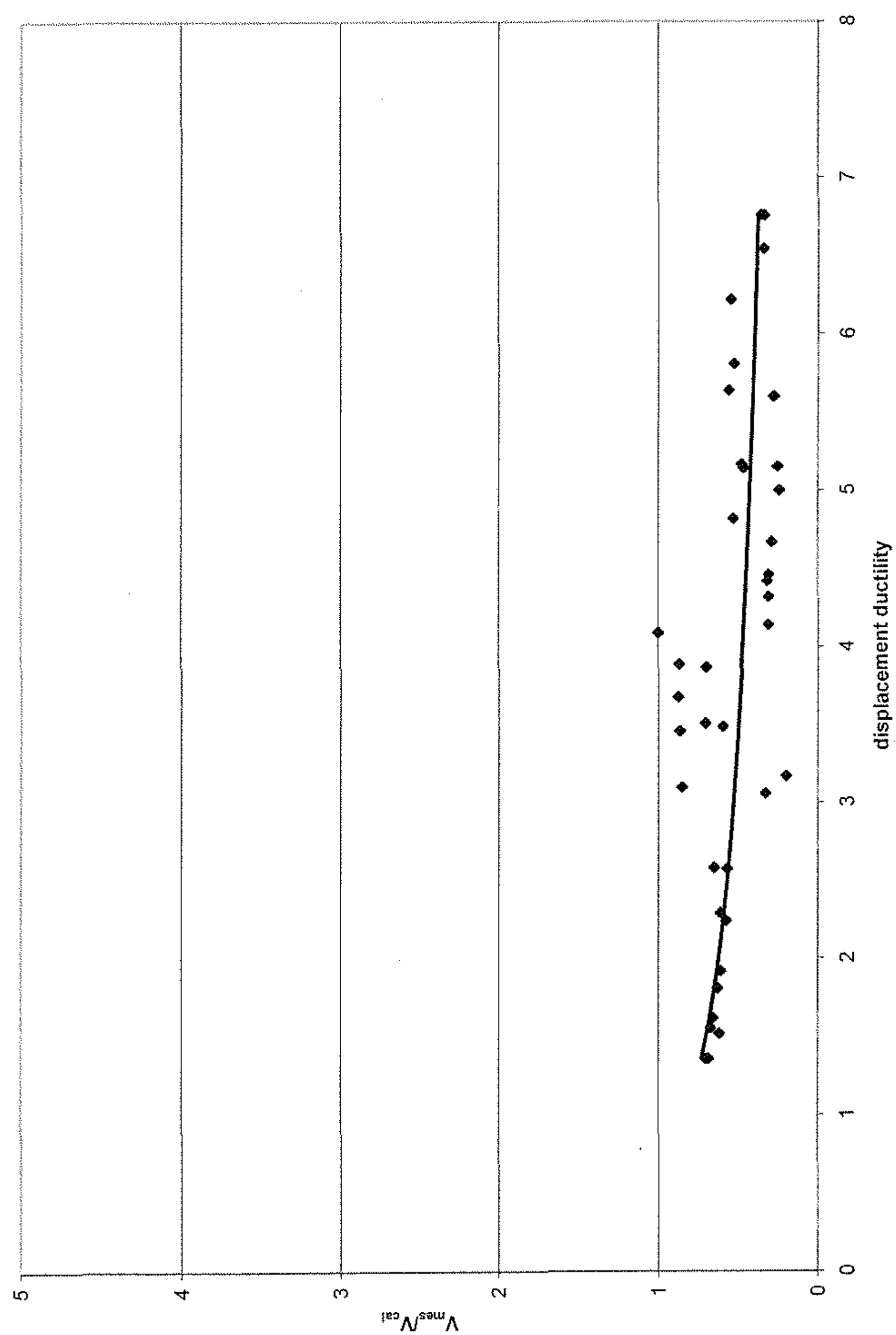

Figure 4-42 Ratio of measured to calculated shear strength versus displacement ductility for RC columns under cyclic load following Priestley's approach

5 Proposed model for the load-carrying mechanism

5.1 Problem statement

To describe the load-carrying mechanism of an RC member under combined axial and cyclic shear load, a model has to be found that represents the different load-carrying components within the member, and which can be easily adjusted to the given design case. Moreover, the concept has to be cohesive, i.e. it has to fulfill requirements set by equilibrium of forces and by compatibility, and the model has to be physically explicable. As a design aid, the model to be developed has to be simple to apply.

An RC member subjected to axial and cyclic lateral load will develop a crack pattern similar to the one shown in Figure 5-1.

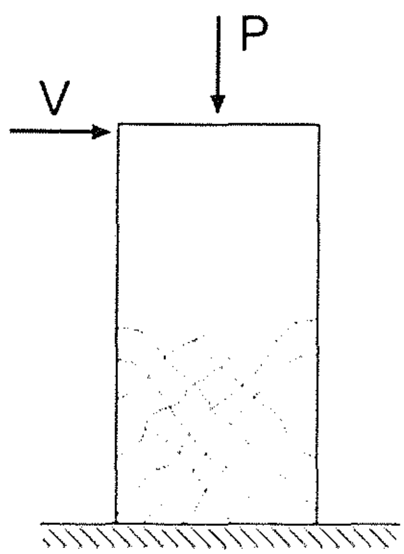

Figure 5-1 Column under axial and lateral load

Resulting from the applied shear load, inclined cracks develop along the member axis, directing from the side of loading towards the opposite corner at the supports. These cracks will as well develop on the opposite side of the member after the shear load is reversed, forming an X-shaped crack pattern in the plane of the lateral load. In general, the member can either fail by a combination of axial load and bending moment (flexural failure), or by shear failure along the described inclined cracks. The latter is of concern in the work at hand. Because of its brittle and sudden nature, a general design objective is to avoid shear failure by keeping the shear resistance of the structural element higher than the flexural resistance. This is one of the aspects of the capacity-design approach as extensively described by Paulay and Bachmann (Bachmann 1995, 2000; Paulay 1990).

To develop a model for the shear resisting mechanisms in an RC member under axial and reversed shear load, the influence of effects from crack geometry, axial load, shear span-to-depth ratio, member depth, and from possible web reinforcement has to be taken into account. One way to illustrate the structural behavior is a representation of the load-carrying mechanism by a combination of arch and truss mechanisms, which was also developed by Watanabe and Aoyama for beams under combined bending and shear load (Aoyama; Watanabe and Ichinose 1991). Using a combination of arch- and truss model ensures the applicability of the model for various member geometries from stocky members with aspect ratios smaller than 2.5 to slender members with $a/d \geq 2.5$.

It is reasonable to distinguish the two load-carrying mechanisms of arch and truss action, since it allows for a wide range of applications. For example, as described in a report by F. Watanabe and T. Kabeyasawa (Watanabe and Kabeyasawa 1998), tests at Tokyo Metropolitan University showed that a relatively small concrete core area within beams reduced the effectiveness of the truss action. It follows that a distinction between the two models and "shifting" the demand on the truss to the capacity of the arch will be able to describe the member behavior more accurately. In the same report, it is stated that as the effective capacity of the transverse reinforcement was increased, the overall shear strength was increased, independent of the amount of axial load (Watanabe and Kabeyasawa 1998). An increase of the amount of axial load had a positive effect on the shear capacity up to load levels of $P = 0.6\ A_c f'_c$.

As tests on slender RC members at the University of Kansas have shown, some shear cracks developed first within the confined area of the column, before propagating towards the exterior surfaces, or before merging with flexural cracks. The crack pattern made clearly visible that an inclined compression field was established between the tensile reinforcement up to the compression zone. As the size of the compression zone was decreasing in the progression of the test, the cracks developed further into the compression side of the member. The cracks developed on the tension side of the column were inclined first and joined flexural cracks normal to the column surfaces. Strut action was not apparent after initial cracking, as expected for these relatively slender members with aspect ratios of $a/d = 3.85$ and 2.5.

In the following, the nominal shear capacity V_n will be described as a superposition of arch-action, truss-action, and a "concrete component" that represents the shear capacity of the uncracked compression zone of the member and friction in the cracked tension zone. In the following, the load-carrying mechanism between two cracked surfaces will be referred to as "friction", instead of the widely used term "aggregate interlock", since this mechanism is as well apparent in higher strength concretes, in which due to the fracture of aggregate particles "aggregate interlock" would be misleading. In general, the nominal shear capacity is expressed as

$$\begin{aligned} V_n &= V_a + V_t + V_c \\ V_n &= V_a + V_t + \left(V_{cz} + V_f\right) \end{aligned} \tag{5.1}$$

A subdivision of the total nominal shear strength into superimposed components allows using various combinations of the components in their respective areas of application. Because of their similar range of application, in the following, the sum of truss-action and concrete component will be called the "truss model".

While the subsequent Sections 5.2 and 5.3 describe the respective load-carrying mechanisms without interaction, Chapter 7 focuses on the calibration of the proposed model and on the combination of the different mechanisms for several member configurations. Several functions that account for the transition between the mechanisms described in Sections 5.2 and 5.3 are described in Chapter 7. It is important to distinguish between the combinations and their respective range of applicability, and the sole load-carrying mechanisms. A summary of the shear-resisting components considered in the proposed model is provided in Section 5.3.

5.2 Proposed combined arch and truss model

5.2.1 Arch-action

A non-reinforced concrete panel under lateral load is able to carry the applied shear force towards the support by a single compression strut C_s as depicted in Figure 5-2. This is the most direct and lowest energy load path. The longitudinal reinforcement along the member axis carries the axial tensile component T_s of the force in the diagonal strut. The strut is inclined at an angle θ. The tensile capacity of the tie (that is, the longitudinal reinforcement), the effective compression strength of the concrete, and the geometry of the member define the maximum force in the strut.

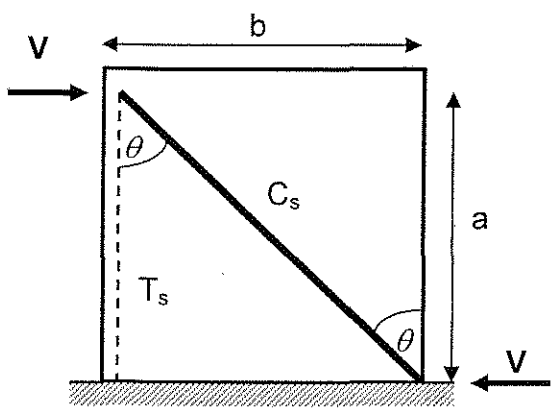

Figure 5-2 Panel with inclined strut

As the angle θ decreases with increasing slenderness of the member, tension in the reinforcement and compression in the strut increases. For a changing amount of shear force and a given tensile capacity of the longitudinal reinforcement, the respective inclination of the strut would need to be changed by varying the width, b, of the member to equilibrate the vertical forces. For example, for an increased lateral force,

V, and a given tensile capacity of the reinforcement, the angle θ needs to be increased to withstand the higher load by lowering the demand on the tensile reinforcement. On the other hand, the maximum load in the strut is limited by its compressive capacity. Thus, the capacity of the arch mechanism is limited by the tensile capacity of the longitudinal reinforcement, and by the compressive capacity of the strut.

In slender members, another possibility to maintain strut action is to cut the part of the strut that extends to the outside of the member, and to move it to the inside of the member, while tying it to the original strut with tension chords as shown in Figure 5-3 a). This was earlier described by Specht (Specht 1986, 1987). As the slenderness of the column increases, an increasing number of strut sections needs to be relocated and tied back to their origin, eventually forming a strut-and-tie truss as depicted in Figure 5-3 b). A strut-and-tie truss model is described in Chapter 5.2.2.

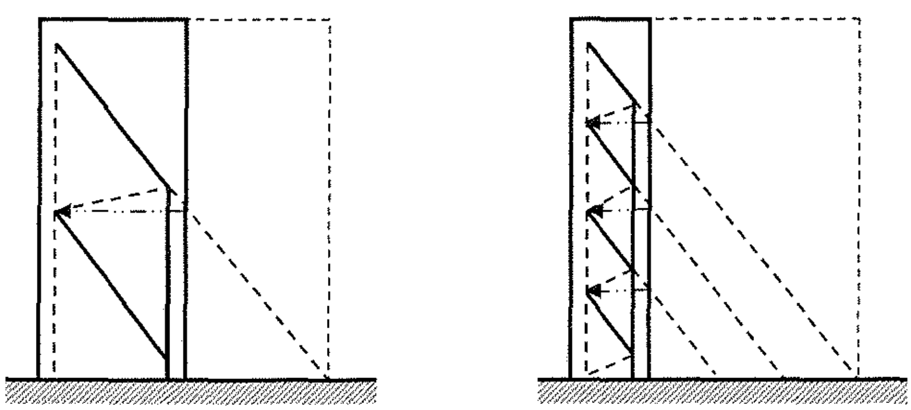

a) cut strut   b) strut-and-tie

Figure 5-3 Transformation from strut model to strut-and-tie model

By definition, a strut can only develop along uncracked areas within the cross section. Therefore, the strut cannot cross cracks, and because the cracks are inclined and can propagate from the column base, the strut has to be formed at an angle equal to or larger than the crack inclination. Commonly, the inclination of shear cracks in a slender laterally loaded RC member without axial load is taken as $\theta = 30° \pm 4°$ (ASCE-ACI Committee 445 1998; Specht 1986), with the smallest crack inclination being approximately 26°. This is consistent with the limiting value of the arch angle in Watanabe's model of $\cot\theta \leq 2$ (Aoyama; Watanabe and Ichinose 1991), which is based on an assumption for the crack width reduction by Thürlimann (Thürlimann 1979). Following this discussion, it is safe to assume that the strut-inclination has to be larger than the angle of the cracks at failure to maintain its compressive capacity. Using the smallest angle within the range of 30° ± 4° results in a lower limit of the strut inclination of

$$\theta \geq 26° \tag{5.2}$$

It can be argued that the angle of the crack inclination is the same as the angle of the axis of principal stresses, which is the basic assumption used in the compression field theory (Collins et al. 1996). However, as reported by ASCE-ACI Committee 445 (ASCE-ACI Committee 445 1998), researchers found that due to tensile stresses normal to the compression struts, or due to shear stresses transferred by friction along the inclined cracks, the angle of the principal compression stress is smaller than the crack inclination (ASCE-ACI Committee 445 1998). Consequently, for the model to be developed, it appears to be more appropriate to use the empirically established limit of $\theta = 30° \pm 4°$.

Further limits are set by the geometry of the member, because the strut certainly has to be located within the member itself if it is not tied back by stirrups, as described before. Since the compression force in the strut is anchored along the tensile reinforcement, it follows that the angle is limited by the effective depth d and the shear-span to:

$$\cot\theta \leq \frac{a}{d} \tag{5.3}$$

It should be noted, though, that arch-action is also possible in RC members with $a/d > 2$. The arch component gradually decreases with increasing slenderness. The ultimate state for small aspect ratios is a direct strut under axial compression with a negligible lateral component. However, it is not advisable to use arch-action as a sole load-carrying mechanism for these members. Additional components as described in the following chapters provide additional strength.

Within the limits defined by equations (5.2) and (5.3), the inclination of the strut can be calculated as follows. Referring to Figure 5-4, the strut inclination θ is given by the connection of the loading point of the lateral force V and its resisting counterpart at the support. This connection forms the centerline of the strut. The width of the strut does not necessarily need to be equal along its length. It is more likely that the strut has a tapered or a "bottle" shape (Schlaich et al. 1987). However, for a given concrete strength and a given applied load V, the capacity of the strut will be limited to the stress at its smallest cross-section. The smallest cross-section of the strut is located at the point of loading or the support.

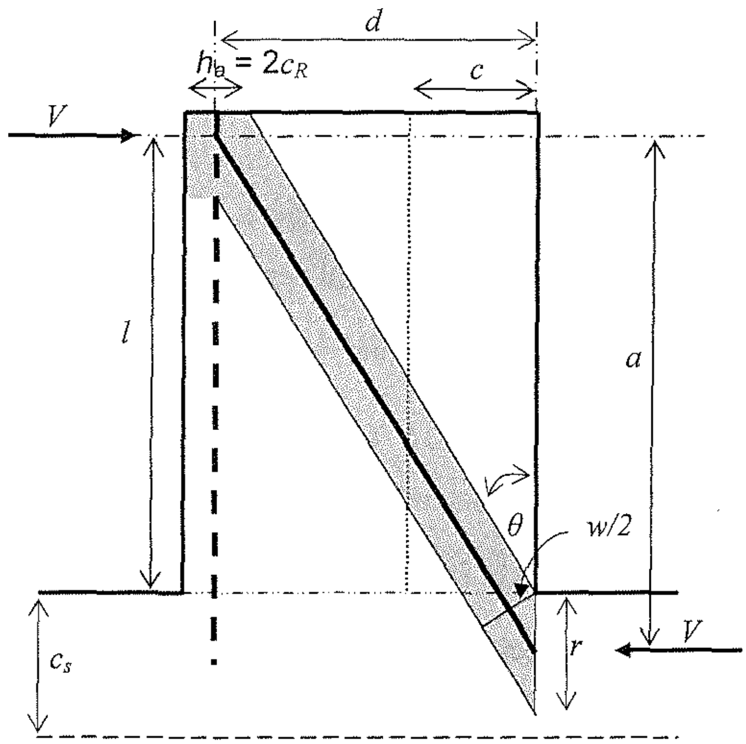

Figure 5-4 Definition of strut inclination

Taking l as the distance from the column base to the loading point and $r/2$ as the distance from the column base to the resisting force in the support, θ can be expressed as

$$\cot\theta = \frac{l + r/2}{d} \tag{5.4}$$

with d = effective depth of the member

r = maximum depth of the strut along the column axis, limited by the effective compressive bearing strength of the concrete at the nodes, $\beta_n f'_c$:

$$r = \frac{V}{\beta_n f'_c b} \tag{5.5}$$

with b = member width

β_n = strength reduction factor

5.2.1.1 Strength reduction factor for monotonic load

The strength reduction factor for the nodal zones, β_n, depends on the support conditions for the member. A common situation is that the member to be designed is located in an RC structural frame and thus is supported by beams on both sides of the members. For the node, this means the strut is supported by one tension zone and two zones under compression as shown in Figure 5-5. The tension zone will be formed by the tensile reinforcement in the beam. A similar situation will occur at the loading point in a cantilevering member supported by a foundation. In Figure 5-4, this is the node on top of the member. For a wall, the governing node, and therefore strut width, is the loading point, since, due to its relative size, the influence of the compression zone depth becomes insignificant to determine the highest amount of stresses.

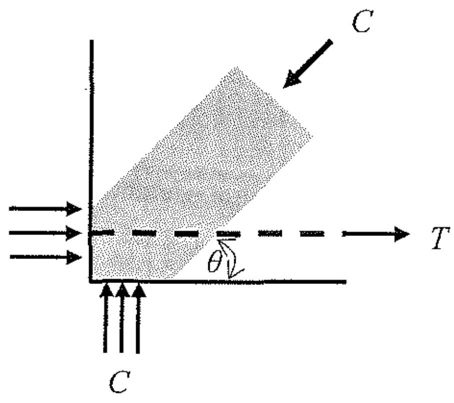

Figure 5-5 CCT Node

According to the ACI Building Code 2002 (ACI-318 2002), the compressive strength of the concrete at CCT nodes is reduced by a factor of $\beta_n = 0.68$. This value agrees with the effective stress level introduced by Schlaich et al. for tensile strains and/or reinforcement at one nodal zone (Schlaich et al. 1987). Based on the state of stresses at the nodes in strut-and-tie models, Schlaich et al. proposed effective strength factors that are depending on the concrete compressive design strength. Those factors are considering the stress distribution, i.e. they reduce the concrete compression design strength, due to tensile stresses at the nodes. The factor of $0.8 f_{cd}^{*} = 0.8 \cdot 0.85 f'_c = 0.68 f'_c$ is applied "if tensile strains in the cross direction or transverse tensile reinforcement may cause cracking parallel to the strut with normal crack width; this applies also to node regions where tension steel bars are anchored or crossing"(Schlaich et al. 1987).

More effective stress levels in concrete struts are listed by the ASCE-ACI Committee 445 on Shear and Torsion (ASCE-ACI Committee 445 1998) in Table 5-1.

In the work at hand, the reduction factor for the effective compressive strength of concrete, β_n, is taken as a function of the compressive strength f'_c. The calibration of the model in Chapter 7 showed that using this function yielded better results for high strength concrete than merely limiting the strength to 68% of the cylinder strength.

The effective concrete strength within the arch is reduced by a coefficient β_n taken as

$$\beta_n = 0.85 - 0.004 f'_c \geq 0.5 \tag{5.6}$$

It should be noted that the reduction factor β_n according to (5.6) is different from the reduction factor for the reduced effective concrete strength in the struts of a truss. The factor β_n accounts for the "bottle-shaped" stress pattern starting at the nodes of the strut, and flexural and shear cracking or tensile deformation in the orthogonal direction of the strut (Kabeyasawa and Hiraishi 1998). However, the compression strength of the struts in the truss is reduced to account for tensile stresses along the cracks and the effects of friction under cyclic loading.

Effective stress level	Concrete struts	Reference
$0.8f'_c$	Undisturbed and uniaxial state of compressive stress that may exist for prismatic struts	(Schlaich et al. 1987)
$0.68f'_c$	Tensile strains and/or reinforcement perpendicular to the axis of the strut may cause cracking parallel to the strut with normal crack width	(Schlaich et al. 1987)
$0.51f'_c$	Tensile strains causing skew cracks and/or reinforcement at skew angles to the strut's axis	(Schlaich et al. 1987)
$0.34f'_c$	For skew cracks with extraordinary crack width. Skew cracks would be expected if modeling of the struts departed significantly from the theory of elasticity's flow of internal forces	(Schlaich et al. 1987)
$0.85f'_c$	Moderately confined diagonal struts going directly from point load to support with shear span to depth ratio less than 2.0	(Alshegeir and Ramirez 1990)
$0.75f'_c$	Struts forming arch mechanism	(Alshegeir and Ramirez 1990)
$0.50f'_c$	Arch members in prestressed beams and fan compression members	(Alshegeir and Ramirez 1990)
$0.95f'_c$	Undisturbed and highly stressed compression struts	(Alshegeir and Ramirez 1990)
$v_2 f'_c$	Uncracked uniaxially stressed struts or fields	(MacGregor 1997)
$v_2(0.80)f'_c$	Struts cracked longitudinally in bulging compression fields with transverse reinforcement	(MacGregor 1997)
$v_2(0.65)f'_c$	Struts cracked longitudinally in bulging compression fields without transverse reinforcement	(MacGregor 1997)
$v_2(0.60)f'_c$	Struts in cracked zone with transverse tensions from transverse reinforcement	(MacGregor 1997)
$v_2(0.30)f'_c$	Severely cracked webs of slender beams with $\theta = 30°$	(MacGregor 1997)
$v_2(0.55)f'_c$	Severely cracked webs of slender beams with $\theta = 45°$	(MacGregor 1997)
Note: $v_2 = 0.5 + 1.25/f'_c$ in MPa after Bergmeister (Bergmeister et al. 1991)		

Table 5-1 Effective stress levels in concrete struts (ASCE-ACI Committee 445 1998)

5.2.1.2 Geometry of the strut

Equation (5.4) equals eq. (5.3), with the shear span, a, being equal to the distance between the loading points

$$a = l + r/2 \tag{5.7}$$

Looking at the supported side of the member, equation (5.4) holds true as long as the length r lies within the compression zone c_s of the supporting member.

$$r \leq c_s \tag{5.8}$$

This condition results from the fact that the strut has to be located within uncracked sections. If r is larger than c_s, it is appropriate to assume that the reaction force V acts at a distance $c_s/2$. This assumption decreases the width of the strut, decreasing the allowable force within the strut. Therefore, this is a safe assumption.

If condition (5.4) holds true, the width of the strut, w, is given by:

$$w = r \cdot \sin\theta \tag{5.9}$$

Following the requirement that the strut is located within sections of the member under compression, the strut width is also limited to the projection of w on the depth of the compression zone, c, of the member. Consequently, the following requirement has to be met:

$$r \leq \frac{c}{\tan\theta} \tag{5.10}$$

If $r > \dfrac{c}{\tan\theta}$, equation (5.4) becomes

$$\cot\theta = \frac{l}{d - c/2} \tag{5.11}$$

Equation (5.11) implies that the resulting force within the strut acts in the center of the strut. The width of the strut is then defined by the projection of *c/2* on an axis normal to the strut as

$$w = c \cdot \cos\theta \tag{5.12}$$

The previous conditions assume that the width of the strut at the support is smaller than the width of the strut at the loading point. This is not necessarily true. Given the situation, a column is fixed at both ends as in a building frame, the afore-mentioned conditions hold true also for the opposite end of the column. Depending on the smallest compression zone depth in the supports, the governing condition from equations (5.4), (5.11) is used.

Additionally, the width of the strut can be limited by the effective development depth of the longitudinal reinforcement, $2c_R$, and the size of the loading plate, l_b (Figure 5-6). It is assumed that the longitudinal tie distributes the stress from the strut onto a horizontal projection of twice the cover of the reinforcement. Following this, the width of the strut is also limited by

$$w = h_a \cdot \cos\theta + l_b \cdot \sin\theta \tag{5.13}$$

where $h_a = 2c_R$ = embedment depth of tensile reinforcement

l_b = length of the loading plate in the plane of the truss

It is noteworthy that the latter case is the most common for deep beams. Using the depth of a support is not sensible, as is the use of the compression zone depth. In very stocky members, especially those in which the arch comes close to a uniaxially loaded member, it is not practical to assume a distinct compression zone depth, since the whole member is under compression. Thus, Eq. (5.13) represents the governing case for deep members.

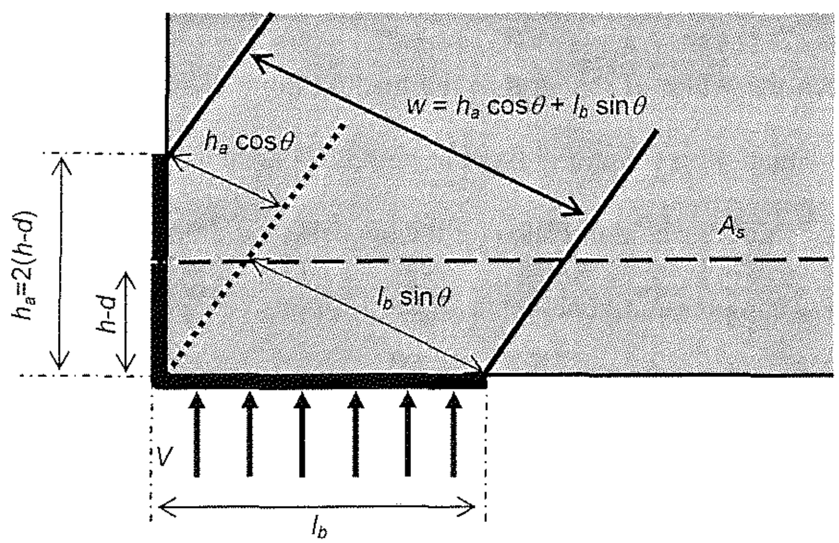

Figure 5-6 Definition of strut width in a deep beam

In summary, the width of the strut is given as the smallest value found from eqs. (5.9), (5.12), or (5.13). This will ensure the smallest possible width of the strut, and is therefore a safe assumption. Depending on the condition of equation (5.10), the strut inclination is given by eqs. (5.4) or (5.11). A sensible simplification is to define the strut inclination by the aspect ratio of the member:

$$\cot\theta = \frac{a}{d} \tag{5.14}$$

5.2.1.3 Influence of aspect ratio

The data analysis and calibration of the proposed model in Chapter 7 revealed a dependency of arch- and truss-action on the aspect ratio a/d. To account for this dependency and to use a function of the aspect ratio for a "smooth" transition between stocky and slender members, a coefficient k_s is introduced. The factor k_s reduces the contribution of the arch with an increasing shear-span-to-depth ratio a/d. The numerical form varies for members with and without transverse reinforcement, as described in the respective chapters dealing with the calibration of the proposed model. The general form for k_s is:

$$k_s = \frac{x}{y + z\left(a/d\right)^w} \tag{5.15}$$

with $k_s = 1.0$ for $a/d = 0$

w, x, y, z = coefficients depending on transverse reinforcement

5.2.1.4 Capacity of the arch in unreinforced stocky members

Using the inclined component of the applied lateral force V, the maximum capacity of the arch is defined by the effective reduced compression strength of concrete and the inclination of the strut, eq. (5.16). An ultimate limit can also be set by the capacity of the longitudinal reinforcement, eq. (5.17):

$$V_a = \beta_n k_s f'_c \cdot w \cdot b \cdot \sin\theta \tag{5.16}$$

$$V_a = T \cdot \tan\theta = A_s f_y \tan\theta \tag{5.17}$$

For members with *a/d* ratios exceeding a value of approximately 2.5, tension members (ties) as described above are necessary to maintain the shear capacity of the member. This can be done by transitioning from a strut into a truss model as mentioned before. This also agrees with the findings of the ASCE-ACI Committee 445 report (ASCE-ACI Committee 445 1998). For a series of beams tested by Kani (Kani et al. 1979), strut models without transverse reinforcement were only accurate for aspect ratios of $a/d < 2.5$. Sectional models were found to be "more appropriate" for larger aspect ratios. As *a/d* increased the resistance of the strut-and-tie models without transverse reinforcement decreased rapidly.

The behavior of the compression strut in a truss mechanism is considerably different from that of concrete loaded uniaxially in compression. A fraction of the total shear is transferred through friction between the cracks, and thus the load-carrying mechanism depends on parameters defined by the conditions in the cracked part of the cross section. Additional strength will be provided by the uncracked compression zone of the member. This makes it necessary to treat the truss and "concrete component" as separate load-carrying mechanisms. The contribution of friction and uncracked compression zone is described in section 5.2.3.

5.2.2 Truss-action

Truss-action is the main load transfer mechanism in lieu of arch-action in slender members, or can provide additional shear strength in deep members. The truss is commonly assumed to consist of a diagonal compression field that is inclined parallel to the cracks, of ties formed by stirrups in the direction of the shear force, and of a force couple in direction of the longitudinal axis (Collins 1991). A general truss is shown in Figure 5-7, in which C_t is the longitudinal resulting force in the compression zone, T_t is the longitudinal tension force in the reinforcement. f_t is the inclined compression stress resulting from the forces in the truss, and f_{ws} is the tensile stress in the web reinforcement. These four components and their respective capacities define the truss-action.

The shear resistance through truss-action can be expressed in a single term, V_t, which considers the diagonal compressive stresses f_t, and the capacity of the web-reinforcement. The longitudinal forces C_t and T_t have a more capacity-limiting character on the direct shear resistance V_t. Subsequently, the shear capacity of the truss-action will be developed as a function of the stresses in the compression struts and in the web reinforcement. The following developed relationships agree with the variable-angle truss model as described by Collins and Mitchell (Collins 1991).

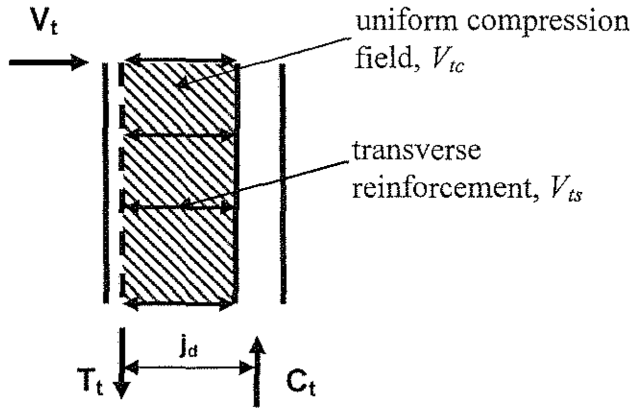

Figure 5-7 General truss

5.2.2.1 Direct load-carrying mechanism V_t

The shear force carried by the truss component is limited by the tensile capacity of the transverse steel, its distribution along the member axis, and by the compressive strength of the concrete in the web. Equilibrium conditions for the truss model at a zero-moment location are shown in Figure 5-8.

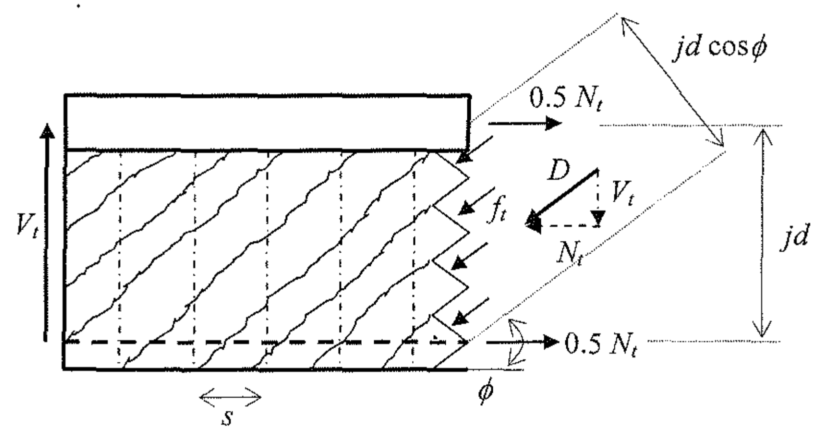

Figure 5-8 Equilibrium conditions within the truss

From the free-body diagram in Figure 5-8, the resulting diagonal force in the web is

$$D = \frac{V_t}{\sin\phi} \tag{5.18}$$

The diagonal force D has to be equal to the diagonal component of the compression stress in the inclined compression field, f_t:

$$D = f_t \cdot b \cdot jd \cdot \cos\phi \tag{5.19}$$

with b = member width

jd = distance between C_t and T_t

ϕ = inclination of the truss

Substituting eq. (5.18) into (5.19) and solving for the compression stress f_t yields

$$\begin{aligned} f_t &= \frac{V_t}{\sin\phi \cdot b \cdot jd \cos\phi} \\ \Leftrightarrow f_t &= \frac{V_t}{b \cdot jd}\left(\tan\phi + \cot\phi\right) \end{aligned} \tag{5.20}$$

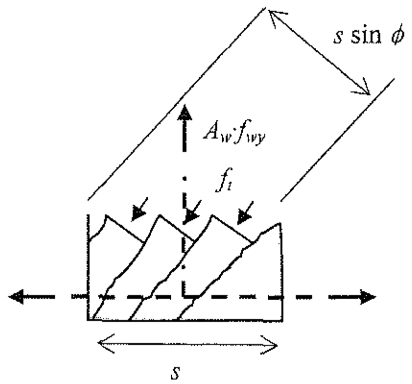

Figure 5-9 Element between stirrups

Figure 5-9 shows the equilibrium conditions in a section of Figure 5-8 enclosing the influence area of one stirrup in the tensile region of the member. Taking equilibrium of forces from the free-body diagram in Figure 5-9, the diagonal compressive force, $f_t \cdot b \cdot s \cdot \sin\phi$, has to be counteracted by the tensile force in the stirrup, its maximum equal to $A_w{\cdot}f_{wy}$. Multiplying the diagonal compression force by sin ϕ yields

$$A_w f_{wy} = f_t \cdot b \cdot s \cdot \sin^2\phi \tag{5.21}$$

with f_{wy} = tensile strength of transverse reinforcement

s = spacing between stirrups

Substituting equation (5.20) into (5.21) results in the shear capacity of the truss as

$$\begin{aligned} A_w f_{wy} &= \frac{V_t \cdot s \cdot \sin\phi}{jd\cos\phi} \\ \Leftrightarrow V_t &= \frac{A_w f_{wy} jd}{s}\cot\phi \end{aligned} \tag{5.22}$$

Equation can also be expressed in terms of the transverse reinforcement ratio, $\rho_w = A_w / b \cdot s$:

$$V_t = \rho_w f_{wy} b \cdot jd \cdot \cot\phi \tag{5.23}$$

In case the transverse reinforcement is inclined at an angle α, eq. (5.22) becomes:

$$V_t = \frac{A_w f_{wy} jd}{s}(\cot\phi + \cot\alpha)\sin\alpha \tag{5.24}$$

In order to express the inclined compression stress in the web in terms of the force in the transverse reinforcement and of the strut inclination, equation (5.22) is substituted into equation (5.20):

$$\begin{aligned} f_t &= \frac{A_w f_{wy}}{s \cdot b \cdot \sin^2\phi} \\ \Leftrightarrow f_t &= \frac{\rho_w f_{wy}}{\sin^2\phi} \end{aligned} \tag{5.25}$$

Equation (5.25) is also obtained by taking the axial projection of the force in the stirrups, $A_w f_{wy} / \sin\phi$, and distributing this force over an area $b \cdot s \cdot \sin\phi$:

$$\begin{aligned} f_t &= \frac{A_w f_{wy}}{\sin\phi}\frac{1}{b \cdot s \cdot \sin\phi} \\ \Leftrightarrow f_t &= \frac{A_w f_{wy}}{s \cdot b \cdot \sin^2\phi} \end{aligned} \tag{5.26}$$

This expression indicates the compression stress in the web as a function of the truss inclination and the stress in the transverse reinforcement.

In addition to the tensile stresses induced by the compression field, stresses are generated in the transverse reinforcement due to lateral expansion of the concrete in the core under axial compression. Pujol indicated that several researchers found that the confinement demand on the stirrups increases with an increasing ductility demand. Furthermore, Pujol found that the function of the confining reinforcement is not only to resist shear forces, but rather to resist a complex state of stresses formed by axial and shear forces (Pujol 2000; Wight and Sözen 1973). Consequently, for high axial loads and high ductility demand, the shear resisting capacity of the web reinforcement will need to be reduced.

5.2.2.2 Axial components of the inclined compression force *D*

From equilibrium in Figure 5-8, the projection of the shear force V_t on the tensile reinforcement in axial direction results in

$$N_t = V_t \cot \phi \tag{5.27}$$

In agreement with the variable angle truss model (Collins 1991), this force is counteracted by forces equal to $0.5N_t$ in the tensile and in the compression cord.

$$0.5N_t = 0.5V_t \cot \phi \tag{5.28}$$

In terms of the diagonal compression force, D, in the web, N_t is described as

$$N_t = D \cdot \cos \phi \tag{5.29}$$

In addition to reacting to the axial force induced by shear, the longitudinal reinforcement carries the moment M applied by the exterior shear force, V. The effect of shear load on the capacity of the longitudinal reinforcement was also mentioned in the ASCE-ACI Committee 445 report on shear and torsion (ASCE-ACI Committee 445 1998). In this report, it is stated that the shear load has to be considered in the design of the tensile reinforcement. Therefore, the normal forces resulting from arch- and truss mechanisms have to be considered in the design of the longitudinal reinforcement. It follows for cases in which linear bending theory is applied that

$$A_s f_y \geq \frac{M}{jd} + 0.5V_t \cot\phi + V_a \cot\theta \tag{5.30}$$

In eq. (5.30), M is the flexural moment, $V_a \cot\theta$ represents the demand on the tensile reinforcement from arch-action. The term $0.5V_t \cot\phi$ is the demand on the tensile reinforcement according to eq. (5.28).

5.2.2.3 Shortcomings of the truss-component

The truss-model as previously described is not able to model the influence of axial load or member depth on shear strength. Axial load generally will increase the shear capacity. Increasing the effective depth also enhances the shear strength of an RC member. Additionally, the shear capacity of members without transverse reinforcement cannot be calculated. A "concrete component" superimposed on the truss component can compensate for these shortcomings.

5.2.3 Concrete components

RC members without transverse reinforcement are considered to have two components that contribute to the shear capacity of the member. These are contributions by the uncracked compression zone, V_{cz}, and by friction between crack surfaces in the tension zone, V_f. The shear-resisting component of friction along crack surfaces in the tensile zone of the RC member, V_f, will be expressed as a modification of the proposal suggested by K.-H. Reineck (Reineck 1990, 1991a, b), described in Chapter 3.3.

The different load-carrying mechanisms in an RC member without transverse reinforcement can be determined by examining the conditions in the cracked member. It is assumed that the uncracked compression zone contributes to the shear capacity of the member by a function related to the area of the compression zone and the tensile strength of concrete, f_{ct}, taken as

$$f_{ct} = \sqrt[3]{f'_c} \tag{5.31}$$

The cracked tension zone of the member contributes to the shear-resistance by friction between two adjacent crack surfaces. Walraven described the friction mechanism by relating the transferable stresses between the cracks to the contact areas of aggregate particles (Walraven 1981b). As the crack width increases, the contact areas become smaller, decreasing the transferable stresses. An ultimate state can be defined by establishing a critical crack width related to a critical slip between surfaces that does not allow for a sufficient stress transfer. Such a critical slip, as presented later in this section, was established by Reineck (Reineck 1990), based on earlier work by Walraven (Walraven 1980, 1981a).

The concrete contribution to shear-resistance will be derived for beams under static load. This basic case will establish the foundation for describing the influence of axial load and cyclic shear later in this thesis.

As depicted in Figure 5-10, the applied shear force V is resisted by a component for dowel-action, V_d, by a friction component V_f along the crack surfaces, and by a shear-carrying component V_{cz} in the uncracked compression zone. The evaluation of Reineck's proposal (Chapter 3.3) has shown that the effect of dowel-action is of minor importance. Focusing on the major contributions of shear-resisting mechanisms, subsequently, dowel-action will be neglected.

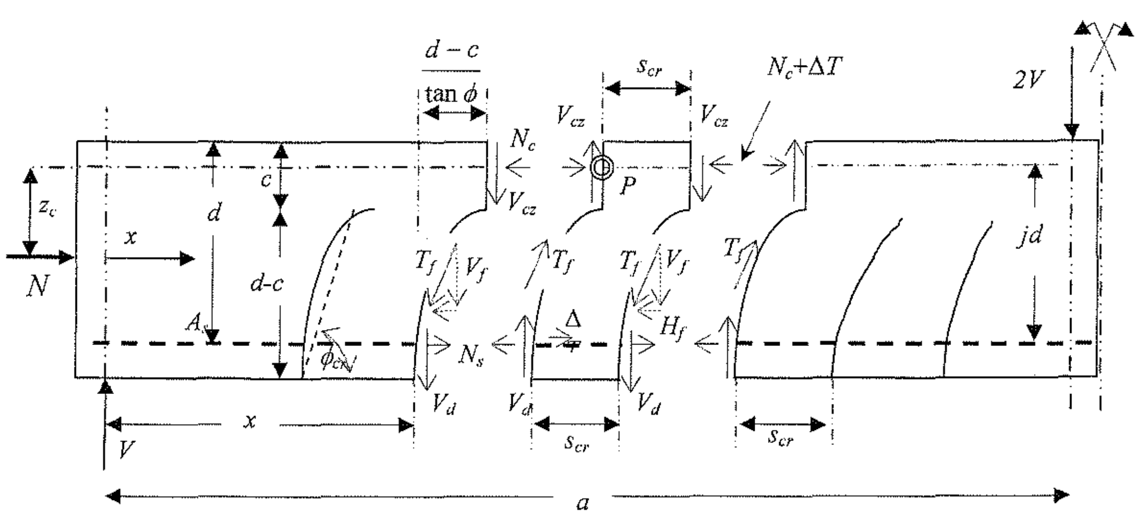

Figure 5-10 Equilibrium and designations in a RC member with tooth element in the center of the figure, adapted from (Reineck 1991b)

The change of the applied bending moment along the member axis leads to shear stresses in the member. As described by Reineck (Reineck 1991b), the shear failure of RC members is constituted when a concrete tooth formed by two cracks breaks away from the member. In order to describe the behavior between two adjacent cracks, the cracks have to be modeled and the spacing between the cracks has to be known. According to Reineck (Reineck 1990, 1991b), the distance between two adjacent cracks is given as a linear function of the depth of the tension zone as

$$s_{cr} = C(d - c) \tag{5.32}$$

The constant C in equation (5.32) is calibrated from the evaluation of the model in Chapter 7 for RC members with and without transverse reinforcement. Following an investigation in (Reineck 1990), and as stated in (Reineck 1991b), "the depth of the compression zone is only slightly influenced by the shear force". Consequently, the depth of the compression zone c is taken as the depth of the compression zone calculated from the flexural analysis of the beam, kd.

Following the procedure proposed by Reineck (Reineck 1991b), first equilibrium conditions of the member in Figure 5-10 are established. Equilibrium of vertical forces and neglecting the minor contribution of dowel-action gives

$$V = V_{cz} + V_f + V_d \approx V_{cz} + V_f \tag{5.33}$$

Taking the sum of moments around point P in the "tooth" depicted in Figure 5-10 yields:

$$
\begin{aligned}
&V_{cz} \cdot s_{cr} + V_f \cdot s_{cr} = \Delta T \cdot jd \\
&\Leftrightarrow V \cdot s_{cr} = \Delta T \cdot jd
\end{aligned}
\tag{5.34}
$$

with ΔT = change of the tensile force in the longitudinal reinforcement within the tooth element.

Equation (5.34) can be expressed in terms of a nominal shear stress, v_n, by dividing both sides of the equation through $s_{cr} jd \cdot b$. This relates the nominal shear stress to the change in force in the reinforcement.

$$
v_n = \frac{V}{jd \cdot b} = \frac{\Delta T}{s_{cr} \cdot b} \tag{5.35}
$$

5.2.3.1 Contribution of the uncracked compression zone

The contribution of the uncracked compression zone is taken as a function of the area of the compression zone and the tensile strength of concrete, f_{ct}.

It is reasonable to assume a linear distribution of axial stresses in the previously described tooth-element, since the element itself is uncracked. Therefore, the depth of the compression zone, c, is calculated from linear elastic bending theory:

$$
c = kd = \left(\sqrt{\rho_s n + 2\rho_s n} - \rho_s n\right) d \tag{5.36}
$$

where $n = \dfrac{E_s}{E_c}$

ρ_s = longitudinal reinforcement ratio

The internal lever arm, jd, between the acting points of axial tension- and compression forces is calculated as:

$$jd = d - \frac{kd}{3} \tag{5.37}$$

The contribution of the uncracked compression zone to the shear resistance of the member is taken as a function of the tensile strength of concrete and the area of the compression zone:

$$\begin{aligned} V_{cz} &= D \cdot f_{ct} \cdot b \cdot c \\ &= D \cdot \sqrt[3]{f'_c} \cdot b \cdot kd \end{aligned} \tag{5.38}$$

The coefficient D is a function of the shear-span-to-depth ratio, which will be established in the calibration of the model. V_{cz} varies with the effective section depth d, and with the longitudinal reinforcement ratio, which is influencing the depth of the compression zone, kd. A possible axial load is increasing the depth of the compression zone, therefore increasing the shear capacity related to the uncracked concrete under compression.

5.2.3.2 Contribution of the friction component

The friction component is calculated from the average shear stress along the cracked tooth. The average shear stress is related to a calculated crack width Δw and a critical crack width Δw_u defined at mid-depth of the crack. The critical crack width was considered by Reineck (Reineck 1990) at mid-depth of the crack to be able to build on the investigations by Walraven, who examined friction under a constant crack width (Walraven 1981b). The dimension of the critical crack width depends on the moment at the considered location.

According to Reineck (Reineck 1990, 1991b), following a proposal by Walraven (Walraven 1980, 1981a), the critical shear stress related to friction is assumed to be given by a linear relationship with the critical crack width Δw_u at mid-depth of the crack as:

$$\tau_{fu} = 0.45 \cdot f_{ct} \left(1 - \frac{\Delta w}{\Delta w_u} \right) \tag{5.39}$$

with f_{ct} = axial tensile strength of concrete

$\Delta w_u = 0.9$ mm

In the calibration of the model in Chapter 7, the critical shear stress will be expressed in a form

$$\tau_{fu} = const \cdot f_{ct} \left(1 - \frac{\Delta w}{\Delta w_u} \right) \tag{5.40}$$

The tensile strength of concrete, f_{ct}, is given by equation (5.31). The constant and the critical crack width Δw_u will be re-established in Chapter 7.

The friction component of the shear resisting forces in the concrete, V_f, is determined by integrating the shear stresses along the crack surfaces. As mentioned earlier, the contribution of dowel-forces from the longitudinal reinforcement was found negligible. Therefore, only the contribution of frictional stresses is considered. In agreement with the proposal by Reineck (Reineck 1990, 1991b), the part of the stresses related to friction is assumed to be constant along the cracked surface as displayed in Figure 5-11 a). Figure 5-11 b) shows the stress field within the tooth related to friction. The friction shear stresses τ_f induce an inclined compression field equilibrated by a tension field perpendicular to the compression field. It follows that the transferable shear stresses are a function of the axial tensile strength of concrete, f_{ct}. The inclination of the compression field is taken as $\phi/2$, half of the crack inclination. As pointed out by Reineck (Reineck 1991b), even though the biaxial tension-compression field is defined by the axial tensile and compression strength of concrete, it will not govern the shear failure. The shear failure is reached when the mechanical transfer of frictional stresses along the crack surfaces is lost (Reineck 1990). This is related to the crack opening and the critical slip between crack surfaces.

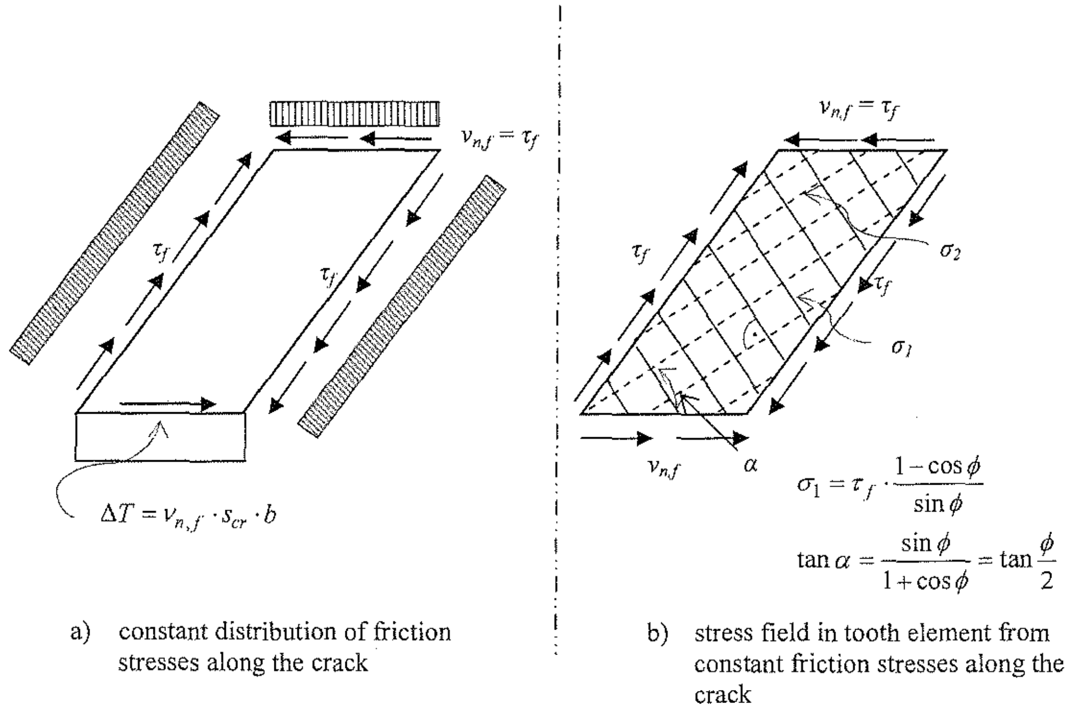

Figure 5-11 Distribution of stresses related to friction at tooth element, adapted from (Reineck 1991b)

The capacity of the friction component of the "concrete contribution" to shear resistance is given by integrating the constant frictional shear stresses τ_{fu} over the area of the cracked region of the member:

$$V_f = \tau_{fu} \cdot b \cdot (d - kd) \tag{5.41}$$

The failure criterion for the friction component is not defined by the crack opening Δw, but rather by the slip between two adjacent crack surfaces due to the rotation while the crack opens. The ultimate state of deformation is adapted from Reineck's proposal (Reineck 1990, 1991b) as

$$\Delta s_u = 0.336\Delta w + 0.01 \text{ [mm]} \tag{5.42}$$

The actual crack width related to the critical slip is determined from geometry within the crack as depicted in Figure 5-12. The critical point is defined at mid-depth of the crack.

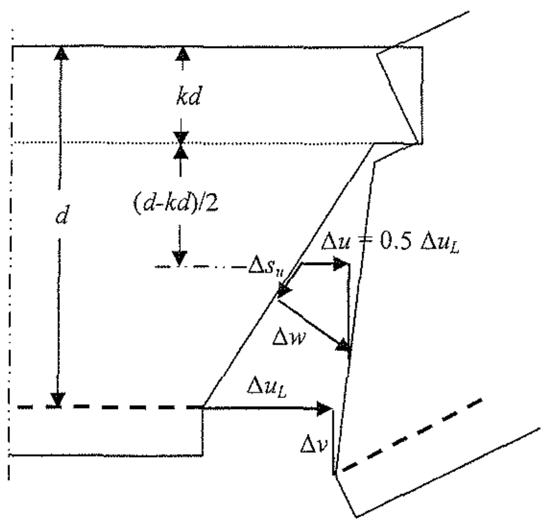

Figure 5-12 Kinematics within the crack, adapted from (Reineck 1991b)

With a given horizontal displacement Δu and the critical slip Δs_u, the corresponding crack width is calculated as

$$\Delta w = \frac{\Delta u}{\sin \phi_u} + \frac{\Delta s}{\tan \phi_u} \tag{5.43}$$

The horizontal displacement at mid-depth, Δu, is calculated from the strain in the longitudinal reinforcement, ε_s, and the crack spacing as

$$\Delta u = 0.5 \cdot \varepsilon_s \cdot s_{cr} \tag{5.44}$$

Inserting equations (5.32) and (5.36),

$$\Delta u = 0.5 \cdot \varepsilon_s \cdot C(d - kd) \tag{5.45}$$

With the critical slip according to eq. (5.42) and the horizontal displacement, the crack width is therefore given as

$$\Delta w = \frac{0.5 \cdot \varepsilon_s \cdot s_{cr}}{\sin \phi_{cr}} + \frac{0.336 \Delta w_u + 0.01}{\tan \phi_{cr}} \text{ [mm]} \tag{5.46}$$

With the strain in the longitudinal reinforcement known, it is possible to monitor the shear strength for different load stages. The ultimate failure crack width is reached for $\Delta w = \Delta w_u$. Solving equation (5.46) for Δw_u yields:

$$\Delta w_u = \frac{0.5 \cdot \varepsilon_s \cdot s_{cr}}{\sin \phi_{cr} \left(1 - 0.336 \cot \phi_{cr}\right)} + \frac{0.01 \cdot \cot \phi_{cr}}{1 - 0.336 \cdot \cot \phi_{cr}} \text{ [mm]} \tag{5.47}$$

The strain in the longitudinal reinforcement is found by taking moment equilibrium of the free-body diagram in Figure 5-10:

$$M = V\left(x + \frac{d - c}{\tan \phi}\right) - f_s A_s \cdot jd + V_f \frac{2}{3} \frac{c}{\tan \phi} - N \cdot z_c = 0$$

with $\varepsilon_s = f_s E_s$ and $c = kd$:

$$\Leftrightarrow \varepsilon_s = \frac{1}{E_s A_s jd}\left[V\left(x + \frac{d - kd}{\tan \phi}\right) + V_f \frac{2}{3} \frac{kd}{\tan \phi} - N \cdot z_c\right]$$

Substituting $V_f = V - V_{cz}$

$$\varepsilon_s = \frac{1}{E_s A_s jd} \cdot \left[V\left(x + \frac{d - kd}{\tan\phi} \right) + \left(\frac{2}{3} \frac{kd}{\tan\phi} \right) - V_{cz}\left(\frac{2}{3} \frac{kd}{\tan\phi} \right) - N \cdot z_c \right]$$

With $jd = d - \frac{kd}{3}$:

$$\Leftrightarrow \varepsilon_s = \frac{1}{E_s A_s jd} \cdot \left[V\left(x + \frac{jd}{\tan\phi} \right) - V_{cz}\left(\frac{2}{3} \frac{kd}{\tan\phi} \right) - N \cdot z_c \right]$$

Since in design it is more common to use the longitudinal reinforcement ratio instead of the amount of reinforcement, the strain becomes:

$$\varepsilon_s = \frac{1}{E_s \cdot \rho_s \cdot bd \cdot jd} \cdot \left[V\left(x + \frac{jd}{\tan\phi} \right) - V_{cz}\left(\frac{2}{3} \frac{kd}{\tan\phi} \right) - N \cdot z_c \right] \qquad (5.48)$$

with $A_s = \rho_s \cdot bd$

z_c = distance from centroid to center of the compression zone

To calculate the strain from equation (5.48) is rather cumbersome for design practice. The evaluation of the model in Chapter 7 has shown that a good agreement between tested and calculated results can also be obtained for members without axial load by calculating the strain from linear bending theory as

$$\varepsilon_s = \frac{f_s}{E_s} = \frac{M}{jd \cdot A_s E_s} = \frac{M}{\rho_s \cdot bd \cdot jd \cdot E_s} \qquad (5.49)$$

Because it is simpler, this way to determine the strain is advised and used for the calibration of the model for members without axial load. An evaluation using equation (5.48) for RC beams under static shear and axial load follows in Chapter 7.3.

According to the ACI code (ACI-318 2002), the critical section for shear design is located at a distance d from the support of a simply supported beam. To be consistent with the code, the moment used to calibrate the model is determined at this location. However, if the strain is calculated at a different location, the critical crack width Δw_u is to be taken as a different value. At the point of a higher (or of the maximum) moment, the strain in the longitudinal reinforcement is larger, opening the crack wider, but a larger critical crack width can also be expected. Values for different locations are provided in the calibration of the proposed model in Chapter 7.

In summary, and anticipating the results from Chapter 7, the shear resistance of the concrete contributions is given by

$$\begin{aligned} & V_c = V_{cz} + V_f \\ & \Leftrightarrow V_c = D \cdot f_{ct} \cdot b \cdot kd + C \cdot f_{ct} \cdot b \cdot (d - kd)\left(1 - \frac{\Delta w}{\Delta w_u}\right) \end{aligned} \tag{5.50}$$

For beams with transverse reinforcement ($V = V_t + V_{cz} + V_f$), the evaluation of a database comprising 168 slender and 66 stocky beams that failed under static shear load yielded

$$\Delta w_u = 1.0 \text{ mm}$$

$$s_{cr} = (d - kd) \text{ [mm]}$$

$$C \cdot f_{ct} = 0.4 \cdot \sqrt[3]{f'_c} \text{ [MPa]}$$

and a critical crack inclination of $\phi_{cr} = 30°$

For beams without transverse reinforcement, the concrete contribution was calibrated from a database comprised of 395 slender and 49 stocky beams that failed in shear. The corresponding coefficients were found to be

$\Delta w_u \quad = 1.0$ mm

$s_{cr} \quad = (d - kd)$ [mm]

$C \cdot f_{ct} = 0.5 \cdot \sqrt[3]{f'_c}$ [MPa]

The critical crack inclination was taken as $\phi_{cr} = 30°$.

Inserting the respective values, equation (5.50) becomes:

- For web-reinforced beams:

$$V_c = 0.4 \cdot f_{ct} \cdot b \cdot kd + 0.4 \cdot f_{ct} \cdot b \cdot (d - kd)\left(1 - \frac{\Delta w}{\Delta w_u}\right) \tag{5.51}$$

wherein

$$\Delta w_u = 1.0 \text{ mm}$$
$$\Delta w = \frac{0.5 \cdot \varepsilon_s \cdot s_{cr}}{\sin 30^\circ \left(1 - 0.336 \cot 30^\circ\right)} + \frac{0.01 \cdot \cot 30^\circ}{1 - 0.336 \cdot \cot 30^\circ} \text{ [mm]}$$
$$s_{cr} = (d - kd) \text{ [mm]}$$
$$\varepsilon_s = \frac{V \cdot d}{\rho_s \cdot bd \cdot jd \cdot E_s}$$

- For beams without web-reinforcement:

$$V_c = 0.5 \cdot f_{ct} \cdot b \cdot kd + 0.5 \cdot f_{ct} \cdot b \cdot (d - kd)\left(1 - \frac{\Delta w}{\Delta w_u}\right) \tag{5.52}$$

with

$$\Delta w_u = 1.0 \text{ mm}$$

$$\Delta w = \frac{0.5 \cdot \varepsilon_s \cdot s_{cr}}{\sin 30^\circ \left(1 - 0.336 \cot 30^\circ\right)} + \frac{0.01 \cdot \cot 30^\circ}{1 - 0.336 \cdot \cot 30^\circ} \text{ [mm]}$$

$$s_{cr} = (d - kd) \text{ [mm]}$$

$$\varepsilon_s = \frac{V \cdot d}{\rho_s \cdot bd \cdot jd \cdot E_s}$$

It should be noted that the values for the coefficients in eqs. (5.51) and (5.52) have been derived considering the contributing arch components, and therefore the respective transition factor related to the aspect ratio *a/d*. The complete derivation of all coefficients is presented in Chapter 7.

5.3 Summary of shear resisting components

In summary, the shear capacity of RC members under axial and cyclic lateral load can be described as the sum of the components for arch-action (Section 5.2.1) and truss-action. The truss-action is subdivided into the traditional truss component (Section 5.2.2), related to the transverse reinforcement, and additional "concrete" components with contributions of the uncracked compression zone and friction in the tension zone (Section 5.2.3).

$$V_n = V_a + V_t + \left(V_{cz} + V_f\right) \qquad \text{((5.1) Repeated)}$$

Each of the components of the nominal shear capacity V_n is limited to its applicability as described in the respective previous sections.

5.3.1 Arch component

Arch-action is formed by a single strut directed from the loading point towards the support. The tensile longitudinal component of the compression strut is formed by the longitudinal reinforcement. From the geometry of the member and test results on the inclination of shear cracks, it can be stated that arch-action can only develop as a single shear resisting mechanism in deep members as walls, deep beams, or columns with an aspect ratio of approximately $a/d \leq 2.5$. The inclination of the strut is calculated by equation (5.14):

$$\cot\theta = \frac{a}{d} \qquad \text{((5.14) Repeated)}$$

The effective shear-span a has to be determined by taking the geometric conditions of the support and loading-points into consideration.

The compressive strength of the strut is defined by the reduced effective compressive strength of concrete as

$$\beta_n = 0.85 - 0.004 f'_c \geq 0.5 \qquad \text{((5.6) Repeated)}$$

The capacity of the strut depends on the width of the strut, w. This width is either calculated from the embedded length of the strut in the compression zone of the supporting member, r, from the depth of the compression zone of the member, c, or from the effective development depth of the longitudinal reinforcement, h_a. The according width w is given by equations (5.9), (5.12), and (5.13), respectively. The smallest width results in the lowest capacity of the strut.

$$w = r \cdot \sin\theta \qquad \text{((5.9) Repeated)}$$

With r given as defined in Figure 5-4, within the limits of

$$r \leq c_s \qquad \text{((5.8) Repeated)}$$

$$r \leq \frac{c}{\tan\theta} \qquad \text{((5.10) Repeated)}$$

If $r > \dfrac{c}{\tan\theta}$, the width of the strut will exceed the depth of the compression zone. The inclination of the strut, altered from eq. (5.4), then becomes

$$\cot\theta = \frac{l}{d - c/2} \qquad \text{((5.11) Repeated)}$$

The width of the strut is then defined by

$$w = c \cdot \cos\theta \qquad \text{((5.12) Repeated)}$$

If the effective development depth of the longitudinal reinforcement governs the width of the strut and/or the dimensions of the loading plates are known, w is calculated as

$$w = h_a \cdot \cos\theta + l_b \cdot \sin\theta \qquad \text{((5.13) Repeated)}$$

The limiting capacity of the strut component as a sole load-carrying mechanism is given by equation (5.16):

$$V_a = \beta_n k_s f'_c \cdot w \cdot b \cdot \sin\theta \qquad \text{((5.16) Repeated)}$$

5.3.2 Truss component

The capacity of the truss component is calculated from equilibrium conditions of the variable angle truss model. From the diagonal force D, the stress in the compression field, f_t, is determined by taking equilibrium of forces in the free-body-diagram in Figure 5-8, page 146. D is given by eqs. (5.18) and (5.19) as

$$D = \frac{V_t}{\sin\phi} \qquad \text{((5.18) Repeated)}$$

$$D = f_t \cdot t \cdot jd \cdot \cos\phi \qquad \text{((5.19) Repeated)}$$

The stress in the compression field is found by equating (5.18) and (5.19):

$$f_t = \frac{V_t}{\sin\phi \cdot t \cdot jd\cos\phi}$$
$$\Leftrightarrow f_t = \frac{V_t}{t \cdot jd}\left(\tan\phi + \cot\phi\right) \qquad \text{((5.20) Repeated)}$$

Equilibrium in the free-body-diagram in Figure 5-9, page 148, yields

$$A_w f_{wy} = f_t \cdot t \cdot s \cdot \sin^2\phi \qquad \text{((5.21) Repeated)}$$

Substituting equation (5.20) into (5.21) results in the shear capacity of the truss as

$$A_w f_{wy} = \frac{V_t \cdot s \cdot \sin\phi}{jd\cos\phi}$$
$$\Leftrightarrow V_t = \frac{A_w f_{wy} jd}{s}\cot\phi \qquad \text{((5.22) Repeated)}$$

Or, in terms of the transverse reinforcement ratio, as

$$V_t = \rho_w f_{wy} b \cdot jd \cdot \cot\phi \qquad \text{((5.23) Repeated)}$$

The stress in the inclined compression field is found from equation (5.25) in terms of the force in the transverse reinforcement and of the angle of the strut.

$$f_t = \frac{A_w f_{wy}}{s \cdot b \cdot \sin^2\phi}$$
$$\Leftrightarrow f_t = \frac{\rho_w f_{wy}}{\sin^2\phi} \qquad \text{((5.25) Repeated)}$$

5.3.3 Concrete components

The shear capacity of RC members without transverse reinforcement is calculated by taking the sum of a component related to the uncracked compression zone, V_{cz}, and a component attributed to friction in the tension zone, V_f.

$$V = V_{cz} + V_f + V_d \approx V_{cz} + V_f \qquad \text{((5.33) Repeated)}$$

The contribution of the compression zone, V_{cz}, is formulated as a function of the tensile strength of concrete, f_{ct}, and the area of the compression zone, $kd \cdot b$.

$$\begin{aligned} V_{cz} &= D \cdot f_{ct} \cdot b \cdot c \\ &= D \cdot \sqrt[3]{f'_c} \cdot b \cdot kd \end{aligned} \qquad \text{((5.38) Repeated)}$$

By defining a critical crack spacing, equilibrium conditions can be used to relate the average shear stress to the tensile force in the longitudinal reinforcement. The critical crack spacing is assumed as a function of the effective depth, d, of the member, and the depth of its compression zone, c:

$$s_{cr} = C(d - c) \qquad \text{((5.32) Repeated)}$$

The average shear stress is related to critical crack spacing and the change in force within the tensile reinforcement:

$$v_n = \frac{V}{jd \cdot b} = \frac{\Delta T}{s_{cr} \cdot b} \qquad \text{((5.35) Repeated)}$$

The friction component is determined from the average friction stress, τ_f, integrated over an area $jd \cdot b$. With the friction stress given by equation (5.40), the friction component becomes

$$V_f = \tau_{fu} \cdot b \cdot (d - kd) \qquad \text{((5.41) Repeated)}$$

$$\text{with } \tau_{fu} = const \cdot f_{ct} \left(1 - \frac{\Delta w}{\Delta w_u}\right) \qquad \text{((5.40) Repeated)}$$

The crack width Δw in the preceding equations results from geometry within the crack. The crack width is determined by equation (5.43) from a critical slip, Δs_u and the horizontal displacement at mid-depth of the crack, Δu.

$$\Delta w = \frac{\Delta u}{\sin \phi_u} + \frac{\Delta s}{\tan \phi_u} \qquad \text{((5.43) Repeated)}$$

$$\Delta s_u = 0.336 \Delta w + 0.01 \text{ [mm]} \qquad \text{((5.42) Repeated)}$$

$$\Delta u = 0.5 \cdot \varepsilon_s \cdot C(d - kd) \qquad \text{((5.45) Repeated)}$$

$$\Delta w = \frac{0.5 \cdot \varepsilon_s \cdot s_{cr}}{\sin \phi_{cr}} + \frac{0.336 \Delta w_u + 0.01}{\tan \phi_{cr}} \text{ [mm]} \qquad \text{((5.46) Repeated)}$$

The various parameters in the aforementioned equations are calibrated for different fields of application in the following chapter. Additionally, the combination of the basic models for arch-action, truss-action, and the concrete component is derived in Chapter 7.

6 Effect of the section depth on shear stresses

Many researchers (ASCE-ACI Committee 445 1998; Bažant and Kim 1984; Collins 1991; Kotsovos and Pavlovic 2004; Tompos and Frosch 2002) found that the magnitude of shear stresses in shear-controlled members is dependent on the effective depth of the section. In the proposed model, from the components contributing to the shear capacity defined in Chapter 5, only the stresses related to the friction component are affected by the effective depth d. Taking the nominal shear stress as $v_u = V_u / bd$, the effective depth cancels out of the terms related to the shear strength of the compression zone and the truss mechanism. According to the proposed model, size effect is not of concern in disturbed regions, because the section depth affects only the stresses related to the friction component V_f.

Equation (6.1) shows the stress related to friction as a function of d in a beam without transverse reinforcement. The strength of the friction component, V_f, is taken from equation (5.52), anticipating results from the calibration on beams without transverse reinforcement in Chapter 7.1.

$$
\begin{aligned}
& v_f = \frac{V_f}{bd} = 0.5 \cdot \sqrt[3]{f'_c}\,(1-k)\left(1-\frac{\Delta w}{\Delta w_u}\right) \\
& \Leftrightarrow v_f = 0.5 \cdot \sqrt[3]{f'_c}\,(1-k)\left(1-\frac{1}{w_u}\left(\frac{0.5\cdot\varepsilon_s\cdot d(1-k)}{\sin\phi(1-0.336\cot\phi)}+\frac{0.01\cot\phi}{1-0.336\cot\phi}\right)\right)
\end{aligned}
\tag{6.1}
$$

Shear strength is affected by the size of the effective depth as long as friction contributes to the strength of the member. The friction component, on the other hand, decreases with increasing strains in the longitudinal reinforcement, increasing the crack width Δw. According to the proposed model, it follows that if the strain in the longitudinal reinforcement increases such that the crack width exceeds the critical crack width, size effect is not of concern, because the friction component has vanished. The section width does not influence the shear stresses resulting from the components considered in the proposed model for shear strength. Dividing any of the contributing components defined in Chapter 5 to gain the average shear stress, cancels out the width b. Thus, the width of the section has no effect on the member strength.

Among test series carried out to investigate the effect of beam depth on the average shear strength are the beams tested by Podgorniak and Stanik and by Yoshida et al., and a test series by Shioya. The beams tested by Podgorniak and Stanik, and by Yoshida et al. (Reineck et al. 2003) were previously mentioned in the evaluation of other models. The test series by Shioya was used by Collins to describe the effect of the section depth (Collins 1991). The tests by Shioya were conducted on five simply supported beams subjected to a distributed vertical load. The specimens did not have transverse reinforcement; the only varying parameters were the section depth and width, which ranged from 203 to 3000 mm, and 152 to 1500 mm, respectively. The widths of the beams were adjusted accordingly to maintain a tensile reinforcement ratio of ρ_s = 0.4 %. Properties and dimensions of the beams are listed in Table 6-1. The average shear stress is given at the critical section, taken at a distance d from the support.

The test series conducted by Podgorniak and Stanik, and by Yoshida (Reineck et al. 2003) was carried out on single-span beams under a concentrated point load. The major variable was the section depth, ranging from 110 to 1890 mm. The beam width was 300 mm for all specimens; all other parameters were approximately equal. The beam properties are listed in Table 6-1.

Test	***b*** [mm]	***d*** [mm]	f'_c [MPa]	f_y [MPa]	ρ_s [%]	$v_{u,test}$ [MPa]
Shioya - 1	1500	3000	24.1	386	0.40	0.37
Shioya - 2	1000	2000	24.1	386	0.40	0.39
Shioya - 3	500	1000	24.1	386	0.40	0.49
Shioya - 4	300	600	24.1	386	0.40	0.78
Shioya - 5	152	203	24.1	386	0.40	1.06
Yoshida et al. - YB2000/0	300	1890	32	455	0.74	0.45
Podgorniak / Stanik BN100	300	925	35	550	0.76	0.69
Podgorniak / Stanik BN50	300	450	35	486	0.81	0.98
Podgorniak / Stanik BN25	300	225	35	437	0.89	1.08
Podgorniak / Stanik BN12.5	300	110	35	458	0.91	1.22

Table 6-1 Properties of beams from test series carried out to investigate size effect

Table 6-2 lists the strains at midspan and at the critical section, as well as the calculated crack width Δw. None of the tested specimens was a flexure-controlled beam according to the ACI code, which requires a strain of $\varepsilon_s \geq 0.005$ in the flexural reinforcement (ACI-318 2002).

The calibration of the proposed model in the following chapter limits the crack width to a value $\Delta w_u = 1.0$ mm. If size effect is only of concern for members that develop a shear resistance related to friction, the effect becomes negligible for members in which the crack width exceeds the critical crack width. This was the case for the first four beams of the test series carried out by Shioya, and the beam tested by Yoshida.

Test	ε_s at d [-]	ε_s at midspan [-]	Δw [mm]
Shioya - 1	0.0005	0.0017	2.86
Shioya - 2	0.0005	0.0016	1.88
Shioya - 3	0.0006	0.0020	1.20
Shioya - 4	0.0010	0.0032	1.14
Shioya - 5	0.0014	0.0044	0.55
Yoshida et al. YB2000/0	0.0003	0.0010	1.12
Podgorniak / Stanik BN100	0.0005	0.0015	0.83
Podgorniak / Stanik BN50	0.0007	0.0019	0.54
Podgorniak / Stanik BN25	0.0007	0.0020	0.29
Podgorniak / Stanik BN12.5	0.0007	0.0022	0.18

Table 6-2 Strains and calculated crack width for beams by Shioya and Podgorniak

According to the model, the change in shear stress with section depth becomes smaller as the friction component decreases. This is represented and confirmed in the curve for the tested specimens in Figure 6-1. Figure 6-1 shows the measured and calculated average shear stresses for the Podgorniak / Yoshida, and the Shioya test series.

For the first four beams tested by Shioya, and the beam tested by Yoshida, the proposed method set a limit to the effect of the section depth in terms of the critical crack width. As the crack width exceeded the limiting value, the contribution from friction became zero. Therefore, the shear stress was only calculated from the contribution of the compression zone. Figure 6-1 shows the measured and calculated average shear stresses, as well as the value of $0.166\sqrt{f'_c}$ [MPa], proposed by the ACI code as the limiting average shear stress (ACI-318 2002). Compared to the results of both test series, the proposed method gave a conservative estimate of the shear stresses. According to the proposed model, arch action contributed to the capacity of the Podgorniak test series with an aspect ratio of approximately $a/d = 2.9$.

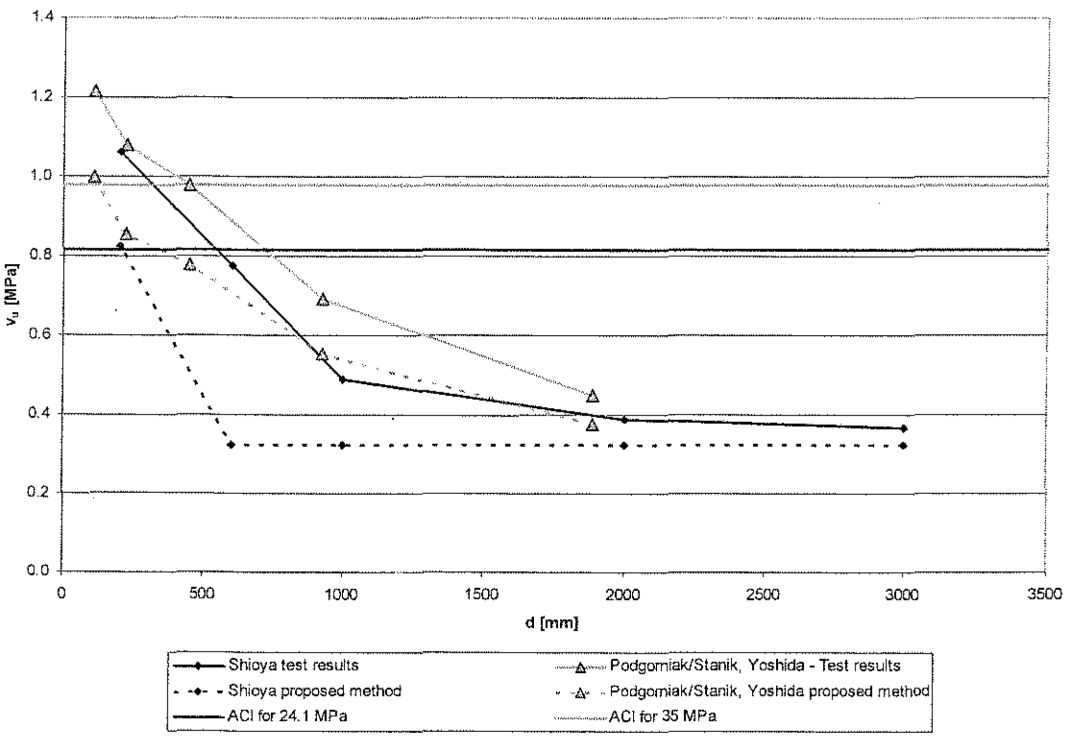

Figure 6-1 Stresses at failure, taken at a distance *d* from the support, versus effective depth

Evaluation of the representation of size effect proposed by Bažant

Figure 6-2 shows the performance of the approach proposed by Bažant as outlined in Section 3.7 on the tests series by Shioya and by Podgorniak / Stanik and Yoshida. The average shear stress was calculated for the beams in the test series according to equation (3.76).

$$v_u = \frac{10\sqrt[3]{\rho_s}}{\sqrt{1+d/25d_a}}\left[\sqrt{f'_c} + 3000\sqrt{\rho_s/(a/d)^5}\right] \quad \text{[psi] ((3.76) Repeated)}$$

The maximum aggregate size d_a in the specimens tested by Shioya was 25 mm (Collins 1991), for the test series by Podgorniak / Stanik and Yoshida, it was assumed d_a = 19 mm. As can be seen from Figure 6-2, the method proposed by Bažant reflected the test results from the series by Shioya well for beams with larger section depths than d = 1000 mm. For beams with d < 1000 mm, Bažant's method was very conservative. The performance on the test series by Podgorniak / Stanik and Yoshida was different. For this test series, the member behavior was modeled relatively well, except a trend to unconservative values with increasing beam depth is discernible.

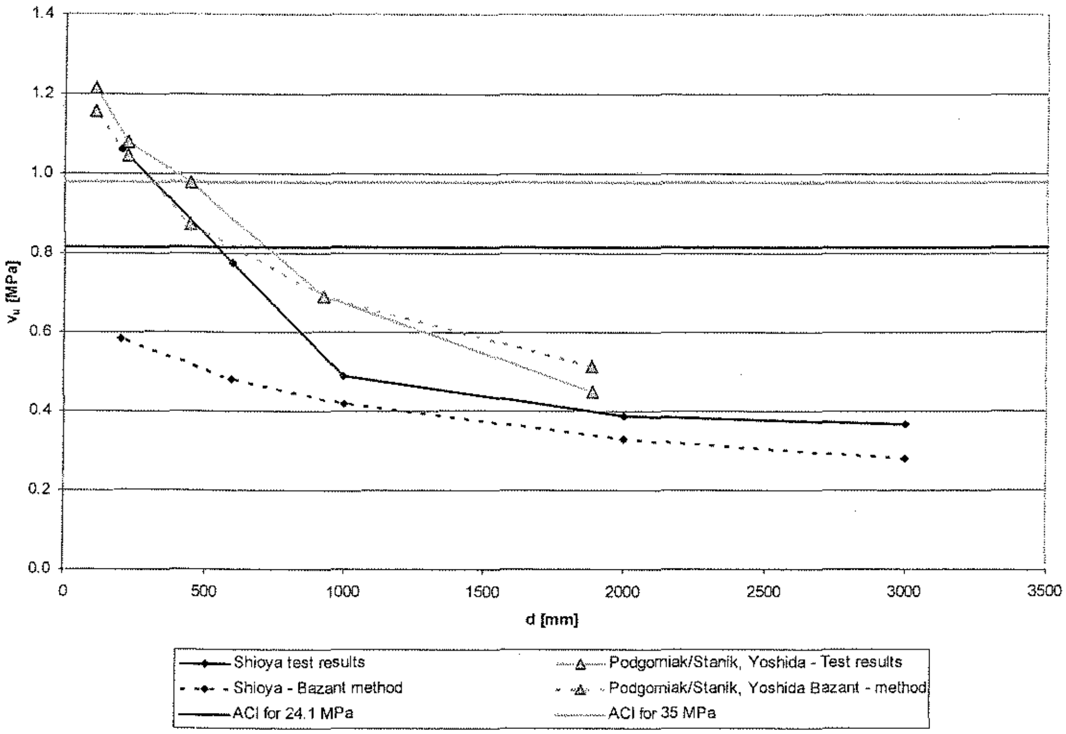

Figure 6-2 Stresses at failure, taken at a distance *d* from the support, versus effective depth; calculated following the proposal by Bažant

The difference in performance for the two test series shows that the term out of the brackets in equation (3.76) does not fully reflect the actual behavior of the tested beams. Table 6-3 lists the calculated values from the first and second terms, as well as the nominal shear stress calculated from equation (3.76). Since the beams in the respective test series were identically scaled, the values resulting from the term within the brackets are equal for each test series. The specimen tested by Yoshida had a slightly lower concrete strength than the specimens tested by Podgorniak and Stanik, resulting in a slightly lower value of the second term of equation (3.76). Because the second terms in each test series are similar, the deviation of the model with respect to the test results has to be related to the first term, defined by the longitudinal reinforcement ratio, the effective depth, and the maximum aggregate size. The values for ρ_s in the test series by Shioya were 0.4 percent. In the test series by Podgorniak / Stanik and Yoshida the longitudinal reinforcement ratio ranged from 0.74 to 0.91 percent (see Table 6-1). The maximum aggregate sizes were equal within each test series. However, the values for d were comparable for the two test series. It follows that the deviation in behavior of the model proposed by Bažant on the two test series must be related to the first term in equation (3.76), which is a function of the section depth and the longitudinal reinforcement. For larger longitudinal reinforcement ratios in combination with larger depths, Bažant's method yields progressively less conservative values; for low values of ρ_s and d, the model was conservative, and appears to become more conservative as the effective depth increases. It should be noted that the reinforcement ratio used in the Podgorniak / Stanik and Yoshida test series is similar to that used in practice, and approximately twice of the amount used in the test series conducted by Shioya.

Test	1st term [-]	2nd term [MPa]	v_u [MPa]
Shioya - 1	0.66	0.42	0.28
Shioya - 2	0.78	0.42	0.33
Shioya - 3	0.99	0.42	0.42
Shioya - 4	1.13	0.42	0.48
Shioya - 5	1.38	0.42	0.58
Yoshida et al. YB2000/0	0.86	0.60	0.51
Podgorniak / Stanik BN100	1.12	0.62	0.69
Podgorniak / Stanik BN50	1.41	0.62	0.87
Podgorniak / Stanik BN25	1.68	0.62	1.04
Podgorniak / Stanik BN12.5	1.86	0.62	1.16

Table 6-3 First and second terms, and nominal shear stress from equation (3.76)

Reduction of the friction component with increasing section depth

Equation (6.1) was solved for an effective depth at which the friction component becomes zero, because the limiting crack-width $\Delta w_u = 1$ mm is reached. This is expressed in equation (6.2) as a function of the strain in the tensile reinforcement and the reinforcement ratio:

$$d = \frac{(500 - 173 \cdot \cot\phi)\sin\phi}{250\varepsilon_s\left(1 + n\rho_s - \sqrt{n\rho_s\,(2 + n\rho_s)}\right)} \tag{6.2}$$

with $n = \dfrac{E_s}{E_c}$

Following eq. (6.2), according to the proposed model, four parameters have an influence on whether size effect is of concern in a beam. The critical crack inclination defines the sliding component of two adjacent crack surfaces due to rotation. If the crack is normal to the beam axis, sliding of the surfaces, and therefore friction, is minimal. The ratio of the modulus of elasticity of the reinforcing steel to that of the concrete and the reinforcement ratio are the two main parameters that affect the depth of the compression zone, and therefore the depth of the crack. The modular ratio may also be expressed in terms of the compressive strength of concrete by adopting a relationship between the modulus of concrete and compressive strength. According to the proposed model, the strain in the longitudinal reinforcement directly influences the width of the crack and therefore the amount of friction. With increasing strains, the effective depth at which the friction component vanishes, decreases.

The term in the brackets in equation (6.1), extracted in (6.3), can be viewed at as a reduction factor for the friction component, depending on the section depth, the strain, the crack inclination, and k.

$$1-R=1-\frac{1}{w_u}\left(\frac{0.5\cdot\varepsilon_s\cdot d(1-k)}{\sin\phi(1-0.336\cot\phi)}+\frac{0.01\cot\phi}{1-0.336\cot\phi}\right) \tag{6.3}$$

Resolving ε_s into the average shear stress v_u at a distance d from the support yields:

$$\varepsilon_s=\frac{v_u}{E_s\rho_s(1-k/3)} \tag{6.4}$$

Therefore, the reduction term in (6.3) becomes:

$$R=\frac{1}{w_u}\cdot\frac{1.5d(k-1)v_u}{(1-0.336\cot\phi)\sin\phi\cdot E_s\rho_s(k-3)} \tag{6.5}$$

Equation (6.5) indicates that the reduction of the friction component, and therefore the average shear stresses, is not only a function of the section depth, but also of the tensile reinforcement ratio, and, if k is taken as in eq. (5.36), of the compressive strength of concrete, with $E_c=4733\sqrt{f'_c}$ [MPa] (Pauw 1960).

Evaluating a critical crack inclination of 30 degrees, E_s = 200,000 MPa, a critical crack width of Δw_u = 1 mm, and neglecting small terms in equation (6.5) yields:

$$R = 0.04 + \frac{v_u d \cdot f'_c}{\rho_s \left(2.35 \cdot 10^6 \cdot \rho_s \sqrt{f'_c} + 83606 f'_c + 55737 \sqrt{\frac{\rho_s \left(1785 \rho_s + 84.5 \sqrt{f'_c}\right)}{f'_c}} \cdot f'_c \right)} \quad (6.6)$$

Equation (6.6) was solved in equation (6.7) for the section depth d in dependence of the reduction R. This could be evaluated for different reduction factors, giving the largest effective depth that allows for the wanted reduction due to the effect of the section depth d.

$$d = \frac{R - 0.04}{v_u f'_c} \rho_s \left(2.35 \cdot 10^6 \cdot \rho_s \sqrt{f'_c} + 83606 f'_c + 55737 \sqrt{\frac{\rho_s \left(1785 \rho_s + 84.5 \sqrt{f'_c}\right)}{f'_c}} \cdot f'_c \right)$$

(6.7)

Equation (6.7) was evaluated for reduction values of R = 0.1, 0.2, and 0.3, which are equivalent to a reduction of the friction component due to "size effect" by 10, 20, and 30 percent, respectively. These values were plotted for several tensile reinforcement ratios and concrete strengths in Figure 6-3 through Figure 6-11. The charts indicate the allowable combination of concrete strength, reinforcement ratio, and section depth for the respective reduction in the average shear stress. The horizontal bold line indicates a limit value of $v_u = 0.166\sqrt{f'_c}$ [MPa], which is the maximum allowable average shear stress according to the current ACI-318 code (ACI-318 2002).

For example, if only a reduction of the friction component by 10 percent is acceptable, a maximum section depth of only $d = 37$ mm is allowable, at a concrete strength of 35 MPa, and a reinforcement ratio of $\rho_s = 0.5$ %, at an average shear stress of $v_u = 0.8$ MPa. An acceptable reduction by 30 percent would allow for $d = 163$ mm, if the other parameters are kept equal to the first case. Alternatively, an increase of the tensile reinforcement ratio to $\rho_s = 2.0$ percent would make a beam depth of 163 mm at a 10 percent reduction of the friction component possible.

Tensile reinforcement ratios ranging from 0.4 to 0.8 percent would be typical values for slabs. According to the proposed model, the effect of the section depth would therefore also be of concern for slabs, if the average shear stresses were close to the permissible value of $v_u = 0.166\sqrt{f'_c}$. Lowering the average shear stress would increase the maximum effective depth for which "size effect" would not reduce the friction component V_f. This is especially true for tensile reinforcement ratios of larger than 0.5 percent, which can be considered typical for beams.

Apparent from the graphs is the considerable effect of concrete strength. According to the proposed model, high-strength concrete beams appeared to be very sensitive with respect to an effect of the section depth on the average shear stress. This is related to the decrease of the depth of the neutral axis with increasing compressive strength. Decreasing the depth of the neutral axis increases the crack width, therefore reducing the friction capacity following the proposed model.

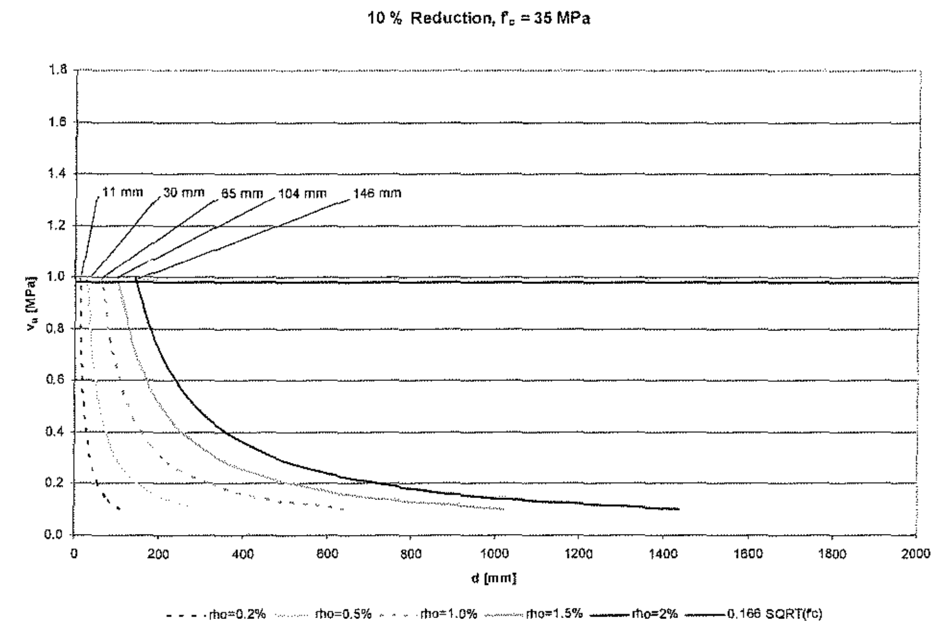

Figure 6-3 Section depth versus average shear stress for a 10 % reduction of the friction component V_f, $f'_c = 35$ MPa

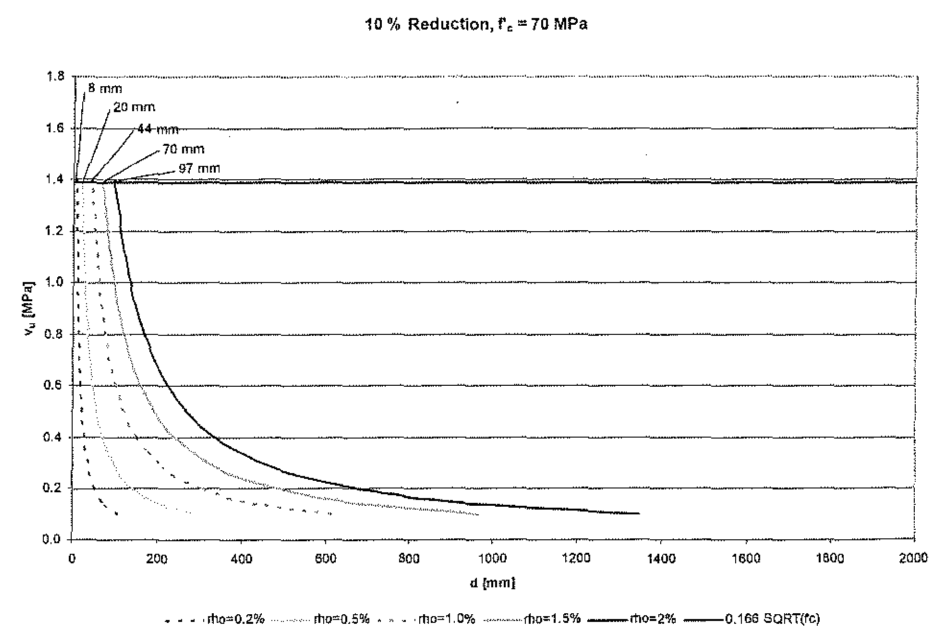

Figure 6-4 Section depth versus average shear stress for a 10 % reduction of the friction component V_f, $f'_c = 70$ MPa

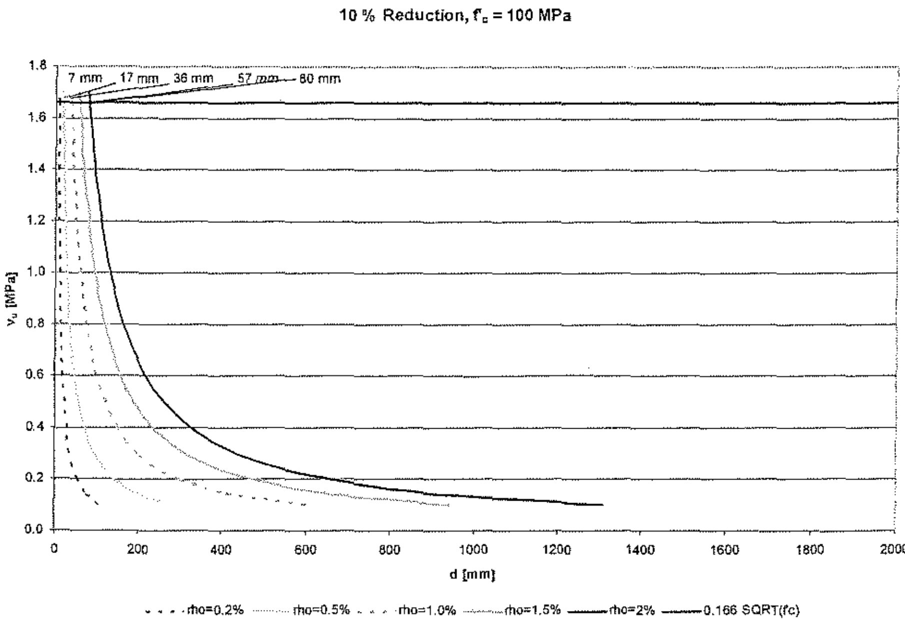

Figure 6-5 Section depth versus average shear stress for a 10 % reduction of the friction component V_f, f'_c = 100 MPa

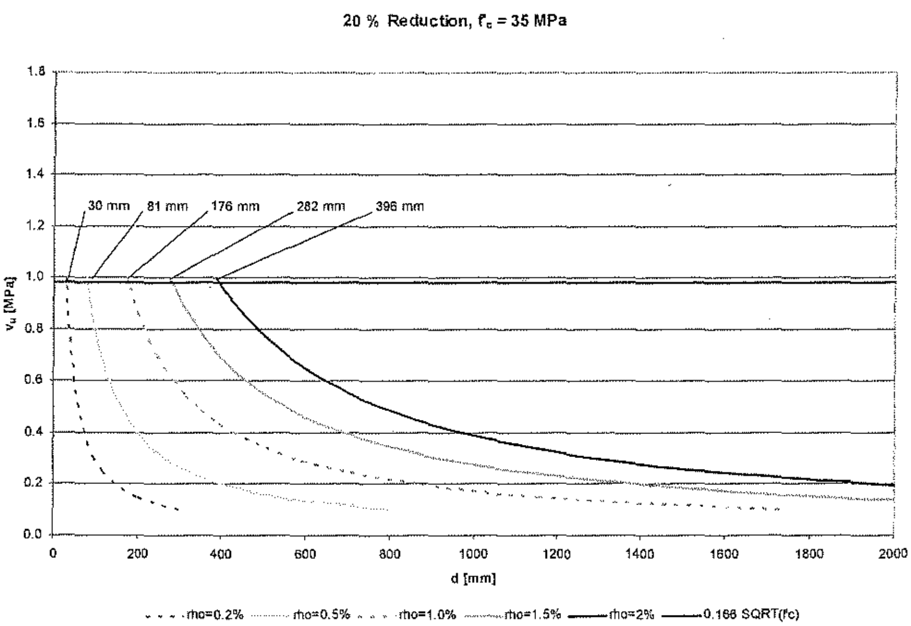

Figure 6-6 Section depth versus average shear stress for a 20 % reduction of the friction component V_f, f'_c = 35 MPa

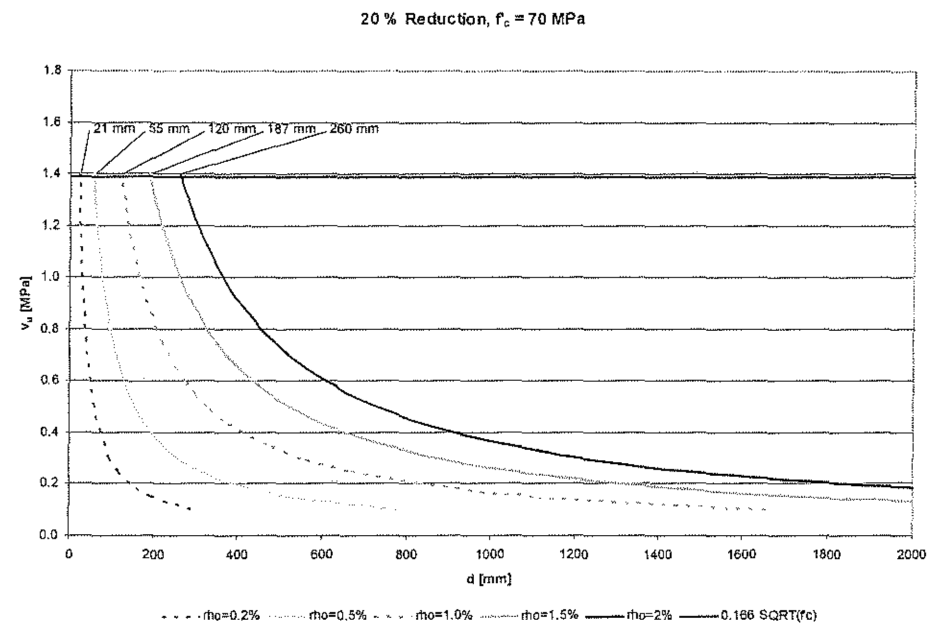

Figure 6-7 Section depth versus average shear stress for a 20 % reduction of the friction component V_f, $f'_c = 70$ MPa

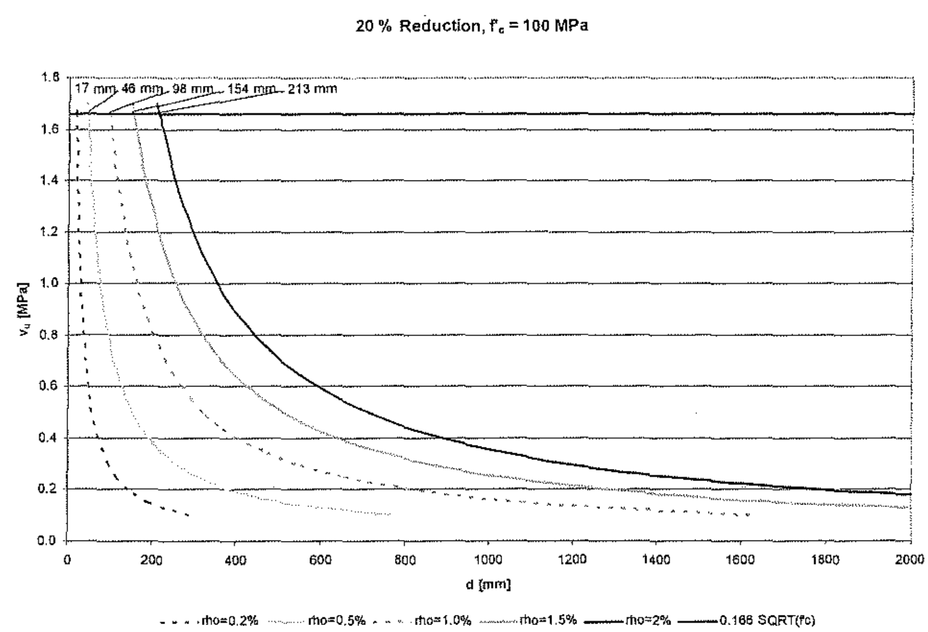

Figure 6-8 Section depth versus average shear stress for a 20 % reduction of the friction component V_f, $f'_c = 100$ MPa

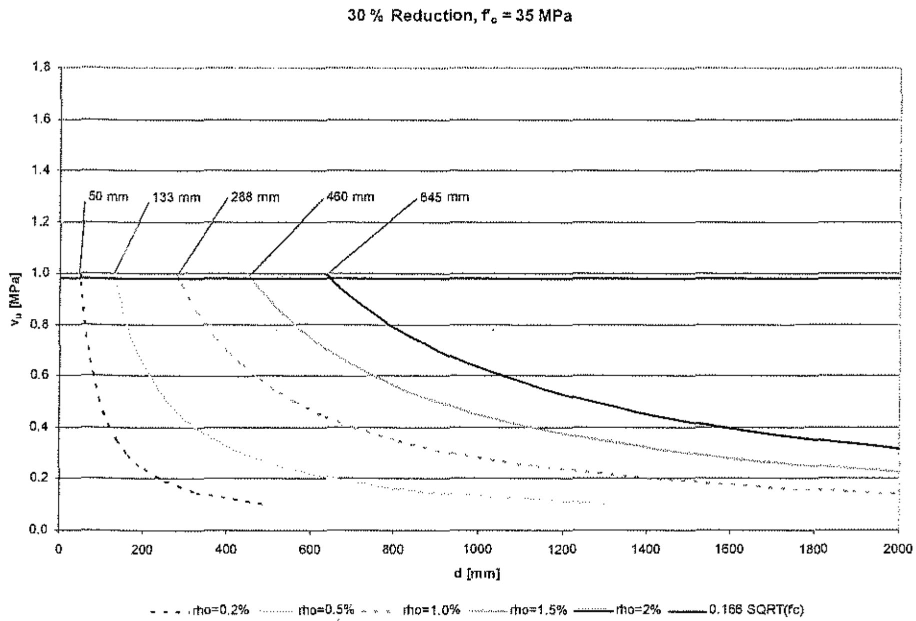

Figure 6-9 Section depth versus average shear stress for a 30 % reduction of the friction component V_f, f'_c = 35 MPa

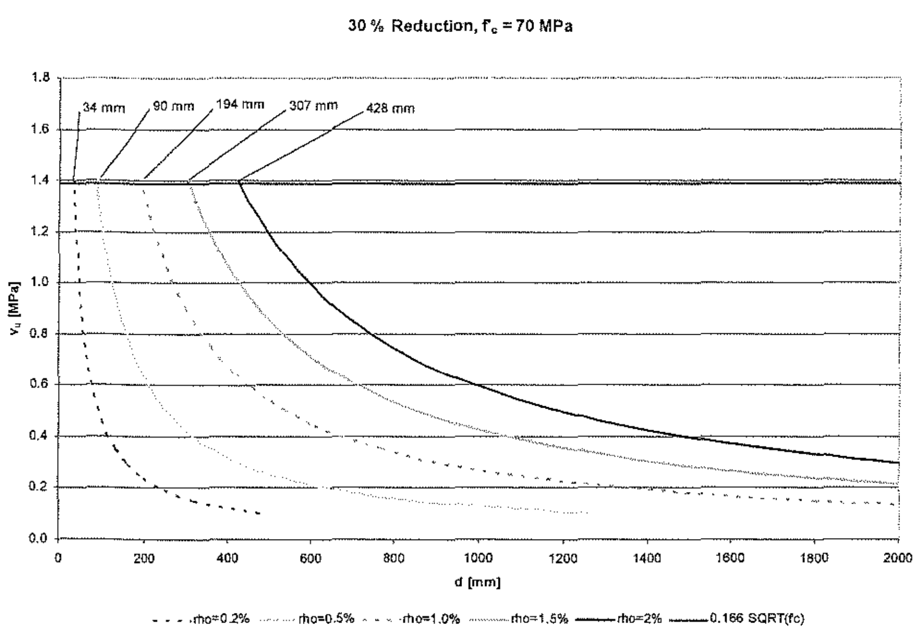

Figure 6-10 Section depth versus average shear stress for a 30 % reduction of the friction component V_f, f'_c = 70 MPa

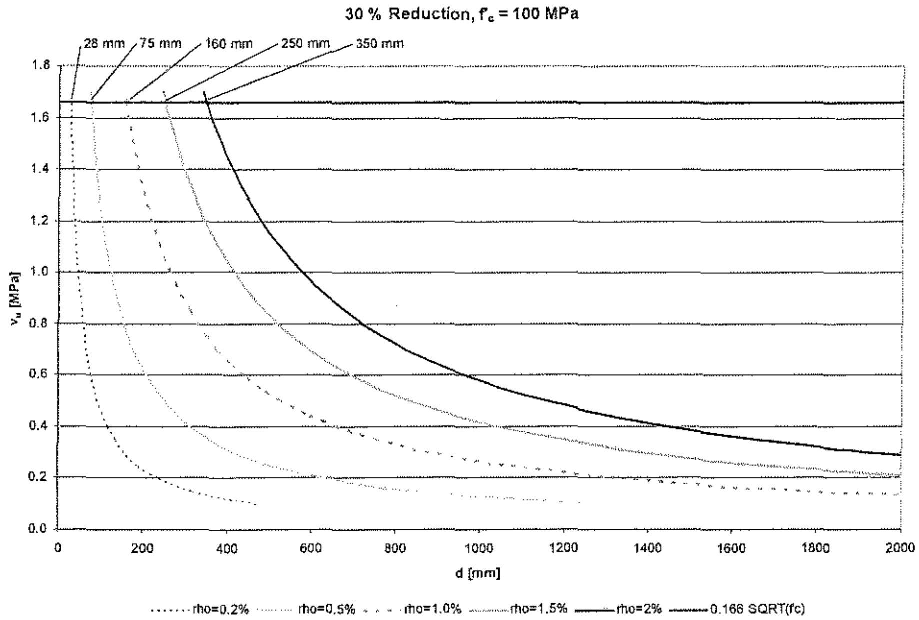

Figure 6-11 Section depth versus average shear stress for a 30 % reduction of the friction component V_f, $f'_c = 100$ MPa

7 Calibration of the proposed model for the static load case

7.1 Members without transverse reinforcement

7.1.1 Transition from contributing components in deep members to slender members

The shear strength of members without transverse reinforcement is contributed to components related to arch-action, V_a, and the concrete contributions, V_{cz} and V_f. The respective contribution of the components is described by transition functions related to the aspect ratio a/d.

In deep members, arch action is the main load-carrying mechanism. It is assumed that in a member with a shear-span-to-depth ratio of a/d smaller than approximately 2.5 no distinct compression and tension zones will develop, chiefly representing "disturbed" D-regions as described by Schlaich (Schlaich et al. 1987). Following this, it appears to be not sensible to attribute a shear capacity to a compression zone while the whole member is mostly under compression. Respectively, the arch is representing the shear resistance taken by the compression zones of the member. Without a distinct tension zone, no flexural cracks will develop that allow for a load carrying mechanism through friction along these cracks.

In slender members, however, distinct compression and tension zones enable a contribution of V_{cz} and V_f. Additionally, an arch component will contribute to the shear resistance in a transition zone, in which V_a decreases with an increasing shear-span-to-depth ratio. For relatively large aspect ratios, the arch contribution is negligible.

To allow for a decrease of the arch component with an increasing value of the aspect ratio *a/d*, a factor k_s as a function of *a/d* was introduced in Section 5.2.1.3, page 143. The factor k_s reduces the contribution of the arch with an increasing shear-span-to-depth ratio *a/d*. The general form for k_s is:

$$k_s = \frac{x}{y + z\left(a/d\right)^w} \qquad \text{((5.15) Repeated)}$$

For a "smooth" transition from arch-action in deep members to the contribution of components related to stresses in the concrete in slender members, k_s has to take a value of one for a theoretical aspect ratio $a/d = 0$ and has to vanish for *a/d* larger than approximately 2.5. The exact values for the variables, as well as the limiting aspect ratio were found from the calibration of the model on a large database comprising deep and slender members without transverse reinforcement that failed in shear. This calibration is described later in this section.

The gradual increase of the components related to the compression zone of the member and friction along crack surfaces with an increasing aspect ratio can be described as a function k_c defined as

$$k_c = 1 + \frac{1}{x + y\left(a/d\right)^w} \geq 0 \qquad (7.1)$$

where the variable w is taken as the same value as in eq. (5.15).

To account for the transition from deep to slender members, the term related to the concrete contributions $V_c = V_{cz} + V_f$ is then reduced by k_c:

$$V_c = k_c\left(V_{cz} + V_f\right) \tag{7.2}$$

Figure 7-1 shows a plot of the reduction factors k_s and k_c versus the aspect ratio with the variable values found from the calibration.

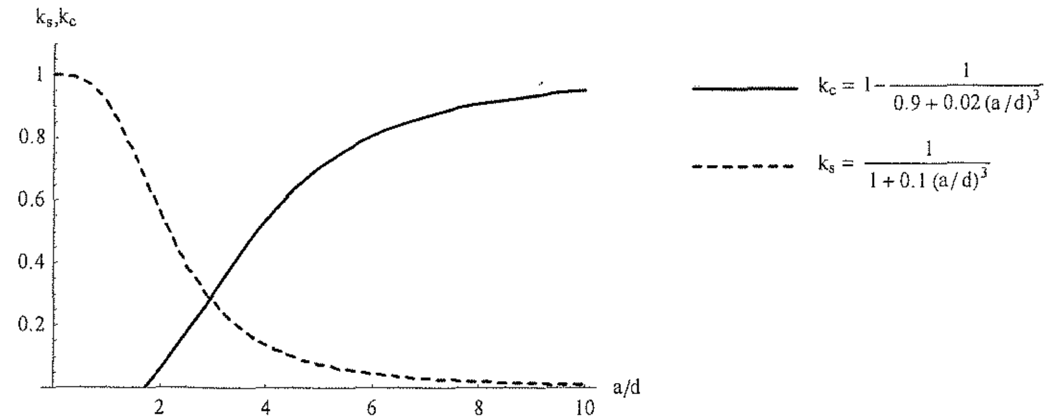

Figure 7-1 Reduction functions related to aspect ratio

7.1.2 Calibration of the model for members without web reinforcement

The coefficients of the proposed model were calibrated on a database collected from a database of slender RC members without transverse reinforcement that failed in shear (Reineck et al. 2003), and a database of RC members with an aspect ratio of $a/d < 2.5$ for the same mode of failure (Matamoros and Wong 2003). The database comprises 395 slender beams and 50 deep beams, resulting in 445 RC members without transverse reinforcement yielding shear failures. Both databases are listed separately in the Appendix and on the supplementary worksheets on the data CD to allow for a comparison with other models.

The calibration was carried out with the goal to achieve relatively small scatter and to give mostly conservative results. The latter seems to be justified by the high variance that RC members without transverse reinforcement generally show with respect to their behavior under shear load.

7.1.2.1 Capacity of deep members

The capacity of the deep members was calculated using equation (5.16)

$$V_a = \beta_n k_s f'_c \cdot w \cdot b \cdot \sin\theta \qquad \text{((5.16) Repeated)}$$

The strut width for the stocky members was calculated from the size of the loading plates and the location of the tensile reinforcement as the governing cases for deep beams. As a safe assumption, the strut width was taken as the smallest value of

$$w = h_a \cdot \cos\theta + l_b \cdot \sin\theta \qquad \text{((5.13) Repeated)}$$

$$w = \frac{l_b}{\sin\theta} \tag{7.3}$$

$$w = h_a \cos\theta \tag{7.4}$$

where $h_a = 2c_R$ = effective embedment depth of tensile reinforcement

l_b = length of the loading plate in direction of the member axis

$$\cot\theta = \frac{a}{d}$$

The reduction factors β_n and k_s were calibrated using the complete database, including deep and slender beams. Taking their functions as follows gave the best fit for the data:

$$\beta_n = 0.85 - 0.004 f'_c \geq 0.5 \qquad \text{((5.6) Repeated)}$$

$$k_s = \frac{1}{1 + 0.1\left(a/d\right)^3} \qquad (7.5)$$

The calibration of the deep beam subset of the database yielded an average value of measure to calculated shear strength of 1.11 ± 0.8 % within a 95 % confidence region. The coefficient of variation was 23 % for a standard deviation of 0.25. These values do not reflect possible contributions from the V_c terms in the transition zone.

Figure 7-2 through Figure 7-4 show graphs plotting the measured versus calculated shear strength, the ratio of measured to calculated shear strength versus aspect ratio, and the ratio of measured to calculated shear strength versus the compressive strength of concrete, respectively, and the respective trend lines. As for the aforementioned average value and coefficient of variation, these graphs show the results for deep members only, with the shear capacity calculated from sole arch-action.

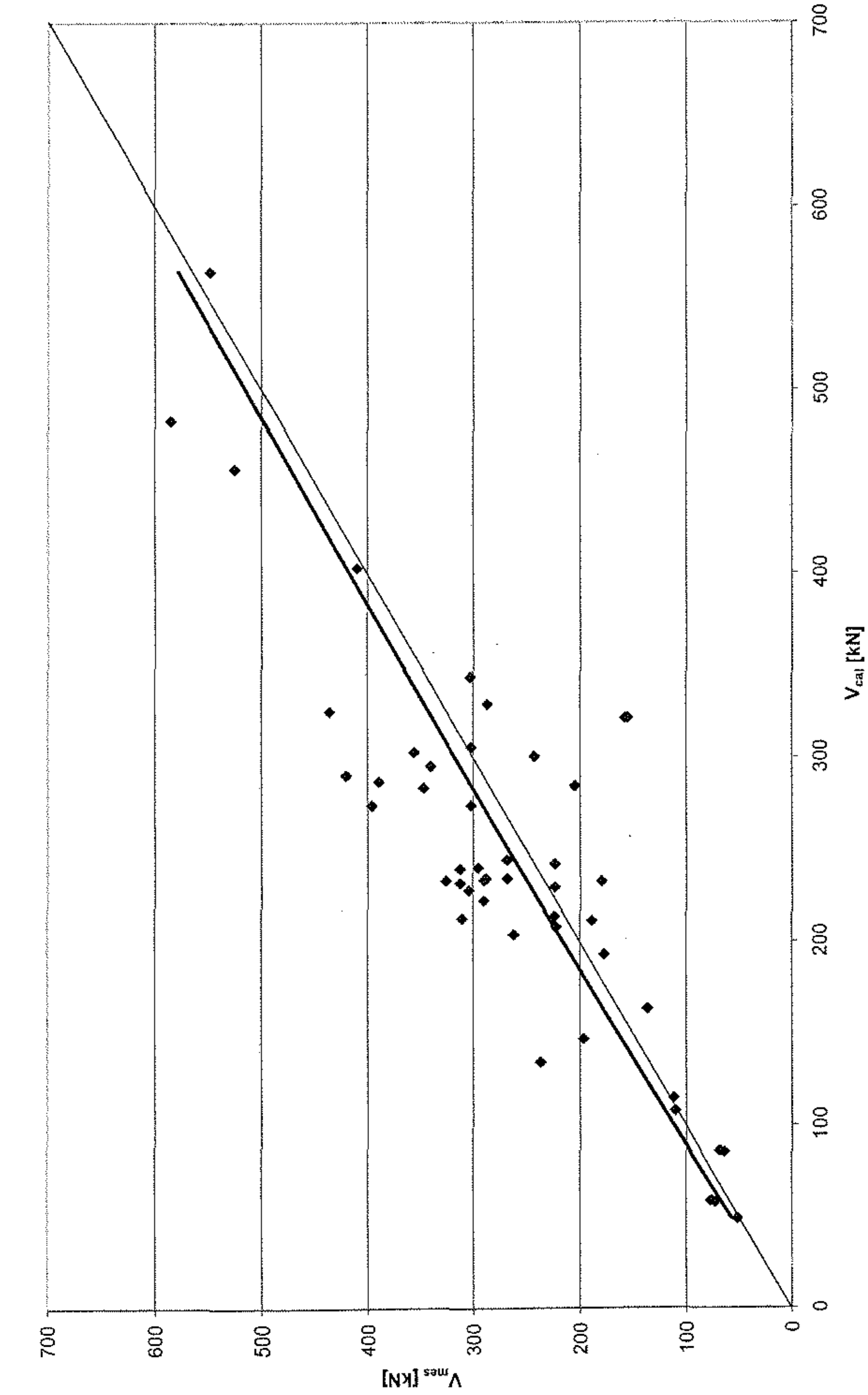

Figure 7-2 Measured versus calculated shear strength from arch action on deep members

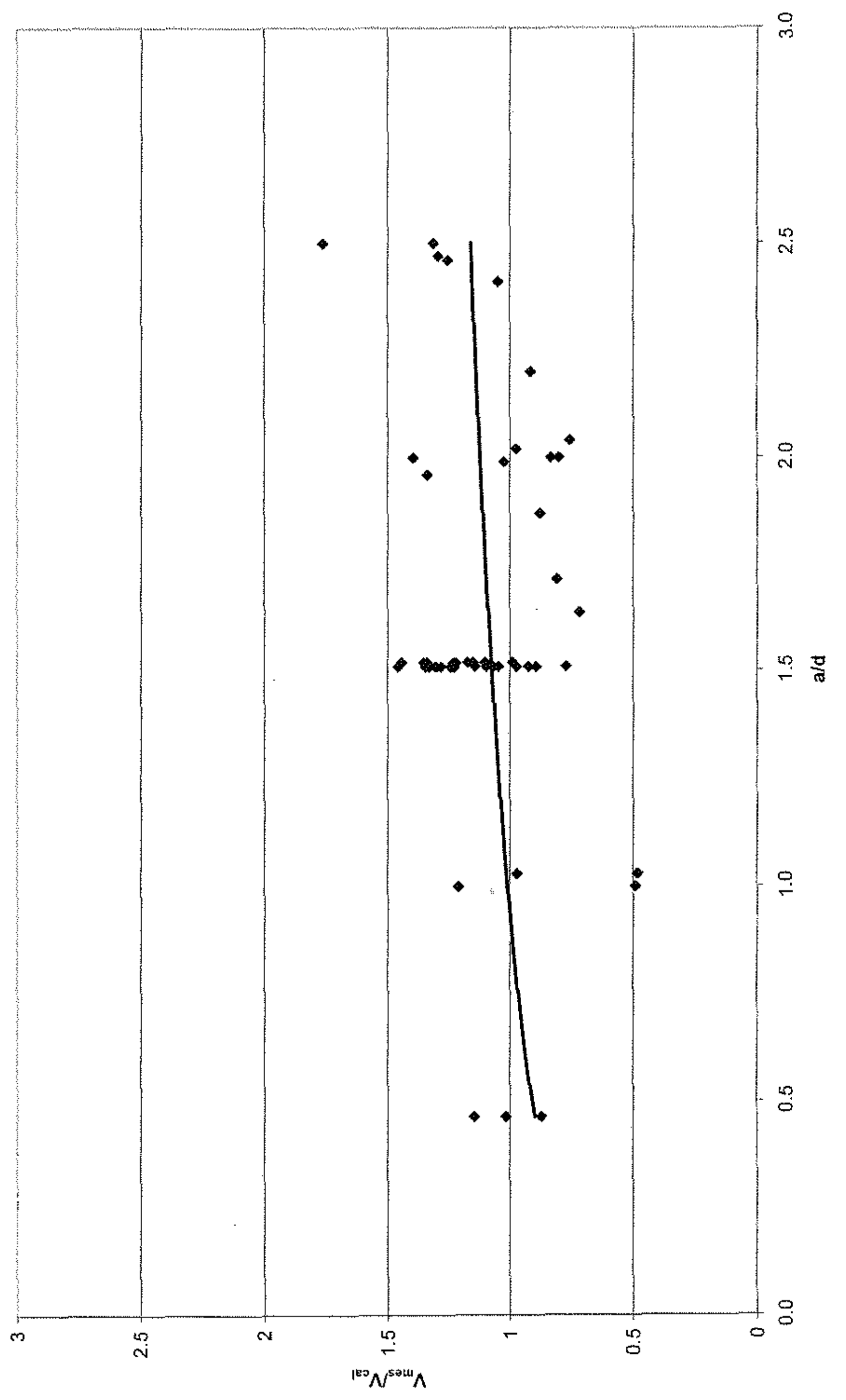

Figure 7-3 Ratio of measured to calculated shear strength versus aspect ratio, deep members, arch-action only

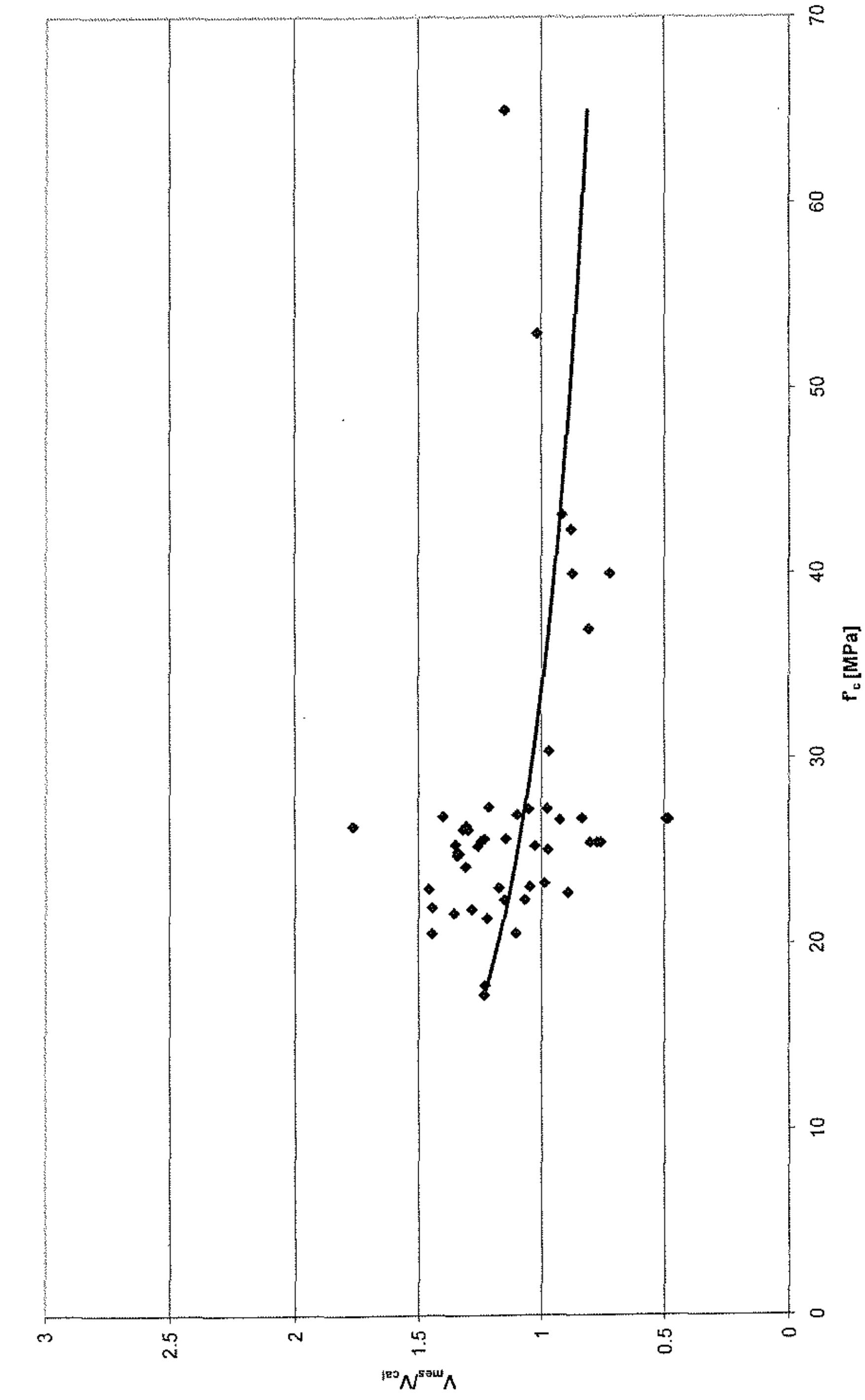

Figure 7-4 Ratio of measured to calculated shear strength versus concrete compressive strength, deep members, arch-action only

7.1.2.2 Capacity of deep and slender members

The main load-carrying mechanisms of slender members without transverse reinforcement are the shear resistance related to the uncracked compression zone, and the shear resistance related to friction as described in Section 5.2.3, page 152. The contributions were previously formulated in equations (5.38) and (5.41):

$$V_{cz} = D \cdot \sqrt[3]{f'_c} \cdot b \cdot kd \qquad \text{((5.38) Repeated)}$$

$$V_f = \tau_{fu} \cdot b \cdot (d - kd) \qquad \text{((5.41) Repeated)}$$

Taking the sum of both components, $V_c = V_{cz} + V_f$, nonlinear regression analysis yielded the following parameters:

$$V_c = 0.5 \cdot f_{ct} \cdot b \cdot kd + 0.5 \cdot f_{ct} \cdot b \cdot (d - kd)\left(1 - \frac{\Delta w}{\Delta w_u}\right) \qquad (7.6)$$

such that

b = width of the beam

kd = depth of the neutral axis from flexural linear analysis

$$f_{ct} = \sqrt[3]{f'_c}$$

$$\Delta w_u = 1.0 \text{ mm}$$

$$\Delta w = \frac{0.5 \cdot \varepsilon_s \cdot s_{cr}}{\sin 30^\circ \left(1 - 0.336 \cot 30^\circ\right)} + \frac{0.01 \cdot \cot 30^\circ}{1 - 0.336 \cdot \cot 30^\circ} \text{ [mm]}$$

$$s_{cr} = (d - kd) \text{ [mm]}$$

$$\varepsilon_s = \frac{V \cdot d}{\rho_s \cdot bd \cdot jd \cdot E_s}$$

The transition from deep members to slender members was done by the factor k_c, introduced in equation (7.1). The nonlinear regression analysis on the full database, including slender and deep members resulted in

$$k_c = 1 - \frac{1}{0.9 + 0.02\left(a/d\right)^3} \geq 0 \tag{7.7}$$

Following equation (7.2), the contribution of the concrete components was reduced as

$$V_c = k_c\left(V_{cz} + V_f\right) \qquad \text{((7.2) Repeated)}$$

The shear strength of all 448 members of the database was calculated by

$$V_n = V_a + k_c\left(V_{cz} + V_f\right) \tag{7.8}$$

No data was available about the size of the loading plates of the slender members. As a safe assumption, the width of the strut for V_a was calculated for the slender members by

$$w = \min\left\{h_a, kd\right\} \cdot \cos\theta \tag{7.9}$$

The mean value of measured to calculated shear strength was calculated as $1.36 \pm 0.33\%$ within a 95 % range of confidence. The standard variation was found as 0.39, resulting in a coefficient of variation of 28.6 percent. As mentioned before, emphasis was put on a conservative estimate, and, reflecting the generally large amount of scatter, on conservative trends. Figure 7-5 through Figure 7-9 show various plots representative of the calibration of the model. Included are five specimens that were scaled to demonstrate the effect of a change in the effective depth. These are indicated in the plots by large grey circles. As can be seen, the proposed model yielded reasonable results considering size effects.

Figure 7-5 shows a plot of measured to calculated shear strength of all specimens in the database. The thick line represents the trend line of the complete data set. Values representative for size effects are lining up along the trend line within reasonable range.

The ratio of measured to calculated shear strength versus aspect ratio is plotted in Figure 7-6. The Scatter is largest in the transition zone ranging between approximately $2.5 \leq a/d \leq 4$. The scatter can partly be attributed to the sum of the two reduction factors k_s and k_c. However, this particular range of aspect ratios also represents the majority of tested beams, such that scatter can be expected to be higher in this area. Since the scatter is only on the conservative side with $V_{mes}/V_{cal} > 1$, it is considered acceptable.

The same as said about a higher variation of V_{mes}/V_{cal} values is discernible in the subsequent plots as Figure 7-7, showing a plot of measured to calculated shear strength versus concrete compressive strength. Also here, the concrete compression strength of the majority of test specimens was in a range of approximately 20 to 30 MPa, representing normal strength concrete in the respective tests. The relatively small amount of variance for higher strength concretes between 40 and 105 MPa with no distinct trend is seen as an indicator for the applicability of the proposed model over an extensive range of concrete strength.

Figure 7-8 shows the influence of the effective depth. The beams that were scaled to demonstrate the effect of the member depth are marked by large grey dots. No trend is apparent over the considered effective depth range between 127 and 1890 mm. The trend line for the beams that were used to evaluate the effect of the effective depth is plotted as the dashed line in Figure 7-8.

The plot of measured to calculated shear strength versus the tensile reinforcement ratio is an indicator for possible bias related to the amount of tensile reinforcement, $\rho_s = A_s/(bd)$. Both components responsible for the shear strength of slender members are influenced by ρ_s. The depth of the neutral axis as calculated by eq. (5.36) is directly related to the tensile reinforcement ratio. The shear resistance component attributed to friction V_f is influenced by the amount of flexural reinforcement, since it is related to the strain in the flexural reinforcement, from which the crack width is calculated. Figure 7-9 shows the plot of V_{mes}/V_{cal} versus the tensile reinforcement ratio of the tested specimens. No distinct trend is perceptible from this graph.

7.1.3 Influence of critical section considered

It was mentioned earlier that if the strain in the longitudinal reinforcement is calculated at a different location than at a distance d measured from the support, the critical crack width, Δw_u, has to be changed due to different crack geometries and wider allowable cracks towards the center of a simply supported beam. As the moment increases, the strain in the longitudinal reinforcement increases. For simply supported beams, the critical crack width has to be changed depending on the considered location where the moment is taken. This effect was studied for different locations. Table 7-1 shows different values of the critical crack width changing with the moment location. For simplicity, only the values for the critical crack width, Δw_u were changed, the critical crack spacing s_{cr} was kept constant with respect to the initial location of the considered moment at a distance d from the support. The calibration was carried out aiming at similar responses in terms of the ratio of measured to calculated shear strength to keep the same level of conservatism. Only the slender members of the database were considered, because an influence of friction in deep members is not relevant, as described before.

Moment	**Δw_u [mm]**	V_{mes} / V_{cal}	**Standard deviation**	**Coefficient of variation [%]**
$M = V \cdot d$	1.0	1.39	0.39	28.0
$M = V \cdot (a - 1.5d)$	2.2	1.38	0.37	27.2
$M = V \cdot a$	3.5	1.38	0.38	27.4

Table 7-1 Alternative values for the critical crack width at different moment locations for members without transverse reinforcement

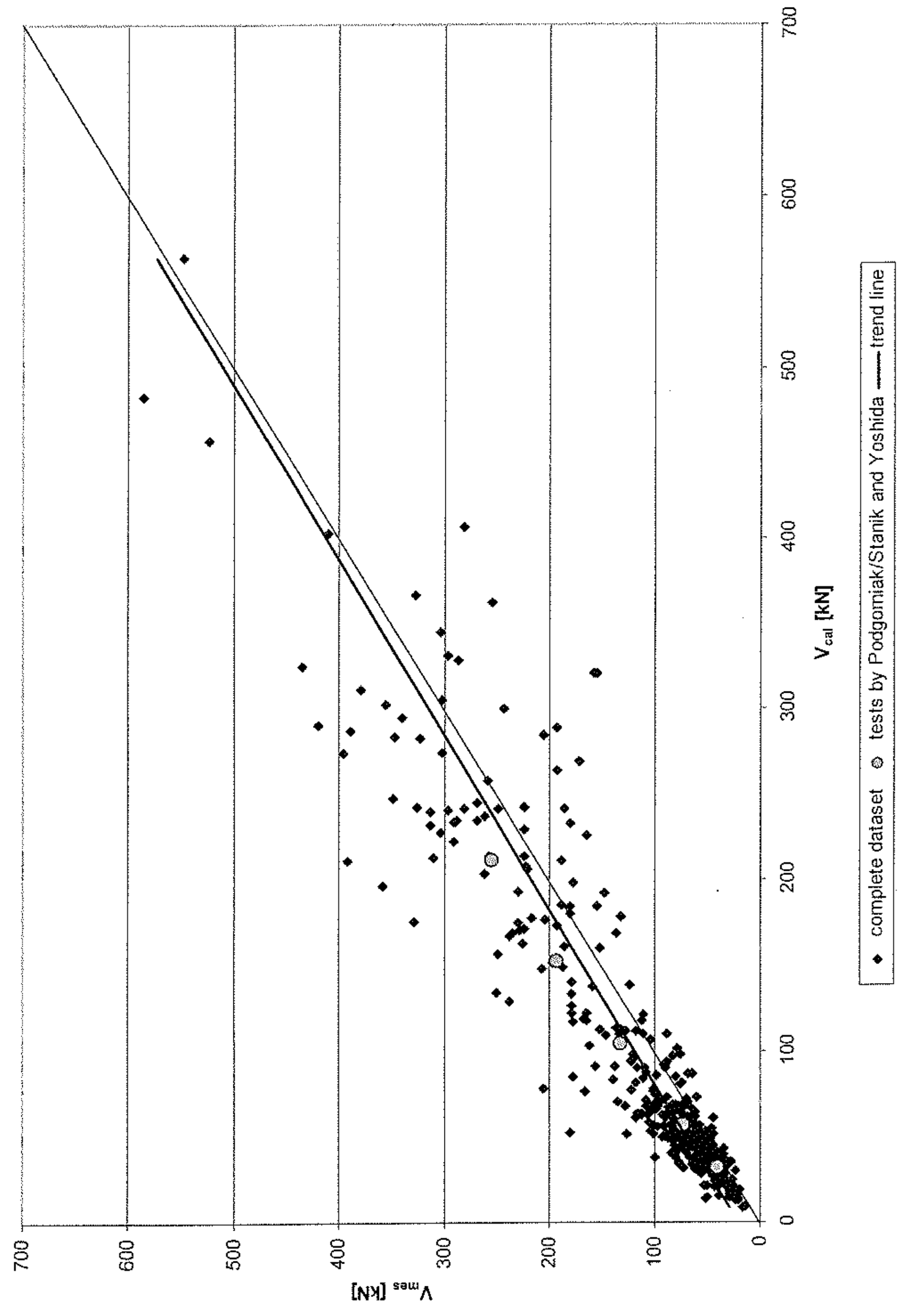

Figure 7-5 Measured versus calculated shear strength for slender and deep members without transverse reinforcement

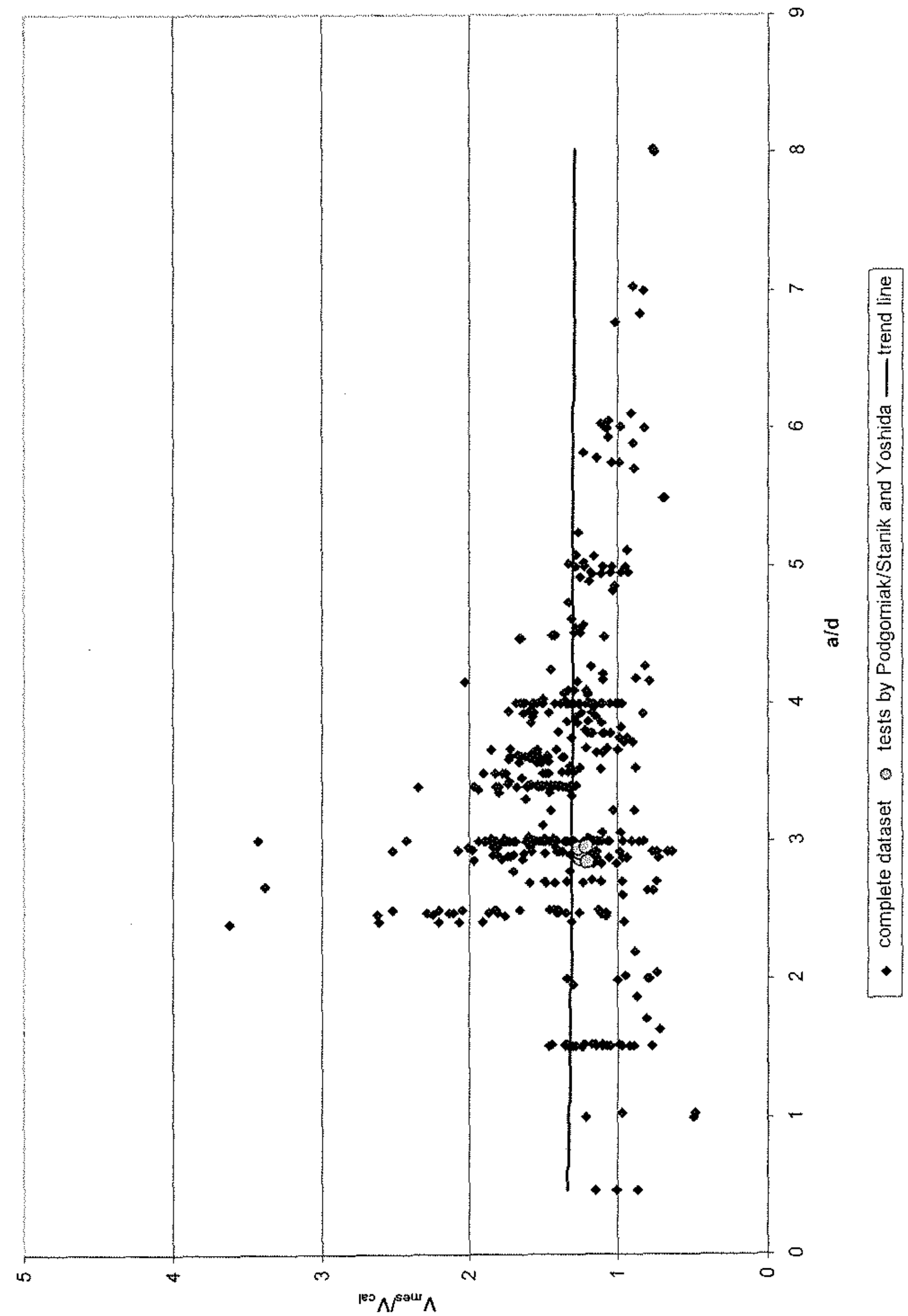

Figure 7-6 Ratio of measured to calculated shear strength versus aspect ratio for deep and slender beams without web reinforcement

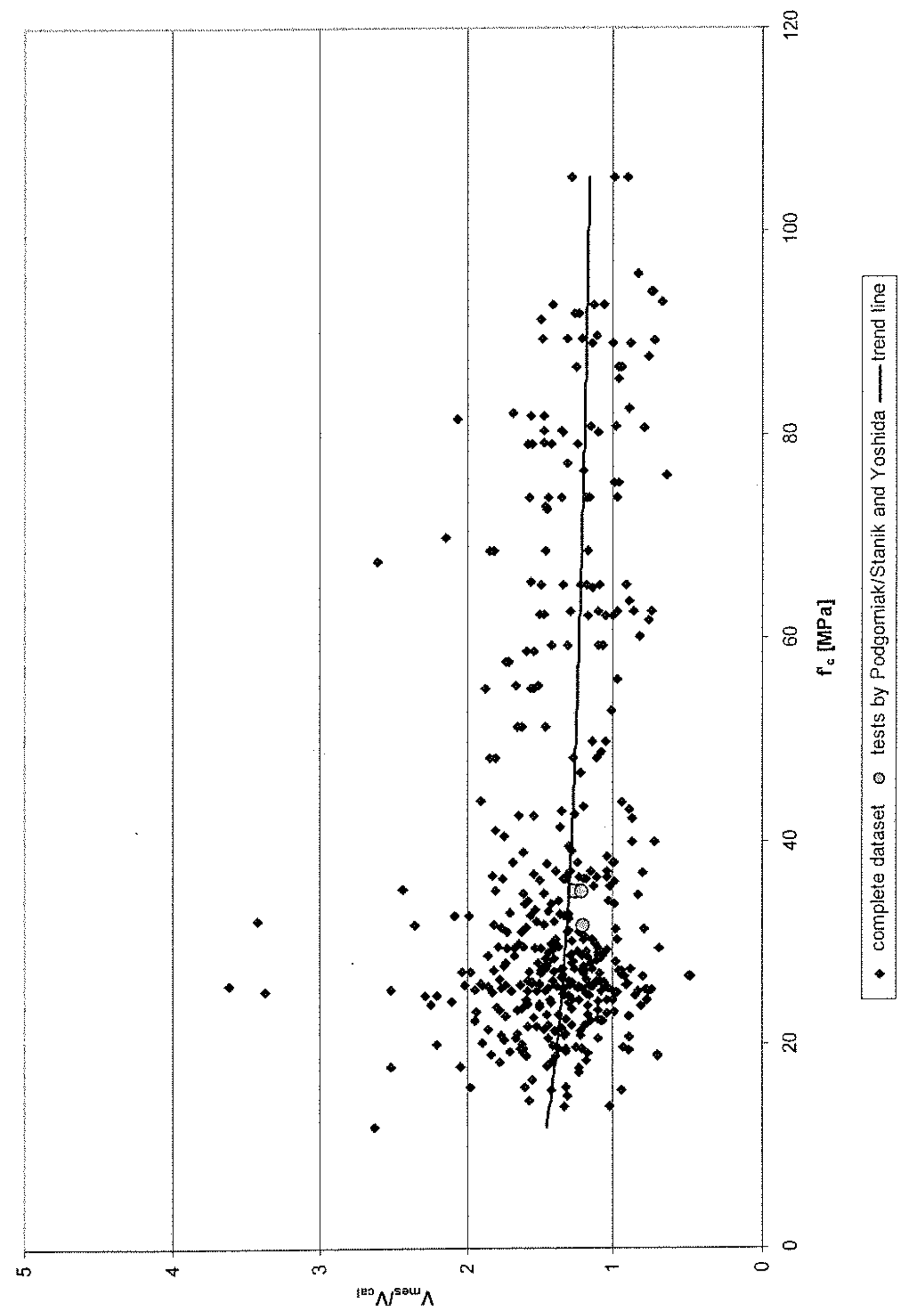

Figure 7-7 Ratio of measured to calculated shear strength versus concrete compressive strength for deep and slender beams without web reinforcement

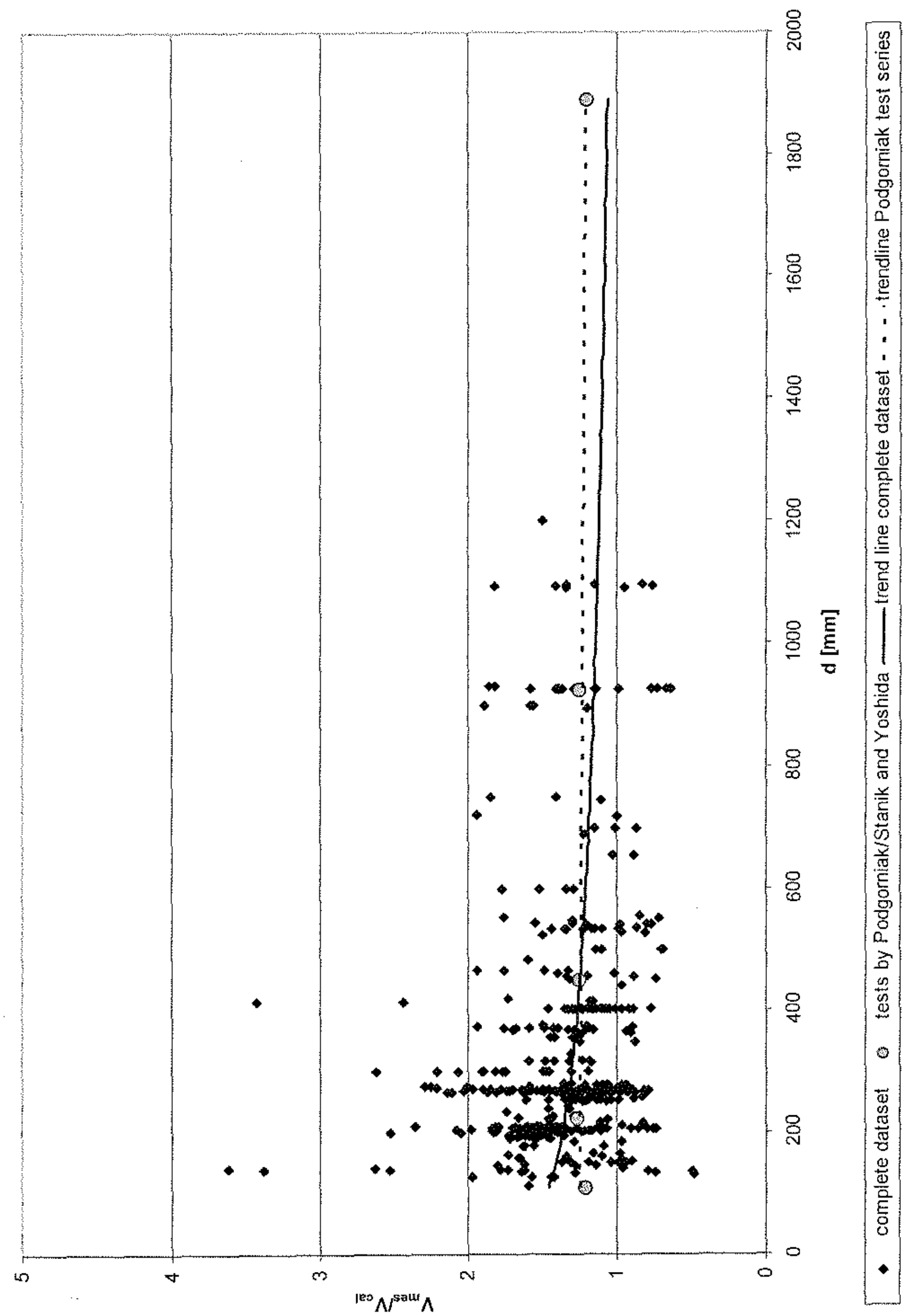

Figure 7-8 Ratio of measured to calculated shear strength versus effective depth for deep and slender beams without web reinforcement

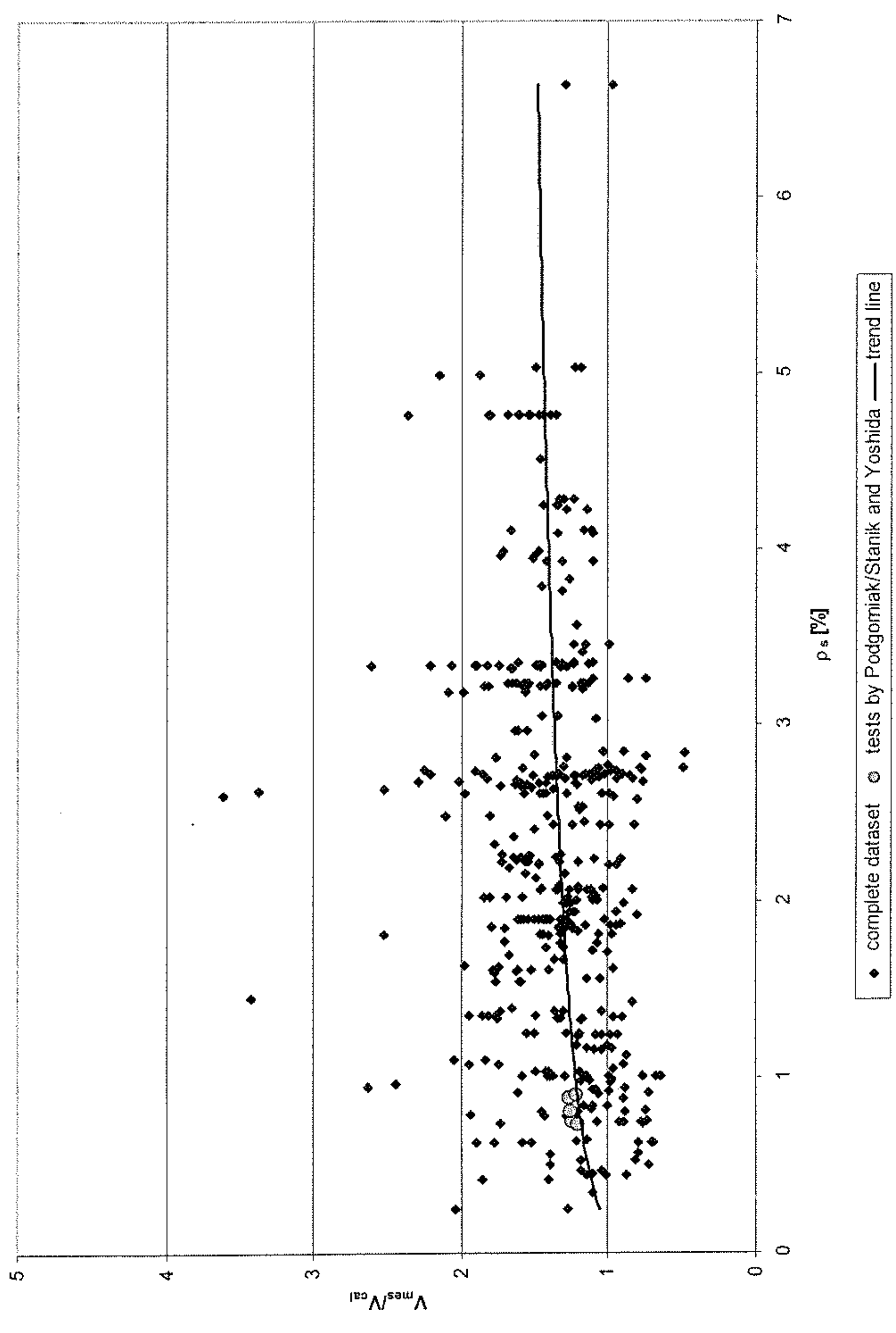

Figure 7-9 Ratio of measured to calculated shear strength versus tensile reinforcement ratio for deep and slender beams without web reinforcement

7.2 Members with transverse reinforcement

Members with web-reinforcement can be handled in a similar way as members without transverse reinforcement. Aside from the contributing concrete and arch-components, the term for the truss was added, yielding the calculated shear strength as previously given:

$$V_n = V_a + V_t + \left(V_{cz} + V_f\right) \qquad \text{((5.1) Repeated)}$$

The form of the expressions for the contributions of friction, uncracked compression zone, and arch-action remains equal to the ones described in the previous section. For simplicity, it was tried to keep most of the coefficients within the equations for arch- and concrete contribution as in the case of RC members without transverse reinforcement. However, introducing truss action to the shear resisting mechanisms of the member results in a different distribution of internal stresses within the member. The calibration made it necessary to change some of the parameters to account for the changed distribution of stresses. Mainly the coefficients in the transition functions (5.15) and (7.1) were changed. This and other changes will be listed later in this section.

Deep members as deep beams and walls are often reinforced with horizontal and vertical web reinforcement. Accordingly, the general term for V_t has to be changed depending on the considered geometry. In addition, the stresses in the inclined compression field induced by the truss interact with the stresses in the inclined strut representing arch-action. If it is assumed that the truss develops its full strength, the allowable stresses in the arch need to be reduced.

7.2.1 Deep members with horizontal and vertical web reinforcement

7.2.1.1 Deep beams

Arch action

The shear capacity of deep beams consists of resistances from arch-action and truss action. Arch-action is represented by a direct strut from the applied shear force V to the support. The inclination of the arch is defined by the shear span, a, and the depth of the member, d. The general geometry for arch action within a deep beam is shown in Figure 7-10.

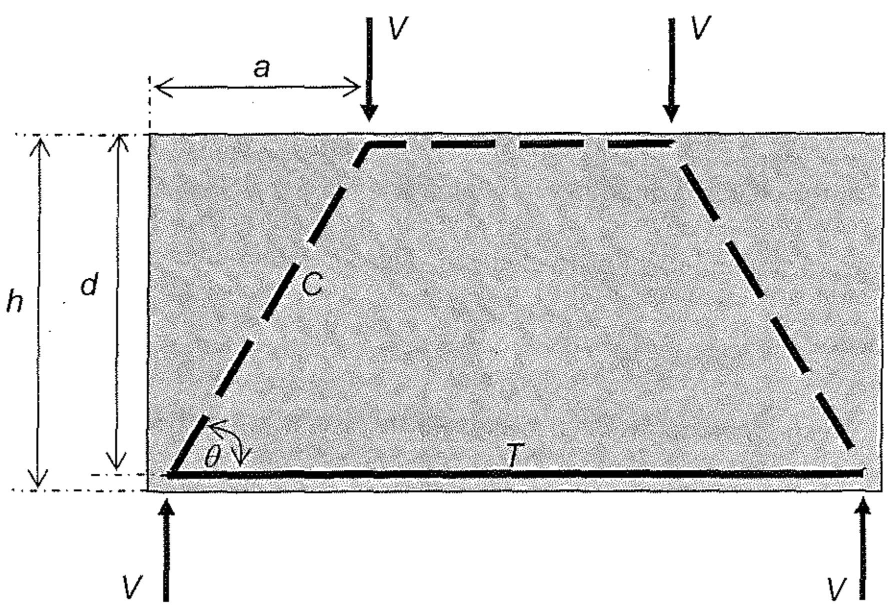

Figure 7-10 Geometry of a deep beam

The inclination of the strut is calculated by

$$\cot\theta = \frac{a}{d} \qquad \text{((5.14) Repeated)}$$

Without considering the transverse reinforcement, the strength of the arch was given before by equation (5.16):

$$V_a = \beta_n k_s f'_c \cdot w \cdot b \cdot \sin\theta \qquad \text{((5.16) Repeated)}$$

The concrete strength related reduction-parameter β_n for the nodal strength is independent of possible transverse reinforcement. Therefore, it is taken as previously derived for equation (5.6). However, the coefficients in the factor for the transition from slender to deep members, k_s, need to be altered, because the internal stress distribution changes by adding transverse reinforcement. The form of k_s is kept constant.

The width of the strut is calculated in the same way as described for members without transverse reinforcement in Section 7.1.2.1.

Truss action

The capacity of the truss within a deep member is calculated according to Chapter 5.2.2 by

$$V_t = \rho_w f_{wy} b \cdot jd \cdot \cot\phi \qquad \text{((5.23) Repeated)}$$

Attention, though, has to be paid to the inclination of the compression field. Figure 7-11 shows the geometry for truss action in a deep member with vertical web reinforcement.

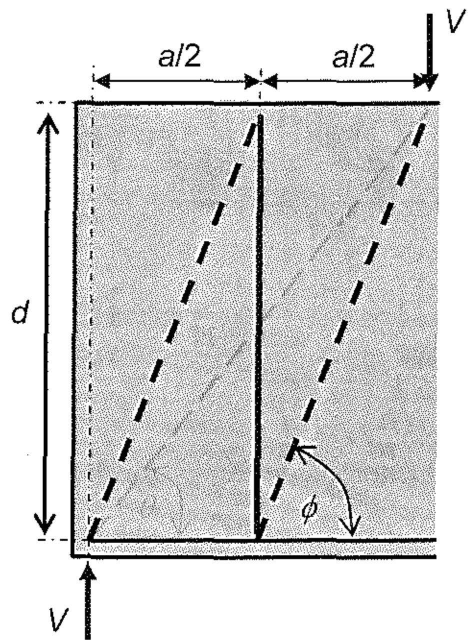

Figure 7-11 Geometry of a vertical truss in a deep beam

The strength of the stirrups is assumed to be bundled in one stirrup at a location $x = a/2$. It is apparent that truss action can only fully develop if the inclined compression field lies within the member, which is only possible if the steel is to act in the center of the section, with the inclination of the compression field given by

$$\cot\phi = \frac{a}{2d} \tag{7.10}$$

with $\theta \le \phi$

The limit of $\theta < \phi$ is set by geometry. If the inclination of the truss-induced compression field, ϕ, becomes smaller than the arch inclination, θ, it is not defined by the shear-span-to-depth ratio anymore, but becomes variable as in a slender member.

It should be noted that it appears justified to use the depth of the member to calculate the capacity in a deep member, because distinct tension and compression zones do not develop. For deep beams, equation (5.23) thus becomes for members with vertical web reinforcement:

$$V_{t,v} = \rho_w f_{wy} b \cdot d \cdot \cot\phi \tag{7.11}$$

Similar to the vertical truss, the geometry of horizontal web reinforcement is depicted in Figure 7-12. It is convenient to introduce a new angle, ψ, for the inclination of the compression field resulting from the horizontal truss.

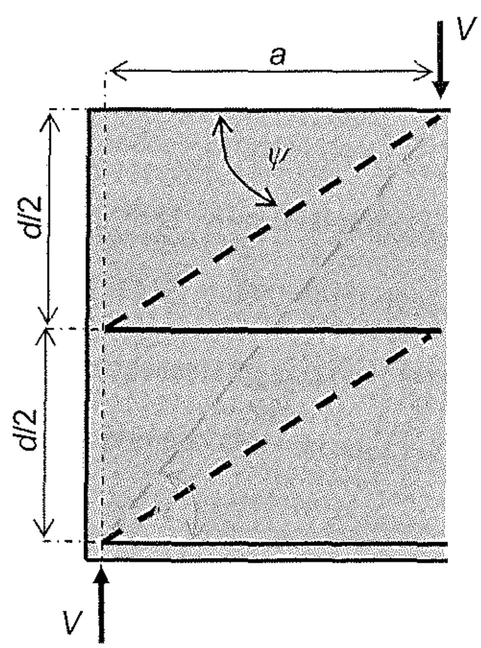

Figure 7-12 Geometry of a horizontal truss in a deep beam

Following Figure 7-12, the inclination of the compression field resulting from horizontal web reinforcement can be calculated as

$$\cot\psi = \frac{2a}{d} \tag{7.12}$$

with $\theta \geq \psi$

Using this angle, the capacity of the horizontal truss is calculated similar to the vertical truss (Section 5.2.2.1) as

$$V_{t,h} = \rho_w f_{wy} b \cdot d \cdot \tan\psi \tag{7.13}$$

The stress in the inclined compression field is given by

$$f_{t,h} = \frac{\rho_h f_{hy}}{\cos^2\psi} \tag{7.14}$$

Combined truss and arch action

If truss- and arch-mechanisms act simultaneously, both mechanisms place a demand on the concrete under compression. In the following, it is assumed that the truss mechanism, as the most reliable shear-carrying mechanism, develops its full capacity. The allowable remaining fraction of the concrete compressive strength can be determined as follows:

Both contributing mechanisms rely on compressive stresses in terms of f_t and $\beta_n f'_c$, for truss and arch components, respectively. The stress f_t is the stress in the diagonal compression field of the truss as defined by eqs. (5.25) and (7.14). The equivalent compressive stress in the arch is the effective compression strength, $\beta_n f'_c$. The contribution of the vertical truss component can be expressed as a function of the fraction of the effective compression strength:

$$R_v = \frac{f_{t,v}}{\beta_n f'_c} \tag{7.15}$$

Where $f_{t,v}$ = stress in the compression field resulting from vertical web reinforcement.

The resistance factor R_v is related to two limitations to the shear-carrying mechanisms:

1) If $f_{t,v} \geq \beta_n f'_c$, the stresses in the inclined compression field exceed the allowable compressive stresses. Accordingly, the contribution from the truss has to be lowered by the fraction that the stresses exceed the capacity. Therefore, V_t has to be reduced by the inverse of the R_v:

$$\frac{\beta_n f'_c}{f_{t,v}} \leq 1.0 \tag{7.16}$$

2) If R_v is viewed at as a resistance factor related to the truss, R_a could be defined as a resistance factor related to arch action. It is sensible to take the sum of resistances as unity (Hwang et al. 2001).

$$R_v + R_a = 1 \tag{7.17}$$

Solving for R_a gives the allowable relative resistance the arch can provide without exceeding the effective compressive strength of concrete in the arch and truss:

$$R_a = 1 - \frac{f_{t,v}}{\beta_n f'_c} \tag{7.18}$$

This factor is in agreement with the term (3.10) described by Watanabe (Watanabe and Ichinose 1991).

Similarly, the relative resistance can be derived for the contribution of a horizontal truss. If the horizontal truss in the deep beam is assumed to develop its full capacity independent of the vertical truss, a resistance fraction can be formulated as

$$R_h = \frac{f_{t,h}}{\beta_n f'_c} \tag{7.19}$$

with $f_{t,h}$ = stress in the compression field resulting from horizontal web reinforcement.

Setting the sum of all three relative resistances equal to unity gives

$$R_a + R_v + R_h = 1 \tag{7.20}$$

Equation (7.20) can be solved for the allowable resistance of the arch, R_a, by calculating the resistance ratios of the vertical truss relative to the arch, and of the horizontal truss relative to the arch mechanism:

$$\frac{R_v}{R_a} = \frac{f_{t,v}}{\beta_n f'_c \left(1 - {f_{t,v}}/{\beta_n f'_c}\right)} \tag{7.21}$$

$$\frac{R_h}{R_a} = \frac{f_{t,h}}{\beta_n f'_c \left(1 - {f_{t,h}}/{\beta_n f'_c}\right)} \tag{7.22}$$

Solving equations (7.20), (7.21) and (7.22) for R_a yields the necessary reduction of the arch contribution due to truss induced compressive stresses:

$$R_a = \frac{\left(\beta_n f'_c - f_{t,h}\right)\left(\beta_n f'_c - f_{t,v}\right)}{\left(\beta_n f'_c\right)^2 - f_{t,h} f_{t,v}} \tag{7.23}$$

Equation (7.23) is the general form for the reduction of the arch if truss action is added. For the case that no horizontal web reinforcement is present, eq. (7.23) becomes equal to (7.18) with $f_{t,h} = 0$.

Following this, the shear capacity of the arch in a deep beam is calculated by reducing the general equation for arch action (5.16) by R_a:

$$V_a = R_a \beta_n k_s f'_c \cdot w \cdot b \cdot \sin\theta \tag{7.24}$$

7.2.2 Calibration of the components

Contributing components

The shear strength of deep and slender RC members with web reinforcement is calculated from a modification of equation (5.1):

$$\begin{aligned} V_n &= V_a + V_t + k_c V_c \\ V_n &= V_a + V_t + k_c\left(V_{cz} + V_f\right) \end{aligned} \tag{7.25}$$

The general forms of the components in equation (5.1) were given previously as

$$V_a = R_a \beta_n k_s f'_c \cdot w \cdot b \cdot \sin\theta \qquad \text{((7.24) Repeated)}$$

with the variable parameter k_s for the transition from deep to slender members

$$k_s = \frac{x}{y + z\left(a/d\right)^w} \qquad \text{((5.15) Repeated)}$$

The contribution of the vertical truss was derived previously as

$$V_{t,v} = \rho_{w,v} f_{wy,v} b \cdot jd \cdot \cot\phi \qquad \text{((5.23) Repeated)}$$

Similarly, the contribution of the horizontal truss is

$$V_{t,h} = \rho_{w,h} f_{wy,h} b \cdot jd \cdot \tan\psi \qquad \text{((7.13) Repeated)}$$

with:

$\rho_{w,v} = \dfrac{A_{s,v}}{b \cdot s} =$ ratio of transverse reinforcement in the vertical direction

$f_{wy,v}$ = yield strength of vertical web reinforcement

$\rho_{w,h} = \dfrac{A_{s,h}}{b \cdot s} =$ ratio of transverse reinforcement in the horizontal direction

$f_{wy,h}$ = yield strength of horizontal web reinforcement

s = spacing of stirrups in the direction considered

As mentioned before, for deep beams it is appropriate to use the full effective depth d instead of the internal lever arm jd. Furthermore, during the calculation the stresses in the inclined compression fields, $f_{t,v}$, and $f_{t,h}$, need to be monitored. If f_t exceeds the allowable effective compressive strength of concrete, $\beta_n f'_c$, V_t has to be reduced by the ratio of effective concrete strength to truss-induced stress in the compression field (eq. (7.16)).

The concrete strength related components apply for slender members only. The contribution of the uncracked compression zone was given previously by equation (5.38):

$$V_{cz} = D \cdot \sqrt[3]{f'_c} \cdot b \cdot kd \qquad \text{((5.38) Repeated)}$$

The constant D was previously found in the calibration of the proposed model for members without transverse reinforcement as $D = 0.5$. Since adding transverse reinforcement does not change the state of stresses in the compression zone considerably, this value should not change drastically. The calibration on members with transverse reinforcement yielded $D = 0.4$.

The friction-related component V_f was derived in Section 5.2.3.2, page 156, as equation (5.41)

$$V_f = \tau_{fu} \cdot b \cdot (d - kd) \qquad \text{((5.41) Repeated)}$$

with
$$\tau_{fu} = const \cdot f_{ct} \left(1 - \frac{\Delta w}{\Delta w_u}\right) \qquad \text{((5.40) Repeated)}$$

in which
$$f_{ct} = \sqrt[3]{f'_c}$$

$$\Delta w_u = \frac{0.5 \cdot \varepsilon_s \cdot s_{cr}}{\sin\phi_{cr}\left(1 - 0.336\cot\phi_{cr}\right)} + \frac{0.01 \cdot \cot\phi_{cr}}{1 - 0.336 \cdot \cot\phi_{cr}} \text{ [mm]} \qquad \text{((5.47) Repeated)}$$

$$s_{cr} = C(d - kd) \qquad \text{((5.32) Repeated)}$$

As for the members without transverse reinforcement, the constant C influencing the critical crack spacing has to be found from the calibration. For simplicity, this value was kept constant for the two different cases.

The concrete contributions V_{cz} and V_f in eq. (7.25) need to be adjusted for the transition from deep to slender members by a factor

$$k_c = 1 + \frac{1}{x + y\left(a/d\right)^{w}} \geq 0 \qquad \text{((7.1) Repeated)}$$

Database of deep and slender beams

The database for the calibration of the model for deep and slender members with web reinforcement was comprised from the open literature. It consists of 168 slender members with vertical web reinforcement, which were taken from (Chen and MacGregor 1993; Zararis 2003). This data was extended by 146 deep beams previously investigated by Matamoros and Wong (Matamoros and Wong 2003). 66 of these deep beams had solely vertical transverse reinforcement. A member was considered a deep beam in the latter database if the shear-span-to-depth ratio was below 2.5. Accordingly, members in the database of slender beams had an aspect ratio exceeding $a/d = 2.5$. The maximum aspect ratio considered was $a/d = 7$. Both databases are provided in Appendices A3 and A4 and the worksheets "Slender beams with web reinforcement", and "Reinforced deep beams" on the accompanying CD, respectively.

The proposed model was calibrated on the combined database of slender beams and deep beams with vertical web reinforcement. Subsequently, it was verified on the complete database of deep beams. The contributions of V_{cz} and V_f were neglected for deep beams.

7.2.3 Calibration for slender and deep beams

The database comprising 168 slender beams and 66 vertically web-reinforced deep beams was calibrated to the components listed in the previous section.

The strut width of the arch in deep beams was calculated as for deep members without transverse reinforcement from the support conditions by equation (5.13)

$$w = h_a \cdot \cos\theta + l_b \cdot \sin\theta \qquad \text{((5.13) Repeated)}$$

Since no data was available for the size of the loading plates of the slender members, the strut width of the arch in slender members was determined by equation (7.9)

$$w = \min\{h_a, kd\} \cdot \cos\theta \qquad \text{((7.9) Repeated)}$$

Nonlinear regression analysis yielded the following coefficients in the various parameters:

The concrete contribution in slender members was found to be

$$V_c = 0.4 \cdot f_{ct} \cdot b \cdot kd + 0.4 \cdot f_{ct} \cdot b \cdot (d - kd)\left(1 - \frac{\Delta w}{\Delta w_u}\right) \qquad (7.26)$$

with

b = width of the beam

kd = depth of the neutral axis from flexural linear analysis

The best fit for the other parameters yielded:

$$f_{ct} = \sqrt[3]{f'_c}$$

$$\Delta w_u = 1.0 \text{ mm}$$

$$\Delta w = \frac{0.5 \cdot \varepsilon_s \cdot s_{cr}}{\sin 30^\circ \left(1 - 0.336 \cot 30^\circ\right)} + \frac{0.01 \cdot \cot 30^\circ}{1 - 0.336 \cdot \cot 30^\circ} \text{ [mm]}$$

$$s_{cr} = (d - kd) \text{ [mm]}$$

$$\varepsilon_s = \frac{V \cdot d}{\rho_s \cdot bd \cdot jd \cdot E_s}$$

Therefore, the parameters that are related to critical crack width and to critical spacing remained constant compared to the equivalent values for deep and slender members without transverse reinforcement (Section 7.1.2.2).

The coefficients related to the transition from deep members to slender members were changed due to the changed relation of stresses in the member. Adding truss-induced stresses changes the relation between arch component and the V_c term, because the arch component is reduced by R_a. The curve fit for the examined data yielded

$$k_s = \frac{4.6}{6.5 + 0.13\left(a/d\right)^5} \qquad (7.27)$$

During the calibration, it was tried to keep the form of k_s such that $k_s = 1$ for a theoretical value of $a/d = 0$. However, this seemed to impose an unconservative trend on the calculated shear strength. A possible explanation for lowering the initial value for k_s might be that the inclined stresses in the arch are not directed in the same direction as the inclined stresses induced by truss action. This could possibly weaken the strut due to a two-axial state of stresses in the arch.

The parameter for the contributions of V_{cz} and V_a in eq. (7.25) was found as

$$k_c = 1 - \frac{1}{0.1 + 0.01(a/d)^5} \geq 0 \tag{7.28}$$

Figure 7-13 shows a plot of the two transition functions against the shear-span-to-depth ratio. The transition function related to the strut, k_s, has an initial value of 0.71 and becomes negligible at approximately $a/d = 3.5$ as it approaches the x-axis asymptotically. This means arch action had no effect for aspect ratios exceeding this value. The transition function for the shear-resistance contributions related to the development of distinct tension and compression zones, k_c, starts at an initial aspect ratio of $a/d = 2.46$. From this point onward, the function increases rapidly until it becomes infinitely close to one at aspect ratios of approximately $a/d = 6$.

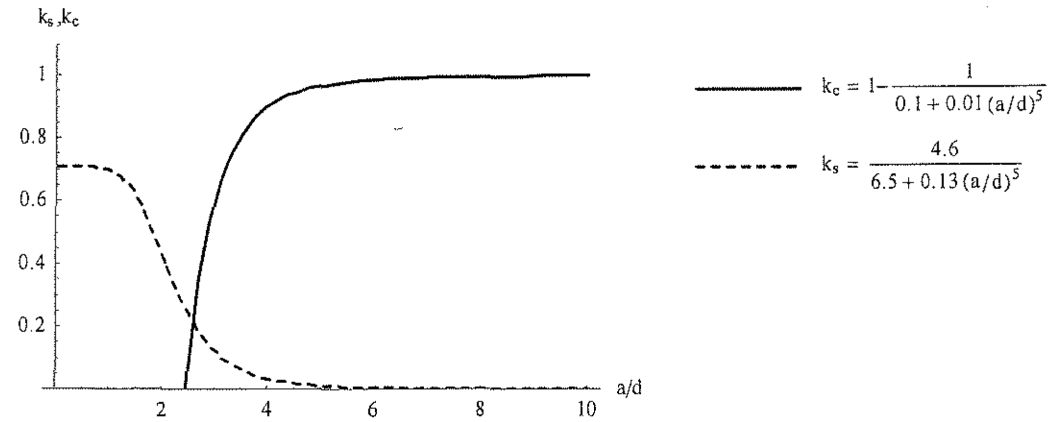

Figure 7-13 Reduction functions related to aspect ratio, web reinforced members

Using the parameters as listed above gave an average value of measured to calculated shear strength of the 243 considered beams of 1.16 ± 0.13 % within a 95 percent confidence interval. The coefficient of variation for the examined data was 14.25 percent with a standard deviation of 0.16. The subset of sole slender beams had a mean value of V_{mes}/V_{cal} = 1.14 ± 0.2 % within a 95 percent confidence interval, and a coefficient of variation of 14.67 % with a standard deviation of 0.17. The subset of deep beams with vertical web reinforcement yielded a mean value of V_{mes}/V_{cal} = 1.22 ± 0.41 % within a 95 % confidence region. The coefficient of variation was 12.1 % at a standard deviation of 0.15.

Figure 7-14 shows a plot of measured to calculated shear strength for all slender and deep beams with vertical web reinforcement. The bold trend line does not show any distinct trend and represents the mean value well. Three of the examined beams show considerably higher measured shear strength than their respective calculated strength. These beams were tested by Roller and Russell (specimens 1, 8, and

9), and were pointed at in the respective publication (Roller and Russell 1990). High strength concrete with f'_c =120.2 for specimen 1, and 125.4 MPa for specimens 8 and 9 was used, while the tensile reinforcement ratio was relatively low at 1.65, 1.88, and 2.35 %, respectively. As mentioned by Roller and Russell, specimens 1 and 8 were reinforced with approximately the minimum amount for web reinforcement required by the ACI-318-83 code; specimen 9 had approximately twice the amount of required transverse reinforcement. The code requirements have changed following the investigation by Roller and Russell, making the minimum required amount of transverse reinforcement a function of the compressive strength of concrete (ACI-318-02, Section 11.1.2). Specimens 1, 8, and 9 do not satisfy the current code provision (ACI-318 2002), and are therefore not considered representative in the work at hand.

The ratio of measured to calculated shear strength versus shear-span-to-depth ratio is shown in Figure 7-15. No trend is discernible as indicated by the trend line running almost parallel to the x-axis at the average value of V_{mes}/V_{cal}. As it was seen before for the beams without transverse reinforcement, scatter was higher around a/d = 3. This can again be attributed to the transition from deep to slender members. It can as well be attributed to the fact that the majority of tested beams fell in this range, thus naturally increasing scatter within this range.

The same can be seen again in Figure 7-16, plotting the ratio of measured to calculated shear strength against the compression strength of concrete. While again it is obvious that the scatter was largest in the range in which the compressive strength of the majority of tested beams fell, no distinct trend can be seen. It is possible that the three previously mentioned specimens tested by Roller and Russell (Roller and Russell 1990) introduced a small amount of bias towards high strength concrete. Aside from these beams, specimens with concrete strengths up to 120 MPa followed the trend line parallel to $V_{mes}/V_{cal} = 1$.

The ratio of measured to calculated shear strength is plotted against the effective depth d in Figure 7-17. Relatively large scatter is visible in the range from approximately $d = 200$ to 400 mm. Due to common design practice, most of the tested specimens fell in this range. Since the scatter is on the conservative side, it is possible that it introduces the negative trend toward larger beam depths. Not enough data is available to make a statement about beams with depths exceeding 800 mm.

Figure 7-18 shows a plot of the ratio of measured to calculated shear strength versus the tensile reinforcement ratio, which is influencing the contributions from V_{cz} and V_f. The scatter that was visible as concentrated over certain ranges in the preceding graphs is now spread evenly over the examined range of $0.5 \le \rho_s \le 4.5$. Figure 7-18 is taken as an indicator that the contributions of uncracked compression zone and friction were calculated appropriately.

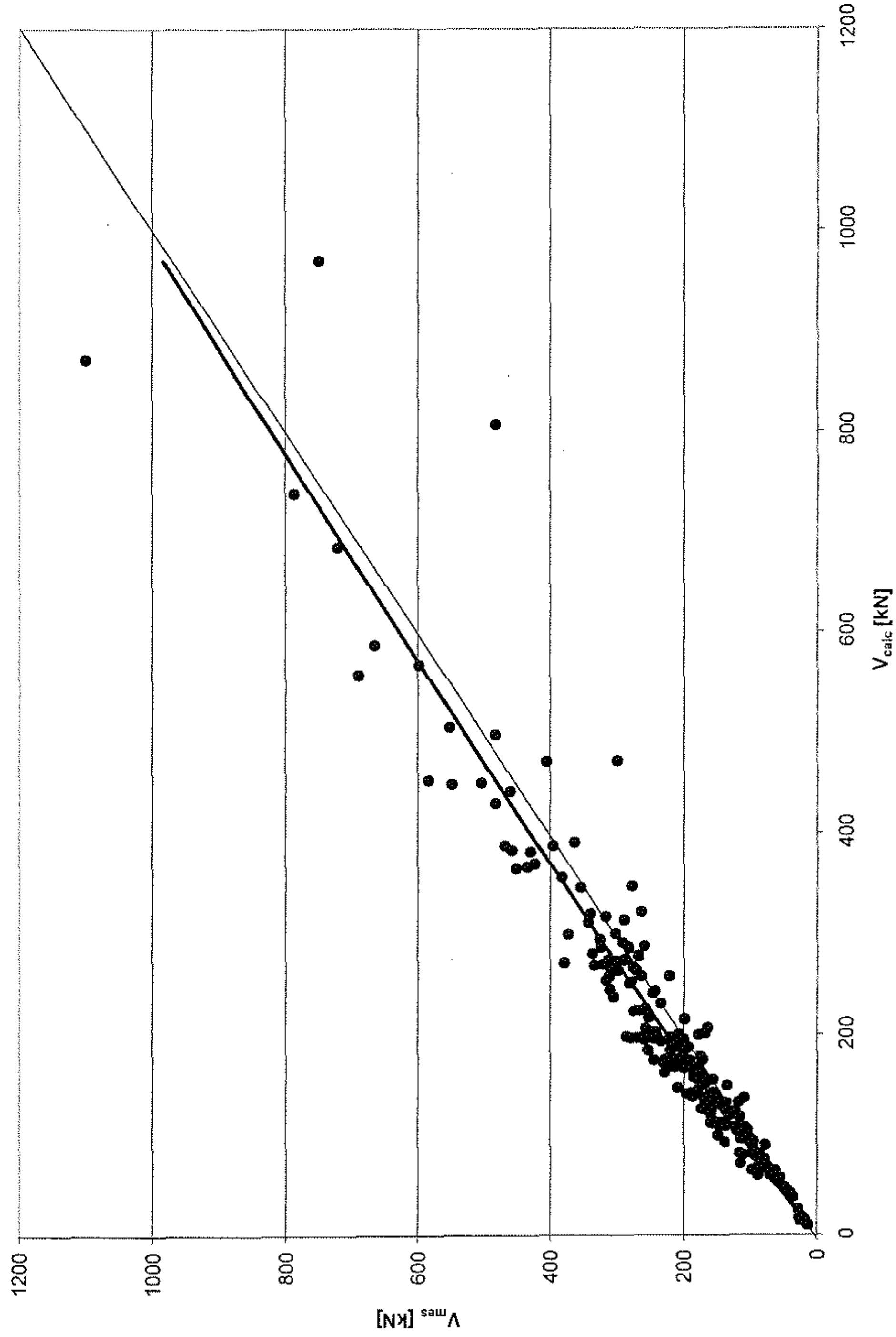

Figure 7-14 Measured versus calculated shear strength for slender and deep beams with vertical web reinforcement

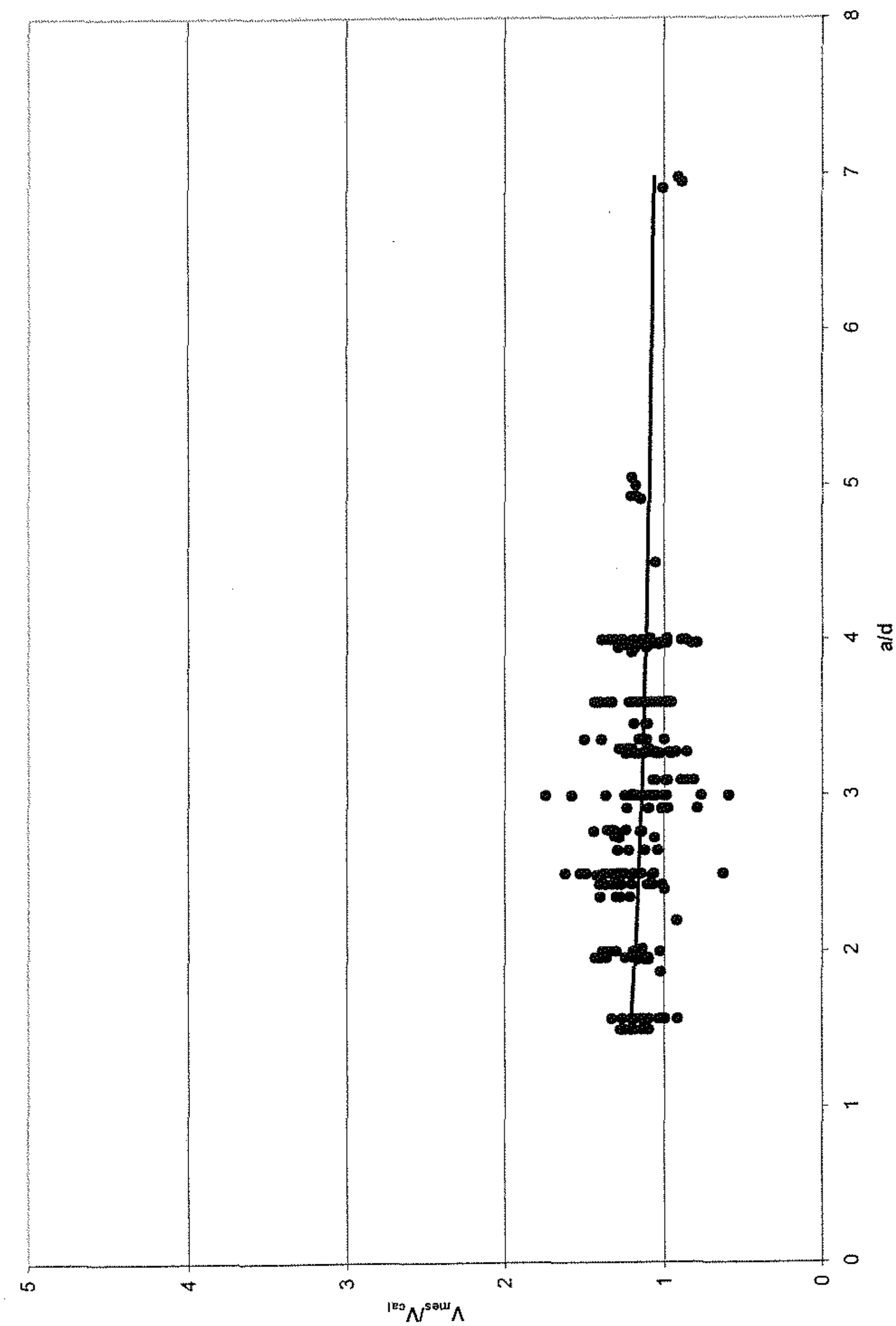

Figure 7-15 Ratio of measured to calculated shear strength versus aspect ratio, deep and slender beams with vertical web reinforcement

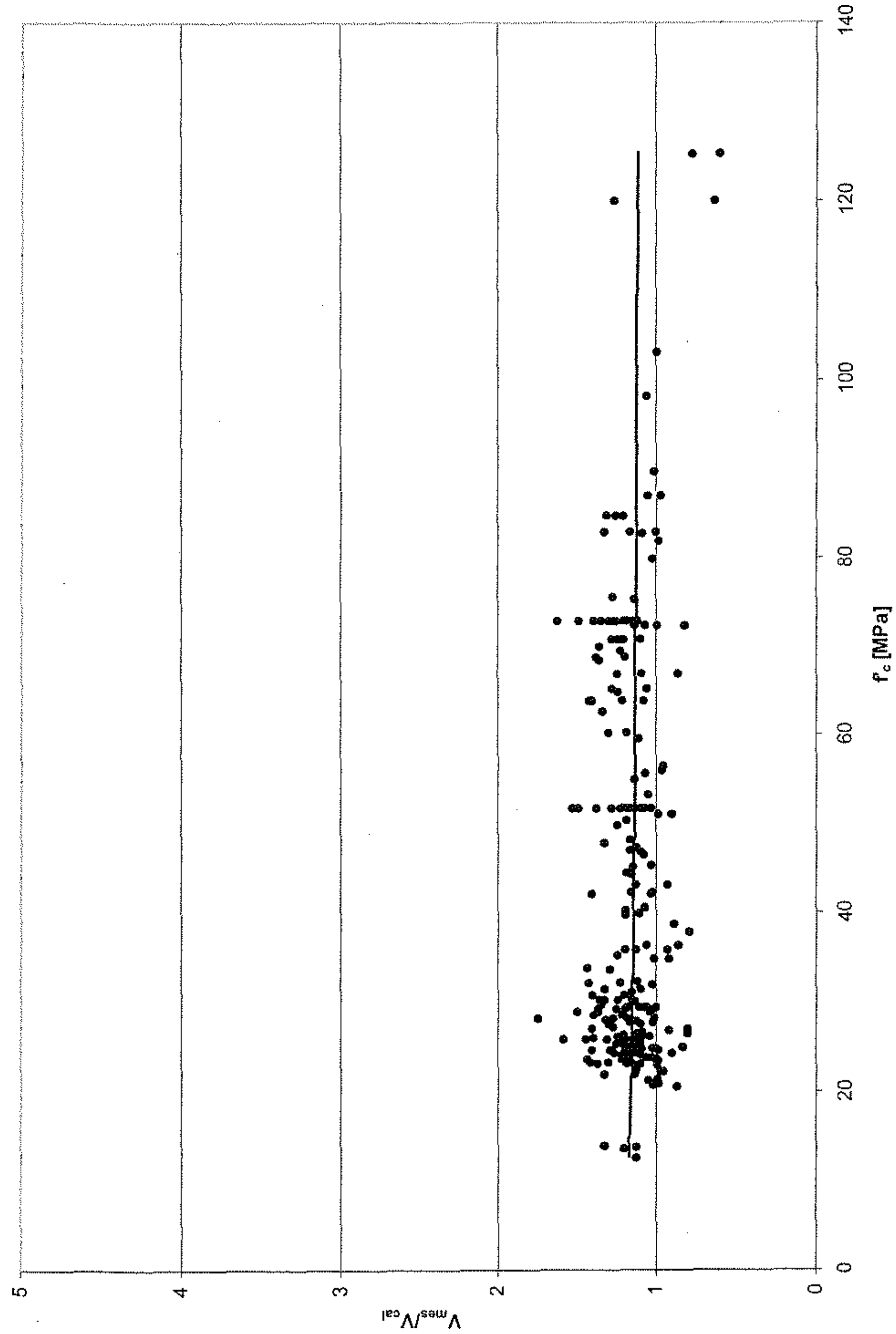

Figure 7-16 Ratio of measured to calculated shear strength versus concrete compressive strength, deep and slender beams with vertical web reinforcement

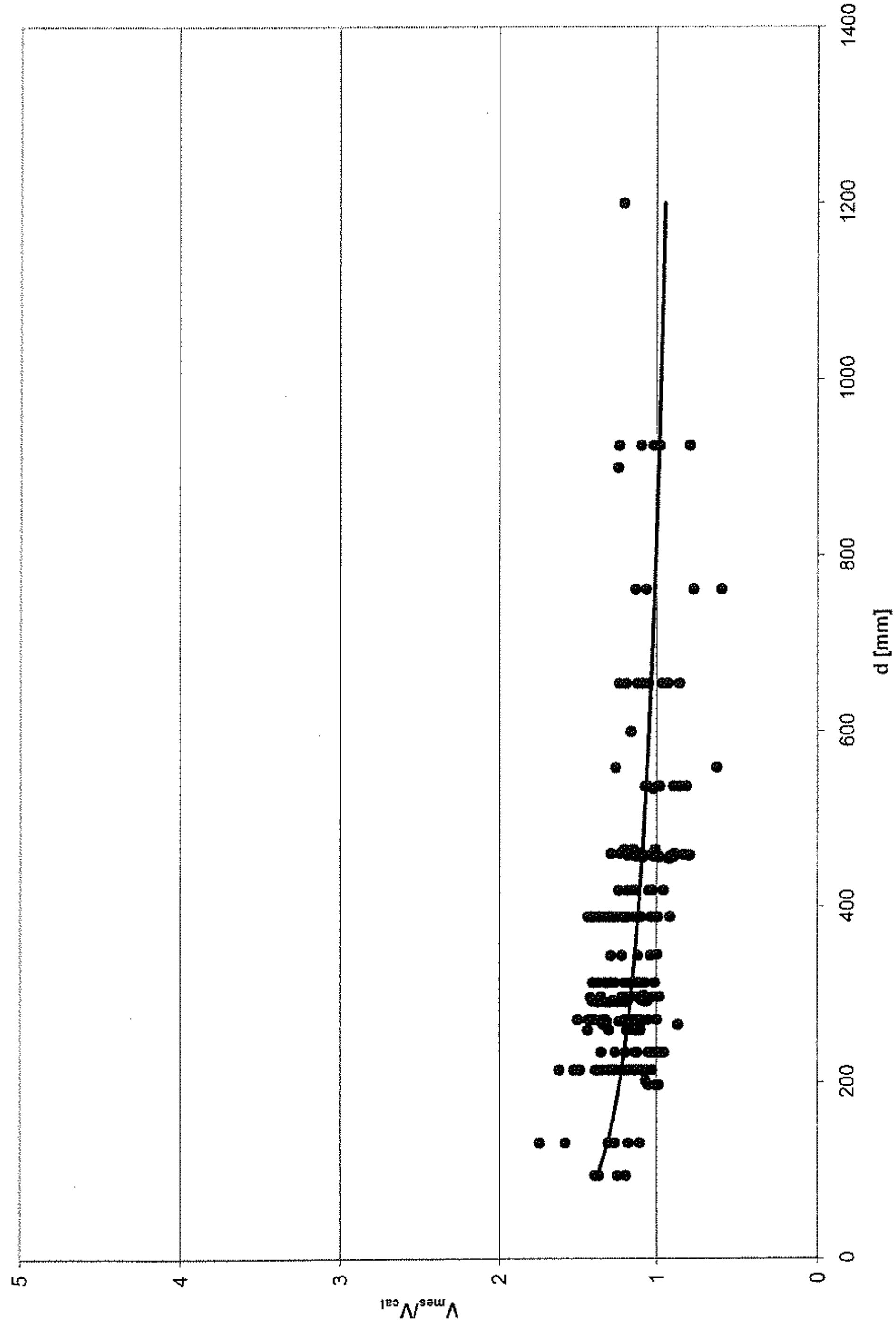

Figure 7-17 Ratio of measured to calculated shear strength versus effective depth, deep and slender beams with vertical web reinforcement

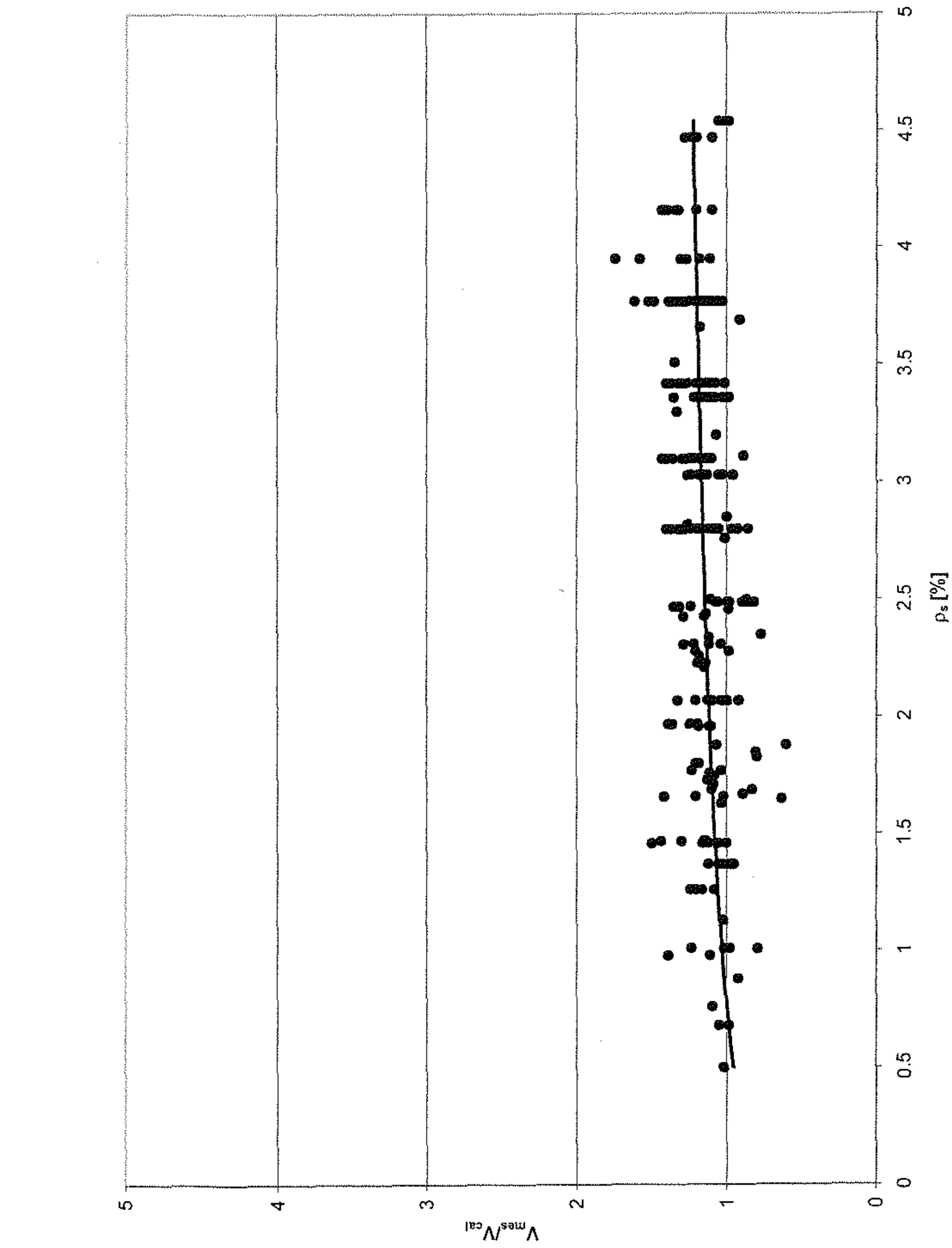

Figure 7-18 Ratio of measured to calculated shear strength versus tensile reinforcement ratio, deep and slender beams with vertical web reinforcement

7.2.4 Influence of critical section considered

As was described in the section on slender and deep members without transverse reinforcement (Section 7.1.3), the critical crack width Δw_u, calculated for the friction component V_f, is dependent on the location of the considered moment. In the calibration of the proposed model on the database described previously, the moment, and therefore the strain in the longitudinal reinforcement, was calculated at a distance d measured from the support. To account for varying crack geometries along the beam span, the critical crack width was calculated for different locations, summarized in Table 7-2. As before for the case of beams without web reinforcement, for simplicity Δw_u was taken as the sole variable. All other factors were kept constant with respect to the calibration for a moment location of $x = d$ measured from the support. Only slender members of the database were considered, since the friction contribution is neglected in deep members due to a lack of a distinct tension zone.

The study of the influence of the considered location for the calculation of strains in the longitudinal reinforcement gave the following values at the sections considered. Criterion was a comparable V_{mes}/V_{cal} ratio to ensure the same degree of safety for the model.

Moment	ϕ_{cr} [deg]	Δw_u [mm]	V_{mes} / V_{cal}	Standard deviation	Coefficient of variation [%]
$M = V \cdot d$	30	1.0	1.14	0.17	14.7
$M = V \cdot (a - 1.5d)$	30	1.7	1.14	0.17	14.6
$M = V \cdot a$	30	2.5	1.14	0.16	14.5

Table 7-2 Alternative values for the critical crack width at different moment locations for members with transverse reinforcement

7.2.5 Evaluation on deep beams and walls

The model as calibrated as before was evaluated on the "complete" database of deep beams and on a database for walls that reportedly failed in shear. The derived parameters were kept constant to verify their applicability on different datasets.

Different components need to be taken into account for deep beams and walls. Deep beams rely on arch action in interaction with horizontal and vertical truss mechanisms, walls rely on the same mechanisms and an additional contribution from the compression zone, which can be very distinct in walls as opposed to deep beams. This is described in Section 7.2.5.2. Furthermore, geometric definitions need to be adjusted to apply the model to walls, because the load is applied horizontally instead of vertically on deep beams.

7.2.5.1 Deep beams with horizontal and vertical reinforcement

The database for deep beams was taken from (Matamoros and Wong 2003). It includes 146 members with horizontal and vertical, and members with vertical web reinforcement only. Properties and computational results are listed in Appendix A4 and in the worksheet "Reinforced deep beams" on the accompanying data CD.

The shear capacity was calculated as the sum of arch- and truss mechanisms,

$$V_n = V_{t,v} + V_{t,h} + V_a \tag{7.29}$$

In which the truss components were calculated from equations (7.11) and (7.13):

$$V_{t,v} = \rho_w f_{wy} b \cdot d \cdot \cot\phi \qquad \text{((7.11) Repeated)}$$

$$V_{t,h} = \rho_w f_{wy} b \cdot d \cdot \tan\psi \qquad \text{((7.13) Repeated)}$$

Depending on the amount of stresses in the respective compression fields, the values were reduced by condition (7.16), if necessary.

$$\frac{\beta_n f'_c}{f_{t,v}} \leq 1.0 \qquad \text{((7.16) Repeated)}$$

The contribution of the arch was calculated from eq. (7.24)

$$V_a = R_a \beta_n k_s f'_c \cdot w \cdot b \cdot \sin\theta \qquad \text{((7.24) Repeated)}$$

With the reduction factors for interaction with the truss mechanisms, and for effective compressive strength, and the transition factors calculated from equations (7.23), (5.6), and (7.27), respectively.

$$R_a = \frac{\left(\beta_n f'_c - f_{t,h}\right)\left(\beta_n f'_c - f_{t,v}\right)}{\left(\beta_n f'_c\right)^2 - f_{t,h} f_{t,v}} \qquad \text{((7.23) Repeated)}$$

$$\beta_n = 0.85 - 0.004 f'_c \geq 0.5 \qquad \text{((5.6) Repeated)}$$

$$k_s = \frac{4.6}{6.5 + 0.13(a/d)^5} \qquad \text{((7.27) Repeated)}$$

Figure 7-19 shows the ratio of measured to calculated shear strength. The average value was V_{mes}/V_{cal} = 1.20 ± 0.24 % within a 95 percent confidence interval. The standard deviation was 0.16, resulting in a coefficient of variation of 12.98 %. As can be seen, the included trend line shows no discernible negative trend, running parallel to the line representing V_{mes}/V_{cal} = 1.0.

This is also true for the plot of the ratio of measured to calculated strength versus aspect ratio. Compared to the respective graph plotted for slender and deep beams (Figure 7-15), Figure 7-20 shows a scatter that is spread out more evenly over the full considered range of $0.2 \leq a/d \leq 2.5$.

The ratio of measured to calculated strength is plotted against the compressive strength of concrete in Figure 7-21. Again, the trend line is parallel to the gridline for V_{mes}/V_{cal} = 1. Figure 7-21 also indicates a larger amount of scatter at relatively low concrete strengths and at two distinct test series (Shin et al. 1999). For both series, the trend line represents the average of the test data accurately.

Figure 7-22 shows the ratio V_{mes}/V_{cal} plotted against the effective depth, d. As in the graphs before, the calculation yielded excellent results, that is, no trend is visible. The considered effective depths ranged from 216 to 940 mm with the whole range well represented in the test data.

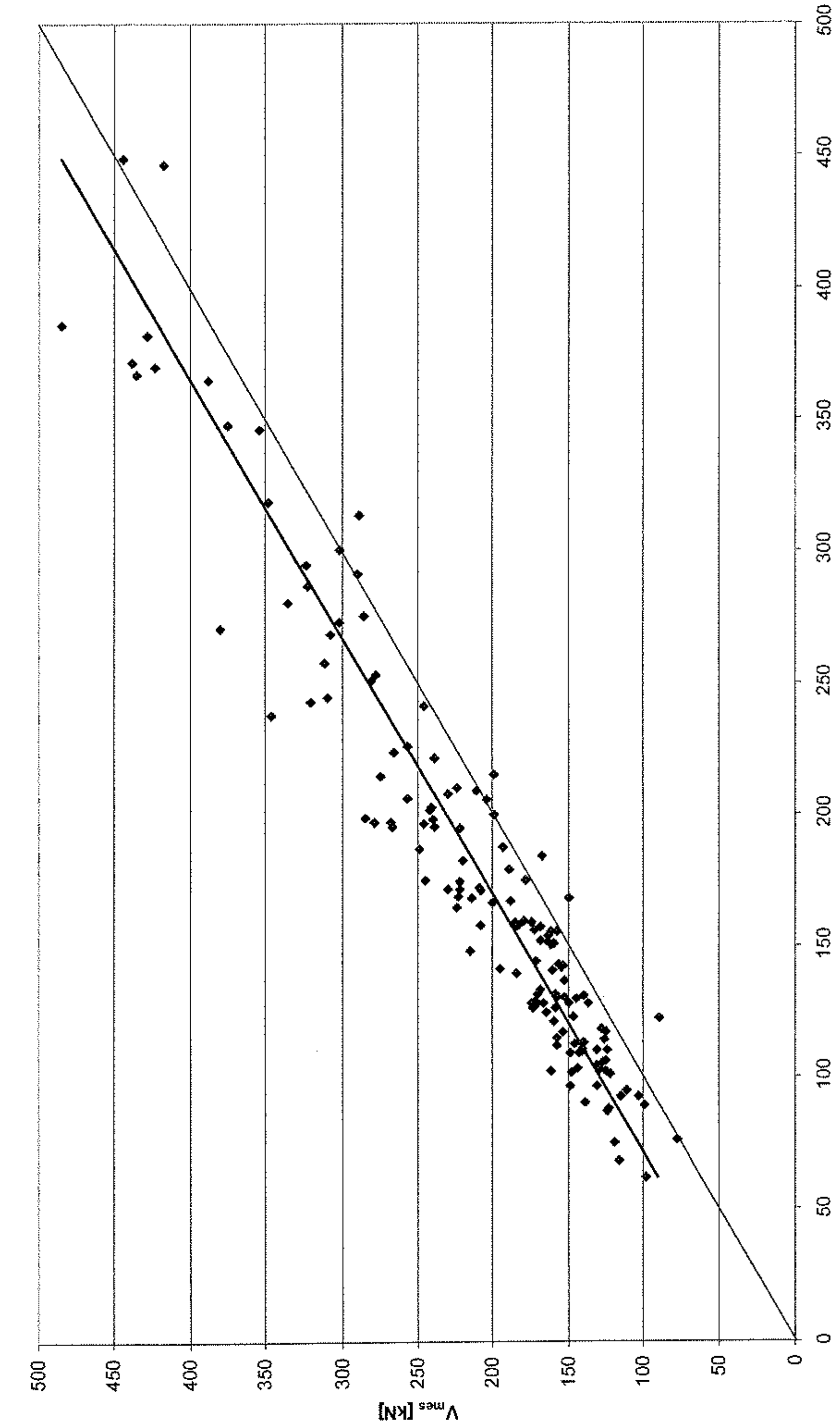

Figure 7-19 Measured versus calculated shear strength for deep beams with web reinforcement

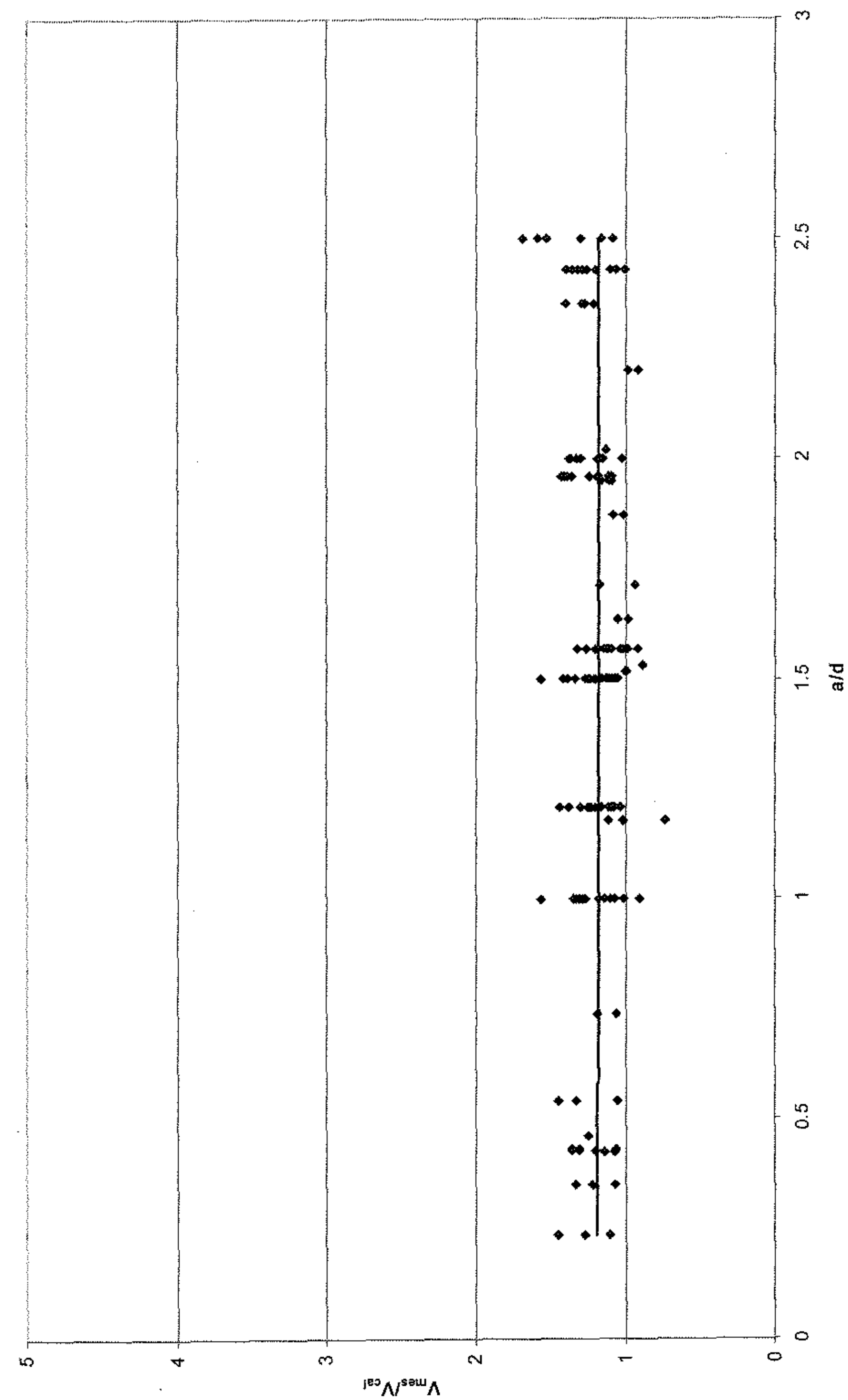

Figure 7-20 Ratio of measured to calculated shear strength versus aspect ratio, deep beams

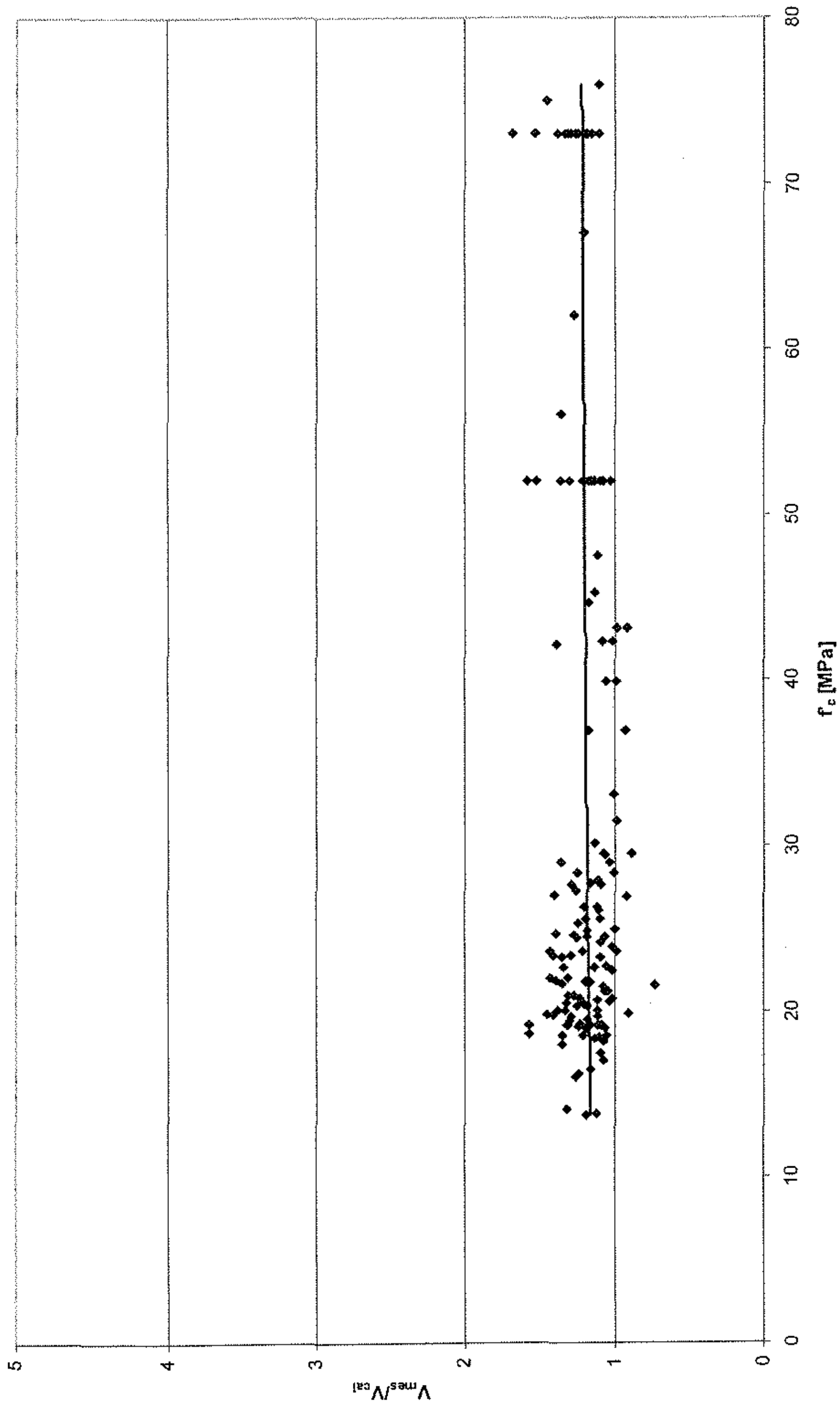

Figure 7-21 Ratio of measured to calculated shear strength versus compressive strength of concrete, deep beams

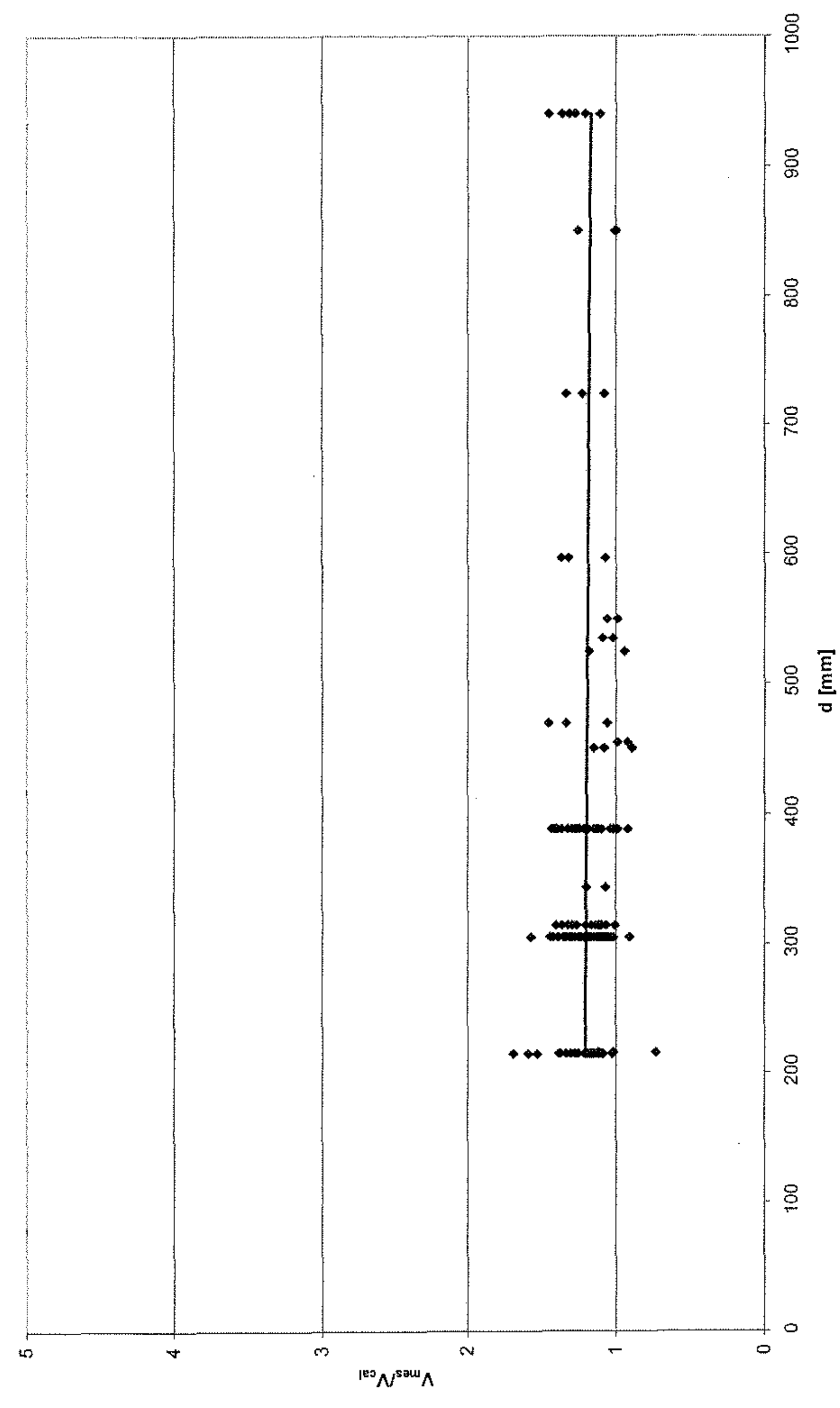

Figure 7-22 Ratio of measured to calculated shear strength versus effective depth, deep beams

7.2.5.2 Walls

The database for walls was comprised from databases collected from the open literature (Kabeyasawa and Hiraishi 1998; Wallace 1998; Wood 1990). 27 of the 146 examined walls were axially loaded with an average axial stress varying from 7 to 18 percent of the compressive strength of concrete; the average applied axial stress was less than 0.5 % in the remaining walls. 56 of the wall specimens were exposed to reversed lateral load, 4 specimens were repeatedly loaded in the same direction; and monotonic lateral load was applied to the remaining 86 specimens. Wall dimensions and properties are provided in Appendix A9 and in the "Wall database" worksheet on the added CD.

It was found that neither the axial load nor the alternating lateral load had a considerable effect on the shear strength of the walls. This might be related to some of the different factors that have to be considered for walls:

(1) The walls were equipped with boundary elements like flanges, heavy reinforcement on the edges of rectangular walls, or were built as barbell sections. Since the axial loads were applied on the whole sections, the boundary elements acted like columns, carrying most of the axial load.

(2) The boundary elements on the opposite side of the load application represent very distinct compression zones. These compression zones are heavily reinforced. Thus, different from deep beams, these boundary elements should be considered in the calculation of

the shear strength. However, the function for the transition from deep to slender members is assumed to be constant with $k_c = 1$.

(3) A contribution from friction in the tensile zone is neglected as a safe assumption for the same reasons it is not considered for the shear capacity of deep beams.

(4) The applied axial loads on the examined walls were very small. Most of the considered walls had no axial load; the majority of axially loaded walls were exposed to an axial load level $P/(A \cdot f'_c)$ of smaller than 0.3 %. Only the walls tested by Kabeyasawa had higher axial load levels between approximately 7 and 14 percent (Kabeyasawa and Hiraishi 1998).

(5) So far, in this work, shear loads had been vertically applied. The horizontal application of shear forces on walls makes it necessary to look at the changed geometry for the considered strength contributions:

Arch-action

For arch-action, the angle of the direct strut is taken as the angle spanning at the support counterclockwise from axial direction as shown in Figure 7-23. The horizontal dimension of the arch is assumed the effective depth *d*. The effective depth *d* is assumed to span between the center of the boundary element in tension and the outer fiber of the wall in compression. The inclination of the strut is thus given by equation (5.14):

$$\cot\theta = \frac{a}{d} \qquad \text{((5.14) Repeated)}$$

No information about dimensions of loading plates was given for the examined walls. However, it is common to apply the lateral load as a line load on top of the wall (Lopes 2001), thus diluting a distinct loading point for the arch and smearing the applied lateral load along the wall length l_w. It appears not sensible to define a strut width from the wall length. However, while the strut width at the location of the load application cannot be defined, the strut has to end at the support within a zone under compression. Such a fan-shaped strut can be idealized as a direct strut forming under the assumed inclination θ, which crosses the compression zone. It is a safe assumption to calculate the strut width solely from the depth of the compression zone, i.e. the boundary element, h_f. Consequently, the strut width for walls can be calculated as

$$w = h_f \cdot \cos\theta \qquad (7.30)$$

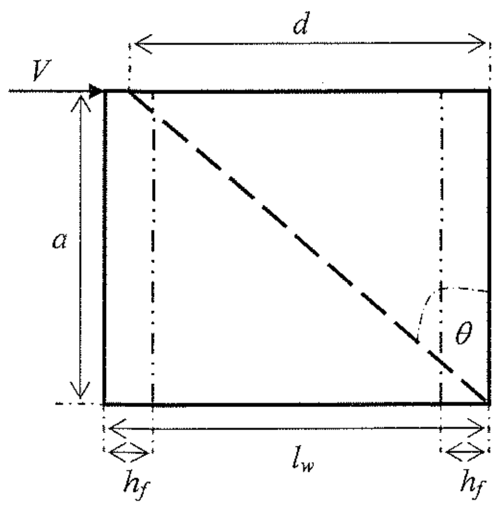

l_w = wall length

h_f = depth of the boundary element

d = effective depth

a = shear span

θ = strut inclination

Figure 7-23 Geometric definitions for arch-action in walls

Truss action

Truss action in walls is defined similar to truss action in deep beams with horizontal and vertical reinforcement. The strength of the trusses is calculated by equations (7.11) through (7.14), with the vertical direction for deep beams becoming the horizontal direction for walls, and the horizontal direction for deep beams becoming the vertical direction for walls.

Shear strength of walls

As previously mentioned, the boundary elements of walls represent a distinct compression zone that has to be reflected in the calculation of the shear strength. The shear strength of walls was calculated by adding the term for the contribution from the compression zone to equation (7.29):

$$V_n = V_{t,v} + V_{t,h} + V_a + V_{cz} \tag{7.31}$$

The contributions of truss action, $V_{t,v}$ and $V_{t,h}$, and from arch action, V_a, are calculated as for deep beams, with the necessary adjustments to the different geometry. These are equations (7.11) through (7.14), with the combination of truss- and arch-action by eq. (7.24). No adjustments were made to the factor k_s describing the decreasing influence of arch-action with an increasing aspect ratio. Thus, k_s is given as for deep and slender beams by eq. (7.27). The contribution related to the compression zone is calculated from the same expression as for slender members with transverse reinforcement:

$$V_{cz} = 0.4 \cdot \sqrt[3]{f'_c} \cdot b \cdot kd \tag{7.32}$$

It should be noted that the width b can change according to the geometry of the boundary element.

Figure 7-24 shows a plot of measured versus calculated shear strength of the 146 walls. Generally, a relatively large amount of scatter can be seen, which is reflected in a standard deviation of 0.47. The average value of V_{mes}/V_{cal} was found to be

$1.28 \pm 0.76\%$ within a 95 % confidence region, yielding a coefficient of variation of 36.6 %. The trend line in Figure 7-24 indicates no distinct negative trend. However, the strength of some walls with higher measured shear capacities between approximately 1700 and 3200 kN was overestimated. It should be noted that all specimens with a higher calculated shear strength than approximately 2500 kN come from a test series by Sugano (Wood 1990). These walls had a very low aspect ratio of $a/d = 0.23$. Their width was 120 mm with a wall length of 3960 mm. While no definite statement can be made, it is assumed that these walls might have failed in a failure mode more related to axially loaded members than to shear. The calculations indicated that as expected, the contributions from vertical truss-action and arch-action are negligible, and the sole horizontal truss component is overestimating the strength of these walls. It is possible that these walls rather failed due to concrete crushing than in shear.

The test series by Sugano is also visible in the graph showing a plot of the ratio of measured to calculated shear strength versus shear-span-to-depth ratio (Figure 7-25). Because these walls have the lowest aspect ratio, they influence the trend line with respect to small aspect ratios. For higher aspect ratios, the scatter was spread out relatively wide, indicating that the trend line gives a good estimate over the whole range.

Figure 7-26 shows a plot of V_{mes}/V_{cal} against concrete compression strength. The concrete strength of the majority of walls ranged from approximately 14 to 50 MPa, seven of the 146 specimens had a concrete strength between 70 and 80 MPa, and the concrete strength of two walls exceeded 100 MPa. The trend line indicates no distinct trend, representing the mean value of V_{mes}/V_{cal}.

Scatter for the length of the tested walls, l_w, is spread out more evenly over the entire range from 430 to 3960 mm. No trend is visible in Figure 7-27. Since the effective depth d was calculated as $d = l_w - h_f / 2$, this graph represents also the plot of the ratio of measured to calculated strength versus d.

Likewise, the graph of the ratio of measured to calculated shear strength against the tensile reinforcement ratio shows no distinct trend with respect to ρ_{be} (Figure 7-28). The reinforcement ratio of the boundary elements ranged from approximately 0.7 to 8.3 percent.

Figure 7-29 shows a plot of the ratio of measured to calculated shear strength against the axial load level. Most of the tested walls had very low or no axial load. Walls with higher axial load levels between 7 and 18 percent do not indicate any trend with respect to axial load.

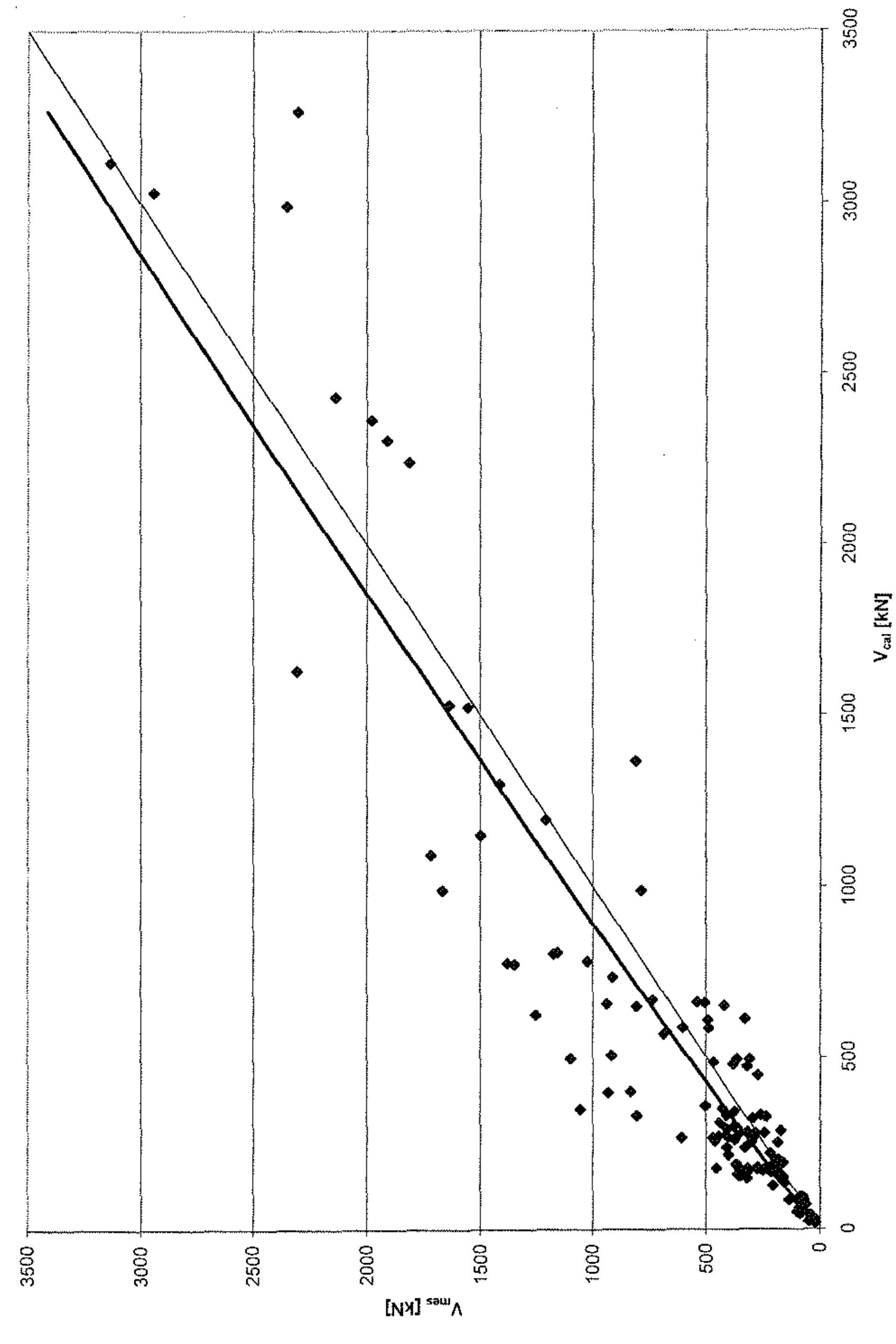

Figure 7-24 Measured versus calculated shear strength for walls

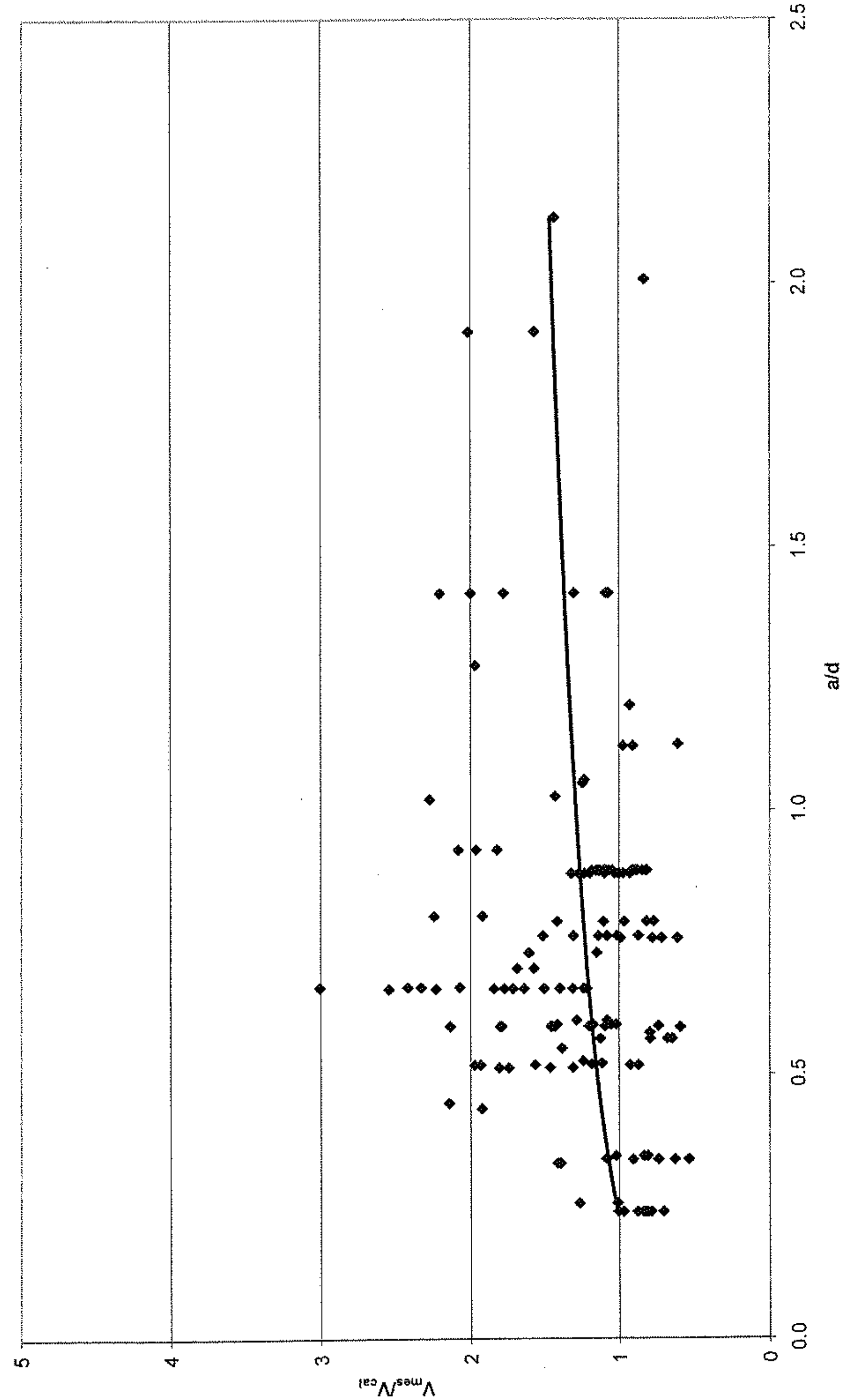

Figure 7-25 Ratio of measured to calculated shear strength versus aspect ratio for walls

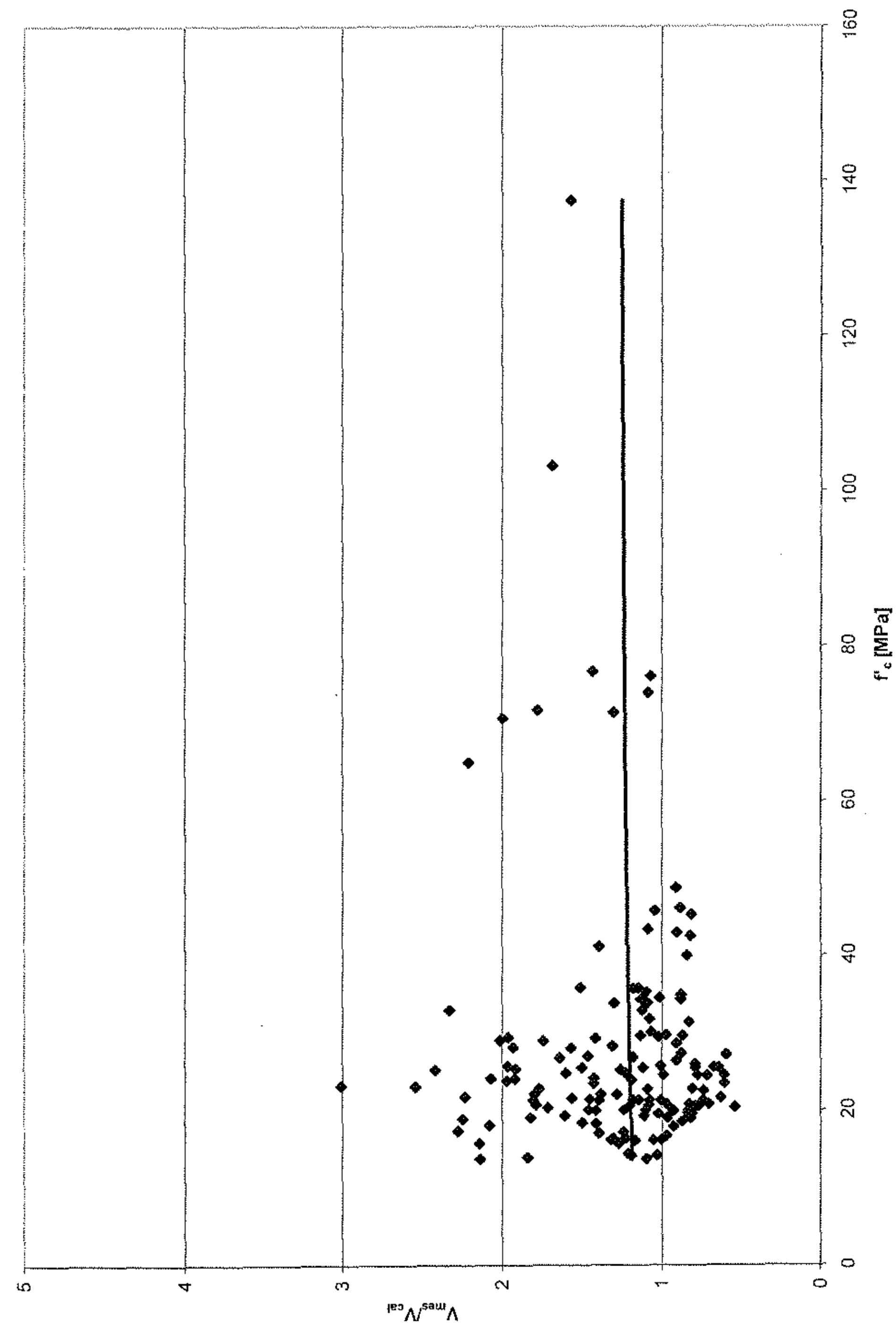

Figure 7-26 Ratio of measured to calculated shear strength versus compressive strength of concrete for walls

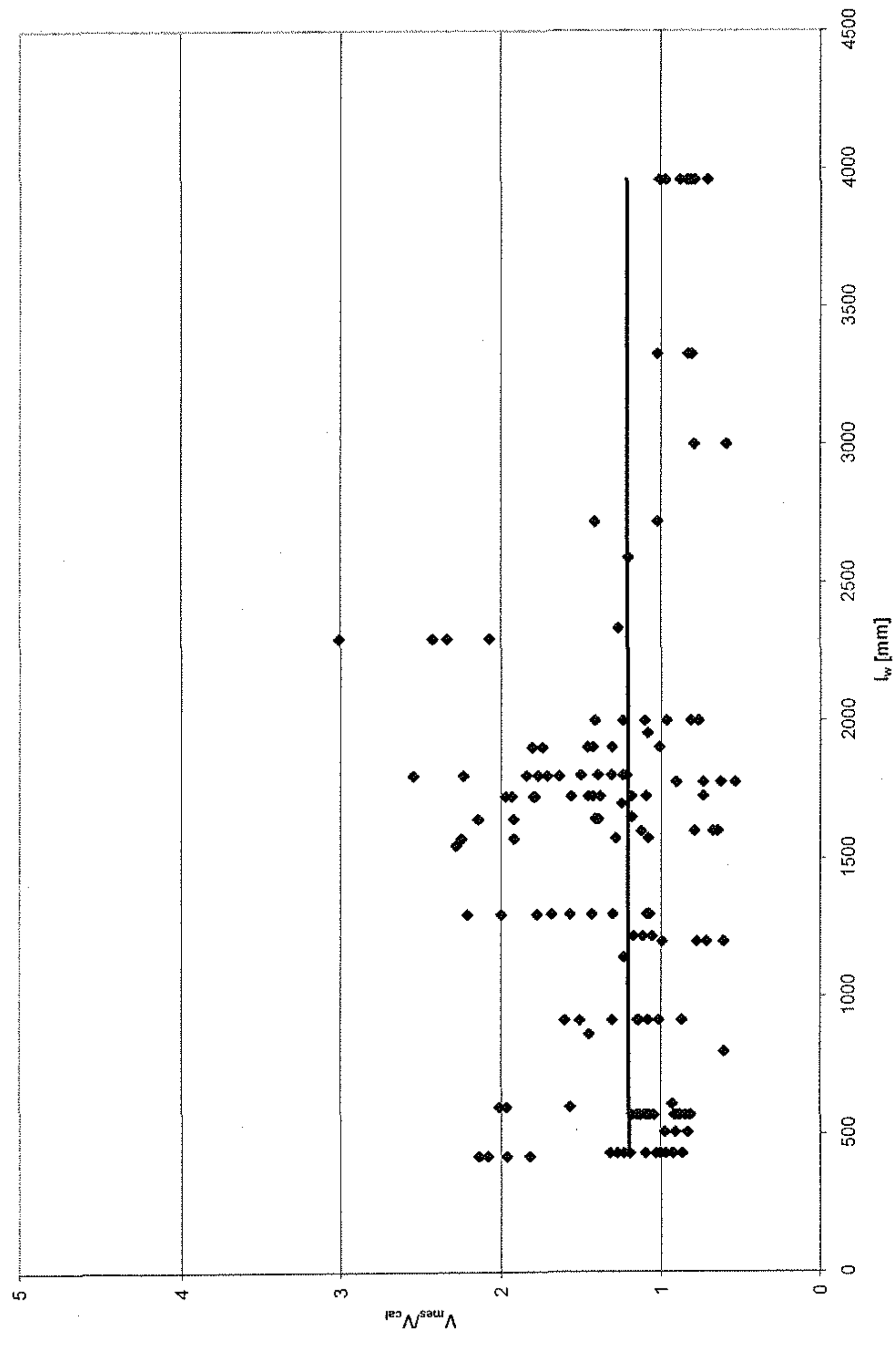

Figure 7-27 Ratio of measured to calculated shear strength versus wall length

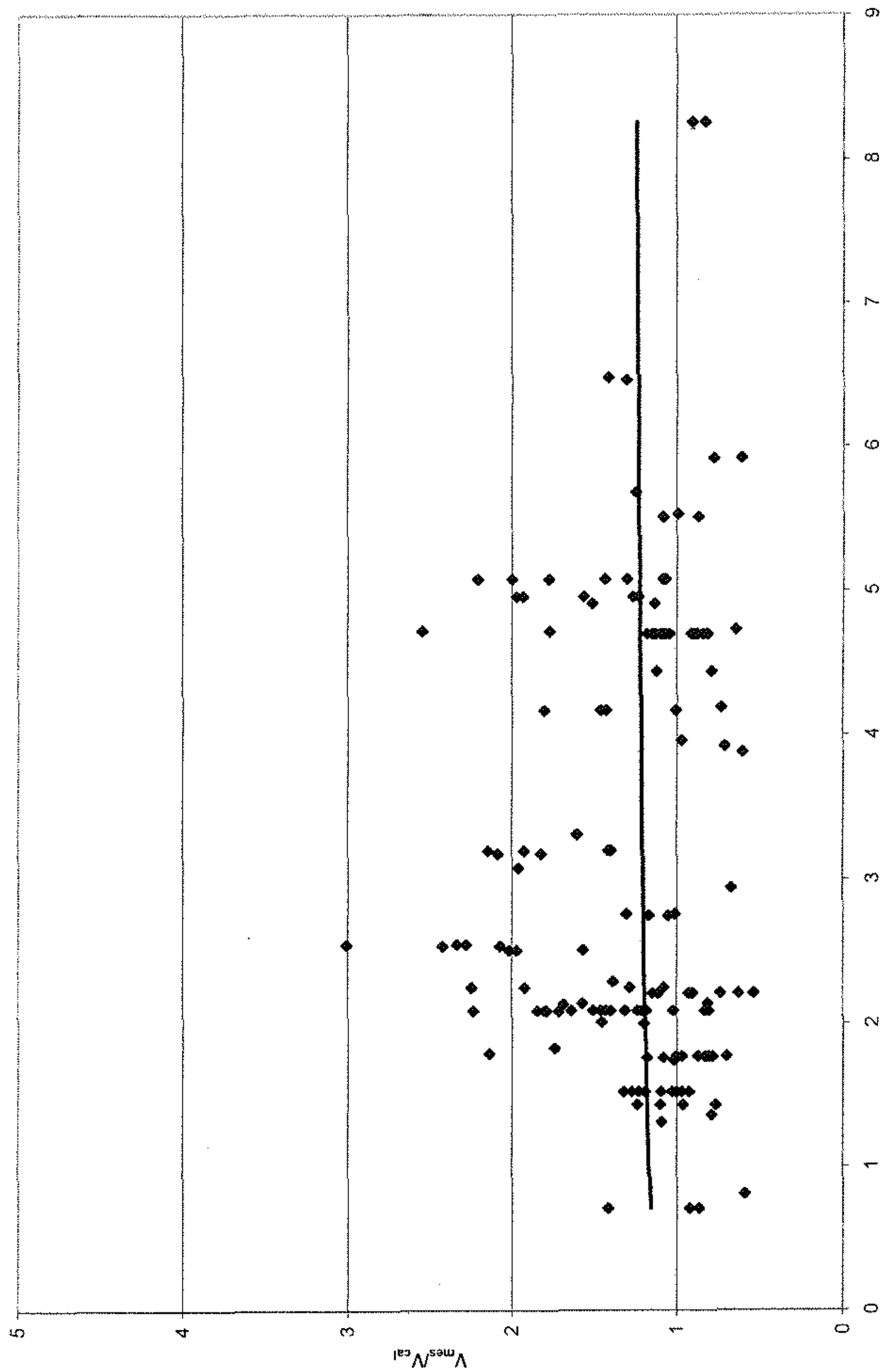

Figure 7-28 Ratio of measured to calculated shear strength versus tensile reinforcement ratio in the boundary elements of walls

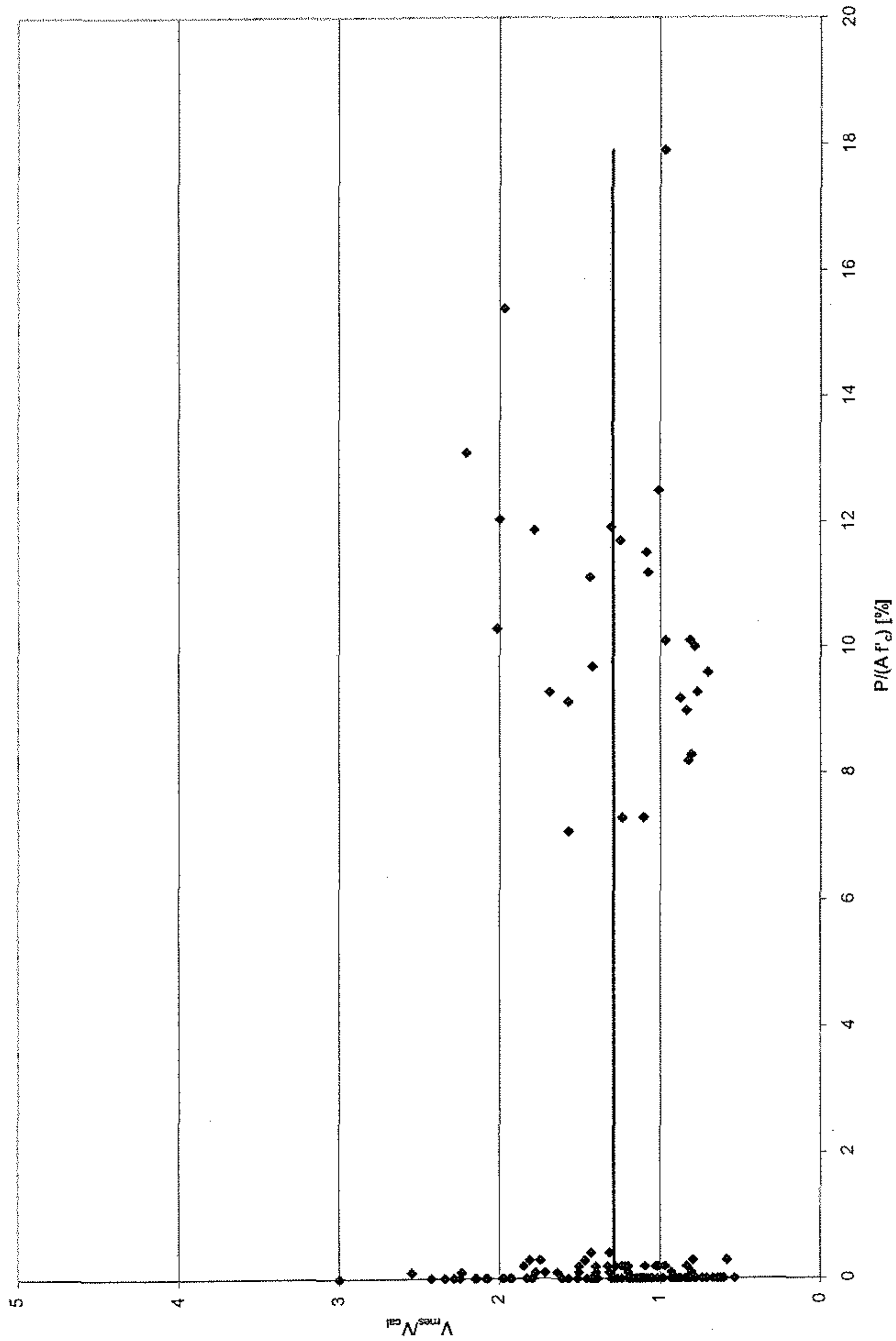

Figure 7-29 Ratio of measured to calculated shear strength versus axial load ratio for walls

7.3 Columns under static shear

No additional parameters are needed to account for effects of axial load with the proposed model. The effect of axial load is already considered in the derived components of the shear capacity. Some considerations have to be pointed out:

Exposing a beam to axial load is reflected in the changed depth of the neutral axis. Therefore, axial load influences the contributions from the uncracked compression zone, V_{cz}, from friction, V_f, and from arch-action, V_a. The compression zone becomes larger, increasing the influence of V_{cz}. Changing the height of the cracks also directly influences the critical crack width related to the friction mechanism, Δ_w. In addition, an axial load is reflected in the equilibrium conditions leading to the friction component in Section 5.2.3.2.

7.3.1 Contribution of the compression zone, V_{cz}

The depth of the neutral axis, c, calculated by flexural analysis for members under axial and flexural load defines a smallest possible compression zone depth, and is therefore a safe assumption. The actual depth of the compression zone under shear loads can be larger than c, and was previously taken as the compression zone depth calculated from linear bending theory, kd. Under axial loads, however, a closed form solution for kd is not readily at hand. It appears sensible to take the smallest possible depth of the compression zone as a conservative assumption. Assuming that the outer fiber of the column in compression has reached the ultimate strain of concrete, the neutral axis depth can be found iteratively as described later in Section 8.1.1 on page

276. The ultimate strain of concrete under compression is taken as $\varepsilon_{cu} = 0.003$. In design practice, a compression zone depth can be determined based on the interaction of moment and axial load. For evaluation purposes, c has to be determined by iterations for the given ultimate shear and axial load. The depth of the compression zone directly influences the contribution of the compression zone to the shear capacity of the member.

7.3.2 Arch-action

The depth of the compression zone also influences arch-action. If the strut width is calculated from the smallest value of either the depth of the compression zone or the embedment depth of the tensile reinforcement, h_a, the strut width is directly influenced by c. Since, however, the smallest value governs to yield the smallest strut width, and therefore the highest stresses in the strut, it is very likely that the embedment depth will govern the definition of the strut width. The values for c and h_a should be compared with this respect.

7.3.3 Friction component, V_f

The friction component V_f is influenced by the depth of the neutral axis, and therefore by axial load, in two ways: First, the depth of the neutral axis defines the depth of the crack, taken as d-c. A larger compression zone decreases the crack width, Δw, increasing the frictional forces. Furthermore, the axial load was already considered in equilibrium conditions of the free body diagram in Figure 5-10, page 153. No additional adjustments need to be made. However, the simplified calculation of the strain in the tensile reinforcement, eq. (5.49), cannot be used anymore, since this formulation does not include axial load. Therefore, the exact formulation in equation (5.48) has to be used.

7.3.4 Evaluation

The performance of the proposed model under static shear strength and axial compression was studied on the set of data that was used to derive the current ACI code provisions for shear under axial load (ACI-318 2002). The data was taken from three test series of beams and knee-frames without web reinforcement (Baldwin and Viest 1958; Diaz De Cossio and Siess 1960; Morrow and Viest 1957), which were later considered for evaluation purposes of the current code (ACI-ASCE committee 326 1962; MacGregor and Hanson 1969). The range of test data covers members that are representative of stocky and slender columns as well. The beam properties and loads are listed in Appendix A5 and the "Axial load" spreadsheet on the supplementary CD. Each of the three test series revealed a distinctly different behavior from the other series. For this reason, the separate series are shown in Figure 7-30 through Figure 7-35. While the series varied in their response to the proposed model, bias with respect to the axial load was not of concern.

Concrete strength, tensile steel ratio and aspect ratio were the considered variables in the 20 tests reported by Diaz De Cossio and Siess (Diaz De Cossio and Siess 1960). Two of the reported specimens failed in a flexural mode. They were not considered in the evaluation. The concrete strength varied from 19.4 to 31.5 MPa, aspect ratios varied from a/d = 2 to 6, and tensile steel ratios of 1 and 3.33 percent were used. The axial load was not varied. However, the beams tested by Diaz De Cossio were cast in pairs, in which one beam of each pair was axially loaded with 89 kN, and the other beam was not axially loaded. This allows for a direct comparison with respect to axial compression. As shown in Figure 7-31, adding axial compression did not have an effect on the accuracy of the proposed model.

The tests reported by Morrow and Viest (Morrow and Viest 1957) and Baldwin and Viest (Baldwin and Viest 1958) are considered to be a continued tests series. The first part of the series, conducted by Morrow and Viest, comprised 33 knee-frames of which 29 failed in shear compression or due to diagonal tension cracks. Test variables were the shear span, concrete compressive strength, and tensile reinforcement ratio. The axial load ratio, $P/(Af'_c)$, varied from 2.5 percent to approximately 10 percent, while the axial load was kept equal to the shear load.

Being a continuation of the preceding test series, the second part conducted by Baldwin and Viest focused almost entirely on a varying axial load, i.e. a varying axial to shear load ratio. The shear-span-to-depth ratio was kept mostly constant at 1.93; only one knee-frame with a/d =1.45 and one member with a/d = 2.62 were additionally tested. Concrete compressive strength was planned as 24 MPa, and varied from 21.2 MPa to 37.6 MPa.

As mentioned previously, scatter among the ratios of measured to calculated shear strength for the three test series was relatively large. As can be seen in Figure 7-30, the largest variation is apparent for the knee-frames tested by Baldwin, indicated by triangular markers. Since only two of the members tested by Baldwin were not under axial compression, no statement can be made concerning the effect of axial load. Figure 7-31, though, shows that a varying amount of axial load did not induce bias on the calculated shear strength. The shear strength of the knee-frames tested by Baldwin was generally overestimated.

A direct comparison between beams with and without load is possible using Diaz De Cossio's data. The same amount of axially loaded members and beams without axial compression is available for similar beams in each category. Marked by a diamond shape in Figure 7-30 and Figure 7-31, the shear capacity was calculated with comparable deviation from the measured values. The same was true for the evaluation of knee-frames of the first investigation by Morrow and Viest. The scatter for this test series was slightly smaller compared to the series by Diaz De Cossio.

The plots of the measured to the calculated shear strength against concrete compressive strength, aspect ratio, effective depth, and tensile reinforcement ratio (Figure 7-30 through Figure 7-35) show no discernible common trends with respect to each parameter. The mean value of measured to calculated shear strength was found to be $1.37 \pm 0.63\%$ within a 95 percent confidence interval. The standard deviation was 0.36, resulting in a coefficient of variation of 26.1 percent. These values are comparable to the values found for deep and slender members without axial load and without transverse reinforcement.

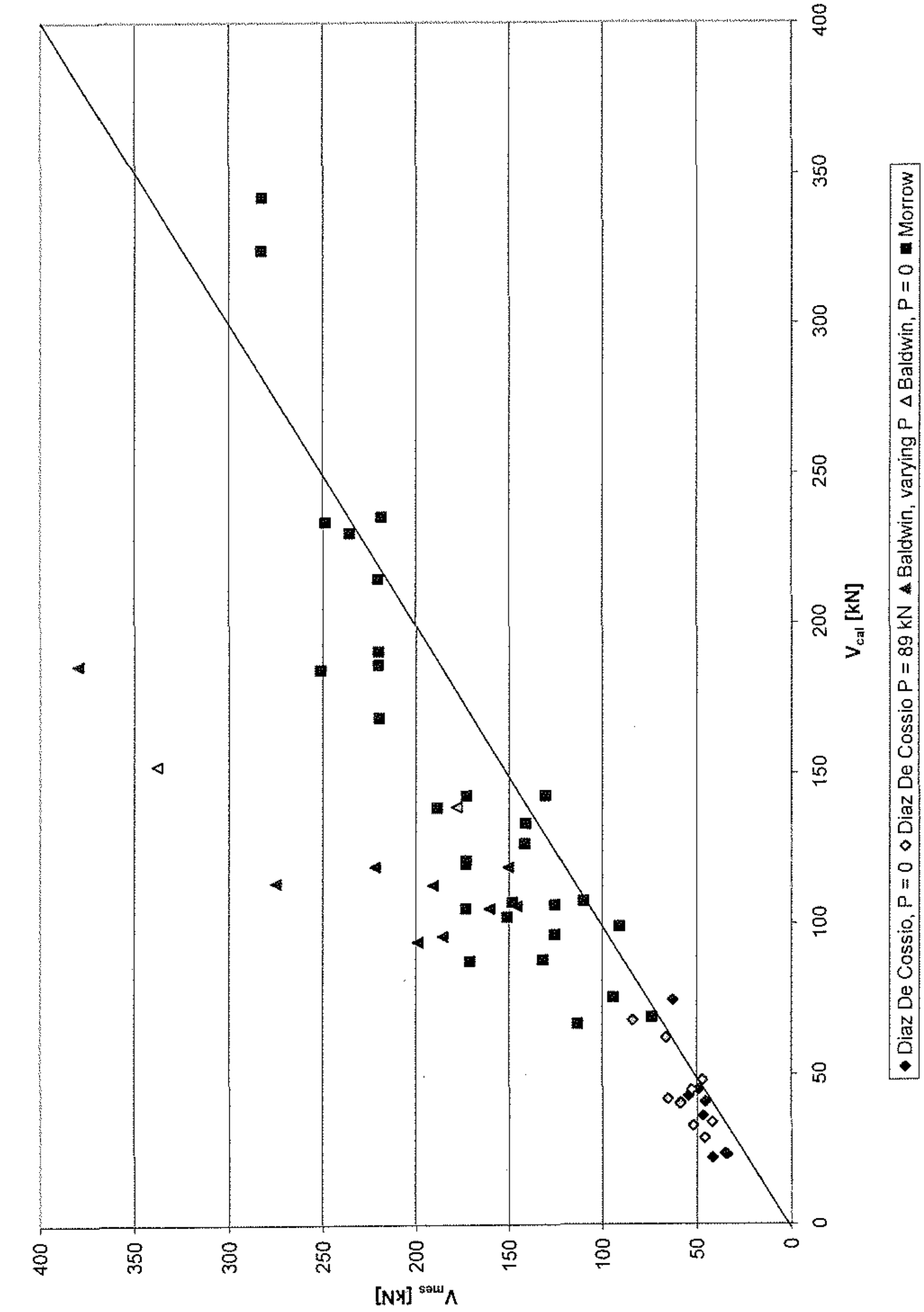

Figure 7-30 Measured to calculated shear strength of axially loaded members without web reinforcement

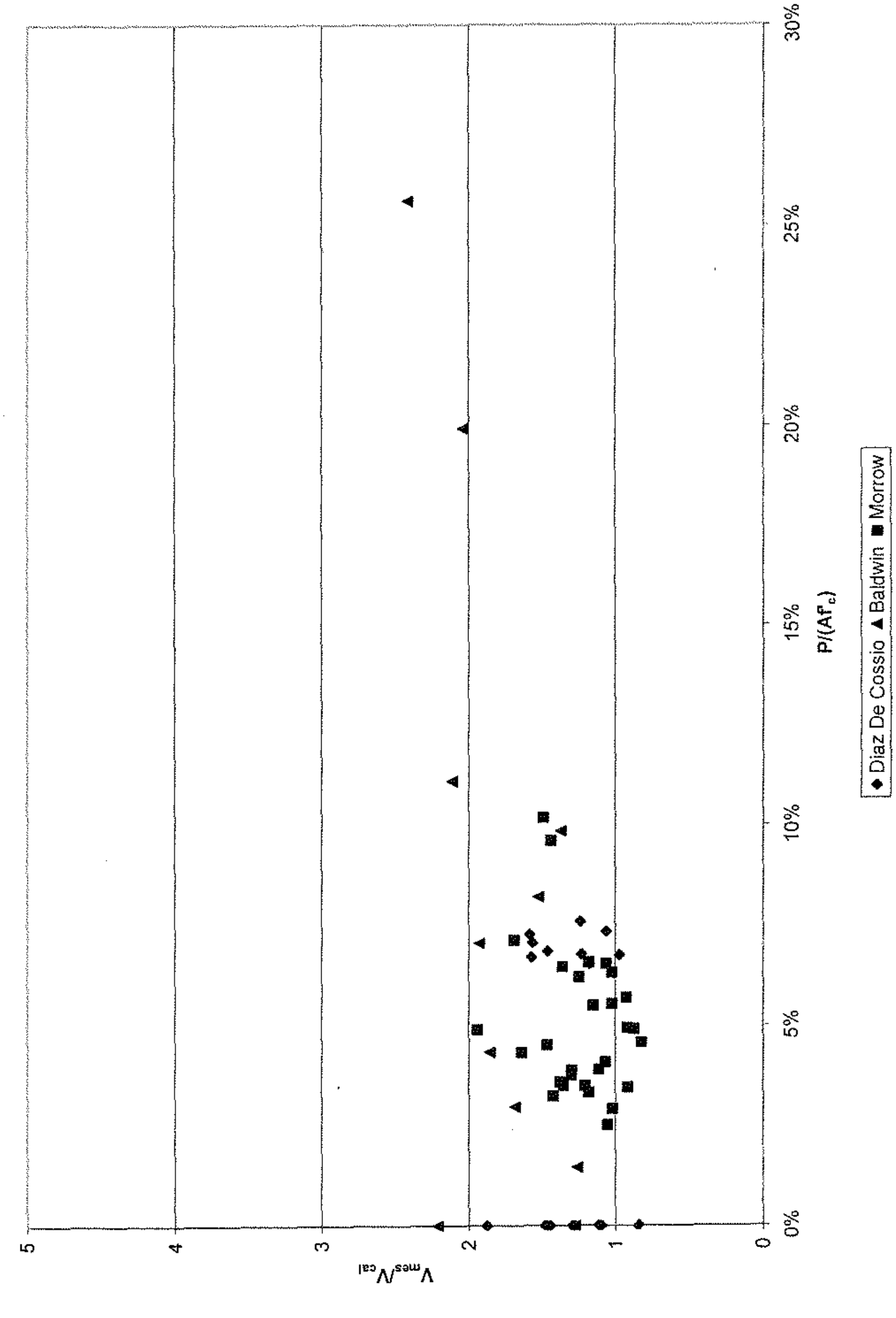

Figure 7-31 Ratio of measured to calculated shear strength versus axial load level of members without web reinforcement

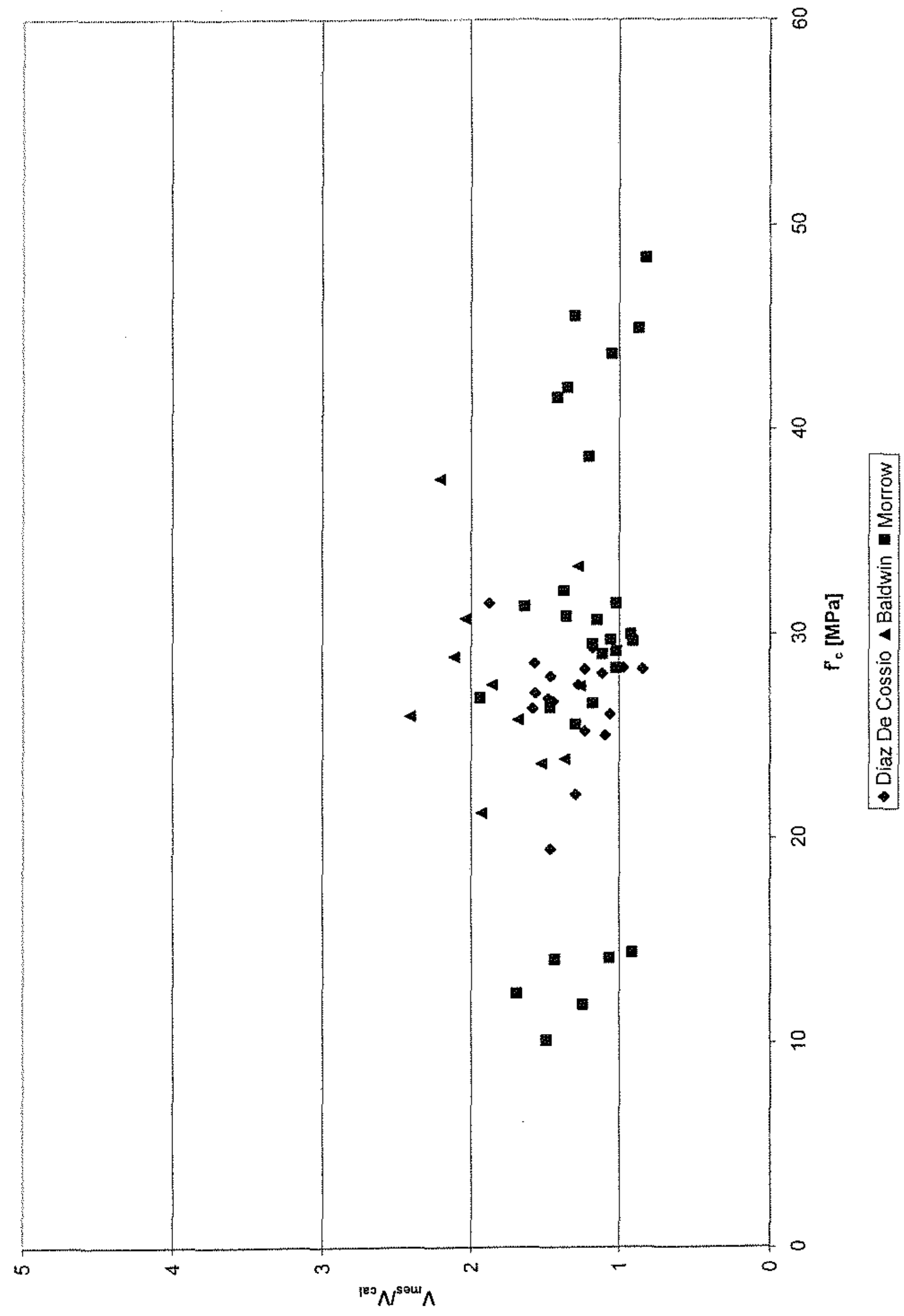

Figure 7-32 Ratio of measured to calculated shear strength versus concrete strength for axially loaded members without web reinforcement

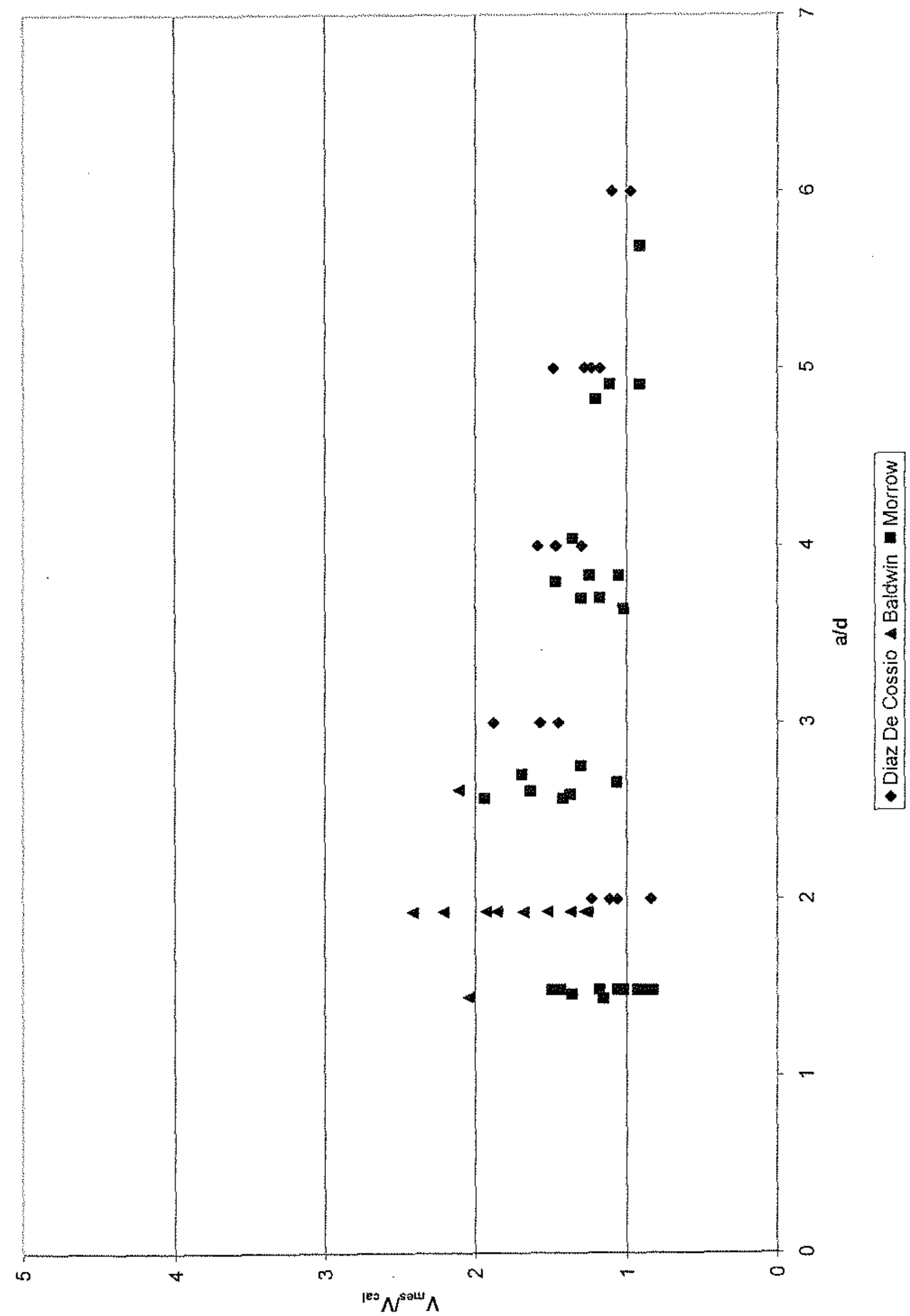

Figure 7-33 Ratio of measured to calculated shear strength versus aspect ratio for axially loaded members without web reinforcement

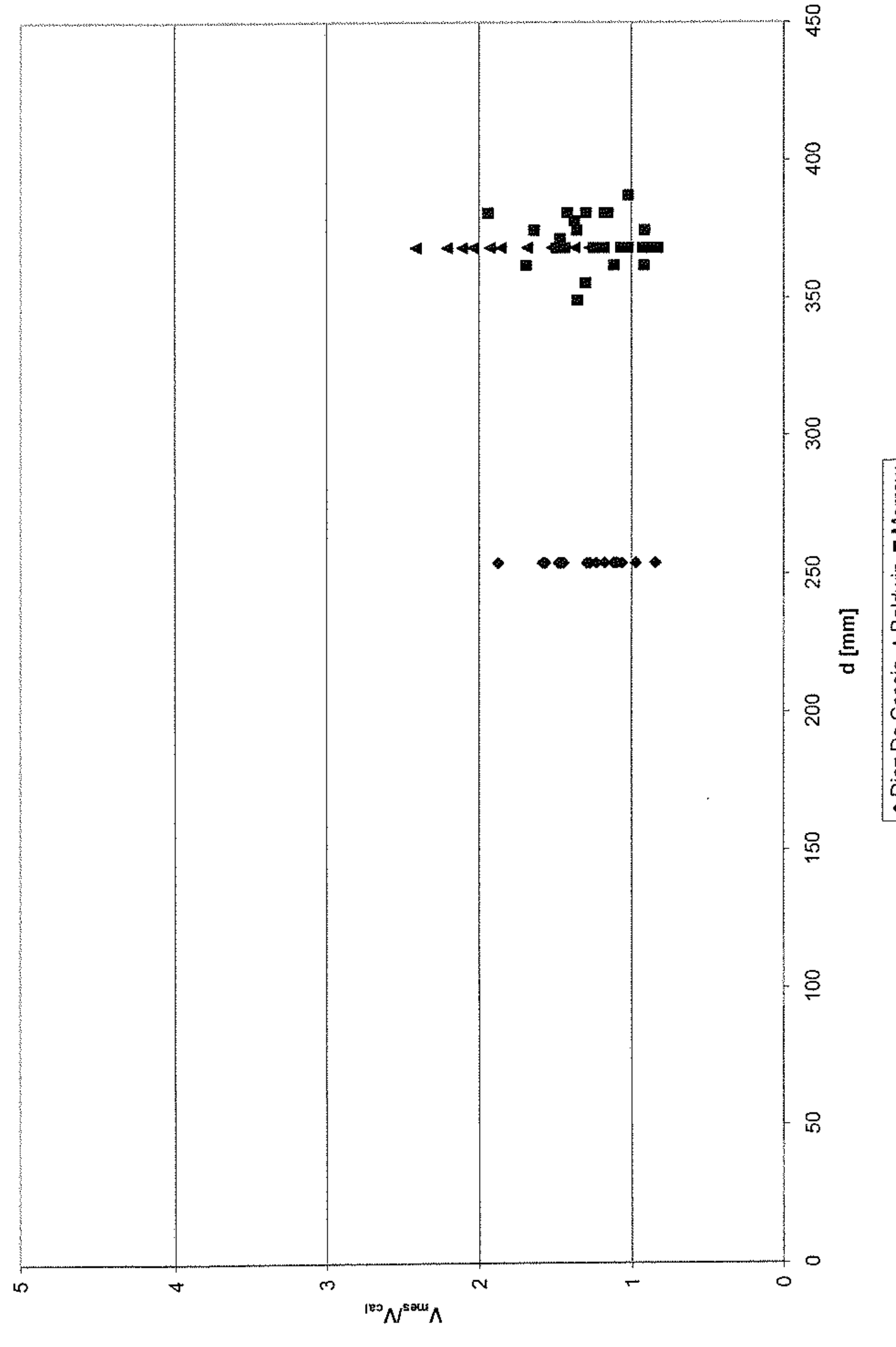

Figure 7-34 Ratio of measured to calculated shear strength versus effective depth of axially loaded members without web reinforcement

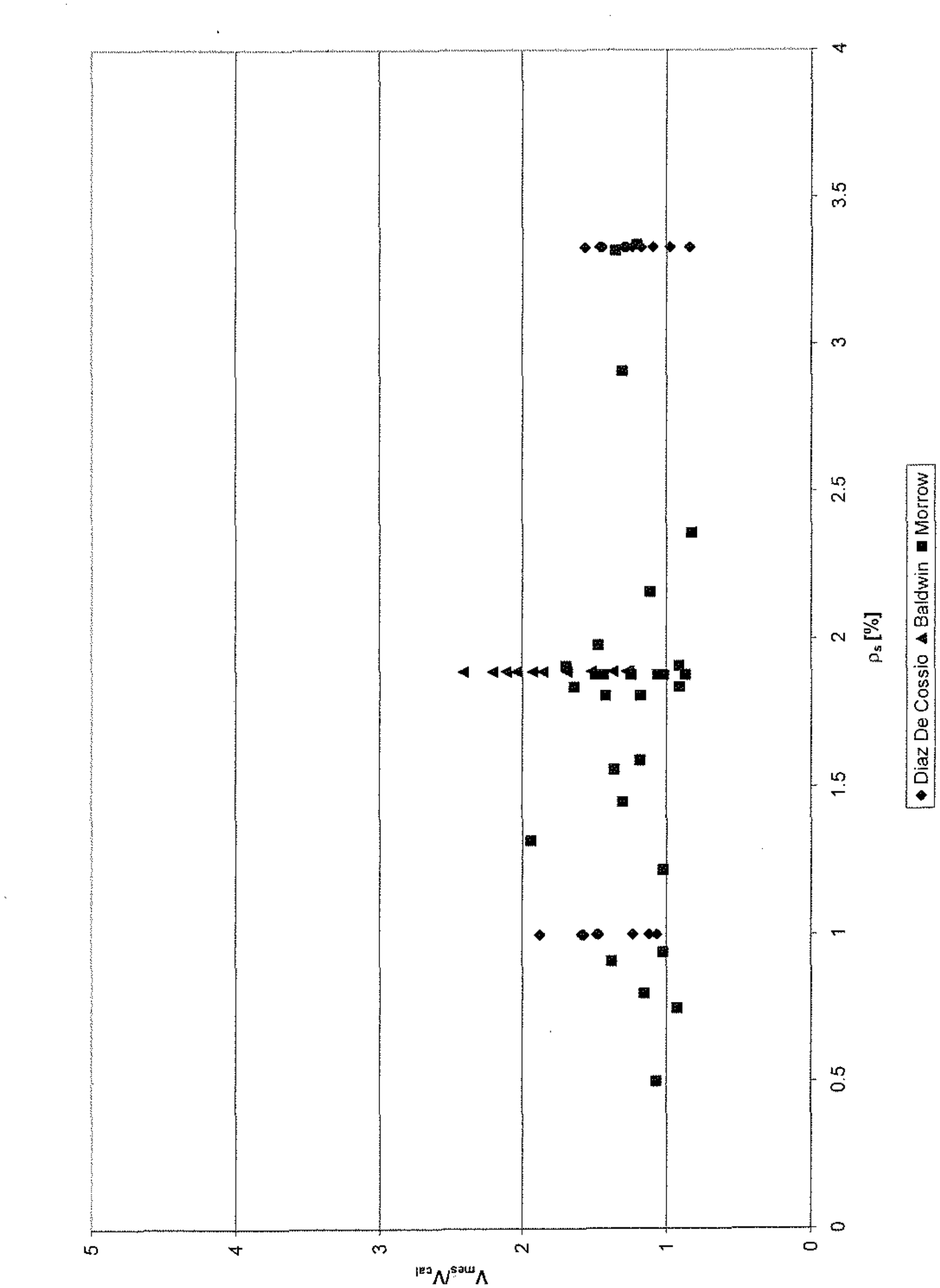

Figure 7-35 Ratio of measured to calculated shear strength versus tensile reinforcement ratio for axially loaded members without web reinforcement

7.4 Evaluation of the calibrated components

Using the results from the previous calibrations, the monotonic shear capacity can be calculated for members with and without web reinforcement in a range from slender to deep members and walls. A possible axial load can be considered following the previous Section 7.3.

7.4.1 Members without web reinforcement

Summarizing, the strength of RC members without web reinforcement was calculated by the superposition of arch-action with the contributions from the compression zone and the friction mechanism.

$$V_n = V_a + k_c\left(V_{cz} + V_f\right) \qquad \text{((7.8) Repeated)}$$

The strength related to arch-action was calculated using equation (5.16), with the effective strength of concrete in the nodal zones given by equation (5.6), and the transition function k_s provided in equation (7.5):

$$V_a = \beta_n k_s f'_c \cdot w \cdot b \cdot \sin\theta \qquad \text{((5.16) Repeated)}$$

$$\beta_n = 0.85 - 0.004 f'_c \geq 0.5 \qquad \text{((5.6) Repeated)}$$

$$k_s = \frac{1}{1 + 0.1\left(a/d\right)^3} \qquad \text{((7.5) Repeated)}$$

The contributions from the compression zone and friction were multiplied by the function k_c to consider the transition from slender to stocky members.

$$k_c = 1 - \frac{1}{0.9 + 0.02\left(a/d\right)^3} \geq 0 \qquad \text{((7.7) Repeated)}$$

The capacity of the combined contributions from the compression zone and friction was given previously in equation (7.6) within the constraints listed in Section 7.1.2.2, page 198.

$$\begin{aligned} V_c &= 0.5 \cdot f_{ct} \cdot b \cdot kd + 0.5 \cdot f_{ct} \cdot b \cdot (d - kd)\left(1 - \frac{\Delta w}{\Delta w_u}\right) \\ \Leftrightarrow V_c &= 0.5 \cdot \sqrt[3]{f'_c} \cdot bd\left[k + (1-k)\left(1 - \frac{\Delta w}{\Delta w_u}\right)\right] \end{aligned} \qquad \text{((7.6) Repeated)}$$

Using an n-fold cross validation, the proposed model can objectively be compared to other proposals outlined in Chapter 3, and evaluated in Chapter 4. The procedure of the n-fold cross validation was described in Section 4.1.1. The individual results for each calibrated member configuration are provided in the respective sections of the Appendix and on the accompanying data CD in the respective worksheets. Table 7-3 summarizes the evaluation in terms of the ratio of measured to calculated strength, V_{mes}/V_{cal}, and the respective coefficient of variation (*C. V.*).

The performance of the proposed model on the deep beam database was compared to the proposal by Watanabe (Watanabe and Ichinose 1991), considering the modifications in (Watanabe and Kabeyasawa 1998). The proposed model revealed less scatter, and less conservatism with respect to the calculated shear capacity of deep beams. Nevertheless, the proposed method provided safe estimates of the shear strength of deep beams.

The performance of the proposed model on the database of slender members without transverse reinforcement showed slightly less scatter compared to the approach proposed by Reineck (Reineck 1990, 1991b), and a significantly smaller coefficient of variation than the Watanabe-model. Contrary to the results for deep beams, the model put forward by Watanabe was the least conservative with a ratio of measured to calculated shear strength of 1.08 ± 0.42 % within a 95 % confidence region. The model proposed by Reineck had the highest ratio of measured to calculated shear strength of 1.55 ± 0.46 % within a 95 % confidence interval; the model in this work gave a conservative estimate of V_{mes}/V_{cal} = 1.36 ± 0.33 % within a 95 % confidence region.

	Researcher	V_{mes}/V_{cal}	*C.V.*
Deep beams	Proposed model	1.11 ± 0.80 %	22.97 %
	Watanabe (Watanabe and Ichinose 1991; Watanabe and Kabeyasawa 1998)	1.52 ± 0.94 %	29.34 %
Slender beams	Proposed model	1.36 ± 0.33 %	28.58 %
	Watanabe (Watanabe and Ichinose 1991; Watanabe and Kabeyasawa 1998)	1.08 ± 0.42 %	34.59 %
	Reineck (Reineck 1990, 1991b)	1.55 ± 0.46 %	27.43 %

Table 7-3 Evaluation of deep and slender members without web reinforcement

7.4.2 Members with web reinforcement

The introduction of an additional term for truss action makes the proposed model applicable to various member configurations with web reinforcement. The general form of the shear capacity of members with web reinforcement was given in equation (5.1):

$$V_n = V_a + V_t + V_c \qquad \text{((5.1) Repeated)}$$

The contribution from the truss-mechanism, V_t, was applied according to Sections 5.2.2 and 7.2, with the modifications necessary for the application of truss-action in deep members described in Section 7.2.1.

According to these sections, the strength of the truss is given in its general form by equation (5.23):

$$V_t = \rho_w f_{wy} b \cdot jd \cdot \cot\phi \qquad \text{((5.23) Repeated)}$$

The inclination of the compression field, ϕ, was assumed equal to 30 degrees.

In deep members, the inclination of the compression field was limited to ensure equilibrium within the compression field. For the vertical truss mechanism, this limit was set by equation (7.10); a possible horizontal truss mechanism in deep beams and walls was assumed to have a limited compression field inclination defined by equation (7.12).

$$\cot\phi = \frac{a}{2d} \qquad \text{((7.10) Repeated)}$$

$$\cot\psi = \frac{2a}{d} \qquad \text{((7.12) Repeated)}$$

The strength of the horizontal truss was provided in equation (7.13):

$$V_{t,h} = \rho_w f_{wy} b \cdot d \cdot \tan\psi \qquad \text{((7.13) Repeated)}$$

To reduce the demand on the nodal zone due to stresses related to the arch mechanism in the presence of truss-induced stresses, a reduction factor R_a was applied to the arch component. The general form of R_a was given in (7.23); the reduced capacity of the arch mechanism was defined in equation (7.24):

$$R_a = \frac{\left(\beta_n f'_c - f_{t,h}\right)\left(\beta_n f'_c - f_{t,v}\right)}{\left(\beta_n f'_c\right)^2 - f_{t,h} f_{t,v}} \qquad \text{((7.23) Repeated)}$$

$$V_a = R_a \beta_n k_s f'_c \cdot w \cdot b \cdot \sin\theta \qquad \text{((7.24) Repeated)}$$

The transition function related to the arch mechanism, k_s, was calibrated as

$$k_s = \frac{4.6}{6.5 + 0.13\left(a/d\right)^5} \qquad \text{((7.27) Repeated)}$$

The calibration of the proposed model on the database of slender and deep members with web reinforcement yielded the parameters listed in Section 7.2.3 on page 220. The strength of the combined contributions from the compression zone and friction components was given in equation (7.26):

$$V_c = 0.4 \cdot f_{ct} \cdot b \cdot kd + 0.4 \cdot f_{ct} \cdot b \cdot (d - kd)\left(1 - \frac{\Delta w}{\Delta w_u}\right)$$
$$\Leftrightarrow V_c = 0.4 \cdot \sqrt[3]{f'_c} bd\left[k + (1-k)\left(1 - \frac{\Delta w}{\Delta w_u}\right)\right] \qquad \text{((7.26) Repeated)}$$

The transition function for the compression zone and friction components was calibrated as

$$k_c = 1 - \frac{1}{0.1 + 0.01(a/d)^5} \geq 0 \qquad \text{((7.28) Repeated)}$$

Similar to the capacity of web reinforced deep beams the capacity of walls was calculated in Section 7.2.5.2.

The calibrated proposed model was compared to other proposed models in an n-fold cross validation. Table 7-4 summarizes the results from this evaluation. With the exception of the application to walls, the proposed model showed smaller scatter than the approach put forward by Watanabe (Watanabe and Ichinose 1991; Watanabe and Kabeyasawa 1998). Applied to the databases for deep and for slender members, the proposed model gave a more conservative estimate with ratios of V_{mes}/V_{cal} = 1.20 ± 0.24 %, and V_{mes}/V_{cal} = 1.14 ± 0.20 %, respectively. This can be attributed to the calibration. One objective of the calibration of the proposed method was to provide a safe assumption of shear strength. Considering the higher amount of scatter in the model proposed by Watanabe, the low ratios of measured to calculated strength resulted in a significant number of members of which the strength was considerably overestimated.

This is especially true for the application of the approach proposed by Watanabe to walls. Even though the coefficient of variation is lower than for the method proposed in this work, the low value of V_{mes}/V_{cal} resulted in a significant number of unsafe estimates of the shear strength of walls.

	Researcher	V_{mes}/V_{cal}	*C.V.*
Deep beams	Proposed model	1.20 ± 0.24 %	12.98 %
	Watanabe (Watanabe and Ichinose 1991; Watanabe and Kabeyasawa 1998)	1.04 ± 0.31%	20.81 %
Slender beams	Proposed model	1.14 ± 0.20 %	14.67 %
	Watanabe (Watanabe and Ichinose 1991; Watanabe and Kabeyasawa 1998)	1.08 ± 0.56%	24.36 %
Walls	Proposed model	1.28 ± 0.76 %	36.63 %
	Watanabe (Watanabe and Ichinose 1991; Watanabe and Kabeyasawa 1998)	0.93 ± 0.43 %	32.38 %

Table 7-4 Evaluation of deep members, slender members, and walls with web reinforcement

It can be concluded that, compared to the models put forward by Watanabe and by Reineck, the proposed model generally resulted in safe estimates of the monotonic shear strength with relatively small coefficients of variation. Independent of the performance with respect to the shear strength, the performance with respect to influencing parameters has to be considered. This was described in detail in the chapter about the evaluation of current proposals, and the calibration of the method proposed in the work at hand.

7.5 Possible simplifications

In the previous sections, it was shown that the contributing components gave a good performance on the available data sets. However, while the forms for truss action, arch-action, and contribution of the uncracked compression zone are relatively simple to use, it can be argued that the friction component is very complex compared to the other components. In the following, suggestions are made to simplify the calculations.

7.5.1 Strain calculations for the friction component

One simplification was already used in the calculation of the V_f term for members without axial load. The strain in the tensile reinforcement, and therefore the horizontal crack opening, was calculated from linear flexural analysis by equation (5.49). The previously described calibrations wêre carried out using this simplified approach. It was pointed out that for axially loaded members the strain has to be calculated according to eq. (5.48) to account for the effect of axial load on the strain in the tensile reinforcement.

Using the simplified form for the calculation of strains leads to another possible simplification. If the strain in the tensile reinforcement is calculated from linear bending theory, it is assumed that the frictional forces do not affect the strains, which is equivalent to assuming the crack is not inclined. If the crack runs perpendicular to the member axis, frictional forces V_f act parallel to the crack, thus reducing the lever arm to zero. The assumption of a perpendicular crack can be used to simplify the friction model further by simplifying the crack width calculation.

7.5.2 Crack width

The crack width Δw was calculated in Chapter 5.2.3.2 by geometric considerations in an inclined crack. The crack opening perpendicular to the crack surface was related to a critical slip Δs parallel to the surface, which made it possible to account for friction between the crack surfaces. This approach can be numerically simplified by assuming a crack normal to the member axis. It should be noted, though, that this is an assumption leading to a numerical simplification. Eliminating the critical slip from the V_f term, means eliminating the frictional stresses along the crack. A crack normal to the member axis cannot develop a contribution to shear resistance without displacement in the same direction. Furthermore, the rotation of the crack opening induces a vertical displacement. To simplify the design process, however, the assumption is made that the crack is not inclined.

The assumed geometry is depicted in Figure 7-36. For an assumed crack inclination of $\phi_u = 90^\circ$, equation (5.43) becomes

$$\Delta w = \Delta u \tag{7.33}$$

with $\tan\phi \to \infty$, and $\sin\phi = 1$

The crack width therefore becomes, with eq. (5.44):

$$\Delta w = 0.5 \cdot \varepsilon_s \cdot s_{cr} \tag{7.34}$$

The strain in the tensile reinforcement is given in its simplified form from linear bending theory by equation (5.49).

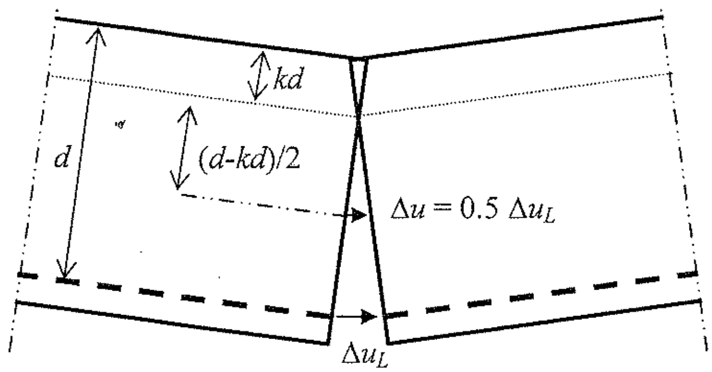

Figure 7-36 Kinematics in an assumed crack with no inclination

Using equation (7.34), the contribution from friction can be calculated as shown in Chapter 5.2.3.2 for members with or without web reinforcement by equations (5.51) and (5.52), respectively.

Because only changes were made to the calculation of the crack width, only parameters related to the crack width should be changed in the evaluation of the proposed simplification. The only parameter directly related to the crack width is the critical crack width Δw_u.

The database mostly related to the calibration of the friction component is the database for deep and slender beams without web reinforcement. A new critical crack width for the simplified approach is found for this database. The established value is expected to give good results also on members with transverse reinforcement.

The calibration on the previously used database for deep and slender members yielded a critical crack width of

$$\Delta w_u = 0.2 \text{ mm} \tag{7.35}$$

It is clear that this is a numerical value with little physical relevance for the reasons described above. Computing the ratio of measured to calculated shear strength for deep and slender members without transverse reinforcement using the simplified approach yielded a mean value of $V_{mes} / V_{cal} = 1.35 \pm 0.34\%$ within a 95 percent confidence interval. The standard deviation for all 448 members was found as 0.39 resulting in a coefficient of variation of 28.65 %. These values indicated only slightly more scatter than found for the same database using the "exact" equations.

Similar results were found using the simplified V_f term on the previously used database for deep and slender members with web reinforcement. Using the established parameters, while changing only the calculation of the crack width and setting the limit value to Δw_u = 0.2 mm, the mean value of measured to calculated strength was found to be $V_{mes} / V_{cal} = 1.16 \pm 0.18\%$ within a 95 % confidence region. The standard deviation was 0.16, resulting in a coefficient of variation of 14.24 %. Values found using the detailed calculation of the crack width were approximately equal to the values using the simplified calculations.

8 Cyclic loading

Columns subjected to cyclic loading can either fail in a mode related to decay of the flexural strength, or due to loss of shear-capacity. Consequently, the possible modes of failure have to be treated using separate procedures.

If the behavior of a column is mainly controlled by flexure, the column is assumed to have reached its limiting capacity at the displacement in which the lateral load is reduced to 80 percent of the maximum applied lateral force. In flexure-controlled members, the maximum lateral load is limited by yielding of the longitudinal reinforcement. An envelope curve for the load – deflection response can be defined as shown by the bold line in Figure 8-1.

For columns with failures related to shear, a 20 percent reduction in shear strength is not the limiting criterion. In the following, it is assumed that a column looses its shear strength if the transverse reinforcement yields. The dashed envelope curve in Figure 8-1 represents the degression of shear strength with increasing displacement under cyclic load. The design objective is that the shear-failure line should not transgress the envelope curve for flexural failure, ensuring a ductile failure mode.

Different parameters influence the reduction in strength due to cyclic loading. These parameters will be discussed in the following sections on flexural failure and shear failure.

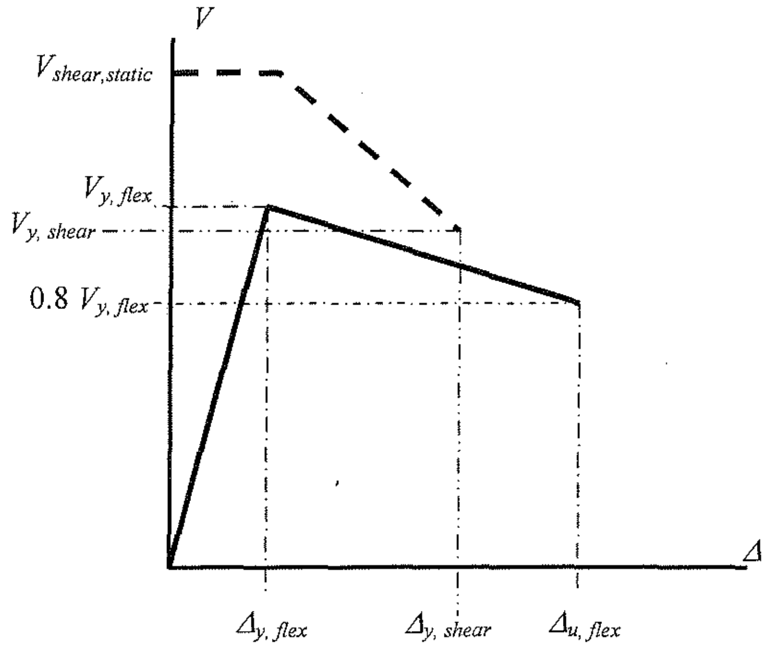

Figure 8-1 Envelope curves for different failure modes under cyclic loading

8.1 Strength degradation in flexure-controlled members

The strength degradation of flexure controlled members has been investigated on a subset of 116 columns from a combined database provided by the University of Washington (UW) (Berry et al. 2003), and by Brachmann (Brachmann 2002). As stated in the UW database, these columns reportedly failed due to flexure. Column properties and calculation results are summarized in Appendix A6 and in the worksheet "Seismic flexural failure" on the accompanying data CD.

8.1.1 Flexural yield load of members with axial loads below balanced load

The flexural capacity of a member can be computed from flexural analysis of the columns as the flexural yield load. Since the column is under axial compression, the neutral axis depth has to be determined from equilibrium conditions within the member, according to Figure 8-2.

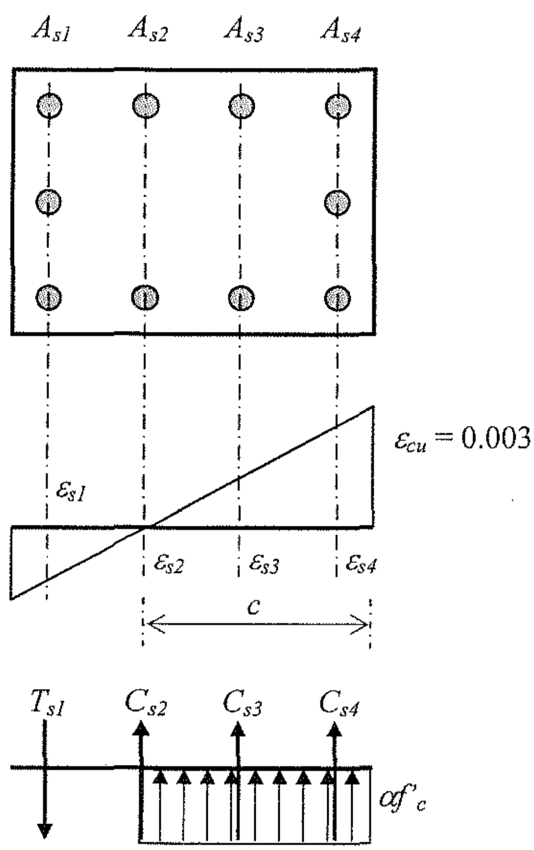

Figure 8-2 Equilibrium conditions and strain distribution in a column

The strain of the longitudinal reinforcement is computed from similar triangles with an (for evaluation purposes) unknown neutral axis depth c. The stress in the reinforcement is then calculated by $f_{si} = \varepsilon_{si} E_s$. Since no information regarding the modulus of elasticity, E_s, was provided in the databases, it was assumed for all specimens E_s = 200,000 MPa. The corresponding forces are found from the provided area of steel. Equilibrium of forces including the axial load P is then used to find the neutral axis depth iteratively. For design purposes, a neutral axis depth is chosen, giving the required moment – axial load interaction. Taking equilibrium of moments about the center of the cross section gives the flexural design moment M_y. The lateral load related to flexural yielding is found from

$$V_{y,flex} = \frac{M_y}{a} \tag{8.1}$$

where a = shear span of the column

The flexural yield load determined for the members of the database is plotted against the measured flexural yield load in Figure 8-3. The mean value of measured to calculated strength is $1.08 \pm 0.39\%$ within a 95 % confidence region. The coefficient of variation of the calculated strength ratio is 14.48 % with a standard deviation of 0.16.

Using the flexural yield load and the drift ratio at yield, $\delta_y = \Delta_y / a$, a dimensionless ratio m can be defined for the strength degradation due to cyclic loading. The flexural degradation ratio m is taken as the ratio of strength degradation to the corresponding change in the displacement:

$$m = \frac{\left(V_{y,flex} - 0.8 \cdot V_{y,flex}\right) / V_{y,flex}}{\Delta_s / a}$$
$$\Leftrightarrow m = \frac{0.2}{\Delta_s / a} \tag{8.2}$$

with

$$\Delta_s = \Delta_{u,flex} - \Delta_{y,flex} \tag{8.3}$$

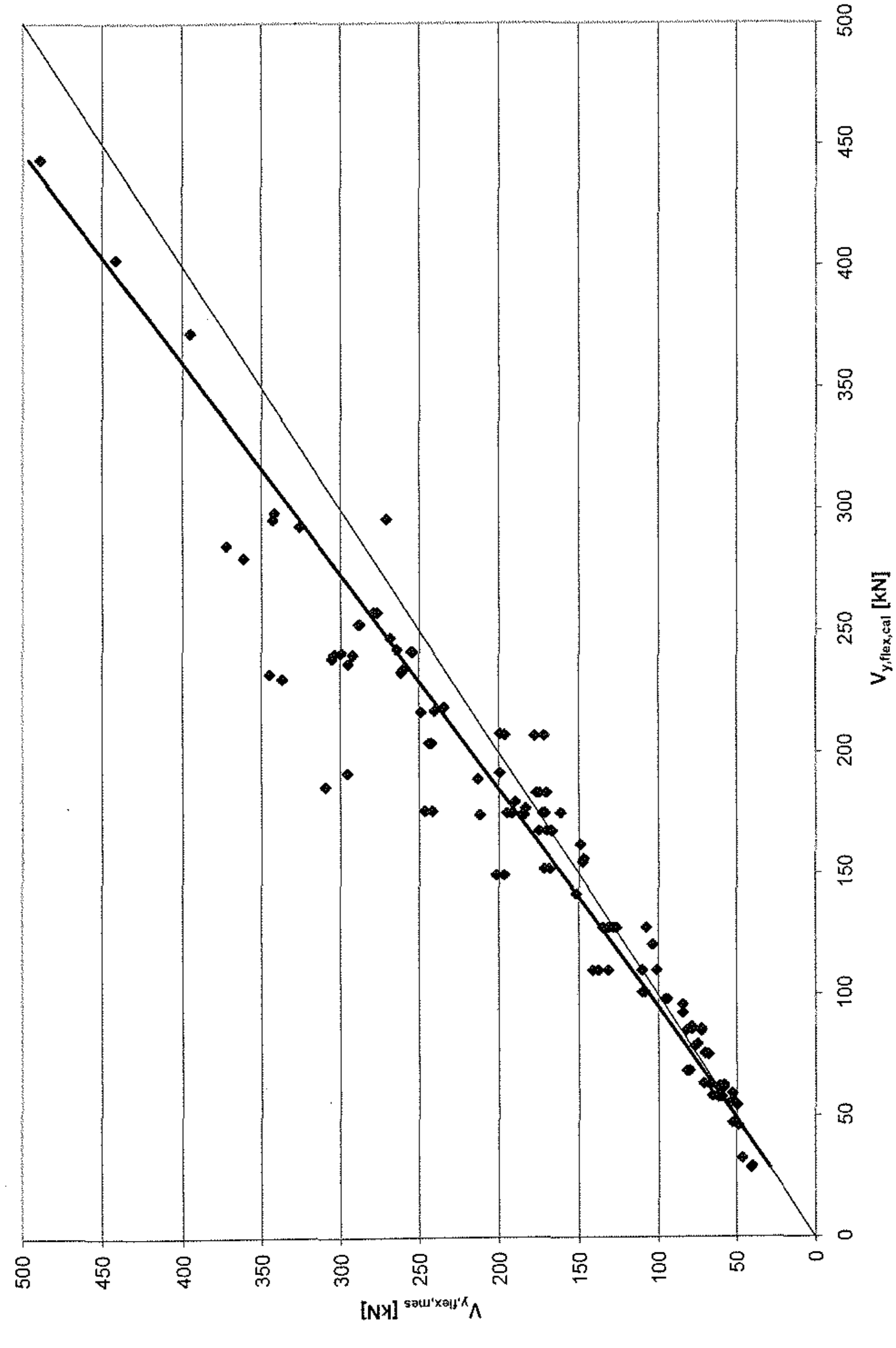

Figure 8-3 Measured versus calculated flexural yield load for columns under cyclic shear

8.1.2 Flexural strength degradation

The strength degradation in flexural members is assumed dependent on five dimensionless parameters:

1) The aspect ratio *a*/*d*: Intuitively, it is expected that the strength of stocky members degrades at a faster rate with respect to displacement than the strength of slender members.

2) The ratio of gross area to core area of the cross section: A relatively larger confined area is expected to sustain larger displacements without significant loss in strength than relatively small cores.

3) The confinement ratio, taken as the effective yield stress in the web reinforcement divided by the compressive strength of concrete, $\rho_w f_{wy} / f'_c$: Low values for $\rho_w f_{wy}$ are expected to yield a larger slope m, that is, a smaller limiting drift ratio.

4) The ratio of flexural to shear strength: A low ratio means the member is flexure-controlled, allowing for a larger limiting drift ratio.

5) The axial load level $P/\left(A_g f'_c\right)$: Large compressive axial stresses are known to reduce the ductility of RC members (Legeron and Paultre 2000).

The flexural degradation ratio m can be used to determine a combination of the previously listed parameters for a chosen limiting drift ratio $\Delta_{lim,flex}$. Alternatively, taking the given conditions, a limiting drift ratio can be calculated.

It is necessary to realize that an exact estimate of the limiting drift ratio, and therefore an accurate estimate of the degradation ratio m in seismic design, is difficult to obtain given the uncertainty of parameters that control the behavior. Nevertheless, in the following, it is attempted to give a safe assumption based on the provided database with an emphasis on safety in a reasonable amount of scatter. This can provide good insight on how strength degradation is affected by the parameters listed above.

Since none of the parameters could be extracted exclusively from the given database, a feedforward neural network was trained on values for m calculated from measured values by eq. (8.2) with measured input values provided by the database. The neural network was trained using 104 training data sets and 12 validation data sets, representing approximately ten percent of the available data. It consisted of one hidden layer with three neurons with an activation function of sigmoid type (Wolfram 2002):

$$f(x) = \frac{1}{1+e^{-x}} \tag{8.4}$$

None of the five input parameters was fixed. A schematic illustration of the used network is shown in Figure 8-4. The values X_i on the left of the figure represent the previously described input parameters. Each parameter, plus a unity bias parameter ("1"), is an input value of the hidden neurons, symbolized by $\Sigma\sigma$. The used network had one hidden layer that consisted of three neurons. Each neuron performs a weighted summation of the inputs following equation (8.5).

$$\hat{y}(\theta) = g(\theta, x) = \sum_{i=1}^{3} w_i^2 \sigma\left(\sum_{j=1}^{5} w_{i,j}^1 x_j + b_{j,i}^1\right) + b^2 \qquad (8.5)$$

The weights w_j and b_j are represented by the arrows from the input parameters to the hidden neurons in Figure 8-4. The inner summation in equation (8.5) is performed on the input parameters, which in the examined case are five; the outer summation is performed on the three hidden neurons. The output of the trained network is performed in an output layer as another weighted summation of the outputs of the respective neurons (Wolfram 2002).

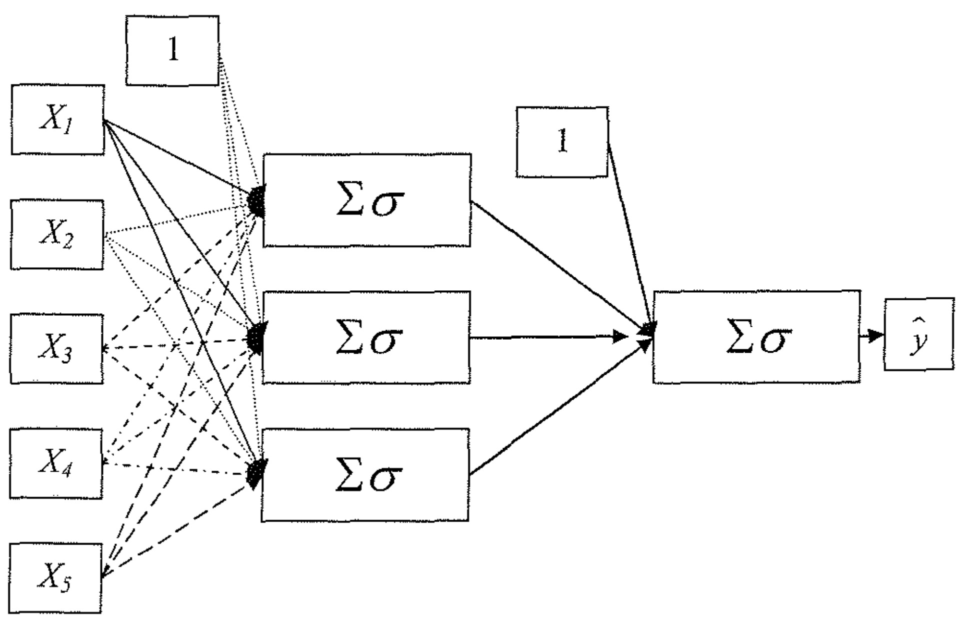

Figure 8-4 Feedforward neural network (FF network) with five input parameters and one hidden layer including three neurons

Using the resulting output function, each one of the five parameters could be varied and plotted against m, while the other parameters were fixed at values representative of the database (for example, $a/d = 4$, $P/(A_g f'_c) = 0.2$). This could be used to give a reasonable assumption about the form of the function relating the considered parameter to the degradation ratio.

Figure 8-5 and Figure 8-6 show the functions of the input parameters as derived from the trained neural network plotted against the degradation ratio. The graphs in Figure 8-5 indicate that the amount of axial load had a very distinct influence on the relation between strength degradation and the ratio of flexural to shear strength at low V_{flex}/V_{shear} ratios.

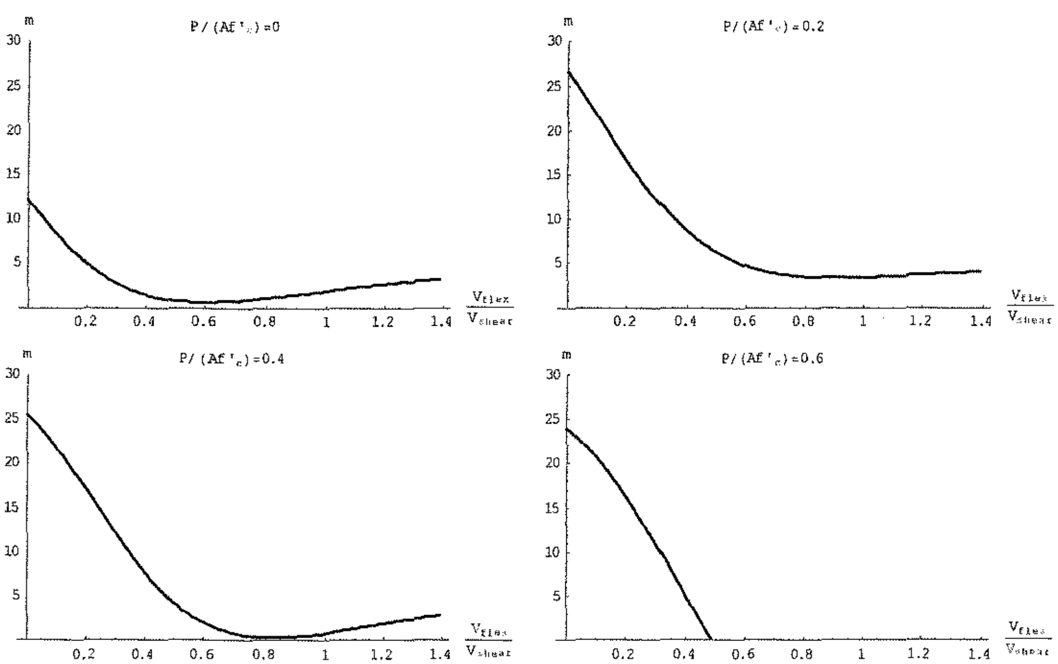

Figure 8-5 Degradation ratio with respect to strength ratio for various axial loads

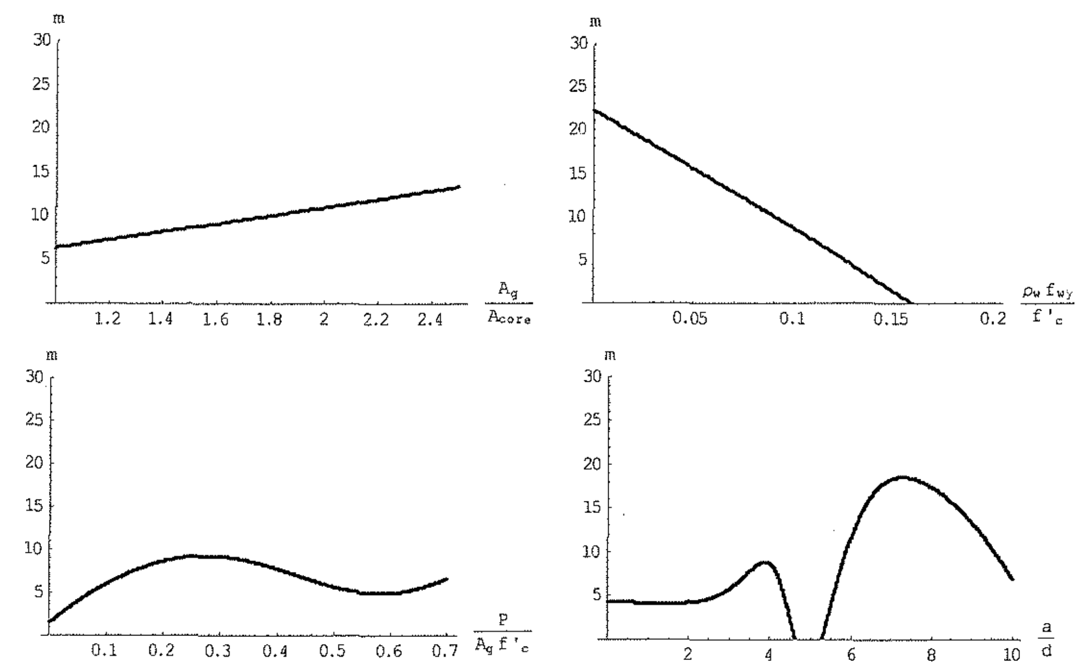

Figure 8-6 Degradation ratio m versus input parameters as calculated by the neural network

Using the exact resulting forms of the respective functions would be too tedious to calculate in relation to the accuracy of the complete estimate of m. Therefore, the functions were further simplified to mostly linear equations. The calculated flexural degradation ratio was then taken as the product of the considered parameters.

$$m_{cal} = C \cdot m_{a/d} \cdot m_{A_g/A_{core}} \cdot m_{confinement} \cdot m_{strengthratio} \cdot m_{P/(A \cdot f'_c)} \tag{8.6}$$

with C = constant, and:

$$
\begin{aligned}
m_{a/d} &= x_1 + y_1 \cdot \frac{a}{d} \\
m_{A_g/A_{core}} &= x_2 + y_2 \frac{A_g}{A_{ore}} \\
m_{confinement} &= x_3 + y_3 \frac{\rho_w f_{wy}}{f'_c} \\
m_{strengthratio} &= \frac{x_4}{y_4 + z_4 \cdot \left(V_{y,flex} / V_{shear} \right)^{w_4}} \\
m_{P/(Af'_c)} &= x_5 + y_5 \cdot \frac{P}{A_g f'_c}
\end{aligned}
\tag{8.7}
$$

The calibration of the variables $\{x, y, w\}_i$ on measured values of the database yielded the following functions:

$$
\begin{aligned}
C &= 0.43 \\
m_{a/d} &= 10 + \frac{a}{d} \equiv k_1 \\
m_{A_g/A_{core}} &= 0.5 + 0.05 \frac{A_g}{A_{ore}} \equiv k_2 \\
m_{confinement} &= 5 - 28 \frac{\rho_w f_{wy}}{f'_c} \equiv k_3 \\
m_{strengthratio} &= \frac{2.5}{-3 + 22 \left(V_{y,flex} / V_{shear} \right)^{0.6}} \equiv k_4 \\
m_{P/(Af'_c)} &= 1 + 6 \frac{P}{A_g f'_c} \equiv k_5
\end{aligned}
\tag{8.8}
$$

The values k_i denominate the respective multiplier in Figure 8-8 through Figure 8-12. As mentioned earlier, emphasis was put on a conservative estimate of the degradation ratio m. Using the parameters listed above to calculate m according to eq. (8.6) yielded an average value of $m_{mes} / m_{cal} = 1.45 \pm 1.24\%$. The standard deviation was found to be 0.62 with a coefficient of variation of 42.5 %. Figure 8-7 shows a graph of measured against calculated values for m. While the scatter is expectedly large, the trend is towards an increasingly conservative estimate for larger m values, i.e. for values representing a greater strength degradation. This was one of the objectives of the calibration to ensure safe estimates for increasingly sensitive members.

Figure 8-8 through Figure 8-12 show graphs of the degradation ratio m_{mes} determined from test results plotted against the contributing parameters in m_{cal}. The "measured" flexural degradation ratio was normalized by the calculated multipliers for all remaining parameters m_i. For example, in the plot of the degradation ratio against the aspect ratio, m_{mes} was normalized to all multipliers of m_{cal} except for the parameter related to the aspect ratio, $m_{a/d}$. These plots were used to determine whether the assumed trends, i.e. the influence of the respective parameters, behaved as expected, or if further adjustments were necessary. The graphs were plotted to the scale of the largest normalized m. This scale does not necessarily represent the actual calculated value for m, normalizing with respect to values smaller than one will increase the scale. Plotting to the same scale can give an indication of the influence of the examined parameter. The shear span was designated L instead of a in the figures to distinguish them from the several variables.

The normalized flexural degradation ratio was plotted against the aspect ratio in Figure 8-8. As can be seen for the range of the columns in the data set, the aspect ratio did not influence the strength degradation as was previously assumed. Therefore, the multiplier $m_{a/d}$ was set equal to one for the subsequent calculations.

In addition, the ratio of gross area to core area, displayed in Figure 8-9, did not have a significant effect on the strength degradation of the examined specimens. This confirms findings by Brachmann (Brachmann 2002). It follows, that also the multiplier related to the ratio of gross to core area will be set equal to one in the following calculations.

The normalized degradation ratio was plotted against the ratio of effective tensile strength of transverse reinforcement to concrete strength in Figure 8-10. The existing form was kept, even though the solid trend line indicates that adopting a similar equation for $m_{confinement}$ and $m_{strengthratio}$ would give results that are more accurate. This had three reasons: First, the existing form is simple. Second, the distinct curvature in the trend line resulted from three specimens with $\rho_w f_{wy}/f'_c \leq 0.3$. Looking at the remaining 114 specimens, a conservative linear curve can give a reasonable estimate on the relation between m and $\rho_w f_{wy}/f'_c$, which is shown by the dashed trend line. Third, a linear form reflects the results from the neural network, shown in Figure 8-6.

Figure 8-11 shows the degradation ratio plotted against the ratio of calculated flexural strength to shear strength. It is apparent that, if compared to the influence of other parameters, the strength ratio did not have a considerable effect on the strength degradation for the examined columns. Thus, the multiplier $m_{strengthratio}$ will be set to unity in a new calibration of the degradation ratio m.

A distinct influence of the axial load level on strength degradation can be seen in Figure 8-12. Even though the scatter is naturally high, it is apparent that an increase in axial load accelerates strength degradation on cyclically loaded members. The form of the function seemed to give a reasonable simplification of the curve plotted in Figure 8-7.

After this evaluation of the considered parameters, the degradation ratio was calculated again with a new calibration of the two remaining parameters, $m_{confinement}$, and $m_{P/(Af'_c)}$. The form of the functions as linear approximations was kept. Since only linear approximation functions were used, the scaling constant C could be set to unity, and the coefficients in the two parameters were used to scale the degradation ratio m, given by the product of the two parameters. Following the new calibration, equations (8.8) become:

$$
\begin{aligned}
&C = 1 \\
&m_{a/d} = 1 \equiv k_1 \\
&m_{A_g/A_{core}} = 1 \equiv k_2 \\
&m_{confinement} = 3 - 10\frac{\rho_w f_{wy}}{f'_c} \equiv k_3 \\
&m_{strengthratio} = 1 \equiv k_4 \\
&m_{P/(Af'_c)} = 1.25 + 5.4\frac{P}{A_g f'_c} \equiv k_5
\end{aligned}
\tag{8.9}
$$

Figure 8-13 shows a plot of the measured against the calculated degradation ratio after elimination of the insignificant parameters. Apparently, scatter became more significant, and the calculated degradation ratio gave a very conservative estimate of the calculated ratio. This is a natural effect of decreasing the number of contributing parameters. The mean value of measured to calculated degradation ratio was $1.67 \pm 1.71\%$; the standard deviation was 0.93, resulting in a coefficient of variation of 55.6 percent.

It can be concluded that even if eqs. (8.6) and (8.9) did not give a very accurate estimate on flexural strength degradation, they gave a safe assumption considering important influence factors in a confirmed form.

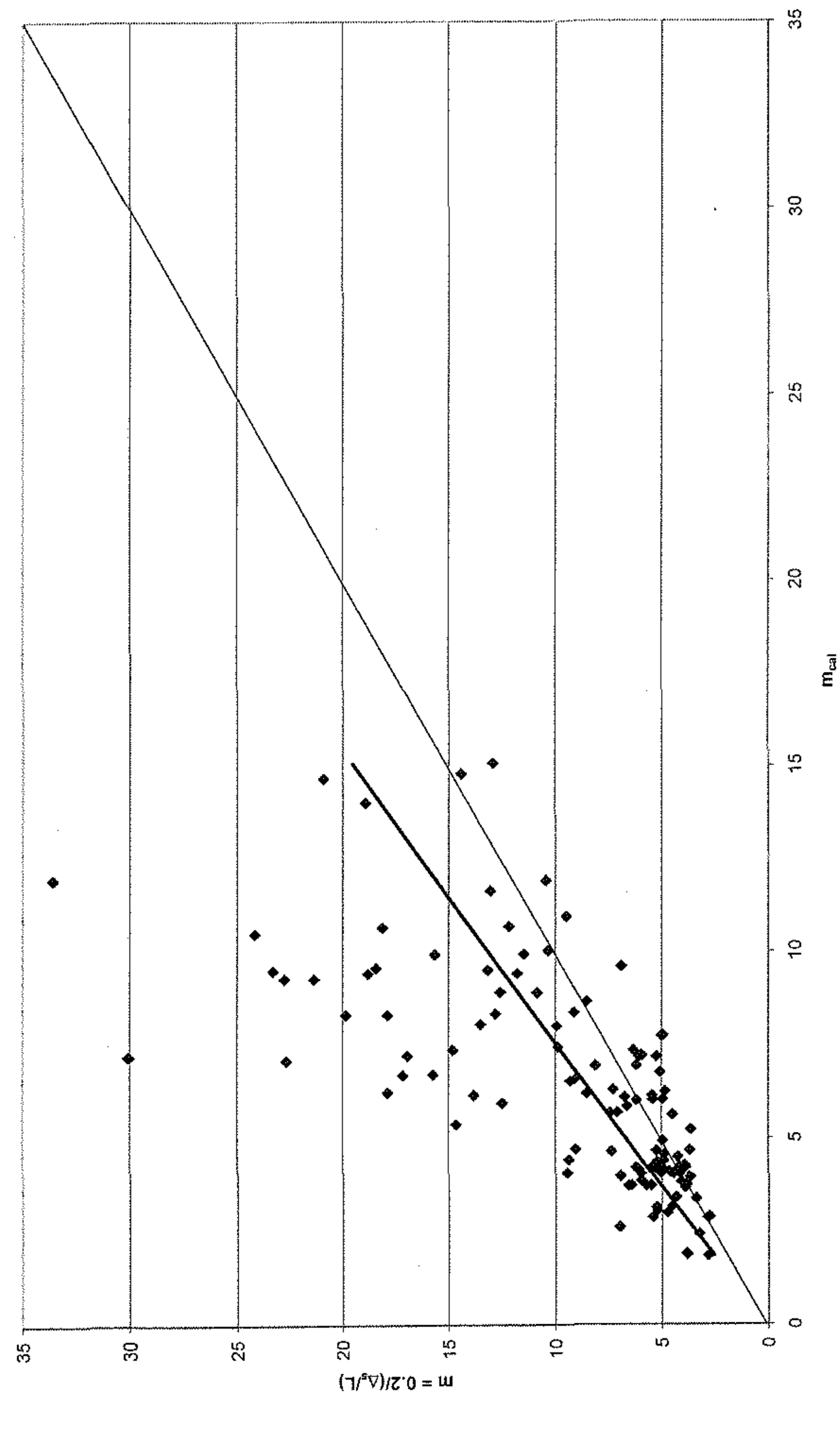

Figure 8-7 Measured versus calculated flexural degradation ratio

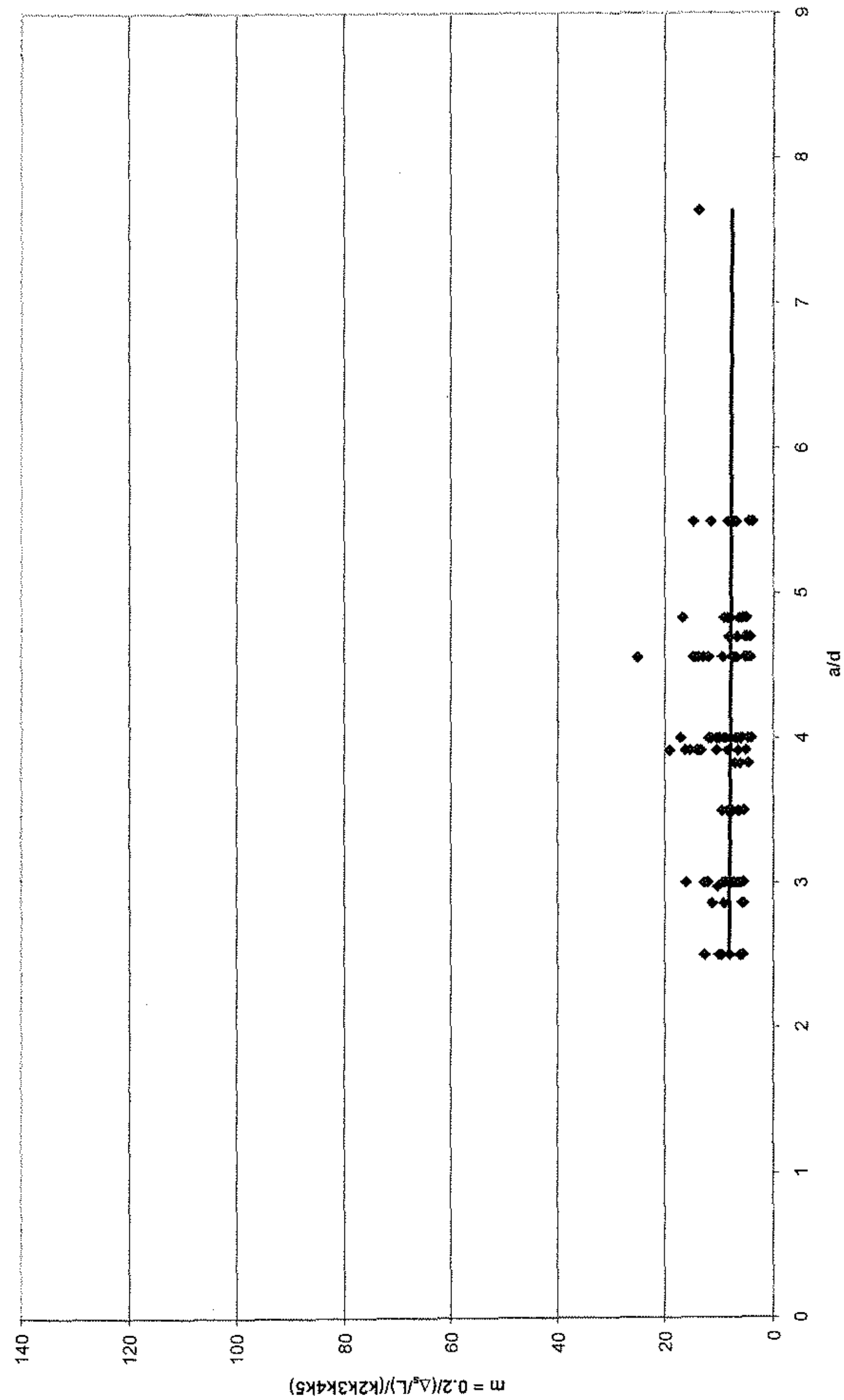

Figure 8-8 Normalized degradation ratio versus aspect ratio

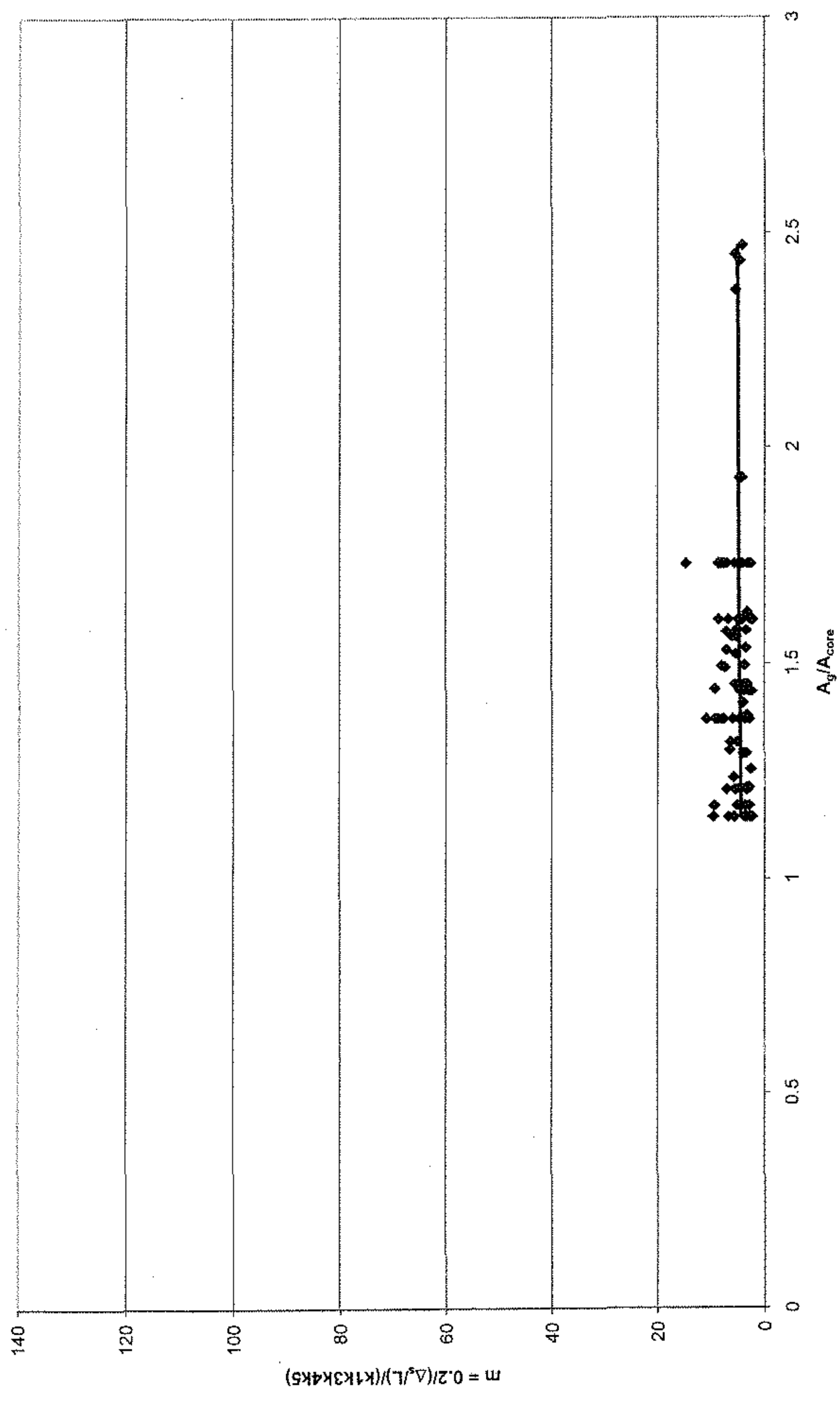

Figure 8-9 Normalized degradation ratio versus the ratio of gross area to core area

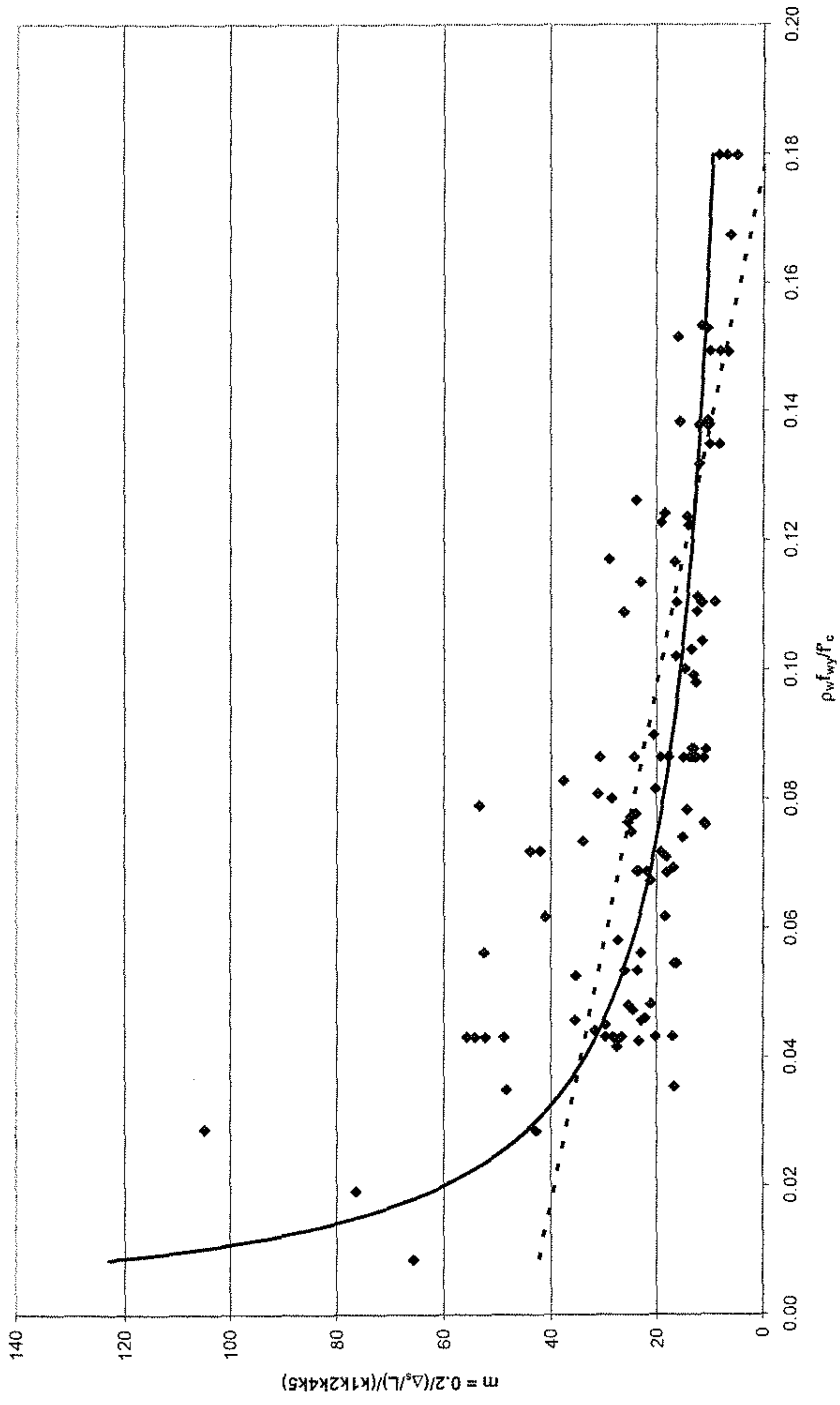

Figure 8-10 Normalized degradation ratio versus the ratio of effective yield strength of transverse reinforcement to core concrete compressive strength

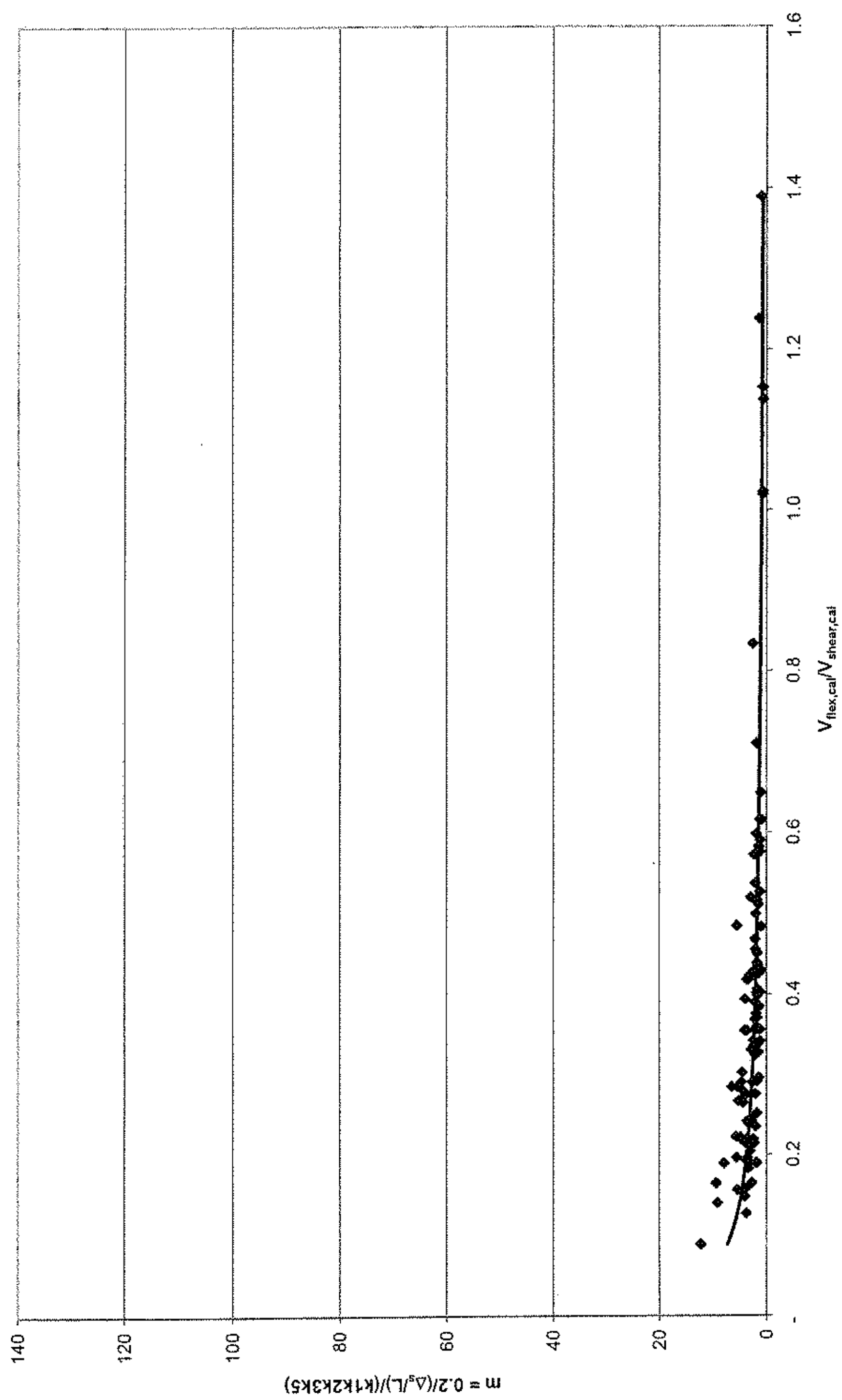

Figure 8-11 Normalized degradation ratio versus the ratio of calculated yield strength to calculated shear strength

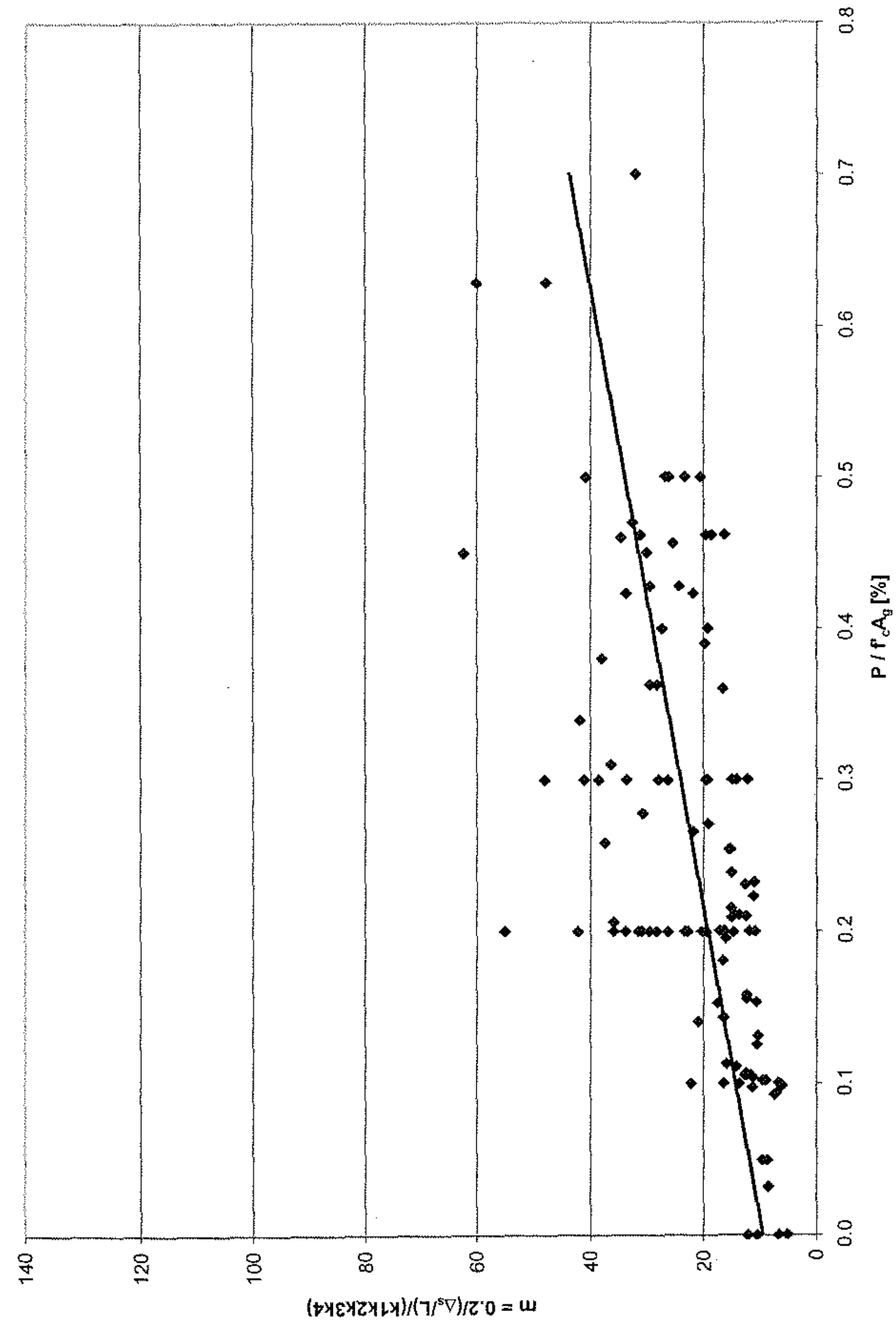

Figure 8-12 Normalized degradation ratio versus axial load level

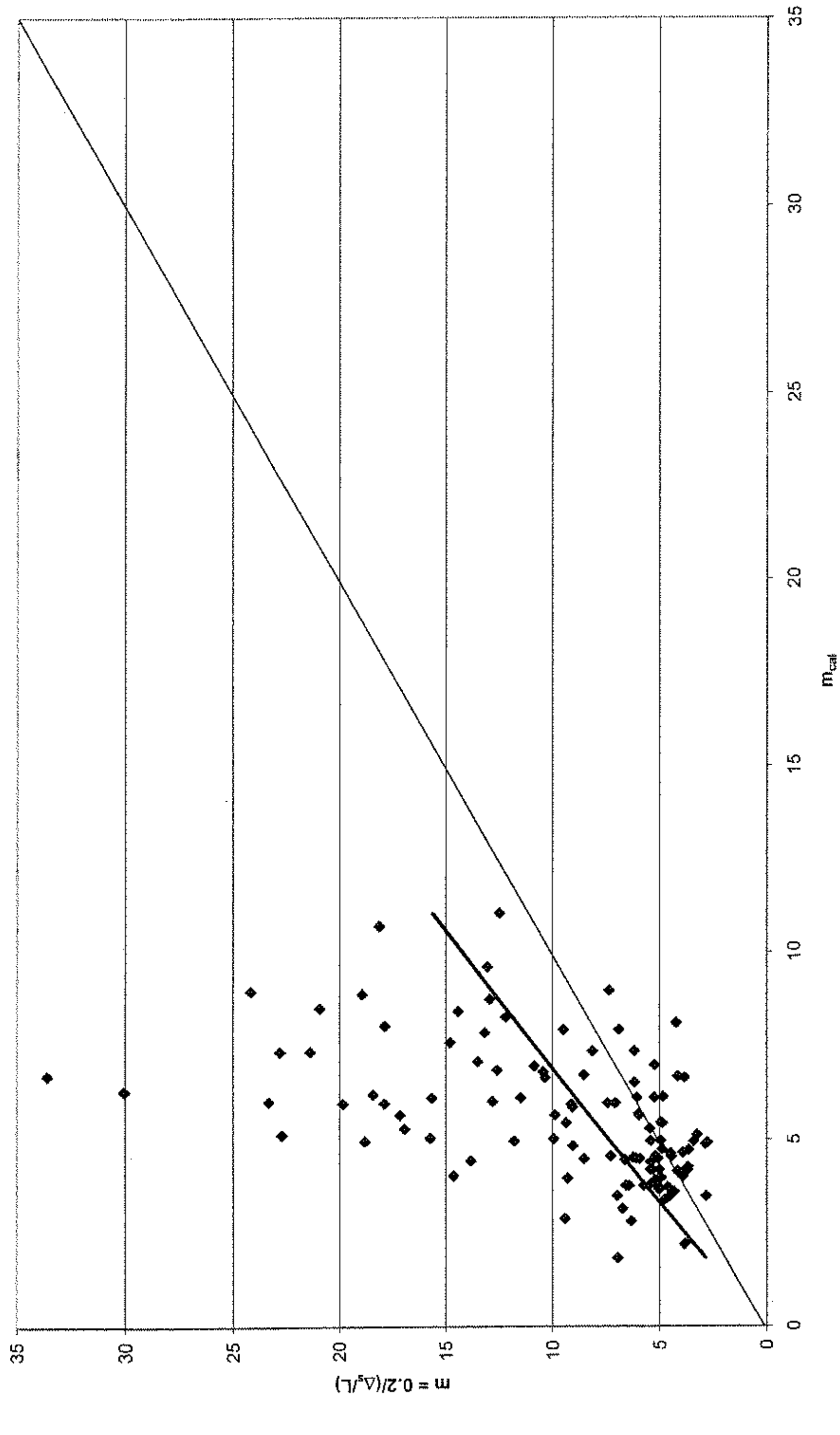

Figure 8-13 Measured versus calculated flexural degradation ratio after eliminating insignificant parameters

8.2 Strength degradation in shear-controlled members

The degradation of shear strength under cyclic lateral load can be described as a function defined by the initial static shear strength of the member (i.e. with no displacement) and the shear force causing yielding of the transverse reinforcement in relation to the drift reached at yielding of the web reinforcement. This was indicated by the dashed line in Figure 8-1. Generally, the design goal is to avoid a brittle shear failure by keeping the initial shear strength well above the flexural yield strength of the member. If, however, the degradation of shear strength with cyclic loading occurs at a higher rate than the degradation of flexural strength, the two failure lines can transgress, making the ultimate failure envelope for the member a combination of the two modes, with the risk of brittle failure in the shear-controlled range. It is therefore important to have a safe estimate for both failure modes.

The initial shear strength is given by the combination of arch-action, truss-action, and the components related to the compression zone of the member and friction. Under cyclic loading, only the first three components contribute to the degrading shear capacity. The contribution from friction as a load-carrying mechanism under cyclic load is neglected, because the load reversals are assumed to destroy the crack surfaces increasingly as cycling progresses, and because the tensile stresses in the reinforcement are significantly high. This degradation mechanism of crack surfaces is not controllable. It is therefore a safe assumption to neglect any contribution from friction for the cyclic load case. A detailed investigation on the friction mechanism under repeated loading was made by Walraven (Walraven 1986; Walraven et al.

1987). With progressing cycling, the contributions from arch-action and concrete in compression decrease, because the initially uncracked compression zone is repeatedly cracked and closed again. Each time the crack is opened wider aggregate particles break off the surface and stay within the crack, thus creating increasingly diverse crack surfaces that do not match upon closing of the crack within the next load cycle. As strength degradation of the arch- and concrete mechanisms progresses, an increased demand is shifted on the truss mechanism at the same rate as the capacity decreases. The increased demand on the truss causes faster strength degradation after the loss of arch and compression zone contributions.

Shear failure in the following is defined as the onset of yielding of the transverse reinforcement. Few data is available about the strength degradation process related to shear strength. Of the 38 members in the collected database that reportedly failed in shear, detailed information about strain in the transverse reinforcement is available for only 20 members (Ichinose et al. 2001; Matamoros 1999; Wight and Sözen 1973). This study will focus on these members.

Even though only limited data with respect to member behavior and the state of stresses and strains within the member is available, the tests by Ichinose give valuable insight in the previously described failure mechanisms. Seven of his eight tests provide useful data to evaluate the degradation process; data provided for one test (specimen D16N) does not show a strain – displacement curve that can be evaluated. Four tests failed in shear after flexural yielding without reaching the yield strain.

Ichinose relates these shear failures to increased axial strains "due to accumulations of residual strain in the longitudinal bars" (Ichinose et al. 2001).

The tests were conducted on eight cantilever columns with an aspect ratio of a/d = 1.93. Tested columns had a cross section of 250 x 250 mm, the force was applied at a distance of 450 mm. Measured yield strength of the transverse reinforcement with 9 mm diameter was 319 MPa. The yield strength of the tensile reinforcement ranged from 377 MPa to 391 MPa, two specimens (P22) with f_y = 1080 MPa were tested. The concrete compressive strength was measured at an average of 28.74 MPa. Details on the test procedure and specimens are provided in (Ichinose et al. 2001). The maximum strain in the transverse reinforcement was measured at a distance x = 160 mm from the support. Additional strain measurements were taken at x = 80 mm and x = 240 mm. However, these strains were smaller than the strains measured at x = 160 mm.

Figure 8-14 shows the strain – deflection diagram for specimen D19S, which will be used as an example for the discussion of strength degradation. Specimen D19S was reinforced with inner and outer ties. The solid black line in Figure 8-14 represents the behavior of the inner ties; the dashed black line shows the behavior of the outer ties, which developed smaller strains and did not yield. The bold grey line represents the calculated yield strain of $\varepsilon_{w,y}$ = 0.0016. The strain – deflection diagram shows how the demand on the stirrups increased up to a strain of ε_w = 0.0014 at a positive deflection of Δ_c = 9.3 mm. Yield strain was not reached so far. This point is assumed to represent the maximum increase of demand on the truss. If it is assumed that with progressive cycling the arch and compression zone contributions decrease, the loss of their contributions is an increasing demand on the truss component. At the deflection of $\Delta_c = 9.3$ mm, the arch and concrete components have degraded to zero contribution, while the demand on the truss mechanism has increased at the same rate. A relationship will be defined later to describe the decay of arch and concrete components.

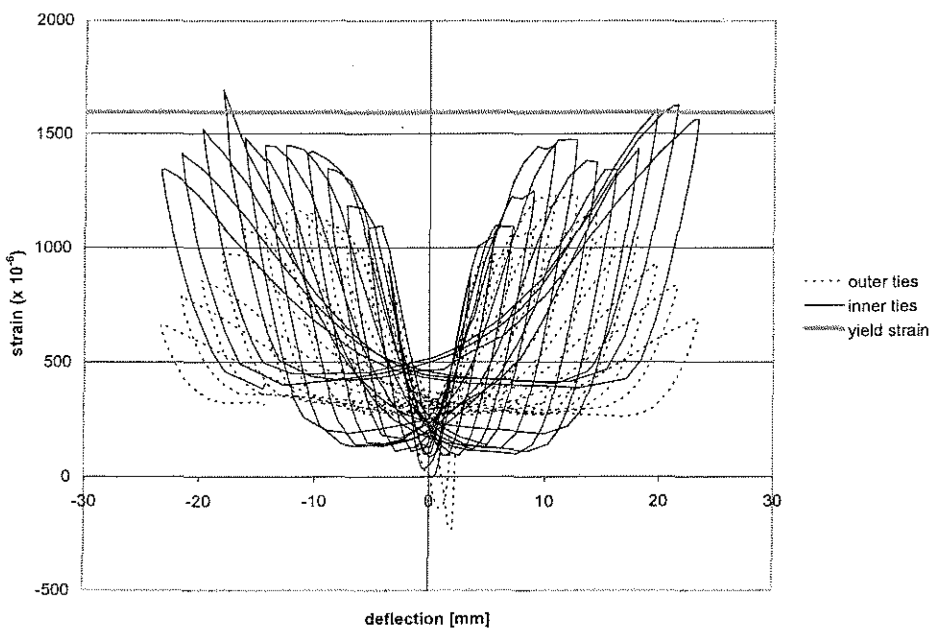

Figure 8-14 Strains in transverse reinforcement, Ichinose specimen D19S (Ichinose et al. 2001)

After reaching a first peak at $\Delta_c = 9.3$ mm, the strain in the ties of specimen D19S decreased under positive deflections. Yielding was first reached under negative deflections, then, with progressing loss of strength, was also reached under positive deflections. Strength degradation of the truss mechanism is even more visible for the outer ties, printed in a dashed line. Because the calculated yield strains were not markedly exceeded, further strength degradation of the truss mechanism is also visible after the peak strain was reached on the negative deflection side. This can also be related to yielding within the same loading cycle in the positive direction.

Figure 8-15 through Figure 8-21 show the deflection – strain diagrams for the other tests conducted by Ichinose (Ichinose et al. 2001). A degradation of the truss mechanism is not only indicated by the decreasing strains at increasing deflections after contributions from V_a and V_{cz} have vanished, but is also clearly visible in each load-cycle. Before the loss of arch and compression zone components, the strain at the peak of each cycle increases at a slower rate with increasing deflections, or, for some specimens does not increase at all. The fact that the strain curves become increasingly horizontal before V_a and V_{cz} have vanished is taken as an indicator that the demand on the truss mechanism was increasing, therefore also increasingly weakening the truss.

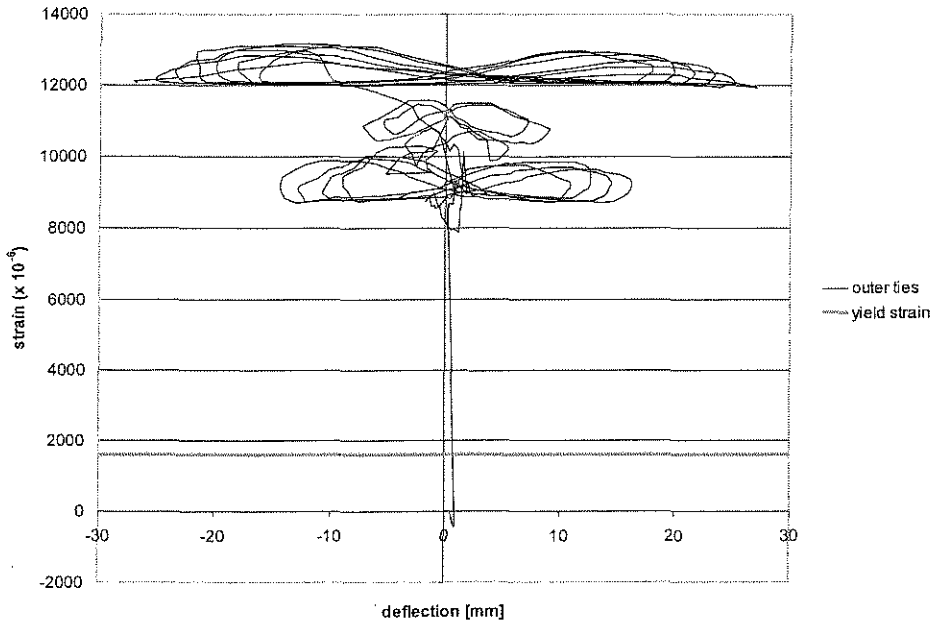

Figure 8-15 Strains in transverse reinforcement, Ichinose specimen D16N (Ichinose et al. 2001)

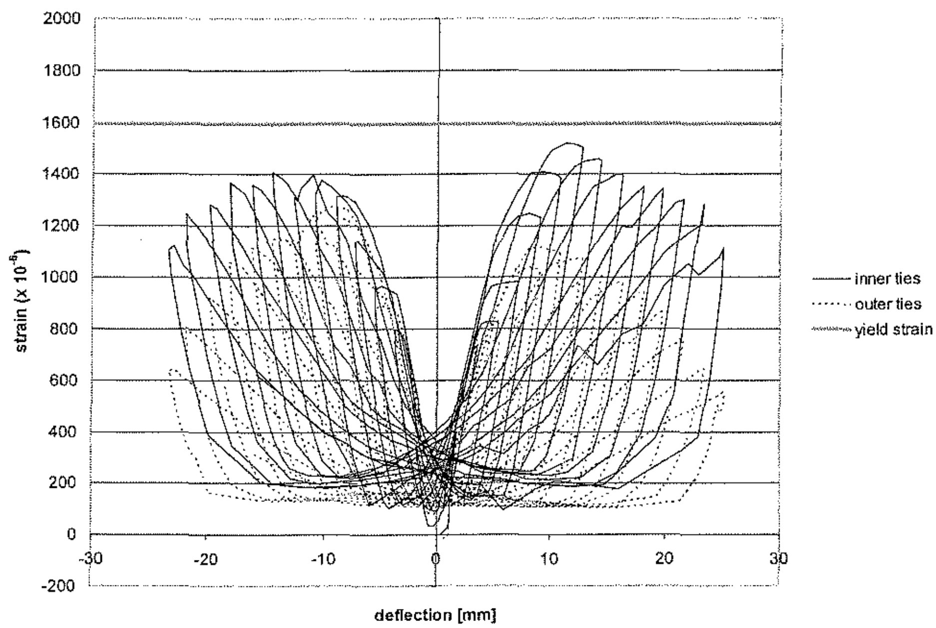

Figure 8-16 Strains in transverse reinforcement, Ichinose specimen D16S (Ichinose et al. 2001)

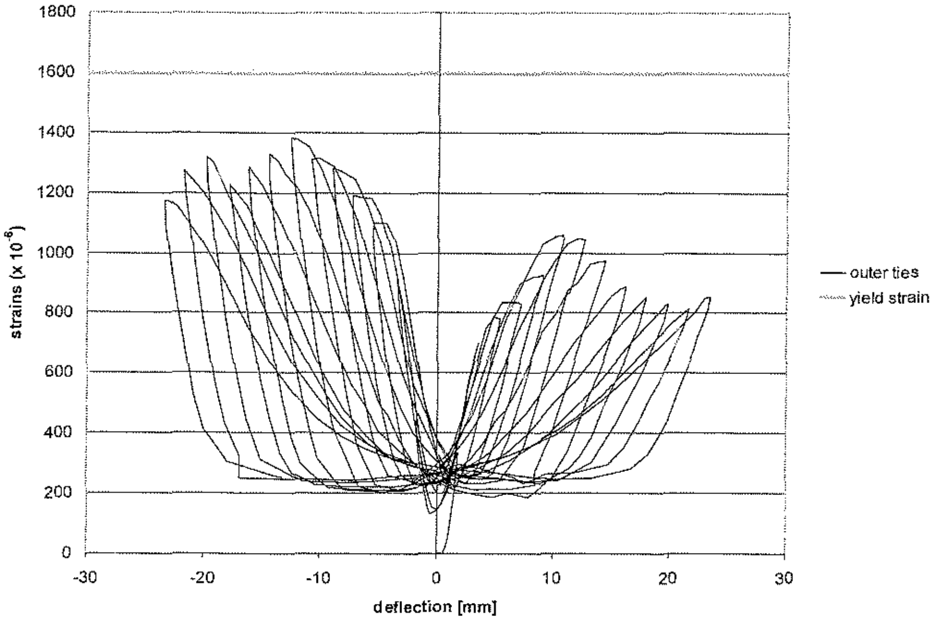

Figure 8-17 Strains in transverse reinforcement, Ichinose specimen D19N (Ichinose et al. 2001)

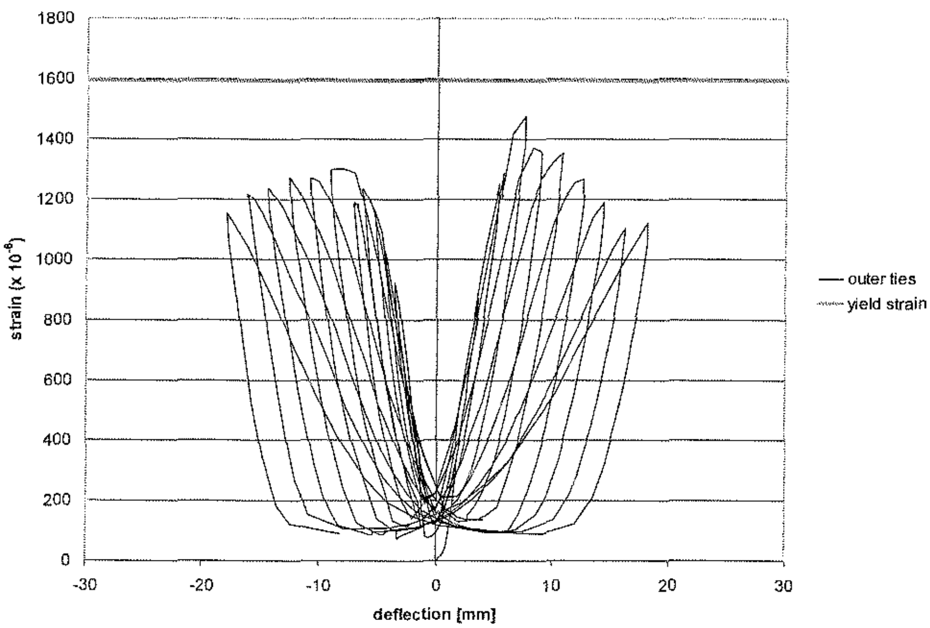

Figure 8-18 Strains in transverse reinforcement, Ichinose specimen D22N (Ichinose et al. 2001)

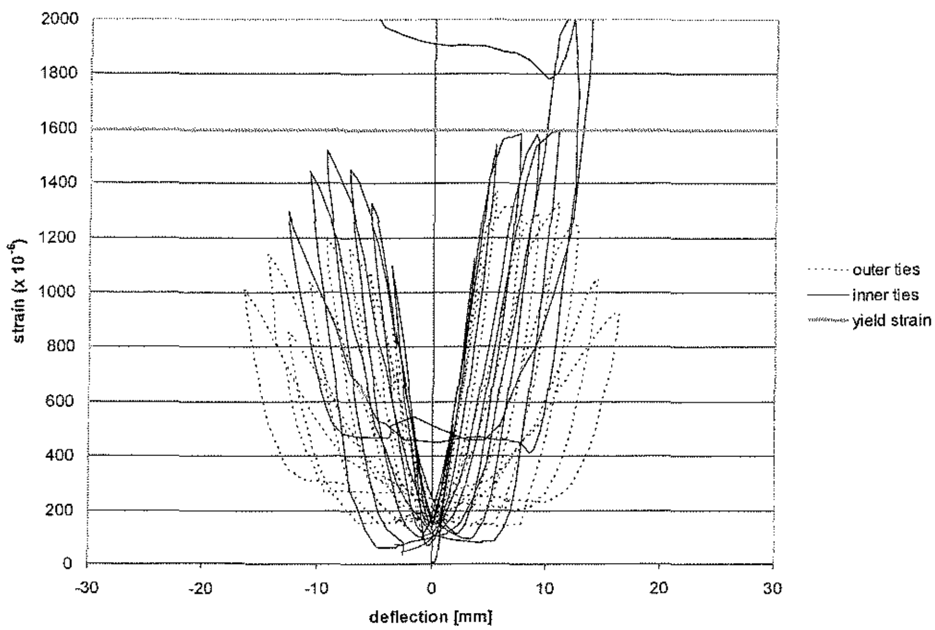

Figure 8-19 Strains in transverse reinforcement, Ichinose specimen D22S (Ichinose et al. 2001)

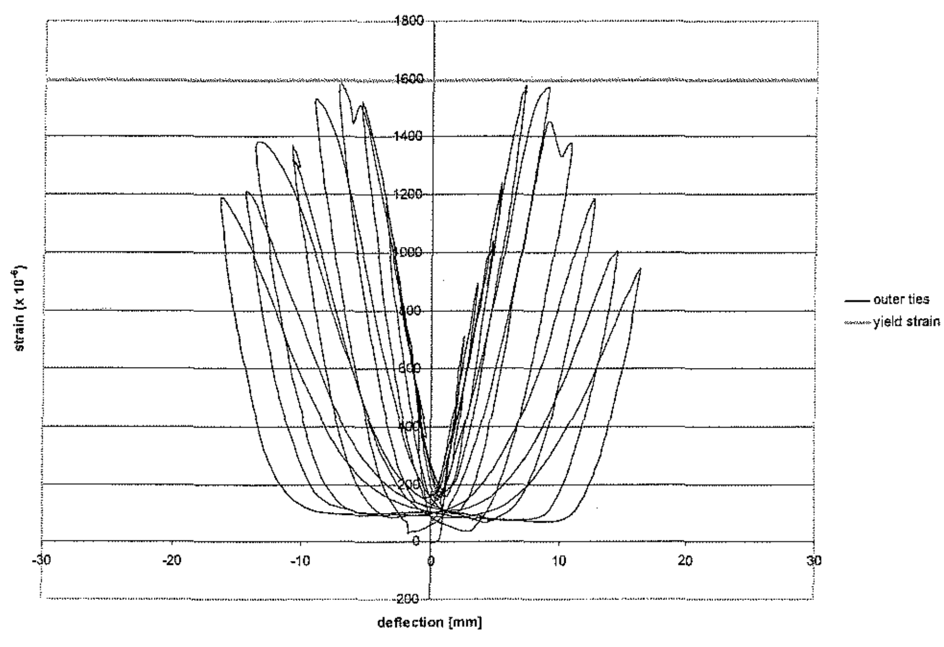

Figure 8-20 Strains in transverse reinforcement, Ichinose specimen P22N (Ichinose et al. 2001)

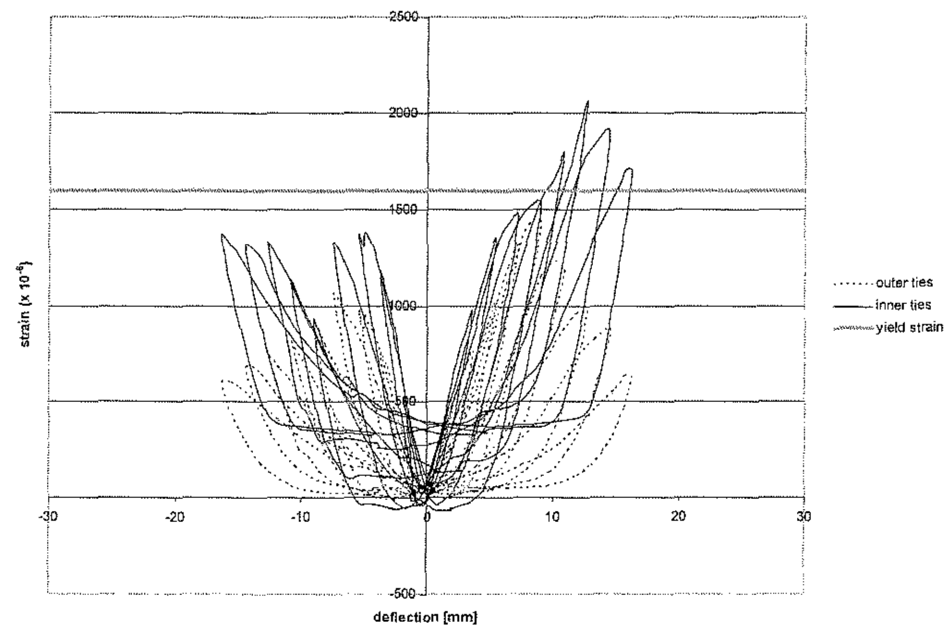

Figure 8-21 Strains in transverse reinforcement, Ichinose specimen P22S (Ichinose et al. 2001)

The calculated contributions of arch-action, compression zone, and truss-action of all members considered in the evaluation are compared in Table 8-1 to the measured yield strengths and maximum shear capacities (Ichinose et al. 2001; Matamoros 1999; Wight and Sözen 1973). For all specimens except for two columns tested by Wight and Sözen, and members in the Ichinose test series, the calculated capacity of the truss was higher than the measured strength at yielding of the transverse reinforcement, V_{yt}. Four of the specimens tested by Ichinose did not reach yielding of the transverse reinforcement, specimens D22S and P22S had larger measured than calculated capacities at yielding of the web reinforcement. It is apparent from the results in Table 8-1 that even with the components for compression zone and arch action fully degraded, i.e. $V_c + V_a = 0$, also the truss component must have degraded to the smaller measured load at yielding of the stirrups.

Specimen		V_c+V_a [kN]	V_t [kN]	V_{yt} [kN]	$(V_{yt}-V_{c+a})/V_t$ [-]	V_{max} [kN]
Wight & Sozen	No. 40.067E	15.9	124.2	92.0	0.61	92.2
Wight & Sozen	No. 40.067W	15.9	124.2	95.0	0.64	91.8
Wight & Sozen	No. 25.033E	15.3	64.2	81.0	1.02	84.9
Wight & Sozen	No. 25.033W	15.3	64.2	93.0	1.21	90.3
Matamoros et al.	C5-20N	21.3	178.7	45.0	0.13	72.5
Matamoros et al.	C10-05N	15.0	197.6	57.0	0.21	70.3
Matamoros et al.	C5-20S	22.2	176.1	49.0	0.15	72.5
Matamoros et al.	C10-10N	16.9	247.6	77.0	0.24	95.6
Matamoros et al.	C5-40N	34.9	202.0	69.0	0.17	84.5
Matamoros et al.	C5-40S	34.9	199.8	69.0	0.17	84.5
Matamoros et al.	C10-20N	34.5	218.3	73.0	0.18	107.6
Matamoros et al.	C10-20S	29.5	221.4	73.0	0.20	103.6
Ichinose et al.	D16S	21.2	211.6	n/a	n/a	140.0
Ichinose et al.	D19S	21.2	209.0	155.0	0.64	191.0
Ichinose et al.	D19N	21.2	209.0	n/a	n/a	196.0
Ichinose et al.	D22S	21.2	205.7	251.0	1.12	254.0
Ichinose et al.	D22N	21.2	205.7	n/a	n/a	252.0
Ichinose et al.	P22S	21.2	180.3	273.0	1.40	309.0
Ichinose et al.	P22N	21.2	180.3	n/a	n/a	290.0

Table 8-1 Measured and calculated shear strength components

The ratio of the difference between yield strength and V_{c+a} is plotted against the drift ratio at yielding of the transverse reinforcement in Figure 8-22. It is clear that, for the specimens considered, the truss mechanism degraded with increasing drift. The capacity of the truss at yielding of the stirrups was considerably lower than the initial strength of the truss for all members, except for specimens 25.033E, and

25.033W tested by Wight and Sozen (Wight and Sözen 1973); and specimens D22S, and P22S from the test series by Ichinose et al. (Ichinose et al. 2001).

Figure 8-23 shows a similar graph for the ratio of the difference between yield strength and V_{c+a} plotted against the axial load. Even though the trend for the degradation of the truss mechanism with increasing axial load is not as apparent as the trend related to drift, an increasing degradation of the truss with increasing axial loads can be noticed. The function for degradation of the truss mechanism will be derived later as a function of the drift ratio at yielding of the transverse reinforcement, and of the axial load.

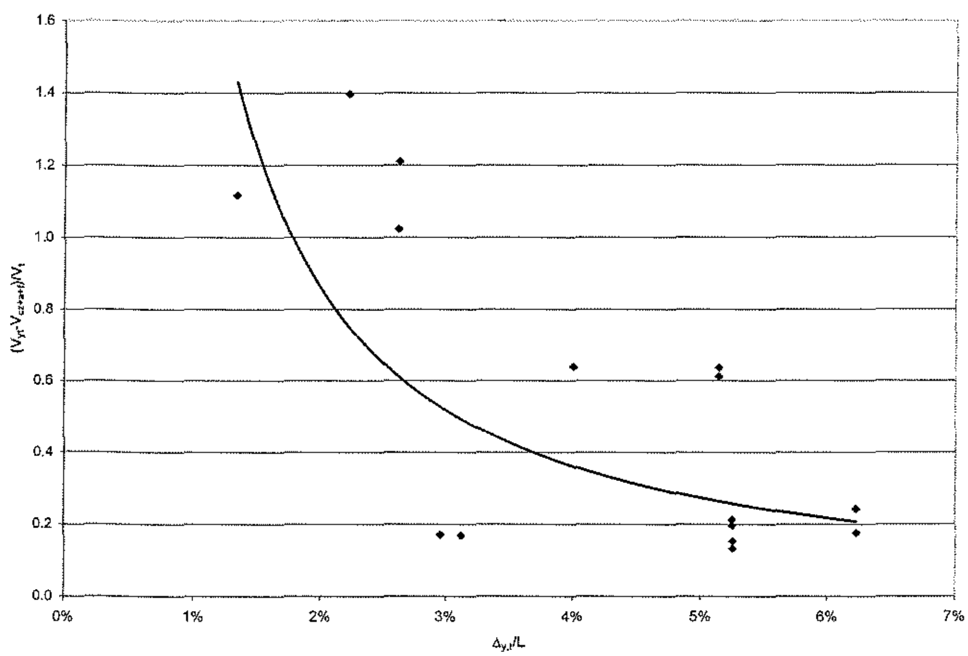

Figure 8-22 Ratio of measured truss strength at yielding of the transverse reinforcement to initial strength of the truss versus drift ratio at yielding

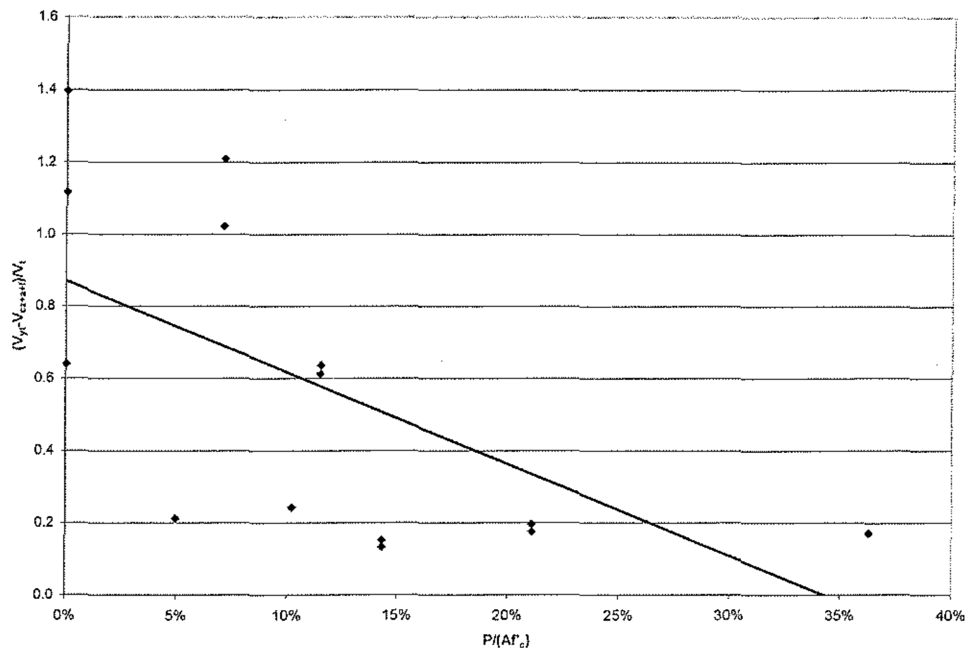

Figure 8-23 Ratio of measured truss strength at yielding of the transverse reinforcement to initial strength of the truss versus axial load level

Table 8-2 lists displacements, strains, and stresses at the first peak strains before yielding, i.e. the point at which $V_{c+a} = 0$, for all specimens tested by Ichinose (Ichinose et al. 2001). The stresses in the stirrups, f_s, were below the yield strength of 319 MPa. Resulting from the stresses in the stirrups, the stresses in the inclined compression field of the truss were calculated. As shown in the last column of Table 8-2, these were approximately one quarter of the compressive strength of concrete. This was taken as an indication that the degradation of truss action was not related to excessive stresses in the compression field.

Specimen	$\delta_c = \Delta_c/a$	$\varepsilon_{\Delta c}$ x 10^{-6}	$f_s(\varepsilon_{\Delta c})$ [MPa]	$f_t(\varepsilon_{\Delta c})$ [MPa]	$f_t(\varepsilon_{\Delta c})/f'_c$
D16S	2.4%	1390	278.0	6.84	0.24
D19S	2.8%	1474	294.8	7.25	0.25
D19N	2.4%	1056	211.2	5.19	0.18
D22S	1.2%	1560	312.0	7.67	0.27
D22N	1.7%	1477	295.4	7.26	0.25
P22S	2.0%	1540	308.0	7.57	0.26
P22N	1.6%	1581	316.2	7.77	0.27

Table 8-2 Properties at loss of arch and compression zone contributions for specimens tested by Ichinose (Ichinose et al. 2001)

To describe the strength degradation of the contributing components, a general model of the following form was adopted:

$$V_n = (1-\eta)(V_{cz} + V_a) + \chi V_t \tag{8.10}$$

In which η and χ are degradation functions for the respective component.

V_n was defined as the capacity of the members at yielding of the transverse reinforcement, V_{yt}.

Because only very limited data was available to establish the respective degradation functions, two assumptions were necessary:

1) The function η for the degradation of the compression zone and arch components was calibrated on the V_a terms calculated for the specimens tested by Ichinose. These members lie in the transition zone between stocky and slender members with $a/d = 1.93$. According to the previously derived transition func-

tion for the static load case, k_c, the compression zone contribution is negligible in these members compared to the contribution from the arch component. Nevertheless, it was assumed that the strength degradation for both components behaves similar in the transition zone. Therefore, it was assumed that, in the transition zone between stocky and slender members, the degradation of the compression zone component could be modeled by the degradation of the arch component. The degradation η is taken as a linear function of the drift ratio δ, and a function of the confinement, $\rho_w f_{wy}/f'_c$.

2) If the compression zone component is derived as a linear function of the displacement Δ_c, taken as the displacement at the first peak in strains from the Ichinose test series, the degraded compression zone component could be calculated for other test specimens at the drift related to yielding of the transverse reinforcement. This was used to establish the degradation of the truss in slender members by subtracting the reduced V_{c+a} component from the strength at maximum displacement and reducing the truss component accordingly (eq. (8.11)). The degradation of the truss, χ, was taken as a function of the axial load and the drift ratio at yielding of the transverse reinforcement.

$$\chi = \frac{V_{yt} - (1-\eta)V_{cz}}{V_t} \tag{8.11}$$

8.2.1 Degradation of the compression zone contribution

According to the previous assumptions, the degradation of the compression zone could be modeled as the degradation of the arch component within the transition zone from stocky to slender members. If a relationship could be found that described the strength degradation of arch and concrete components, and this degradation was linear, it would also be applicable to determine the strength degradation up to the yield deflection of the transverse reinforcement. For the members from the Ichinose test series the strength degradation was known. The shear strength component V_{cz} degraded to zero at a drift ratio of $\delta_c = \Delta_c/a$, where Δ_c is the displacement at the first peak strain in the stirrups before yielding and a is the shear span. The function describing the strength degradation, η, was calibrated on the displacements related to the peak strain before yielding from the tests conducted by Ichinose. Its general form was taken as

$$\eta = \frac{x \cdot \delta}{\rho_w f_{wy} / f'_c + y} \tag{8.12}$$

where x, y = variables depending on the calibration

$\rho_w f_{wy}$ = effective yield strength of the transverse reinforcement

f'_c = compressive strength of concrete

δ = drift ratio

With the shear strength at the first peak before yielding of the stirrups known to be V_{cz}, η can be determined by

$$
\begin{aligned}
&(1-\eta)V_{c+a} = V_{c+a,reduced} \\
&\Leftrightarrow \eta = 1 \text{ for } \delta = \delta_c = \Delta_c / a \text{ and } V_{c+a,reduced} = 0
\end{aligned} \tag{8.13}
$$

The calibration on the seven tests by Ichinose yielded

$$
\eta = \frac{8\delta}{\left(\rho_w f_{wy} / f'_c\right) + 0.01} \tag{8.14}
$$

Equation (8.14) implements that the degradation is larger for small confinement ratios, and that the combined contributions from compression zone and arch action degrade at a fast rate, if no confinement is provided. For simplicity, the added term in the denominator of eq. (8.14) can be neglected. However, in this case, arch action and compression zone would not contribute to shear strength under cyclic loading, if no confinement is provided.

This function for η provided a safe assumption for condition (8.13) with a mean value of $\bar{\eta} = 1.07 \pm 4.3\%$ within a 95 % confidence interval. The standard variation was expectedly high for a small data set at 0.3; the coefficient of variation was 28.1 %.

Figure 8-24 shows a plot of η with versus the confinement ratio and the drift ratio for the range of input data considered in the Ichinose tests. The form of equation (8.13) sets a limit of η = 1, which defines when the contributions from compression zone and arch action are fully degraded. The degradation function for the compression zone increases with increasing drift ratios, reducing the compression zone component; η is very large at a theoretical confinement ratio of zero and decreases with increasing confinement ratios, diminishing the reduction.

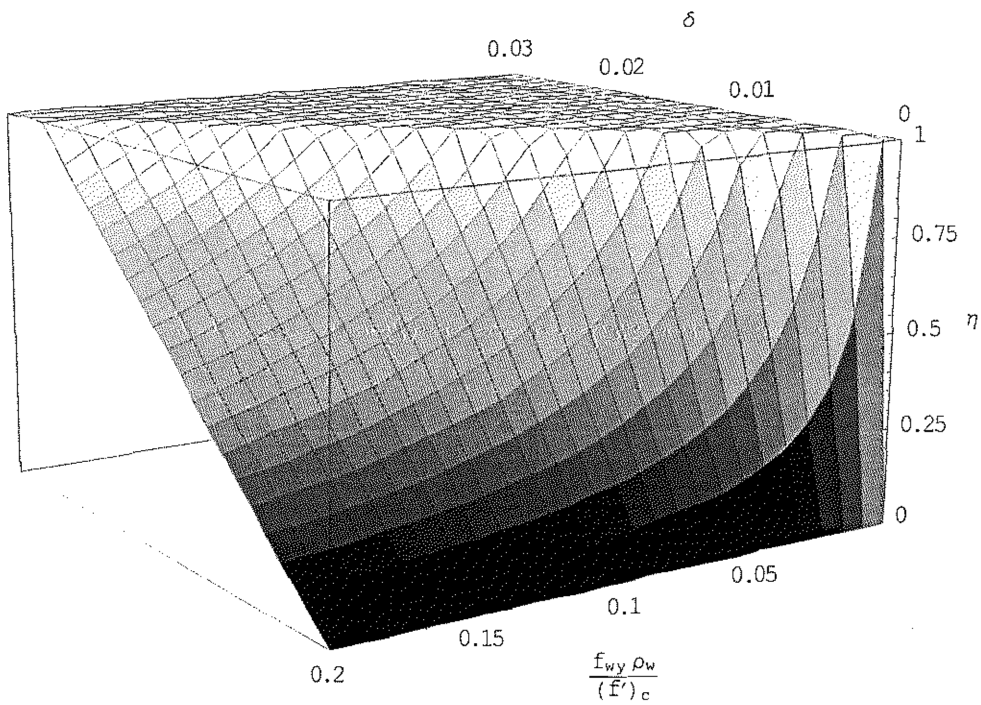

Figure 8-24 Strength degradation function for the compression zone component, η

The degradation of arch and compression zone is plotted against the confinement ratio for varying drift ratios from 1 to 2.5 percent in Figure 8-25. This graph can be used to determine the rate of degradation in relation with the confinement. It can be seen that, according to the proposed model, a relatively high amount of confinement is necessary to allow for contributions of arch-action and compression zone at large drift ratios. Doubling the drift ratio would require more than twice as much confinement to result in the same rate of degradation, η.

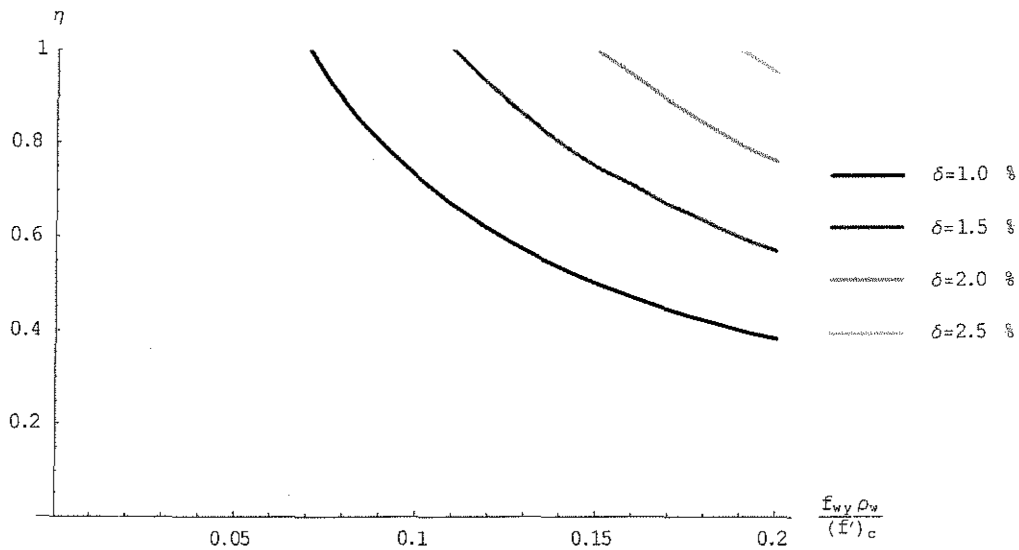

Figure 8-25 Strength degradation function for the compression zone component, η, for different drift ratios

If the strength degradation of the compression zone and arch resistances is assumed linear, η describes the degradation over the entire range of displacements. The degraded contribution from the compression zone is then given by

$$\begin{aligned} &V_{c+a,red} = V_{c+a} - \eta V_{c+a} \\ &\Leftrightarrow V_{c+a,red} = (1-\eta) V_{c+a} \end{aligned} \tag{8.15}$$

with $\eta \leq 1$

Using the degradation of the V_{c+a} term, the degradation of the truss up to yielding of the transverse reinforcement was found as follows.

8.2.2 Degradation of the truss mechanism

Detailed information about strain in the transverse reinforcement was available for all 20 of the specimens in the database. The yield strain in the transverse reinforcement was reached in 15 of these. The respective capacities of the columns are listed in Table 8-1. For all 15 columns, the reduced contributions from the compression zone and arch-action were calculated at the deflection related to yielding of the web reinforcement. Using this value, the ratio of measured applied load at yielding to the sum of truss-action and $V_{c+a,red}$ was calculated. For eleven specimens, the measured load at yielding of the web reinforcement was smaller than $V_t + (1-\eta)V_{c+a}$ (see Table 8-1). A function describing the strength degradation of the truss component from initial strength to yielding was established for these members.

As seen before in Figure 8-22 and Figure 8-23, the degradation of truss action was found dependent on the level of axial load and on the drift ratio. Moreover, according to those graphs, the strength of the truss degraded at an increasingly faster rate due to increasing axial stresses and drift. The truss has to develop its full static capacity if the drift is zero, independent of the amount of axial load. According to the proposed model, for the monotonic load case, the axial load is carried by the relatively larger compression zone and by a larger friction contribution. A function that results in a degradation coefficient equal to one for various amounts of axial load at no deflection, but in a faster degradation at increasing drift demand is expressed in equation (8.16):

$$\chi = \frac{1}{1 + a \cdot \delta_{yt} \cdot b^{\lambda}} \tag{8.16}$$

with

$$\delta_{yt} = \frac{\Delta_{yt}}{L} = \text{ drift ratio at yielding of the transverse reinforcement.}$$
$$\lambda = c + d \cdot P/(Af'_c)^e$$

The influence of the confinement ratio on the degradation of the truss component was considered as well, but it was found negligible for the specimens considered.

Equation (8.16) was calibrated on the eleven columns of the available dataset, in which the strains were known to exceed the yield strain. The following degradation function showed a good fit for the measured values of the examined specimens:

$$\chi = \frac{1}{1 + 1.5 \cdot \delta_{yt} \cdot 6^{\lambda}} \quad \text{and } \lambda = 1 + 2 \cdot P/(Af'_c)^{0.35} \tag{8.17}$$

Figure 8-26 shows the degradation function (8.17) plotted against the input parameters. An increase of both, axial load demand and drift ratio, decreases χ, reducing the truss contribution. For a drift ratio $\delta_{yt} = 0$, the degradation function is zero, independent of the axial load. According to the proposed model, an increased drift ratio results in a fast degradation of the arch and compression zone components. A fast degradation of the arch and compression zone components results in an increasing demand on the truss under axial load, therefore degrading the truss component at a fast rate under axial load. The influence of the axial load on the degradation rate is displayed in Figure 8-27 for drift ratios varying from 0 to 5 percent. This graph also shows the decreasing influence of the drift ratio, discernible in the decreasing distances between the respective curves.

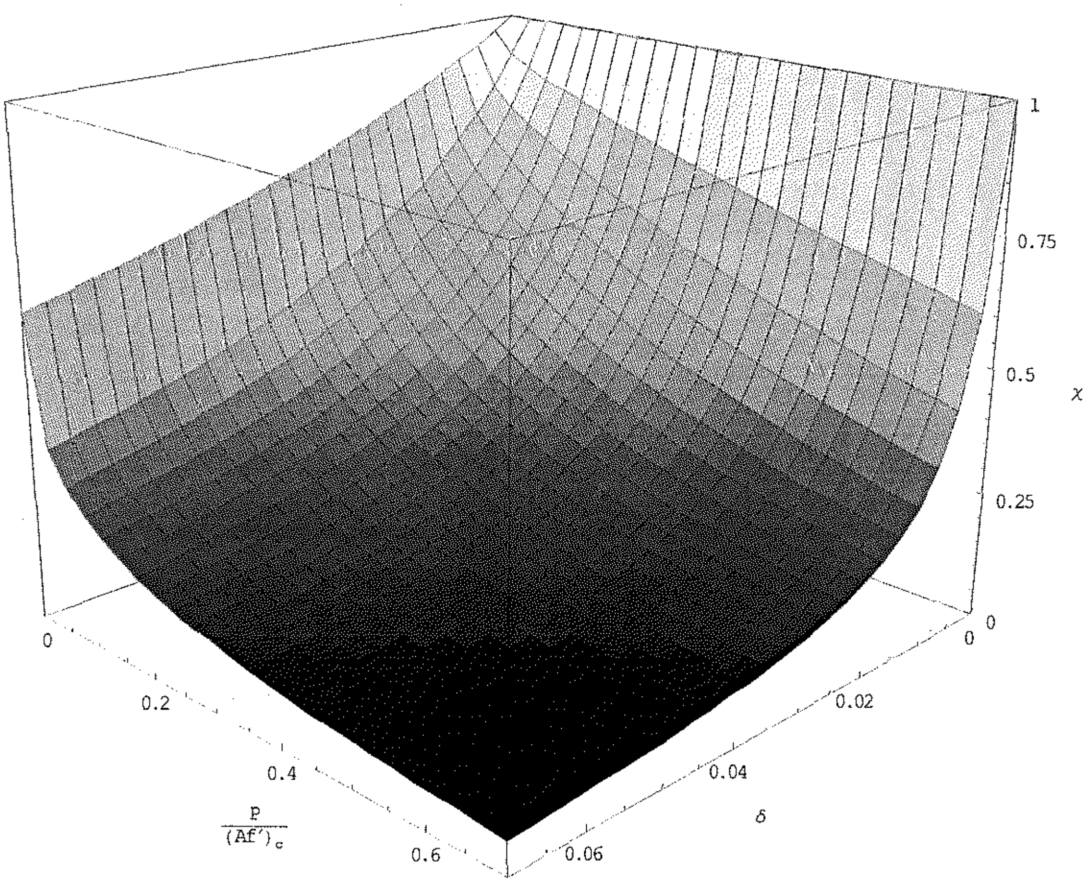

Figure 8-26 Degradation function of the truss component

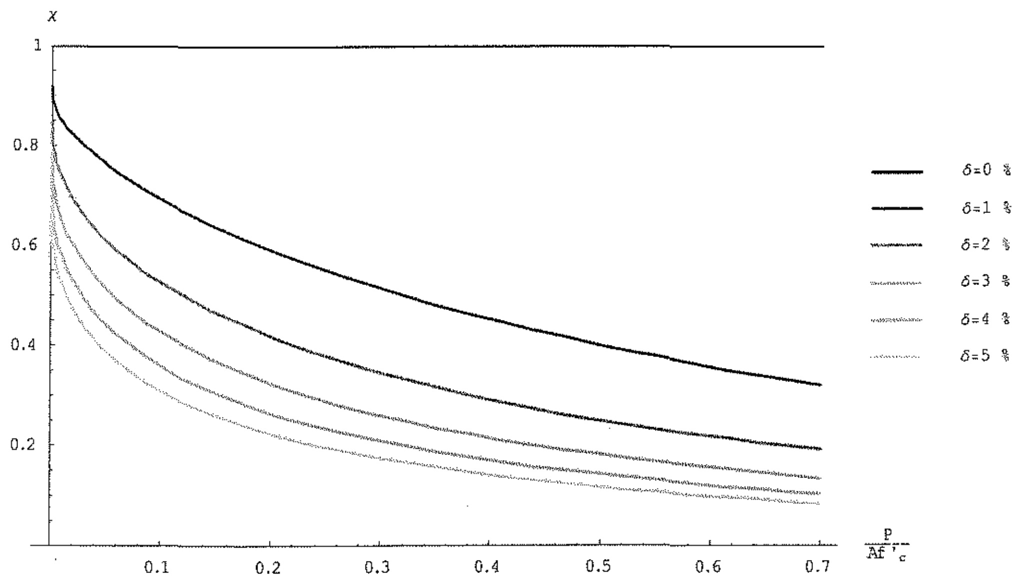

Figure 8-27 Degradation function of the truss component for different drift ratios

The calculated shear strength at yielding of the transverse reinforcement was calculated for the considered columns by eq. (8.18):

$$V_{yt,cal} = \chi V_t + (1-\eta) V_{c+a} \tag{8.18}$$

Because the dataset used for calibration was very limited, the objectives of the calibration were a conservative estimate, and to capture the influence of axial load and drift ratio accurately.

Comparison of the measured to the calculated shear load at yielding of the web reinforcement resulted in a mean value of $V_{yt,mes} / V_{yt,cal} = 1.51 \pm 2.8\%$ within a 95 percent confidence interval. The standard variation was 0.63, resulting in a relatively high coefficient of variation of 41.6 percent. The mean value reflects the multiplicator a = 1.5 of the drift ratio in equations (8.16) and (8.17). Figure 8-28 shows a graph of measured against calculated shear strength at yielding of the reinforcement. Statements about trends should be made carefully for very small amounts of data as considered here. Overall, the method seemed to give a reasonable assumption of the shear strength at yielding of the reinforcement.

For the examined columns, the ultimate reported shear strength was slightly higher than the reported strength at yielding of the web reinforcement. This is especially true for the members tested by Matamoros (Matamoros 1999), which failed due to buckling of the axial reinforcement after yielding of the stirrups. This type of failure was still considered a shear related failure, since the tensile reinforcement would not have buckled without yielding of the stirrups. However, it is obvious that such specimens could still sustain a certain amount of additional loads, even after the shear resistance was lost. Such extended capacity should not be relied on though, since the failure is not controllable after the loss of shear strength.

Figure 8-29 shows a plot of the measured ultimate shear strength against the calculated strength V_{yt}. The scatter decreased slightly, while the level of conservatism increased considerably. The mean of measured to calculated strength ratio was $V_{u,mes} / V_{yt,cal} = 1.87 \pm 2.1\%$, the standard deviation 0.58, and the coefficient of variation 31.2 % for the eleven considered specimens.

The ratio of measured to calculated yield strength was plotted against the drift ratio at yielding in Figure 8-30. For the specimens considered, no negative trend was visible. The same ratio was plotted against the axial load in Figure 8-31. Here, a slight trend to increasingly conservative values with increasing axial load can be seen. However, as mentioned before, it is difficult to make a clear statement about distinct trends in a very small dataset.

The application of the proposed functions for degradation of the truss mechanism, and for arch- and compression zone components will be demonstrated on tested shear walls in the following section.

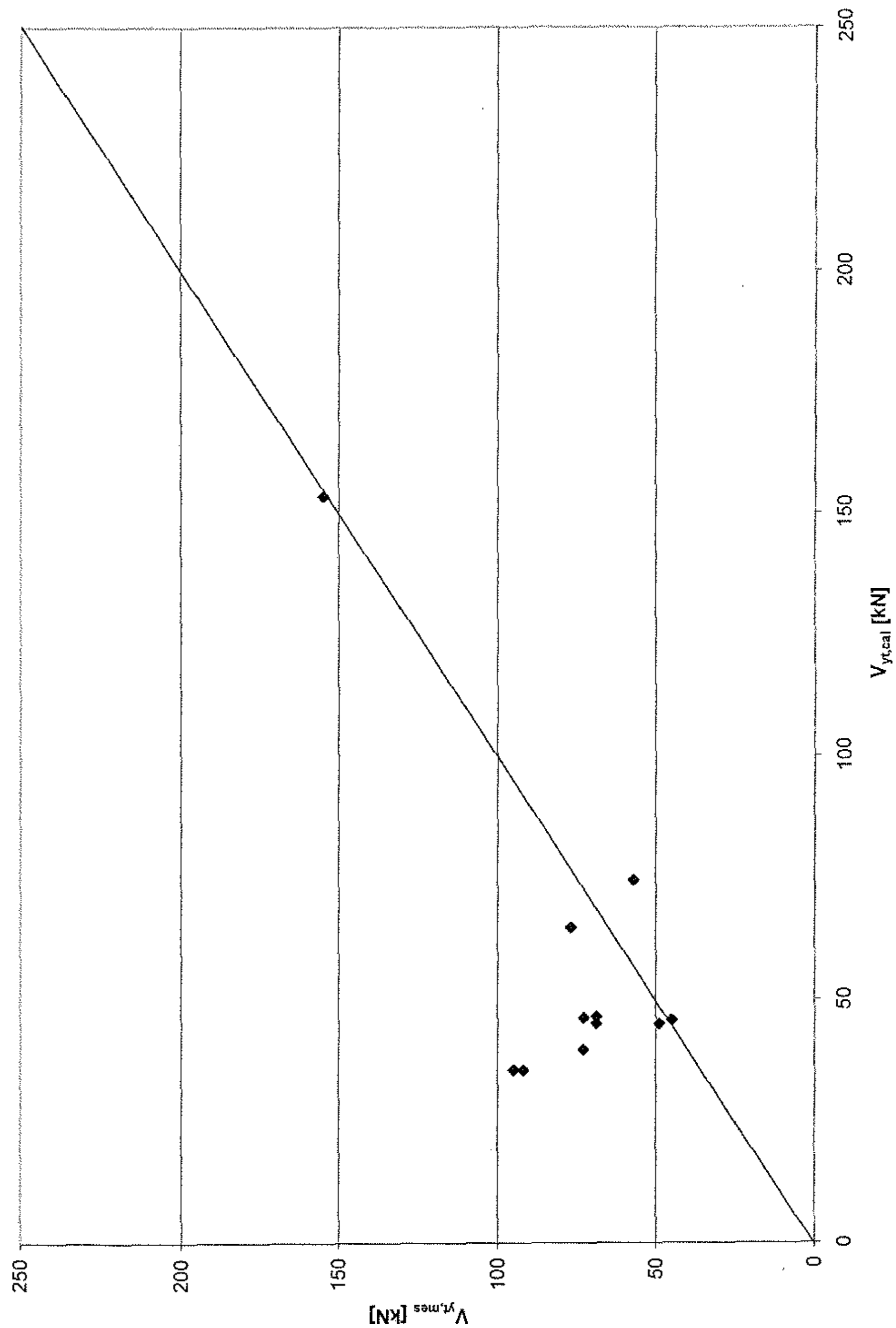

Figure 8-28 Measured versus calculated shear strength at yielding of transverse reinforcement

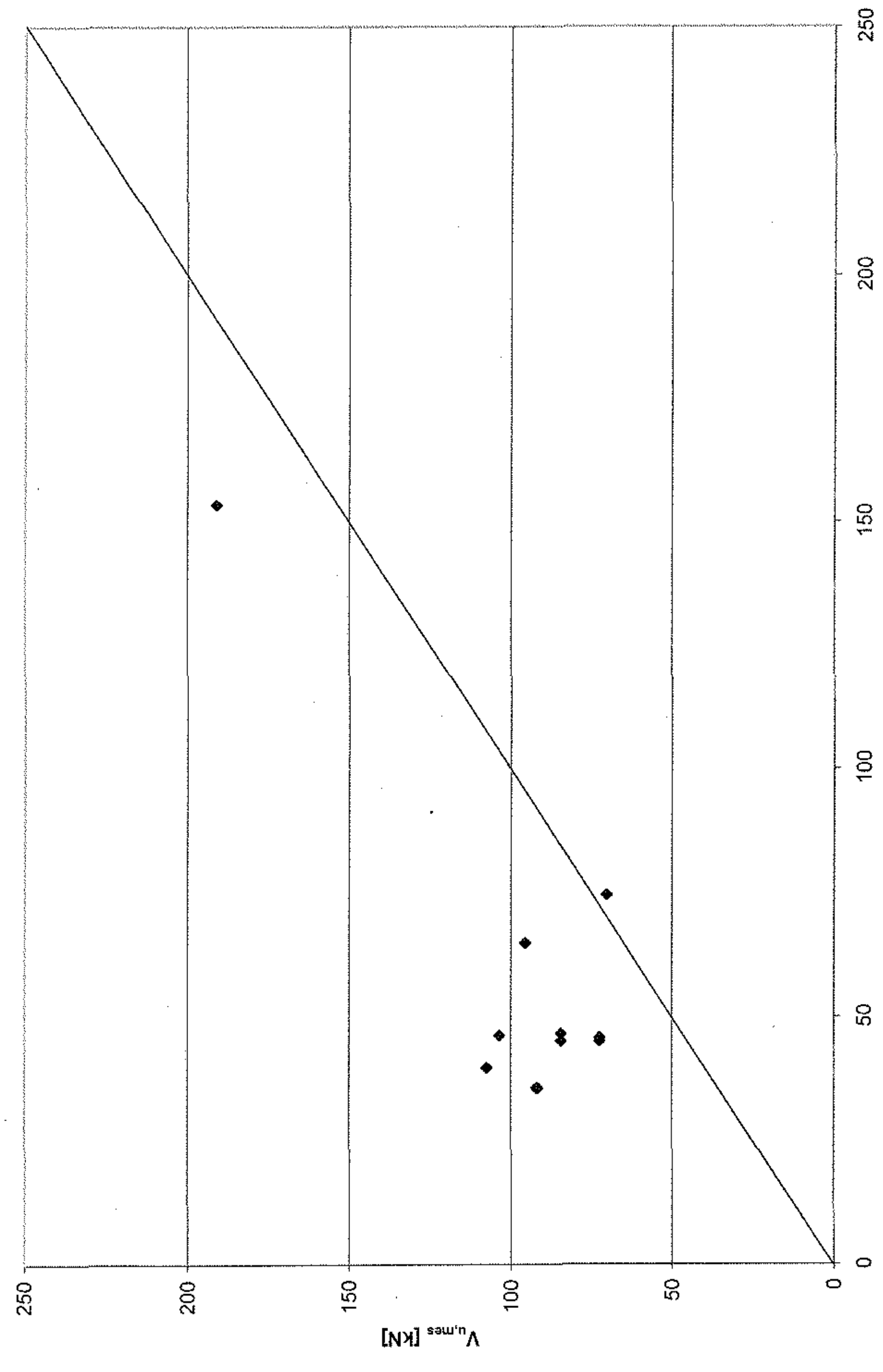

Figure 8-29 Measured ultimate shear strength versus shear strength at yielding of transverse reinforcement

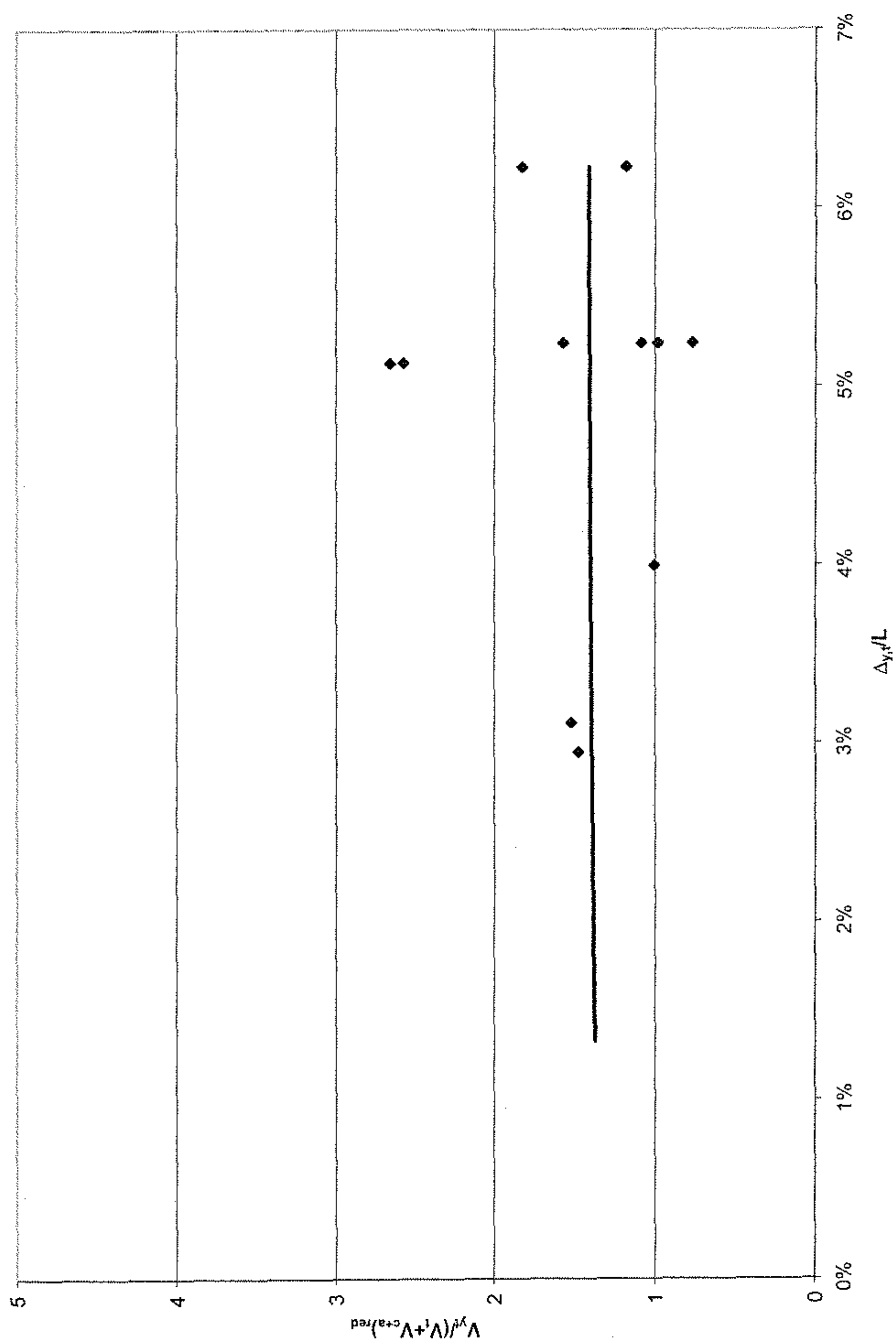

Figure 8-30 Ratio of measured to calculated strength versus drift ratio at yielding of the transverse reinforcement

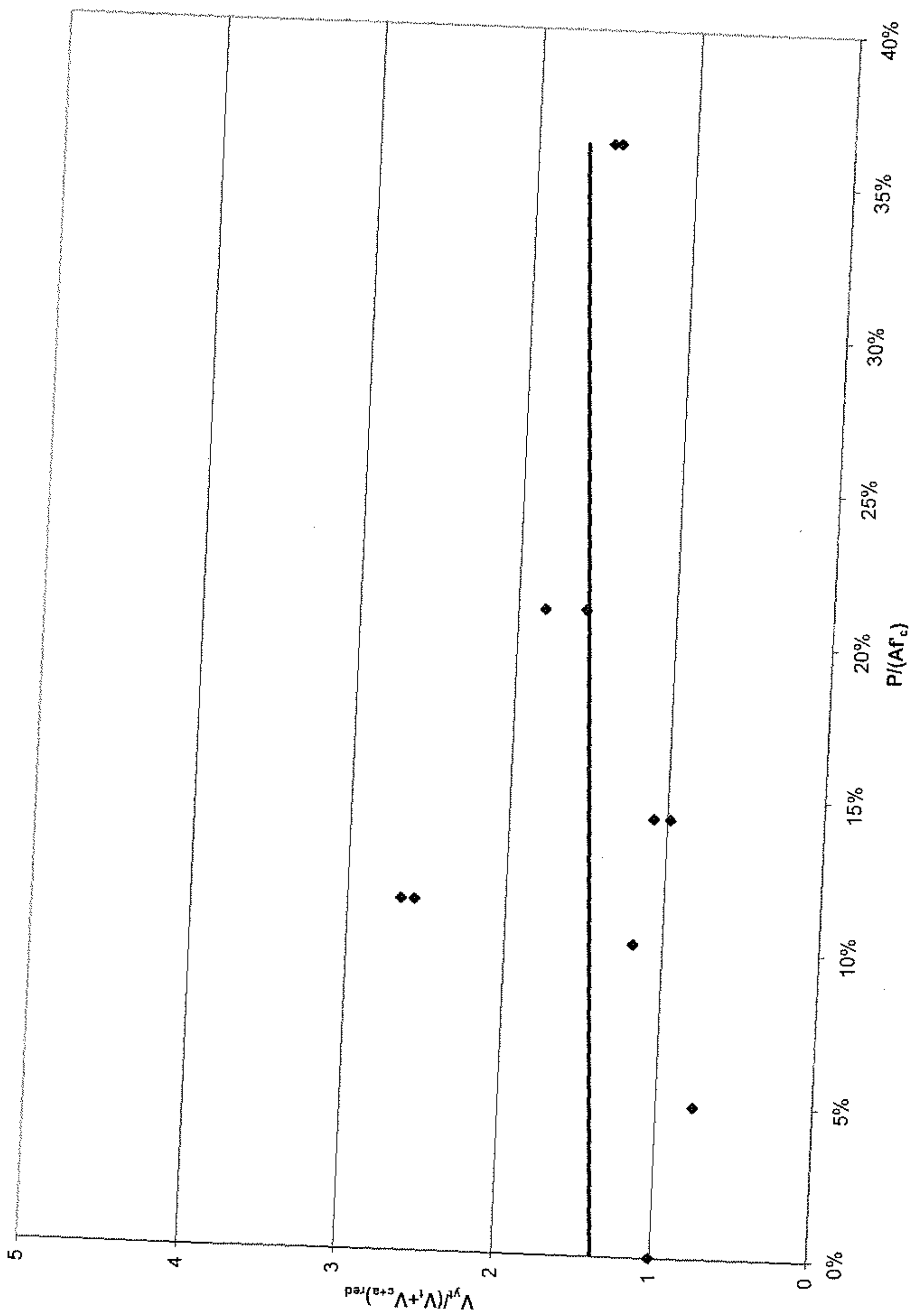

Figure 8-31 Ratio of measured to calculated strength at yielding of the transverse reinforcement versus axial load level

8.3 Application to shear walls

The degradation functions developed in the previous sections can be used to estimate the reduced shear strength for a limiting drift ratio (Figure 8-1). In slender walls, the initial shear strength has to be large enough to ensure safe behavior of the member under cyclic loading. The envelope curve for the flexural response is determined using the slope m as described in Section 8.1.2. The calculated shear strength at yielding of the transverse reinforcement would have to be larger than the respective flexural value to ensure that the member would not fail in shear.

In walls with low aspect ratios, it is unlikely that yielding of the vertical reinforcement due to flexure will be the limiting factor. In these cases, walls must be proportioned so that the elastic seismic demand is smaller than the shear capacity of the wall.

The proposed procedure was applied to several walls that failed in shear either before or after yielding of the longitudinal reinforcement. The capacity of the walls under monotonic loads and the strength degradation due to cyclic loads were calculated and compared with the envelope of the measured hysteresis curve.

To determine the failure envelope, the following values have to be computed first: The elastic deflection, the flexural strength at yielding of the longitudinal reinforcement, and the initial shear strength.

The total deflection at the onset of yielding was calculated as the sum of deflections due to flexure, bar slip, and shear deformations. Deformations due to sliding of the wall panel along its base were not considered, because the related mode of failure was not an objective in the study at hand. Nevertheless, the failure envelope was calculated for specimen K4, tested by Ogata et al. (Ogata and Kabeyasawa 1985), which failed in sliding shear. The calculated envelope curve for this wall shows a change from flexure-controlled behavior to shear-controlled behavior.

The component of the drift ratio related to yielding of the longitudinal reinforcement was calculated as

$$\delta_y = \frac{1}{L}\varphi_y \frac{L^2}{3} = \varphi_y \frac{L}{3} \tag{8.19}$$

where L = wall height

φ_y = curvature at yielding determined from eq. (8.20):

$$\varphi_y = \frac{\varepsilon_s}{d(1-k)} \tag{8.20}$$

The drift ratio resulting from slip in the longitudinal reinforcement was calculated by (Lopez 1988):

$$\delta_{slip} = \frac{L}{L(d-kd)} \frac{f_y}{0.498\sqrt{f'_c}} \frac{1}{8} \varepsilon_s d_b \tag{8.21}$$

The component of the drift ratio related to shear was calculated as (von Ramin et al. 2002):

$$\delta_{shear} = \frac{V_{ys}}{A_{eff} \cdot G_c} \tag{8.22}$$

with V_{ys} = shear related to yielding of the longitudinal reinforcement

A_{eff} = total area of the wall

$G_c = \frac{E_c}{2(1+\nu)}$ and $\nu = 1/6$

The moment at yielding of the longitudinal reinforcement was calculated from an approximate design equation, which is based on flexural theory (Kabeyasawa and Hiraishi 1998):

$$M_{ys} = A_{s,be} f_{y,be} l_w + 0.5 A_v f_{vy} l_w + 0.5 N \cdot l_w \tag{8.23}$$

where $A_{s,be}$ = area of steel in the boundary element

A_v = area of vertical steel in the web

$f_{y,be}$ = yield strength of longitudinal steel in the boundary element

f_{vy} = yield strength of vertical steel in the web

N = axial load

l_w = wall length

Dividing M_{ys} by the shear span, i.e. in this case the wall height, results in the respective shear force, V_{ys}.

The initial shear strength of the walls was determined following the procedure described in Section 7.2.5.2.

The functions proposed for the degradation of flexural strength (equations (8.6) and (8.9)), and for the reduction of shear strength (equations (8.15) and (8.17)) were then used to construct the respective envelope lines.

Two different failure definitions were applied:

- If the calculated shear strength was below the flexural strength at yielding of the reinforcement, the wall response was considered elastic, because the wall displacement was smaller than the displacement at yielding of the longitudinal reinforcement. The shear capacity at this displacement is then given by the shear capacity under monotonic loading, according to the proposed model.
- If the calculated shear strength exceeded the flexural strength, the strength at failure was defined as the strength at which the degrading envelope of the shear strength transgressed the flexural envelope.

The calculated failure envelopes are indicated by a solid black line in the following figures, showing the calculated and measured envelope curves.

According to the proposed method, the reduction of the shear strength is a direct function of the drift ratio. The maximum displacement reached in the tests was used to determine the reduced shear strength. In a design situation, this value would have to be chosen. The reduced flexural strength, however, was assumed as 80 percent of the initial strength at yielding of the longitudinal reinforcement, following the proposed method. The flexural degradation slope m was calculated and used to obtain the change in displacements between to V_{ys} and $0.8V_{ys}$:

$$
\begin{aligned}
m &= \frac{0.2}{\Delta_u - \Delta_y} \\
\Leftrightarrow \Delta_u &= \frac{0.2}{m} + \Delta_y
\end{aligned}
\tag{8.24}
$$

The described procedure was carried out on walls tested by Barda et al. (Barda et al. 1977), by Ogata and Kabeyasawa (Ogata and Kabeyasawa 1985), by Kabeyasawa and Hiraishi (Kabeyasawa and Hiraishi 1998), and by Oesterle et al. (Oesterle et al. 1980; Oesterle et al. 1976). The walls tested by Barda, and by Ogata failed in shear before yielding of the longitudinal reinforcement; the specimens tested by Kabeyasawa failed after yielding of the longitudinal reinforcement. The specimens tested by Oesterle et al. are representative cases of slender wall behavior. Properties of the set of walls are provided in Appendix A10 and in the respective worksheet on the provided data CD.

Figure 8-32 shows the calculated and measured response of specimen B7-5 tested by Barda et al. The wall panel had a very low aspect ratio of 0.25, and failed in shear before reaching its flexural yield strength. Figure 8-33 shows the dimensions and cross-sectional properties representative for the test series by Barda (Barda et al. 1977). The reinforcement ratio of the horizontal and vertical web reinforcement was 0.5 percent; the reinforcement ratio in the boundary elements was very high with 4.17 percent. The axial load applied to specimen B7-5 was relatively low with an axial stress demand of $P/(Af'_c) = 0.2$ %.

The flexural capacity of specimen B7-5 greatly exceeded the calculated and the measured shear strength. This case is representative of a squat wall, where the wall would be proportioned based on the monotonic shear strength obtained with the proposed model. A hysteresis curve for this specimen is therefore not provided. Because failure will occur at a small fraction of the flexural yield load, it is assumed that the wall looses its load carrying capacity after shear failure. The calculated shear strength, indicated by the solid grey line, was slightly conservative. The measured failure envelope is displayed as a straight line from the origin to the limiting drift at the maximum load.

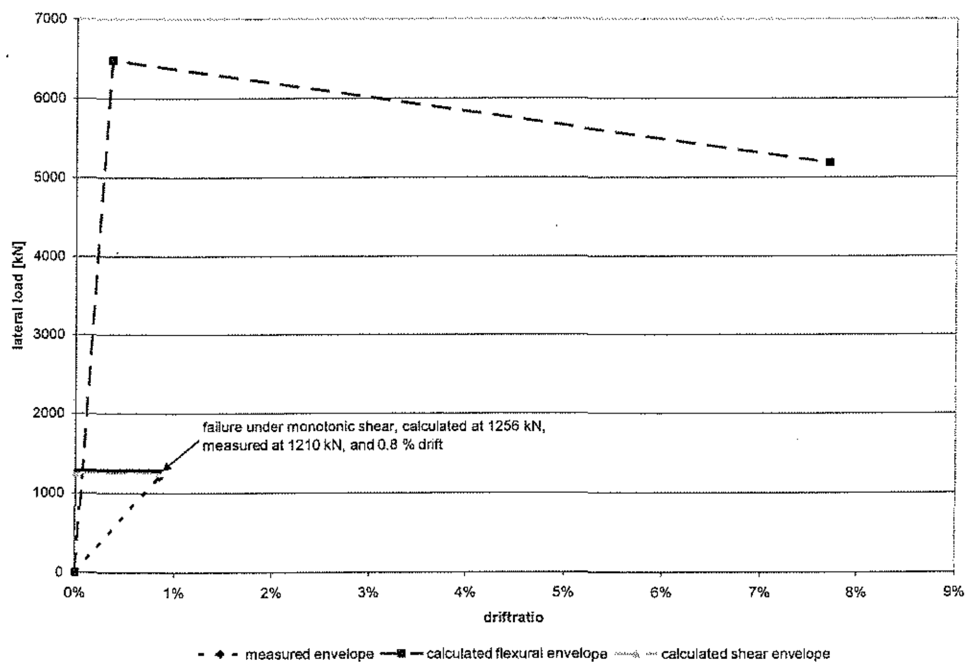

Figure 8-32 Measured and calculated failure envelope for specimen B7-5 (Barda et al. 1977)

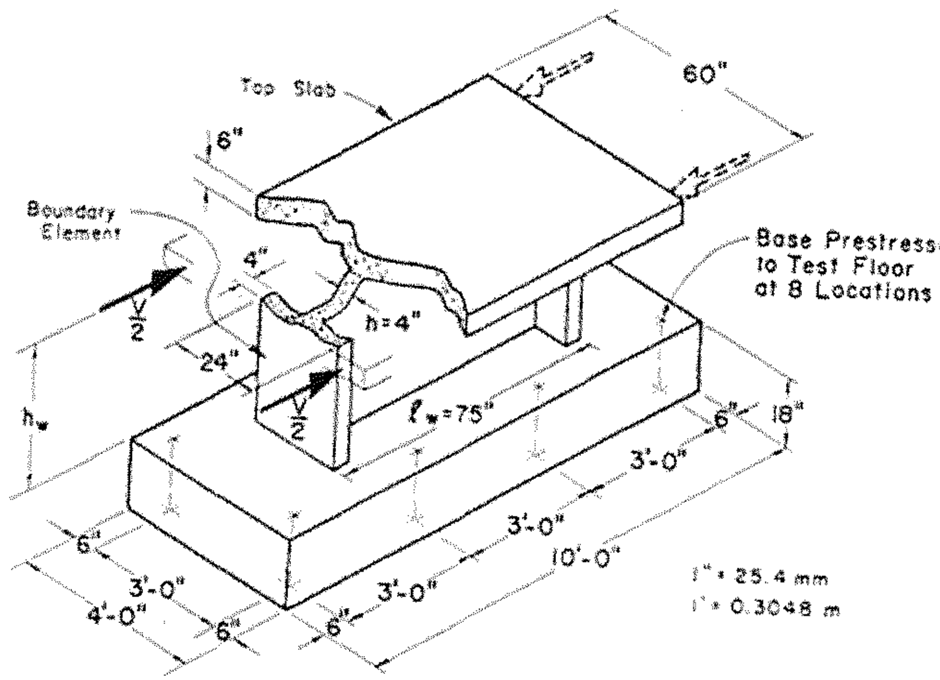

Figure 8-33 Cross-sectional properties of specimens in test series by Barda (Barda et al. 1977)

The envelope curve for a specimen with a higher calculated shear capacity than flexural capacity is shown in Figure 8-35. Specimen K4 failed in sliding shear before yielding of the longitudinal reinforcement (Ogata and Kabeyasawa 1985). Specimen K4 had a low shear span ratio of 0.75; normal strength concrete and normal strength reinforcement was used. The axial stress demand for specimen K4 was relatively high with 9.3 percent. The web reinforcement ratio was comparatively high. With 0.8 percent, the web reinforcement ratio was higher than in any other test specimen described in this section. The longitudinal reinforcement ratio in the boundary element was 1.43 precent, which is low compared to the other described test specimens. Figure 8-34 shows reinforcement details and cross-sectional dimensions of specimen K4 as provided in (Ogata and Kabeyasawa 1985).

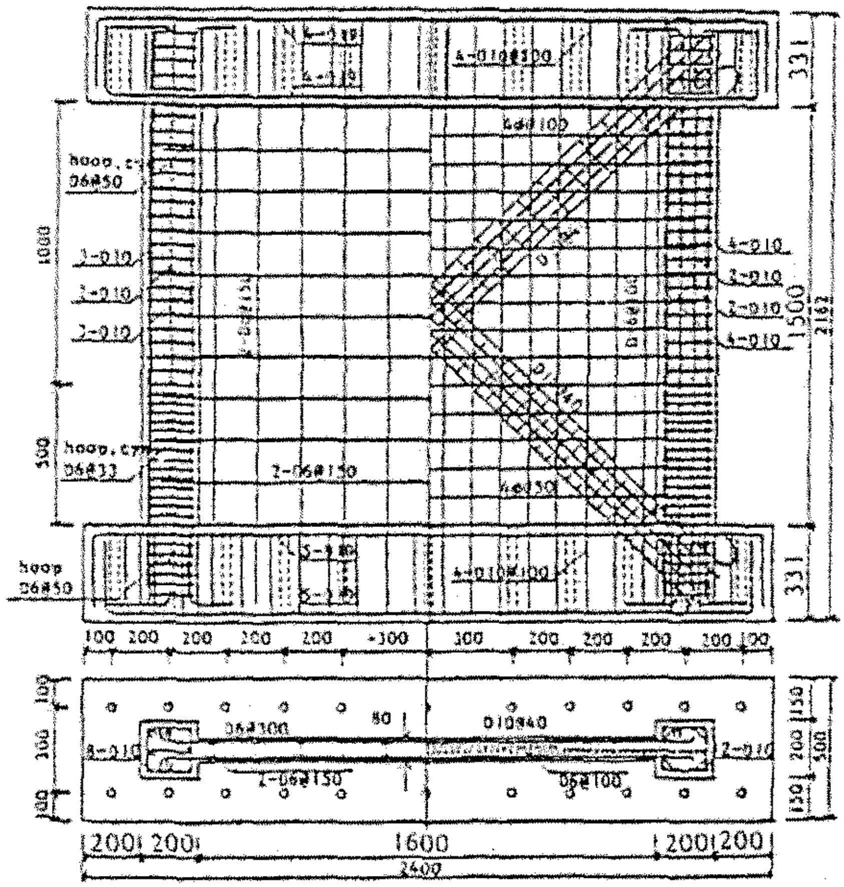

Figure 8-34 Dimensions and reinforcement details of specimen K4 (Ogata and Kabeyasawa 1985)

The calculated failure envelope for specimen K4, plotted in Figure 8-35, is represented by a line connecting the origin with points A to C. The calculated response is first dominated by the flexural capacity, i.e. until point B. However, the failure line related to the shear strength transgresses the flexural curve very soon, and dominates the response between points B and C. The calculated displacement at the onset of yielding of the longitudinal reinforcement was much smaller than the measured drift. This could be related to the failure mode. Since the wall failed in sliding shear, a considerable amount of the lateral deflection has to be attributed to sliding of the wall panel. As mentioned earlier, the method used to determine the drift ratio at yielding does not account for these deformations. The hysteresis curve for specimen K4, provided by (Ogata and Kabeyasawa 1985), is shown in Figure 8-36.

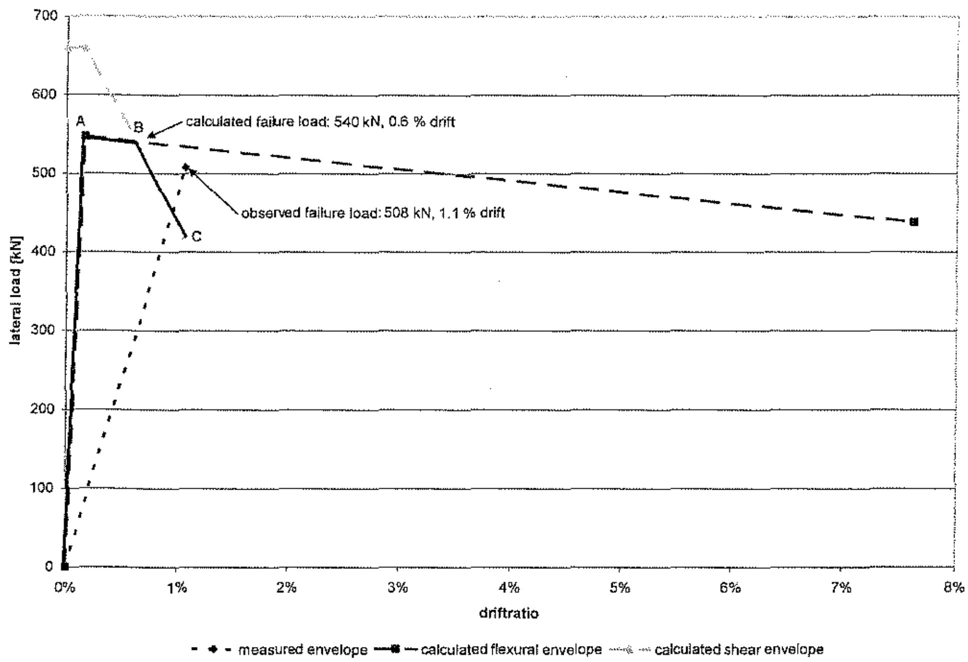

Figure 8-35 Measured and calculated failure envelope for specimen K4 (Ogata and Kabeyasawa 1985)

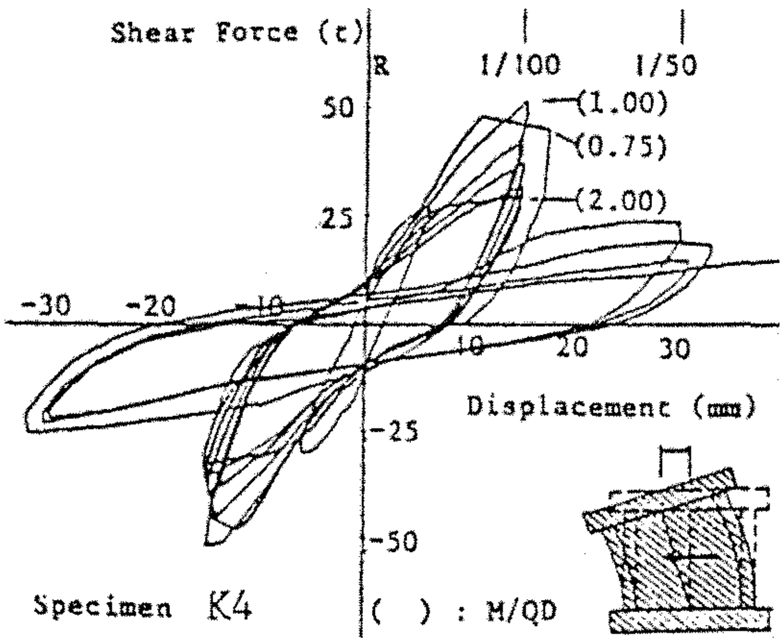

Figure 8-36 Hysteresis curve for specimen K4 (Ogata and Kabeyasawa 1985)

An example for a wall that reached yielding of the longitudinal reinforcement is shown for specimen NW1 (Kabeyasawa and Hiraishi 1998) in Figure 8-38. This wall failed after the tensile reinforcement in the boundary element and the longitudinal reinforcement in the web ruptured. Specimen NW1 had a shear span ratio of 2 and was axially loaded with P = 1764 kN, which is equivalent to an axial stress demand of approximately 11 percent. As stated by Kabeyasawa, the axial load was chosen equivalent to an axial load imposed on the wall by 20 to 30 stories. The wall specimen had a barbell – cross section with a longitudinal reinforcement in the boundary element of ρ_{be} = 2.14 %. The yield strength of the longitudinal reinforcement in the boundary element was $f_{y,be}$ = 776 MPa, the yield strength of the vertical and horizontal web reinforcement was 1001 MPa. High-strength concrete was used with a compressive strength of f'_c = 87.6 MPa. The wall panel was framed by the vertical boundary elements and by horizontal boundary elements to accommodate the load application. Cross-sectional drawings of specimen NW1 are shown in Figure 8-37 (Kabeyasawa and Hiraishi 1998).

The calculated flexural and shear response were similar to specimen K4, i.e. the calculated failure envelope was first dominated by the flexural response, and, starting at point B, the calculated response was limited by the shear capacity. In this case, the estimate of strength was conservative. It appears appropriate to assume that the high axial load and the heavily reinforced boundary elements suppressed the failure of the wall until the boundary element and the vertical web reinforcement ultimately ruptured. Figure 8-39 shows the measured hysteresis curve for specimen NW1 (Kabeyasawa and Hiraishi 1998). The measured failure envelope curve for specimen NW1 is compared to the calculated failure envelope in Figure 8-38.

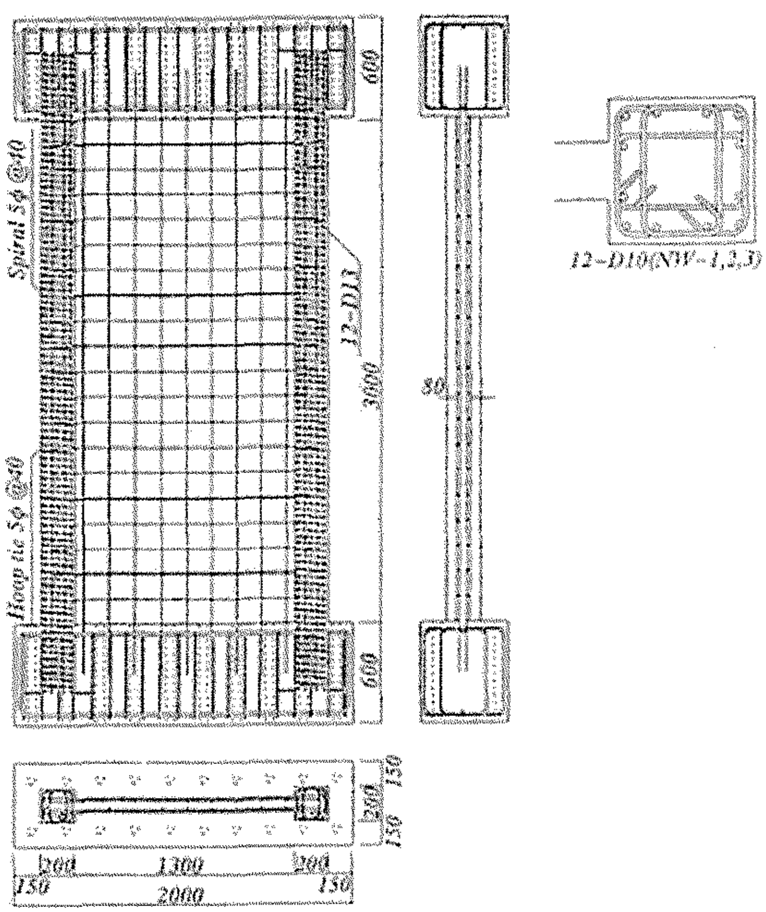

Figure 8-37 Cross-sectional properties of specimen NW1 (Kabeyasawa and Hiraishi 1998)

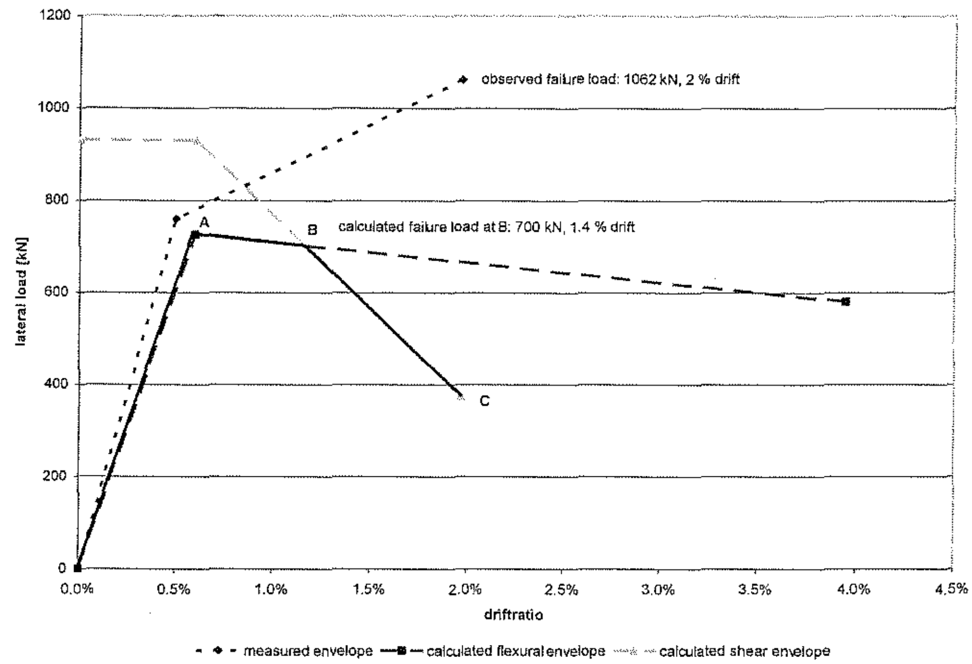

Figure 8-38 Measured and calculated failure envelope for specimen NW1 (Kabeyasawa and Hiraishi 1998)

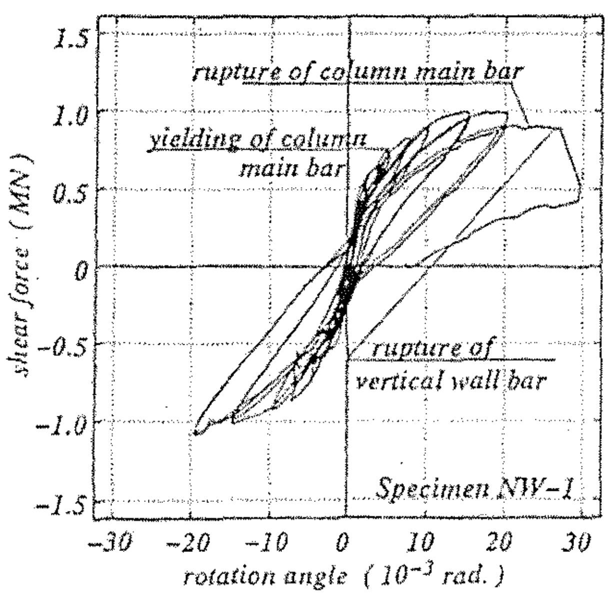

Figure 8-39 Hysteresis curve for specimen NW1 (Kabeyasawa and Hiraishi 1998)

The behavior of slender walls is illustrated using specimens that were tested by Oesterle et al. (Oesterle et al. 1980; Oesterle et al. 1976). These walls, designated B1, B2, B3, and B5, had barbell cross-sections, and an aspect ratio of 2.4. The cross-sectional dimensions of the wall panels are shown in Figure 8-40, taken from (Oesterle et al. 1980). No axial load was applied to the walls tested by Oesterle et al. The wall panels had web reinforcement in the vertical and horizontal directions of approximately 0.3 percent, the horizontal web reinforcement in specimens B2 and B5 was more than twice as much with $\rho_h = 0.625$ percent.

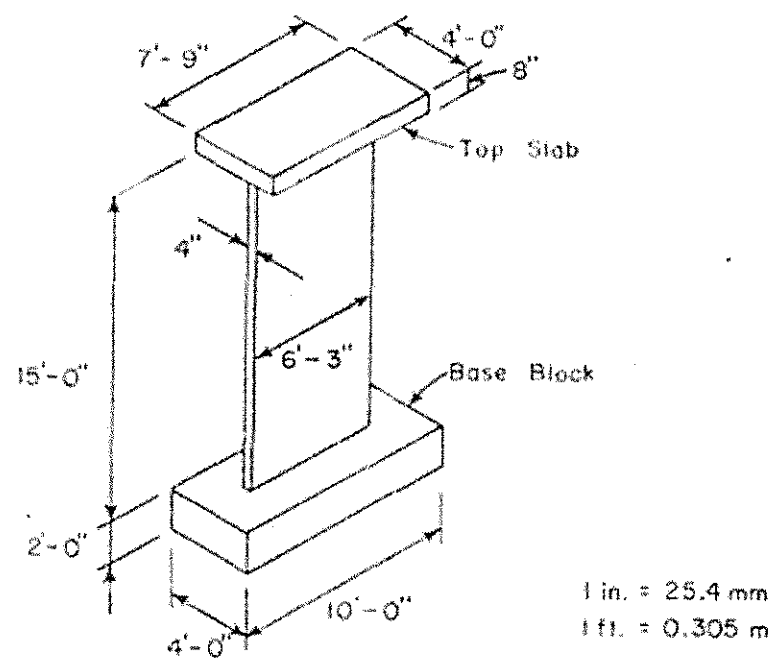

Figure 8-40 Dimensions of specimens B1, B2, B3, B5 as provided in (Oesterle et al. 1980)

Specimens B1 and B3 developed considerable flexural strength after yielding of the longitudinal reinforcement. Both specimens were identically constructed, except that more confinement was provided in the boundary element of specimen B3.

Wall B1 failed because of buckling of the main vertical reinforcement in a boundary element, after the boundary column core lost concrete while it was loaded in tension. The comparable specimen B3 provided more confinement in the boundary elements and could develop larger displacements. The computed and measured failure envelopes for specimens B1 and B3 are shown in Figure 8-41 and Figure 8-42, respectively. Figure 8-43 shows the hysteresis behavior of specimens B1 and B3 as provided in (Oesterle et al. 1980). The calculated initial shear strength of specimen B1 greatly exceeded the flexural capacity. After yielding of the longitudinal reinforcement, the calculated shear strength degraded at a very fast rate; however, the calculated shear strength at the measured maximum drift ratio was slightly larger than the measured strength of 271 kN. The calculated strength at failure is indicated by point B.

A similar response as for specimen B1 can be seen in Figure 8-42 for specimen B3. As previously mentioned, the wall developed higher ductility, but failed at essentially the same load. The calculated flexural capacity and the calculated initial shear strength are equal to the strengths calculated for specimen B1. Because the wall B3 was able to withstand larger deformations than B1, the slope of the shear degradation function changed accordingly. Since the larger drift ratio yielded a larger reduction of shear strength, the calculated failure load at the obtained drift ratio provided a safe estimate of the failure load. The calculated failure point C is in relatively good agreement with the measured limiting shear strength.

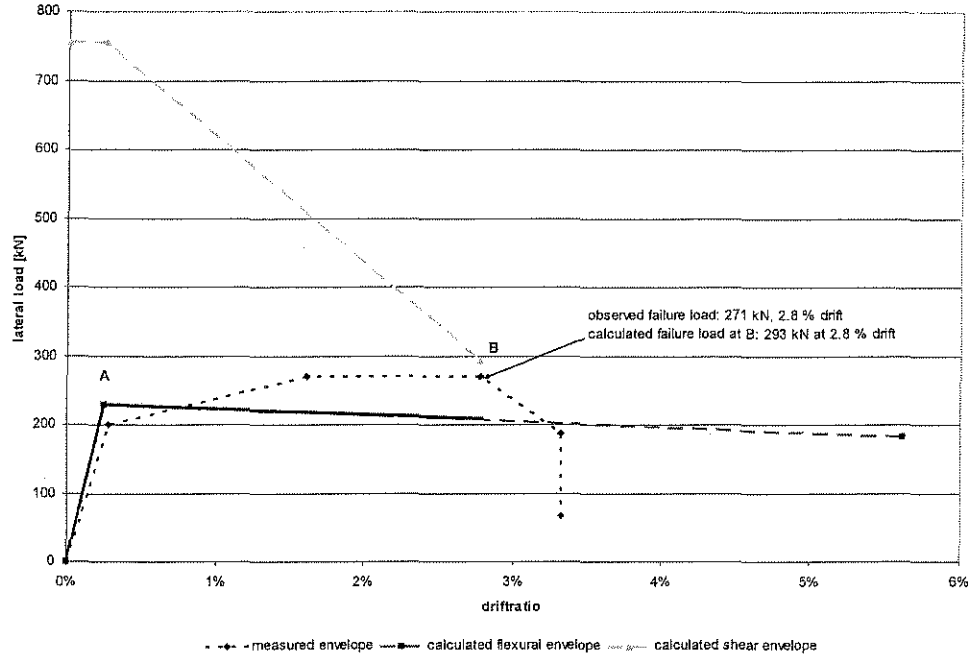

Figure 8-41 Measured and calculated failure envelope for specimen B1 (Oesterle et al. 1980)

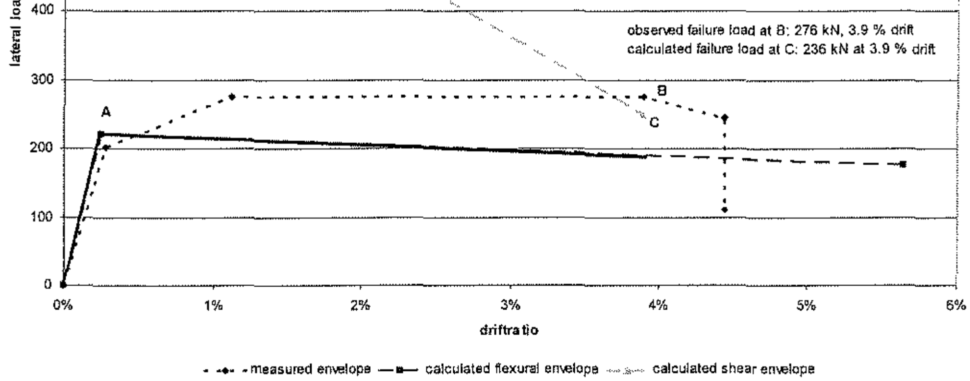

Figure 8-42 Measured and calculated failure envelope for specimen B3 (Oesterle et al. 1980)

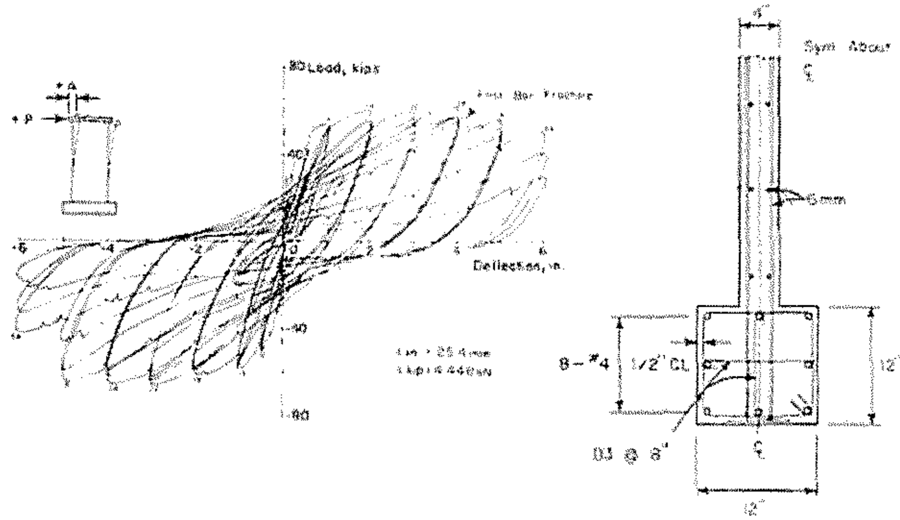

Specimen B1.

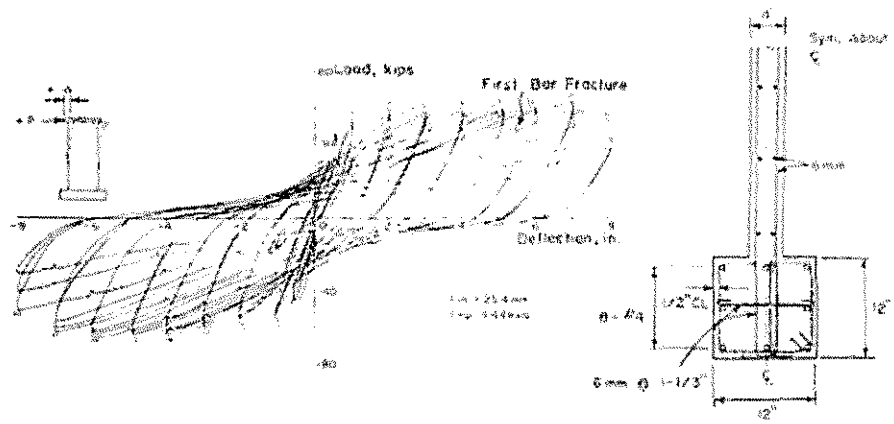

Specimen B3.

Figure 8-43 Hysteretic response of specimens B1 and B3 as provided in (Oesterle et al. 1980)

Wall specimens B2 and B5 were built similar to walls B1 and B3. The difference was that these walls had a higher amount of longitudinal reinforcement in the boundary elements, which changed from ρ_{be} = 1.1 % in specimens B1 and B3 to ρ_{be} = 3.7 % in specimens B2 and B5. Similar to the first pair of walls, the amount of transverse reinforcement in the boundary element was higher in specimen B5 than in specimen B2. According to Oesterle et al., the capacity of both walls was limited by web crushing. The boundary elements in specimen B2 lost their strength prior to web crushing; in specimen B5, they maintained their strength until after web crushing (Oesterle et al. 1976).

Figure 8-44 shows the measured and calculated capacity of wall specimen B2. The calculated flexural strength was higher than the measured strength at yielding of the longitudinal reinforcement. The initial shear strength was considerably higher than the flexural strength; however, the calculated shear strength degraded rapidly with increasing drift ratio. The calculated ultimate shear strength, indicated by point B, gave a conservative estimate of the measured response. Point B is very close to the calculated flexural failure envelope, indicating a change in member behavior from a flexure- to a shear-controlled member. This was consistent with the experimental observations. The measured hysteresis curve for specimen B2, taken from (Oesterle et al. 1980), is shown in Figure 8-45. The higher amount of transverse reinforcement in the boundary elements of specimens B2 and B5 is also shown in Figure 8-45.

The concrete compressive strength, and the yield strength of the web reinforcement, of specimen B5 were lower than in B2, resulting in different calculated failure envelopes. The limiting shear strength of this specimen, indicated by point B in Figure 8-46, was underestimated, whereas the calculated flexural strength (point A) exceeded the measured capacity. Point B represents the point at which the calculated member behavior changes from flexural to shear-controlled behavior. The measured hysteresis curve for specimen B5 is displayed in Figure 8-47 (Oesterle et al. 1980).

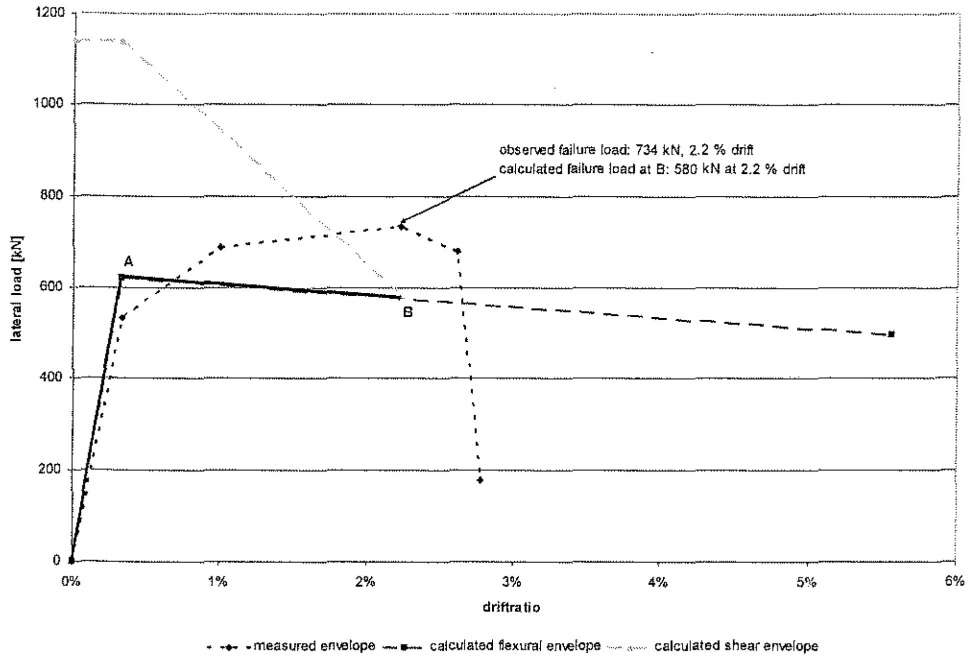

Figure 8-44 Measured and calculated failure envelope for specimen B2 (Oesterle et al. 1980)

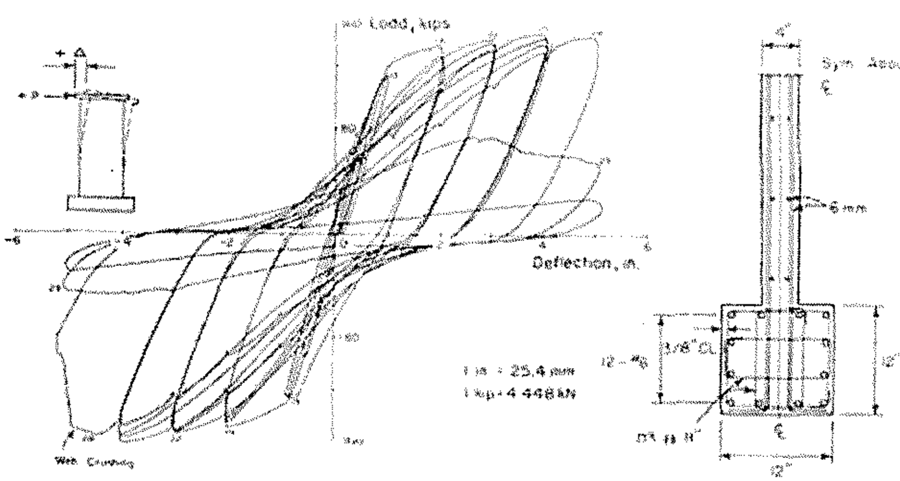

Figure 8-45 Hysteresis curve for specimen B2 as provided in (Oesterle et al. 1980)

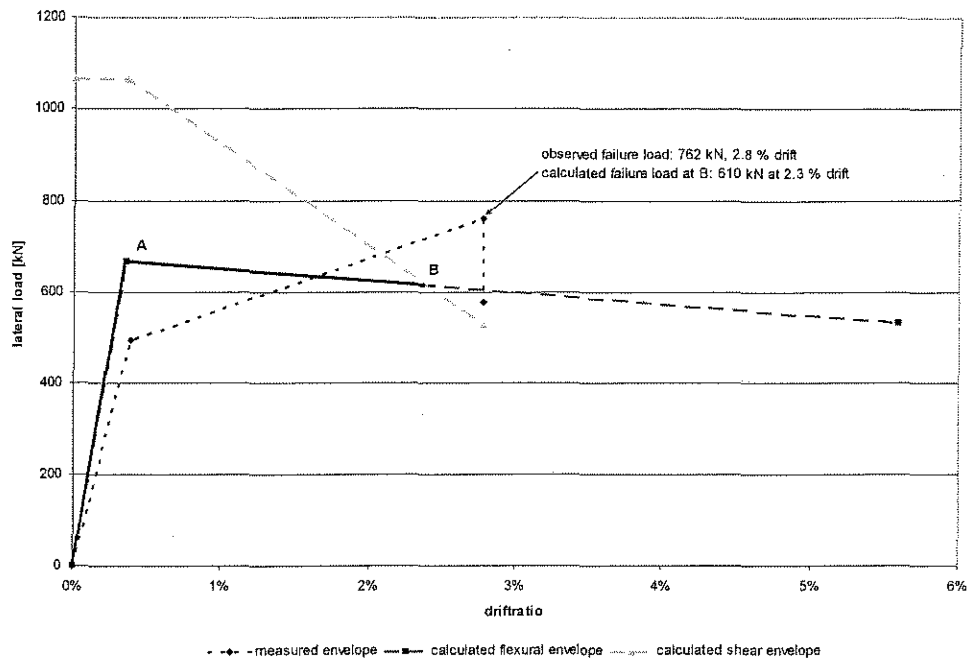

Figure 8-46 Measured and calculated failure envelope for specimen B5 (Oesterle et al. 1980)

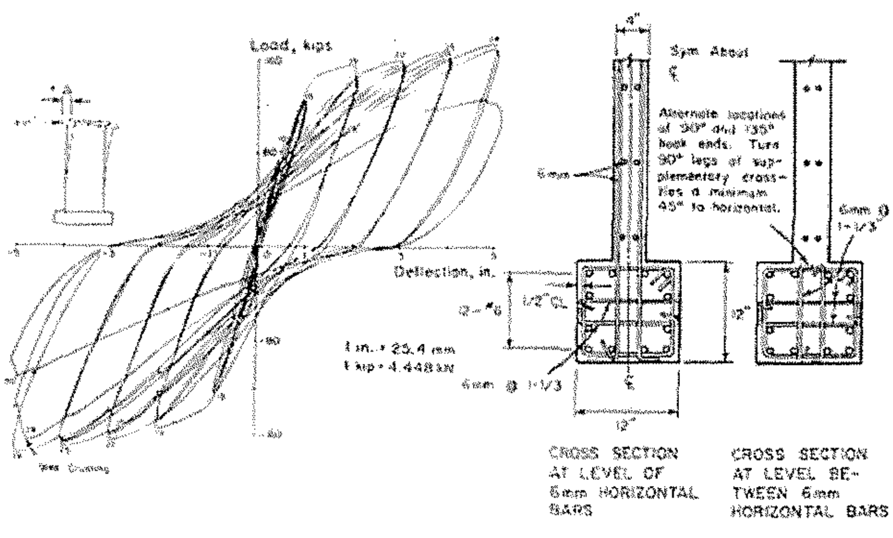

Figure 8-47 Hysteresis curve for specimen B5 as provided in (Oesterle et al. 1980)

The proposed model is sensitive to the chosen limiting drift ratio, because the slope and amount of the shear strength degradation are controlled by the limiting drift ratio. Figure 8-48 shows the envelope curves for the shear strength degradation at hypothetical drift ratios of 1.0, 1.5, 2.0, and 3.0 % for specimen B5. According to the proposed method, the change in the response of the wall from flexure- to shear-controlled behavior would have set in at points A through D. The end-points of the respective curves for shear strength degradation indicate, compared to flexural strength degradation, a faster degradation of the shear strength with increasing drift ratio.

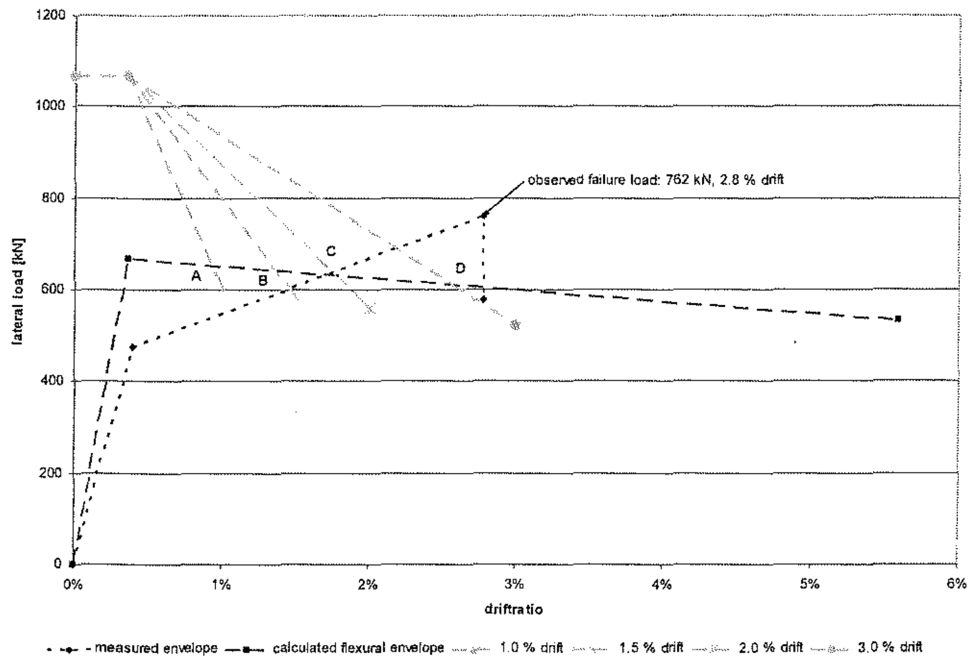

Figure 8-48 Change in shear response of specimen B5 at different drift ratios

It can be concluded that the application of the proposed method on walls gave relatively accurate results in terms of the developed strength at the limiting drift ratio. However, the proposed method is only able to give estimates of the strength at the limiting drift ratio. Increases in lateral load after yielding of the longitudinal reinforcement cannot be modeled with the proposed method.

For some walls, the calculated estimate of shear strength was very conservative. An example for this is specimen NW1, tested by Kabeyasawa et al. According to the proposed model, the wall would have failed at point B in Figure 8-38. The tested wall, though, developed a considerable amount of strength exceeding the reduced capacity determined following the proposed model. The calculated ultimate flexural displacement was largely overestimated; however, for the walls considered, this was not of concern, because their strength was limited by the shear capacity. The change between flexural and shear-controlled response was modeled well for the walls B2 and B5 tested by Oesterle et al. The displacement at yielding of the longitudinal reinforcement was underestimated for the walls that failed in shear and in sliding shear, because displacements related to sliding shear were not taken into account by the proposed model.

9 Summary and conclusions

The static shear capacity of reinforced concrete members was modeled using the superposition of different shear carrying mechanisms. The degradation of shear strength under cyclic load was calculated based on the calculated static shear strength.

Five different approaches to shear design of RC members were examined with respect to their applicability to various design configurations. Approaches by Watanabe and Reineck were found useful as a basis for further investigations (Reineck 1990; Watanabe and Ichinose 1991). However, a narrow range of applicability or conceptual shortcomings made it necessary to develop their conceptual ideas further into a general analysis tool for the design of RC members under monotonic shear load. This model was shown to be applicable to members of different geometries, with or without shear reinforcement, or with or without axial load. The strength degradation under seismic loads was modeled by considering the most significant parameters.

All components of the developed model were calibrated using available test data. The derived parameters were evaluated using *n*-fold cross validation, yielding good results with respect to the examined databases.

9.1 Monotonic shear capacity

It was shown that the shear capacity of RC members subjected to monotonic loads could be modeled by a superposition of arch-action, truss-action, and resistances related to the uncracked compression zone and friction between crack surfaces.

Depending on the existence of transverse reinforcement, the previously listed components contribute differently to the shear capacity of an RC member.

9.1.1 Members without web reinforcement

The load carrying mechanisms in members without web reinforcement were assumed as arch-action, friction, and the contribution from the uncracked compression zone, which is related to the tensile strength of concrete.

The strength of the arch component was chiefly related to the strut width, defined by the depth of the compression zone, or by the cover of the tensile reinforcement. The geometry of the loading plates also was important for the strut geometry in deep members, because it defines the axial dimension of the strut width. According to the proposed model, the strut has to be located in a section of the member that is under compression, because the compressive strut cannot transfer stresses across cracks.

For squat members, it was assumed that the main load carrying mechanism is arch-action; for slender members, the shear strength was calculated from the other two remaining components, friction and the shear carried by the compression zone. Furthermore, it was assumed that arch-action is present to some extent in slender members, and the contributions from friction and compression zone are present to some extent in deep members as well. To account for the transition from deep to slender members, two transition functions, k_s and k_c, were introduced that decrease the arch component and increase the friction and compression zone components with an increasing aspect ratio. In the transitional range of shear-span-to-depth ratios of approximately $2 \leq a/d \leq 6$, all three components contribute to the shear capacity of the member.

9.1.2 Members with web reinforcement

For members with web reinforcement, the contribution from the truss model was added to the aforementioned components. While in slender beams only a vertical truss component is present, the web of deep beams and walls is often reinforced vertically and horizontally. Both truss mechanisms have to be considered. However, simply adding the truss components yielded too high demand for the compression field in the web. A resistance fraction R was established that controls the demand on the individual shear-carrying contributions. It was assumed that the truss mechanisms develop their full capacity; the stresses in the compressive strut were reduced accordingly through R_a.

Additionally, the geometry of the truss in deep beams and walls was considered. The angle of the inclined compression field was limited in such a way that two compressive struts can develop to assure equilibrium within the member. This effectively limited the inclination of the compression field in deep members to $\cot\phi \leq a/2d$.

To compensate for the lack of a distinct compression and tension zone in deep beams, the contributions from friction and uncracked compression zone were neglected. In walls, however, it was assumed that boundary elements form distinct load paths for the vertical load couple. Thus, in walls, a contribution from the compression zone was considered.

9.1.3 Axial load

The effect of axial load was considered in the modeling of the shear-resisting mechanisms. Following the proposed model, applying axial compression increases the depth of the compression zone, and therefore the contributions from uncracked compression zone and friction. According to the proposed method, the contribution of arch action generally does not increase with axial load, because although the depth of the compression zone increases, it becomes more likely that the cover of the tensile reinforcement governs the effective strut width.

Moreover, axial load was considered in the equilibrium conditions related to the friction component. Axial compression reduces the strain in the tensile reinforcement, and therefore the crack width. Decreasing the crack width increases the shear resistance related to friction consistent with the proposed model.

9.1.4 Effect of the section depth

The decrease of the average shear stress with increasing section depth is treated in the proposed model by the friction component. The decrease of average shear stresses was found not only related to the effective depth of the members, but also related to a combination of section depth, average shear stress, compressive strength of concrete, and tensile reinforcement ratio. The proposed model represented the decrease of average shear stresses with increasing section depth well. Design charts were provided which give the allowable combination of effective depth, concrete strength, tensile reinforcement, and average shear stress for reductions of the friction component by 10, 20, and 30 percent.

9.2 Seismic shear capacity

The main objective in seismic design is to maintain a higher static shear strength than flexural capacity. However, the different degradation rate of both capacities due to cyclic loading results in either flexural or shear failure under lateral load reversals. It was concluded that the strength degradation for both capacities had to be examined.

9.2.1 Degradation of flexural strength

It was shown that the flexural strength found from elastic analysis was a good estimate of the lateral load at yielding of the longitudinal reinforcement in the cyclically loaded columns that were considered. The lateral load at failure was taken as 80 percent of the flexural capacity. A dimensionless strength reduction function, m, was introduced that represents the degradation of shear strength between the displacement at yielding of the tensile reinforcement and the reduced strength at 80 % of V_y.

Out of several variables that were examined, two parameters were found to have an important effect on strength degradation: The confinement ratio, taken as the ratio of effective yield strength of the transverse reinforcement, $\rho_w f_{wy}$, to the compressive strength of concrete, f'_c, and the axial load level, $P/(Af'_c)$. The slope representing the flexural strength degradation was computed as the product of functions of these parameters.

9.2.2 Degradation of shear strength

Similar to flexural strength degradation, the decay of shear strength can be viewed as a function of the static shear strength. The shear corresponding to yielding of the transverse reinforcement was assumed as the ultimate shear capacity. It was assumed that the additional contributions from arch-action and compression zone would have degraded partially or totally at this loading stage.

According to the proposed model, the degradation of shear strength stems from the degradation of the contributions from arch-action and compression zone, and a degradation of the truss mechanism. Using test data by Ichinose (Ichinose et al. 2001), the degradation of the arch and compression zone contributions was calculated as a function of the drift at the point of loss of arch- and compression zone contributions, and the confinement ratio, $\rho_w f_{wy}/f'_c$.

The test data showed that a full degradation of concrete-related components of shear strength was not sufficient to account for the total reduction in strength, and that degradation of the truss mechanism took place.

Available information about the drift at yielding of the transverse reinforcement was used to describe further strength decay as a function of the axial load level, $P/(Af'_c)$, and the drift ratio at yielding of the transverse reinforcement, Δ_{yt}/L.

The proposed model was applied to walls that failed in shear before and after yielding of the longitudinal reinforcement, and to walls that lost their capacity in a flexural failure mode. The calculated strengths of the wall specimens were within reasonable limits compared to the measured failure envelope curves.

9.3 Conclusions

1. The monotonic shear capacity for a wide range of member configurations can be modeled by a superposition of arch-action, truss-action, friction, and a contribution of the compression zone. However, simply superimposing the individual components does not reflect the actual member behavior. Functions transitioning between squat and slender members, as well as between reinforced members and members without web reinforcement, are necessary to model the member behavior accurately.

2. According to the proposed model, the contribution from the friction component can be used to control the so-called "size effect." It was found that the "size effect" is not only an effect of the section depth, but is also influenced by the com-

pressive strength of concrete, the tensile reinforcement ratio, and the average shear stress.

3. In the cyclic load case, the shear strength degradation under reversed lateral loads was found to be not only a strength reduction of the components related to friction and the compression zone, but also as a reduction of the truss mechanism. Flexural strength and shear strength degrade at different rates. To define a failure envelope curve in the design case, the envelopes for flexural and shear strength degradation have to be constructed separately. If the member behavior changes from flexure-controlled to shear-controlled behavior, the interception of the two curves gives the design strength.

4. The shear analysis according to the proposed model gives more accurate results than the other models considered in the study at hand. Moreover, with the exception of the approach proposed by Watanabe, compared to other methods, it is the only model applicable to a wide range of member configurations.

5. The proposed model has the following limitations: Applicable member geometries range from axially loaded walls to slender beams. Within the scope of this work, only members subjected to point loads with a single shear span, such as simply supported beams or cantilever columns, were investigated. To account for distributed loads, changes to the arch mechanism would be necessary. The calibration was carried out at a critical location of a distance d from the support. The application of the proposed model at different locations with different strains in the longitudinal reinforcement would yield different contributions from the friction component. For RC

members subjected to point loads altered values of the critical crack width related to the friction component were presented.

6. The proposed model does not reflect safety factors used for shear analysis. Nevertheless, one objective of the respective calibrations was to provide a certain level of conservatism. However, the level of conservatism attributed to the various components reflects mostly the scatter in the calculated response of the investigated data set.

9.4 Suggested further research

Test data on the degradation of shear strength under seismic load is very limited. The shear strength degradation under cyclic load in this work was treated as empirical relationships of important parameters influencing strength decay. Additional tests with focus on the physical behavior within a member could provide helpful information for physically modeling the degradation process. In order to obtain this, strains in the transverse reinforcement and in the concrete core would have to be measured and correlated to lateral load. In addition, changes are necessary to make the proposed model applicable to different loading types. For example, the arch-model has to be adjusted to reflect a distributed lateral load.

10 References

ACI-318. (2002). *ACI 318-02 Building code requirements for structural concrete*, American Concrete Institute, Farmington Hills, Michigan.

ACI-ASCE committee 326. (1962). "Shear and diagonal tension -- Report of ACI-ASCE committee 326." *American Concrete Institute -- Journal*, 59(3), 353-395.

AIJ. (1988). "AIJ Design Guidelines for Earthquake Resistant Reinforced Concrete Buildings based on Ultimate Strength Concept, with Commentary." Architectural Institute of Japan.

Alshegeir, A., and Ramirez, J. A. (1990). "Analysis of disturbed regions in strut-and-tie models." Purdue University, West Lafayette, Ind.

Ang, Beng Ghee, Priestley, M.J.N., and Paulay, T. (1989). "Seismic shear strength of circular reinforced concrete columns." *ACI Structural Journal (American Concrete Institute)*, 86(1), 45-59.

Aoyama, H. (1993). "Design philosophy for shear in earthquake resistance in Japan." Earthquake resistance of reinforced concrete structures, T. Okada, ed., Dept. of Architecture, Faculty of engineering, University of Tokyo, Tokyo, 407-418.

ASCE-ACI Committee 445. (1998). "Recent approaches to shear design of structural concrete." *Journal of Structural Engineering*, 124(12), 1375-1417.

Aschheim, M. (2000). "Towards improved models of shear strength degradation in reinforced concrete members." *Structural Engineering and Mechanics*, 9(6), 601-613.

Bachmann, Hugo. (1995). *Erdbebensicherung von Bauwerken*, Birkhäuser Verlag, Basel, Boston, Berlin.

Bachmann, Hugo. (2000). "Grundsätze für Ingenieure und Architekten für den erdbebengerechten Entwurf von Hochbauten." Eidgenössische Technische Hochschule Zürich, Zürich.

Baldwin, Jr., J.W., and Viest, I.M. (1958). "Effect of axial compression on shear strength of reinforced concrete frame members." *American Concrete Institute -- Journal*, 30(5), 635-654.

Barda, Felix, Hanson, John M., and Corley, W. Gene. (1977). "Shear Strength of Low-Rise Walls with Boundary Elements." *Publ SP Am Concr Inst SP-53, Symp on Reinf Concr Struct in Seism Zones, 1974*, 149-202.

Bažant, Zdenek P. (1984). "Size effect in blunt fracture: Concrete, rock, metal." *Journal of Engineering Mechanics*, 110(4), 518-535.

Bažant, Zdenek P. (1997). "Fracturing truss model: Size effect in shear failure of reinforced concrete." *Journal of Engineering Mechanics*, 123(12), 1276-1288.

Bažant, Zdenek P., and Kim, Jin-Keun. (1984). "Size effect in shear failure of longitudinally reinforced beams." *ACI Structural Journal*, 81(5), 456-468.

Bergmeister, K., Breen, J. E., and Jirsa, J. O. (1991). "Dimensioning of the nodes and development of reinforcement." IABSE, Zürich.

Berry, M., Camarillo, H., Mookerjeee, A., and Parrish, M. (2003). "Structural Performance Database." University of Washington.Internet database.http://maximus.ce.washington.edu/~peera1/

Brachmann, Ingo. (2002). "Drift Limits of Rectangular Reinforced Concrete Columns subjected to Cyclic Loading," M.S. Thesis, University of Kansas, Lawrence.

Chen, Simon A., and MacGregor, James G. (1993). "Shear-friction truss model for reinforced concrete beams subjected to shear."

Collins, Michael P., Mitchell, Denis, Adebar, Perry, and Vecchio, Frank J. (1996). "General shear design method." *ACI Structural Journal*, 93(1), 36-45.

Collins, Michael P., Mitchell, Denis. (1991). *Prestressed concrete structures*, D. Mitchell, translator, Prentice Hall, Englewood Cliffs, N.J.

Diaz De Cossio, R., and Siess, C.P. (1960). "Behavior and strength in shear of beams and frames without web reinforcement." *American Concrete Institute -- Journal*, 31(8), 695-735.

Hwang, Shyh-Jiann, Fang, Wen-Hung, Lee, Hung-Jen, and Yu, Hsin-Wan. (2001). "Analytical model for predicting shear strength of squat walls." *Journal of Structural Engineering*, 127(1), 43-50.

Ichinose, T., Imai, M., Okano, T., and Ohashi, K. (2001). "Three-Dimensional Shear Failure of RC Columns after Cyclic Loading." Modeling of Inelastic Behavior of RC Structures under Seismic Loads, B. P. Shing, ed., ASCE, Reston, VA, 546-561.

Kabeyasawa, T., and Hiraishi, H. (1998). "Tests and Analyses of High-Strength Reinforced Concrete Shear Walls in Japan." *ACI Special Publication*, 176(176-13), 281-310.

Kani, M. W., Huggins, M. W., and Wiltkopp, P. F. (1979). "Kani on shear in reinforced concrete." Dept. of Civil Engineering, University of Toronto, Toronto.

Kinugasa, H.; Nomura, S. (2001). "Failure mechanism of RC beam under reversed cyclic loading after flexural yielding caused by lateral strain accumulation in plastic-hinging region." *Advances in Earthquake Engineering*, 9(Earthquake Resistant Engineering Structures III), 377-386.

Kong, Fung-Kew, Robins, P.J., and Cole, D.F. (1970). "Web Reinforcement effects on deep beams." *Journal of the American Concrete Institute*, 67(12), 1010-17.

Kong, Fung-Kew, Teng, Susanto, Maimba, P.P., Tan, K.H., and Guan, Lingwei. (1994). "Single-Span, Continuous, and Slender Deep Beams Made of High-Strength Concrete." *ACI Special Publication*, SP149-23, 413-431.

Kotsovos, Michael D., and Pavlovic, Milija N. (2004). "Size effects in beams with small shear span-to-depth ratios." *Computers and Structures*, 82(2-3), 143-156.

Lee, J.Y., Watanabe, F., Nishiyama, M. "Theoretical Prediction of Shear Strength and Ductility of Reinforced Concrete Beams." *Eleventh World Conference on Earthquake Engineering*.

Legeron, Frederic, and Paultre, Patrick. (2000). "Behavior of high-strength concrete columns under cyclic flexure and constant axial load." *ACI Structural Journal*, 97(4), 591-601.

Lopes, M.S. (2001). "Experimental shear-dominated response of RC walls. Part I: Objectives, methodology and results." *Engineering Structures*, 23(3), 229-239.

Lopez, Ricardo Rafael. (1988). "A Numerical Model for Nonlinear Response of R/C Frame-Wall Structures," Dissertation, University of Illinois, Urbana-Champaign.

MacGregor, J.G. (1997). *Reinforced Concrete: Mechanics and Design*, Prentice-Hall, Inc., Englewood Cliffs, New Jersey.

MacGregor, J.G., and Hanson, J.M. (1969). "Proposed changes in shear provisions for reinforced and prestressed concrete beams." *Journal of the American Concrete Institute*, 66(4), 276-288.

Matamoros, Adolfo B. (1999). "Study of Drift Limits for High-Strength Concrete Columns," Doctoral thesis, University of Illinois, Urbana-Champaign.

Matamoros, Adolfo B., and Wong, Kuok Hong. (2003). "Design of Simply Supported Deep Beams Using Strut-and-Tie Models." *ACI Structural Journal*, 100(6), 704-712.

Morrow, J., and Viest, I.M. (1957). "Shear strength of reinforced concrete frame members without web reinforcement." *American Concrete Institute -- Journal*, 28(9), 833-869.

Nielsen, M.P. (1999). *Limit Analysis and Concrete Plasticity*, CRC Press, Boca Raton.

Oesterle, R. G., Fiorato, A. E., and Corley, W. G. (1980). "Reinforcement Details for Earthquake-Resistant Structural Walls." 2(12), 55-66.

Oesterle, R. G., Fiorato, A. E., Johal, L. S., Carpenter, J. E., Russell, H. G., and Corley, W. G. (1976). "Earthquake resistant structural walls - tests of isolated walls." *PB-271 467*, Research and Development Construction Technology Laboratories Portland Cement Association, Skokie, Ill.

Ogata, Kyoko, and Kabeyasawa, Toshimi. (1985). "Experimental Study on the Hysteretic Behavior of Reinforced Concrete Shear Walls under the Loading of different Moment-to-Shear Ratios." *Transactions of the Japan Concrete Institute*, 6, 717-724.

Paulay, T.; Bachmann, H.; Moser, K. (1990). *Erdbebenbemessung von Stahlbetonhochbauten*, Birkhäuser Verlag, Basel, Boston, Berlin.

Pauw, A. (1960). "Static modulus of elasticity of concrete as affected by density." *American Concrete Institute -- Journal*, 32(6), 679-687.

Priestley, M.J.N., Verma, R., Xiao, Y. (1994). "Seismic Shear Strength of Reinforced Concrete Columns." *Journal of Structural Engineering*, 120(8), 2310-2329.

Pujol, S. (1997). "Drift capacity of reinforced concrete columns," MS thesis, Purdue University, West Lafayette, Ind.

Pujol, S., Sözen, M., Ramírez, J. (2000). "Transverse Reinforcement for Columns of RC Frames to resist Earthquakes." *Journal of Structural Engineering*, 126(4), 461-466.

Reineck, Karl-Heinz. (1990). "Ein mechanisches Modell für den Querkraftbereich von Stahlbetonbauteilen," Diss., Universität Stuttgart, Stuttgart.

Reineck, Karl-Heinz. (1991a). "Modelling of members with transverse reinforcement." IABSE Colloquium "Structural Concrete", Stuttgart.

Reineck, Karl-Heinz. (1991b). "Ultimate shear force of structural concrete members without transverse reinforcement derived from a mechanical model." *ACI Structural Journal (American Concrete Institute)*, 88(5), 592-602.

Reineck, Karl-Heinz, Kuchma, Daniel A., Kim, Kang Su, and Marx, Sina. (2003). "Shear database for reinforced concrete members without shear reinforcement." *ACI Structural Journal*, 100(2), 240-249.

Richart, F.E., Brandtzaeg, A., Brown, R.L. (1929). "The failure of plain and spirally reinforced concrete in compression." *Bulletin No. 190*, University of Illinois, Engrg. Experiment Station, 26(31).

Roller, John J., and Russell, Henry G. (1990). "Shear strength of high-strength concrete beams with web reinforcement." *ACI Structural Journal (American Concrete Institute)*, 87(2), 191-198.

Schlaich, Jörg, Schäfer, Kurt, and Jennewein, Mattias. (1987). "Toward a consistent design of structural concrete." *PCI Journal (Prestressed Concrete Institute)*, 32(3), 74-150.

Schneider, Klaus-Jürgen. (1998). "Bautabellen für Ingenieure." Werner Verlag, Düsseldorf.

Selby, Robert G., Vecchio, Frank J., and Collins, Michael P. (1996). "Analysis of reinforced concrete members subject to shear and axial compression." *ACI Structural Journal*, 93(3), 306-315.

Shin, Sung-Woo, Lee, Kwang-Soo, Moon, Jung-Ill, and Ghosh, S.K. (1999). "Shear strength of reinforced high-strength concrete beams with shear span-to-depth ratios between 1.5 and 2.5." *ACI Structural Journal*, 96(4), 549-556.

Specht, Manfred. (1986). "Modellstudie zur Querkrafttragfähigkeit von Stahlbetonträgern ohne Schubbewehrung im Bruchzustand. (Model To Study The Shear Force Capacity Of Reinforced Concrete Members Without Shear Reinforcement Under Ultimate Bending Load.)." *Bautechnik*, 63(10), 339-350.

Specht, Manfred. (1987). "Ingenieurmodelle zur Beschreibung der Querkrafttragfähigkeit von Stahlbetonträgern im Bruchzustand. (Engineering Models for Describing the Transverse Force Load-bearing Capacity of Reinforced Concrete Girders in the Fracture State.)." *Bautechnik*, 64(11), 371-378.

Thürlimann, B. (1979). "Plastic analysis of Reinforced Concrete Beams." Copenhagen.

Tompos, Eric J., and Frosch, Robert J. (2002). "Influence of beam size, longitudinal reinforcement, and stirrup effectiveness on concrete shear strength." *ACI Structural Journal*, 99(5), 559-567.

von Ramin, Malte, Matamoros, Adolfo B., and Browning, JoAnn. (2002). "Effect of shear strength and geometry on performance of short-period systems." *SL Report 02-1*, Dpt. of Civil, Environmental, and Architectural Engineering, University of Kansas, Lawrence, KS.

Wallace, J.W. (1998). "Behavior and Design of High-Strength RC Walls." *ACI Special Publication*, 176-12, 259-279.

Walraven, Joost C. (1980). "Aggregate Interlock: A theoretical and experimental analysis," PhD thesis, Delft University.

Walraven, Joost C. (1981a). "Behaviour of cracks in plain and reinforced concrete subjected to shear." IABSE Colloquium, Delft.

Walraven, Joost C. (1981b). "Fundamental Analysis of Aggregate Interlock." *ASCE Journal of the Structural Division*, 107(11), 2245-2270.

Walraven, Joost C. (1986). "Aggregate interlock under dynamic loads." *Darmstadt Concrete, Annual Journal on Concrete and Concrete Structures*, 1, 143-156.

Walraven, Joost C., Frenay, Jerome, and Pruijssers, Arjan. (1987). "Influence of concrete strength and load history on the shear friction capacity of concrete members." *PCI Journal (Prestressed Concrete Institute)*, 32(1), 66-84.

Watanabe, F., and Ichinose, T. "Strength and ductility design of RC members subjected to combined bending and shear." *International Workshop on concrete shear in earthquake*, University of Houston, Houston, Texas.

Watanabe, Fumio, and Kabeyasawa, T. (1998). "Shear Strength of RC Members with High-Strength Concrete." *ACI Special Publication*, 176(176-17), 379-396.

Watanabe, Fumio, and Lee, Jung-Yoon. (1998). "Theoretical prediction of shear strength and failure mode of reinforced concrete beams." *ACI Structural Journal*, 95(6), 749-757.

Wight, J. K., and Sözen, M. A. (1973). "Shear strength decay in reinforced concrete columns subjected to large deflection reversals." *Struct. Res. No. 403*, University of Illinois at Urbana-Champaign, Ill., Urbana-Champaign.

Wolfram. (2002). "Mathematica Neural Networks Add-On." Wolfram Research, Inc., Champaign, Ill.

Wong, Y.L., Paulay, T., Priestley, M.J.N. (1993). "Response of Circular Reinforced Concrete Columns to multi-directional Seismic Attack." *ACI Structural Journal*, 90(2), 183-191.

Wood, Sharon L. (1990). "Shear strength of low-rise reinforced concrete walls." *ACI Structural Journal (American Concrete Institute)*, 87(1), 99-107.

Zararis, Prodromes D. (2003). "Shear strength and minimum shear reinforcement of reinforced concrete slender beams." *ACI Structural Journal*, 100(2), 203-214.

11 Appendix: list of specimen properties

A1. Deep beams without web reinforcement

No.	Researcher	Specimen ID	Loading conditions		b	d	a	a/d
			l_b [mm]	h_a [mm]	[mm]	[mm]	[mm]	
1	Moody et al. (1954)	24a	203.2	153.2	178	533	810	1.52
2	Moody et al. (1954)	24b	203.2	153.2	178	533	810	1.52
3	Moody et al. (1954)	25b	203.2	153.2	178	533	810	1.52
4	Moody et al. (1954)	26a	203.2	153.2	178	533	810	1.52
5	Moody et al. (1954)	26b	203.2	153.2	178	533	810	1.52
6	Moody et al. (1954)	27a	203.2	153.2	178	533	810	1.52
7	Moody et al. (1954)	27b	203.2	153.2	178	533	810	1.52
8	Moody et al. (1954)	28a	203.2	153.2	178	533	810	1.52
9	Moody et al. (1954)	28b	203.2	153.2	178	533	810	1.52
10	Moody et al. (1954)	29a	203.2	153.2	178	533	810	1.52
11	Moody et al. (1954)	29b	203.2	153.2	178	533	810	1.52
12	Mathey and Watstein (1963)	I - 1	101.6	108.5	203	403	609	1.51
13	Mathey and Watstein (1963)	I - 2	101.6	108.5	203	403	609	1.51
14	Mathey and Watstein (1963)	II - 3	101.6	108.5	203	403	609	1.51
15	Mathey and Watstein (1963)	II - 4	101.6	108.5	203	403	609	1.51
16	Mathey and Watstein (1963)	III - 5	101.6	108.5	203	403	609	1.51
17	Mathey and Watstein (1963)	III - 6	101.6	108.5	203	403	609	1.51
18	Mathey and Watstein (1963)	IV - 7	101.6	108.5	203	403	609	1.51
19	Mathey and Watstein (1963)	IV - 8	101.6	108.5	203	403	609	1.51
20	Mathey and Watstein (1963)	V - 9	101.6	108.5	203	403	609	1.51
21	Mathey and Watstein (1963)	V - 10	101.6	108.5	203	403	609	1.51

No.	Researcher	Specimen ID	Loading conditions		b	d	a	a/d
			l_b [mm]	h_a [mm]	[mm]	[mm]	[mm]	
22	Mathey and Watstein (1963)	VI - 11	101.6	108.5	203	403	609	1.51
23	Mathey and Watstein (1963)	VI - 12	101.6	108.5	203	403	609	1.51
24	Mathey and Watstein (1963)	V - 13	101.6	108.5	203	403	609	1.51
25	Mathey and Watstein (1963)	V - 14	101.6	108.5	203	403	609	1.51
26	Mathey and Watstein (1963)	VI - 15	101.6	108.5	203	403	609	1.51
27	Mathey and Watstein (1963)	VI - 16	101.6	108.5	203	403	609	1.51
28	Kani (1967)	41.00	203.2	22.9	153	141	340	2.41
29	Kani (1967)	45.00	203.2	38.9	151	133	271	2.04
30	Kani (1967)	46.00	203.2	32.8	151	136	272	2.00
31	Kani (1967)	53.00	203.2	40.9	151	132	136	1.03
32	Kani (1967)	54.00	203.2	32.8	151	136	136	1.00
33	Kani (1967)	94.00	203.2	63.5	153	273	543	1.99
34	Kani (1967)	95.00	203.2	59.7	153	275	677	2.46
35	Kani (1967)	98.00	203.2	59.7	153	275	679	2.47
36	Kani (1967)	99.00	203.2	65.5	152	272	680	2.50
37	Kani (1967)	100.00	203.2	69.6	153	270	545	2.02
38	Kani (1967)	61.00	203.2	135.1	156	542	1084	2.00
39	Kani (1967)	67.00	203.2	163.3	157	528	544	1.03
40	Kani (1967)	69.00	203.2	135.1	155	542	542	1.00
41	Kani (1967)	72.00	203.2	121.2	152	549	1076	1.96
42	Kani (1967)	3041.00	203.2	244.3	152	1097	2194	2.00
43	Kani (1967)	3042.00	203.2	248.4	154	1095	2738	2.50
44	Rogowsky et al. (1986)	BM1/1.5T1	200.0	130.0	200	535	1000	1.87
45	Rogowsky et al. (1986)	BM1/2.0T1	200.0	89.9	200	455	1001	2.20
46	Kong and Teng (1994)	N-1a	200.0	150.0	150	525	900	1.71
47	Kong and Teng (1994)	N-1b	200.0	100.0	150	550	900	1.64
48	Kong and Teng (1994)	DB1	100.0	100.0	100	700	325	0.46
49	Kong and Teng (1994)	DB2	100.0	100.0	100	700	325	0.46
50	Kong and Teng (1994)	DB3	100.0	100.0	100	700	325	0.46

No.	Researcher	Specimen ID	f'_c [MPa]	Longitudinal reinf. ρ_s [%]	V_{mes} [kN]	V_{mes}/V_{cal} [-]	V_{mes}/V_{cal} Watanabe [-]
1	Moody et al. (1954)	24a	18	2.7	296	1.23	1.80
2	Moody et al. (1954)	24b	21	2.7	303	1.10	1.67
3	Moody et al. (1954)	25b	17	3.5	289	1.23	1.79
4	Moody et al. (1954)	26a	22	4.3	420	1.45	2.22
5	Moody et al. (1954)	26b	21	4.3	396	1.44	2.18
6	Moody et al. (1954)	27a	21	2.7	347	1.22	1.86
7	Moody et al. (1954)	27b	23	2.7	356	1.17	1.82
8	Moody et al. (1954)	28a	23	3.5	303	0.99	1.54
9	Moody et al. (1954)	28b	22	3.5	340	1.15	1.77
10	Moody et al. (1954)	29a	22	4.3	389	1.36	2.07
11	Moody et al. (1954)	29b	25	4.3	436	1.34	2.11
12	Mathey and Watstein (1963)	I - 1	25	3.1	313	1.35	1.73
13	Mathey and Watstein (1963)	I - 2	23	3.1	311	1.46	1.84
14	Mathey and Watstein (1963)	II - 3	22	1.9	262	1.28	1.60
15	Mathey and Watstein (1963)	II - 4	26	1.9	313	1.30	1.69
16	Mathey and Watstein (1963)	III - 5	26	1.9	289	1.23	1.58
17	Mathey and Watstein (1963)	III - 6	26	1.9	291	1.24	1.60
18	Mathey and Watstein (1963)	IV - 7	24	1.9	291	1.31	1.66
19	Mathey and Watstein (1963)	IV - 8	25	1.9	304	1.33	1.70
20	Mathey and Watstein (1963)	V - 9	23	1.2	224	1.05	1.32
21	Mathey and Watstein (1963)	V - 10	27	1.2	269	1.10	1.43
22	Mathey and Watstein (1963)	VI - 11	25	1.2	224	0.97	1.25
23	Mathey and Watstein (1963)	VI - 12	26	1.2	269	1.15	1.47
24	Mathey and Watstein (1963)	V - 13	22	0.8	222	1.07	1.34
25	Mathey and Watstein (1963)	V - 14	27	0.8	224	0.92	1.20
26	Mathey and Watstein (1963)	VI - 15	25	0.8	180	0.77	0.99
27	Mathey and Watstein (1963)	VI - 16	23	0.8	189	0.89	1.12

No.	Researcher	Specimen ID	f'c [MPa]	Longitudinal reinf. ρ_s [%]	V_{mes} [kN]	V_{mes}/V_{cal} [-]	V_{mes}/V_{cal} Watanabe [-]
28	Kani (1967)	41.00	27	2.6	51	1.05	1.55
29	Kani (1967)	45.00	25	2.8	65	0.76	1.88
30	Kani (1967)	46.00	25	2.8	69	0.80	1.93
31	Kani (1967)	53.00	27	2.8	155	0.48	2.53
32	Kani (1967)	54.00	27	2.8	158	0.49	2.44
33	Kani (1967)	94.00	25	2.8	111	1.03	1.52
34	Kani (1967)	95.00	25	2.8	73	1.26	1.21
35	Kani (1967)	98.00	26	2.7	76	1.30	1.24
36	Kani (1967)	99.00	26	2.7	77	1.32	1.29
37	Kani (1967)	100.00	27	2.7	112	0.98	1.50
38	Kani (1967)	61.00	27	2.6	136	0.83	0.90
39	Kani (1967)	67.00	30	2.8	548	0.97	1.97
40	Kani (1967)	69.00	27	2.7	586	1.21	2.18
41	Kani (1967)	72.00	25	2.7	197	1.34	1.36
42	Kani (1967)	3041.00	27	2.7	326	1.40	1.09
43	Kani (1967)	3042.00	26	2.7	237	1.77	0.97
44	Rogowsky et al. (1986)	BM1/1.5T1	42	1.1	303	0.88	1.09
45	Rogowsky et al. (1986)	BM1/2.0T1	43	0.9	177	0.92	0.86
46	Kong and Teng (1994)	N-1a	37	1.9	243	0.81	1.21
47	Kong and Teng (1994)	N-1b	40	0.9	205	0.72	0.89
48	Kong and Teng (1994)	DB1	40	0.5	287	0.87	0.65
49	Kong and Teng (1994)	DB2	53	0.5	410	1.02	0.77
50	Kong and Teng (1994)	DB3	65	0.5	525	1.15	0.86
					mean	1.11 ± 0.8%	1.52 ± 0.94%
					std-dev	0.25	0.45
					c.v.	22.97%	29.34%

(Kong et al. 1994; Matamoros and Wong 2003)

A2. Slender beams without web reinforcement

No.	Researcher	Specimen ID	b [mm]	h [mm]	d [mm]	h_a [mm]	a [mm]	a/d [-]
1	Adebar P., Collins M.P. (1996)	ST1	360	310	278	64	800	2.88
2	Adebar P., Collins M.P. (1996)	ST2	360	310	278	64	800	2.88
3	Adebar P., Collins M.P. (1996)	ST3	290	310	278	64	800	2.88
4	Adebar P., Collins M.P. (1996)	ST8	290	310	278	64	800	2.88
5	Adebar P., Collins M.P. (1996)	ST16	290	210	178	64	800	4.49
6	Adebar P., Collins M.P. (1996)	ST23	290	310	278	64	800	2.88
7	Ahmad, Kahloo (1986)	A1	127	254	203	102	813	4.00
8	Ahmad, Kahloo (1986)	A2	127	254	203	102	610	3.00
9	Ahmad, Kahloo (1986)	A3	127	254	203	102	549	2.70
10	Ahmad, Kahloo (1986)	A8	127	254	208	92	624	3.00
11	Ahmad, Kahloo (1986)	B1	127	254	202	105	807	4.00
12	Ahmad, Kahloo (1986)	B2	127	254	202	105	605	3.00
13	Ahmad, Kahloo (1986)	B3	127	254	202	105	545	2.70
14	Ahmad, Kahloo (1986)	B7	127	254	208	92	832	4.00
15	Ahmad, Kahloo (1986)	B8	127	254	208	92	624	3.00
16	Ahmad, Kahloo (1986)	B9	127	254	208	92	562	2.70
17	Ahmad, Kahloo (1986)	C1	127	254	184	140	737	4.00
18	Ahmad, Kahloo (1986)	C2	127	254	184	140	552	3.00
19	Ahmad, Kahloo (1986)	C3	127	254	184	140	497	2.70
20	Ahmad, Kahloo (1986)	C7	127	254	207	95	826	4.00
21	Ahmad, Kahloo (1986)	C8	127	254	207	95	620	3.00
22	Ahmad, Kahloo (1986)	C9	127	254	207	95	558	2.70

No.	Researcher	Specimen ID	b [mm]	h [mm]	d [mm]	h_a [mm]	a [mm]	a/d [-]
23	Al-Alusi A.F. (1957)	7	76	146	127	38	572	4.50
24	Al-Alusi A.F. (1957)	10	76	146	127	38	508	4.00
25	Al-Alusi A.F. (1957)	11	76	146	127	38	432	3.40
26	Al-Alusi A.F. (1957)	18	76	146	127	38	572	4.50
27	Angelakos D., Bentz E. C. , Collins M. P. ()	DB120	300	1000	925	150	2700	2.92
28	Angelakos D., Bentz E. C. , Collins M. P. ()	DB130	300	1000	925	150	2700	2.92
29	Angelakos D., Bentz E. C. , Collins M. P. ()	DB140	300	1000	925	150	2700	2.92
30	Angelakos D., Bentz E. C. , Collins M. P. ()	DB165	300	1000	925	150	2700	2.92
31	Angelakos D., Bentz E. C. , Collins M. P. ()	DB180	300	1000	925	150	2700	2.92
32	Angelakos D., Bentz E. C. , Collins M. P. ()	DB230	300	1000	895	210	2700	3.02
33	Angelakos D., Bentz E. C. , Collins M. P. (2000)	DBO530	300	1000	925	150	2700	2.92
34	Aster; Koch (1974)	2	1000	281	250	62	920	3.68
35	Aster; Koch (1974)	3	1000	289	250	77	920	3.68
36	Aster; Koch (1974)	8	1000	544	500	88	2750	5.50
37	Aster; Koch (1974)	9	1000	544	500	88	2750	5.50
38	Aster; Koch (1974)	10	1000	544	500	88	2750	5.50
39	Aster; Koch (1974)	11	1000	539	500	77	1825	3.65
40	Aster; Koch (1974)	12	1000	540	500	80	1825	3.65
41	Aster; Koch (1974)	16	1000	794	750	88	2750	3.67
42	Aster; Koch (1974)	17	1000	794	750	88	2750	3.67
43	Bhal (1968)	B1	240	350	300	100	900	3.00
44	Bhal (1968)	B2	240	650	600	100	1800	3.00
45	Bhal (1968)	B3	240	950	900	100	2700	3.00
46	Bhal (1968)	B4	240	1250	1200	100	3600	3.00
47	Bhal (1968)	B5	240	650	600	100	1800	3.00
48	Bhal (1968)	B6	240	650	600	100	1800	3.00
49	Bhal (1968)	B7	240	950	900	100	2700	3.00
50	Bhal (1968)	B8	240	950	900	100	2700	3.00
51	Bresler, Scordelis (1963)	0A-1	310	556	461	191	1753	3.80

No.	Researcher	Specimen ID	b [mm]	h [mm]	d [mm]	h_a [mm]	a [mm]	a/d [-]
52	Bresler, Scordelis (1963)	0A-2	305	561	466	191	2210	4.74
53	Bresler, Scordelis (1963)	0A-3	307	556	462	189	3124	6.77
54	Cederwall K., Hedman O., Losberg A. (1974)	734-34	135	260	234	52	800	3.42
55	Chana (1981)	37623	203	406	356	100	1068	3.00
56	Chana (1981)	37654	203	406	356	100	1068	3.00
57	Chana (1981)	37682	203	406	356	100	1068	3.00
58	Collins, Kuchma (1999)	B100	300	1000	925	150	2701	2.92
59	Collins, Kuchma (1999)	B100H	300	1000	925	150	2701	2.92
60	Collins, Kuchma (1999)	B100B	300	1000	925	150	2701	2.92
61	Collins, Kuchma (1999)	B100L	300	1000	925	150	2701	2.92
62	Collins, Kuchma (1999)	B100-R	300	1000	925	150	2701	2.92
63	Collins, Kuchma (1999)	B100L-R	300	1000	925	150	2701	2.92
64	Diaz de Cossio, Siess (1960)	A2	152	305	254	102	762	3.00
65	Diaz de Cossio, Siess (1960)	A3	152	305	254	102	1016	4.00
66	Diaz de Cossio, Siess (1960)	A-12	152	305	254	102	762	3.00
67	Diaz de Cossio, Siess (1960)	A-13	152	305	254	102	1016	4.00
68	Diaz de Cossio, Siess (1960)	A-14	152	305	254	102	1270	5.00
69	Elzanaty, Nilson, Slate (1986)	F1	178	305	270	70	1080	4.00
70	Elzanaty, Nilson, Slate (1986)	F2	178	305	268	73	1073	4.00
71	Elzanaty, Nilson, Slate (1986)	F10	178	305	267	76	1067	4.00
72	Elzanaty, Nilson, Slate (1986)	F9	178	305	268	73	1073	4.00
73	Elzanaty, Nilson, Slate (1986)	F15	178	305	268	73	1073	4.00
74	Elzanaty, Nilson, Slate (1986)	F6	178	305	268	73	1610	6.00
75	Elzanaty, Nilson, Slate (1986)	F11	178	305	270	70	1080	4.00
76	Elzanaty, Nilson, Slate (1986)	F12	178	305	268	73	1073	4.00

No.	Researcher	Specimen ID	b [mm]	h [mm]	d [mm]	h_a [mm]	a [mm]	a/d [-]
77	Elzanaty, Nilson, Slate (1986)	F8	178	305	273	64	1092	4.00
78	Elzanaty, Nilson, Slate (1986)	F13	178	305	270	70	1080	4.00
79	Elzanaty, Nilson, Slate (1986)	F14	178	305	268	73	1073	4.00
80	Feldman, Siess (1955)	L-2A	152	305	252	105	762	3.02
81	Feldman, Siess (1955)	L-3	152	305	252	105	1016	4.02
82	Feldman, Siess (1955)	L-4	152	305	252	105	1270	5.03
83	Feldman, Siess (1955)	L-5	152	305	252	105	1524	6.04
84	Ferguson P.M. (1956)	F2	101	210	189	41	610	3.23
85	Ferguson P.M., Thompson N.J. (1953)	A1	102	241	210	64	711	3.39
86	Ferguson P.M., Thompson N.J. (1953)	A2	102	241	210	64	711	3.39
87	Ferguson P.M., Thompson N.J. (1953)	A3	102	241	210	64	711	3.39
88	Ferguson P.M., Thompson N.J. (1953)	A4	102	241	210	64	711	3.39
89	Ferguson P.M., Thompson N.J. (1953)	A5	102	241	210	64	711	3.39
90	Ferguson P.M., Thompson N.J. (1953)	A6	102	241	210	64	711	3.39
91	Ferguson P.M., Thompson N.J. (1953)	D1	178	241	210	64	711	3.39
92	Ferguson P.M., Thompson N.J. (1953)	D2	178	241	210	64	711	3.39
93	Ferguson P.M., Thompson N.J. (1953)	N1	108	191	178	25	711	4.00
94	Ferguson P.M., Thompson N.J. (1953)	N2	108	191	178	25	711	4.00

No.	Researcher	Specimen ID	b [mm]	h [mm]	d [mm]	h_a [mm]	a [mm]	a/d [-]
95	Ferguson P.M., Thompson N.J. (1953)	N3	108	191	178	25	711	4.00
96	Ferguson P.M., Thompson N.J. (1953)	B1	102	241	210	64	711	3.39
97	Ferguson P.M., Thompson N.J. (1953)	B2	102	241	210	64	711	3.39
98	Ferguson P.M., Thompson N.J. (1953)	B3	102	241	210	64	711	3.39
99	Ferguson P.M., Thompson N.J. (1953)	B4	102	241	210	64	711	3.39
100	Ferguson P.M., Thompson N.J. (1953)	B5	102	241	210	64	711	3.39
101	Ferguson P.M., Thompson N.J. (1953)	C1	102	241	210	64	711	3.39
102	Ferguson P.M., Thompson N.J. (1953)	C2	102	241	210	64	711	3.39
103	Ferguson P.M., Thompson N.J. (1953)	L1	108	191	159	64	711	4.48
104	Ferguson P.M., Thompson N.J. (1953)	L3	108	191	159	64	711	4.48
105	Grimm, R. (1997)	s1.1	300	200	153	94	570	3.73
106	Grimm, R. (1997)	s1.2	300	200	152	96	570	3.75
107	Grimm, R. (1997)	s1.3	300	200	146	108	570	3.90
108	Grimm, R. (1997)	s2.2	300	400	348	104	1230	3.53
109	Grimm, R. (1997)	s2.3	300	400	348	104	1230	3.53
110	Grimm, R. (1997)	s2.4	300	400	328	144	1230	3.75
111	Grimm, R. (1997)	s3.2	300	800	718	164	2630	3.66
112	Grimm, R. (1997)	s3.3	300	800	746	108	2630	3.53
113	Grimm, R. (1997)	s3.4	300	800	690	220	2630	3.81
114	Grimm, R. (1997)	s4.1	300	200	153	94	570	3.73
115	Grimm, R. (1997)	s4.2	300	200	152	96	570	3.75
116	Grimm, R. (1997)	s4.3	300	200	146	108	570	3.90
117	Hallgren (1994)	B90SB13-2-86	163	233	192	82	700	3.65
118	Hallgren (1994)	B90SB14-2-86	158	235	194	82	700	3.61

No.	Researcher	Specimen ID	b [mm]	h [mm]	d [mm]	h_a [mm]	a [mm]	a/d [-]
119	Hallgren (1994)	B90SB22-2-85	158	234	193	82	700	3.63
120	Hallgren (1994)	B91SC2-2-62	155	237	196	82	700	3.57
121	Hallgren (1994)	B91SC4-2-69	156	236	195	82	700	3.59
122	Hallgren (1994)	B90SB17-2-45	157	232	191	82	700	3.66
123	Hallgren (1994)	B90SB18-2-45	155	235	194	82	700	3.61
124	Hallgren (1994)	B90SB21-2-85	155	235	194	82	700	3.61
125	Hallgren (1994)	B91SC1-2-62	156	234	193	82	700	3.63
126	Hallgren (1994)	B91SD1-4-61	156	247	194	106	700	3.61
127	Hallgren (1994)	B91SD2-4-61	156	248	195	106	700	3.59
128	Hallgren (1994)	B91SD3-4-66	156	248	195	106	700	3.59
129	Hallgren (1994)	B91SD4-4-66	155	248	195	106	700	3.59
130	Hallgren (1994)	B91SD5-4-58	156	249	196	106	700	3.57
131	Hallgren (1994)	B91SD6-4-58	150	249	196	106	700	3.57
132	Hallgren (1994)	B90SB5-2-33	156	232	191	82	700	3.66
133	Hallgren (1994)	B90SB6-2-33	156	235	194	82	700	3.61
134	Hallgren (1994)	B90SB9-2-31	156	233	192	82	700	3.65
135	Hallgren (1994)	B90SB10-2-31	157	234	193	82	700	3.63
136	Hallgren (1996)	B3	262	240	208	64	550	2.64
137	Hallgren (1996)	B5	283	240	211	58	550	2.61
138	Hallgren (1996)	B7	337	240	208	64	550	2.64
139	Hamadi; Regan (1980)	G1	100	400	370	60	1255	3.39
140	Hamadi; Regan (1980)	G2	100	400	372	56	1255	3.37
141	Hamadi; Regan (1980)	G4	100	400	372	56	2195	5.90
142	Hanson J.A. (1958)	8A-X	152	305	267	76	660	2.48
143	Hanson J.A. (1958)	8A	152	305	267	76	660	2.48
144	Hanson J.A. (1958)	8B	152	305	267	76	660	2.48
145	Hanson J.A. (1958)	8C	152	305	267	76	660	2.48
146	Hanson J.A. (1958)	8D	152	305	267	76	660	2.48
147	Hanson (1961)	8A4	152	305	267	76	1321	4.95
148	Hanson (1961)	8B4	152	305	267	76	1321	4.95
149	Hanson (1961)	8BW4	152	305	267	76	1321	4.95
150	Hanson (1961)	8B2	152	305	267	76	1321	4.95
151	Hanson (1961)	8B3	152	305	267	76	660	2.48
152	Islam M.S., Pam H.J., Kwan A.K.H. (1998)	M100-S0	150	250	203	94	800	3.94

No.	Researcher	Specimen ID	b [mm]	h [mm]	d [mm]	h_a [mm]	a [mm]	a/d [-]
153	Islam M.S., Pam H.J., Kwan A.K.H. (1998)	M100-S1	150	250	203	94	600	2.96
154	Islam M.S., Pam H.J., Kwan A.K.H. (1998)	M100-S3	150	250	203	94	600	2.96
155	Islam M.S., Pam H.J., Kwan A.K.H. (1998)	M100-S4	150	250	203	94	800	3.94
156	Islam M.S., Pam H.J., Kwan A.K.H. (1998)	M80-S0	150	250	203	94	800	3.94
157	Islam M.S., Pam H.J., Kwan A.K.H. (1998)	M80-S1	150	250	203	94	600	2.96
158	Islam M.S., Pam H.J., Kwan A.K.H. (1998)	M80-S3	150	250	203	94	600	2.96
159	Islam M.S., Pam H.J., Kwan A.K.H. (1998)	M80-S4	150	250	203	94	800	3.94
160	Islam M.S., Pam H.J., Kwan A.K.H. (1998)	M60-S0	150	250	207	86	800	3.86
161	Islam M.S., Pam H.J., Kwan A.K.H. (1998)	M60-S1	150	250	207	86	600	2.90
162	Islam M.S., Pam H.J., Kwan A.K.H. (1998)	M60-S3	150	250	207	86	600	2.90
163	Islam M.S., Pam H.J., Kwan A.K.H. (1998)	M60-S4	150	250	207	86	800	3.86
164	Islam M.S., Pam H.J., Kwan A.K.H. (1998)	M40-S0	150	250	205	90	800	3.90
165	Islam M.S., Pam H.J., Kwan A.K.H. (1998)	M40-S1	150	250	205	90	600	2.93
166	Islam M.S., Pam H.J., Kwan A.K.H. (1998)	M40-S3	150	250	205	90	600	2.93
167	Islam M.S., Pam H.J., Kwan A.K.H. (1998)	M25-S0	150	250	207	86	800	3.86
168	Islam M.S., Pam H.J., Kwan A.K.H. (1998)	M25-S3	150	250	207	86	600	2.90

No.	Researcher	Specimen ID	b [mm]	h [mm]	d [mm]	h_a [mm]	a [mm]	a/d [-]
169	Kani (1967)	3044	152	1219	1097	244	4364	3.98
170	Kani (1967)	3045	155	1219	1092	254	5461	5.00
171	Kani (1967)	3046	155	1219	1097	244	7681	7.00
172	Kani (1967)	3047	155	1219	1095	249	8758	8.00
173	Kani (1967)	63	154	610	543	134	2170	4.00
174	Kani (1967)	64	156	610	541	138	4340	8.03
175	Kani (1967)	66	156	610	541	137	3255	6.01
176	Kani (1967)	79	153	610	556	107	3805	6.84
177	Kani (1967)	1	152	610	524	171	1631	3.11
178	Kani (1967)	71	155	610	544	131	1628	2.99
179	Kani (1967)	272	611	305	271	68	1359	5.02
180	Kani (1967)	273	612	305	271	67	1087	4.01
181	Kani (1967)	274	612	305	270	69	815	3.02
182	Kani (1967)	52	152	152	138	28	544	3.93
183	Kani (1967)	48	151	152	133	38	678	5.09
184	Kani (1967)	81	153	305	274	61	1628	5.93
185	Kani (1967)	84	151	305	271	68	1085	4.00
186	Kani (1967)	96	153	305	275	59	1085	3.94
187	Kani (1967)	83	156	305	271	67	814	3.00
188	Kani (1967)	97	152	305	276	57	815	2.95
189	Kani (1967)	3043	154	1219	1092	254	3277	3.00
190	Kani (1967)	56	153	152	137	30	476	3.46
191	Kani (1967)	58	152	152	138	28	476	3.44
192	Kani (1967)	60	155	152	139	27	407	2.93
193	Kani (1967)	91	154	305	269	72	1628	6.06
194	Kani (1967)	92	152	305	270	70	1899	7.03
195	Kani (1967)	41	152	152	141	22	340	2.41
196	Kani (1967)	59	154	152	140	25	373	2.67
197	Kani (1967)	65	150	610	552	114	1359	2.46
198	Kani (1967)	95	153	305	275	59	678	2.47
199	Kani (1967)	98	153	305	275	60	679	2.47
200	Kani (1967)	99	152	305	272	66	679	2.50
201	Kani (1967)	3042	154	1219	1095	249	2737	2.50
202	Krefeld, Thurston (1966)	11A2	152	381	314	134	851	2.71
203	Krefeld, Thurston (1966)	12A2	152	305	238	135	851	3.58
204	Krefeld, Thurston (1966)	18A2	152	381	316	130	851	2.69
205	Krefeld, Thurston (1966)	18B2	152	381	316	130	851	2.69
206	Krefeld, Thurston (1966)	18C2	152	381	316	130	851	2.69

No.	Researcher	Specimen ID	b [mm]	h [mm]	d [mm]	h_a [mm]	a [mm]	a/d [-]
207	Krefeld, Thurston (1966)	18D2	152	381	316	130	851	2.69
208	Krefeld, Thurston (1966)	16A2	152	305	240	130	851	3.55
209	Krefeld, Thurston (1966)	17A2	152	305	243	124	851	3.50
210	Krefeld, Thurston (1966)	3AC	152	305	256	99	1156	4.52
211	Krefeld, Thurston (1966)	3CC	152	305	256	99	1461	5.72
212	Krefeld, Thurston (1966)	3AAC	152	305	256	99	851	3.33
213	Krefeld, Thurston (1966)	4AAC	152	305	254	102	851	3.35
214	Krefeld, Thurston (1966)	5AAC	152	305	252	105	851	3.37
215	Krefeld, Thurston (1966)	6AAC	152	305	250	109	851	3.40
216	Krefeld, Thurston (1966)	3AC	152	305	256	99	1156	4.52
217	Krefeld, Thurston (1966)	4AC	152	305	254	102	1156	4.55
218	Krefeld, Thurston (1966)	5AC	152	305	252	105	1156	4.58
219	Krefeld, Thurston (1966)	6AC	152	305	250	109	1156	4.61
220	Krefeld, Thurston (1966)	4CC	152	305	254	102	1461	5.75
221	Krefeld, Thurston (1966)	5CC	152	305	252	105	1461	5.78
222	Krefeld, Thurston (1966)	6CC	152	305	250	109	1461	5.83
223	Krefeld, Thurston (1966)	C	203	533	483	102	1461	3.03
224	Krefeld, Thurston (1966)	OCA	152	305	254	102	1461	5.75
225	Krefeld, Thurston (1966)	OCB	152	305	254	102	1461	5.75
226	Krefeld, Thurston (1966)	OCA	254	508	456	105	1765	3.87
227	Krefeld, Thurston (1966)	OCB	254	508	456	105	1765	3.87
228	Krefeld, Thurston (1966)	15A2	152	381	316	130	914	2.89
229	Krefeld, Thurston (1966)	15B2	152	381	316	130	914	2.89
230	Kulkarni S.M., Shah S.P. (1998)	B4JL20-S	102	178	152	52	760	5.00

No.	Researcher	Specimen ID	b [mm]	h [mm]	d [mm]	h_a [mm]	a [mm]	a/d [-]
231	Kulkarni S.M., Shah S.P. (1998)	B3NO15-S	102	178	152	52	608	4.00
232	Kulkarni S.M., Shah S.P. (1998)	B3NO30-S	102	178	152	52	532	3.50
233	Küng (1985)	C	140	230	200	60	500	2.50
234	Küng (1985)	D	140	230	200	60	500	2.50
235	Küng (1985)	E	140	230	200	60	500	2.50
236	Küng (1985)	F	140	230	200	60	500	2.50
237	Küng (1985)	E-1	140	230	200	60	500	2.50
238	Lambotte H., Taerwe L.R. (1990)	NS-0.97	200	450	415	70	1250	3.01
239	Lambotte H., Taerwe L.R. (1990)	NS-1.45	200	450	415	70	1250	3.01
240	Laupa, Siess (1953)	S2	152	305	269	72	1295	4.82
241	Laupa, Siess (1953)	S3	152	305	265	79	1295	4.89
242	Laupa, Siess (1953)	S4	152	305	263	83	1295	4.92
243	Laupa, Siess (1953)	S5	152	305	262	86	1295	4.95
244	Laupa, Siess (1953)	S11	152	305	267	76	1295	4.85
245	Laupa, Siess (1953)	S13	152	305	262	86	1295	4.95
246	Leonhardt (1962)	P8	502	168	148	40	490	3.31
247	Leonhardt (1962)	P9	500	166	146	40	490	3.36
248	Leonhardt (1962)	5l	190	320	270	100	810	3.00
249	Leonhardt (1962)	5r	190	320	270	100	810	3.00
250	Leonhardt (1962)	6l	190	320	270	100	1100	4.07
251	Leonhardt (1962)	6r	190	320	270	100	1100	4.07
252	Leonhardt (1962)	7-1	190	320	278	84	1390	5.00
253	Leonhardt (1962)	7-2	190	320	278	84	1390	5.00
254	Leonhardt (1962)	8-1	190	320	278	84	1668	6.00
255	Leonhardt (1962)	8-2	190	320	274	92	1644	6.00
256	Leonhardt (1962)	D2/1	100	160	140	40	420	3.00
257	Leonhardt (1962)	D2/2	100	160	140	40	420	3.00
258	Leonhardt (1962)	D3/1	150	240	210	60	630	3.00
259	Leonhardt (1962)	D3/2l	150	240	210	60	630	3.00
260	Leonhardt (1962)	D3/2r	150	240	210	60	630	3.00
261	Leonhardt (1962)	D4/1	200	320	280	80	840	3.00
262	Leonhardt (1962)	D4/2l	200	320	280	80	840	3.00
263	Leonhardt (1962)	D4/2r	200	320	280	80	840	3.00
264	Leonhardt (1962)	C1	100	180	150	60	450	3.00
265	Leonhardt (1962)	C2	150	330	300	60	900	3.00
266	Leonhardt (1962)	C3	200	500	450	100	1350	3.00
267	Leonhardt (1962)	C4	225	670	600	140	1800	3.00
268	Leonhardt (1962)	P12	501	162	142	40	350	2.46
269	Leonhardt (1962)	4l	190	320	270	100	670	2.48

No.	Researcher	Specimen ID	b [mm]	h [mm]	d [mm]	h_a [mm]	a [mm]	a/d [-]
270	Leonhardt (1962)	4r	190	320	270	100	670	2.48
271	Leonhardt (1962)	EA1	190	320	270	100	750	2.78
272	Leonhardt (1962)	EA2	190	320	270	100	750	2.78
273	Marti; Pralong; Thürlimann (1977)	PS11	400	180	162	36	640	3.95
274	Mathey, Watstein (1963)	IIIa- 17	203	457	403	109	1524	3.78
275	Mathey, Watstein (1963)	IIIa-18	203	457	403	109	1524	3.78
276	Mathey, Watstein (1963)	Va-19	203	457	403	109	1524	3.78
277	Mathey, Watstein (1963)	Va-20	203	457	403	109	1524	3.78
278	Mathey, Watstein (1963)	VIa-24	203	457	403	109	1524	3.78
279	Mathey, Watstein (1963)	VIa-25	203	457	403	109	1524	3.78
280	Mathey, Watstein (1963)	VIb-21	203	457	403	109	1143	2.84
281	Mathey, Watstein (1963)	VIb-22	203	457	403	109	1143	2.84
282	Mathey, Watstein (1963)	VIb-23	203	457	403	109	1143	2.84
283	Moody K.G. (1954)	A1	178	305	262	86	775	2.96
284	Moody K.G. (1954)	A2	178	305	267	76	775	2.90
285	Moody K.G. (1954)	A3	178	305	268	74	775	2.89
286	Moody K.G. (1954)	A4	178	305	270	70	775	2.87
287	Moody K.G. (1954)	B1	178	305	267	76	775	2.90
288	Moody K.G. (1954)	B2	178	305	268	74	775	2.89
289	Moody K.G. (1954)	B3	178	305	270	70	775	2.87
290	Moody K.G. (1954)	B4	178	305	272	67	775	2.85
291	Moody K.G. (1954)	1	152	305	268	73	914	3.41
292	Moody K.G. (1954)	2	152	305	268	73	914	3.41
293	Moody K.G. (1954)	3	152	305	268	73	914	3.41
294	Moody K.G. (1954)	4	152	305	268	73	914	3.41
295	Moody K.G. (1954)	5	152	305	268	73	914	3.41
296	Moody K.G. (1954)	6	152	305	268	73	914	3.41
297	Moody K.G. (1954)	7	152	305	268	73	914	3.41
298	Moody K.G. (1954)	9	152	305	268	73	914	3.41
299	Moody K.G. (1954)	10	152	305	268	73	914	3.41
300	Moody K.G. (1954)	11	152	305	268	73	914	3.41
301	Moody K.G. (1954)	12	152	305	268	73	914	3.41
302	Moody K.G. (1954)	14	152	305	268	73	914	3.41
303	Moody K.G. (1954)	15	152	305	268	73	914	3.41
304	Moody K.G. (1954)	16	152	305	268	73	914	3.41

No.	Researcher	Specimen ID	b [mm]	h [mm]	d [mm]	h_a [mm]	a [mm]	a/d [-]
305	Morrow, Viest (1957)	B56 B2	305	406	368	76	1511	4.10
306	Morrow, Viest (1957)	B56 A4	305	406	375	64	1511	4.03
307	Morrow, Viest (1957)	B56 B4	305	406	368	76	1511	4.10
308	Morrow, Viest (1957)	B56 E4	305	406	368	76	1511	4.10
309	Morrow, Viest (1957)	B56 A6	308	406	356	102	1511	4.25
310	Morrow, Viest (1957)	B56 B6	305	406	372	70	1511	4.07
311	Morrow, Viest (1957)	B70 B2	305	406	365	82	1867	5.11
312	Morrow, Viest (1957)	B70 A4	305	406	368	76	1867	5.07
313	Morrow, Viest (1957)	B70 A6	305	406	356	102	1867	5.25
314	Morrow, Viest (1957)	B84 B4	305	406	363	86	2222	6.11
315	Morrow, Viest (1957)	B40 B4	305	406	368	76	1105	3.00
316	Mphonde, Frantz (1984)	AO-3-3b	152	337	298	76	1041	3.49
317	Mphonde, Frantz (1984)	AO-3-3c	152	337	298	76	1041	3.49
318	Mphonde, Frantz (1984)	AO-7-3a	152	337	298	76	1041	3.49
319	Mphonde, Frantz (1984)	AO-7-3b	152	337	298	76	1041	3.49
320	Mphonde, Frantz (1984)	AO-11-3a	152	337	298	76	1041	3.49
321	Mphonde, Frantz (1984)	AO-11-3b	152	337	298	76	1041	3.49
322	Mphonde, Frantz (1984)	AO-15-3a	152	337	298	76	1041	3.49
323	Mphonde, Frantz (1984)	AO-15-3b	152	337	298	76	1041	3.49
324	Mphonde, Frantz (1984)	AO-15-3c	152	337	298	76	1041	3.49
325	Mphonde, Frantz (1984)	AO-3-2	152	337	298	76	721	2.41
326	Mphonde, Frantz (1984)	AO-7-2	152	337	298	76	721	2.41
327	Mphonde, Frantz (1984)	AO-11-2	152	337	298	76	721	2.41
328	Mphonde, Frantz (1984)	AO-15-2a	152	337	298	76	721	2.41

No.	Researcher	Specimen ID	b [mm]	h [mm]	d [mm]	h_a [mm]	a [mm]	a/d [-]
329	Mphonde, Frantz (1984)	AO-15-2b	152	337	298	76	721	2.41
330	Podgorniak-Stanik B.A. (1998)	BRL100	300	1000	925	150	2663	2.88
331	Podgorniak-Stanik B.A. (1998)	BN100	300	1000	925	150	2663	2.88
332	Podgorniak-Stanik B.A. (1998)	BH100	300	1000	925	150	2663	2.88
333	Podgorniak-Stanik B.A. (1998)	BN50	300	500	450	100	1313	2.92
334	Podgorniak-Stanik B.A. (1998)	BH50	300	500	450	100	1313	2.92
335	Podgorniak-Stanik B.A. (1998)	BN25	300	250	225	50	664	2.95
336	Podgorniak-Stanik B.A. (1998)	BN12.5	300	125	110	30	326	2.96
337	Rajagopalan; Ferguson (1968)	S-13	152	311	265	92	1118	4.22
338	Rajagopalan; Ferguson (1968)	S-1	154	311	259	105	1016	3.93
339	Rajagopalan; Ferguson (1968)	S-2	154	311	265	92	1016	3.83
340	Rajagopalan; Ferguson (1968)	S-3	152	311	267	89	1118	4.19
341	Rajagopalan; Ferguson (1968)	S-4	152	311	268	86	1118	4.17
342	Rajagopalan; Ferguson (1968)	S-5	152	311	262	99	1118	4.27
343	Rajagopalan; Ferguson (1968)	S-9	152	311	262	99	1118	4.27
344	Rajagopalan; Ferguson (1968)	S-6	151	311	267	87	1118	4.18
345	Rajagopalan; Ferguson (1968)	S-7	152	311	268	86	1118	4.17
346	Rajagopalan; Ferguson (1968)	S-12	153	311	268	85	1118	4.16
347	Reineck; Koch; Schlaich (1978)	N8	500	250	226	48	791	3.50
348	Reineck; Koch; Schlaich (1978)	N6	500	250	226	48	565	2.50
349	Reineck; Koch; Schlaich (1978)	N7	500	250	225	50	563	2.50
350	Remmel (1991)	s1_1	150	200	165	70	660	4.00
351	Remmel (1991)	s1_2	150	200	165	70	505	3.06
352	Remmel (1991)	s1_4	150	200	160	80	640	4.00
353	Remmel (1991)	s1_5	150	200	160	80	490	3.06

No.	Researcher	Specimen ID	b [mm]	h [mm]	d [mm]	h_a [mm]	a [mm]	a/d [-]
354	Ruesch, Haugli (1962)	X	90	134	111	46	400	3.60
355	Ruesch, Haugli (1962)	Y	120	229	199	60	717	3.60
356	Ruesch, Haugli (1962)	Z	180	302	262	80	947	3.62
357	Scholz (1994)	A-2	200	400	372	56	1116	3.00
358	Scholz (1994)	D-2	200	400	362	76	1086	3.00
359	Scholz (1994)	D-3	200	400	362	76	1448	4.00
360	Taylor (1968)	1A	203	406	370	73	1118	3.02
361	Taylor (1968)	2A	203	406	370	73	1118	3.02
362	Taylor (1968)	1B	203	406	370	73	1118	3.02
363	Taylor (1968)	2B	203	406	370	73	1118	3.02
364	Taylor (1968)	3B	203	406	370	73	1118	3.02
365	Taylor (1968)	5A	203	406	370	73	914	2.47
366	Taylor (1968)	5B	203	406	370	73	914	2.47
367	Taylor (1972)	B1	200	500	465	70	1395	3.00
368	Taylor (1972)	B2	200	500	465	70	1395	3.00
369	Taylor (1972)	B3	200	500	465	70	1395	3.00
370	Taylor (1972)	A1	400	1000	930	140	2790	3.00
371	Taylor (1972)	A2	400	1000	930	140	2790	3.00
372	Thorenfeldt, Drangshold (1990)	B11	150	250	221	58	663	3.00
373	Thorenfeldt, Drangshold (1990)	B13	150	250	207	86	828	4.00
374	Thorenfeldt, Drangshold (1990)	B14	150	250	207	86	621	3.00
375	Thorenfeldt, Drangshold (1990)	B21	150	250	221	58	663	3.00
376	Thorenfeldt, Drangshold (1990)	B23	150	250	207	86	828	4.00
377	Thorenfeldt, Drangshold (1990)	B24	150	250	207	86	621	3.00
378	Thorenfeldt, Drangshold (1990)	B33	150	250	207	86	828	4.00
379	Thorenfeldt, Drangshold (1990)	B34	150	250	207	86	621	3.00
380	Thorenfeldt, Drangshold (1990)	B43	150	250	207	86	828	4.00
381	Thorenfeldt, Drangshold (1990)	B44	150	250	207	86	621	3.00
382	Thorenfeldt, Drangshold (1990)	B51	150	250	221	58	663	3.00
383	Thorenfeldt, Drangshold (1990)	B53	150	250	207	86	828	4.00

No.	Researcher	Specimen ID	b [mm]	h [mm]	d [mm]	h_s [mm]	a [mm]	a/d [-]
384	Thorenfeldt, Drangshold (1990)	B54	150	250	207	86	621	3.00
385	Thorenfeldt, Drangshold (1990)	B61	300	500	442	116	1326	3.00
386	Thorenfeldt, Drangshold (1990)	B63	300	500	414	172	1656	4.00
387	Thorenfeldt, Drangshold (1990)	B64	300	500	414	172	1242	3.00
388	Walraven (1978)	A2	200	450	420	60	1260	3.00
389	Walraven (1978)	A3	200	750	720	60	2160	3.00
390	Xie, Ahmad, Yu (1994)	NNN-3	127	254	216	76	648	3.00
391	Xie, Ahmad, Yu (1994)	NHN-3	127	254	216	76	648	3.00
392	Yoon, Y.S.; Cook, W.D.; Mitchell, D. (1996)	NI-S	375	750	655	190	2113	3.23
393	Yoon, Y.S.; Cook, W.D.; Mitchell, D. (1996)	M1-S	375	750	655	190	2113	3.23
394	Yoon, Y.S.; Cook, W.D.; Mitchell, D. (1996)	H1-S	375	750	655	190	2113	3.23
395	Yoshida Y., Bentz E., Collins M. (2000)	YB2000/0	300	2000	1890	220	5405	2.86

No.	Researcher	Specimen ID	f'_c [MPa]	Longitudinal reinforcement ρ_s [%]	ε_s at d [-]	f_{sy} [MPa]	kd [mm]	s_{cr} [mm]	Δw [mm]
1	Adebar P., Collins M.P. (1996)	ST1	50	1.6	0.0005	536	109	169	0.2
2	Adebar P., Collins M.P. (1996)	ST2	50	1.6	0.0004	536	109	169	0.2
3	Adebar P., Collins M.P. (1996)	ST3	47	1.9	0.0004	536	118	160	0.2
4	Adebar P., Collins M.P. (1996)	ST8	44	1.9	0.0003	536	118	160	0.2
5	Adebar P., Collins M.P. (1996)	ST16	49	3.0	0.0003	536	88	90	0.1
6	Adebar P., Collins M.P. (1996)	ST23	56	1.0	0.0006	536	91	187	0.3
7	Ahmad, Kahloo (1986)	A1	59	3.9	0.0003	414	109	94	0.1
8	Ahmad, Kahloo (1986)	A2	59	3.9	0.0004	414	109	94	0.1
9	Ahmad, Kahloo (1986)	A3	59	3.9	0.0004	414	109	94	0.1
10	Ahmad, Kahloo (1986)	A8	59	1.8	0.0006	414	85	123	0.2
11	Ahmad, Kahloo (1986)	B1	65	5.0	0.0002	414	117	85	0.1
12	Ahmad, Kahloo (1986)	B2	65	5.0	0.0003	414	117	85	0.1
13	Ahmad, Kahloo (1986)	B3	65	5.0	0.0005	414	117	85	0.1
14	Ahmad, Kahloo (1986)	B7	65	2.2	0.0004	414	93	115	0.2
15	Ahmad, Kahloo (1986)	B8	65	2.2	0.0005	414	93	115	0.2
16	Ahmad, Kahloo (1986)	B9	65	2.2	0.0008	414	93	115	0.3
17	Ahmad, Kahloo (1986)	C1	63	6.6	0.0002	414	116	68	0.1
18	Ahmad, Kahloo (1986)	C2	63	6.6	0.0003	414	116	68	0.1
19	Ahmad, Kahloo (1986)	C3	63	6.6	0.0003	414	116	68	0.1
20	Ahmad, Kahloo (1986)	C7	63	3.3	0.0003	414	105	102	0.1

No.	Researcher	Specimen ID	f'_c [MPa]	Longitudinal reinforcement ρ_s [%]	ε_s at d [-]	f_{sy} [MPa]	kd [mm]	s_{cr} [mm]	Δw [mm]
21	Ahmad, Kahloo (1986)	C8	63	3.3	0.0003	414	105	102	0.1
22	Ahmad, Kahloo (1986)	C9	63	3.3	0.0003	414	105	102	0.1
23	Al-Alusi A.F. (1957)	7	24	2.6	0.0003	366	60	67	0.1
24	Al-Alusi A.F. (1957)	10	27	2.6	0.0003	366	60	67	0.1
25	Al-Alusi A.F. (1957)	11	27	2.6	0.0004	366	60	67	0.1
26	Al-Alusi A.F. (1957)	18	26	2.6	0.0003	366	60	67	0.1
27	Angelakos D., Bentz E. C. , Collins M. P. ()	DB120	20	1.0	0.0004	550	304	621	0.6
28	Angelakos D., Bentz E. C. , Collins M. P. ()	DB130	30	1.0	0.0004	550	304	621	0.6
29	Angelakos D., Bentz E. C. , Collins M. P. ()	DB140	36	1.0	0.0004	550	304	621	0.6
30	Angelakos D., Bentz E. C. , Collins M. P. ()	DB165	62	1.0	0.0004	550	304	621	0.6
31	Angelakos D., Bentz E. C. , Collins M. P. ()	DB180	76	1.0	0.0003	550	304	621	0.6
32	Angelakos D., Bentz E. C. , Collins M. P. ()	DB230	30	2.1	0.0003	550	389	506	0.4
33	Angelakos D., Bentz E. C. , Collins M. P. (2000)	DBO530	30	0.5	0.0006	550	228	697	1.0
34	Aster; Koch (1974)	2	26	0.6	0.0007	554	68	182	0.4
35	Aster; Koch (1974)	3	26	0.9	0.0005	535	79	171	0.3
36	Aster; Koch (1974)	8	30	0.6	0.0005	536	135	365	0.5
37	Aster; Koch (1974)	9	19	0.6	0.0004	536	135	365	0.4
38	Aster; Koch (1974)	10	19	0.6	0.0004	536	135	365	0.4
39	Aster; Koch (1974)	11	23	0.5	0.0006	535	118	382	0.6

No.	Researcher	Specimen ID	f'_c [MPa]	Longitudinal reinforcement ρ_s [%]	ε_s at d [-]	f_{sy} [MPa]	kd [mm]	s_{cr} [mm]	Δw [mm]
40	Aster; Koch (1974)	12	26	0.7	0.0005	535	138	362	0.5
41	Aster; Koch (1974)	16	29	0.4	0.0007	536	171	579	1.0
42	Aster; Koch (1974)	17	27	0.4	0.0006	536	171	579	0.9
43	Bhal (1968)	B1	22	1.3	0.0004	434	108	192	0.2
44	Bhal (1968)	B2	28	1.3	0.0004	434	215	385	0.4
45	Bhal (1968)	B3	26	1.3	0.0003	434	323	577	0.5
46	Bhal (1968)	B4	24	1.3	0.0003	434	431	769	0.6
47	Bhal (1968)	B5	25	0.6	0.0006	434	162	438	0.7
48	Bhal (1968)	B6	23	0.6	0.0007	430	162	438	0.8
49	Bhal (1968)	B7	26	0.6	0.0005	434	244	656	0.9
50	Bhal (1968)	B8	26	0.6	0.0005	430	244	656	0.8
51	Bresler, Scordelis (1963)	0A-1	21	1.8	0.0004	555	190	271	0.3
52	Bresler, Scordelis (1963)	0A-2	23	2.3	0.0003	555	209	257	0.2
53	Bresler, Scordelis (1963)	0A-3	36	2.7	0.0003	552	220	241	0.2
54	Cederwall K., Hedman O., Losberg A. (1974)	734-34	28	1.1	0.0007	818	79	155	0.3
55	Chana (1981)	37623	37	1.7	0.0004	478	145	211	0.3
56	Chana (1981)	37654	31	1.7	0.0004	478	145	211	0.2
57	Chana (1981)	37682	34	1.7	0.0005	478	145	211	0.3
58	Collins, Kuchma (1999)	B100	34	1.0	0.0005	550	304	621	0.7
59	Collins, Kuchma (1999)	B100H	93	1.0	0.0004	550	304	621	0.6
60	Collins, Kuchma (1999)	B100B	37	1.0	0.0004	550	304	621	0.6
61	Collins, Kuchma (1999)	B100L	37	1.0	0.0004	483	304	621	0.7
62	Collins, Kuchma (1999)	B100-R	34	1.0	0.0005	550	304	621	0.8
63	Collins, Kuchma (1999)	B100L-R	37	1.0	0.0005	483	304	621	0.7
64	Diaz de Cossio, Siess (1960)	A2	30	1.0	0.0006	469	83	171	0.3
65	Diaz de Cossio, Siess (1960)	A3	18	1.0	0.0005	452	83	171	0.2

No.	Researcher	Specimen ID	f'_c [MPa]	Longitudinal reinforcement ρ_s [%]	ε_s at d [-]	f_{sy} [MPa]	kd [mm]	s_{cr} [mm]	Δw [mm]
66	Diaz de Cossio, Siess (1960)	A-12	25	3.3	0.0003	314	130	124	0.1
67	Diaz de Cossio, Siess (1960)	A-13	21	3.3	0.0002	393	130	124	0.1
68	Diaz de Cossio, Siess (1960)	A-14	26	3.3	0.0003	364	130	124	0.1
69	Elzanaty, Nilson, Slate (1986)	F1	62	1.2	0.0006	434	95	175	0.3
70	Elzanaty, Nilson, Slate (1986)	F2	62	2.4	0.0003	434	123	145	0.2
71	Elzanaty, Nilson, Slate (1986)	F10	62	3.2	0.0003	434	134	132	0.1
72	Elzanaty, Nilson, Slate (1986)	F9	75	1.6	0.0005	434	106	162	0.2
73	Elzanaty, Nilson, Slate (1986)	F15	75	2.4	0.0003	434	123	145	0.2
74	Elzanaty, Nilson, Slate (1986)	F6	60	2.4	0.0003	434	123	145	0.1
75	Elzanaty, Nilson, Slate (1986)	F11	20	1.2	0.0004	434	95	175	0.2
76	Elzanaty, Nilson, Slate (1986)	F12	20	2.4	0.0003	434	123	145	0.1
77	Elzanaty, Nilson, Slate (1986)	F8	38	0.9	0.0006	434	87	186	0.3
78	Elzanaty, Nilson, Slate (1986)	F13	38	1.2	0.0005	434	95	175	0.2
79	Elzanaty, Nilson, Slate (1986)	F14	38	2.4	0.0003	434	123	145	0.2
80	Feldman, Siess (1955)	L-2A	35	3.4	0.0004	283	129	123	0.2
81	Feldman, Siess (1955)	L-3	27	3.4	0.0002	310	129	123	0.1
82	Feldman, Siess (1955)	L-4	25	3.4	0.0002	303	129	123	0.1
83	Feldman, Siess (1955)	L-5	27	3.4	0.0002	331	129	123	0.1

No.	Researcher	Specimen ID	f'_c [MPa]	Longitudinal reinforcement ρ_s [%]	ε_s at d [-]	f_{sy} [MPa]	kd [mm]	s_{cr} [mm]	Δw [mm]
84	Ferguson P.M. (1956)	F2	28	2.1	0.0003	310	82	107	0.1
85	Ferguson P.M., Thompson N.J. (1953)	A1	28	4.8	0.0002	276	120	90	0.1
86	Ferguson P.M., Thompson N.J. (1953)	A2	26	4.8	0.0002	276	120	90	0.1
87	Ferguson P.M., Thompson N.J. (1953)	A3	33	4.8	0.0002	276	120	90	0.1
88	Ferguson P.M., Thompson N.J. (1953)	A4	33	4.8	0.0002	276	120	90	0.1
89	Ferguson P.M., Thompson N.J. (1953)	A5	43	4.8	0.0002	276	120	90	0.1
90	Ferguson P.M., Thompson N.J. (1953)	A6	37	4.8	0.0002	276	120	90	0.1
91	Ferguson P.M., Thompson N.J. (1953)	D1	30	2.7	0.0003	276	100	110	0.1
92	Ferguson P.M., Thompson N.J. (1953)	D2	28	2.7	0.0003	276	100	110	0.1
93	Ferguson P.M., Thompson N.J. (1953)	N1	20	3.0	0.0002	276	87	90	0.1
94	Ferguson P.M., Thompson N.J. (1953)	N2	20	3.0	0.0003	276	87	90	0.1
95	Ferguson P.M., Thompson N.J. (1953)	N3	17	3.0	0.0002	276	87	90	0.1
96	Ferguson P.M., Thompson N.J. (1953)	B1	34	4.8	0.0002	276	120	90	0.1
97	Ferguson P.M., Thompson N.J. (1953)	B2	32	4.8	0.0002	276	120	90	0.1
98	Ferguson P.M., Thompson N.J. (1953)	B3	38	4.8	0.0002	276	120	90	0.1
99	Ferguson P.M., Thompson N.J. (1953)	B4	41	4.8	0.0003	276	120	90	0.1

No.	Researcher	Specimen ID	f'_c [MPa]	Longitudinal reinforcement ρ_s [%]	ε_s at d [-]	f_{sy} [MPa]	kd [mm]	s_{cr} [mm]	Δw [mm]
100	Ferguson P.M., Thompson N.J. (1953)	B5	39	4.8	0.0002	276	120	90	0.1
101	Ferguson P.M., Thompson N.J. (1953)	C1	32	4.8	0.0003	276	120	90	0.1
102	Ferguson P.M., Thompson N.J. (1953)	C2	32	4.8	0.0002	276	120	90	0.1
103	Ferguson P.M., Thompson N.J. (1953)	L1	21	3.3	0.0003	276	81	78	0.1
104	Ferguson P.M., Thompson N.J. (1953)	L3	21	3.3	0.0003	276	81	78	0.1
105	Grimm, R. (1997)	s1.1	86	1.3	0.0006	660	56	97	0.2
106	Grimm, R. (1997)	s1.2	87	2.2	0.0004	517	67	85	0.1
107	Grimm, R. (1997)	s1.3	89	4.2	0.0003	487	80	66	0.1
108	Grimm, R. (1997)	s2.2	87	1.9	0.0006	469	145	203	0.3
109	Grimm, R. (1997)	s2.3	89	0.9	0.0007	469	111	237	0.4
110	Grimm, R. (1997)	s2.4	89	3.8	0.0004	487	174	154	0.2
111	Grimm, R. (1997)	s3.2	89	1.7	0.0004	487	290	428	0.5
112	Grimm, R. (1997)	s3.3	90	0.8	0.0006	487	226	520	0.8
113	Grimm, R. (1997)	s3.4	89	3.6	0.0003	487	360	330	0.3
114	Grimm, R. (1997)	s4.1	105	1.3	0.0007	660	56	97	0.2
115	Grimm, R. (1997)	s4.2	105	2.2	0.0005	517	67	85	0.1
116	Grimm, R. (1997)	s4.3	105	4.2	0.0004	487	80	66	0.1
117	Hallgren (1994)	B90SB13-2-86	82	2.2	0.0007	630	85	107	0.2
118	Hallgren (1994)	B90SB14-2-86	82	2.2	0.0007	630	86	108	0.2
119	Hallgren (1994)	B90SB22-2-85	80	2.2	0.0007	630	86	107	0.2
120	Hallgren (1994)	B91SC2-2-62	59	2.2	0.0006	443	87	109	0.2

No.	Researcher	Specimen ID	f'_c [MPa]	Longitudinal reinforcement ρ_s [%]	ε_s at d [-]	f_{sy} [MPa]	kd [mm]	s_{cr} [mm]	Δw [mm]
121	Hallgren (1994)	B91SC4-2-69	66	2.2	0.0006	443	87	108	0.2
122	Hallgren (1994)	B90SB17-2-45	43	2.3	0.0005	630	85	106	0.2
123	Hallgren (1994)	B90SB18-2-45	43	2.3	0.0005	630	87	107	0.2
124	Hallgren (1994)	B90SB21-2-85	80	2.3	0.0006	630	87	107	0.2
125	Hallgren (1994)	B91SC1-2-62	59	2.3	0.0006	443	86	107	0.2
126	Hallgren (1994)	B91SD1-4-61	58	4.0	0.0004	494	105	89	0.1
127	Hallgren (1994)	B91SD2-4-61	58	4.0	0.0005	494	105	90	0.1
128	Hallgren (1994)	B91SD3-4-66	62	4.0	0.0004	494	105	90	0.1
129	Hallgren (1994)	B91SD4-4-66	62	4.0	0.0004	494	106	89	0.1
130	Hallgren (1994)	B91SD5-4-58	55	3.9	0.0004	494	106	90	0.1
131	Hallgren (1994)	B91SD6-4-58	55	4.1	0.0004	494	107	89	0.1
132	Hallgren (1994)	B90SB5-2-33	31	2.3	0.0005	651	86	105	0.2
133	Hallgren (1994)	B90SB6-2-33	31	2.2	0.0005	651	86	108	0.2
134	Hallgren (1994)	B90SB9-2-31	30	2.3	0.0004	651	86	106	0.1
135	Hallgren (1994)	B90SB10-2-31	30	2.2	0.0005	651	85	108	0.2
136	Hallgren (1996)	B3	88	0.7	0.0010	632	60	148	0.4
137	Hallgren (1996)	B5	87	1.1	0.0009	604	71	140	0.4
138	Hallgren (1996)	B7	81	0.6	0.0012	630	54	154	0.5
139	Hamadi; Regan (1980)	G1	29	1.7	0.0004	400	149	221	0.3
140	Hamadi; Regan (1980)	G2	22	1.1	0.0006	460	126	246	0.4
141	Hamadi; Regan (1980)	G4	21	1.1	0.0004	800	126	246	0.3
142	Hanson J.A. (1958)	8A-X	24	2.5	0.0005	333	123	143	0.2
143	Hanson J.A. (1958)	8A	26	2.5	0.0003	333	123	143	0.2
144	Hanson J.A. (1958)	8B	35	2.5	0.0005	333	123	143	0.2
145	Hanson J.A. (1958)	8C	55	5.0	0.0004	333	155	112	0.1

No.	Researcher	Specimen ID	f'_c [MPa]	Longitudinal reinforcement ρ_s [%]	ε_s at d [-]	f_{sy} [MPa]	kd [mm]	s_{cr} [mm]	Δw [mm]
146	Hanson J.A. (1958)	8D	70	5.0	0.0005	333	155	112	0.2
147	Hanson (1961)	8A4	20	1.2	0.0004	611	95	171	0.2
148	Hanson (1961)	8B4	29	1.2	0.0005	611	95	171	0.2
149	Hanson (1961)	8BW4	28	1.2	0.0004	611	95	171	0.2
150	Hanson (1961)	8B2	29	2.5	0.0003	637	124	143	0.1
151	Hanson (1961)	8B3	29	1.2	0.0005	334	95	171	0.3
152	Islam M.S., Pam H.J., Kwan A.K.H. (1998)	M100-S0	79	3.2	0.0004	532	103	100	0.1
153	Islam M.S., Pam H.J., Kwan A.K.H. (1998)	M100-S1	79	3.2	0.0007	532	103	100	0.2
154	Islam M.S., Pam H.J., Kwan A.K.H. (1998)	M100-S3	79	3.2	0.0006	532	103	100	0.2
155	Islam M.S., Pam H.J., Kwan A.K.H. (1998)	M100-S4	79	3.2	0.0005	532	103	100	0.2
156	Islam M.S., Pam H.J., Kwan A.K.H. (1998)	M80-S0	69	3.2	0.0004	532	103	100	0.1
157	Islam M.S., Pam H.J., Kwan A.K.H. (1998)	M80-S1	69	3.2	0.0007	532	103	100	0.2
158	Islam M.S., Pam H.J., Kwan A.K.H. (1998)	M80-S3	69	3.2	0.0007	532	103	100	0.2
159	Islam M.S., Pam H.J., Kwan A.K.H. (1998)	M80-S4	69	3.2	0.0004	532	103	100	0.1
160	Islam M.S., Pam H.J., Kwan A.K.H. (1998)	M60-S0	48	2.0	0.0004	554	89	118	0.2
161	Islam M.S., Pam H.J., Kwan A.K.H. (1998)	M60-S1	48	2.0	0.0009	554	89	118	0.3
162	Islam M.S., Pam H.J., Kwan A.K.H. (1998)	M60-S3	48	2.0	0.0008	554	89	118	0.3
163	Islam M.S., Pam H.J., Kwan A.K.H. (1998)	M60-S4	48	2.0	0.0005	554	89	118	0.2
164	Islam M.S., Pam H.J., Kwan A.K.H. (1998)	M40-S0	33	3.2	0.0003	320	103	102	0.1

No.	Researcher	Specimen ID	f'_c [MPa]	Longitudinal reinforcement ρ_s [%]	ε_s at d [-]	f_{sy} [MPa]	kd [mm]	s_{cr} [mm]	Δw [mm]
165	Islam M.S., Pam H.J., Kwan A.K.H. (1998)	M40-S1	33	3.2	0.0005	320	103	102	0.2
166	Islam M.S., Pam H.J., Kwan A.K.H. (1998)	M40-S3	33	3.2	0.0005	320	103	102	0.2
167	Islam M.S., Pam H.J., Kwan A.K.H. (1998)	M25-S0	25	2.0	0.0004	350	89	118	0.2
168	Islam M.S., Pam H.J., Kwan A.K.H. (1998)	M25-S3	25	2.0	0.0005	350	89	118	0.2
169	Kani (1967)	3044	28	2.7	0.0002	376	524	574	0.3
170	Kani (1967)	3045	27	2.7	0.0002	381	520	573	0.3
171	Kani (1967)	3046	25	2.7	0.0002	360	522	575	0.3
172	Kani (1967)	3047	25	2.7	0.0002	376	520	575	0.3
173	Kani (1967)	63	25	2.8	0.0002	352	261	282	0.2
174	Kani (1967)	64	24	2.8	0.0002	352	259	282	0.2
175	Kani (1967)	66	25	2.7	0.0002	352	259	282	0.2
176	Kani (1967)	79	25	2.7	0.0002	381	265	291	0.2
177	Kani (1967)	1	26	2.8	0.0003	367	254	270	0.2
178	Kani (1967)	71	26	2.7	0.0003	373	258	286	0.2
179	Kani (1967)	272	26	2.7	0.0003	377	129	141	0.1
180	Kani (1967)	273	26	2.7	0.0003	377	129	142	0.1
181	Kani (1967)	274	26	2.7	0.0003	377	129	141	0.2
182	Kani (1967)	52	24	2.7	0.0003	392	66	73	0.1
183	Kani (1967)	48	24	2.8	0.0003	392	64	69	0.1
184	Kani (1967)	81	26	2.8	0.0003	343	132	143	0.1
185	Kani (1967)	84	26	2.8	0.0003	342	131	140	0.1
186	Kani (1967)	96	24	2.8	0.0003	335	132	143	0.1
187	Kani (1967)	83	26	2.7	0.0003	343	130	141	0.2
188	Kani (1967)	97	26	2.7	0.0003	366	131	145	0.2
189	Kani (1967)	3043	26	2.7	0.0002	376	521	572	0.3
190	Kani (1967)	56	26	2.7	0.0003	403	65	72	0.1
191	Kani (1967)	58	26	2.7	0.0003	417	66	73	0.1
192	Kani (1967)	60	25	2.6	0.0004	392	66	73	0.1
193	Kani (1967)	91	26	2.7	0.0003	364	128	141	0.1
194	Kani (1967)	92	26	2.7	0.0002	369	129	141	0.1
195	Kani (1967)	41	26	2.6	0.0005	381	66	75	0.1
196	Kani (1967)	59	25	2.6	0.0005	392	66	74	0.1
197	Kani (1967)	65	26	2.8	0.0003	374	267	286	0.2
198	Kani (1967)	95	24	2.8	0.0004	338	132	143	0.2
199	Kani (1967)	98	25	2.7	0.0004	366	130	144	0.2

No.	Researcher	Specimen ID	f'_c [MPa]	Longitudinal reinforcement ρ_s [%]	ε_s at d [-]	f_{sy} [MPa]	kd [mm]	s_{cr} [mm]	Δw [mm]
200	Kani (1967)	99	25	2.7	0.0004	366	130	142	0.2
201	Kani (1967)	3042	25	2.7	0.0003	375	521	574	0.5
202	Krefeld, Thurston (1966)	11A2	29	3.4	0.0003	401	162	152	0.1
203	Krefeld, Thurston (1966)	12A2	29	4.5	0.0002	401	134	104	0.1
204	Krefeld, Thurston (1966)	18A2	18	2.7	0.0003	478	150	166	0.2
205	Krefeld, Thurston (1966)	18B2	19	2.7	0.0003	478	150	166	0.2
206	Krefeld, Thurston (1966)	18C2	21	2.7	0.0003	478	150	166	0.2
207	Krefeld, Thurston (1966)	18D2	21	2.7	0.0003	478	150	166	0.2
208	Krefeld, Thurston (1966)	16A2	21	1.8	0.0004	478	98	142	0.2
209	Krefeld, Thurston (1966)	17A2	21	2.1	0.0003	408	106	137	0.2
210	Krefeld, Thurston (1966)	3AC	20	2.0	0.0003	386	109	146	0.2
211	Krefeld, Thurston (1966)	3CC	19	2.0	0.0003	386	109	146	0.1
212	Krefeld, Thurston (1966)	3AAC	33	2.0	0.0004	386	109	146	0.2
213	Krefeld, Thurston (1966)	4AAC	28	2.6	0.0003	401	120	134	0.2
214	Krefeld, Thurston (1966)	5AAC	31	3.4	0.0003	378	129	123	0.1
215	Krefeld, Thurston (1966)	6AAC	33	4.3	0.0002	368	139	112	0.1
216	Krefeld, Thurston (1966)	3AC	30	2.0	0.0004	386	109	146	0.2
217	Krefeld, Thurston (1966)	4AC	29	2.6	0.0003	401	120	134	0.1
218	Krefeld, Thurston (1966)	5AC	31	3.4	0.0003	378	129	123	0.1
219	Krefeld, Thurston (1966)	6AC	32	4.3	0.0002	368	139	112	0.1
220	Krefeld, Thurston (1966)	4CC	36	2.6	0.0003	401	120	134	0.1
221	Krefeld, Thurston (1966)	5CC	36	3.4	0.0003	378	129	123	0.1
222	Krefeld, Thurston (1966)	6CC	36	4.3	0.0002	368	139	112	0.1
223	Krefeld, Thurston (1966)	C	16	1.6	0.0003	401	188	295	0.3

No.	Researcher	Specimen ID	f'_c [MPa]	Longitudinal reinforcement ρ_s [%]	ε_s at d [-]	f_{sy} [MPa]	kd [mm]	s_{cr} [mm]	Δw [mm]
224	Krefeld, Thurston (1966)	OCA	34	2.6	0.0003	369	120	134	0.1
225	Krefeld, Thurston (1966)	OCB	37	2.6	0.0003	368	120	134	0.1
226	Krefeld, Thurston (1966)	OCA	36	2.2	0.0003	367	203	253	0.2
227	Krefeld, Thurston (1966)	OCB	36	2.2	0.0003	366	203	253	0.2
228	Krefeld, Thurston (1966)	15A2	19	1.3	0.0004	386	116	200	0.2
229	Krefeld, Thurston (1966)	15B2	20	1.3	0.0005	386	116	200	0.3
230	Kulkarni S.M., Shah S.P. (1998)	B4JL20-S	39	1.4	0.0005	518	57	95	0.2
231	Kulkarni S.M., Shah S.P. (1998)	B3NO15-S	40	1.4	0.0006	518	57	95	0.2
232	Kulkarni S.M., Shah S.P. (1998)	B3NO30-S	41	1.4	0.0006	518	57	95	0.2
233	Küng (1985)	C	19	0.6	0.0009	504	52	148	0.4
234	Küng (1985)	D	18	0.8	0.0007	497	60	140	0.3
235	Küng (1985)	E	18	1.1	0.0008	492	68	132	0.3
236	Küng (1985)	F	18	1.8	0.0006	507	83	117	0.2
237	Küng (1985)	E-1	19	1.1	0.0007	492	68	132	0.3
238	Lambotte H., Taerwe L.R. (1990)	NS-0.97	35	1.0	0.0009	545	134	281	0.6
239	Lambotte H., Taerwe L.R. (1990)	NS-1.45	32	1.5	0.0009	545	158	257	0.6
240	Laupa, Siess (1953)	S2	26	2.1	0.0003	284	117	152	0.1
241	Laupa, Siess (1953)	S3	31	2.5	0.0003	410	123	142	0.1
242	Laupa, Siess (1953)	S4	29	3.2	0.0003	309	133	130	0.1
243	Laupa, Siess (1953)	S5	28	4.1	0.0002	315	143	119	0.1
244	Laupa, Siess (1953)	S11	14	1.9	0.0003	328	112	155	0.1
245	Laupa, Siess (1953)	S13	25	4.1	0.0002	304	143	119	0.1
246	Leonhardt (1962)	P8	24	0.9	0.0007	427	47	101	0.2

No.	Researcher	Specimen ID	f'_c [MPa]	Longitudinal reinforcement ρ_s [%]	ε_s at d [-]	f_{sy} [MPa]	kd [mm]	s_{cr} [mm]	Δw [mm]
247	Leonhardt (1962)	P9	24	1.9	0.0005	427	61	85	0.1
248	Leonhardt (1962)	5l	27	2.1	0.0003	465	117	153	0.2
249	Leonhardt (1962)	5r	27	2.1	0.0004	465	117	153	0.2
250	Leonhardt (1962)	6l	27	2.1	0.0003	465	117	153	0.2
251	Leonhardt (1962)	6r	27	2.1	0.0004	465	117	153	0.2
252	Leonhardt (1962)	7-1	29	2.0	0.0003	465	119	159	0.2
253	Leonhardt (1962)	7-2	29	2.0	0.0004	465	119	159	0.2
254	Leonhardt (1962)	8-1	29	2.0	0.0004	465	119	159	0.2
255	Leonhardt (1962)	8-2	29	2.0	0.0004	465	118	156	0.2
256	Leonhardt (1962)	D2/1	30	1.6	0.0005	427	55	85	0.2
257	Leonhardt (1962)	D2/2	30	1.6	0.0006	427	55	85	0.2
258	Leonhardt (1962)	D3/1	32	1.6	0.0005	413	83	127	0.2
259	Leonhardt (1962)	D3/2l	32	1.6	0.0005	413	83	127	0.2
260	Leonhardt (1962)	D3/2r	32	1.6	0.0005	413	83	127	0.2
261	Leonhardt (1962)	D4/1	33	1.7	0.0005	439	112	168	0.2
262	Leonhardt (1962)	D4/2l	33	1.7	0.0004	439	112	168	0.2
263	Leonhardt (1962)	D4/2r	33	1.7	0.0004	439	112	168	0.2
264	Leonhardt (1962)	C1	36	1.3	0.0006	425	55	95	0.2
265	Leonhardt (1962)	C2	36	1.3	0.0006	425	110	190	0.3
266	Leonhardt (1962)	C3	36	1.3	0.0005	425	166	284	0.4
267	Leonhardt (1962)	C4	36	1.3	0.0005	425	221	379	0.5
268	Leonhardt (1962)	P12	12	1.0	0.0008	427	46	96	0.2
269	Leonhardt (1962)	4l	27	2.1	0.0004	465	117	153	0.2

No.	Researcher	Specimen ID	f'_c [MPa]	Longitudinal reinforcement ρ_s [%]	ε_s at d [-]	f_{sy} [MPa]	kd [mm]	s_{cr} [mm]	Δw [mm]
270	Leonhardt (1962)	4r	27	2.1	0.0005	465	117	153	0.2
271	Leonhardt (1962)	EA1	19	1.8	0.0004	439	112	158	0.2
272	Leonhardt (1962)	EA2	19	1.8	0.0005	490	111	159	0.2
273	Marti; Pralong; Thürlimann (1977)	PS11	28	1.4	0.0006	542	60	102	0.2
274	Mathey, Watstein (1963)	IIIa- 17	28	2.5	0.0003	505	188	215	0.2
275	Mathey, Watstein (1963)	IIIa-18	24	2.5	0.0002	505	188	215	0.2
276	Mathey, Watstein (1963)	Va-19	22	0.9	0.0005	690	128	274	0.3
277	Mathey, Watstein (1963)	Va-20	24	0.9	0.0005	690	128	274	0.4
278	Mathey, Watstein (1963)	VIa-24	25	0.5	0.0008	696	96	307	0.6
279	Mathey, Watstein (1963)	VIa-25	25	0.5	0.0007	696	96	307	0.6
280	Mathey, Watstein (1963)	VIb-21	25	0.8	0.0006	707	123	280	0.4
281	Mathey, Watstein (1963)	VIb-22	25	0.8	0.0005	707	123	280	0.4
282	Mathey, Watstein (1963)	VIb-23	29	0.8	0.0006	707	123	280	0.4
283	Moody K.G. (1954)	A1	29	2.2	0.0003	310	115	146	0.2
284	Moody K.G. (1954)	A2	29	2.1	0.0004	310	117	150	0.2
285	Moody K.G. (1954)	A3	29	2.2	0.0004	310	119	149	0.2
286	Moody K.G. (1954)	A4	30	2.4	0.0004	310	123	147	0.2
287	Moody K.G. (1954)	B1	20	1.6	0.0004	310	105	162	0.2
288	Moody K.G. (1954)	B2	21	1.6	0.0004	310	106	162	0.2
289	Moody K.G. (1954)	B3	18	1.6	0.0004	310	106	164	0.2
290	Moody K.G. (1954)	B4	16	1.6	0.0004	310	108	164	0.2
291	Moody K.G. (1954)	1	35	1.9	0.0004	310	113	156	0.2
292	Moody K.G. (1954)	2	16	1.9	0.0003	310	113	156	0.1

No.	Researcher	Specimen ID	f'_c [MPa]	Longitudinal reinforcement ρ_s [%]	ε_s at d [-]	f_{sy} [MPa]	kd [mm]	s_{cr} [mm]	Δw [mm]
293	Moody K.G. (1954)	3	25	1.9	0.0004	310	113	156	0.2
294	Moody K.G. (1954)	4	15	1.9	0.0003	310	113	156	0.2
295	Moody K.G. (1954)	5	29	1.9	0.0004	310	113	156	0.2
296	Moody K.G. (1954)	6	15	1.9	0.0003	310	113	156	0.1
297	Moody K.G. (1954)	7	29	1.9	0.0004	310	113	156	0.2
298	Moody K.G. (1954)	9	39	1.9	0.0004	310	113	156	0.2
299	Moody K.G. (1954)	10	23	1.9	0.0004	310	113	156	0.2
300	Moody K.G. (1954)	11	36	1.9	0.0005	310	113	156	0.2
301	Moody K.G. (1954)	12	19	1.9	0.0004	310	113	156	0.2
302	Moody K.G. (1954)	14	21	1.9	0.0003	310	113	156	0.2
303	Moody K.G. (1954)	15	36	1.9	0.0004	310	113	156	0.2
304	Moody K.G. (1954)	16	16	1.9	0.0003	310	113	156	0.1
305	Morrow, Viest (1957)	B56 B2	14	1.9	0.0003	471	153	215	0.2
306	Morrow, Viest (1957)	B56 A4	24	2.4	0.0003	330	171	203	0.2
307	Morrow, Viest (1957)	B56 B4	26	1.9	0.0003	441	153	215	0.2
308	Morrow, Viest (1957)	B56 E4	27	1.2	0.0004	429	131	237	0.3
309	Morrow, Viest (1957)	B56 A6	38	3.8	0.0003	439	189	166	0.1
310	Morrow, Viest (1957)	B56 B6	43	1.8	0.0004	466	154	218	0.2
311	Morrow, Viest (1957)	B70 B2	16	1.9	0.0002	462	152	213	0.2
312	Morrow, Viest (1957)	B70 A4	26	2.5	0.0003	436	170	199	0.2
313	Morrow, Viest (1957)	B70 A6	43	3.8	0.0003	435	190	166	0.1
314	Morrow, Viest (1957)	B84 B4	26	1.9	0.0003	465	152	212	0.2
315	Morrow, Viest (1957)	B40 B4	33	1.9	0.0004	378	153	215	0.3

No.	Researcher	Specimen ID	f'_c [MPa]	Longitudinal reinforcement ρ_s [%]	ε_s at d [-]	f_{sy} [MPa]	kd [mm]	s_{cr} [mm]	Δw [mm]
316	Mphonde, Frantz (1984)	AO-3-3b	20	3.3	0.0003	414	153	146	0.1
317	Mphonde, Frantz (1984)	AO-3-3c	26	2.3	0.0004	414	135	164	0.2
318	Mphonde, Frantz (1984)	AO-7-3a	37	3.3	0.0003	414	153	146	0.2
319	Mphonde, Frantz (1984)	AO-7-3b	41	3.3	0.0003	414	153	146	0.2
320	Mphonde, Frantz (1984)	AO-11-3a	73	3.3	0.0004	414	153	146	0.2
321	Mphonde, Frantz (1984)	AO-11-3b	73	3.3	0.0004	414	153	146	0.2
322	Mphonde, Frantz (1984)	AO-15-3a	79	3.3	0.0004	414	153	146	0.2
323	Mphonde, Frantz (1984)	AO-15-3b	91	3.3	0.0004	414	153	146	0.2
324	Mphonde, Frantz (1984)	AO-15-3c	89	3.3	0.0004	414	153	146	0.2
325	Mphonde, Frantz (1984)	AO-3-2	20	3.3	0.0003	414	153	146	0.1
326	Mphonde, Frantz (1984)	AO-7-2	44	3.3	0.0005	414	153	146	0.2
327	Mphonde, Frantz (1984)	AO-11-2	77	3.3	0.0004	414	153	146	0.2
328	Mphonde, Frantz (1984)	AO-15-2a	82	3.3	0.0007	414	153	146	0.3
329	Mphonde, Frantz (1984)	AO-15-2b	68	3.3	0.0008	414	153	146	0.3
330	Podgorniak-Stanik B.A. (1998)	BRL100	89	0.5	0.0006	550	228	697	1.0
331	Podgorniak-Stanik B.A. (1998)	BN100	35	0.8	0.0005	550	271	654	0.8
332	Podgorniak-Stanik B.A. (1998)	BH100	94	0.8	0.0005	550	271	654	0.8
333	Podgorniak-Stanik B.A. (1998)	BN50	35	0.8	0.0007	486	136	314	0.5
334	Podgorniak-Stanik B.A. (1998)	BH50	94	0.8	0.0007	486	136	314	0.5
335	Podgorniak-Stanik B.A. (1998)	BN25	35	0.9	0.0007	437	70	155	0.3

No.	Researcher	Specimen ID	f'_c [MPa]	Longitudinal reinforcement ρ_s [%]	ε_s at d [-]	f_{sy} [MPa]	kd [mm]	s_{cr} [mm]	Δw [mm]
336	Podgorniak-Stanik B.A. (1998)	BN12.5	35	0.9	0.0007	458	35	75	0.2
337	Rajagopalan; Ferguson (1968)	S-13	23	1.7	0.0003	655	107	157	0.2
338	Rajagopalan; Ferguson (1968)	S-1	35	1.4	0.0004	655	97	161	0.2
339	Rajagopalan; Ferguson (1968)	S-2	31	1.0	0.0005	655	86	179	0.3
340	Rajagopalan; Ferguson (1968)	S-3	28	0.8	0.0005	524	80	186	0.3
341	Rajagopalan; Ferguson (1968)	S-4	31	0.6	0.0006	524	73	195	0.3
342	Rajagopalan; Ferguson (1968)	S-5	27	0.5	0.0009	1779	66	196	0.4
343	Rajagopalan; Ferguson (1968)	S-9	24	0.5	0.0006	1779	66	196	0.3
344	Rajagopalan; Ferguson (1968)	S-6	29	0.3	0.0010	1779	56	211	0.6
345	Rajagopalan; Ferguson (1968)	S-7	27	0.3	0.0015	1779	49	219	0.9
346	Rajagopalan; Ferguson (1968)	S-12	28	0.3	0.0013	1779	49	220	0.7
347	Reineck; Koch; Schlaich (1978)	N8	24	0.8	0.0006	501	67	159	0.3
348	Reineck; Koch; Schlaich (1978)	N6	24	0.8	0.0007	501	67	159	0.3
349	Reineck; Koch; Schlaich (1978)	N7	23	1.4	0.0005	441	84	141	0.2
350	Remmel (1991)	s1_1	81	1.9	0.0006	523	69	96	0.2
351	Remmel (1991)	s1_2	81	1.9	0.0006	523	69	96	0.2
352	Remmel (1991)	s1_4	80	4.1	0.0004	474	87	73	0.1
353	Remmel (1991)	s1_5	80	4.1	0.0004	474	87	73	0.1
354	Ruesch, Haugli (1962)	X	22	2.7	0.0003	481	52	59	0.1
355	Ruesch, Haugli (1962)	Y	22	2.7	0.0003	407	94	105	0.1

No.	Researcher	Specimen ID	f'_c [MPa]	Longitudinal reinforcement ρ_s [%]	ε_s at d [-]	f_{sy} [MPa]	kd [mm]	s_{cr} [mm]	Δw [mm]
356	Ruesch, Haugli (1962)	Z	23	2.6	0.0003	412	124	138	0.1
357	Scholz (1994)	A-2	77	0.8	0.0008	500	112	260	0.5
358	Scholz (1994)	D-2	92	1.9	0.0005	500	153	209	0.3
359	Scholz (1994)	D-3	92	1.9	0.0005	500	153	209	0.3
360	Taylor (1968)	1A	27	1.0	0.0004	350	123	247	0.3
361	Taylor (1968)	2A	32	1.5	0.0005	350	144	226	0.3
362	Taylor (1968)	1B	27	1.0	0.0005	350	123	247	0.4
363	Taylor (1968)	2B	32	1.5	0.0005	350	144	226	0.3
364	Taylor (1968)	3B	30	1.0	0.0006	350	123	247	0.4
365	Taylor (1968)	5A	28	1.0	0.0006	350	123	247	0.4
366	Taylor (1968)	5B	28	1.0	0.0006	350	123	247	0.4
367	Taylor (1972)	B1	26	1.4	0.0005	420	172	293	0.4
368	Taylor (1972)	B2	21	1.4	0.0004	420	172	293	0.3
369	Taylor (1972)	B3	27	1.4	0.0004	420	172	293	0.3
370	Taylor (1972)	A1	27	1.4	0.0004	420	343	587	0.6
371	Taylor (1972)	A2	22	1.4	0.0004	420	343	587	0.6
372	Thorenfeldt, Drangshold (1990)	B11	51	1.8	0.0006	500	91	130	0.2
373	Thorenfeldt, Drangshold (1990)	B13	51	3.2	0.0004	500	105	102	0.1
374	Thorenfeldt, Drangshold (1990)	B14	51	3.2	0.0005	500	105	102	0.2
375	Thorenfeldt, Drangshold (1990)	B21	74	1.8	0.0007	500	91	130	0.2
376	Thorenfeldt, Drangshold (1990)	B23	74	3.2	0.0005	500	105	102	0.2
377	Thorenfeldt, Drangshold (1990)	B24	74	3.2	0.0005	500	105	102	0.2
378	Thorenfeldt, Drangshold (1990)	B33	55	3.2	0.0004	500	105	102	0.1
379	Thorenfeldt, Drangshold (1990)	B34	55	3.2	0.0005	500	105	102	0.2
380	Thorenfeldt, Drangshold (1990)	B43	82	3.2	0.0005	500	105	102	0.2

No.	Researcher	Specimen ID	f'_c [MPa]	Longitudinal reinforcement ρ_s [%]	ε_s at d [-]	f_{sy} [MPa]	kd [mm]	s_{cr} [mm]	Δw [mm]
381	Thorenfeldt, Drangshold (1990)	B44	82	3.2	0.0006	500	105	102	0.2
382	Thorenfeldt, Drangshold (1990)	B51	93	1.8	0.0005	500	91	130	0.2
383	Thorenfeldt, Drangshold (1990)	B53	93	3.2	0.0005	500	105	102	0.2
384	Thorenfeldt, Drangshold (1990)	B54	93	3.2	0.0005	500	105	102	0.2
385	Thorenfeldt, Drangshold (1990)	B61	74	1.8	0.0004	500	183	259	0.3
386	Thorenfeldt, Drangshold (1990)	B63	74	3.2	0.0003	500	209	205	0.2
387	Thorenfeldt, Drangshold (1990)	B64	74	3.2	0.0004	500	209	205	0.2
388	Walraven (1978)	A2	23	0.7	0.0006	440	122	298	0.5
389	Walraven (1978)	A3	23	0.8	0.0005	440	215	505	0.6
390	Xie, Ahmad, Yu (1994)	NNN-3	37	2.1	0.0004	421	94	122	0.2
391	Xie, Ahmad, Yu (1994)	NHN-3	96	2.1	0.0005	421	94	122	0.2
392	Yoon, Y.S.; Cook, W.D.; Mitchell, D. (1996)	NI-S	34	2.8	0.0002	400	317	338	0.2
393	Yoon, Y.S.; Cook, W.D.; Mitchell, D. (1996)	M1-S	64	2.8	0.0003	400	317	338	0.2
394	Yoon, Y.S.; Cook, W.D.; Mitchell, D. (1996)	H1-S	83	2.8	0.0003	400	317	338	0.3
395	Yoshida Y., Bentz E., Collins M. (2000)	YB2000/0	32	0.7	0.0003	455	548	1342	1.0

No.	Researcher	Specimen ID	V_{mes} [kN]	V_{mes}/V_{cal} Proposed model [-]	V_{mes}/V_{cal} Watanabe [-]	V_{mes}/V_{cal} Reineck [-]
1	Adebar P., Collins M.P. (1996)	ST1	128	1.14	0.65	1.08
2	Adebar P., Collins M.P. (1996)	ST2	119	1.06	0.60	1.01
3	Adebar P., Collins M.P. (1996)	ST3	108	1.22	0.71	1.16
4	Adebar P., Collins M.P. (1996)	ST8	81	0.94	0.55	0.90
5	Adebar P., Collins M.P. (1996)	ST16	75	1.09	1.08	1.21
6	Adebar P., Collins M.P. (1996)	ST23	90	0.97	0.52	0.93
7	Ahmad, Kahloo (1986)	A1	58	1.42	1.24	1.62
8	Ahmad, Kahloo (1986)	A2	69	1.32	1.12	1.90
9	Ahmad, Kahloo (1986)	A3	69	1.11	1.01	1.89
10	Ahmad, Kahloo (1986)	A8	49	1.07	0.79	1.38
11	Ahmad, Kahloo (1986)	B1	51	1.19	1.03	1.34
12	Ahmad, Kahloo (1986)	B2	69	1.22	1.05	1.79
13	Ahmad, Kahloo (1986)	B3	100	1.49	1.38	2.58
14	Ahmad, Kahloo (1986)	B7	44	1.10	0.89	1.19
15	Ahmad, Kahloo (1986)	B8	47	0.91	0.71	1.22
16	Ahmad, Kahloo (1986)	B9	80	1.34	1.10	2.07
17	Ahmad, Kahloo (1986)	C1	54	1.29	1.12	1.58
18	Ahmad, Kahloo (1986)	C2	76	1.29	1.18	2.18
19	Ahmad, Kahloo (1986)	C3	69	0.97	0.98	1.98

No.	Researcher	Specimen ID	V_{mes} [kN]	V_{mes}/V_{cal} **Proposed model** [-]	V_{mes}/V_{cal} **Watanabe** [-]	V_{mes}/V_{cal} **Reineck** [-]
20	Ahmad, Kahloo (1986)	C7	45	1.11	0.93	1.22
21	Ahmad, Kahloo (1986)	C8	44	0.86	0.70	1.17
22	Ahmad, Kahloo (1986)	C9	45	0.75	0.64	1.19
23	Al-Alusi A.F. (1957)	7	14	1.42	1.71	1.81
24	Al-Alusi A.F. (1957)	10	15	1.58	1.53	1.81
25	Al-Alusi A.F. (1957)	11	17	1.98	1.55	2.13
26	Al-Alusi A.F. (1957)	18	14	1.44	1.71	1.80
27	Angelakos D., Bentz E. C. , Collins M. P. ()	DB120	179	1.41	0.63	1.17
28	Angelakos D., Bentz E. C. , Collins M. P. ()	DB130	185	1.14	0.49	0.98
29	Angelakos D., Bentz E. C. , Collins M. P. ()	DB140	180	1.00	0.43	0.88
30	Angelakos D., Bentz E. C. , Collins M. P. ()	DB165	185	0.77	0.31	0.71
31	Angelakos D., Bentz E. C. , Collins M. P. ()	DB180	172	0.64	0.25	0.61
32	Angelakos D., Bentz E. C. , Collins M. P. ()	DB230	257	1.20	0.70	1.22
33	Angelakos D., Bentz E. C. , Collins M. P. (2000)	DBO530	165	1.40	0.44	1.11
34	Aster; Koch (1974)	2	216	1.21	0.86	1.25
35	Aster; Koch (1974)	3	221	1.07	0.84	1.20
36	Aster; Koch (1974)	8	281	0.69	0.77	1.06
37	Aster; Koch (1974)	9	254	0.70	0.94	1.16
38	Aster; Koch (1974)	10	255	0.70	0.94	1.16

No.	Researcher	Specimen ID	V_{mes} [kN]	V_{mes}/V_{cal} Proposed model [-]	V_{mes}/V_{cal} Watanabe [-]	V_{mes}/V_{cal} Reineck [-]
39	Aster; Koch (1974)	I1	261	1.10	0.57	1.01
40	Aster; Koch (1974)	I2	324	1.14	0.66	1.07
41	Aster; Koch (1974)	I6	392	1.85	0.51	1.14
42	Aster; Koch (1974)	I7	349	1.41	0.47	1.03
43	Bhal (1968)	B1	70	1.20	0.85	1.41
44	Bhal (1968)	B2	117	1.29	0.65	1.10
45	Bhal (1968)	B3	162	1.56	0.64	1.13
46	Bhal (1968)	B4	177	1.51	0.56	1.04
47	Bhal (1968)	B5	104	1.52	0.62	1.19
48	Bhal (1968)	B6	112	1.78	0.70	1.32
49	Bhal (1968)	B7	135	1.90	0.54	1.15
50	Bhal (1968)	B8	123	1.58	0.48	1.04
51	Bresler, Scordelis (1963)	0A-1	167	1.40	1.25	1.77
52	Bresler, Scordelis (1963)	0A-2	178	1.33	1.61	1.86
53	Bresler, Scordelis (1963)	0A-3	189	1.02	1.79	1.58
54	Cederwall K., Hedman O., Losberg A. (1974)	734-34	41	1.74	1.15	1.64
55	Chana (1981)	37623	96	1.30	0.84	1.38
56	Chana (1981)	37654	87	1.31	0.85	1.39
57	Chana (1981)	37682	99	1.42	0.92	1.50
58	Collins, Kuchma (1999)	B100	225	1.38	0.55	1.13
59	Collins, Kuchma (1999)	B100H	193	0.67	0.24	0.63
60	Collins, Kuchma (1999)	B100B	204	1.15	0.47	0.98
61	Collins, Kuchma (1999)	B100L	223	1.30	0.52	1.07
62	Collins, Kuchma (1999)	B100-R	249	1.58	0.61	1.25
63	Collins, Kuchma (1999)	B100L-R	235	1.39	0.55	1.13
64	Diaz de Cossio, Siess (1960)	A2	42	1.13	0.74	1.30
65	Diaz de Cossio, Siess (1960)	A3	34	1.19	1.11	1.48

No.	Researcher	Specimen ID	V_{mes} [kN]	V_{mes}/V_{cal} Proposed model [-]	V_{mes}/V_{cal} Watanabe [-]	V_{mes}/V_{cal} Reineck [-]
66	Diaz de Cossio, Siess (1960)	A-12	59	1.47	1.17	1.90
67	Diaz de Cossio, Siess (1960)	A-13	47	1.33	1.39	1.73
68	Diaz de Cossio, Siess (1960)	A-14	55	1.29	1.74	1.78
69	Elzanaty, Nilson, Slate (1986)	F1	57	1.01	0.71	0.98
70	Elzanaty, Nilson, Slate (1986)	F2	66	1.05	0.81	1.02
71	Elzanaty, Nilson, Slate (1986)	F10	75	1.18	0.92	1.14
72	Elzanaty, Nilson, Slate (1986)	F9	62	0.97	0.68	0.91
73	Elzanaty, Nilson, Slate (1986)	F15	66	0.99	0.72	0.92
74	Elzanaty, Nilson, Slate (1986)	F6	60	0.82	1.12	1.01
75	Elzanaty, Nilson, Slate (1986)	F11	44	1.22	1.16	1.45
76	Elzanaty, Nilson, Slate (1986)	F12	53	1.38	1.41	1.69
77	Elzanaty, Nilson, Slate (1986)	F8	45	0.99	0.77	1.04
78	Elzanaty, Nilson, Slate (1986)	F13	48	1.01	0.81	1.07
79	Elzanaty, Nilson, Slate (1986)	F14	63	1.25	1.09	1.33
80	Feldman, Siess (1955)	L-2A	80	1.62	1.29	2.11
81	Feldman, Siess (1955)	L-3	53	1.35	1.36	1.70
82	Feldman, Siess (1955)	L-4	51	1.23	1.71	1.74
83	Feldman, Siess (1955)	L-5	51	1.11	1.94	1.68
84	Ferguson P.M. (1956)	F2	22	1.45	0.98	1.39
85	Ferguson P.M., Thompson N.J. (1953)	A1	29	1.45	1.14	1.57
86	Ferguson P.M., Thompson N.J. (1953)	A2	27	1.40	1.12	1.54

No.	Researcher	Specimen ID	V_{mes} [kN]	V_{mes}/V_{cal} Proposed model [-]	V_{mes}/V_{cal} Watanabe [-]	V_{mes}/V_{cal} Reineck [-]
87	Ferguson P.M., Thompson N.J. (1953)	A3	34	1.54	1.19	1.63
88	Ferguson P.M., Thompson N.J. (1953)	A4	32	1.45	1.12	1.54
89	Ferguson P.M., Thompson N.J. (1953)	A5	34	1.36	1.01	1.39
90	Ferguson P.M., Thompson N.J. (1953)	A6	36	1.55	1.18	1.62
91	Ferguson P.M., Thompson N.J. (1953)	D1	49	1.37	1.06	1.48
92	Ferguson P.M., Thompson N.J. (1953)	D2	52	1.51	1.18	1.64
93	Ferguson P.M., Thompson N.J. (1953)	N1	24	1.62	1.66	1.83
94	Ferguson P.M., Thompson N.J. (1953)	N2	24	1.64	1.68	1.85
95	Ferguson P.M., Thompson N.J. (1953)	N3	21	1.56	1.68	1.84
96	Ferguson P.M., Thompson N.J. (1953)	B1	35	1.61	1.24	1.70
97	Ferguson P.M., Thompson N.J. (1953)	B2	32	1.48	1.15	1.58
98	Ferguson P.M., Thompson N.J. (1953)	B3	39	1.69	1.27	1.76
99	Ferguson P.M., Thompson N.J. (1953)	B4	44	1.80	1.34	1.86
100	Ferguson P.M., Thompson N.J. (1953)	B5	38	1.62	1.22	1.68
101	Ferguson P.M., Thompson N.J. (1953)	C1	50	2.36	1.82	2.51

No.	Researcher	Specimen ID	V_{mes} [kN]	V_{mes}/V_{cal} Proposed model [-]	V_{mes}/V_{cal} Watanabe [-]	V_{mes}/V_{cal} Reineck [-]
102	Ferguson P.M., Thompson N.J. (1953)	C2	39	1.82	1.41	1.94
103	Ferguson P.M., Thompson N.J. (1953)	L1	27	1.67	2.07	2.28
104	Ferguson P.M., Thompson N.J. (1953)	L3	27	1.65	2.04	2.25
105	Grimm, R. (1997)	s1.1	70	0.96	0.59	0.93
106	Grimm, R. (1997)	s1.2	76	0.94	0.64	0.96
107	Grimm, R. (1997)	s1.3	99	1.15	0.84	1.23
108	Grimm, R. (1997)	s2.2	187	1.26	0.74	1.15
109	Grimm, R. (1997)	s2.3	123	0.89	0.48	0.87
110	Grimm, R. (1997)	s2.4	230	1.31	0.94	1.35
111	Grimm, R. (1997)	s3.2	259	1.00	0.52	0.93
112	Grimm, R. (1997)	s3.3	193	1.11	0.37	0.89
113	Grimm, R. (1997)	s3.4	379	1.22	0.79	1.18
114	Grimm, R. (1997)	s4.1	74	0.91	0.54	0.87
115	Grimm, R. (1997)	s4.2	90	1.00	0.66	1.01
116	Grimm, R. (1997)	s4.3	122	1.28	0.94	1.37
117	Hallgren (1994)	B90SB13-2-86	83	1.57	1.10	1.60
118	Hallgren (1994)	B90SB14-2-86	77	1.48	1.04	1.52
119	Hallgren (1994)	B90SB22-2-85	76	1.47	1.05	1.52
120	Hallgren (1994)	B91SC2-2-62	70	1.54	1.18	1.70
121	Hallgren (1994)	B91SC4-2-69	74	1.57	1.17	1.69
122	Hallgren (1994)	B90SB17-2-45	59	1.54	1.28	1.79

No.	Researcher	Specimen ID	V_{mes} [kN]	V_{mes}/V_{cal} Proposed model [-]	V_{mes}/V_{cal} Watanabe [-]	V_{mes}/V_{cal} Reineck [-]
123	Hallgren (1994)	B90SB18-2-45	63	1.65	1.35	1.90
124	Hallgren (1994)	B90SB21-2-85	69	1.36	0.97	1.41
125	Hallgren (1994)	B91SC1-2-62	71	1.60	1.23	1.76
126	Hallgren (1994)	B91SD1-4-61	89	1.72	1.46	2.13
127	Hallgren (1994)	B91SD2-4-61	90	1.74	1.47	2.16
128	Hallgren (1994)	B91SD3-4-66	82	1.51	1.26	1.86
129	Hallgren (1994)	B91SD4-4-66	79	1.47	1.23	1.81
130	Hallgren (1994)	B91SD5-4-58	78	1.52	1.30	1.91
131	Hallgren (1994)	B91SD6-4-58	83	1.67	1.43	2.10
132	Hallgren (1994)	B90SB5-2-33	56	1.73	1.51	2.08
133	Hallgren (1994)	B90SB6-2-33	54	1.63	1.40	1.96
134	Hallgren (1994)	B90SB9-2-31	49	1.54	1.35	1.88
135	Hallgren (1994)	B90SB10-2-31	54	1.67	1.45	2.03
136	Hallgren (1996)	B3	76	0.76	0.43	0.88
137	Hallgren (1996)	B5	104	0.97	0.54	1.05
138	Hallgren (1996)	B7	89	0.80	0.41	0.88
139	Hamadi; Regan (1980)	G1	45	1.68	1.06	1.48
140	Hamadi; Regan (1980)	G2	41	1.95	1.15	1.66
141	Hamadi; Regan (1980)	G4	30	0.90	1.53	1.43
142	Hanson J.A. (1958)	8A-X	80	2.11	1.37	2.55
143	Hanson J.A. (1958)	8A	58	1.42	0.93	1.73
144	Hanson J.A. (1958)	8B	90	1.81	1.20	2.25
145	Hanson J.A. (1958)	8C	127	1.88	1.26	2.32
146	Hanson J.A. (1958)	8D	165	2.15	1.39	2.58
147	Hanson (1961)	8A4	34	0.93	1.28	1.35

No.	Researcher	Specimen ID	V_{mes} [kN]	V_{mes}/V_{cal} Proposed model [-]	V_{mes}/V_{cal} Watanabe [-]	V_{mes}/V_{cal} Reineck [-]
148	Hanson (1961)	8B4	43	1.05	1.25	1.36
149	Hanson (1961)	8BW4	40	0.99	1.20	1.30
150	Hanson (1961)	8B2	52	1.19	1.53	1.54
151	Hanson (1961)	8B3	46	1.08	0.70	1.35
152	Islam M.S., Pam H.J., Kwan A.K.H. (1998)	M100-S0	65	1.25	0.97	1.30
153	Islam M.S., Pam H.J., Kwan A.K.H. (1998)	M100-S1	108	1.59	1.22	2.11
154	Islam M.S., Pam H.J., Kwan A.K.H. (1998)	M100-S3	97	1.43	1.10	1.90
155	Islam M.S., Pam H.J., Kwan A.K.H. (1998)	M100-S4	81	1.56	1.21	1.62
156	Islam M.S., Pam H.J., Kwan A.K.H. (1998)	M80-S0	58	1.17	0.95	1.27
157	Islam M.S., Pam H.J., Kwan A.K.H. (1998)	M80-S1	117	1.85	1.46	2.52
158	Islam M.S., Pam H.J., Kwan A.K.H. (1998)	M80-S3	115	1.81	1.44	2.48
159	Islam M.S., Pam H.J., Kwan A.K.H. (1998)	M80-S4	72	1.47	1.19	1.58
160	Islam M.S., Pam H.J., Kwan A.K.H. (1998)	M60-S0	46	1.11	0.93	1.26
161	Islam M.S., Pam H.J., Kwan A.K.H. (1998)	M60-S1	92	1.85	1.43	2.48
162	Islam M.S., Pam H.J., Kwan A.K.H. (1998)	M60-S3	90	1.81	1.40	2.43
163	Islam M.S., Pam H.J., Kwan A.K.H. (1998)	M60-S4	52	1.27	1.06	1.43
164	Islam M.S., Pam H.J., Kwan A.K.H. (1998)	M40-S0	55	1.57	1.47	1.91
165	Islam M.S., Pam H.J., Kwan A.K.H. (1998)	M40-S1	85	2.08	1.72	2.90

No.	Researcher	Specimen ID	V_{mes} [kN]	V_{mes}/V_{cal} Proposed model [-]	V_{mes}/V_{cal} Watanabe [-]	V_{mes}/V_{cal} Reineck [-]
166	Islam M.S., Pam H.J., Kwan A.K.H. (1998)	M40-S3	81	1.99	1.64	2.76
167	Islam M.S., Pam H.J., Kwan A.K.H. (1998)	M25-S0	48	1.59	1.49	1.96
168	Islam M.S., Pam H.J., Kwan A.K.H. (1998)	M25-S3	57	1.70	1.35	2.29
169	Kani (1967)	3044	159	1.15	0.97	1.33
170	Kani (1967)	3045	152	0.95	1.17	1.38
171	Kani (1967)	3046	154	0.84	1.72	1.59
172	Kani (1967)	3047	147	0.76	1.87	1.60
173	Kani (1967)	63	93	1.30	1.22	1.51
174	Kani (1967)	64	79	0.77	2.05	1.45
175	Kani (1967)	66	91	0.98	1.74	1.55
176	Kani (1967)	79	84	0.85	1.87	1.47
177	Kani (1967)	1	108	1.51	1.09	1.73
178	Kani (1967)	71	102	1.56	0.98	1.56
179	Kani (1967)	272	228	1.33	1.84	1.78
180	Kani (1967)	273	206	1.38	1.33	1.57
181	Kani (1967)	274	250	1.86	1.23	1.88
182	Kani (1967)	52	29	1.63	1.56	1.79
183	Kani (1967)	48	27	1.28	1.90	1.77
184	Kani (1967)	81	51	1.06	1.92	1.58
185	Kani (1967)	84	55	1.50	1.44	1.70
186	Kani (1967)	96	56	1.59	1.50	1.77
187	Kani (1967)	83	65	1.90	1.24	1.90
188	Kani (1967)	97	62	2.02	1.20	1.84
189	Kani (1967)	3043	165	1.34	0.81	1.36
190	Kani (1967)	56	28	1.64	1.25	1.63
191	Kani (1967)	58	29	1.73	1.29	1.68
192	Kani (1967)	60	39	2.52	1.50	2.26
193	Kani (1967)	91	51	1.06	1.94	1.60
194	Kani (1967)	92	46	0.91	2.05	1.48
195	Kani (1967)	41	51	3.62	1.64	2.90
196	Kani (1967)	59	50	3.38	1.76	2.87
197	Kani (1967)	65	112	1.77	0.94	1.73
198	Kani (1967)	95	73	2.25	1.24	2.22
199	Kani (1967)	98	76	2.29	1.27	2.29
200	Kani (1967)	99	77	2.21	1.31	2.35
201	Kani (1967)	3042	237	1.83	0.99	1.91

No.	Researcher	Specimen ID	V_{mes} [kN]	V_{mes}/V_{cal} Proposed model [-]	V_{mes}/V_{cal} Watanabe [-]	V_{mes}/V_{cal} Reineck [-]
202	Krefeld, Thurston (1966)	11A2	73	1.18	0.98	1.77
203	Krefeld, Thurston (1966)	12A2	64	1.47	1.39	2.03
204	Krefeld, Thurston (1966)	18A2	63	1.43	1.12	2.04
205	Krefeld, Thurston (1966)	18B2	72	1.60	1.26	2.28
206	Krefeld, Thurston (1966)	18C2	73	1.48	1.18	2.14
207	Krefeld, Thurston (1966)	18D2	60	1.23	0.98	1.78
208	Krefeld, Thurston (1966)	16A2	42	1.32	1.10	1.66
209	Krefeld, Thurston (1966)	17A2	44	1.34	1.15	1.72
210	Krefeld, Thurston (1966)	3AC	44	1.25	1.53	1.74
211	Krefeld, Thurston (1966)	3CC	36	0.89	1.58	1.45
212	Krefeld, Thurston (1966)	3AAC	56	1.31	1.03	1.56
213	Krefeld, Thurston (1966)	4AAC	58	1.46	1.20	1.79
214	Krefeld, Thurston (1966)	5AAC	57	1.32	1.10	1.62
215	Krefeld, Thurston (1966)	6AAC	60	1.33	1.13	1.66
216	Krefeld, Thurston (1966)	3AC	53	1.29	1.40	1.62
217	Krefeld, Thurston (1966)	4AC	54	1.29	1.46	1.65
218	Krefeld, Thurston (1966)	5AC	54	1.24	1.41	1.58
219	Krefeld, Thurston (1966)	6AC	59	1.31	1.51	1.67
220	Krefeld, Thurston (1966)	4CC	53	1.05	1.54	1.43
221	Krefeld, Thurston (1966)	5CC	57	1.14	1.72	1.56
222	Krefeld, Thurston (1966)	6CC	63	1.23	1.88	1.68
223	Krefeld, Thurston (1966)	C	85	1.61	0.99	1.55
224	Krefeld, Thurston (1966)	OCA	49	0.99	1.49	1.38

No.	Researcher	Specimen ID	V_{mes} [kN]	V_{mes}/V_{cal} Proposed model [-]	V_{mes}/V_{cal} Watanabe [-]	V_{mes}/V_{cal} Reineck [-]
225	Krefeld, Thurston (1966)	OCB	53	1.04	1.52	1.42
226	Krefeld, Thurston (1966)	OCA	147	1.34	1.05	1.38
227	Krefeld, Thurston (1966)	OCB	134	1.21	0.96	1.25
228	Krefeld, Thurston (1966)	15A2	46	1.18	0.85	1.49
229	Krefeld, Thurston (1966)	15B2	52	1.32	0.95	1.67
230	Kulkarni S.M., Shah S.P. (1998)	B4JL20-S	20	1.05	1.23	1.28
231	Kulkarni S.M., Shah S.P. (1998)	B3NO15-S	23	1.31	1.13	1.43
232	Kulkarni S.M., Shah S.P. (1998)	B3NO30-S	24	1.37	1.03	1.47
233	Küng (1985)	C	26	1.40	0.78	1.52
234	Küng (1985)	D	30	1.46	0.93	1.76
235	Küng (1985)	E	43	2.05	1.31	2.45
236	Küng (1985)	F	54	2.52	1.64	3.02
237	Küng (1985)	E-1	40	1.83	1.18	2.21
238	Lambotte H., Taerwe L.R. (1990)	NS-0.97	127	2.44	1.05	1.79
239	Lambotte H., Taerwe L.R. (1990)	NS-1.45	180	3.43	1.58	2.52
240	Laupa, Siess (1953)	S2	42	1.03	1.33	1.37
241	Laupa, Siess (1953)	S3	53	1.19	1.49	1.52
242	Laupa, Siess (1953)	S4	56	1.25	1.62	1.63
243	Laupa, Siess (1953)	S5	50	1.11	1.49	1.47
244	Laupa, Siess (1953)	S11	34	1.02	1.59	1.60
245	Laupa, Siess (1953)	S13	50	1.17	1.62	1.60
246	Leonhardt (1962)	P8	91	1.62	1.15	1.66
247	Leonhardt (1962)	P9	106	1.80	1.37	1.90
248	Leonhardt (1962)	51	60	1.14	0.87	1.42

No.	Researcher	Specimen ID	V_{mes} [kN]	V_{mes}/V_{cal} Proposed model [-]	V_{mes}/V_{cal} Watanabe [-]	V_{mes}/V_{cal} Reineck [-]
249	Leonhardt (1962)	5r	77	1.46	1.10	1.81
250	Leonhardt (1962)	6l	61	1.20	1.17	1.47
251	Leonhardt (1962)	6r	68	1.36	1.32	1.65
252	Leonhardt (1962)	7-1	62	1.11	1.42	1.46
253	Leonhardt (1962)	7-2	68	1.22	1.56	1.60
254	Leonhardt (1962)	8-1	66	1.07	1.79	1.58
255	Leonhardt (1962)	8-2	66	1.08	1.79	1.60
256	Leonhardt (1962)	D2/1	21	1.62	1.10	1.71
257	Leonhardt (1962)	D2/2	23	1.78	1.20	1.88
258	Leonhardt (1962)	D3/1	46	1.53	1.02	1.62
259	Leonhardt (1962)	D3/2l	43	1.41	0.94	1.49
260	Leonhardt (1962)	D3/2r	43	1.41	0.94	1.49
261	Leonhardt (1962)	D4/1	74	1.36	0.90	1.45
262	Leonhardt (1962)	D4/2l	71	1.31	0.86	1.40
263	Leonhardt (1962)	D4/2r	71	1.31	0.86	1.40
264	Leonhardt (1962)	C1	22	1.19	0.87	1.45
265	Leonhardt (1962)	C2	65	1.75	0.95	1.52
266	Leonhardt (1962)	C3	102	1.33	0.74	1.25
267	Leonhardt (1962)	C4	152	1.34	0.73	1.30
268	Leonhardt (1962)	P12	100	2.63	1.57	2.90
269	Leonhardt (1962)	4l	82	1.26	0.98	1.90
270	Leonhardt (1962)	4r	87	1.35	1.05	2.03
271	Leonhardt (1962)	EA1	58	1.32	0.98	1.72

No.	Researcher	Specimen ID	V_{mes} [kN]	V_{mes}/V_{cal} Proposed model [-]	V_{mes}/V_{cal} Watanabe [-]	V_{mes}/V_{cal} Reineck [-]
272	Leonhardt (1962)	EA2	75	1.71	1.26	2.20
273	Marti; Pralong; Thürlimann (1977)	PS11	97	1.74	1.51	1.82
274	Mathey, Watstein (1963)	IIIa- 17	88	1.20	1.03	1.34
275	Mathey, Watstein (1963)	IIIa-18	81	1.17	1.04	1.34
276	Mathey, Watstein (1963)	Va-19	63	1.09	0.85	1.23
277	Mathey, Watstein (1963)	Va-20	66	1.10	0.84	1.22
278	Mathey, Watstein (1963)	VIa-24	54	1.18	0.68	1.17
279	Mathey, Watstein (1963)	VIa-25	50	1.05	0.63	1.08
280	Mathey, Watstein (1963)	VIb-21	71	1.16	0.68	1.25
281	Mathey, Watstein (1963)	VIb-22	62	1.01	0.60	1.10
282	Mathey, Watstein (1963)	VIb-23	75	1.11	0.65	1.20
283	Moody K.G. (1954)	A1	60	1.29	0.93	1.51
284	Moody K.G. (1954)	A2	67	1.50	1.00	1.62
285	Moody K.G. (1954)	A3	76	1.73	1.12	1.83
286	Moody K.G. (1954)	A4	71	1.64	1.04	1.68
287	Moody K.G. (1954)	B1	56	1.63	1.08	1.77
288	Moody K.G. (1954)	B2	60	1.75	1.14	1.85
289	Moody K.G. (1954)	B3	56	1.78	1.13	1.83
290	Moody K.G. (1954)	B4	56	1.97	1.23	1.99
291	Moody K.G. (1954)	1	58	1.48	1.05	1.50
292	Moody K.G. (1954)	2	36	1.33	1.09	1.51
293	Moody K.G. (1954)	3	52	1.59	1.20	1.69

No.	Researcher	Specimen ID	V_{mes} [kN]	V_{mes}/V_{cal} Proposed model [-]	V_{mes}/V_{cal} Watanabe [-]	V_{mes}/V_{cal} Reineck [-]
294	Moody K.G. (1954)	4	40	1.58	1.31	1.81
295	Moody K.G. (1954)	5	52	1.45	1.06	1.51
296	Moody K.G. (1954)	6	34	1.32	1.10	1.52
297	Moody K.G. (1954)	7	51	1.42	1.04	1.48
298	Moody K.G. (1954)	9	53	1.28	0.90	1.29
299	Moody K.G. (1954)	10	49	1.54	1.18	1.66
300	Moody K.G. (1954)	11	60	1.51	1.06	1.52
301	Moody K.G. (1954)	12	47	1.62	1.27	1.78
302	Moody K.G. (1954)	14	43	1.39	1.08	1.52
303	Moody K.G. (1954)	15	51	1.29	0.92	1.31
304	Moody K.G. (1954)	16	38	1.43	1.18	1.63
305	Morrow, Viest (1957)	B56 B2	100	1.33	1.50	1.74
306	Morrow, Viest (1957)	B56 A4	138	1.51	1.43	1.66
307	Morrow, Viest (1957)	B56 B4	122	1.29	1.21	1.46
308	Morrow, Viest (1957)	B56 E4	109	1.21	1.05	1.33
309	Morrow, Viest (1957)	B56 A6	178	1.45	1.40	1.62
310	Morrow, Viest (1957)	B56 B6	137	1.20	0.95	1.19
311	Morrow, Viest (1957)	B70 B2	89	0.94	1.54	1.49
312	Morrow, Viest (1957)	B70 A4	132	1.17	1.61	1.57
313	Morrow, Viest (1957)	B70 A6	178	1.26	1.61	1.55
314	Morrow, Viest (1957)	B84 B4	111	0.91	1.63	1.42
315	Morrow, Viest (1957)	B40 B4	156	1.71	0.97	1.54
316	Mphonde, Frantz (1984)	AO-3-3b	65	1.90	1.56	2.07

No.	Researcher	Specimen ID	V_{mes} [kN]	V_{mes}/V_{cal} Proposed model [-]	V_{mes}/V_{cal} Watanabe [-]	V_{mes}/V_{cal} Reineck [-]
317	Mphonde, Frantz (1984)	AO-3-3c	67	1.78	1.35	1.84
318	Mphonde, Frantz (1984)	AO-7-3a	82	1.82	1.33	1.80
319	Mphonde, Frantz (1984)	AO-7-3b	83	1.75	1.26	1.71
320	Mphonde, Frantz (1984)	AO-11-3a	90	1.46	0.92	1.28
321	Mphonde, Frantz (1984)	AO-11-3b	89	1.46	0.92	1.28
322	Mphonde, Frantz (1984)	AO-15-3a	93	1.48	0.91	1.27
323	Mphonde, Frantz (1984)	AO-15-3b	100	1.50	0.88	1.25
324	Mphonde, Frantz (1984)	AO-15-3c	98	1.48	0.88	1.23
325	Mphonde, Frantz (1984)	AO-3-2	78	2.21	1.33	2.47
326	Mphonde, Frantz (1984)	AO-7-2	118	1.91	1.20	2.25
327	Mphonde, Frantz (1984)	AO-11-2	111	1.31	0.78	1.48
328	Mphonde, Frantz (1984)	AO-15-2a	178	2.07	1.20	2.29
329	Mphonde, Frantz (1984)	AO-15-2b	206	2.61	1.57	2.98
330	Podgorniak-Stanik B.A. (1998)	BRL100	164	0.73	0.21	0.76
331	Podgorniak-Stanik B.A. (1998)	BN100	192	1.25	0.46	1.03
332	Podgorniak-Stanik B.A. (1998)	BH100	193	0.73	0.24	0.71
333	Podgorniak-Stanik B.A. (1998)	BN50	132	1.26	0.63	1.19
334	Podgorniak-Stanik B.A. (1998)	BH50	132	0.74	0.33	0.73
335	Podgorniak-Stanik B.A. (1998)	BN25	73	1.26	0.71	1.18
336	Podgorniak-Stanik B.A. (1998)	BN12.5	40	1.22	0.78	1.25

No.	Researcher	Specimen ID	V_{mes} [kN]	V_{mes}/V_{cal} Proposed model [-]	V_{mes}/V_{cal} Watanabe [-]	V_{mes}/V_{cal} Reineck [-]
337	Rajagopalan; Ferguson (1968)	S-13	40	1.10	1.17	1.41
338	Rajagopalan; Ferguson (1968)	S-1	36	0.83	0.72	0.99
339	Rajagopalan; Ferguson (1968)	S-2	37	0.99	0.79	1.12
340	Rajagopalan; Ferguson (1968)	S-3	31	0.88	0.79	1.06
341	Rajagopalan; Ferguson (1968)	S-4	28	0.79	0.65	0.93
342	Rajagopalan; Ferguson (1968)	S-5	34	1.18	0.89	1.30
343	Rajagopalan; Ferguson (1968)	S-9	24	0.82	0.70	1.00
344	Rajagopalan; Ferguson (1968)	S-6	27	1.11	0.67	1.11
345	Rajagopalan; Ferguson (1968)	S-7	30	2.04	0.76	1.40
346	Rajagopalan; Ferguson (1968)	S-12	25	1.27	0.61	1.13
347	Reineck; Koch; Schlaich (1978)	N8	102	1.29	0.89	1.26
348	Reineck; Koch; Schlaich (1978)	N6	118	1.44	0.75	1.39
349	Reineck; Koch; Schlaich (1978)	N7	140	1.66	0.92	1.66
350	Remmel (1991)	s1_1	46	1.16	0.87	1.16
351	Remmel (1991)	s1_2	48	0.98	0.69	1.17
352	Remmel (1991)	s1_4	58	1.34	1.08	1.41
353	Remmel (1991)	s1_5	60	1.10	0.87	1.46
354	Ruesch, Haugli (1962)	X	15	1.59	1.47	1.99
355	Ruesch, Haugli (1962)	Y	30	1.53	1.33	1.74
356	Ruesch, Haugli (1962)	Z	55	1.37	1.18	1.57
357	Scholz (1994)	A-2	83	1.21	0.46	0.88
358	Scholz (1994)	D-2	121	1.23	0.59	1.00
359	Scholz (1994)	D-3	121	1.26	0.78	1.07
360	Taylor (1968)	1A	62	1.19	0.66	1.08
361	Taylor (1968)	2A	92	1.60	0.89	1.41
362	Taylor (1968)	1B	76	1.50	0.81	1.32
363	Taylor (1968)	2B	101	1.77	0.98	1.55
364	Taylor (1968)	3B	76	1.43	0.76	1.26
365	Taylor (1968)	5A	81	1.40	0.69	1.33

No.	Researcher	Specimen ID	V_{mes} [kN]	V_{mes}/V_{cal} Proposed model [-]	V_{mes}/V_{cal} Watanabe [-]	V_{mes}/V_{cal} Reineck [-]
366	Taylor (1968)	5B	81	1.40	0.69	1.33
367	Taylor (1972)	B1	104	1.94	0.96	1.53
368	Taylor (1972)	B2	87	1.76	0.91	1.44
369	Taylor (1972)	B3	85	1.50	0.75	1.21
370	Taylor (1972)	A1	358	1.82	0.79	1.41
371	Taylor (1972)	A2	328	1.86	0.84	1.47
372	Thorenfeldt, Drangshold (1990)	B11	58	1.46	0.89	1.43
373	Thorenfeldt, Drangshold (1990)	B13	70	1.66	1.43	1.82
374	Thorenfeldt, Drangshold (1990)	B14	83	1.63	1.27	2.10
375	Thorenfeldt, Drangshold (1990)	B21	68	1.44	0.82	1.33
376	Thorenfeldt, Drangshold (1990)	B23	78	1.58	1.24	1.60
377	Thorenfeldt, Drangshold (1990)	B24	83	1.35	1.00	1.66
378	Thorenfeldt, Drangshold (1990)	B33	68	1.55	1.31	1.68
379	Thorenfeldt, Drangshold (1990)	B34	83	1.56	1.21	2.00
380	Thorenfeldt, Drangshold (1990)	B43	86	1.69	1.28	1.66
381	Thorenfeldt, Drangshold (1990)	B44	107	1.69	1.20	2.01
382	Thorenfeldt, Drangshold (1990)	B51	56	1.06	0.58	0.96
383	Thorenfeldt, Drangshold (1990)	B53	77	1.42	1.05	1.37
384	Thorenfeldt, Drangshold (1990)	B54	78	1.14	0.80	1.35

No.	Researcher	Specimen ID	V_{mes} [kN]	V_{mes}/V_{cal} Proposed model [-]	V_{mes}/V_{cal} Watanabe [-]	V_{mes}/V_{cal} Reineck [-]
385	Thorenfeldt, Drangshold (1990)	B61	180	0.97	0.54	0.96
386	Thorenfeldt, Drangshold (1990)	B63	229	1.18	0.91	1.26
387	Thorenfeldt, Drangshold (1990)	B64	281	1.16	0.85	1.47
388	Walraven (1978)	A2	71	1.74	0.77	1.31
389	Walraven (1978)	A3	101	1.94	0.66	1.19
390	Xie, Ahmad, Yu (1994)	NNN-3	37	1.11	0.82	1.34
391	Xie, Ahmad, Yu (1994)	NHN-3	46	0.83	0.54	0.91
392	Yoon, Y.S.; Cook, W.D.; Mitchell, D. (1996)	NI-S	249	1.03	0.72	1.12
393	Yoon, Y.S.; Cook, W.D.; Mitchell, D. (1996)	M1-S	296	0.89	0.56	0.93
394	Yoon, Y.S.; Cook, W.D.; Mitchell, D. (1996)	H1-S	327	0.89	0.52	0.89
395	Yoshida Y., Bentz E., Collins M. (2000)	YB2000/0	255	1.20	0.32	0.94
			mean	1.36 ± 0.33 %	1.08 ± 0.42 %	1.55 ± 0.46 %
			std-dev	0.39	0.37	0.42
			c.v.	28.58 %	34.59 %	27.43 %

(Reineck et al. 2003)

A3. Slender beams with web reinforcement

No.	Researcher	Specimen ID	b [mm]	d [mm]	a/d [-]	f'$_c$ [MPa]	Longitudinal reinforcement ρ_s [%]	Longitudinal reinforcement ε_s at d [-]
1	Scordelis	A-1	307	466	3.92	24	1.8	0.0005
2		A-2	305	464	4.93	24	2.3	0.0004
3		A-3	307	466	6.91	35	2.8	0.0004
4		B-1	231	461	3.95	25	2.4	0.0005
5		B-2	229	466	4.91	23	2.4	0.0005
6		B-3	229	461	6.95	39	3.1	0.0003
7		C-1	156	464	3.95	30	1.8	0.0007
8		C-2	152	464	4.93	24	3.7	0.0004
9		C-3	155	459	6.98	35	3.7	0.0003
10		XB-1	231	458	4	25	2.4	0.0005
11		CA-1	307	459	3.98	27	1.8	0.0004
12		CB-1	229	458	3.98	25	2.5	0.0004
13		CC-1	152	459	3.98	27	1.9	0.0005
14		RA-1	305	458	3.98	25	1.7	0.0005
15		RB-1	229	459	3.98	25	2.2	0.0005
16		RC-1	155	459	3.98	29	1.6	0.0007
17	Leonhard and Walther	E21	190	270	2.78	30	2.5	0.0008
18		E31	190	270	2.78	28	2.5	0.0009
19		E41	190	270	2.78	30	2.5	0.0009
20		E51	190	270	2.78	30	2.5	0.0009
21	Bresler and Scordelis	CRA-1	305	460	3.98	25	1.7	0.0004
22		CRB-1	229	457	4.01	24	2.3	0.0004
23		CRC-1	155	458	4	24	1.7	0.0006
24		1WCRA-1	305	457	4.01	26	1.7	0.0005
25		1WCRB-1	229	459	3.99	23	2.3	0.0005
26		1WCRC-1	152	460	3.98	27	1.7	0.0007
27		1WCA-1	305	462	3.95	25	1.8	0.0005
28		1WCB-1	231	460	3.97	27	2.3	0.0005
29		1WCC-1	155	460	3.97	25	1.8	0.0007
30		2WCA-1	305	461	3.96	26	1.8	0.0006
31		3WCA-1	305	460	3.97	26	1.8	0.0005
32	Bahl	B15	240	300	3	27	1.3	0.0008
33		B25	240	600	3	25	1.3	0.0008
34		B35	240	900	3	26	1.3	0.0008
35		B45	240	1200	3	25	1.3	0.0007
36	Placas and Regan	R8	152	272	3.36	27	1.5	0.0008
37		R9	152	272	3.36	30	1.5	0.0010
38		R10	152	272	3.36	30	1.0	0.0010

No.	Researcher	Specimen ID	b [mm]	d [mm]	a/d [-]	f'_c [MPa]	Longitudinal reinforcement ρ_s [%]	Longitudinal reinforcement ε_s at d [-]
39		R11	152	272	3.36	26	1.0	0.0012
40		R12	152	272	3.6	34	4.2	0.0004
41		R13	152	272	3.6	32	4.2	0.0006
42		R14	152	272	3.36	29	1.5	0.0008
43		R15	152	272	3.6	30	4.2	0.0005
44		R16	152	272	3.6	32	4.2	0.0005
45		R17	152	272	3.36	13	1.5	0.0007
46		R18	152	272	3.36	31	1.5	0.0008
47		R19	152	272	3.36	30	1.5	0.0011
48		R20	152	272	3.36	43	1.5	0.0009
49		R21	152	272	3.6	48	4.2	0.0006
50		R22	152	272	4.5	30	1.5	0.0008
51		R24	152	272	5.05	31	4.2	0.0004
52		R25	152	272	3.6	31	4.2	0.0004
53		R28	152	272	3.6	32	4.2	0.0007
54	Swamy and Andriopoulos	C3	76	95	3	29	2.0	0.0006
55		R3	76	95	3	29	2.0	0.0007
56		J3	76	95	3	29	2.0	0.0008
57		C4	76	95	4	29	2.0	0.0006
58		O3	76	132	3	28	4.0	0.0004
59		Z3	76	132	3	26	4.0	0.0004
60		Y3	76	132	3	26	4.0	0.0004
61		O4	76	132	4	28	4.0	0.0003
62		Z4	76	132	4	26	4.0	0.0004
63		O5	76	132	5	28	4.0	0.0003
64	Mphonde and Frantz	B50-3-3	152	298	3.6	22	3.4	0.0003
65		B50-7-3	152	298	3.6	40	3.4	0.0004
66		B50-11-3	152	298	3.6	60	3.4	0.0004
67		B50-15-3	152	298	3.6	83	3.4	0.0004
68		B100-3-3	152	298	3.6	28	3.4	0.0004
69		B100-7-3	152	298	3.6	47	3.4	0.0005
70		B100-11-3	152	298	3.6	69	3.4	0.0006
71		B100-15-3	152	298	3.6	82	3.4	0.0005
72		B150-3-3	152	298	3.6	29	3.4	0.0005
73		B150-7-3	152	298	3.6	47	3.4	0.0005
74		B150-11-3	152	298	3.6	70	3.4	0.0006
75		B150-15-3	152	298	3.6	83	3.4	0.0006
76	Elzanaty, Nilson, and Slate	G4	178	266	4	63	3.3	0.0006
77		G5	178	266	4	40	2.5	0.0006
78		G6	178	266	4	21	2.5	0.0004
79	Johnson and Ramirez	1	304	538	3.1	36	2.5	0.0005
80		2	304	538	3.1	36	2.5	0.0003

No.	Researcher	Specimen ID	b [mm]	d [mm]	a/d [-]	f'_c [MPa]	Longitudinal reinforcement ρ_s [%]	Longitudinal reinforcement ε_s at d [-]
81	Johnson and Ramirez	3	304	538	3.1	72	2.5	0.0004
82		4	304	538	3.1	72	2.5	0.0005
83		5	304	538	3.1	56	2.5	0.0006
84		7	304	538	3.1	51	2.5	0.0004
85		8	304	538	3.1	51	2.5	0.0004
86	Anderson and Ramirez	W1	406	345	2.65	29	2.3	0.0008
87		W2	406	345	2.65	32	2.3	0.0010
88		W3	406	345	2.65	32	2.3	0.0009
89		W4	406	345	2.65	34	2.3	0.0011
90	Roller and Russel	1	356	559	2.5	120	1.7	0.0005
91		2	356	559	2.5	120	3.0	0.0011
92		6	457	762	3	72	1.7	0.0006
93		7	457	762	3	72	1.9	0.0007
94		8	457	762	3	125	1.9	0.0004
95		9	457	762	3	125	2.4	0.0005
96	Sarzam and Al-Musawi	AL2-N	180	235	4	40	2.2	0.0007
97		AL2-H	180	235	4	75	2.2	0.0008
98		BL2-H	180	235	4	76	2.8	0.0007
99		CL2-H	180	235	4	70	3.5	0.0006
100	Xie et al.	NNW-3	127	203	3	41	3.2	0.0006
101		NHW-3	127	198	3	98	4.5	0.0006
102		NHW-3a	127	198	3	90	4.5	0.0006
103		NHW-3b	127	198	3	103	4.5	0.0007
104	McGormley, Creary, and Ramirez	BUS-1	203	419	3.27	42	3.0	0.0006
105		EUS-1	203	419	3.27	43	3.0	0.0007
106		BUH-1	203	419	3.27	46	3.0	0.0006
107		EUH-1	203	419	3.27	44	3.0	0.0007
108		BUIS-2	203	419	3.27	35	3.0	0.0007
109		EUIS-2	203	419	3.27	48	3.0	0.0007
110		BUIH-2	203	419	3.27	50	3.0	0.0008
111		EUIH-2	203	419	3.27	51	3.0	0.0007
112		BUH-3	203	419	3.27	53	3.0	0.0007
113		EUH-3	203	419	3.27	55	3.0	0.0007
114		BUIS-3	203	419	3.27	57	3.0	0.0006
115		EUIS-3	203	419	3.27	56	3.0	0.0006
116	Yoon, Cook, and Mitchell	N1-N	375	655	3.28	36	2.8	0.0004
117		N2-S	375	655	3.28	36	2.8	0.0003
118		N2-N	375	655	3.28	36	2.8	0.0004
119		M1-N	375	655	3.28	67	2.8	0.0004
120		M2-S	375	655	3.28	67	2.8	0.0005
121		M2-N	375	655	3.28	67	2.8	0.0006
122		H1-N	375	655	3.28	87	2.8	0.0004

No.	Researcher	Specimen ID	b [mm]	d [mm]	a/d [-]	f'$_c$ [MPa]	Longitudinal reinforcement ρ_s [%]	ε_s at d [-]
123		H2-S	375	655	3.28	87	2.8	0.0005
124		H2-N	375	655	3.28	87	2.8	0.0006
125	Kong and Rangan	S1-1	250	292	2.5	60	2.8	0.0007
126		S1-2	250	292	2.5	60	2.8	0.0006
127		S2-3	250	292	2.5	69	2.8	0.0007
128		S2-4	250	292	2.5	69	2.8	0.0006
129		S3-1	250	297	2.49	64	1.7	0.0010
130		S3-2	250	297	2.49	64	1.7	0.0008
131		S3-3	250	293	2.49	64	2.8	0.0007
132		S3-3	250	293	2.49	64	2.8	0.0005
133		S4-3	250	346	2.4	83	2.9	0.0006
134		S4-4	250	292	2.5	83	2.8	0.0008
135		S5-1	250	292	3.01	85	2.8	0.0007
136		S5-2	250	292	2.74	85	2.8	0.0008
137		S5-3	250	292	2.5	85	2.8	0.0007
138		S6-3	250	293	2.73	65	2.8	0.0005
139		S6-4	250	293	2.73	65	2.8	0.0006
140		S7-1	250	294	3.3	71	4.5	0.0004
141		S7-2	250	294	3.3	71	4.5	0.0004
142		S7-3	250	294	3.3	71	4.5	0.0005
143		S7-4	250	294	3.3	71	4.5	0.0005
144		S7-5	250	294	3.3	71	4.5	0.0006
145		S7-6	250	294	3.3	71	4.5	0.0006
146	Zararis and Papadakis	A033	140	235	3.6	22	1.4	0.0005
147		A050	140	235	3.6	24	1.4	0.0006
148		A066	140	235	3.6	23	1.4	0.0007
149		A1	140	235	3.6	23	1.4	0.0008
150		B033	140	235	3.6	22	1.4	0.0005
151		B050	140	235	3.6	24	1.4	0.0006
152		B066	140	235	3.6	21	1.4	0.0006
153		C5	140	235	3.6	22	0.7	0.0014
154		C6	140	235	3.6	21	0.7	0.0012
155	Karayiannis and Chalioris	A24	200	260	2.77	26	1.5	0.0005
156		A36	200	260	2.77	26	1.5	0.0007
157		A48	200	260	2.77	26	1.5	0.0007
158		A72	200	260	2.77	26	1.5	0.0007
159		B30	200	260	3.46	26	2.0	0.0004
160		B45	200	260	3.46	26	2.0	0.0004
161		B60	200	260	3.46	26	2.0	0.0004
162		B90	200	260	3.46	26	2.0	0.0005
163	Angelakos, Bentz,	DB0.530M	300	925	2.92	32	0.5	0.0010
164		DB120M	300	925	2.92	21	1.0	0.0006

No.	Researcher	Specimen ID	b [mm]	d [mm]	a/d [-]	f'_c [MPa]	Longitudinal reinforcement ρ_s [%]	ε_s at d [-]
165	and Collins	DB140	300	925	2.92	38	1.0	0.0006
166		DB165	300	925	2.92	65	1.0	0.0009
167		DB180M	300	925	2.92	80	1.0	0.0008
168		BM100	300	925	2.92	47	0.8	0.0009

No.	Researcher	Specimen ID	Transverse reinf. f_{wy} [MPa]	ρ_w [%]	kd [mm]	s_{cr} [mm]	Δw [mm]
1	Scordelis	A-1	330	0.1	192	274	0.4
2		A-2	328	0.1	208	256	0.3
3		A-3	330	0.1	223	243	0.2
4		B-1	328	0.15	211	250	0.3
5		B-2	325	0.15	214	252	0.3
6		B-3	325	0.15	230	231	0.2
7		C-1	330	0.2	191	273	0.5
8		C-2	327	0.2	244	220	0.2
9		C-3	323	0.2	242	217	0.2
10		XB-1	337	0.15	210	248	0.3
11		CA-1	335	0.1	190	269	0.3
12		CB-1	341	0.15	211	247	0.3
13		CC-1	342	0.2	191	268	0.4
14		RA-1	343	0.1	183	275	0.4
15		RB-1	341	0.15	204	255	0.4
16		RC-1	338	0.2	182	277	0.5
17	Leonhard and Walther	E21	371	0.41	125	145	0.2
18		E31	388	0.42	125	145	0.3
19		E41	261	0.59	125	145	0.3
20		E51	278	0.58	125	145	0.3
21	Bresler and Scordelis	CRA-1	350	0.1	185	275	0.3
22		CRB-1	340	0.15	205	252	0.3
23		CRC-1	345	0.2	183	275	0.4
24		1WCRA-1	350	0.1	185	272	0.4
25		1WCRB-1	340	0.15	205	254	0.3
26		1WCRC-1	350	0.2	185	275	0.5
27		1WCA-1	350	0.1	189	273	0.4
28		1WCB-1	340	0.15	208	252	0.3
29		1WCC-1	345	0.2	187	273	0.5
30		2WCA-1	350	0.1	189	272	0.4
31		3WCA-1	350	0.1	188	272	0.4
32	Bahl	B15	440	0.15	108	192	0.3
33		B25	440	0.15	216	384	0.6
34		B35	440	0.15	323	577	0.9
35		B45	440	0.15	431	769	1.2
36	Placas and Regan	R8	276	0.21	103	169	0.3
37		R9	267	0.43	103	169	0.4
38		R10	276	0.21	88	184	0.5
39		R11	276	0.21	88	184	0.6
40		R12	276	0.21	149	123	0.2
41		R13	267	0.43	149	123	0.2

No.	Researcher	Specimen ID	Transverse reinf.		kd	s_{cr}	Δw
			f_{wy} [MPa]	ρ_w [%]	[mm]	[mm]	[mm]
42	Placas and Regan	R14	271	0.14	103	169	0.4
43		R15	267	0.43	149	123	0.2
44		R16	267	0.43	149	123	0.2
45		R17	276	0.21	103	169	0.3
46		R18	276	0.21	103	169	0.3
47		R19	267	0.43	103	169	0.5
48		R20	276	0.21	103	169	0.4
49		R21	267	0.43	149	123	0.2
50		R22	276	0.21	103	169	0.3
51		R24	276	0.21	149	123	0.1
52		R25	276	0.21	149	123	0.2
53		R28	268	0.84	149	123	0.2
54	Swamy and Andriopoulos	C3	275	0.16	40	55	0.1
55		R3	208	0.38	40	55	0.1
56		J3	253	0.43	40	55	0.1
57		C4	283	0.06	40	55	0.1
58		O3	258	0.12	71	61	0.1
59		Z3	179	0.34	71	61	0.1
60		Y3	222	0.6	71	61	0.1
61		O4	258	0.12	71	61	0.1
62		Z4	179	0.34	71	61	0.1
63		O5	258	0.12	71	61	0.1
64	Mphonde and Frantz	B50-3-3	292	0.12	153	145	0.1
65		B50-7-3	292	0.12	153	145	0.2
66		B50-11-3	292	0.12	153	145	0.2
67		B50-15-3	292	0.12	153	145	0.2
68		B100-3-3	269	0.26	153	145	0.2
69		B100-7-3	269	0.26	153	145	0.2
70		B100-11-3	269	0.26	153	145	0.2
71		B100-15-3	269	0.26	153	145	0.2
72		B150-3-3	271	0.38	153	145	0.2
73		B150-7-3	271	0.38	153	145	0.2
74		B150-11-3	271	0.38	153	145	0.3
75		B150-15-3	271	0.38	153	145	0.2
76	Elzanaty, Nilson, and Slate	G4	382	0.17	135	131	0.2
77		G5	382	0.17	123	143	0.2
78		G6	382	0.17	123	143	0.2
79	Johnson and Ramirez	1	493	0.14	249	289	0.3
80		2	500	0.07	249	289	0.2
81		3	500	0.07	249	289	0.3
82		4	500	0.07	249	289	0.3
83		5	493	0.14	249	289	0.4

No.	Researcher	Specimen ID	Transverse reinf.		kd	s_{cr}	Δw
			f_{wy} [MPa]	ρ_w [%]	[mm]	[mm]	[mm]
84	Johnson and Ramirez	7	500	0.07	249	289	0.3
85		8	500	0.07	249	289	0.3
86	Anderson and Ramirez	W1	549	0.39	155	190	0.3
87		W2	549	0.39	155	190	0.4
88		W3	549	0.39	155	190	0.3
89		W4	549	0.39	155	190	0.4
90	Roller and Russel	1	400	0.07	223	336	0.3
91		2	451	0.43	277	282	0.6
92		6	450	0.08	309	453	0.6
93		7	444	0.16	319	443	0.7
94		8	450	0.08	319	443	0.4
95		9	444	0.16	345	417	0.5
96	Sarzam and Al-Musawi	AL2-N	844	0.09	105	130	0.3
97		AL2-H	844	0.09	105	130	0.3
98		BL2-H	844	0.09	114	121	0.2
99		CL2-H	844	0.09	122	113	0.2
100	Xie et al.	NNW-3	322	0.49	102	101	0.2
101		NHW-3	324	0.51	112	86	0.1
102		NHW-3a	323	0.65	112	86	0.1
103		NHW-3b	324	0.78	112	86	0.1
104	McGormley, Creary, and Ramirez	BUS-1	426	0.34	207	212	0.3
105		EUS-1	426	0.34	207	212	0.4
106		BUH-1	426	0.34	207	212	0.3
107		EUH-1	426	0.34	207	212	0.4
108		BUIS-2	426	0.34	207	212	0.4
109		EUIS-2	426	0.34	207	212	0.4
110		BUIH-2	426	0.34	207	212	0.4
111		EUIH-2	426	0.34	207	212	0.4
112		BUH-3	426	0.34	207	212	0.4
113		EUH-3	426	0.34	207	212	0.4
114		BUIS-3	426	0.34	207	212	0.3
115		EUIS-3	426	0.34	207	212	0.3
116	Yoon, Cook, and Mitchell	N1-N	438	0.08	316	339	0.3
117		N2-S	438	0.08	316	339	0.3
118		N2-N	417	0.12	316	339	0.4
119		M1-N	438	0.08	316	339	0.3
120		M2-S	417	0.12	316	339	0.4
121		M2-N	438	0.16	316	339	0.5
122		H1-N	438	0.08	316	339	0.4
123		H2-S	429	0.14	316	339	0.4
124		H2-N	435	0.23	316	339	0.5

No.	Researcher	Specimen ID	Transverse reinf. f_{wy} [MPa]	ρ_w [%]	kd [mm]	s_{cr} [mm]	Δw [mm]
125	Kong and Rangan	S1-1	556	0.16	141	151	0.2
126		S1-2	556	0.16	141	151	0.2
127		S2-3	556	0.16	141	151	0.2
128		S2-4	556	0.16	141	151	0.2
129		S3-1	640	0.1	119	178	0.3
130		S3-2	640	0.1	119	178	0.3
131		S3-3	640	0.1	141	152	0.2
132		S3-3	640	0.1	141	152	0.2
133		S4-3	556	0.16	168	178	0.2
134		S4-4	556	0.16	141	151	0.2
135		S5-1	556	0.16	141	151	0.2
136		S5-2	556	0.16	141	151	0.2
137		S5-3	556	0.16	141	151	0.2
138		S6-3	640	0.1	141	152	0.2
139		S6-4	640	0.1	141	152	0.2
140		S7-1	600	0.1	165	129	0.2
141		S7-2	554	0.13	165	129	0.1
142		S7-3	556	0.16	165	129	0.2
143		S7-4	560	0.2	165	129	0.2
144		S7-5	577	0.22	165	129	0.2
145		S7-6	573	0.26	165	129	0.2
146	Zararis and Papadakis	A033	267	0.09	87	148	0.2
147		A050	264	0.14	87	148	0.3
148		A066	263	0.19	87	148	0.3
149		A1	270	0.27	87	148	0.3
150		B033	267	0.06	87	148	0.2
151		B050	256	0.09	87	148	0.2
152		B066	258	0.12	87	148	0.2
153		C5	270	0.27	66	169	0.6
154		C6	271	0.17	66	169	0.5
155	Karayiannis and Chalioris	A24	263	0.08	99	161	0.2
156		A36	267	0.12	99	161	0.2
157		A48	269	0.16	99	161	0.2
158		A72	256	0.25	99	161	0.2
159		B30	275	0.04	110	150	0.2
160		B45	243	0.07	110	150	0.2
161		B60	256	0.09	110	150	0.2
162		B90	262	0.13	110	150	0.2
163	Angelakos, Bentz, and Collins	DB0.530M	500	0.08	227	698	1.4
164		DB120M	500	0.08	305	620	0.7
165		DB140	500	0.08	305	620	0.7
166		DB165	500	0.08	305	620	1.1

No.	Researcher	Specimen ID	Transverse reinf.				
			f_{wy} [MPa]	ρ_w [%]	kd [mm]	s_{cr} [mm]	Δw [mm]
167		DB180M	500	0.08	305	620	1.0
168		BM100	500	0.08	271	654	1.2

No.	Researcher	Specimen ID	V_{mes} [kN]	V_{mes}/V_{cal} Proposed model [-]	V_{mes}/V_{cal} Watanabe [-]
1	Scordelis	A-1	233	1.21	1.32
2		A-2	245	1.21	1.59
3		A-3	234	1.01	1.56
4		B-1	223	1.29	1.47
5		B-2	200	1.15	1.48
6		B-3	178	0.89	1.31
7		C-1	156	1.18	1.23
8		C-2	162	1.18	1.54
9		C-3	136	0.91	1.32
10		XB-1	200	1.14	1.32
11		CA-1	165	0.80	0.91
12		CB-1	176	0.99	1.15
13		CC-1	110	0.81	0.89
14		RA-1	200	1.02	1.13
15		RB-1	200	1.15	1.31
16		RC-1	137	1.03	1.08
17	Leonhard and Walther	E21	171	1.24	1.09
18		E31	186	1.32	1.16
19		E41	188	1.35	1.19
20		E51	189	1.33	1.17
21	Bresler and Scordelis	CRA-1	168	0.83	0.94
22		CRB-1	173	0.99	1.15
23		CRC-1	119	0.89	0.98
24		1WCRA-1	215	1.09	1.19
25		1WCRB-1	204	1.18	1.36
26		1WCRC-1	143	1.10	1.16
27		1WCA-1	220	1.11	1.22
28		1WCB-1	202	1.12	1.27
29		1WCC-1	143	1.09	1.17
30		2WCA-1	242	1.23	1.32
31		3WCA-1	208	1.04	1.14
32	Bahl	B15	130	1.08	0.93
33		B25	253	1.17	0.93
34		B35	373	1.24	0.90
35		B45	468	1.21	0.86
36	Placas and Regan	R8	80	1.12	1.11
37		R9	105	1.00	1.00
38		R10	76	1.11	1.00
39		R11	90	1.39	1.24
40		R12	117	1.43	1.59
41		R13	160	1.42	1.60

No.	Researcher	Specimen ID	V_{mes} [kN]	V_{mes}/V_{cal} Proposed model [-]	V_{mes}/V_{cal} Watanabe [-]
42	Placas and Regan	R14	90	1.50	1.40
43		R15	150	1.34	1.53
44		R16	150	1.33	1.50
45		R17	70	1.13	1.26
46		R18	85	1.15	1.10
47		R19	120	1.16	1.14
48		R20	90	1.15	1.03
49		R21	160	1.33	1.41
50		R22	80	1.05	1.21
51		R24	99	1.21	1.61
52		R25	112	1.40	1.57
53		R28	192	1.10	1.25
54	Swamy and Andriopoulos	C3	16	1.37	1.25
55		R3	18	1.25	1.17
56		J3	21	1.20	1.14
57		C4	14	1.39	1.69
58		O3	25	1.74	1.67
59		Z3	28	1.58	1.55
60		Y3	29	1.11	1.11
61		O4	20	1.27	1.58
62		Z4	26	1.31	1.62
63		O5	19	1.18	1.70
64	Mphonde and Frantz	B50-3-3	76	1.14	1.35
65		B50-7-3	94	1.20	1.25
66		B50-11-3	98	1.11	1.06
67		B50-15-3	111	1.16	1.01
68		B100-3-3	95	1.02	1.16
69		B100-7-3	121	1.16	1.20
70		B100-11-3	151	1.35	1.28
71		B100-15-3	116	0.98	0.90
72		B150-3-3	138	1.22	1.37
73		B150-7-3	133	1.08	1.13
74		B150-11-3	162	1.22	1.18
75		B150-15-3	150	1.09	1.02
76	Elzanaty, Nilson, and Slate	G4	149	1.34	1.01
77		G5	111	1.11	1.22
78		G6	78	0.87	1.07
79	Johnson and Ramirez	1	339	1.06	0.96
80		2	222	0.86	0.78
81		3	263	0.82	0.54
82		4	316	1.00	0.54
83		5	383	1.07	0.90

No.	Researcher	Specimen ID	V_{mes} [kN]	V_{mes}/V_{cal} Proposed model [-]	V_{mes}/V_{cal} Watanabe [-]
84	Johnson and Ramirez	7	281	0.98	0.82
85		8	258	0.90	0.75
86	Anderson and Ramirez	W1	460	1.04	0.87
87		W2	549	1.22	1.02
88		W3	505	1.12	0.93
89		W4	585	1.29	1.07
90	Roller and Russel	1	298	0.63	0.38
91		2	1100	1.26	0.96
92		6	666	1.13	0.73
93		7	788	1.07	0.75
94		8	483	0.60	0.39
95		9	750	0.77	0.54
96	Sarzam and Al-Musawi	AL2-N	115	1.20	1.30
97		AL2-H	123	1.14	1.09
98		BL2-H	138	1.26	1.23
99		CL2-H	147	1.35	1.36
100	Xie et al.	NNW-3	87	1.07	1.02
101		NHW-3	102	1.06	0.90
102		NHW-3a	108	1.01	0.89
103		NHW-3b	123	0.99	0.88
104	McGormley, Creary, and Ramirez	BUS-1	272	1.03	1.03
105		EUS-1	298	1.13	1.12
106		BUH-1	276	1.03	1.02
107		EUH-1	307	1.16	1.14
108		BUIS-2	316	1.24	1.26
109		EUIS-2	312	1.16	1.13
110		BUIH-2	334	1.24	1.20
111		EUIH-2	320	1.19	1.14
112		BUH-3	289	1.05	1.01
113		EUH-3	312	1.13	1.08
114		BUIS-3	267	0.96	0.92
115		EUIS-3	267	0.96	0.92
116	Yoon, Cook, and Mitchell	N1-N	457	1.19	1.11
117		N2-S	363	0.93	0.88
118		N2-N	483	1.12	1.06
119		M1-N	405	0.86	0.71
120		M2-S	552	1.09	0.90
121		M2-N	689	1.24	1.03
122		H1-N	483	0.97	0.73
123		H2-S	598	1.05	0.82
124		H2-N	721	1.05	0.85

No.	Researcher	Specimen ID	V_{mes} [kN]	V_{mes}/V_{cal} Proposed model [-]	V_{mes}/V_{cal} Watanabe [-]
125	Kong and Rangan	S1-1	228	1.30	0.96
126		S1-2	208	1.19	0.87
127		S2-3	253	1.38	1.00
128		S2-4	219	1.19	0.86
129		S3-1	209	1.42	0.90
130		S3-2	178	1.21	0.77
131		S3-3	229	1.41	1.01
132		S3-3	175	1.08	0.77
133		S4-3	243	1.00	0.72
134		S4-4	258	1.33	0.93
135		S5-1	242	1.20	0.96
136		S5-2	260	1.31	0.98
137		S5-3	244	1.25	0.87
138		S6-3	178	1.06	0.83
139		S6-4	214	1.28	0.99
140		S7-1	217	1.24	1.11
141		S7-2	205	1.10	1.00
142		S7-3	247	1.22	1.12
143		S7-4	274	1.22	1.15
144		S7-5	304	1.28	1.21
145		S7-6	311	1.20	1.15
146	Zararis and Papadakis	A033	40	0.97	1.07
147		A050	50	1.04	1.12
148		A066	59	1.12	1.21
149		A1	64	0.99	1.08
150		B033	36	0.96	1.05
151		B050	44	1.06	1.13
152		B066	45	1.02	1.14
153		C5	56	0.99	0.95
154		C6	47	1.05	1.01
155	Karayiannis and Chalioris	A24	64	1.14	0.86
156		A36	89	1.44	1.09
157		A48	89	1.30	1.01
158		A72	93	1.15	0.92
159		B30	71	1.19	1.25
160		B45	71	1.11	1.17
161		B60	77	1.12	1.18
162		B90	85	1.11	1.18
163	Angelakos, Bentz, and Collins	DB0.530M	263	1.02	0.52
164		DB120M	282	0.98	0.69
165		DB140	277	0.80	0.51
166		DB165	452	1.24	0.63

No.	Researcher	Specimen ID	V_{mes} [kN]	V_{mes}/V_{cal} Proposed model [-]	V_{mes}/V_{cal} Watanabe [-]
167		DB180M	395	1.02	0.49
168		BM100	342	1.10	0.56
			mean	1.14 ± 0.20 %	1.08 ± 0.56 %
			std-dev	0.17	0.26
			c.v.	14.6 7%	24.36 %

(Chen and MacGregor 1993; Krefeld and Thurston 1966; Zararis 2003)

A4. Deep beams with web reinforcement

No.	Researcher	Specimen ID	Loading conditions l_b [mm]	h_a [mm]	b [mm]	d [mm]	a [mm]	a/d
1	Smith and Vantsiotis (1982)	1A1-10	102	60	102	305	305	1.00
2	Smith and Vantsiotis (1982)	1A3-11	102	60	102	305	305	1.00
3	Smith and Vantsiotis (1982)	1A4-12	102	60	102	305	305	1.00
4	Smith and Vantsiotis (1982)	1A4-51	102	60	102	305	305	1.00
5	Smith and Vantsiotis (1982)	1A6-37	102	60	102	305	305	1.00
6	Smith and Vantsiotis (1982)	2A1-38	102	60	102	305	305	1.00
7	Smith and Vantsiotis (1982)	2A3-39	102	60	102	305	305	1.00
8	Smith and Vantsiotis (1982)	2A4-40	102	60	102	305	305	1.00
9	Smith and Vantsiotis (1982)	2A6-61	102	60	102	305	305	1.00
10	Smith and Vantsiotis (1982)	3A1-42	102	60	102	305	305	1.00
11	Smith and Vantsiotis (1982)	3A3-43	102	60	102	305	305	1.00
12	Smith and Vantsiotis (1982)	3A4-45	102	60	102	305	305	1.00
13	Smith and Vantsiotis (1982)	3A6-46	102	60	102	305	305	1.00
14	Smith and Vantsiotis (1982)	1B1-04	102	60	102	305	368	1.21
15	Smith and Vantsiotis (1982)	1B3-29	102	60	102	305	368	1.21
16	Smith and Vantsiotis (1982)	1B4-40	102	60	102	305	368	1.21
17	Smith and Vantsiotis (1982)	1B6-31	102	60	102	305	368	1.21
18	Smith and Vantsiotis (1982)	2B1-05	102	60	102	305	368	1.21
19	Smith and Vantsiotis (1982)	2B3-06	102	60	102	305	368	1.21
20	Smith and Vantsiotis (1982)	2B4-07	102	60	102	305	368	1.21
21	Smith and Vantsiotis (1982)	2B4-52	102	60	102	305	368	1.21

No.	Researcher	Specimen ID	Loading conditions		b	d	a	a/d
			l_b [mm]	h_a [mm]	[mm]	[mm]	[mm]	
22	Smith and Vantsiotis (1982)	2B6-32	102	60	102	305	368	1.21
23	Smith and Vantsiotis (1982)	3B1-08	102	60	102	305	368	1.21
24	Smith and Vantsiotis (1982)	3B1-36	102	60	102	305	368	1.21
25	Smith and Vantsiotis (1982)	3B3-33	102	60	102	305	368	1.21
26	Smith and Vantsiotis (1982)	3B4-34	102	60	102	305	368	1.21
27	Smith and Vantsiotis (1982)	3B6-35	102	60	102	305	368	1.21
28	Smith and Vantsiotis (1982)	4B1-09	102	60	102	305	368	1.21
29	Smith and Vantsiotis (1982)	1C1-14	102	60	102	305	457	1.50
30	Smith and Vantsiotis (1982)	1C3-02	102	60	102	305	457	1.50
31	Smith and Vantsiotis (1982)	1C4-15	102	60	102	305	457	1.50
32	Smith and Vantsiotis (1982)	1C6-16	102	60	102	305	457	1.50
33	Smith and Vantsiotis (1982)	2C1-17	102	60	102	305	457	1.50
34	Smith and Vantsiotis (1982)	2C3-03	102	60	102	305	457	1.50
35	Smith and Vantsiotis (1982)	2C3-27	102	60	102	305	457	1.50
36	Smith and Vantsiotis (1982)	2C4-18	102	60	102	305	457	1.50
37	Smith and Vantsiotis (1982)	2C6-19	102	60	102	305	457	1.50
38	Smith and Vantsiotis (1982)	3C1-20	102	60	102	305	457	1.50
39	Smith and Vantsiotis (1982)	3C3-21	102	60	102	305	457	1.50
40	Smith and Vantsiotis (1982)	3C4-22	102	60	102	305	457	1.50
41	Smith and Vantsiotis (1982)	3C6-23	102	60	102	305	457	1.50
42	Smith and Vantsiotis (1982)	4C1-24	102	60	102	305	457	1.50
43	Smith and Vantsiotis (1982)	4C3-04	102	60	102	305	457	1.50
44	Smith and Vantsiotis (1982)	4C3-28	102	60	102	305	457	1.50

No.	Researcher	Specimen ID	Loading conditions					
			l_b [mm]	h_a [mm]	b [mm]	d [mm]	a [mm]	a/d
45	Smith and Vantsiotis (1982)	4C4-25	102	60	102	305	457	1.50
46	Smith and Vantsiotis (1982)	4C6-26	102	60	102	305	457	1.50
47	Kong, Robins and Cole (1970)	1-30	76	76	76	724	254	0.35
48	Kong, Robins and Cole (1970)	1-25	76	76	76	597	254	0.43
49	Kong, Robins and Cole (1970)	1-20	76	76	76	470	254	0.54
50	Kong, Robins and Cole (1970)	1-15	76	76	76	343	254	0.74
51	Kong, Robins and Cole (1970)	1-10	76	76	76	216	254	1.18
52	Kong, Robins and Cole (1970)	2-30	76	76	76	724	254	0.35
53	Kong, Robins and Cole (1970)	2-25	76	76	76	597	254	0.43
54	Kong, Robins and Cole (1970)	2-20	76	76	76	470	254	0.54
55	Kong, Robins and Cole (1970)	2-15	76	76	76	343	254	0.74
56	Kong, Robins and Cole (1970)	2-10	76	76	76	216	254	1.18
57	Kong, Robins and Cole (1970)	5-30	76	76	76	724	254	0.35
58	Kong, Robins and Cole (1970)	5-25	76	76	76	597	254	0.43
59	Kong, Robins and Cole (1970)	5-20	76	76	76	470	254	0.54
60	Kong, Robins and Cole (1970)	5-15	76	76	76	343	254	0.74
61	Kong, Robins and Cole (1970)	5-10	76	76	76	216	254	1.18
62	Clark (1951)	A1-1	89	136	203	389	914	2.35
63	Clark (1951)	A1-2	89	136	203	389	914	2.35
64	Clark (1951)	A1-3	89	136	203	389	914	2.35
65	Clark (1951)	A1-4	89	136	203	389	914	2.35
66	Clark (1951)	B1-1	89	136	203	389	762	1.96
67	Clark (1951)	B1-2	89	136	203	389	762	1.96
68	Clark (1951)	B1-3	89	136	203	389	762	1.96
69	Clark (1951)	B1-4	89	136	203	389	762	1.96
70	Clark (1951)	B1-5	89	136	203	389	762	1.96
71	Clark (1951)	B2-1	89	136	203	389	762	1.96
72	Clark (1951)	B2-2	89	136	203	389	762	1.96
73	Clark (1951)	B2-3	89	136	203	389	762	1.96

No.	Researcher	Specimen ID	Loading conditions					
			l_b [mm]	h_a [mm]	b [mm]	d [mm]	a [mm]	a/d
74	Clark (1951)	B6-1	89	136	203	389	762	1.96
75	Clark (1951)	C1-1	89	136	203	389	611	1.57
76	Clark (1951)	C1-2	89	136	203	389	611	1.57
77	Clark (1951)	C1-3	89	136	203	389	611	1.57
78	Clark (1951)	C1-4	89	136	203	389	611	1.57
79	Clark (1951)	C2-1	89	136	203	389	611	1.57
80	Clark (1951)	C2-2	89	136	203	389	611	1.57
81	Clark (1951)	C2-3	89	136	203	389	611	1.57
82	Clark (1951)	C2-4	89	136	203	389	611	1.57
83	Clark (1951)	C3-1	89	136	203	389	611	1.57
84	Clark (1951)	C3-2	89	136	203	389	611	1.57
85	Clark (1951)	C3-3	89	136	203	389	611	1.57
86	Clark (1951)	C4-1	89	136	203	389	611	1.57
87	Clark (1951)	C6-2	89	136	203	389	611	1.57
88	Clark (1951)	C6-3	89	136	203	389	611	1.57
89	Clark (1951)	C6-4	89	136	203	389	611	1.57
90	Clark (1951)	D1-6	89	134	152	314	612	1.95
91	Clark (1951)	D1-7	89	134	152	314	612	1.95
92	Clark (1951)	D1-8	89	134	152	314	612	1.95
93	Clark (1951)	E1-2	89	134	152	314	634	2.02
94	Clark (1951)	D2-6	89	134	152	314	763	2.43
95	Clark (1951)	D2-7	89	134	152	314	763	2.43
96	Clark (1951)	D2-8	89	134	152	314	763	2.43
97	Clark (1951)	D4-1	89	134	152	314	763	2.43
98	Clark (1951)	D4-2	89	134	152	314	763	2.43
99	Clark (1951)	D4-3	89	134	152	314	763	2.43
100	Clark (1951)	D5-1	89	134	152	314	763	2.43
101	Clark (1951)	D5-2	89	134	152	314	763	2.43
102	Clark (1951)	D5-3	89	134	152	314	763	2.43
103	Shin et al. (1999)	MHB1.5-2.5	44	68	125	215	323	1.50
104	Shin et al. (1999)	MHB1.5-50	44	68	125	215	323	1.50
105	Shin et al. (1999)	MHB1.5-75	44	68	125	215	323	1.50
106	Shin et al. (1999)	MHB1.5-100	44	68	125	215	323	1.50
107	Shin et al. (1999)	MHB2.0-25	44	68	125	215	430	2.00
108	Shin et al. (1999)	MHB2.0-50	44	68	125	215	430	2.00
109	Shin et al. (1999)	MHB2.0-75	44	68	125	215	430	2.00

No.	Researcher	Specimen ID	Loading conditions l_b [mm]	h_a [mm]	b [mm]	d [mm]	a [mm]	a/d
110	Shin et al. (1999)	MHB2.0-100	44	68	125	215	430	2.00
111	Shin et al. (1999)	MHB2.5-25	44	68	125	215	538	2.50
112	Shin et al. (1999)	MHB2.5-50	44	68	125	215	538	2.50
113	Shin et al. (1999)	MHB2.5-75	44	68	125	215	538	2.50
114	Shin et al. (1999)	MHB2.5-100	44	68	125	215	538	2.50
115	Shin et al. (1999)	HB1.5-25	44	68	125	215	323	1.50
116	Shin et al. (1999)	HB1.5-50	44	68	125	215	323	1.50
117	Shin et al. (1999)	HB1.5-75	44	68	125	215	323	1.50
118	Shin et al. (1999)	HB1.5-100	44	68	125	215	323	1.50
119	Shin et al. (1999)	HB2.0-25	44	68	125	215	430	2.00
120	Shin et al. (1999)	HB2.0-50	44	68	125	215	430	2.00
121	Shin et al. (1999)	HB2.0-75	44	68	125	215	430	2.00
122	Shin et al. (1999)	HB2.0-100	44	68	125	215	430	2.00
123	Shin et al. (1999)	HB2.5-25	44	68	125	215	538	2.50
124	Shin et al. (1999)	HB2.5-50	44	68	125	215	538	2.50
125	Shin et al. (1999)	HB2.5-75	44	68	125	215	538	2.50
126	Shin et al. (1999)	HB2.5-100	44	68	125	215	538	2.50
127	Rogowsky et al. (1986)	BM1/1.5T2	200	130	200	535	1000	1.87
128	Rogowsky et al. (1986)	BM2/1.5T2	102	130	200	535	1000	1.87
129	Rogowsky et al. (1986)	BM1/2.0T2	200	90	200	455	1001	2.20
130	Rogowsky et al. (1986)	BM2/2.0T2	102	86	200	455	1001	2.20
131	Subedi, Vardy and Kubota (1986)	1A2	150	180	100	450	190	0.42
132	Subedi, Vardy and Kubota (1986)	2A2	150	180	100	450	190	0.42
133	Subedi, Vardy and Kubota (1986)	1B2	150	100	100	450	690	1.53
134	Subedi, Vardy and Kubota (1986)	1C2	150	225	100	850	390	0.46
135	Subedi, Vardy and Kubota (1986)	1D2	150	100	100	850	1290	1.52

No.	Researcher	Specimen ID	Loading conditions					
			l_b [mm]	h_a [mm]	b [mm]	d [mm]	a [mm]	a/d
136	Subedi, Vardy and Kubota (1986)	2D2	150	100	100	850	1290	1.52
137	Kong and Teng (1994)	N-2a	200	150	150	525	900	1.71
138	Kong and Teng (1994)	N-3a	200	150	150	525	900	1.71
139	Kong and Teng (1994)	N-2b	200	100	150	550	900	1.64
140	Kong and Teng (1994)	N-3b	200	100	150	550	900	1.64
141	Kong and Teng (1994)	A33-0.05	180	120	30	940	400	0.43
142	Kong and Teng (1994)	B33-0.05	80	120	30	940	220	0.23
143	Kong and Teng (1994)	A40-0.05	180	120	25	940	400	0.43
144	Kong and Teng (1994)	B40-0.05	80	120	25	940	220	0.23
145	Kong and Teng (1994)	A50-0.05	180	120	20	940	400	0.43
146	Kong and Teng (1994)	B50-0.05	80	120	20	940	220	0.23

No.	Researcher	Specimen ID	f'_c [MPa]	Horizontal web reinforcement f_{wyh} [MPa]	ρ_{wh} [%]	Vertical web reinforcement f_{wyv} [MPa]	ρ_{wv} [%]	Long. reinf. ρ_s [%]
1	Smith and Vantsiotis (1982)	1A1-10	19	431	0.2	437	0.3	1.9
2	Smith and Vantsiotis (1982)	1A3-11	18	431	0.5	437	0.3	1.9
3	Smith and Vantsiotis (1982)	1A4-12	16	431	0.7	437	0.3	1.9
4	Smith and Vantsiotis (1982)	1A4-51	21	431	0.7	437	0.3	1.9
5	Smith and Vantsiotis (1982)	1A6-37	21	431	0.9	437	0.3	1.9
6	Smith and Vantsiotis (1982)	2A1-38	22	431	0.2	437	0.6	1.9
7	Smith and Vantsiotis (1982)	2A3-39	20	431	0.5	437	0.6	1.9
8	Smith and Vantsiotis (1982)	2A4-40	20	431	0.7	437	0.6	1.9
9	Smith and Vantsiotis (1982)	2A6-61	19	431	0.9	437	0.6	1.9
10	Smith and Vantsiotis (1982)	3A1-42	18	431	0.2	437	1.3	1.9
11	Smith and Vantsiotis (1982)	3A3-43	19	431	0.5	437	1.3	1.9
12	Smith and Vantsiotis (1982)	3A4-45	21	431	0.7	437	1.3	1.9
13	Smith and Vantsiotis (1982)	3A6-46	20	431	0.9	437	1.3	1.9
14	Smith and Vantsiotis (1982)	1B1-04	22	431	0.2	437	0.2	1.9
15	Smith and Vantsiotis (1982)	1B3-29	20	431	0.5	437	0.2	1.9
16	Smith and Vantsiotis (1982)	1B4-40	21	431	0.7	437	0.2	1.9
17	Smith and Vantsiotis (1982)	1B6-31	20	431	0.9	437	0.2	1.9
18	Smith and Vantsiotis (1982)	2B1-05	19	431	0.2	437	0.4	1.9
19	Smith and Vantsiotis (1982)	2B3-06	19	431	0.5	437	0.4	1.9
20	Smith and Vantsiotis (1982)	2B4-07	17	431	0.7	437	0.4	1.9
21	Smith and Vantsiotis (1982)	2B4-52	22	431	0.7	437	0.4	1.9
22	Smith and Vantsiotis (1982)	2B6-32	20	431	0.9	437	0.4	1.9
23	Smith and Vantsiotis (1982)	3B1-08	16	431	0.2	437	0.6	1.9

No.	Researcher	Specimen ID	f'_c [MPa]	Horizontal web reinforcement f_{wyh} [MPa]	ρ_{wh} [%]	Vertical web reinforcement f_{wyv} [MPa]	ρ_{wv} [%]	Long. reinf. ρ_s [%]
24	Smith and Vantsiotis (1982)	3B1-36	20	431	0.2	437	0.8	1.9
25	Smith and Vantsiotis (1982)	3B3-33	19	431	0.5	437	0.8	1.9
26	Smith and Vantsiotis (1982)	3B4-34	19	431	0.7	437	0.8	1.9
27	Smith and Vantsiotis (1982)	3B6-35	21	431	0.9	437	0.8	1.9
28	Smith and Vantsiotis (1982)	4B1-09	17	431	0.2	437	1.3	1.9
29	Smith and Vantsiotis (1982)	1C1-14	19	431	0.2	437	0.2	1.9
30	Smith and Vantsiotis (1982)	1C3-02	22	431	0.5	437	0.2	1.9
31	Smith and Vantsiotis (1982)	1C4-15	23	431	0.7	437	0.2	1.9
32	Smith and Vantsiotis (1982)	1C6-16	22	431	0.9	437	0.2	1.9
33	Smith and Vantsiotis (1982)	2C1-17	20	431	0.2	437	0.3	1.9
34	Smith and Vantsiotis (1982)	2C3-03	19	431	0.5	437	0.3	1.9
35	Smith and Vantsiotis (1982)	2C3-27	19	431	0.5	437	0.3	1.9
36	Smith and Vantsiotis (1982)	2C4-18	20	431	0.7	437	0.3	1.9
37	Smith and Vantsiotis (1982)	2C6-19	21	431	0.9	437	0.3	1.9
38	Smith and Vantsiotis (1982)	3C1-20	21	431	0.2	437	0.6	1.9
39	Smith and Vantsiotis (1982)	3C3-21	17	431	0.5	437	0.6	1.9
40	Smith and Vantsiotis (1982)	3C4-22	18	431	0.7	437	0.6	1.9
41	Smith and Vantsiotis (1982)	3C6-23	19	431	0.9	437	0.6	1.9
42	Smith and Vantsiotis (1982)	4C1-24	20	431	0.2	437	0.8	1.9
43	Smith and Vantsiotis (1982)	4C3-04	19	431	0.5	437	0.6	1.9
44	Smith and Vantsiotis (1982)	4C3-28	19	431	0.5	437	0.8	1.9
45	Smith and Vantsiotis (1982)	4C4-25	19	431	0.7	437	0.8	1.9
46	Smith and Vantsiotis (1982)	4C6-26	21	431	0.9	437	0.8	1.9

No.	Researcher	Specimen ID	f'_c [MPa]	Horizontal web reinforcement f_{wyh} [MPa]	ρ_{wh} [%]	Vertical web reinforcement f_{wyv} [MPa]	ρ_{wv} [%]	Long. reinf. ρ_s [%]
47	Kong, Robins and Cole (1970)	1-30	22	287	0.5	280	2.5	0.5
48	Kong, Robins and Cole (1970)	1-25	25	287	0.6	280	2.5	0.6
49	Kong, Robins and Cole (1970)	1-20	21	287	0.8	280	2.5	0.8
50	Kong, Robins and Cole (1970)	1-15	21	287	1.1	280	2.5	1.1
51	Kong, Robins and Cole (1970)	1-10	22	287	1.7	280	2.5	1.7
52	Kong, Robins and Cole (1970)	2-30	19	287	0.5	303	0.9	0.5
53	Kong, Robins and Cole (1970)	2-25	19	287	0.6	303	0.9	0.6
54	Kong, Robins and Cole (1970)	2-20	20	287	0.8	303	0.9	0.8
55	Kong, Robins and Cole (1970)	2-15	23	287	1.1	303	0.9	1.1
56	Kong, Robins and Cole (1970)	2-10	20	287	1.7	303	0.9	1.7
57	Kong, Robins and Cole (1970)	5-30	19	287	0.6	280	0.6	0.5
58	Kong, Robins and Cole (1970)	5-25	19	287	0.6	280	0.6	0.6
59	Kong, Robins and Cole (1970)	5-20	20	287	0.6	280	0.6	0.8
60	Kong, Robins and Cole (1970)	5-15	22	287	0.6	280	0.6	1.1
61	Kong, Robins and Cole (1970)	5-10	23	287	0.6	280	0.6	1.7
62	Clark (1951)	A1-1	25			331	0.4	3.1
63	Clark (1951)	A1-2	24			331	0.4	3.1
64	Clark (1951)	A1-3	23			331	0.4	3.1
65	Clark (1951)	A1-4	25			331	0.4	3.1
66	Clark (1951)	B1-1	23			331	0.4	3.1
67	Clark (1951)	B1-2	25			331	0.4	3.1
68	Clark (1951)	B1-3	24			331	0.4	3.1
69	Clark (1951)	B1-4	23			331	0.4	3.1
70	Clark (1951)	B1-5	25			331	0.4	3.1
71	Clark (1951)	B2-1	23			331	0.7	3.1
72	Clark (1951)	B2-2	26			331	0.7	3.1
73	Clark (1951)	B2-3	25			331	0.7	3.1
74	Clark (1951)	B6-1	42			331	0.4	3.1
75	Clark (1951)	C1-1	26			331	0.3	2.1
76	Clark (1951)	C1-2	26			331	0.3	2.1

No.	Researcher	Specimen ID	f'_c [MPa]	Horizontal web reinforcement f_{wyh} [MPa]	Horizontal web reinforcement ρ_{wh} [%]	Vertical web reinforcement f_{wyv} [MPa]	Vertical web reinforcement ρ_{wv} [%]	Long. reinf. ρ_s [%]
77	Clark (1951)	C1-3	24			331	0.3	2.1
78	Clark (1951)	C1-4	29			331	0.3	2.1
79	Clark (1951)	C2-1	24			331	0.7	2.1
80	Clark (1951)	C2-2	25			331	0.7	2.1
81	Clark (1951)	C2-3	24			331	0.7	2.1
82	Clark (1951)	C2-4	27			331	0.7	2.1
83	Clark (1951)	C3-1	14			331	0.3	2.1
84	Clark (1951)	C3-2	14			331	0.3	2.1
85	Clark (1951)	C3-3	14			331	0.3	2.1
86	Clark (1951)	C4-1	24			331	0.3	3.1
87	Clark (1951)	C6-2	45			331	0.3	3.1
88	Clark (1951)	C6-3	45			331	0.3	3.1
89	Clark (1951)	C6-4	48			331	0.3	3.1
90	Clark (1951)	D1-6	28			331	0.5	3.4
91	Clark (1951)	D1-7	28			331	0.5	3.4
92	Clark (1951)	D1-8	28			331	0.5	3.4
93	Clark (1951)	E1-2	30			331	0.7	3.4
94	Clark (1951)	D2-6	29			331	0.6	3.4
95	Clark (1951)	D2-7	28			331	0.6	3.4
96	Clark (1951)	D2-8	26			331	0.6	3.4
97	Clark (1951)	D4-1	27			331	0.5	3.4
98	Clark (1951)	D4-2	26			331	0.5	3.4
99	Clark (1951)	D4-3	22			331	0.5	3.4
100	Clark (1951)	D5-1	28			331	0.4	3.4
101	Clark (1951)	D5-2	29			331	0.4	3.4
102	Clark (1951)	D5-3	27			331	0.4	3.4
103	Shin et al. (1999)	MHB1.5-2.5	52			414	0.5	3.8
104	Shin et al. (1999)	MHB1.5-50	52			414	0.9	3.8
105	Shin et al. (1999)	MHB1.5-75	52			414	1.4	3.8
106	Shin et al. (1999)	MHB1.5-100	52			414	1.8	3.8
107	Shin et al. (1999)	MHB2.0-25	52			414	0.3	3.8
108	Shin et al. (1999)	MHB2.0-50	52			414	0.7	3.8
109	Shin et al. (1999)	MHB2.0-75	52			414	1.0	3.8
110	Shin et al. (1999)	MHB2.0-100	52			414	1.3	3.8
111	Shin et al. (1999)	MHB2.5-25	52			414	0.3	3.8

No.	Researcher	Specimen ID	f'_c [MPa]	Horizontal web reinforcement f_{wyh} [MPa]	ρ_{wh} [%]	Vertical web reinforcement f_{wyv} [MPa]	ρ_{wv} [%]	Long. reinf. ρ_s [%]
112	Shin et al. (1999)	MHB2.5-50	52			414	0.5	3.8
113	Shin et al. (1999)	MHB2.5-75	52			414	0.7	3.8
114	Shin et al. (1999)	MHB2.5-100	52			414	0.9	3.8
115	Shin et al. (1999)	HB1.5-25	73			414	0.5	3.8
116	Shin et al. (1999)	HB1.5-50	73			414	0.9	3.8
117	Shin et al. (1999)	HB1.5-75	73			414	1.4	3.8
118	Shin et al. (1999)	HB1.5-100	73			414	1.8	3.8
119	Shin et al. (1999)	HB2.0-25	73			414	0.3	3.8
120	Shin et al. (1999)	HB2.0-50	73			414	0.7	3.8
121	Shin et al. (1999)	HB2.0-75	73			414	1.0	3.8
122	Shin et al. (1999)	HB2.0-100	73			414	1.3	3.8
123	Shin et al. (1999)	HB2.5-25	73			414	0.3	3.8
124	Shin et al. (1999)	HB2.5-50	73			414	0.5	3.8
125	Shin et al. (1999)	HB2.5-75	73			414	0.7	3.8
126	Shin et al. (1999)	HB2.5-100	73			414	0.9	3.8
127	Rogowsky et al. (1986)	BM1/1.5T2	42			570	0.2	1.1
128	Rogowsky et al. (1986)	BM2/1.5T2	42	570	0.3	570	0.2	1.1
129	Rogowsky et al. (1986)	BM1/2.0T2	43			570	0.2	0.9
130	Rogowsky et al. (1986)	BM2/2.0T2	43	570	0.3	570	0.2	0.9
131	Subedi, Vardy and Kubota (1986)	1A2	30	493	0.5	454	0.2	0.9
132	Subedi, Vardy and Kubota (1986)	2A2	23	322	0.5	438	0.2	0.9
133	Subedi, Vardy and Kubota (1986)	1B2	30	493	0.5	454	0.2	0.9
134	Subedi, Vardy and Kubota (1986)	1C2	28	330	0.4	454	0.2	1.2
135	Subedi, Vardy and Kubota (1986)	1D2	33	330	0.4	454	0.2	1.2
136	Subedi, Vardy and Kubota (1986)	2D2	32	303	0.4	438	0.2	1.2
137	Kong and Teng (1994)	N-2a	37	600	0.0	350	0.7	1.9

No.	Researcher	Specimen ID	f'_c [MPa]	Horizontal web reinforcement f_{wyh} [MPa]	ρ_{wh} [%]	Vertical web reinforcement f_{wyv} [MPa]	ρ_{wv} [%]	Long. reinf. ρ_s [%]
138	Kong and Teng (1994)	N-3a	37	600	0.8	350	0.7	1.9
139	Kong and Teng (1994)	N-2b	40	600	0.0	350	0.7	0.9
140	Kong and Teng (1994)	N-3b	40	600	0.8	350	0.7	0.9
141	Kong and Teng (1994)	A33-0.05	73	430	0.7	314	0.4	1.2
142	Kong and Teng (1994)	B33-0.05	75	430	0.7	314	0.4	1.2
143	Kong and Teng (1994)	A40-0.05	56	430	0.8	314	0.5	1.4
144	Kong and Teng (1994)	B40-0.05	62	430	0.8	314	0.5	1.4
145	Kong and Teng (1994)	A50-0.05	67	430	1.0	314	0.7	1.8
146	Kong and Teng (1994)	B50-0.05	76	430	1.0	314	0.7	1.8

No.	Researcher	Specimen ID	V_{mes} [kN]	V_{mes}/V_{cal} Proposed model [-]	V_{mes}/V_{cal} Watanabe [-]
1	Smith and Vantsiotis (1982)	1A1-10	161.2	1.57	1.49
2	Smith and Vantsiotis (1982)	1A3-11	148.3	1.36	1.40
3	Smith and Vantsiotis (1982)	1A4-12	141.2	1.27	1.40
4	Smith and Vantsiotis (1982)	1A4-51	170.9	1.33	1.51
5	Smith and Vantsiotis (1982)	1A6-37	184.1	1.32	1.61
6	Smith and Vantsiotis (1982)	2A1-38	174.5	1.36	1.12
7	Smith and Vantsiotis (1982)	2A3-39	170.6	1.30	1.14
8	Smith and Vantsiotis (1982)	2A4-40	171.9	1.19	1.13
9	Smith and Vantsiotis (1982)	2A6-61	161.9	1.08	1.09
10	Smith and Vantsiotis (1982)	3A1-42	161.0	1.15	0.63
11	Smith and Vantsiotis (1982)	3A3-43	172.7	1.11	0.68
12	Smith and Vantsiotis (1982)	3A4-45	178.5	1.02	0.70
13	Smith and Vantsiotis (1982)	3A6-46	168.1	0.91	0.66
14	Smith and Vantsiotis (1982)	1B1-04	147.5	1.44	1.41
15	Smith and Vantsiotis (1982)	1B3-29	143.6	1.39	1.44
16	Smith and Vantsiotis (1982)	1B4-40	140.3	1.24	1.38
17	Smith and Vantsiotis (1982)	1B6-31	153.3	1.31	1.56
18	Smith and Vantsiotis (1982)	2B1-05	129.0	1.25	1.08
19	Smith and Vantsiotis (1982)	2B3-06	131.2	1.19	1.10
20	Smith and Vantsiotis (1982)	2B4-07	126.1	1.10	1.09
21	Smith and Vantsiotis (1982)	2B4-52	149.9	1.17	1.19
22	Smith and Vantsiotis (1982)	2B6-32	145.2	1.12	1.20
23	Smith and Vantsiotis (1982)	3B1-08	130.8	1.25	0.94

No.	Researcher	Specimen ID	V_{mes} [kN]	V_{mes}/V_{cal} Proposed model [-]	V_{mes}/V_{cal} Watanabe [-]
24	Smith and Vantsiotis (1982)	3B1-36	158.9	1.26	0.96
25	Smith and Vantsiotis (1982)	3B3-33	158.3	1.21	0.97
26	Smith and Vantsiotis (1982)	3B4-34	155.0	1.09	0.95
27	Smith and Vantsiotis (1982)	3B6-35	161.7	1.04	0.97
28	Smith and Vantsiotis (1982)	4B1-09	153.5	1.08	0.60
29	Smith and Vantsiotis (1982)	1C1-14	119.0	1.58	1.45
30	Smith and Vantsiotis (1982)	1C3-02	123.4	1.40	1.42
31	Smith and Vantsiotis (1982)	1C4-15	131.0	1.35	1.48
32	Smith and Vantsiotis (1982)	1C6-16	122.3	1.21	1.41
33	Smith and Vantsiotis (1982)	2C1-17	124.1	1.42	1.23
34	Smith and Vantsiotis (1982)	2C3-03	103.6	1.12	1.04
35	Smith and Vantsiotis (1982)	2C3-27	115.3	1.24	1.16
36	Smith and Vantsiotis (1982)	2C4-18	124.5	1.21	1.22
37	Smith and Vantsiotis (1982)	2C6-19	124.1	1.12	1.21
38	Smith and Vantsiotis (1982)	3C1-20	140.8	1.28	1.03
39	Smith and Vantsiotis (1982)	3C3-21	125.0	1.17	0.97
40	Smith and Vantsiotis (1982)	3C4-22	127.7	1.08	0.97
41	Smith and Vantsiotis (1982)	3C6-23	137.2	1.07	1.03
42	Smith and Vantsiotis (1982)	4C1-24	146.6	1.19	0.90
43	Smith and Vantsiotis (1982)	4C3-04	124.5	1.06	0.88
44	Smith and Vantsiotis (1982)	4C3-28	152.3	1.17	0.94
45	Smith and Vantsiotis (1982)	4C4-25	152.6	1.12	0.95
46	Smith and Vantsiotis (1982)	4C6-26	159.5	1.05	0.96

No.	Researcher	Specimen ID	V_{mes} [kN]	V_{mes}/V_{cal} Proposed model [-]	V_{mes}/V_{cal} Watanabe [-]
47	Kong, Robins and Cole (1970)	1-30	238.9	1.08	0.42
48	Kong, Robins and Cole (1970)	1-25	224.2	1.07	0.48
49	Kong, Robins and Cole (1970)	1-20	189.5	1.06	0.51
50	Kong, Robins and Cole (1970)	1-15	164.2	1.07	0.61
51	Kong, Robins and Cole (1970)	1-10	89.4	0.73	0.53
52	Kong, Robins and Cole (1970)	2-30	249.1	1.33	0.86
53	Kong, Robins and Cole (1970)	2-25	224.2	1.36	0.97
54	Kong, Robins and Cole (1970)	2-20	215.3	1.46	1.18
55	Kong, Robins and Cole (1970)	2-15	139.7	1.06	1.02
56	Kong, Robins and Cole (1970)	2-10	99.7	1.12	1.30
57	Kong, Robins and Cole (1970)	5-30	239.3	1.22	0.90
58	Kong, Robins and Cole (1970)	5-25	208.2	1.32	0.96
59	Kong, Robins and Cole (1970)	5-20	172.6	1.34	1.03
60	Kong, Robins and Cole (1970)	5-15	127.2	1.20	1.08
61	Kong, Robins and Cole (1970)	5-10	77.9	1.02	1.17
62	Clark (1951)	A1-1	222.6	1.28	0.96
63	Clark (1951)	A1-2	209.2	1.22	0.91
64	Clark (1951)	A1-3	222.6	1.30	0.98
65	Clark (1951)	A1-4	244.8	1.40	1.05
66	Clark (1951)	B1-1	278.9	1.41	1.17
67	Clark (1951)	B1-2	256.7	1.25	1.04
68	Clark (1951)	B1-3	284.8	1.43	1.18
69	Clark (1951)	B1-4	268.2	1.36	1.12
70	Clark (1951)	B1-5	241.5	1.19	0.99
71	Clark (1951)	B2-1	301.2	1.10	0.88
72	Clark (1951)	B2-2	322.3	1.12	0.91
73	Clark (1951)	B2-3	335.0	1.19	0.96
74	Clark (1951)	B6-1	379.5	1.40	1.25
75	Clark (1951)	C1-1	277.8	1.10	1.06
76	Clark (1951)	C1-2	311.2	1.21	1.18

No.	Researcher	Specimen ID	V_{mes} [kN]	V_{mes}/V_{cal} Proposed model [-]	V_{mes}/V_{cal} Watanabe [-]
77	Clark (1951)	C1-3	246.0	1.02	0.97
78	Clark (1951)	C1-4	286.1	1.04	1.04
79	Clark (1951)	C2-1	290.1	1.00	0.84
80	Clark (1951)	C2-2	301.2	1.00	0.85
81	Clark (1951)	C2-3	323.8	1.10	0.93
82	Clark (1951)	C2-4	288.3	0.92	0.80
83	Clark (1951)	C3-1	223.7	1.33	1.09
84	Clark (1951)	C3-2	200.4	1.20	0.98
85	Clark (1951)	C3-3	188.2	1.13	0.92
86	Clark (1951)	C4-1	309.4	1.26	1.21
87	Clark (1951)	C6-2	424.0	1.15	1.25
88	Clark (1951)	C6-3	435.1	1.19	1.29
89	Clark (1951)	C6-4	428.8	1.12	1.23
90	Clark (1951)	D1-6	174.8	1.10	1.03
91	Clark (1951)	D1-7	179.2	1.12	1.05
92	Clark (1951)	D1-8	185.9	1.17	1.09
93	Clark (1951)	E1-2	221.8	1.14	1.00
94	Clark (1951)	D2-6	168.5	1.07	0.89
95	Clark (1951)	D2-7	157.4	1.01	0.84
96	Clark (1951)	D2-8	168.5	1.11	0.91
97	Clark (1951)	D4-1	168.5	1.27	1.03
98	Clark (1951)	D4-2	157.3	1.21	0.98
99	Clark (1951)	D4-3	165.1	1.32	1.07
100	Clark (1951)	D5-1	146.2	1.30	1.03
101	Clark (1951)	D5-2	157.3	1.37	1.09
102	Clark (1951)	D5-3	157.3	1.40	1.11
103	Shin et al. (1999)	MHB1.5-2.5	156.7	1.10	1.07
104	Shin et al. (1999)	MHB1.5-50	208.0	1.22	1.05
105	Shin et al. (1999)	MHB1.5-75	239.7	1.21	0.96
106	Shin et al. (1999)	MHB1.5-100	257.4	1.14	0.85
107	Shin et al. (1999)	MHB2.0-25	110.7	1.16	0.96
108	Shin et al. (1999)	MHB2.0-50	173.9	1.37	1.12
109	Shin et al. (1999)	MHB2.0-75	185.4	1.18	0.95
110	Shin et al. (1999)	MHB2.0-100	193.2	1.03	0.82
111	Shin et al. (1999)	MHB2.5-25	98.6	1.59	1.05

No.	Researcher	Specimen ID	V_{mes} [kN]	V_{mes}/V_{cal} Proposed model [-]	V_{mes}/V_{cal} Watanabe [-]
112	Shin et al. (1999)	MHB2.5-50	138.6	1.53	1.12
113	Shin et al. (1999)	MHB2.5-75	159.3	1.31	1.03
114	Shin et al. (1999)	MHB2.5-100	164.2	1.08	0.89
115	Shin et al. (1999)	HB1.5-25	214.2	1.27	1.25
116	Shin et al. (1999)	HB1.5-50	246.2	1.25	1.10
117	Shin et al. (1999)	HB1.5-75	265.8	1.19	0.97
118	Shin et al. (1999)	HB1.5-100	280.3	1.12	0.87
119	Shin et al. (1999)	HB2.0-25	142.7	1.30	1.07
120	Shin et al. (1999)	HB2.0-50	195.9	1.39	1.12
121	Shin et al. (1999)	HB2.0-75	230.0	1.34	1.07
122	Shin et al. (1999)	HB2.0-100	242.1	1.20	0.95
123	Shin et al. (1999)	HB2.5-25	115.6	1.69	1.05
124	Shin et al. (1999)	HB2.5-50	148.9	1.54	1.07
125	Shin et al. (1999)	HB2.5-75	166.9	1.30	0.98
126	Shin et al. (1999)	HB2.5-100	183.8	1.16	0.91
127	Rogowsky et al. (1986)	BM1/1.5T2	354.0	1.02	0.94
128	Rogowsky et al. (1986)	BM2/1.5T2	348.0	1.09	0.92
129	Rogowsky et al. (1986)	BM1/2.0T2	199.0	0.92	0.67
130	Rogowsky et al. (1986)	BM2/2.0T2	204.0	0.99	0.69
131	Subedi, Vardy and Kubota (1986)	1A2	375.0	1.08	1.42
132	Subedi, Vardy and Kubota (1986)	2A2	307.5	1.14	1.38
133	Subedi, Vardy and Kubota (1986)	1B2	149.5	0.89	0.97
134	Subedi, Vardy and Kubota (1986)	1C2	485.0	1.26	1.04
135	Subedi, Vardy and Kubota (1986)	1D2	211.0	1.01	0.70
136	Subedi, Vardy and Kubota (1986)	2D2	199.0	1.00	0.68
137	Kong and Teng (1994)	N-2a	438.0	1.18	1.08

No.	Researcher	Specimen ID	V_{mes} [kN]	V_{mes}/V_{cal} Proposed model [-]	V_{mes}/V_{cal} Watanabe [-]
138	Kong and Teng (1994)	N-3a	418.0	0.94	1.03
139	Kong and Teng (1994)	N-2b	388.0	1.06	0.88
140	Kong and Teng (1994)	N-3b	444.0	0.99	1.01
141	Kong and Teng (1994)	A33-0.05	320.0	1.32	1.09
142	Kong and Teng (1994)	B33-0.05	346.0	1.45	1.00
143	Kong and Teng (1994)	A40-0.05	267.0	1.37	1.27
144	Kong and Teng (1994)	B40-0.05	275.0	1.28	1.07
145	Kong and Teng (1994)	A50-0.05	220.0	1.21	1.15
146	Kong and Teng (1994)	B50-0.05	230.0	1.11	0.98
			mean	1.20 ± 0.24 %	1.04 ± 0.31 %
			std-dev	0.16	0.22
			c.v.	12.98 %	20.81 %

(Kong et al. 1994; Matamoros and Wong 2003)

A5. Axially loaded members

No.	Researcher	Specimen ID	b [mm]	h [mm]	d [mm]	h_a [mm]	a [mm]	a/d [-]
1	Diaz De Cossio & Siess, 1960	A-1	152	305	254	102	508	2.0
2	Diaz De Cossio & Siess, 1960	A-2	152	305	254	102	762	3.0
3	Diaz De Cossio & Siess, 1960	A-3	152	305	254	102	1016	4.0
4	Diaz De Cossio & Siess, 1960	A-4	152	305	254	102	1270	5.0
5	Diaz De Cossio & Siess, 1960	B-1	152	305	254	102	508	2.0
6	Diaz De Cossio & Siess, 1960	B-2	152	305	254	102	762	3.0
7	Diaz De Cossio & Siess, 1960	B-3	152	305	254	102	1016	4.0
8	Diaz De Cossio & Siess, 1960	B-4	152	305	254	102	1270	5.0
9	Diaz De Cossio & Siess, 1960	A-11	152	305	254	102	508	2.0
10	Diaz De Cossio & Siess, 1960	A-12	152	305	254	102	762	3.0
11	Diaz De Cossio & Siess, 1960	A-13	152	305	254	102	1016	4.0
12	Diaz De Cossio & Siess, 1960	A-14	152	305	254	102	1270	5.0
13	Diaz De Cossio & Siess, 1960	A-15	152	305	254	102	1524	6.0
14	Diaz De Cossio & Siess, 1960	B-11	152	305	254	102	508	2.0
15	Diaz De Cossio & Siess, 1960	B-12	152	305	254	102	762	3.0
16	Diaz De Cossio & Siess, 1960	B-13	152	305	254	102	1016	4.0
17	Diaz De Cossio & Siess, 1960	B-14	152	305	254	102	1270	5.0
18	Diaz De Cossio & Siess, 1960	B-15	152	305	254	102	1524	6.0
19	Baldwin & Viest	0B28	305	406	368	76	711	1.9
20	Baldwin & Viest	0F28	305	406	368	76	711	1.9
21	Baldwin & Viest	2F28	305	406	368	76	711	1.9
22	Baldwin & Viest	3F28	305	406	368	76	711	1.9
23	Baldwin & Viest	4F28	305	406	368	76	711	1.9
24	Baldwin & Viest	6F28	305	406	368	76	711	1.9

No.	Researcher	Specimen ID	b [mm]	h [mm]	d [mm]	h_a [mm]	a [mm]	a/d [-]
25	Baldwin & Viest	9F28	305	406	368	76	711	1.9
26	Baldwin & Viest	12F28	305	406	368	76	711	1.9
27	Baldwin & Viest	18F28	305	406	368	76	711	1.9
28	Baldwin & Viest	12F21	305	406	368	76	533	1.4
29	Baldwin & Viest	12F38	305	406	368	76	965	2.6
30	Morrow & Viest, 1957	F21B2	305	419	368	102	549	1.5
31	Morrow & Viest, 1957	B2R	305	419	368	102	549	1.5
32	Morrow & Viest, 1957	B4	305	419	368	102	549	1.5
33	Morrow & Viest, 1957	B4R	305	419	368	102	549	1.5
34	Morrow & Viest, 1957	C4	305	413	368	89	549	1.5
35	Morrow & Viest, 1957	C4R	305	413	375	76	549	1.5
36	Morrow & Viest, 1957	D4	305	413	368	89	549	1.5
37	Morrow & Viest, 1957	E4	311	419	381	76	549	1.4
38	Morrow & Viest, 1957	F4	305	419	368	102	549	1.5
39	Morrow & Viest, 1957	A6	305	419	368	102	549	1.5
40	Morrow & Viest, 1957	B6	305	419	368	102	549	1.5
41	Morrow & Viest, 1957	F38B2	305	419	362	114	980	2.7
42	Morrow & Viest, 1957	E2	305	419	368	102	980	2.7
43	Morrow & Viest, 1957	B4	305	416	375	83	980	2.6
44	Morrow & Viest, 1957	D4	308	416	381	70	980	2.6
45	Morrow & Viest, 1957	E4	305	419	378	82	980	2.6
46	Morrow & Viest, 1957	A6	305	419	356	127	980	2.8
47	Morrow & Viest, 1957	B6	305	419	381	76	980	2.6
48	Morrow & Viest, 1957	F55B2	305	419	368	102	1412	3.8
49	Morrow & Viest, 1957	A4	308	410	372	76	1412	3.8
50	Morrow & Viest, 1957	B4	305	419	381	76	1412	3.7
51	Morrow & Viest, 1957	D4	308	410	381	57	1412	3.7
52	Morrow & Viest, 1957	E4	308	429	387	83	1412	3.6
53	Morrow & Viest, 1957	A6	305	419	349	140	1412	4.0
54	Morrow & Viest, 1957	B6	305	419	368	102	1412	3.8
55	Morrow & Viest, 1957	F70B2	305	419	362	114	1778	4.9
56	Morrow & Viest, 1957	A4	305	410	362	96	1778	4.9
57	Morrow & Viest, 1957	B6	305	419	368	102	1778	4.8
58	Morrow & Viest, 1957	F84B4	305	416	375	83	2134	5.7

No.	Researcher	Specimen ID	f'c [MPa]	Long. reinf. ρs [%]	εs at d [-]	fsy [MPa]	c [mm]	scr [mm]	Δw [mm]
1	Diaz De Cossio & Siess, 1960	A-1	28.1	1.0	0.0017	459	56.8	197.2	0.84
2	Diaz De Cossio & Siess, 1960	A-2	31.5	1.0	0.0015	469	53.2	200.8	0.77
3	Diaz De Cossio & Siess, 1960	A-3	19.4	1.0	0.0012	452	80.6	173.4	0.56
4	Diaz De Cossio & Siess, 1960	A-4	26.8	1.0	0.0013	459	59.3	194.7	0.63
5	Diaz De Cossio & Siess, 1960	B-1	26.1	1.0	0.0019	459	92.0	162.0	0.79
6	Diaz De Cossio & Siess, 1960	B-2	28.5	1.0	0.0013	459	84.7	169.3	0.58
7	Diaz De Cossio & Siess, 1960	B-3	26.3	1.0	0.0011	394	82.6	171.4	0.48
8	Diaz De Cossio & Siess, 1960	B-4	28.3	1.0	0.0009	459	85.3	168.7	0.41
9	Diaz De Cossio & Siess, 1960	A-11	28.3	3.3	0.0008	341	141.9	112.1	0.24
10	Diaz De Cossio & Siess, 1960	A-12	26.7	3.3	0.0007	314	137.4	116.6	0.23
11	Diaz De Cossio & Siess, 1960	A-13	22.1	3.3	0.0005	393	166.5	87.5	0.15
12	Diaz De Cossio & Siess, 1960	A-14	27.5	3.3	0.0006	364	154.7	99.3	0.18
13	Diaz De Cossio & Siess, 1960	A-15	25.0	3.3	0.0005	332	154.9	99.1	0.16
14	Diaz De Cossio & Siess, 1960	B-11	25.2	3.3	0.0009	332	169.8	84.2	0.22
15	Diaz De Cossio & Siess, 1960	B-12	27.1	3.3	0.0006	392	166.3	87.7	0.17
16	Diaz De Cossio & Siess, 1960	B-13	27.9	3.3	0.0005	354	165.0	89.0	0.15
17	Diaz De Cossio & Siess, 1960	B-14	29.3	3.3	0.0004	363	163.2	90.8	0.13
18	Diaz De Cossio & Siess, 1960	B-15	28.3	3.3	0.0003	326	164.2	89.8	0.11
19	Baldwin & Viest	0B28	37.6	1.9	0.0000	519	367.1	1.2	0.04
20	Baldwin & Viest	0F28	33.3	1.9	0.0000	313	367.2	1.1	0.04
21	Baldwin & Viest	2F28	27.4	1.9	0.0000	532	367.3	1.0	0.04
22	Baldwin & Viest	3F28	25.8	1.9	0.0000	543	367.4	0.9	0.04
23	Baldwin & Viest	4F28	27.5	1.9	0.0000	523	367.4	0.9	0.04
24	Baldwin & Viest	6F28	21.2	1.9	0.0000	519	367.6	0.7	0.04
25	Baldwin & Viest	9F28	23.6	1.9	0.0000	523	367.6	0.7	0.04
26	Baldwin & Viest	12F28	23.9	1.9	0.0000	519	367.7	0.6	0.04

No.	Researcher	Specimen ID	f'c [MPa]	Long. reinf. ρ_s [%]	ε_s at d [-]	f_{sy} [MPa]	c [mm]	s_{cr} [mm]	Δw [mm]
27	Baldwin & Viest	18F28	26.0	1.9	0.0000	532	367.7	0.6	0.04
28	Baldwin & Viest	12F21	30.8	1.9	0.0000	313	367.6	0.7	0.04
29	Baldwin & Viest	12F38	28.9	1.9	0.0000	313	367.4	0.9	0.04
30	Morrow & Viest, 1957	F21B2	10.1	1.9	0.0000	376	368.0	0.3	0.04
31	Morrow & Viest, 1957	B2R	14.1	1.9	0.0000	376	367.9	0.4	0.04
32	Morrow & Viest, 1957	B4	29.7	1.9	0.0000	378	367.4	0.9	0.04
33	Morrow & Viest, 1957	B4R	29.2	1.9	0.0000	378	367.4	0.9	0.04
34	Morrow & Viest, 1957	C4	26.6	1.6	0.0000	434	367.3	1.0	0.04
35	Morrow & Viest, 1957	C4R	30.9	1.6	0.0000	447	373.5	1.2	0.04
36	Morrow & Viest, 1957	D4	31.5	1.2	0.0000	452	366.8	1.5	0.04
37	Morrow & Viest, 1957	E4	30.7	0.8	0.0000	432	378.6	2.4	0.04
38	Morrow & Viest, 1957	F4	30.0	0.8	0.0000	427	365.9	2.4	0.04
39	Morrow & Viest, 1957	A6	48.4	2.4	0.0000	376	367.2	1.1	0.04
40	Morrow & Viest, 1957	B6	45.0	1.9	0.0000	378	367.0	1.3	0.04
41	Morrow & Viest, 1957	F38B2	12.4	1.9	0.0000	374	361.6	0.4	0.04
42	Morrow & Viest, 1957	E2	14.1	0.5	0.0000	388	366.5	1.8	0.04
43	Morrow & Viest, 1957	B4	31.4	1.8	0.0000	385	373.6	1.1	0.04
44	Morrow & Viest, 1957	D4	26.9	1.3	0.0000	368	379.7	1.3	0.04
45	Morrow & Viest, 1957	E4	32.1	0.9	0.0000	368	375.7	2.2	0.04
46	Morrow & Viest, 1957	A6	45.6	2.9	0.0000	364	354.8	0.8	0.04
47	Morrow & Viest, 1957	B6	41.6	1.8	0.0000	379	379.6	1.4	0.04
48	Morrow & Viest, 1957	F55B2	11.9	1.9	0.0000	374	367.9	0.4	0.04
49	Morrow & Viest, 1957	A4	26.4	2.0	0.0000	405	370.7	0.9	0.04
50	Morrow & Viest, 1957	B4	29.5	1.8	0.0000	384	379.9	1.1	0.04

No.	Researcher	Specimen ID	f'_c [MPa]	Long. reinf. ρ_s [%]	ε_s at d [-]	f_{sy} [MPa]	c [mm]	s_{cr} [mm]	Δw [mm]
51	Morrow & Viest, 1957	D4	25.6	1.5	0.0000	432	379.8	1.2	0.04
52	Morrow & Viest, 1957	E4	28.3	0.9	0.0000	423	385.3	2.0	0.04
53	Morrow & Viest, 1957	A6	42.1	3.3	0.0000	379	348.6	0.7	0.04
54	Morrow & Viest, 1957	B6	43.7	1.9	0.0000	376	367.0	1.3	0.04
55	Morrow & Viest, 1957	F70B2	14.4	1.9	0.0000	383	361.5	0.5	0.04
56	Morrow & Viest, 1957	A4	29.0	2.2	0.0000	376	361.1	0.8	0.04
57	Morrow & Viest, 1957	B6	38.7	3.3	0.0000	354	367.6	0.7	0.04
58	Morrow & Viest, 1957	F84B4	29.6	1.8	0.0000	381	373.6	1.0	0.04

No.	Researcher	Specimen ID	P [kN]	$P/(Af'_c)$ [-]	V_{mes} [kN]	V_{mes}/V_{cal} Proposed model [-]
1	Diaz De Cossio & Siess, 1960	A-1	0	0.0%	46	1.12
2	Diaz De Cossio & Siess, 1960	A-2	0	0.0%	42	1.88
3	Diaz De Cossio & Siess, 1960	A-3	0	0.0%	34	1.47
4	Diaz De Cossio & Siess, 1960	A-4	0	0.0%	35	1.48
5	Diaz De Cossio & Siess, 1960	B-1	89	7.3%	66	1.07
6	Diaz De Cossio & Siess, 1960	B-2	89	6.7%	52	1.57
7	Diaz De Cossio & Siess, 1960	B-3	89	7.3%	46	1.59
8	Diaz De Cossio & Siess, 1960	B-4	89	6.8%	42	1.23
9	Diaz De Cossio & Siess, 1960	A-11	0	0.0%	63	0.84
10	Diaz De Cossio & Siess, 1960	A-12	0	0.0%	59	1.45
11	Diaz De Cossio & Siess, 1960	A-13	0	0.0%	47	1.30
12	Diaz De Cossio & Siess, 1960	A-14	0	0.0%	55	1.28
13	Diaz De Cossio & Siess, 1960	A-15	0	0.0%	49	1.10
14	Diaz De Cossio & Siess, 1960	B-11	89	7.6%	84	1.24
15	Diaz De Cossio & Siess, 1960	B-12	89	7.1%	66	1.57
16	Diaz De Cossio & Siess, 1960	B-13	89	6.9%	59	1.46
17	Diaz De Cossio & Siess, 1960	B-14	89	6.5%	53	1.18
18	Diaz De Cossio & Siess, 1960	B-15	89	6.8%	47	0.97
19	Baldwin & Viest	0B28	0	0.0%	338	2.21
20	Baldwin & Viest	0F28	0	0.0%	178	1.28
21	Baldwin & Viest	2F28	50	1.5%	150	1.26
22	Baldwin & Viest	3F28	95	3.0%	191	1.69
23	Baldwin & Viest	4F28	148	4.3%	222	1.86
24	Baldwin & Viest	6F28	186	7.1%	186	1.93
25	Baldwin & Viest	9F28	241	8.2%	160	1.52
26	Baldwin & Viest	12F28	291	9.9%	146	1.37
27	Baldwin & Viest	18F28	825	25.6%	275	2.42

No.	Researcher	Specimen ID	P [kN]	P/(Af'c) [-]	V_{mes} [kN]	V_{mes}/V_{cal} Proposed model [-]
28	Baldwin & Viest	12F21	760	19.9%	380	2.04
29	Baldwin & Viest	12F38	398	11.1%	199	2.11
30	Morrow & Viest, 1957	F21B2	132	10.2%	132	1.49
31	Morrow & Viest, 1957	B2R	173	9.6%	173	1.44
32	Morrow & Viest, 1957	B4	248	6.5%	248	1.06
33	Morrow & Viest, 1957	B4R	236	6.3%	236	1.02
34	Morrow & Viest, 1957	C4	220	6.6%	220	1.18
35	Morrow & Viest, 1957	C4R	252	6.5%	251	1.36
36	Morrow & Viest, 1957	D4	220	5.6%	220	1.02
37	Morrow & Viest, 1957	E4	220	5.5%	220	1.15
38	Morrow & Viest, 1957	F4	219	5.7%	218	0.93
39	Morrow & Viest, 1957	A6	283	4.6%	283	0.83
40	Morrow & Viest, 1957	B6	283	4.9%	283	0.87
41	Morrow & Viest, 1957	F38B2	113	7.1%	113	1.69
42	Morrow & Viest, 1957	E2	74	4.1%	74	1.07
43	Morrow & Viest, 1957	B4	173	4.3%	173	1.64
44	Morrow & Viest, 1957	D4	169	4.9%	171	1.94
45	Morrow & Viest, 1957	E4	148	3.6%	148	1.38
46	Morrow & Viest, 1957	A6	220	3.8%	220	1.30
47	Morrow & Viest, 1957	B6	173	3.3%	173	1.42
48	Morrow & Viest, 1957	F55B2	94	6.2%	94	1.25
49	Morrow & Viest, 1957	A4	151	4.5%	151	1.47
50	Morrow & Viest, 1957	B4	126	3.3%	126	1.18
51	Morrow & Viest, 1957	D4	126	3.9%	126	1.30
52	Morrow & Viest, 1957	E4	110	2.9%	110	1.02
53	Morrow & Viest, 1957	A6	189	3.5%	189	1.36
54	Morrow & Viest, 1957	B6	142	2.5%	141	1.05
55	Morrow & Viest, 1957	F70B2	91	5.0%	91	0.92
56	Morrow & Viest, 1957	A4	142	3.9%	142	1.11
57	Morrow & Viest, 1957	B6	173	3.5%	173	1.21
58	Morrow & Viest, 1957	F84B4	131	3.5%	131	0.91
					mean	1.37 ± 0.36 %
					std-dev	0.36
					c.v.	26.09 %

(Baldwin and Viest 1958; Diaz De Cossio and Siess 1960; Morrow and Viest 1957)

A6. Cyclic flexural failure

No.	Researcher	Year	Specimen ID	Geometry						
				b [mm]	h [mm]	d [mm]	h_a [mm]	L [mm]	A_g/A_{core} [-]	a/d [-]
1	Park and Paulay	1990	No. 9	400	600	564	72	1784	1.24	3.0
2	Ohno and Nishioka	1984	L2	400	400	359	82	1600	1.41	4.0
3	Ohno and Nishioka	1984	L3	400	400	359	82	1600	1.41	4.0
4	Atalay and Penzien	1975	No. 4S1	305	305	262	86	1676	1.60	5.5
5	Atalay and Penzien	1975	No. 1S1	305	305	262	86	1676	1.60	5.5
6	Atalay and Penzien	1975	No. 3S1	305	305	262	86	1676	1.60	5.5
7	Atalay and Penzien	1975	No. 2S1	305	305	262	86	1676	1.60	5.5
8	Saatcioglu and Ozcebe	1989	U6	350	350	312	77	1000	1.38	2.9
9	Saatcioglu and Ozcebe	1989	U7	350	350	312	77	1000	1.38	2.9
10	Wehbe et al.	1998	A1	380	610	572	75	2335	1.29	3.8
11	Wehbe et al.	1998	B1	380	610	575	69	2335	1.25	3.8
12	Mo and Wang	2000	C1-1	400	400	356	87	1400	1.45	3.5
13	Mo and Wang	2000	C2-1	400	400	356	87	1400	1.45	3.5
14	Mo and Wang	2000	C3-1	400	400	356	87	1400	1.45	3.5
15	Mo and Wang	2000	C3-2	400	400	356	87	1400	1.45	3.5
16	Saatcioglu and Ozcebe	1989	U4	350	350	315	70	1000	1.32	2.9
17	Saatcioglu and Ozcebe	1989	U3	350	350	315	70	1000	1.32	2.9
18	Kanda et al.	1987	85STC-1	250	250	209	83	750	1.93	3.0
19	Kanda et al.	1987	85STC-2	250	250	209	83	750	1.93	3.0
20	Kanda et al.	1987	85STC-3	250	250	209	83	750	1.93	3.0
21	Matamoros et al.	1999	C5-00N	203	203	171	64	610	1.53	3.0
22	Matamoros et al.	1999	C5-00S	203	203	167	72	610	1.57	3.0
23	Soesianawati et al.	1986	No. 1	400	400	379	42	1600	1.14	4.0

No.	Researcher	Year	Specimen ID	Geometry						
				b [mm]	h [mm]	d [mm]	h_a [mm]	L [mm]	A_g/A_{core} [-]	a/d [-]
24	Matamoros et al.	1999	C5-20N	203	203	157	92	610	2.37	3.0
25	Matamoros et al.	1999	C10-05N	203	203	155	96	610	2.43	3.0
26	Matamoros et al.	1999	C10-05S	203	203	155	95	610	2.47	3.0
27	Matamoros et al.	1999	C5-20S	203	203	156	94	610	2.45	3.0
28	Matamoros et al.	1999	C10-10N	203	203	169	68	610	1.62	3.0
29	Matamoros et al.	1999	C10-10S	203	203	171	63	610	1.58	3.0
30	Thomsen and Wallace	1994	B2	152.4	152.4	137	32	597	1.37	3.9
31	Thomsen and Wallace	1994	B1	152.4	152.4	137	32	597	1.37	3.9
32	Thomsen and Wallace	1994	A1	152.4	152.4	137	32	597	1.37	3.9
33	Thomsen and Wallace	1994	C1	152.4	152.4	137	32	597	1.37	3.9
34	Thomsen and Wallace	1994	C2	152.4	152.4	137	32	597	1.37	3.9
35	Soesianawati et al.	1986	No. 4	400	400	379	42	1600	1.14	4.0
36	Tanaka and Park	1990	No. 1	400	400	350	100	1600	1.56	4.0
37	Tanaka and Park	1990	No. 2	400	400	350	100	1600	1.56	4.0
38	Tanaka and Park	1990	No. 3	400	400	350	100	1600	1.56	4.0
39	Tanaka and Park	1990	No. 4	400	400	350	100	1600	1.56	4.0
40	Atalay and Penzien	1975	No. 11	305	305	262	86	1676	1.60	5.5
41	Atalay and Penzien	1975	No. 12	305	305	262	86	1676	1.60	5.5
42	Atalay and Penzien	1975	No. 5S1	305	305	262	86	1676	1.60	5.5
43	Atalay and Penzien	1975	No. 6S1	305	305	262	86	1676	1.60	5.5
44	Atalay and Penzien	1975	No. 10	305	305	262	86	1676	1.60	5.5
45	Atalay and Penzien	1975	No. 9	305	305	262	86	1676	1.60	5.5
46	Wehbe et al.	1998	A2	380	610	572	75	2335	1.29	3.8
47	Wehbe et al.	1998	B2	380	610	575	69	2335	1.25	3.8

No.	Researcher	Year	Specimen ID	Geometry						
				b [mm]	h [mm]	d [mm]	h_a [mm]	L [mm]	A_g/A_{core} [-]	a/d [-]
48	Azizinamini et al.	1988	NC-2	457	457	406	102	1372	1.44	3.0
49	Mo and Wang	2000	C1-3	400	400	356	87	1400	1.45	3.5
50	Mo and Wang	2000	C1-2	400	400	356	87	1400	1.45	3.5
51	Mo and Wang	2000	C2-3	400	400	356	87	1400	1.45	3.5
52	Mo and Wang	2000	C3-3	400	400	356	87	1400	1.45	3.5
53	Mo and Wang	2000	C2-2	400	400	356	87	1400	1.45	3.5
54	Zahn et al.	1986	No. 9	400	400	379	42	1600	1.14	4.0
55	Saatcioglu and Grira	1999	BG-3	350	350	311	78	1645	1.44	4.7
56	Saatcioglu and Grira	1999	BG-8	350	350	311	78	1645	1.44	4.7
57	Muguruma et al.	1989	BL-1	200	200	185	31	500	1.21	2.5
58	Soesianawati et al.	1986	No. 2	400	400	379	42	1600	1.14	4.0
59	Soesianawati et al.	1986	No. 3	400	400	379	42	1600	1.14	4.0
60	Galeota et al.	1996	AA4	250	250	215	70	1140	1.73	4.6
61	Galeota et al.	1996	BA1	250	250	215	70	1140	1.73	4.6
62	Galeota et al.	1996	BA4	250	250	215	70	1140	1.73	4.6
63	Galeota et al.	1996	CA1	250	250	215	70	1140	1.73	4.6
64	Galeota et al.	1996	CA3	250	250	215	70	1140	1.73	4.6
65	Galeota et al.	1996	BB1	250	250	210	80	1140	1.73	4.6
66	Galeota et al.	1996	BB2	250	250	210	80	1140	1.73	4.6
67	Galeota et al.	1996	CB1	250	250	210	80	1140	1.73	4.6
68	Galeota et al.	1996	CB2	250	250	210	80	1140	1.73	4.6
69	Galeota et al.	1996	BA2	250	250	215	70	1140	1.73	4.6
70	Galeota et al.	1996	BA3	250	250	215	70	1140	1.73	4.6
71	Galeota et al.	1996	CA2	250	250	215	70	1140	1.73	4.6

No.	Researcher	Year	Specimen ID	Geometry						
				b [mm]	h [mm]	d [mm]	h_a [mm]	L [mm]	A_g/A_{core} [-]	a/d [-]
72	Galeota et al.	1996	CA4	250	250	215	70	1140	1.73	4.6
73	Galeota et al.	1996	BB4	250	250	210	80	1140	1.73	4.6
74	Galeota et al.	1996	BB4B	250	250	210	80	1140	1.73	4.6
75	Galeota et al.	1996	CB3	250	250	210	80	1140	1.73	4.6
76	Galeota et al.	1996	CB4	250	250	210	80	1140	1.73	4.6
77	Matamoros et al.	1999	C10-20N	203	203	173	60	610	1.50	3.0
78	Matamoros et al.	1999	C10-20S	203	203	180	45	610	1.54	3.0
79	Muguruma et al.	1989	BH-1	200	200	185	31	500	1.21	2.5
80	Thomsen and Wallace	1994	A3	152.4	152.4	137	32	597	1.37	3.9
81	Thomsen and Wallace	1994	B3	152.4	152.4	137	32	597	1.37	3.9
82	Thomsen and Wallace	1994	D3	152.4	152.4	137	32	597	1.37	3.9
83	Thomsen and Wallace	1994	D1	152.4	152.4	137	32	597	1.37	3.9
84	Thomsen and Wallace	1994	C3	152.4	152.4	137	32	597	1.37	3.9
85	Thomsen and Wallace	1994	D2	152.4	152.4	137	32	597	1.37	3.9
86	Watson and Park	1989	No. 9	400	400	379	42	1600	1.14	4.0
87	Ang et al.	1981	No. 3	400	400	368	65	1600	1.30	4.0
88	Nosho et al.	1996	No. 1	279.4	279.4	246	67	2134	1.49	7.6
89	Watson and Park	1989	No. 5	400	400	379	42	1600	1.14	4.0
90	Watson and Park	1989	No. 6	400	400	379	42	1600	1.14	4.0
91	Zahn et al.	1986	No. 10	400	400	379	42	1600	1.14	4.0
92	Matamoros et al.	1999	C5-40N	203	203	174	57	610	1.52	3.0
93	Matamoros et al.	1999	C5-40S	203	203	174	57	610	1.58	3.0
94	Saatcioglu and Grira	1999	BG-1	350	350	311	78	1645	1.44	4.7
95	Saatcioglu and Grira	1999	BG-2	350	350	311	78	1645	1.44	4.7
96	Saatcioglu and Grira	1999	BG-6	350	350	306	88	1645	1.44	4.7

No.	Researcher	Year	Specimen ID	Geometry						
				b [mm]	h [mm]	d [mm]	h_a [mm]	L [mm]	A_g/A_{core} [-]	a/d [-]
97	Saatcioglu and Grira	1999	BG-4	350	350	311	78	1645	1.44	4.7
98	Saatcioglu and Grira	1999	BG-5	350	350	311	78	1645	1.44	4.7
99	Saatcioglu and Grira	1999	BG-10	350	350	313	74	1645	1.44	4.7
100	Saatcioglu and Grira	1999	BG-7	350	350	311	78	1645	1.44	4.7
101	Saatcioglu and Grira	1999	BG-9	350	350	313	74	1645	1.44	4.7
102	Azizinamini et al.	1988	NC-4	457	457	403	108	1372	1.49	3.0
103	Muguruma et al.	1989	AL-1	200	200	185	31	500	1.21	2.5
104	Muguruma et al.	1989	AL-2	200	200	185	31	500	1.21	2.5
105	Muguruma et al.	1989	BL-2	200	200	185	31	500	1.21	2.5
106	Bayrak and Sheikh	1996	AS-4HT	305	305	284	43	1842	1.17	4.8
107	Bayrak and Sheikh	1996	ES-1HT	305	305	284	43	1842	1.17	4.8
108	Bayrak and Sheikh	1996	AS-5HT	305	305	284	43	1842	1.17	4.8
109	Bayrak and Sheikh	1996	AS-6HT	305	305	284	43	1842	1.17	4.8
110	Bayrak and Sheikh	1996	ES-8HT	305	305	284	43	1842	1.17	4.8
111	Bayrak and Sheikh	1996	AS-2HT	305	305	281	48	1842	1.21	4.8
112	Bayrak and Sheikh	1996	AS-3HT	305	305	281	48	1842	1.21	4.8
113	Bayrak and Sheikh	1996	AS-7HT	305	305	281	48	1842	1.21	4.8
114	Muguruma et al.	1989	AH-1	200	200	185	31	500	1.21	2.5
115	Muguruma et. al	1989	AH-2	200	200	185	31	500	1.21	2.5
116	Muguruma et al.	1989	BH-2	200	200	185	31	500	1.21	2.5

No.	Researcher	Year	Specimen ID	f'_c [MPa]	Longitudinal reinforcement ρ_s [-]	Longitudinal reinforcement f_{sy} [MPa]	Web reinforcement ρ_w [-]	Web reinforcement f_{wy} [MPa]
1	Park and Paulay	1990	No. 9	27	0.019	432	0.0071	305
2	Ohno and Nishioka	1984	L2	25	0.014	362	0.0032	325
3	Ohno and Nishioka	1984	L3	25	0.014	362	0.0032	325
4	Atalay and Penzien	1975	No. 4S1	28	0.016	429	0.0037	363
5	Atalay and Penzien	1975	No. 1S1	29	0.016	367	0.0061	363
6	Atalay and Penzien	1975	No. 3S1	29	0.016	367	0.0061	363
7	Atalay and Penzien	1975	No. 2S1	31	0.016	367	0.0037	363
8	Saatcioglu and Ozcebe	1989	U6	37	0.032	437	0.0042	425
9	Saatcioglu and Ozcebe	1989	U7	39	0.032	437	0.0042	425
10	Wehbe et al.	1998	A1	27	0.022	448	0.0027	428
11	Wehbe et al.	1998	B1	28	0.022	448	0.0036	428
12	Mo and Wang	2000	C1-1	25	0.021	497	0.0063	459.5
13	Mo and Wang	2000	C2-1	25	0.021	497	0.0061	459.5
14	Mo and Wang	2000	C3-1	26	0.021	497	0.0059	459.5
15	Mo and Wang	2000	C3-2	27	0.021	497	0.0059	459.5
16	Saatcioglu and Ozcebe	1989	U4	32	0.032	438	0.0090	470
17	Saatcioglu and Ozcebe	1989	U3	35	0.032	430	0.0060	470
18	Kanda et al.	1987	85STC-1	28	0.016	374	0.0038	506
19	Kanda et al.	1987	85STC-2	28	0.016	374	0.0038	506
20	Kanda et al.	1987	85STC-3	28	0.016	374	0.0038	506
21	Matamoros et al.	1999	C5-00N	38	0.019	572	0.0092	513.7
22	Matamoros et al.	1999	C5-00S	38	0.019	573	0.0090	514.7
23	Soesianawati et al.	1986	No. 1	47	0.015	446	0.0045	364
24	Matamoros et al.	1999	C5-20N	48	0.019	586	0.0092	406.8
25	Matamoros et al.	1999	C10-05N	70	0.019	586	0.0092	406.8

No.	Researcher	Year	Specimen ID	f'_c [MPa]	Longitudinal reinforcement ρ_s [-]	Longitudinal reinforcement f_{sy} [MPa]	Web reinforcement ρ_w [-]	Web reinforcement f_{wy} [MPa]
26	Matamoros et al.	1999	C10-05S	70	0.019	586	0.0092	406.8
27	Matamoros et al.	1999	C5-20S	48	0.019	587	0.0090	407.8
28	Matamoros et al.	1999	C10-10N	68	0.019	572	0.0092	513.7
29	Matamoros et al.	1999	C10-10S	68	0.019	573	0.0090	514.7
30	Thomsen and Wallace	1994	B2	83	0.025	455	0.0082	793
31	Thomsen and Wallace	1994	B1	88	0.025	455	0.0082	793
32	Thomsen and Wallace	1994	A1	103	0.025	517	0.0061	793
33	Thomsen and Wallace	1994	C1	68	0.025	476	0.0082	1262
34	Thomsen and Wallace	1994	C2	75	0.025	476	0.0082	1262
35	Soesianawati et al.	1986	No. 4	40	0.015	446	0.0030	255
36	Tanaka and Park	1990	No. 1	26	0.016	474	0.0106	333
37	Tanaka and Park	1990	No. 2	26	0.016	474	0.0106	333
38	Tanaka and Park	1990	No. 3	26	0.016	474	0.0106	333
39	Tanaka and Park	1990	No. 4	26	0.016	474	0.0106	333
40	Atalay and Penzien	1975	No. 11	31	0.016	363	0.0061	373
41	Atalay and Penzien	1975	No. 12	32	0.016	363	0.0037	373
42	Atalay and Penzien	1975	No. 5S1	29	0.016	429	0.0061	392
43	Atalay and Penzien	1975	No. 6S1	32	0.016	429	0.0037	392
44	Atalay and Penzien	1975	No. 10	32	0.016	363	0.0037	392
45	Atalay and Penzien	1975	No. 9	33	0.016	363	0.0061	392
46	Wehbe et al.	1998	A2	27	0.022	448	0.0027	428
47	Wehbe et al.	1998	B2	28	0.022	448	0.0036	428
48	Azizinamini et al.	1988	NC-2	39	0.019	439	0.0131	454
49	Mo and Wang	2000	C1-3	26	0.021	497	0.0063	459.5

No.	Researcher	Year	Specimen ID	f'_c [MPa]	Longitudinal reinforcement ρ_s [-]	Longitudinal reinforcement f_{sy} [MPa]	Web reinforcement ρ_w [-]	Web reinforcement f_{wy} [MPa]
50	Mo and Wang	2000	C1-2	27	0.021	497	0.0063	459.5
51	Mo and Wang	2000	C2-3	27	0.021	497	0.0061	459.5
52	Mo and Wang	2000	C3-3	27	0.021	497	0.0059	459.5
53	Mo and Wang	2000	C2-2	27	0.021	497	0.0061	459.5
54	Zahn et al.	1986	No. 9	28	0.015	440	0.0067	466
55	Saatcioglu and Grira	1999	BG-3	34	0.020	456	0.0080	570
56	Saatcioglu and Grira	1999	BG-8	34	0.029	456	0.0051	580
57	Muguruma et al.	1989	BL-1	116	0.038	400	0.0162	328.4
58	Soesianawati et al.	1986	No. 2	44	0.015	446	0.0064	360
59	Soesianawati et al.	1986	No. 3	44	0.015	446	0.0042	364
60	Galeota et al.	1996	AA4	80	0.015	430	0.0054	430
61	Galeota et al.	1996	BA1	80	0.015	430	0.0080	430
62	Galeota et al.	1996	BA4	80	0.015	430	0.0080	430
63	Galeota et al.	1996	CA1	80	0.015	430	0.0161	430
64	Galeota et al.	1996	CA3	80	0.015	430	0.0161	430
65	Galeota et al.	1996	BB1	80	0.060	430	0.0080	430
66	Galeota et al.	1996	BB2	80	0.060	430	0.0080	430
67	Galeota et al.	1996	CB1	80	0.060	430	0.0161	430
68	Galeota et al.	1996	CB2	80	0.060	430	0.0161	430
69	Galeota et al.	1996	BA2	80	0.015	430	0.0080	430
70	Galeota et al.	1996	BA3	80	0.015	430	0.0080	430
71	Galeota et al.	1996	CA2	80	0.015	430	0.0161	430
72	Galeota et al.	1996	CA4	80	0.015	430	0.0161	430
73	Galeota et al.	1996	BB4	80	0.060	430	0.0080	430
74	Galeota et al.	1996	BB4B	80	0.060	430	0.0080	430
75	Galeota et al.	1996	CB3	80	0.060	430	0.0161	430
76	Galeota et al.	1996	CB4	80	0.060	430	0.0161	430
77	Matamoros et al.	1999	C10-20N	66	0.019	572	0.0092	513.7
78	Matamoros et al.	1999	C10-20S	66	0.019	573	0.0090	514.7
79	Muguruma et al.	1989	BH-1	116	0.038	400	0.0162	792.3
80	Thomsen and Wallace	1994	A3	86	0.025	517	0.0061	793

No.	Researcher	Year	Specimen ID	f'_c [MPa]	Longitudinal reinforcement ρ_s [-]	Longitudinal reinforcement f_{sy} [MPa]	Web reinforcement ρ_w [-]	Web reinforcement f_{wy} [MPa]
81	Thomsen and Wallace	1994	B3	90	0.025	455	0.0082	793
82	Thomsen and Wallace	1994	D3	71	0.025	476	0.0047	1262
83	Thomsen and Wallace	1994	D1	76	0.025	476	0.0065	1262
84	Thomsen and Wallace	1994	C3	82	0.025	476	0.0082	1262
85	Thomsen and Wallace	1994	D2	87	0.025	476	0.0055	1262
86	Watson and Park	1989	No. 9	40	0.015	474	0.0217	308
87	Ang et al.	1981	No. 3	24	0.015	427	0.0113	320
88	Nosho et al.	1996	No. 1	41	0.010	407	0.0010	351
89	Watson and Park	1989	No. 5	41	0.015	474	0.0062	372
90	Watson and Park	1989	No. 6	40	0.015	474	0.0029	388
91	Zahn et al.	1986	No. 10	40	0.015	440	0.0085	466
92	Matamoros et al.	1999	C5-40N	38	0.019	572	0.0092	513.7
93	Matamoros et al.	1999	C5-40S	38	0.019	573	0.0090	514.7
94	Saatcioglu and Grira	1999	BG-1	34	0.020	456	0.0040	570
95	Saatcioglu and Grira	1999	BG-2	34	0.020	456	0.0080	570
96	Saatcioglu and Grira	1999	BG-6	34	0.023	478	0.0107	570
97	Saatcioglu and Grira	1999	BG-4	34	0.029	456	0.0054	570
98	Saatcioglu and Grira	1999	BG-5	34	0.029	456	0.0107	570
99	Saatcioglu and Grira	1999	BG-10	34	0.033	428	0.0107	570
100	Saatcioglu and Grira	1999	BG-7	34	0.029	456	0.0051	580
101	Saatcioglu and Grira	1999	BG-9	34	0.033	428	0.0051	580
102	Azizinamini et al.	1988	NC-4	40	0.019	439	0.0073	616
103	Muguruma et al.	1989	AL-1	86	0.038	400	0.0162	328.4
104	Muguruma et al.	1989	AL-2	86	0.038	400	0.0162	328.4
105	Muguruma et al.	1989	BL-2	116	0.038	400	0.0162	328.4

No.	Researcher	Year	Specimen ID	f'_c [MPa]	Longitudinal reinforcement ρ_s [-]	Longitudinal reinforcement f_{sy} [MPa]	Web reinforcement ρ_w [-]	Web reinforcement f_{wy} [MPa]
106	Bayrak and Sheikh	1996	AS-4HT	72	0.027	454	0.0232	463
107	Bayrak and Sheikh	1996	ES-1HT	72	0.027	454	0.0122	463
108	Bayrak and Sheikh	1996	AS-5HT	102	0.027	454	0.0258	463
109	Bayrak and Sheikh	1996	AS-6HT	102	0.027	454	0.0305	463
110	Bayrak and Sheikh	1996	ES-8HT	102	0.027	454	0.0166	463
111	Bayrak and Sheikh	1996	AS-2HT	72	0.027	454	0.0114	542
112	Bayrak and Sheikh	1996	AS-3HT	72	0.027	454	0.0114	542
113	Bayrak and Sheikh	1996	AS-7HT	102	0.027	454	0.0110	542
114	Muguruma et al.	1989	AH-1	86	0.038	400	0.0162	792.3
115	Muguruma et. al	1989	AH-2	86	0.038	400	0.0162	792.3
116	Muguruma et al.	1989	BH-2	116	0.038	400	0.0162	792.3

No.	Researcher	Year	Specimen ID	Axial Load		Maximum capacity		Yield capacity	
				P [kN]	P / ($A_g f'_c$) [-]	V_{max} [kN]	80% V_{max} [kN]	$M_{y,flex}$ [kNmm]	$V_{y,flex}$ [kN]
1	Park and Paulay	1990	No. 9	646	0.10	395	314	664,834	373
2	Ohno and Nishioka	1984	L2	127	0.03	109	84	161,633	101
3	Ohno and Nishioka	1984	L3	127	0.03	110	81	161,633	101
4	Atalay and Penzien	1975	No. 4S1	267	0.10	71	39	106,355	63
5	Atalay and Penzien	1975	No. 1S1	267	0.10	62	46	96,912	58
6	Atalay and Penzien	1975	No. 3S1	267	0.10	60	46	96,944	58
7	Atalay and Penzien	1975	No. 2S1	267	0.09	61	43	97,418	58
8	Saatcioglu and Ozcebe	1989	U6	600	0.13	343	259	295,843	296
9	Saatcioglu and Ozcebe	1989	U7	600	0.13	342	262	298,677	299
10	Wehbe et al.	1998	A1	615	0.10	337	261	538,297	231
11	Wehbe et al.	1998	B1	601	0.09	345	271	543,008	233
12	Mo and Wang	2000	C1-1	450	0.11	249	199	303,535	217
13	Mo and Wang	2000	C2-1	450	0.11	241	191	304,305	217
14	Mo and Wang	2000	C3-1	450	0.11	235	188	306,338	219
15	Mo and Wang	2000	C3-2	675	0.15	260	208	328,859	235
16	Saatcioglu and Ozcebe	1989	U4	600	0.15	326	244	293,086	293
17	Saatcioglu and Ozcebe	1989	U3	600	0.14	271	214	296,017	296
18	Kanda et al.	1987	85STC-1	184	0.11	82	61	51,458	69
19	Kanda et al.	1987	85STC-2	184	0.11	80	61	51,458	69
20	Kanda et al.	1987	85STC-3	184	0.11	82	61	51,458	69
21	Matamoros et al.	1999	C5-00N	0	0.00	59	46	37,530	62
22	Matamoros et al.	1999	C5-00S	0	0.00	58	45	38,217	63
23	Soesianawati et al.	1986	No. 1	744	0.10	200	149	306,830	192
24	Matamoros et al.	1999	C5-20N	285	0.14	73	57	52,283	86
25	Matamoros et al.	1999	C10-05N	142	0.05	70	53	46,210	76

No.	Researcher	Year	Specimen ID	Axial Load		Maximum capacity		Yield capacity	
				P [kN]	$P/(A_g f'_c)$ [-]	V_{max} [kN]	80% V_{max} [kN]	$M_{y,flex}$ [kNmm]	$V_{y,flex}$ [kN]
26	Matamoros et al.	1999	C10-05S	142	0.05	68	53	45,940	75
27	Matamoros et al.	1999	C5-20S	285	0.14	73	56	51,789	85
28	Matamoros et al.	1999	C10-10N	285	0.10	96	75	59,755	98
29	Matamoros et al.	1999	C10-10S	285	0.10	94	74	59,814	98
30	Thomsen and Wallace	1994	B2	194	0.10	53	38	28,205	47
31	Thomsen and Wallace	1994	B1	0	0.00	41	26	17,024	29
32	Thomsen and Wallace	1994	A1	0	0.00	46	35	19,391	32
33	Thomsen and Wallace	1994	C1	0	0.00	40	30	17,472	29
34	Thomsen and Wallace	1994	C2	173	0.10	49	35	27,450	46
35	Soesianawati et al.	1986	No. 4	1920	0.30	265	190	388,198	243
36	Tanaka and Park	1990	No. 1	819	0.20	167	133	268,566	168
37	Tanaka and Park	1990	No. 2	819	0.20	168	128	268,566	168
38	Tanaka and Park	1990	No. 3	819	0.20	175	136	268,566	168
39	Tanaka and Park	1990	No. 4	819	0.20	170	134	268,566	168
40	Atalay and Penzien	1975	No. 11	801	0.28	82	62	142,603	85
41	Atalay and Penzien	1975	No. 12	801	0.27	79	62	143,625	86
42	Atalay and Penzien	1975	No. 5S1	534	0.20	77	59	131,697	79
43	Atalay and Penzien	1975	No. 6S1	534	0.18	75	56	133,276	80
44	Atalay and Penzien	1975	No. 10	801	0.27	78	61	144,358	86
45	Atalay and Penzien	1975	No. 9	801	0.26	79	63	145,409	87
46	Wehbe et al.	1998	A2	1505	0.24	361	276	654,226	280
47	Wehbe et al.	1998	B2	1514	0.23	372	298	666,256	285
48	Azizinamini et al.	1988	NC-2	1690	0.21	441	323	552,546	403
49	Mo and Wang	2000	C1-3	900	0.22	305	244	334,375	239

No.	Researcher	Year	Specimen ID	Axial Load		Maximum capacity		Yield capacity	
				P [kN]	$P / (A_g f'_c)$ [-]	V_{max} [kN]	80% V_{max} [kN]	$M_{y,flex}$ [kNmm]	$V_{y,flex}$ [kN]
50	Mo and Wang	2000	C1-2	675	0.16	261	209	326,215	233
51	Mo and Wang	2000	C2-3	900	0.21	304	243	336,951	241
52	Mo and Wang	2000	C3-3	900	0.21	300	240	337,471	241
53	Mo and Wang	2000	C2-2	675	0.16	261	208	327,894	234
54	Zahn et al.	1986	No. 9	1010	0.22	213	157	303,055	189
55	Saatcioglu and Grira	1999	BG-3	831	0.20	152	111	232,633	141
56	Saatcioglu and Grira	1999	BG-8	961	0.23	183	146	291,514	177
57	Muguruma et al.	1989	BL-1	1176	0.25	255	193	120,828	242
58	Soesianawati et al.	1986	No. 2	2112	0.30	279	200	412,377	258
59	Soesianawati et al.	1986	No. 3	2112	0.30	277	214	412,377	258
60	Galeota et al.	1996	AA4	1000	0.20	138	105	125,404	110
61	Galeota et al.	1996	BA1	1000	0.20	141	109	125,404	110
62	Galeota et al.	1996	BA4	1000	0.20	110	84	125,404	110
63	Galeota et al.	1996	CA1	1000	0.20	101	80	125,404	110
64	Galeota et al.	1996	CA3	1000	0.20	132	101	125,404	110
65	Galeota et al.	1996	BB1	1000	0.20	162	126	199,715	175
66	Galeota et al.	1996	BB2	1000	0.20	195	150	199,715	175
67	Galeota et al.	1996	CB1	1000	0.20	172	133	199,715	175
68	Galeota et al.	1996	CB2	1000	0.20	173	134	199,715	175
69	Galeota et al.	1996	BA2	1500	0.30	128	100	145,410	128
70	Galeota et al.	1996	BA3	1500	0.30	131	105	145,410	128
71	Galeota et al.	1996	CA2	1500	0.30	126	101	145,410	128
72	Galeota et al.	1996	CA4	1500	0.30	135	100	145,410	128
73	Galeota et al.	1996	BB4	1500	0.30	175	139	209,275	184
74	Galeota et al.	1996	BB4B	1500	0.30	171	134	209,275	184
75	Galeota et al.	1996	CB3	1500	0.30	170	133	209,275	184
76	Galeota et al.	1996	CB4	1500	0.30	177	138	209,275	184
77	Matamoros et al.	1999	C10-20N	569	0.21	108	81	77,798	128
78	Matamoros et al.	1999	C10-20S	569	0.21	104	81	73,538	121
79	Muguruma et al.	1989	BH-1	1176	0.25	256	197	120,828	242
80	Thomsen and Wallace	1994	A3	401	0.20	67	42	37,360	63

No.	Researcher	Year	Specimen ID	Axial Load		Maximum capacity		Yield capacity	
				P [kN]	$P/(A_g f'_c)$ [-]	V_{max} [kN]	80% V_{max} [kN]	$M_{y,flex}$ [kNmm]	$V_{y,flex}$ [kN]
81	Thomsen and Wallace	1994	B3	418	0.20	61	46	37,151	62
82	Thomsen and Wallace	1994	D3	331	0.20	50	39	32,393	54
83	Thomsen and Wallace	1994	D1	352	0.20	53	42	33,659	56
84	Thomsen and Wallace	1994	C3	380	0.20	53	40	35,309	59
85	Thomsen and Wallace	1994	D2	404	0.20	58	43	36,737	62
86	Watson and Park	1989	No. 9	4480	0.70	310	216	298,137	186
87	Ang et al.	1981	No. 3	1435	0.38	192	149	280,083	175
88	Nosho et al.	1996	No. 1	1076	0.34	66	44	124,600	58
89	Watson and Park	1989	No. 5	3280	0.50	292	225	384,590	240
90	Watson and Park	1989	No. 6	3200	0.50	295	229	378,693	237
91	Zahn et al.	1986	No. 10	2502	0.39	269	207	395,510	247
92	Matamoros et al.	1999	C5-40N	569	0.36	85	64	58,382	96
93	Matamoros et al.	1999	C5-40S	569	0.36	85	62	56,364	92
94	Saatcioglu and Grira	1999	BG-1	1782	0.43	172	138	250,044	152
95	Saatcioglu and Grira	1999	BG-2	1782	0.43	169	134	250,044	152
96	Saatcioglu and Grira	1999	BG-6	1900	0.46	190	143	295,925	180
97	Saatcioglu and Grira	1999	BG-4	1923	0.46	185	142	287,091	175
98	Saatcioglu and Grira	1999	BG-5	1923	0.46	212	141	287,091	175
99	Saatcioglu and Grira	1999	BG-10	1923	0.46	202	139	246,038	150
100	Saatcioglu and Grira	1999	BG-7	1923	0.46	186	143	287,091	175
101	Saatcioglu and Grira	1999	BG-9	1923	0.46	197	151	246,038	150
102	Azizinamini et al.	1988	NC-4	2580	0.31	489	386	609,163	444
103	Muguruma et al.	1989	AL-1	1371	0.40	243	191	102,091	204
104	Muguruma et al.	1989	AL-2	2156	0.63	242	189	88,124	176

No.	Researcher	Year	Specimen ID	Axial Load		Maximum capacity		Yield capacity	
				P [kN]	P / ($A_g f'_c$) [-]	V_{max} [kN]	80% V_{max} [kN]	$M_{y,flex}$ [kNmm]	$V_{y,flex}$ [kN]
105	Muguruma et al.	1989	BL-2	1959	0.42	289	227	126,402	253
106	Bayrak and Sheikh	1996	AS-4HT	3344	0.50	148	111	287,148	156
107	Bayrak and Sheikh	1996	ES-1HT	3354	0.50	147	109	287,731	156
108	Bayrak and Sheikh	1996	AS-5HT	4261	0.45	199	146	383,059	208
109	Bayrak and Sheikh	1996	AS-6HT	4360	0.46	197	136	382,067	207
110	Bayrak and Sheikh	1996	ES-8HT	4468	0.47	178	135	381,506	207
111	Bayrak and Sheikh	1996	AS-2HT	2401	0.36	149	119	298,516	162
112	Bayrak and Sheikh	1996	AS-3HT	3340	0.50	148	115	284,969	155
113	Bayrak and Sheikh	1996	AS-7HT	4270	0.45	172	127	381,571	207
114	Muguruma et al.	1989	AH-1	1371	0.40	244	195	102,091	204
115	Muguruma et. al	1989	AH-2	2156	0.63	247	194	88,124	176
116	Muguruma et al.	1989	BH-2	1959	0.42	288	230	126,402	253

No.	Researcher	Year	Specimen ID	Δ_y [mm]	$\delta_y = \Delta_y/L$ [-]	Δ_u [mm]	$\Delta_s = \Delta_u - \Delta_y$ [mm]	Δ_s / Δ_u [-]	m = 0.2/ (Δ_s/L) [-]
1	Park and Paulay	1990	No. 9	16	0.047	84	68.1	0.81	5.24
2	Ohno and Nishioka	1984	L2	10	0.046	74	63.4	0.86	5.05
3	Ohno and Nishioka	1984	L3	9	0.046	73	63.6	0.87	5.03
4	Atalay and Penzien	1975	No. 4S1	15	0.036	61	46.0	0.75	7.29
5	Atalay and Penzien	1975	No. 1S1	15	0.049	81	66.7	0.82	5.03
6	Atalay and Penzien	1975	No. 3S1	14	0.048	81	67.8	0.83	4.95
7	Atalay and Penzien	1975	No. 2S1	15	0.048	81	65.9	0.81	5.09
8	Saatcioglu and Ozcebe	1989	U6	18	0.090	90	72.0	0.80	2.78
9	Saatcioglu and Ozcebe	1989	U7	18	0.088	88	70.0	0.80	2.86
10	Wehbe et al.	1998	A1	32	0.052	121	89.6	0.74	5.21
11	Wehbe et al.	1998	B1	35	0.069	161	126.5	0.79	3.69
12	Mo and Wang	2000	C1-1	26	0.061	85	58.9	0.69	4.76
13	Mo and Wang	2000	C2-1	37	0.070	99	61.9	0.63	4.52
14	Mo and Wang	2000	C3-1	33	0.070	98	64.4	0.66	4.35
15	Mo and Wang	2000	C3-2	24	0.071	100	75.9	0.76	3.69
16	Saatcioglu and Ozcebe	1989	U4	19	0.090	90	70.6	0.78	2.83
17	Saatcioglu and Ozcebe	1989	U3	14	0.051	51	36.8	0.72	5.43
18	Kanda et al.	1987	85STC-1	7	0.046	35	28.0	0.81	5.36
19	Kanda et al.	1987	85STC-2	5	0.046	35	29.9	0.87	5.02
20	Kanda et al.	1987	85STC-3	7	0.046	35	27.5	0.80	5.45
21	Matamoros et al.	1999	C5-00N	9	0.066	40	31.7	0.78	3.85
22	Matamoros et al.	1999	C5-00S	9	0.066	40	31.9	0.79	3.82
23	Soesianawati et al.	1986	No. 1	10	0.061	98	87.6	0.90	3.65
24	Matamoros et al.	1999	C5-20N	6	0.043	26	19.9	0.77	6.12
25	Matamoros et al.	1999	C10-05N	8	0.052	32	24.1	0.76	5.05

No.	Researcher	Year	Specimen ID	Δ_y [mm]	$\delta_y = \Delta_y/L$ [-]	Δ_u [mm]	$\Delta_s = \Delta_u - \Delta_y$ [mm]	Δ_s / Δ_u [-]	$m = 0.2/(\Delta_s/L)$ [-]
26	Matamoros et al.	1999	C10-05S	8	0.056	34	26.3	0.77	4.63
27	Matamoros et al.	1999	C5-20S	6	0.041	25	19.5	0.77	6.25
28	Matamoros et al.	1999	C10-10N	7	0.062	38	31.3	0.82	3.90
29	Matamoros et al.	1999	C10-10S	7	0.060	36	29.3	0.80	4.17
30	Thomsen and Wallace	1994	B2	3	0.027	16	12.8	0.81	9.30
31	Thomsen and Wallace	1994	B1	7	0.043	26	18.8	0.73	6.34
32	Thomsen and Wallace	1994	A1	10	0.047	28	17.7	0.63	6.75
33	Thomsen and Wallace	1994	C1	10	0.046	27	17.1	0.63	6.98
34	Thomsen and Wallace	1994	C2	4	0.029	17	12.7	0.74	9.44
35	Soesianawati et al.	1986	No. 4	9	0.017	27	17.9	0.66	17.88
36	Tanaka and Park	1990	No. 1	11	0.041	66	55.7	0.84	5.75
37	Tanaka and Park	1990	No. 2	13	0.039	63	49.7	0.79	6.44
38	Tanaka and Park	1990	No. 3	10	0.037	59	48.5	0.83	6.59
39	Tanaka and Park	1990	No. 4	12	0.043	70	57.9	0.83	5.53
40	Atalay and Penzien	1975	No. 11	12	0.018	30	18.2	0.60	18.44
41	Atalay and Penzien	1975	No. 12	12	0.026	43	30.9	0.72	10.86
42	Atalay and Penzien	1975	No. 5S1	16	0.030	50	33.7	0.67	9.95
43	Atalay and Penzien	1975	No. 6S1	16	0.030	50	33.9	0.68	9.89
44	Atalay and Penzien	1975	No. 10	14	0.024	41	26.6	0.66	12.58
45	Atalay and Penzien	1975	No. 9	16	0.018	30	14.4	0.47	23.31
46	Wehbe et al.	1998	A2	25	0.043	100	75.4	0.75	6.19
47	Wehbe et al.	1998	B2	28	0.053	124	96.3	0.78	4.85
48	Azizinamini et al.	1988	NC-2	9	0.035	48	39.2	0.81	7.00
49	Mo and Wang	2000	C1-3	20	0.059	82	62.6	0.76	4.47

No.	Researcher	Year	Specimen ID	Δ_y [mm]	$\delta_y = \Delta_y/L$ [-]	Δ_u [mm]	$\Delta_s = \Delta_u - \Delta_y$ [mm]	Δ_s / Δ_u [-]	m = 0.2/ (Δ_s/L) [-]
50	Mo and Wang	2000	C1-2	22	0.067	93	71.4	0.76	3.92
51	Mo and Wang	2000	C2-3	22	0.067	93	71.3	0.76	3.93
52	Mo and Wang	2000	C3-3	32	0.063	89	57.1	0.64	4.90
53	Mo and Wang	2000	C2-2	30	0.070	98	68.1	0.69	4.11
54	Zahn et al.	1986	No. 9	15	0.054	86	71.0	0.83	4.51
55	Saatcioglu and Grira	1999	BG-3	13	0.046	75	62.6	0.83	5.25
56	Saatcioglu and Grira	1999	BG-8	21	0.049	81	60.2	0.74	5.47
57	Muguruma et al.	1989	BL-1	2	0.057	28	26.0	0.92	3.85
58	Soesianawati et al.	1986	No. 2	10	0.021	34	23.7	0.71	13.50
59	Soesianawati et al.	1986	No. 3	9	0.019	30	21.6	0.71	14.81
60	Galeota et al.	1996	AA4	8	0.014	16	7.6	0.48	30.06
61	Galeota et al.	1996	BA1	9	0.018	20	11.5	0.57	19.85
62	Galeota et al.	1996	BA4	11	0.020	23	12.7	0.55	17.89
63	Galeota et al.	1996	CA1	10	0.019	22	12.1	0.56	18.81
64	Galeota et al.	1996	CA3	9	0.025	28	19.3	0.68	11.79
65	Galeota et al.	1996	BB1	15	0.042	47	32.1	0.68	7.09
66	Galeota et al.	1996	BB2	13	0.038	44	30.6	0.70	7.44
67	Galeota et al.	1996	CB1	16	0.054	62	45.9	0.75	4.97
68	Galeota et al.	1996	CB2	15	0.050	57	41.9	0.74	5.44
69	Galeota et al.	1996	BA2	10	0.018	21	10.7	0.51	21.38
70	Galeota et al.	1996	BA3	8	0.016	18	10.0	0.56	22.78
71	Galeota et al.	1996	CA2	9	0.021	24	14.6	0.61	15.67
72	Galeota et al.	1996	CA4	9	0.025	29	19.8	0.69	11.49
73	Galeota et al.	1996	BB4	13	0.044	50	36.8	0.74	6.20
74	Galeota et al.	1996	BB4B	13	0.036	41	28.0	0.69	8.14
75	Galeota et al.	1996	CB3	13	0.049	56	43.4	0.77	5.26
76	Galeota et al.	1996	CB4	14	0.045	51	37.6	0.73	6.07
77	Matamoros et al.	1999	C10-20N	7	0.052	32	25.0	0.79	4.88
78	Matamoros et al.	1999	C10-20S	7	0.052	32	24.6	0.78	4.97
79	Muguruma et al.	1989	BH-1	3	0.065	32	29.3	0.90	3.41
80	Thomsen and Wallace	1994	A3	5	0.020	12	7.0	0.57	17.17

No.	Researcher	Year	Specimen ID	Δ_y [mm]	$\delta_y = \Delta_y/L$ [-]	Δ_u [mm]	$\Delta_s = \Delta_u - \Delta_y$ [mm]	Δ_s / Δ_u [-]	m = 0.2/ (Δ_s/L) [-]
81	Thomsen and Wallace	1994	B3	3	0.017	10	7.0	0.68	16.95
82	Thomsen and Wallace	1994	D3	4	0.019	11	7.6	0.68	15.74
83	Thomsen and Wallace	1994	D1	4	0.020	12	8.6	0.71	13.83
84	Thomsen and Wallace	1994	C3	3	0.019	12	8.2	0.71	14.64
85	Thomsen and Wallace	1994	D2	6	0.018	11	5.3	0.48	22.70
86	Watson and Park	1989	No. 9	7	0.024	38	30.9	0.81	10.36
87	Ang et al.	1981	No. 3	10	0.028	45	35.3	0.79	9.06
88	Nosho et al.	1996	No. 1	17	0.016	34	17.7	0.51	24.18
89	Watson and Park	1989	No. 5	9	0.021	34	24.5	0.73	13.05
90	Watson and Park	1989	No. 6	8	0.016	25	17.6	0.70	18.14
91	Zahn et al.	1986	No. 10	12	0.031	50	37.4	0.76	8.55
92	Matamoros et al.	1999	C5-40N	5	0.042	26	20.4	0.80	5.97
93	Matamoros et al.	1999	C5-40S	5	0.041	25	20.3	0.81	6.00
94	Saatcioglu and Grira	1999	BG-1	6	0.020	33	27.0	0.82	12.18
95	Saatcioglu and Grira	1999	BG-2	7	0.026	43	36.2	0.84	9.08
96	Saatcioglu and Grira	1999	BG-6	12	0.037	61	49.6	0.81	6.64
97	Saatcioglu and Grira	1999	BG-4	16	0.025	41	25.0	0.61	13.17
98	Saatcioglu and Grira	1999	BG-5	12	0.031	50	38.5	0.77	8.53
99	Saatcioglu and Grira	1999	BG-10	13	0.042	68	55.4	0.81	5.94
100	Saatcioglu and Grira	1999	BG-7	12	0.036	59	47.5	0.80	6.92
101	Saatcioglu and Grira	1999	BG-9	17	0.031	51	34.6	0.67	9.50
102	Azizinamini et al.	1988	NC-4	9	0.028	38	29.3	0.76	9.37
103	Muguruma et al.	1989	AL-1	5	0.057	28	23.5	0.83	4.25
104	Muguruma et al.	1989	AL-2	3	0.021	11	8.0	0.76	12.48

No.	Researcher	Year	Specimen ID	Δ_y [mm]	$\delta_y = \Delta_y/L$ [-]	Δ_u [mm]	$\Delta_s = \Delta_u - \Delta_y$ [mm]	Δ_s / Δ_u [-]	$m = 0.2/(\Delta_s/L)$ [-]
105	Muguruma et al.	1989	BL-2	4	0.035	17	13.6	0.79	7.37
106	Bayrak and Sheikh	1996	AS-4HT	8	0.026	48	40.3	0.84	9.13
107	Bayrak and Sheikh	1996	ES-1HT	5	0.018	33	28.5	0.86	12.93
108	Bayrak and Sheikh	1996	AS-5HT	4	0.008	15	11.0	0.74	33.60
109	Bayrak and Sheikh	1996	AS-6HT	9	0.020	37	28.8	0.77	12.81
110	Bayrak and Sheikh	1996	ES-8HT	6	0.013	23	17.6	0.75	20.93
111	Bayrak and Sheikh	1996	AS-2HT	8	0.024	44	35.2	0.81	10.46
112	Bayrak and Sheikh	1996	AS-3HT	6	0.017	32	25.5	0.80	14.42
113	Bayrak and Sheikh	1996	AS-7HT	8	0.015	27	19.4	0.71	18.95
114	Muguruma et al.	1989	AH-1	5	0.072	36	30.7	0.86	3.26
115	Muguruma et. al	1989	AH-2	3	0.044	22	19.0	0.87	5.25
116	Muguruma et al.	1989	BH-2	3	0.054	27	24.0	0.89	4.17

No.	Researcher	Year	Specimen ID	$V_{n,shear}$ [kN]	$V_{mes} / V_{y,flex}$ [-]	m Eq. (8.9) [-]	m_{mes} / m_{cal} [-]
1	Park and Paulay	1990	No. 9	693.7	1.06	3.94	1.33
2	Ohno and Nishioka	1984	L2	268.9	1.08	3.68	1.37
3	Ohno and Nishioka	1984	L3	268.8	1.09	3.68	1.37
4	Atalay and Penzien	1975	No. 4S1	195.7	1.12	4.56	1.60
5	Atalay and Penzien	1975	No. 1S1	304.3	1.07	3.99	1.26
6	Atalay and Penzien	1975	No. 3S1	304.4	1.03	3.99	1.24
7	Atalay and Penzien	1975	No. 2S1	196.2	1.05	4.51	1.13
8	Saatcioglu and Ozcebe	1989	U6	290.3	1.16	4.93	0.56
9	Saatcioglu and Ozcebe	1989	U7	292.1	1.14	4.89	0.58
10	Wehbe et al.	1998	A1	451.0	1.46	4.57	1.14
11	Wehbe et al.	1998	B1	577.6	1.48	4.29	0.86
12	Mo and Wang	2000	C1-1	655.5	1.15	3.41	1.40
13	Mo and Wang	2000	C2-1	634.5	1.11	3.51	1.29
14	Mo and Wang	2000	C3-1	616.5	1.07	3.61	1.20
15	Mo and Wang	2000	C3-2	612.6	1.10	4.20	0.88
16	Saatcioglu and Ozcebe	1989	U4	586.9	1.11	3.49	0.81
17	Saatcioglu and Ozcebe	1989	U3	416.8	0.92	4.41	1.23
18	Kanda et al.	1987	85STC-1	152.0	1.19	4.20	1.27
19	Kanda et al.	1987	85STC-2	152.1	1.17	4.20	1.19
20	Kanda et al.	1987	85STC-3	152.0	1.19	4.20	1.30
21	Matamoros et al.	1999	C5-00N	232.4	0.96	2.20	1.75
22	Matamoros et al.	1999	C5-00S	225.2	0.93	2.22	1.72
23	Soesianawati et al.	1986	No. 1	446.5	1.04	4.74	0.77
24	Matamoros et al.	1999	C5-20N	166.7	0.85	4.51	1.36
25	Matamoros et al.	1999	C10-05N	172.5	0.93	3.74	1.35

No.	Researcher	Year	Specimen ID	$V_{n,shear}$ [kN]	$V_{mes} / V_{y,flex}$ [-]	m Eq. (8.9) [-]	m_{mes} / m_{cal} [-]
26	Matamoros et al.	1999	C10-05S	172.8	0.90	3.74	1.24
27	Matamoros et al.	1999	C5-20S	164.3	0.85	4.52	1.38
28	Matamoros et al.	1999	C10-10N	229.6	0.98	4.15	0.94
29	Matamoros et al.	1999	C10-10S	230.3	0.96	4.17	1.00
30	Thomsen and Wallace	1994	B2	214.1	1.11	3.98	2.34
31	Thomsen and Wallace	1994	B1	224.1	1.42	2.82	2.24
32	Thomsen and Wallace	1994	A1	170.3	1.43	3.16	2.14
33	Thomsen and Wallace	1994	C1	330.1	1.37	1.84	3.80
34	Thomsen and Wallace	1994	C2	328.0	1.06	2.89	3.26
35	Soesianawati et al.	1986	No. 4	291.0	1.09	8.06	2.22
36	Tanaka and Park	1990	No. 1	770.3	1.00	3.78	1.52
37	Tanaka and Park	1990	No. 2	770.2	1.00	3.78	1.71
38	Tanaka and Park	1990	No. 3	769.5	1.04	3.78	1.75
39	Tanaka and Park	1990	No. 4	770.0	1.02	3.78	1.46
40	Atalay and Penzien	1975	No. 11	310.5	0.97	6.23	2.96
41	Atalay and Penzien	1975	No. 12	213.2	0.92	6.97	1.56
42	Atalay and Penzien	1975	No. 5S1	323.8	0.98	5.03	1.98
43	Atalay and Penzien	1975	No. 6S1	215.8	0.94	5.67	1.74
44	Atalay and Penzien	1975	No. 10	220.8	0.91	6.87	1.83
45	Atalay and Penzien	1975	No. 9	324.9	0.91	6.03	3.86
46	Wehbe et al.	1998	A2	474.5	1.29	6.54	0.95
47	Wehbe et al.	1998	B2	590.0	1.31	6.15	0.79
48	Azizinamini et al.	1988	NC-2	1417.1	1.10	3.51	2.00
49	Mo and Wang	2000	C1-3	643.8	1.28	4.55	0.98

No.	Researcher	Year	Specimen ID	$V_{n,shear}$ [kN]	V_{mes} / $V_{y,flex}$ [-]	m Eq. (8.9) [-]	m_{mes} / m_{cal} [-]
50	Mo and Wang	2000	C1-2	652.9	1.12	4.02	0.98
51	Mo and Wang	2000	C2-3	624.2	1.26	4.66	0.84
52	Mo and Wang	2000	C3-3	605.0	1.24	4.75	1.03
53	Mo and Wang	2000	C2-2	632.0	1.11	4.11	1.00
54	Zahn et al.	1986	No. 9	752.2	1.13	4.65	0.97
55	Saatcioglu and Grira	1999	BG-3	771.2	1.07	3.84	1.37
56	Saatcioglu and Grira	1999	BG-8	524.9	1.04	5.30	1.03
57	Muguruma et al.	1989	BL-1	209.7	1.05	6.66	0.58
58	Soesianawati et al.	1986	No. 2	602.0	1.08	7.10	1.90
59	Soesianawati et al.	1986	No. 3	450.1	1.07	7.61	1.95
60	Galeota et al.	1996	AA4	226.9	1.25	6.32	4.76
61	Galeota et al.	1996	BA1	310.0	1.28	5.98	3.32
62	Galeota et al.	1996	BA4	310.0	1.00	5.98	2.99
63	Galeota et al.	1996	CA1	559.4	0.92	4.98	3.78
64	Galeota et al.	1996	CA3	559.4	1.20	4.98	2.37
65	Galeota et al.	1996	BB1	301.2	0.92	5.98	1.19
66	Galeota et al.	1996	BB2	300.3	1.11	5.98	1.24
67	Galeota et al.	1996	CB1	534.4	0.98	4.98	1.00
68	Galeota et al.	1996	CB2	534.3	0.99	4.98	1.09
69	Galeota et al.	1996	BA2	304.9	1.01	7.37	2.90
70	Galeota et al.	1996	BA3	304.9	1.03	7.37	3.09
71	Galeota et al.	1996	CA2	527.4	0.99	6.13	2.56
72	Galeota et al.	1996	CA4	527.4	1.06	6.13	1.87
73	Galeota et al.	1996	BB4	298.1	0.95	7.37	0.84
74	Galeota et al.	1996	BB4B	298.1	0.93	7.37	1.10
75	Galeota et al.	1996	CB3	515.4	0.93	6.13	0.86
76	Galeota et al.	1996	CB4	515.4	0.96	6.13	0.99
77	Matamoros et al.	1999	C10-20N	221.5	0.84	5.45	0.90
78	Matamoros et al.	1999	C10-20S	228.8	0.86	5.47	0.91
79	Muguruma et al.	1989	BH-1	459.2	1.06	4.97	0.69
80	Thomsen and Wallace	1994	A3	159.0	1.07	5.68	3.02

No.	Researcher	Year	Specimen ID	$V_{n,shear}$ [kN]	$V_{mes} / V_{y,flex}$ [-]	m Eq. (8.9) [-]	m_{mes} / m_{cal} [-]
81	Thomsen and Wallace	1994	B3	205.7	0.98	5.31	3.19
82	Thomsen and Wallace	1994	D3	186.8	0.92	5.06	3.11
83	Thomsen and Wallace	1994	D1	253.5	0.94	4.45	3.11
84	Thomsen and Wallace	1994	C3	312.3	0.90	4.05	3.62
85	Thomsen and Wallace	1994	D2	216.2	0.95	5.15	4.41
86	Watson and Park	1989	No. 9	1164.1	1.66	6.67	1.55
87	Ang et al.	1981	No. 3	788.7	1.10	4.84	1.87
88	Nosho et al.	1996	No. 1	112.4	1.13	8.99	2.69
89	Watson and Park	1989	No. 5	591.2	1.21	9.63	1.36
90	Watson and Park	1989	No. 6	395.7	1.25	10.72	1.69
91	Zahn et al.	1986	No. 10	896.4	1.09	6.74	1.27
92	Matamoros et al.	1999	C5-40N	204.5	0.88	5.66	1.06
93	Matamoros et al.	1999	C5-40S	202.7	0.91	5.70	1.05
94	Saatcioglu and Grira	1999	BG-1	423.2	1.13	8.28	1.47
95	Saatcioglu and Grira	1999	BG-2	715.9	1.11	5.88	1.54
96	Saatcioglu and Grira	1999	BG-6	881.4	1.06	4.46	1.49
97	Saatcioglu and Grira	1999	BG-4	519.8	1.06	7.86	1.67
98	Saatcioglu and Grira	1999	BG-5	901.0	1.21	4.50	1.90
99	Saatcioglu and Grira	1999	BG-10	904.0	1.35	4.50	1.32
100	Saatcioglu and Grira	1999	BG-7	510.5	1.07	7.94	0.87
101	Saatcioglu and Grira	1999	BG-9	512.9	1.32	7.94	1.20
102	Azizinamini et al.	1988	NC-4	1048.5	1.10	5.45	1.72
103	Muguruma et al.	1989	AL-1	179.5	1.19	8.12	0.52
104	Muguruma et al.	1989	AL-2	142.4	1.37	11.06	1.13
105	Muguruma et al.	1989	BL-2	181.9	1.14	8.98	0.82

No.	Researcher	Year	Specimen ID	$V_{n,shear}$ [kN]	V_{mes} / $V_{y,flex}$ [-]	m Eq. (8.9) [-]	m_{mes} / m_{cal} [-]
106	Bayrak and Sheikh	1996	AS-4HT	1051.9	0.95	5.96	1.53
107	Bayrak and Sheikh	1996	ES-1HT	663.9	0.94	8.76	1.48
108	Bayrak and Sheikh	1996	AS-5HT	1263.3	0.96	6.73	4.99
109	Bayrak and Sheikh	1996	AS-6HT	1325.9	0.95	6.03	2.12
110	Bayrak and Sheikh	1996	ES-8HT	866.8	0.86	8.52	2.46
111	Bayrak and Sheikh	1996	AS-2HT	754.5	0.92	6.82	1.53
112	Bayrak and Sheikh	1996	AS-3HT	704.3	0.96	8.44	1.71
113	Bayrak and Sheikh	1996	AS-7HT	713.6	0.83	8.90	2.13
114	Muguruma et al.	1989	AH-1	395.3	1.20	5.14	0.63
115	Muguruma et. al	1989	AH-2	307.8	1.40	7.00	0.75
116	Muguruma et al.	1989	BH-2	389.6	1.14	6.70	0.62
				mean	1.08 ± 0.33%		1.67 ± 1.71%
				std-dev	0.16		0.93
				c.v.	14.48%		55.62%

(Berry et al. 2003; Brachmann 2002)

A7. Cyclic shear failure

No.	Researcher, Specimen ID	Geometry			
		b [mm]	h [mm]	L [mm]	a/d [-]
1	Zhou et al. 1987, No. 302-07	160	160	480	3.0
2	Zhou et al. 1987, No. 312-07	160	160	480	3.0
3	Zhou et al. 1987, No. 322-07	160	160	480	3.0
4	Wight and Sozen 1973, No. 40.048(East)	152	305	876	2.9
5	Wight and Sozen 1973, No. 40.048(West)	152	305	876	2.9
6	Wight and Sozen 1973, No. 40.033(East)	152	305	876	2.9
7	Wight and Sozen 1973, No. 40.033(West)	152	305	876	2.9
8	Wight and Sozen 1973, No. 25.033(East)	152	305	876	2.9
9	Wight and Sozen 1973, No. 25.033(West)	152	305	876	2.9
10	Wight and Sozen 1973, No. 40.067(East)	152	305	876	2.9
11	Wight and Sozen 1973, No. 40.067(West)	152	305	876	2.9
12	Wight and Sozen 1973, No. 40.092(East)	152	305	876	2.9
13	Wight and Sozen 1973, No. 40.092(West)	152	305	876	2.9
14	Lynn et al. 1998, 3CLH18	457	457	1473	3.2
15	Lynn et al. 1998, 2CLH18	457	457	1473	3.2
16	Lynn et al. 1998, 2CMH18	457	457	1473	3.2
17	Lynn et al. 1998, 3CMH18	457	457	1473	3.2
18	Lynn et al. 1998, 3CMD12	457	457	1473	3.2
19	Lynn et al. 1996, 3SLH18	457	457	1473	3.2
20	Lynn et al. 1996, 2SLH18	457	457	1473	3.2
21	Lynn et al. 1996, 3SMD12	457	457	1473	3.2
22	Matamoros et al. 1999,C10-05N	203	203	610	3.0
23	Matamoros et al. 1999,C10-10N	203	203	610	3.0
24	Matamoros et al. 1999,C10-20N	203	203	610	3.0
25	Matamoros et al. 1999,C10-20S	203	203	610	3.0
26	Matamoros et al. 1999,C5-20N	203	203	610	3.0
27	Matamoros et al. 1999,C5-20S	203	203	610	3.0
28	Matamoros et al. 1999,C5-40N	203	203	610	3.0
29	Matamoros et al. 1999,C5-40S	203	203	610	3.0
30	Aboutaha et al. 1999, SC3	914	457	1219	2.7
31	Ichinose et al. 2001, D16S	250	250	450	1.8
32	Ichinose et al. 2001, D16n	250	250	450	1.8
33	Ichinose et al. 2001, D19S	250	250	450	1.8
34	Ichinose et al. 2001, D19N	250	250	450	1.8
35	Ichinose et al. 2001, D22S	250	250	450	1.8
36	Ichinose et al. 2001, D22N	250	250	450	1.8
37	Ichinose et al. 2001, P22S	250	250	450	1.8
38	Ichinose et al. 2001, P22N	250	250	450	1.8

No.	Researcher, Specimen ID	f'_c [MPa]	Longitudinal reinforcement ρ_s [-]	f_{sy} [MPa]	Web reinforcement ρ_w [-]	f_{wy} [MPa]
1	Zhou et al. 1987, No. 302-07	29	0.022	341	0.006	559
2	Zhou et al. 1987, No. 312-07	29	0.022	341	0.006	559
3	Zhou et al. 1987, No. 322-07	29	0.022	341	0.015	559
4	Wight and Sozen 1973, No. 40.048(East)	26	0.024	496	0.005	345
5	Wight and Sozen 1973, No. 40.048(West)	26	0.024	496	0.005	345
6	Wight and Sozen 1973, No. 40.033(East)	34	0.024	496	0.003	345
7	Wight and Sozen 1973, No. 40.033(West)	34	0.024	496	0.003	345
8	Wight and Sozen 1973, No. 25.033(East)	34	0.024	496	0.003	345
9	Wight and Sozen 1973, No. 25.033(West)	34	0.024	496	0.003	345
10	Wight and Sozen 1973, No. 40.067(East)	33	0.024	496	0.006	345
11	Wight and Sozen 1973, No. 40.067(West)	33	0.024	496	0.006	345
12	Wight and Sozen 1973, No. 40.092(East)	34	0.024	496	0.009	317
13	Wight and Sozen 1973, No. 40.092(West)	34	0.024	496	0.009	317
14	Lynn et al. 1998, 3CLH18	27	0.030	331	0.001	400
15	Lynn et al. 1998, 2CLH18	33	0.019	331	0.001	400
16	Lynn et al. 1998, 2CMH18	26	0.019	331	0.001	400
17	Lynn et al. 1998, 3CMH18	28	0.030	331	0.001	400
18	Lynn et al. 1998, 3CMD12	28	0.030	331	0.002	400
19	Lynn et al. 1996, 3SLH18	27	0.030	331	0.001	400
20	Lynn et al. 1996, 2SLH18	33	0.019	331	0.001	400
21	Lynn et al. 1996, 3SMD12	26	0.030	331	0.002	400
22	Matamoros et al. 1999,C10-05N	70	0.019	586	0.010	407
23	Matamoros et al. 1999,C10-10N	68	0.019	572	0.010	514
24	Matamoros et al. 1999,C10-20N	66	0.019	572	0.010	514
25	Matamoros et al. 1999,C10-20S	66	0.019	573	0.010	515
26	Matamoros et al. 1999,C5-20N	48	0.019	586	0.010	407
27	Matamoros et al. 1999,C5-20S	48	0.019	587	0.010	408
28	Matamoros et al. 1999,C5-40N	38	0.019	572	0.010	514
29	Matamoros et al. 1999,C5-40S	38	0.019	573	0.010	515
30	Aboutaha et al. 1999, SC3	22	0.019	434	0.001	400
31	Ichinose et al. 2001, D16S	29	0.026	377	0.013	319
32	Ichinose et al. 2001, D16n	29	0.026	377	0.013	319
33	Ichinose et al. 2001, D19S	29	0.036	374	0.013	319
34	Ichinose et al. 2001, D19N	29	0.036	374	0.013	319
35	Ichinose et al. 2001, D22S	29	0.049	391	0.013	319
36	Ichinose et al. 2001, D22N	29	0.049	391	0.013	319
37	Ichinose et al. 2001, P22S	29	0.049	1080	0.013	319
38	Ichinose et al. 2001, P22N	29	0.049	1080	0.013	319

No.	Researcher, Specimen ID	Axial Load P [kN]	Axial Load $P/(A_g f'_c)$ [-]	Δ_{max} [mm]	$\delta_{max} = \Delta_{max}/L$ [-]
1	Zhou et al. 1987, No. 302-07	517	0.70	7	1.5%
2	Zhou et al. 1987, No. 312-07	517	0.70	7	1.5%
3	Zhou et al. 1987, No. 322-07	517	0.70	11	2.2%
4	Wight and Sozen 1973, No. 40.048(East)	178	0.15	43	4.9%
5	Wight and Sozen 1973, No. 40.048(West)	178	0.15	47	5.4%
6	Wight and Sozen 1973, No. 40.033(East)	178	0.11	47	5.4%
7	Wight and Sozen 1973, No. 40.033(West)	178	0.11	49	5.6%
8	Wight and Sozen 1973, No. 25.033(East)	111	0.07	31	3.6%
9	Wight and Sozen 1973, No. 25.033(West)	111	0.07	30	3.4%
10	Wight and Sozen 1973, No. 40.067(East)	178	0.11	59	6.7%
11	Wight and Sozen 1973, No. 40.067(West)	178	0.11	59	6.7%
12	Wight and Sozen 1973, No. 40.092(East)	178	0.11	52	5.9%
13	Wight and Sozen 1973, No. 40.092(West)	178	0.11	50	5.7%
14	Lynn et al. 1998, 3CLH18	503	0.09	31	2.1%
15	Lynn et al. 1998, 2CLH18	503	0.07	38	2.6%
16	Lynn et al. 1998, 2CMH18	1512	0.28	15	1.0%
17	Lynn et al. 1998, 3CMH18	1512	0.26	30	2.1%
18	Lynn et al. 1998, 3CMD12	1512	0.26	33	2.3%
19	Lynn et al. 1996, 3SLH18	503	0.09	46	3.1%
20	Lynn et al. 1996, 2SLH18	503	0.07	54	3.7%
21	Lynn et al. 1996, 3SMD12	1512	0.28	25	1.7%
22	Matamoros et al. 1999,C10-05N	142	0.05	32	5.2%
23	Matamoros et al. 1999,C10-10N	285	0.10	38	6.2%
24	Matamoros et al. 1999,C10-20N	569	0.21	32	5.2%
25	Matamoros et al. 1999,C10-20S	569	0.21	32	5.2%
26	Matamoros et al. 1999,C5-20N	285	0.14	44	7.2%
27	Matamoros et al. 1999,C5-20S	285	0.14	44	7.2%
28	Matamoros et al. 1999,C5-40N	569	0.36	26	4.3%
29	Matamoros et al. 1999,C5-40S	569	0.36	25	4.2%
30	Aboutaha et al. 1999, SC3	0	0.00	36	3.0%
31	Ichinose et al. 2001, D16S	0	0.00	22	4.8%
32	Ichinose et al. 2001, D16n	0	0.00	25	5.6%
33	Ichinose et al. 2001, D19S	0	0.00	22	4.8%
34	Ichinose et al. 2001, D19N	0	0.00	22	4.8%
35	Ichinose et al. 2001, D22S	0	0.00	14	3.1%
36	Ichinose et al. 2001, D22N	0	0.00	16	3.5%
37	Ichinose et al. 2001, P22S	0	0.00	13	2.8%
38	Ichinose et al. 2001, P22N	0	0.00	16	3.6%

No.	Researcher, Specimen ID	V_{mes} [kN]	V_{mes}/ V_{cal} Watanabe [-]	V_{mes}/ V_{cal} Priestley [-]	V_{mes}/ V_{cal} Pujol [-]
1	Zhou et al. 1987, No. 302-07	57	0.35	0.36	n/a
2	Zhou et al. 1987, No. 312-07	55	0.34	0.33	n/a
3	Zhou et al. 1987, No. 322-07	52	0.25	0.20	n/a
4	Wight and Sozen 1973, No. 40.048(East)	105	1.38	0.71	n/a
5	Wight and Sozen 1973, No. 40.048(West)	98	1.39	0.70	n/a
6	Wight and Sozen 1973, No. 40.033(East)	94	1.40	0.61	11.62
7	Wight and Sozen 1973, No. 40.033(West)	105	1.56	0.88	14.81
8	Wight and Sozen 1973, No. 25.033(East)	88	0.86	0.66	3.70
9	Wight and Sozen 1973, No. 25.033(West)	93	0.88	0.87	3.79
10	Wight and Sozen 1973, No. 40.067(East)	102	0.97	0.56	8.16
11	Wight and Sozen 1973, No. 40.067(West)	99	0.95	0.55	7.95
12	Wight and Sozen 1973, No. 40.092(East)	121	0.79	0.53	4.45
13	Wight and Sozen 1973, No. 40.092(West)	121	0.79	0.53	4.30
14	Lynn et al. 1998, 3CLH18	277	0.66	0.71	n/a
15	Lynn et al. 1998, 2CLH18	241	0.58	1.00	n/a
16	Lynn et al. 1998, 2CMH18	306	0.49	0.66	n/a
17	Lynn et al. 1998, 3CMH18	328	0.62	0.86	n/a
18	Lynn et al. 1998, 3CMD12	356	0.62	0.62	n/a
19	Lynn et al. 1996, 3SLH18	270	0.81	0.69	n/a
20	Lynn et al. 1996, 2SLH18	233	0.73	0.58	n/a
21	Lynn et al. 1996, 3SMD12	367	0.59	0.62	n/a
22	Matamoros et al. 1999,C10-05N	70	0.41	0.31	1.67
23	Matamoros et al. 1999,C10-10N	96	0.48	0.28	1.76
24	Matamoros et al. 1999,C10-20N	108	0.60	0.29	2.57
25	Matamoros et al. 1999,C10-20S	104	0.65	0.31	n/a
26	Matamoros et al. 1999,C5-20N	73	0.52	0.31	n/a
27	Matamoros et al. 1999,C5-20S	73	0.53	0.32	n/a
28	Matamoros et al. 1999,C5-40N	85	0.54	0.25	n/a
29	Matamoros et al. 1999,C5-40S	85	0.53	0.26	n/a
30	Aboutaha et al. 1999, SC3	407	0.74	0.87	n/a

No.	Researcher, Specimen ID	V_{mes} [kN]	V_{mes} / V_{cal} Watanabe [-]	V_{mes} / V_{cal} Priestley [-]	V_{mes} / V_{cal} Pujol [-]
31	Ichinose et al. 2001, D16S	140	0.70	0.34	1.61
32	Ichinose et al. 2001, D16n	139	0.78	0.34	1.81
33	Ichinose et al. 2001, D19S	191	0.95	0.47	2.24
34	Ichinose et al. 2001, D19N	196	0.99	0.48	2.31
35	Ichinose et al. 2001, D22S	254	0.68	0.57	2.40
36	Ichinose et al. 2001, D22N	252	0.74	0.60	2.51
37	Ichinose et al. 2001, P22S	309	0.83	0.68	n/a
38	Ichinose et al. 2001, P22N	290	0.89	0.63	n/a
		mean	0.75 ± 1.31%	0.55 ± 1.67%	4.47 ± 3.12%
		std-dev	0.30	0.21	3.84
		c.v.	39.77%	38.12%	86.1%

(Berry et al. 2003; Brachmann 2002; Ichinose et al. 2001; Matamoros 1999; Wight and Sözen 1973)

A8. Shear strength degradation

No.	Researcher	Year	Specimen ID	Geometry					
				b [mm]	h [mm]	d [mm]	h_a [mm]	L [mm]	a/d [-]
1	Wight and Sozen	1973	No. 40.067 (East)	152	305	273	64	876	3.2
2	Wight and Sozen	1973	No. 40.067 (West)	152	305	273	64	876	3.2
3	Wight and Sozen	1973	No. 25.033 (East)	152	305	273	64	876	3.2
4	Wight and Sozen	1973	No. 25.033 (West)	152	305	273	64	876	3.2
5	Matamoros et al.	1999	C5-20N	203	203	157	92	610	3.9
6	Matamoros et al.	1999	C10-05N	203	203	155	96	610	3.9
7	Matamoros et al.	1999	C5-20S	203	203	156	94	610	3.9
8	Matamoros et al.	1999	C10-10N	203	203	169	68	610	3.6
9	Matamoros et al.	1999	C5-40N	203	203	174	57	610	3.5
10	Matamoros et al.	1999	C5-40S	203	203	174	57	610	3.5
11	Matamoros et al.	1999	C10-20N	203	203	173	60	610	3.5
12	Matamoros et al.	1999	C10-20S	203	203	180	45	610	3.4
13	Ichinose et al.	2001	D16S	250	250	233	34	450	1.9
14	Ichinose et al.	2001	D19S	250	250	233	34	450	1.9
15	Ichinose et al.	2001	D19N	250	250	233	34	450	1.9
16	Ichinose et al.	2001	D22S	250	250	233	34	450	1.9
17	Ichinose et al.	2001	D22N	250	250	233	34	450	1.9
18	Ichinose et al.	2001	P22S	250	250	233	34	450	1.9
19	Ichinose et al.	2001	P22N	250	250	233	34	450	1.9

No.	Researcher	Year	Specimen ID	f'_c [MPa]	Tensile reinf. ρ_s [-]	f_{sy} [MPa]	Web reinforcement ρ_w [-]	f_{wy} [MPa]	$\rho_w f_{wy} / f'_c$ [-]
1	Wight and Sozen	1973	No. 40.067 (East)	33	0.024	496	0.006	345	0.07
2	Wight and Sozen	1973	No. 40.067 (West)	33	0.024	496	0.006	345	0.07
3	Wight and Sozen	1973	No. 25.033 (East)	34	0.024	496	0.003	345	0.03
4	Wight and Sozen	1973	No. 25.033 (West)	34	0.024	496	0.003	345	0.03
5	Matamoros et al.	1999	C5-20N	48	0.019	586	0.009	407	0.08
6	Matamoros et al.	1999	C10-05N	70	0.019	586	0.009	407	0.05
7	Matamoros et al.	1999	C5-20S	48	0.019	587	0.009	408	0.08
8	Matamoros et al.	1999	C10-10N	68	0.019	572	0.009	514	0.07
9	Matamoros et al.	1999	C5-40N	38	0.019	572	0.009	514	0.12
10	Matamoros et al.	1999	C5-40S	38	0.019	573	0.009	515	0.12
11	Matamoros et al.	1999	C10-20N	66	0.019	572	0.009	514	0.07
12	Matamoros et al.	1999	C10-20S	66	0.019	573	0.009	515	0.07
13	Ichinose et al.	2001	D16S	29	0.026	377	0.013	319	0.14
14	Ichinose et al.	2001	D19S	29	0.036	374	0.013	319	0.14
15	Ichinose et al.	2001	D19N	29	0.036	374	0.013	319	0.14
16	Ichinose et al.	2001	D22S	29	0.049	391	0.013	319	0.14
17	Ichinose et al.	2001	D22N	29	0.049	391	0.013	319	0.14
18	Ichinose et al.	2001	P22S	29	0.049	1080	0.013	319	0.14
19	Ichinose et al.	2001	P22N	29	0.049	1080	0.013	319	0.14

No.	Researcher	Year	Specimen ID	Axial Load		Measured capacity	
				P [kN]	$P/(A_g f'_c)$ [-]	V_{max} [kN]	$80\%V_{max}$ [kN]
1	Wight and Sozen	1973	No. 40.067 (East)	178	0.11	92	72
2	Wight and Sozen	1973	No. 40.067 (West)	178	0.11	92	72
3	Wight and Sozen	1973	No. 25.033 (East)	111	0.07	85	65
4	Wight and Sozen	1973	No. 25.033 (West)	111	0.07	90	70
5	Matamoros et al.	1999	C5-20N	285	0.14	73	57
6	Matamoros et al.	1999	C10-05N	142	0.05	70	53
7	Matamoros et al.	1999	C5-20S	285	0.14	73	56
8	Matamoros et al.	1999	C10-10N	285	0.10	96	75
9	Matamoros et al.	1999	C5-40N	569	0.36	85	64
10	Matamoros et al.	1999	C5-40S	569	0.36	85	62
11	Matamoros et al.	1999	C10-20N	569	0.21	108	81
12	Matamoros et al.	1999	C10-20S	569	0.21	104	81
13	Ichinose et al.	2001	D16S	0	0.00	140	112
14	Ichinose et al.	2001	D19S	0	0.00	191	153
15	Ichinose et al.	2001	D19N	0	0.00	196	157
16	Ichinose et al.	2001	D22S	0	0.00	254	203
17	Ichinose et al.	2001	D22N	0	0.00	252	202
18	Ichinose et al.	2001	P22S	0	0.00	309	247
19	Ichinose et al.	2001	P22N	0	0.00	290	232

No.	Researcher	Year	Specimen ID	Yield displ. Δ_y [mm]	Drift ratio $\delta_u=\Delta_u/L$ [-]	Δ_u [mm]	Yield capacity $M_{y,flex}$ [kNmm]	$V_{y,flex}$ [kN]
1	Wight and Sozen	1973	No. 40.067 (East)	11	0.068	60	82,972	95
2	Wight and Sozen	1973	No. 40.067 (West)	10	0.069	60	82,972	95
3	Wight and Sozen	1973	No. 25.033 (East)	12	0.036	32	76,556	87
4	Wight and Sozen	1973	No. 25.033 (West)	11	0.048	42	76,556	87
5	Matamoros et al.	1999	C5-20N	6	0.043	26	52,283	86
6	Matamoros et al.	1999	C10-05N	8	0.052	32	46,210	76
7	Matamoros et al.	1999	C5-20S	6	0.041	25	51,789	85
8	Matamoros et al.	1999	C10-10N	7	0.062	38	59,755	98
9	Matamoros et al.	1999	C5-40N	5	0.042	26	58,382	96
10	Matamoros et al.	1999	C5-40S	5	0.041	25	56,364	92
11	Matamoros et al.	1999	C10-20N	7	0.052	32	77,798	128
12	Matamoros et al.	1999	C10-20S	7	0.052	32	73,538	121
13	Ichinose et al.	2001	D16S	3	0.048	22	62,550	139
14	Ichinose et al.	2001	D19S	4	0.048	22	85,586	190
15	Ichinose et al.	2001	D19N	4	0.048	22	85,586	190
16	Ichinose et al.	2001	D22S	5	0.031	14	117,254	261
17	Ichinose et al.	2001	D22N	5	0.035	16	117,254	261
18	Ichinose et al.	2001	P22S	8	0.028	13	217,181	483
19	Ichinose et al.	2001	P22N	9	0.036	16	217,181	483

No.	Researcher	Year	Specimen ID	Transverse reinforcement		
				Δ_{wy} [mm]	$\delta_{wy}=\Delta_{wy}/L$ [-]	$V_{wy,shear}$ [kN]
1	Wight and Sozen	1973	No. 40.067 (East)	45	0.05	92
2	Wight and Sozen	1973	No. 40.067 (West)	45	0.05	95
3	Wight and Sozen	1973	No. 25.033 (East)	23	0.03	81
4	Wight and Sozen	1973	No. 25.033 (West)	23	0.03	93
5	Matamoros et al.	1999	C5-20N	32	0.05	45
6	Matamoros et al.	1999	C10-05N	32	0.05	57
7	Matamoros et al.	1999	C5-20S	32	0.05	49
8	Matamoros et al.	1999	C10-10N	38	0.06	77
9	Matamoros et al.	1999	C5-40N	19	0.03	69
10	Matamoros et al.	1999	C5-40S	18	0.03	69
11	Matamoros et al.	1999	C10-20N	38	0.06	73
12	Matamoros et al.	1999	C10-20S	32	0.05	73
13	Ichinose et al.	2001	D16S	n/a	n/a	n/a
14	Ichinose et al.	2001	D19S	18	0.04	155
15	Ichinose et al.	2001	D19N	n/a	n/a	n/a
16	Ichinose et al.	2001	D22S	6	0.01	251
17	Ichinose et al.	2001	D22N	n/a	n/a	n/a
18	Ichinose et al.	2001	P22S	10	0.02	273
19	Ichinose et al.	2001	P22N	n/a	n/a	n/a

No.	Researcher	Year	Specimen ID	$V_{shear,cal}$ [kN]	V_t [kN]	V_c+V_a [kN]	$(V_{wy,shear}-(V_c+V_a))/V_t$
1	Wight and Sozen	1973	No. 40.067 (East)	140	124	16	0.61
2	Wight and Sozen	1973	No. 40.067 (West)	140	124	16	0.64
3	Wight and Sozen	1973	No. 25.033 (East)	80	64	15	1.02
4	Wight and Sozen	1973	No. 25.033 (West)	80	64	15	1.21
5	Matamoros et al.	1999	C5-20N	200	179	21	0.13
6	Matamoros et al.	1999	C10-05N	213	198	15	0.21
7	Matamoros et al.	1999	C5-20S	198	176	22	0.15
8	Matamoros et al.	1999	C10-10N	264	248	17	0.24
9	Matamoros et al.	1999	C5-40N	237	202	35	0.17
10	Matamoros et al.	1999	C5-40S	235	200	35	0.17
11	Matamoros et al.	1999	C10-20N	253	218	35	0.18
12	Matamoros et al.	1999	C10-20S	251	221	30	0.20
13	Ichinose et al.	2001	D16S	233	212	21	n/a
14	Ichinose et al.	2001	D19S	230	209	21	0.64
15	Ichinose et al.	2001	D19N	230	209	21	n/a
16	Ichinose et al.	2001	D22S	227	206	21	1.12
17	Ichinose et al.	2001	D22N	227	206	21	n/a
18	Ichinose et al.	2001	P22S	202	180	21	1.40
19	Ichinose et al.	2001	P22N	202	180	21	n/a

No.	Researcher	Year	Specimen ID	Δ_c/L [-]	$\varepsilon_{\Delta c}$ [-]	f_{ws} $(\varepsilon_{\Delta c})$ [MPa]	$f_t(\varepsilon_{\Delta c})$ [MPa]	$f_t(\varepsilon_{\Delta c})$ / f'_c [-]	$\eta(\Delta_c)$ Eq. (7-13)
1	Wight and Sozen	1973	No. 40.067 (East)						
2	Wight and Sozen	1973	No. 40.067 (West)						
3	Wight and Sozen	1973	No. 25.033 (East)						
4	Wight and Sozen	1973	No. 25.033 (West)						
5	Matamoros et al.	1999	C5-20N						
6	Matamoros et al.	1999	C10-05N						
7	Matamoros et al.	1999	C5-20S						
8	Matamoros et al.	1999	C10-10N						
9	Matamoros et al.	1999	C5-40N						
10	Matamoros et al.	1999	C5-40S						
11	Matamoros et al.	1999	C10-20N						
12	Matamoros et al.	1999	C10-20S						
13	Ichinose et al.	2001	D16S	0.02	0.001	278	6.84	0.24	1.29
14	Ichinose et al.	2001	D19S	0.03	0.001	295	7.25	0.25	1.49
15	Ichinose et al.	2001	D19N	0.02	0.001	211	5.19	0.18	1.27
16	Ichinose et al.	2001	D22S	0.01	0.002	312	7.67	0.27	0.63
17	Ichinose et al.	2001	D22N	0.02	0.001	295	7.26	0.25	0.88
18	Ichinose et al.	2001	P22S	0.02	0.002	308	7.57	0.26	1.05
19	Ichinose et al.	2001	P22N	0.02	0.002	316	7.77	0.27	0.85
								mean	1.07 ± 4.34 %
								std-dev	0.300
								c.v.	28.14 %

No.	Researcher	Year	Specimen ID	$\eta(\Delta_{wy})$ [-]	$V_t+\eta(V_{cz}+V_a)$ [kN]	$V_{wy}/V_t+\eta(V_{cz}+V_a)$ [-]
1	Wight and Sozen	1973	No. 40.067 (East)	0.00	124	0.74
2	Wight and Sozen	1973	No. 40.067 (West)	0.00	124	0.76
3	Wight and Sozen	1973	No. 25.033 (East)	0.00	64	1.26
4	Wight and Sozen	1973	No. 25.033 (West)	0.00	64	1.45
5	Matamoros et al.	1999	C5-20N	0.00	179	0.25
6	Matamoros et al.	1999	C10-05N	0.00	198	0.29
7	Matamoros et al.	1999	C5-20S	0.00	176	0.28
8	Matamoros et al.	1999	C10-10N	0.00	248	0.31
9	Matamoros et al.	1999	C5-40N	0.00	202	0.34
10	Matamoros et al.	1999	C5-40S	0.00	200	0.35
11	Matamoros et al.	1999	C10-20N	0.00	218	0.33
12	Matamoros et al.	1999	C10-20S	0.00	221	0.33
13	Ichinose et al.	2001	D16S	n/a	n/a	n/a
14	Ichinose et al.	2001	D19S	0.00	209	0.74
15	Ichinose et al.	2001	D19N	n/a	n/a	n/a
16	Ichinose et al.	2001	D22S	0.29	212	1.18
17	Ichinose et al.	2001	D22N	n/a	n/a	n/a
18	Ichinose et al.	2001	P22S	0.00	180	1.51
19	Ichinose et al.	2001	P22N	n/a	n/a	n/a

No.	Researcher	Year	Specimen ID	χ Eq. (7-17)	$V_{wy,cal} = \chi V_t + \eta(V_{cz}+V_a)$ [kN]	$V_{wy,mes} / V_{wy,cal}$ [-]	$V_{mes} / V_{wy,cal}$ [-]
1	Wight and Sozen	1973	No. 40.067 (East)	0.29	35.7	2.58	2.58
2	Wight and Sozen	1973	No. 40.067 (West)	0.29	35.7	2.66	2.57
3	Wight and Sozen	1973	No. 25.033 (East)	n/a	n/a	n/a	n/a
4	Wight and Sozen	1973	No. 25.033 (West)	n/a	n/a	n/a	n/a
5	Matamoros et al.	1999	C5-20N	0.26	45.8	0.98	1.58
6	Matamoros et al.	1999	C10-05N	0.38	74.6	0.76	0.94
7	Matamoros et al.	1999	C5-20S	0.26	45.1	1.09	1.61
8	Matamoros et al.	1999	C10-10N	0.26	65.0	1.19	1.47
9	Matamoros et al.	1999	C5-40N	0.22	45.3	1.52	1.87
10	Matamoros et al.	1999	C5-40S	0.23	46.7	1.48	1.81
11	Matamoros et al.	1999	C10-20N	0.18	39.8	1.83	2.70
12	Matamoros et al.	1999	C10-20S	0.21	46.4	1.57	2.23
13	Ichinose et al.	2001	D16S	n/a	n/a	n/a	n/a
14	Ichinose et al.	2001	D19S	0.74	153.7	1.01	1.24
15	Ichinose et al.	2001	D19N	n/a	n/a	n/a	n/a
16	Ichinose et al.	2001	D22S	n/a	n/a	n/a	n/a
17	Ichinose et al.	2001	D22N	n/a	n/a	n/a	n/a
18	Ichinose et al.	2001	P22S	n/a	n/a	n/a	n/a
19	Ichinose et al.	2001	P22N	n/a	n/a	n/a	n/a
					mean	1.51 ± 2.80 %	1.87 ± 2.10 %
					std-dev	0.629	0.583
					c.v.	41.61 %	31.21 %

(Ichinose et al. 2001; Matamoros 1999; Wight and Sözen 1973)

A9. Wall database

No.	Researcher	Specimen ID	Section type	Loading type	Boundary Element b_f [mm]	h_f [mm]	Web thick. t [mm]	Wall Length l_w [mm]
1	Hirosawa	9	Barbell	Alternating	100	100	30	600
2		15	Barbell	Alternating	150	100	30	600
3		16	Barbell	Alternating	150	100	30	600
4	Rye	29	Barbell	Repeated	250	250	78	2300
5		30	Barbell	Alternating	250	250	75	2300
6		31	Barbell	Alternating	250	250	80	1550
7	Kobusho	46	Flanged	Alternating	145	30	23	430
8		47	Flanged	Alternating	145	30	24	430
9		50	Flanged	Alternating	145	30	27	430
10		51	Flanged	Alternating	145	30	24	430
11		52	Flanged	Alternating	145	30	22	430
12		53	Flanged	Alternating	145	30	16	430
13		54	Flanged	Alternating	145	30	22	430
14		55	Flanged	Alternating	145	30	22	430
15		56	Flanged	Alternating	145	30	24	430
16		57	Flanged	Alternating	145	30	23	430
17		58	Flanged	Alternating	145	30	23	430
18		59	Flanged	Alternating	145	30	21	430
19		61	Barbell	Alternating	60	60	20	420
20		64	Barbell	Alternating	60	60	20	420
21		65	Barbell	Alternating	60	60	20	420
22		69	Barbell	Alternating	60	60	20	420
23	Sugano	70	Barbell	Alternating	250	250	74	2300
24		71	Barbell	Alternating	250	250	83	2300
25	Hirosawa	72	Rectangular	Alternating	160	170	160	1700
26	Tanabe	101	Barbell	Monotonic	60	60	20	570
27		102	Barbell	Monotonic	60	60	20	570
28		103	Barbell	Monotonic	60	60	20	570
29		104	Barbell	Monotonic	60	60	30	570
30		105	Barbell	Monotonic	60	60	30	570
31		106	Barbell	Monotonic	60	60	30	570
32		107	Barbell	Monotonic	60	60	40	570
33		108	Barbell	Monotonic	60	60	40	570
34		109	Barbell	Monotonic	60	60	40	570
35		110	Barbell	Monotonic	60	60	10	570
36		111	Barbell	Monotonic	60	60	10	570
37		112	Barbell	Monotonic	60	60	20	570
38		113	Barbell	Monotonic	60	60	20	570

No.	Researcher	Specimen ID	Section type	Loading type	Boundary Element b_f [mm]	h_f [mm]	Web thick. t [mm]	Wall Length l_w [mm]
39	Tanabe	114	Barbell	Monotonic	60	60	30	570
40		115	Barbell	Monotonic	60	60	30	570
41		116	Barbell	Monotonic	60	60	40	570
42		117	Barbell	Monotonic	60	60	40	570
43	Tsuboi	131	Barbell	Repeated	107	120	67	507
44		134	Barbell	Repeated	107	120	67	507
45		135	Barbell	Repeated	107	120	67	507
46	Sugano	140	Barbell	Monotonic	360	360	120	3960
47		141	Barbell	Monotonic	360	360	120	3960
48		142	Barbell	Monotonic	360	360	120	3960
49		143	Barbell	Monotonic	360	360	120	3960
50		144	Barbell	Monotonic	360	360	120	3960
51		145	Barbell	Monotonic	360	360	120	3960
52		146	Barbell	Monotonic	360	360	120	3960
53		147	Barbell	Monotonic	360	360	120	3960
54	Aoyagi	150	Barbell	Alternating	320	320	160	2720
55		152	Barbell	Alternating	320	320	160	2720
56	Yoshizaki	169	Rectangular	Alternating	60	80	60	800
57		171	Rectangular	Alternating	60	120	60	1200
58		172	Rectangular	Alternating	60	120	60	1200
59		173	Rectangular	Alternating	60	120	60	1200
60		174	Rectangular	Alternating	60	120	60	1200
61		176	Rectangular	Alternating	60	160	60	1600
62		177	Rectangular	Alternating	60	160	60	1600
63		178	Rectangular	Alternating	60	160	60	1600
64		179	Rectangular	Alternating	60	160	60	1600
65	Kabeyasawa	K1	Barbell	Alternating	200	200	80	2000
66		K2	Barbell	Alternating	200	200	80	2000
67		K3	Barbell	Alternating	200	200	80	2000
68		K4	Barbell	Alternating	200	200	80	2000
69		K7	Barbell	Alternating	200	200	120	2000
70		K8	Barbell	Alternating	200	200	120	2000
71	Paulay	W1	Rectangular	Alternating	100	200	100	3000
72		W3	Flanged	Alternating	500	100	100	3000
73	Antebi	6	Barbell	Monotonic	191	127	51	1803
74		10	Barbell	Monotonic	191	127	51	1803
75		13	Barbell	Monotonic	191	127	51	1803
76		25	Barbell	Monotonic	191	127	51	1803
77		32	Barbell	Monotonic	191	127	51	1803
78		35	Barbell	Monotonic	191	127	51	1803
79		37	Barbell	Monotonic	191	127	51	1803
80		41	Barbell	Monotonic	191	127	51	1803

No.	Researcher	Specimen ID	Section type	Loading type	Boundary Element b_f [mm]	h_f [mm]	Web thick. t [mm]	Wall Length l_w [mm]
81	Antebi	45	Barbell	Monotonic	191	127	76	1803
82		49	Barbell	Monotonic	191	127	76	1803
83		50	Barbell	Monotonic	191	127	76	1803
84		51	Barbell	Monotonic	191	127	76	1803
85		54	Barbell	Monotonic	191	127	76	1803
86		55	Barbell	Monotonic	191	127	51	3327
87		58	Barbell	Monotonic	191	127	51	3327
88		60	Barbell	Monotonic	191	127	51	3327
89	Barda	B1-1	Flanged	Monotonic	610	102	102	1905
90		B2-1	Flanged	Monotonic	610	102	102	1905
91		B3-2	Flanged	Alternating	610	102	102	1905
92		B6-4	Flanged	Alternating	610	102	102	1905
93		B7-5	Flanged	Alternating	610	102	102	1905
94		B8-5	Flanged	Alternating	610	102	102	1905
95	Benjamin	4BII-1	Barbell	Monotonic	127	102	51	610
96		4BII-2	Barbell	Monotonic	127	102	51	914
97		4BII-3	Barbell	Monotonic	127	102	51	1219
98		4BII-4	Barbell	Monotonic	127	102	51	1778
99		3BI-1	Barbell	Monotonic	95	127	51	1727
100		1BII-1	Barbell	Monotonic	191	127	51	1727
101		1BII-2a	Barbell	Monotonic	191	127	51	1727
102		1BII-2b	Barbell	Monotonic	191	127	51	1727
103		3BI-3	Barbell	Monotonic	305	127	51	1727
104		3AII-1	Barbell	Monotonic	127	102	44	914
105		3AII-2	Barbell	Monotonic	127	102	44	914
106		1BII-1a	Barbell	Monotonic	95	64	25	864
107		1BII-3	Barbell	Monotonic	286	191	76	2591
108		NV-1	Barbell	Monotonic	127	127	51	1651
109		NV-11	Barbell	Monotonic	127	127	51	1143
110		NV-18	Barbell	Monotonic	127	127	51	1956
111		VR-3	Barbell	Monotonic	191	127	51	1727
112		R-1	Barbell	Monotonic	191	127	51	1727
113		A1-A	Barbell	Monotonic	127	102	44	1778
114		A1-B	Barbell	Monotonic	127	102	44	1778
115		A2-B	Barbell	Monotonic	127	102	44	1778
116		M-1	Barbell	Monotonic	191	121	51	1575
117		M-2	Barbell	Monotonic	191	121	51	1575
118		M-3	Barbell	Monotonic	191	121	51	1575
119		M-4	Barbell	Monotonic	191	121	51	1575
120		MR-1	Barbell	Monotonic	127	127	44	1645
121		MR-2	Barbell	Monotonic	127	127	44	1645
122		MR-3	Barbell	Monotonic	127	127	44	1645

No.	Researcher	Specimen ID	Section type	Loading type	Boundary Element b_f [mm]	h_f [mm]	Web thick. t [mm]	Wall Length l_w [mm]
123	Benjamin	MR-4	Barbell	Monotonic	127	127	44	1645
124		VRR-1	Barbell	Monotonic	178	127	51	1727
125		MS-1	Barbell	Monotonic	127	127	51	1727
126		MS-2	Barbell	Monotonic	127	127	51	1727
127		MS-2-2	Barbell	Monotonic	127	127	51	1727
128		MS-5	Barbell	Monotonic	127	127	51	2337
129		SD-1A	Barbell	Monotonic	102	102	51	1219
130		SD-1B	Barbell	Monotonic	102	102	51	1219
131		SD-1C	Barbell	Monotonic	102	102	51	1219
132	Gallerly	A-8	Barbell	Monotonic	102	102	44	914
133		A-4	Barbell	Monotonic	102	102	44	914
134		B-8	Barbell	Monotonic	102	102	44	914
135		B-4	Barbell	Monotonic	102	102	44	914
136		C-8	Barbell	Monotonic	102	102	44	914
137		C-4	Barbell	Monotonic	102	102	44	914
138	Kabeyasawa, Hiraishi 1997	W08	Barbell	Alternating	200	200	80	1300
139		W12	Barbell	Alternating	200	200	80	1300
140		No. 1	Barbell	Alternating	200	200	80	1300
141		No. 2	Barbell	Alternating	200	200	80	1300
142		No. 3	Barbell	Alternating	200	200	80	1300
143		No. 5	Barbell	Alternating	200	200	80	1300
144		No. 6	Barbell	Alternating	200	200	80	1300
145		No. 7	Barbell	Alternating	200	200	80	1300
146		No. 8	Barbell	Alternating	200	200	80	1300

No.	Researcher	Specimen ID	M/Vl_w (a/l_w)	a [mm]	$P/(Af'_c)$ [%]	f'_c [MPa]
1	Hirosawa	9	1.17	702	15.4	26
2		15	1.75	1050	7.1	28
3		16	1.75	1050	10.3	29
4	Rye	29	0.63	1449	0.0	23
5		30	0.63	1449	0.0	33
6		31	0.94	1457	0.0	17
7	Kobusho	46	0.50	215	0.0	20
8		47	0.50	215	0.0	19
9		50	0.85	366	0.2	14
10		51	0.85	366	0.2	14
11		52	0.85	366	0.2	16
12		53	0.85	366	0.2	14
13		54	0.85	366	0.1	18
14		55	0.85	366	0.2	17
15		56	0.85	366	0.1	24
16		57	0.85	366	0.2	16
17		58	0.85	366	0.2	16
18		59	0.85	366	0.2	16
19		61	0.55	231	0.0	14
20		64	0.86	361	0.0	19
21		65	0.86	361	0.0	18
22		69	0.86	361	0.0	29
23	Sugano	70	0.63	1449	0.0	24
24		71	0.63	1449	0.0	25
25	Hirosawa	72	1.00	1700	11.7	17
26	Tanabe	101	0.84	479	0.0	34
27		102	0.84	479	0.0	30
28		103	0.84	479	0.0	35
29		104	0.84	479	0.0	36
30		105	0.84	479	0.0	34
31		106	0.84	479	0.0	34
32		107	0.84	479	0.0	33
33		108	0.84	479	0.0	35
34		109	0.84	479	0.0	36
35		110	0.84	479	0.0	46
36		111	0.84	479	0.0	43
37		112	0.84	479	0.0	43
38		113	0.84	479	0.0	49
39		114	0.84	479	0.0	40
40		115	0.84	479	0.0	46
41		116	0.84	479	0.0	45

No.	Researcher	Specimen ID	M/Vl$_w$ (a/l$_w$)	a [mm]	P/(Af'$_c$) [%]	f'$_c$ [MPa]
42	Tanabe	117	0.84	479	0.0	43
43	Tsuboi	131	1.77	897	0.0	31
44		134	0.99	502	0.0	30
45		135	0.99	502	0.0	29
46	Sugano	140	0.23	911	10.0	21
47		141	0.23	911	17.9	21
48		142	0.23	911	12.5	21
49		143	0.23	911	8.3	20
50		144	0.23	911	8.2	21
51		145	0.23	911	9.2	27
52		146	0.23	911	9.0	20
53		147	0.23	911	9.6	21
54	Aoyagi	150	0.56	1523	0.0	29
55		152	0.56	1523	0.0	29
56	Yoshizaki	169	1.07	856	0.0	24
57		171	0.72	864	0.0	25
58		172	0.72	864	0.0	25
59		173	0.72	864	0.0	25
60		174	0.72	864	0.0	25
61		176	0.54	864	0.0	26
62		177	0.54	864	0.0	26
63		178	0.54	864	0.0	26
64		179	0.54	864	0.0	26
65	Kabeyasawa	K1	0.75	1500	9.7	18
66		K2	0.75	1500	10.1	19
67		K3	0.75	1500	10.1	19
68		K4	0.75	1500	9.3	21
69		K7	0.75	1500	7.3	20
70		K8	0.50	1000	7.3	20
71	Paulay	W1	0.57	1710	0.3	27
72		W3	0.57	1710	0.3	26
73	Antebi	6	0.64	1154	0.1	22
74		10	0.64	1154	0.1	23
75		13	0.64	1154	0.2	18
76		25	0.64	1154	0.1	41
77		32	0.64	1154	0.1	27
78		35	0.64	1154	0.1	26
79		37	0.64	1154	0.1	28
80		41	0.64	1154	0.1	23
81		45	0.64	1154	0.1	20
82		49	0.64	1154	0.2	14
83		50	0.64	1154	0.2	16

No.	Researcher	Specimen ID	M/Vl_w (a/l_w)	a [mm]	$P/(Af'_c)$ [%]	f'_c [MPa]
84	Antebi	51	0.64	1154	0.2	17
85		54	0.64	1154	0.2	14
86		55	0.34	1131	0.1	23
87		58	0.34	1131	0.2	20
88		60	0.34	1131	0.2	20
89	Barda	B1-1	0.50	953	0.3	29
90		B2-1	0.50	953	0.4	16
91		B3-2	0.50	953	0.3	27
92		B6-4	0.50	953	0.3	21
93		B7-5	0.25	476	0.2	26
94		B8-5	1.00	1905	0.4	23
95	Benjamin	4BII-1	1.10	671	0.0	20
96		4BII-2	0.69	631	0.0	21
97		4BII-3	0.50	610	0.0	19
98		4BII-4	0.33	587	0.0	26
99		3BI-1	0.57	985	0.0	21
100		1BII-1	0.57	985	0.0	20
101		1BII-2a	0.57	985	0.0	22
102		1BII-2b	0.57	985	0.0	24
103		3BI-3	0.57	985	0.0	23
104		3AII-1	0.69	631	0.0	25
105		3AII-2	0.69	631	0.0	19
106		1BII-1a	0.57	492	0.0	21
107		1BII-3	0.57	1477	0.0	21
108		NV-1	0.50	826	0.0	27
109		NV-11	1.00	1143	0.0	25
110		NV-18	0.33	645	0.0	21
111		VR-3	0.57	985	0.0	21
112		R-1	0.57	985	0.0	21
113		A1-A	0.33	587	0.0	22
114		A1-B	0.33	587	0.0	23
115		A2-B	0.33	587	0.0	20
116		M-1	0.58	913	0.0	22
117		M-2	0.77	1213	0.0	19
118		M-3	0.77	1213	0.0	25
119		M-4	0.58	913	0.0	21
120		MR-1	0.42	691	0.0	24
121		MR-2	0.32	526	0.0	20
122		MR-3	0.43	707	0.0	16
123		MR-4	0.32	526	0.0	21
124		VRR-1	0.53	915	0.0	22
125		MS-1	0.50	864	0.0	22

No.	Researcher	Specimen ID	M/Vl_w (a/l_w)	a [mm]	$P/(Af'_c)$ [%]	f'_c [MPa]
126	Benjamin	MS-2	0.50	864	0.0	28
127		MS-2-2	0.50	864	0.0	24
128		MS-5	0.25	584	0.0	25
129		SD-1A	0.57	695	0.0	16
130		SD-1B	0.57	695	0.0	16
131		SD-1C	0.57	695	0.0	16
132	Gallerly	A-8	0.72	658	0.0	36
133		A-4	0.72	658	0.0	30
134		B-8	0.72	658	0.0	34
135		B-4	0.72	658	0.0	34
136		C-8	0.72	658	0.0	32
137		C-4	0.72	658	0.0	30
138	Kabeyasawa, Hiraishi 1997	W08	0.66	1122	9.3	103
139		W12	0.66	1122	7.0	138
140		No. 1	1.33	2261	14.7	65
141		No. 2	1.33	2261	13.5	71
142		No. 3	1.33	2261	13.4	72
143		No. 5	2	3400	12.5	77
144		No. 6	1.33	2261	12.9	74
145		No. 7	1.33	2261	13.4	72
146		No. 8	1.33	2261	12.6	76

No.	Researcher	Specimen ID	ρ_{be} [%]	ρ_v [%]	ρ_h [%]	$f_{y,be}$ [MPa]	$f_{y,v}$ [MPa]	$f_{y,h}$ [MPa]
1	Hirosawa	9	2.5	0.2	0.2	208.9	293.0	293.0
2		15	2.5	0.2	0.2	221.3	475.7	475.7
3		16	2.5	0.2	0.2	221.3	475.7	475.7
4	Rye	29	2.6	0.2	0.2	467.5	335.1	335.1
5		30	2.6	0.2	0.2	467.5	335.1	335.1
6		31	2.6	0.2	0.2	467.5	485.4	485.4
7	Kobusho	46	0.7	0.7	0.7	402.0	323.4	323.4
8		47	0.7	0.7	0.7	402.0	323.4	323.4
9		50	1.5	0.4	0.4	407.5	402.0	402.0
10		51	1.5	0.5	0.4	407.5	323.4	323.4
11		52	1.5	0.5	0.5	407.5	323.4	323.4
12		53	1.5	0.7	0.7	407.5	323.4	323.4
13		54	1.5	0.7	0.7	407.5	323.4	323.4
14		55	1.5	0.7	0.7	407.5	323.4	323.4
15		56	1.5	0.5	0.5	407.5	323.4	323.4
16		57	1.5	0.5	0.5	407.5	323.4	323.4
17		58	1.5	0.5	0.5	407.5	323.4	323.4
18		59	1.5	0.5	0.5	407.5	323.4	323.4
19		61	1.8	0.5	0.5	342.7	323.4	323.4
20		64	3.2	0.5	0.5	334.4	323.4	323.4
21		65	3.2	0.5	0.5	334.4	323.4	323.4
22		69	3.1	0.3	0.3	294.4	372.3	372.3
23	Sugano	70	2.5	0.2	0.2	418.5	548.8	548.8
24		71	2.5	0.1	0.1	418.5	460.6	460.6
25	Hirosawa	72	5.7	0.5	0.3	376.5	419.2	419.2
26	Tanabe	101	4.7	1.8	1.8	367.5	284.1	284.1
27		102	4.7	1.8	1.8	367.5	284.1	284.1
28		103	4.7	1.8	1.8	367.5	284.1	284.1
29		104	4.7	1.2	1.2	367.5	284.1	284.1
30		105	4.7	1.2	1.2	367.5	284.1	284.1
31		106	4.7	1.2	1.2	367.5	284.1	284.1
32		107	4.7	0.9	0.9	367.5	284.1	284.1
33		108	4.7	0.9	0.9	367.5	284.1	284.1
34		109	4.7	0.9	0.9	367.5	284.1	284.1
35		110	4.7	1.8	1.8	293.0	294.4	294.4
36		111	4.7	1.8	1.8	293.0	294.4	294.4
37		112	4.7	1.8	1.8	293.0	294.4	294.4
38		113	4.7	1.8	1.8	293.0	294.4	294.4
39		114	4.7	1.2	1.2	293.0	294.4	294.4
40		115	4.7	1.2	1.2	293.0	294.4	294.4
41		116	4.7	0.9	0.9	293.0	294.4	294.4

No.	Researcher	Specimen ID	ρ_{be} [%]	ρ_v [%]	ρ_h [%]	$f_{y,be}$ [MPa]	$f_{y,v}$ [MPa]	$f_{y,h}$ [MPa]
42	Tanabe	117	4.7	0.9	0.9	293.0	294.4	294.4
43	Tsuboi	131	8.3	2.0	1.9	302.0	296.5	296.5
44		134	4.0	2.0	1.9	260.6	296.5	296.5
45		135	8.3	2.0	1.9	302.0	296.5	296.5
46	Sugano	140	1.8	0.7	0.7	397.1	571.6	571.6
47		141	1.8	0.7	0.7	397.1	571.6	571.6
48		142	1.8	0.7	0.7	397.1	571.6	571.6
49		143	1.8	0.3	0.3	397.1	571.6	571.6
50		144	1.8	0.3	0.3	397.1	571.6	571.6
51		145	1.8	0.7	0.7	397.1	284.1	284.1
52		146	1.8	0.7	0.7	397.1	284.1	284.1
53		147	1.8	0.8	0.7	397.1	397.1	397.1
54	Aoyagi	150	1.7	0.6	0.6	362.7	339.2	339.2
55		152	6.5	0.6	0.6	272.3	339.2	339.2
56	Yoshizaki	169	3.9	1.2	1.2	345.4	433.7	433.7
57		171	3.9	0.8	0.8	342.7	433.7	433.7
58		172	5.5	0.4	0.4	342.7	433.7	433.7
59		173	5.9	0.8	0.8	345.4	433.7	433.7
60		174	5.9	1.2	1.2	345.4	433.7	433.7
61		176	2.9	0.8	0.8	342.7	433.7	433.7
62		177	4.4	0.4	0.4	345.4	433.7	433.7
63		178	4.4	0.8	0.8	345.4	433.7	433.7
64		179	4.7	1.2	1.2	350.9	433.7	433.7
65	Kabeyasawa	K1	0.7	0.3	0.3	391.6	395.1	395.1
66		K2	1.4	0.5	0.5	391.6	395.1	395.1
67		K3	2.1	0.8	0.8	391.6	395.1	395.1
68		K4	1.4	0.8	0.8	391.6	395.1	395.1
69		K7	1.4	0.5	0.5	377.8	356.5	356.5
70		K8	1.4	0.5	0.5	377.8	356.5	356.5
71	Paulay	W1	0.8	0.8	1.6	299.9	341.3	341.3
72		W3	1.4	0.4	1.6	299.9	341.3	341.3
73	Antebi	6	2.1	0.3	0.3	324.1	271.0	271.0
74		10	4.7	0.3	0.3	305.4	271.0	271.0
75		13	2.1	0.5	0.5	296.5	393.0	393.0
76		25	2.1	0.5	0.5	275.8	330.9	330.9
77		32	2.1	0.5	0.5	344.7	344.7	344.7
78		35	2.1	0.5	0.5	344.7	344.7	344.7
79		37	2.1	0.5	0.5	344.7	344.7	344.7
80		41	4.7	0.5	0.5	337.8	323.4	323.4
81		45	2.1	0.3	0.3	295.8	313.7	313.7
82		49	2.1	0.3	0.3	313.7	319.2	319.2
83		50	2.1	0.5	0.5	319.2	306.1	306.1

No.	Researcher	Specimen ID	ρ_{be} [%]	ρ_v [%]	ρ_h [%]	$f_{y,be}$ [MPa]	$f_{y,v}$ [MPa]	$f_{y,h}$ [MPa]
84	Antebi	51	2.1	0.5	0.5	318.5	343.4	343.4
85		54	2.1	0.5	0.5	312.3	346.1	346.1
86		55	2.1	0.5	0.5	320.6	360.6	360.6
87		58	2.1	0.5	0.5	335.8	348.2	348.2
88		60	2.1	0.5	0.5	318.5	350.3	350.3
89	Barda	B1-1	1.8	0.5	0.5	525.4	543.3	495.7
90		B2-1	6.5	0.5	0.5	486.8	551.6	499.2
91		B3-2	4.2	0.5	0.5	413.7	544.7	513.0
92		B6-4	4.2	0.3	0.5	528.8	496.4	496.4
93		B7-5	4.2	0.5	0.5	539.2	530.9	501.2
94		B8-5	4.2	0.5	0.5	488.8	527.4	495.7
95	Benjamin	4BII-1	2.2	0.5	0.5	312.3	341.3	341.3
96		4BII-2	2.2	0.5	0.5	312.3	341.3	341.3
97		4BII-3	2.2	0.5	0.5	312.3	341.3	341.3
98		4BII-4	2.2	0.5	0.5	312.3	341.3	341.3
99		3BI-1	4.2	0.5	0.5	312.3	341.3	341.3
100		1BII-1	2.1	0.3	0.3	312.3	341.3	341.3
101		1BII-2a	2.1	0.5	0.5	312.3	341.3	341.3
102		1BII-2b	2.1	0.5	0.5	312.3	341.3	341.3
103		3BI-3	1.3	0.5	0.5	312.3	341.3	341.3
104		3AII-1	3.3	0.5	0.5	312.3	341.3	341.3
105		3AII-2	3.3	0.3	0.3	312.3	341.3	341.3
106		1BII-1a	2.0	0.5	0.5	312.3	341.3	341.3
107		1BII-3	2.0	0.5	0.5	312.3	341.3	341.3
108		NV-1	1.8	0.5	0.5	312.3	341.3	341.3
109		NV-11	5.0	0.5	0.5	312.3	341.3	341.3
110		NV-18	1.8	0.5	0.5	312.3	341.3	341.3
111		VR-3	2.1	0.5	0.5	312.3	341.3	341.3
112		R-1	2.1	0.3	0.3	324.1	358.5	358.5
113		A1-A	2.2	1.0	1.0	296.5	341.3	341.3
114		A1-B	2.2	1.0	1.0	296.5	341.3	341.3
115		A2-B	2.2	1.5	1.5	296.5	341.3	341.3
116		M-1	2.3	0.3	0.3	324.1	358.5	358.5
117		M-2	2.3	0.3	0.3	324.1	358.5	358.5
118		M-3	2.3	0.3	0.3	324.1	358.5	358.5
119		M-4	2.3	0.3	0.3	324.1	358.5	358.5
120		MR-1	3.2	0.3	0.3	324.1	358.5	358.5
121		MR-2	3.2	0.3	0.3	324.1	358.5	358.5
122		MR-3	3.2	0.3	0.3	324.1	358.5	358.5
123		MR-4	3.2	0.3	0.3	324.1	358.5	358.5
124		VRR-1	2.3	0.5	0.5	293.0	293.0	293.0
125		MS-1	5.0	0.3	0.3	293.0	293.0	293.0

No.	Researcher	Specimen ID	ρ_{be} [%]	ρ_v [%]	ρ_h [%]	$f_{y,be}$ [MPa]	$f_{y,v}$ [MPa]	$f_{y,h}$ [MPa]
126	Benjamin	MS-2	5.0	0.3	0.3	293.0	293.0	293.0
127		MS-2-2	5.0	0.3	0.3	293.0	293.0	293.0
128		MS-5	5.0	0.3	0.3	293.0	293.0	293.0
129		SD-1A	2.8	0.5	0.5	293.0	293.0	293.0
130		SD-1B	2.8	0.5	0.5	293.0	293.0	293.0
131		SD-1C	2.8	0.5	0.5	293.0	293.0	293.0
132	Gallerly	A-8	4.9	0.8	0.8	317.2	344.7	344.7
133		A-4	4.9	1.6	1.6	312.3	344.7	344.7
134		B-8	2.8	0.8	0.8	342.7	344.7	344.7
135		B-4	2.8	1.6	1.6	342.7	344.7	344.7
136		C-8	5.5	0.8	0.8	368.9	344.7	344.7
137		C-4	5.5	1.6	1.6	366.8	344.7	344.7
138	Kabeyasawa, Hiraishi 1997	W08	2.1	0.5	0.5	761	1079	1079
139		W12	2.1	0.5	0.5	761	1079	1079
140		No. 1	5.1	0.2	0.2	1009	792	792
141		No. 2	5.1	0.3	0.3	1009	792	792
142		No. 3	5.1	0.5	0.5	1009	792	792
143		No. 5	5.1	0.5	0.5	1009	792	792
144		No. 6	5.1	0.7	0.7	1009	1420	1420
145		No. 7	5.1	1.0	1.0	1009	792	792
146		No. 8	5.1	1.5	1.5	1009	792	792

No.	Researcher	Specimen ID	V_{mes} [kN]	V_{mes}/V_{cal} [-]	V_{mes}/V_{cal} Watanabe [-]
1	Hirosawa	9	86.30	1.97	1.61
2		15	78.29	1.57	1.66
3		16	101.86	2.02	2.12
4	Rye	29	1055.12	3.01	1.48
5		30	931.90	2.33	1.08
6		31	608.07	2.28	1.79
7	Kobusho	46	29.36	0.93	0.65
8		47	27.58	0.87	0.62
9		50	24.47	1.03	0.67
10		51	23.58	1.19	0.75
11		52	20.02	1.00	0.63
12		53	19.57	1.10	0.83
13		54	24.91	0.93	0.67
14		55	25.80	0.97	0.71
15		56	26.69	1.20	0.64
16		57	26.69	1.32	0.81
17		58	25.80	1.27	0.79
18		59	24.47	1.23	0.79
19		61	48.93	2.14	1.90
20		64	43.15	1.82	1.54
21		65	48.49	2.08	1.79
22		69	44.93	1.96	1.33
23	Sugano	70	833.60	2.07	1.17
24		71	804.24	2.42	1.02
25	Hirosawa	72	809.13	1.25	1.02
26	Tanabe	101	62.72	0.88	0.86
27		102	74.73	1.07	1.06
28		103	62.72	0.88	0.85
29		104	94.30	1.18	0.95
30		105	89.85	1.14	0.93
31		106	86.30	1.09	0.90
32		107	97.86	1.13	0.83
33		108	96.97	1.10	0.79
34		109	101.86	1.15	0.82
35		110	42.70	1.05	1.02
36		111	44.04	1.09	1.07
37		112	68.50	0.91	0.84
38		113	70.73	0.92	0.82
39		114	70.73	0.85	0.67
40		115	76.51	0.89	0.68
41		116	78.29	0.82	0.55

No.	Researcher	Specimen ID	V_{mes} [kN]	V_{mes}/V_{cal} [-]	V_{mes}/V_{cal} Watanabe [-]
42	Tanabe	117	77.40	0.82	0.57
43	Tsuboi	131	161.92	0.83	1.08
44		134	195.28	0.97	1.30
45		135	184.60	0.91	1.23
46	Sugano	140	2355.33	0.79	1.02
47		141	2942.05	0.97	1.27
48		142	3138.22	1.01	1.33
49		143	1814.43	0.81	0.80
50		144	1912.29	0.83	0.81
51		145	2137.82	0.88	0.75
52		146	1981.24	0.84	0.87
53		147	2304.62	0.71	0.98
54	Aoyagi	150	1554.65	1.02	0.69
55		152	2309.52	1.42	1.03
56	Yoshizaki	169	174.37	0.61	0.60
57		171	235.31	0.72	0.66
58		172	219.74	0.99	0.70
59		173	259.78	0.78	0.72
60		174	274.46	0.61	0.63
61		176	321.61	0.68	0.64
62		177	318.94	1.12	0.69
63		178	382.55	0.79	0.76
64		179	421.69	0.65	0.72
65	Kabeyasawa	K1	439.48	1.42	0.82
66		K2	470.62	0.97	0.77
67		K3	541.35	0.82	0.80
68		K4	507.99	0.77	0.72
69		K7	738.40	1.10	0.79
70		K8	911.89	1.24	0.89
71	Paulay	W1	809.58	0.59	0.38
72		W3	786.45	0.79	0.34
73	Antebi	6	360.31	2.23	1.01
74		10	453.72	2.55	1.22
75		13	413.68	1.50	1.12
76		25	409.24	1.40	0.72
77		32	444.82	1.64	1.00
78		35	404.79	1.51	0.94
79		37	360.31	1.31	0.79
80		41	471.51	1.77	1.17
81		45	409.24	1.71	0.79
82		49	400.34	1.84	0.96
83		50	409.24	1.24	0.82

No.	Researcher	Specimen ID	V_{mes} [kN]	V_{mes}/V_{cal} [-]	V_{mes}/V_{cal} Watanabe [-]
84	Antebi	51	502.65	1.40	0.97
85		54	427.47	1.21	0.90
86		55	493.75	0.81	0.55
87		58	489.30	0.83	0.59
88		60	600.51	1.02	0.74
89	Barda	B1-1	1347.81	1.74	1.20
90		B2-1	1023.54	1.31	1.25
91		B3-2	1175.67	1.46	1.09
92		B6-4	915.44	1.81	0.97
93		B7-5	1209.03	1.01	1.05
94		B8-5	939.46	1.43	1.07
95	Benjamin	4BII-1	88.96	0.93	0.94
96		4BII-2	154.80	1.15	0.84
97		4BII-3	201.50	1.11	0.77
98		4BII-4	293.58	0.91	0.57
99		3BI-1	186.83	0.74	0.49
100		1BII-1	249.10	1.46	0.72
101		1BII-2a	462.62	1.80	1.18
102		1BII-2b	373.65	1.43	0.91
103		3BI-3	293.58	1.09	0.74
104		3AII-1	204.62	1.60	1.16
105		3AII-2	137.89	1.61	0.98
106		1BII-1a	92.52	1.45	0.96
107		1BII-3	685.03	1.20	0.81
108		NV-1	301.14	1.18	0.69
109		NV-11	222.41	1.23	1.00
110		NV-18	373.65	1.08	0.77
111		VR-3	302.48	1.18	0.79
112		R-1	315.82	1.79	0.89
113		A1-A	311.38	0.63	0.74
114		A1-B	366.98	0.74	0.85
115		A2-B	329.17	0.54	0.61
116		M-1	213.51	1.28	0.64
117		M-2	346.96	2.25	1.28
118		M-3	324.72	1.92	1.01
119		M-4	177.93	1.08	0.55
120		MR-1	317.16	1.92	0.89
121		MR-2	244.65	1.41	0.72
122		MR-3	318.05	2.14	1.18
123		MR-4	244.65	1.39	0.69
124		VRR-1	329.17	1.38	0.84
125		MS-1	274.46	1.56	0.73

No.	Researcher	Specimen ID	V_{mes} [kN]	V_{mes}/V_{cal} [-]	V_{mes}/V_{cal} Watanabe [-]
126	Benjamin	MS-2	368.31	1.93	0.83
127		MS-2-2	358.53	1.97	0.89
128		MS-5	380.32	1.27	0.56
129		SD-1A	177.93	1.17	0.80
130		SD-1B	177.93	1.17	0.80
131		SD-1C	160.14	1.05	0.72
132	Gallerly	A-8	273.57	1.51	1.19
133		A-4	318.05	1.14	1.24
134		B-8	226.86	1.31	1.02
135		B-4	284.69	1.01	1.09
136		C-8	191.27	1.08	0.89
137		C-4	244.65	0.87	0.95
138	Kabeyasawa, Hiraishi 1997	W08	1670	1.69	1.17
139		W12	1719	1.57	1.05
140		No. 1	1101	2.21	1.73
141		No. 2	1255	2.00	1.61
142		No. 3	1379	1.78	1.48
143		No. 5	1159	1.44	1.34
144		No. 6	1412	1.09	0.97
145		No. 7	1499	1.30	1.16
146		No. 8	1639	1.07	0.91
			mean	1.28 ± 0.76 %	0.93 ± 0.43 %
			std-dev	0.47	0.30
			c.v.	36.63 %	32.38 %

(Kabeyasawa and Hiraishi 1998; Wood 1990)

A10. Cyclically loaded walls

Researcher	Specimen ID	Boundary Element b_f [mm]	Boundary Element h_f [mm]	Web thickness t [mm]	Wall length l_w [mm]	M/Vl_w (a/l_w)	a [mm]
Kabeyasawa & Hiraishi, 1998	NW1	200	200	80	1300	2	3400
Ogata & Kabeyasawa, 1985	K4	200	200	80	2000	0.75	1500
Barda et al., 1977	B3-2	610	102	102	1905	0.50	953
	B6-4	610	102	102	1905	0.50	953
	B7-5	610	102	102	1905	0.25	476
	B8-5	610	102	102	1905	1.00	1905
Oesterle et al., 1980	B1	305	305	102	1905	2.4	4572
	B2	305	305	102	1905	2.4	4572
	B3	305	305	102	1905	2.4	4572
	B5	305	305	102	1905	2.4	4572

Researcher	Specimen ID	$P/(Af'_c)$ [%]	f'_c [MPa]	ρ_{be} [%]	ρ_v [%]	ρ_h [%]
Kabeyasawa & Hiraishi, 1998	NW1	10.9	87.6	2.14	0.53	0.53
Ogata & Kabeyasawa, 1985	K4	9.3	20.6	1.43	0.8	0.8
Barda et al., 1977	B3-2	0.3	27.0	4.17	0.5	0.5
	B6-4	0.3	21.2	4.17	0.25	0.5
	B7-5	0.2	25.7	4.17	0.5	0.5
	B8-5	0.4	23.4	4.17	0.5	0.5
Oesterle et al., 1980	B1	0.0	53.0	1.1	0.28	0.3
	B2	0.0	53.6	3.67	0.28	0.625
	B3	0.0	47.3	1.1	0.28	0.3
	B5	0.0	45.3	3.67	0.28	0.625

Researcher	Specimen ID	$f_{y,be}$ [MPa]	$f_{y,v}$ [MPa]	$f_{y,h}$ [MPa]	$\rho_v f_{yv}/f'_c$ [-]
Kabeyasawa & Hiraishi, 1998	NW1	776	1001	1001	0.06
Ogata & Kabeyasawa, 1985	K4	392	395	395	0.15
Barda et al., 1977	B3-2	414	545	513	0.10
	B6-4	529	496	496	0.06
	B7-5	539	531	501	0.10
	B8-5	489	527	496	0.11
Oesterle et al., 1980	B1	449.5	520.5	520.5	0.03
	B2	410	532.3	532.3	0.03
	B3	438	478.5	478.5	0.03
	B5	444	502	502	0.03

Researcher	Specimen ID	Measured values			
		$\delta_{ys} = \Delta_y/a$ [-]	V_{ys} [kN]	$\delta_{limit} = \Delta_{limit}/a$ [-]	$V_{u,shear}$ [kN]
Kabeyasawa & Hiraishi, 1998	NW1	0.005	760	0.020	1062
Ogata & Kabeyasawa, 1985	K4	n/a	508	0.011	508
Barda et al., 1977	B3-2	n/a	n/a	0.006	1176
	B6-4	n/a	n/a	0.006	915
	B7-5	n/a	n/a	0.009	1209
	B8-5	n/a	n/a	0.006	939
Oesterle et al., 1980	B1	0.003	201	0.028	271
	B2	0.003	533	0.022	680
	B3	0.003	201	0.039	276
	B5	0.004	495	0.028	762

Researcher	Specimen ID	ϕy [-]	$\delta(\phi_y)$ [-]	δ_{slip} [-]	δ_{shear} [-]	$\delta_{ys,total}$ [-]
Kabeyasawa & Hiraishi, 1998	NW1	4.32E-06	0.005	0.001	0.000	0.006
Ogata & Kabeyasawa, 1985	K4	1.66E-06	0.001	0.001	0.000	0.002
Barda et al., 1977	B3-2	2.47E-06	0.001	0.001	0.001	0.002
	B6-4	3.16E-06	0.001	0.001	0.001	0.003
	B7-5	3.22E-06	0.001	0.001	0.002	0.004
	B8-5	2.92E-06	0.002	0.001	0.001	0.004
Oesterle et al., 1980	B1	1.44E-06	0.002	0.000	0.000	0.003
	B2	1.83E-06	0.003	0.000	0.000	0.003
	B3	1.41E-06	0.002	0.000	0.000	0.002
	B5	1.99E-06	0.003	0.000	0.000	0.004

Researcher	Specimen ID	M_{ys} [kNmm]	V_{ys} [kN]	$0.8V_{ys,cal}$ [kN]	m (Eq. 8.9) [-]	$\Delta_{limit,cal}$ $0.2/m$-δ_{ys} [-]
Kabeyasawa & Hiraishi, 1998	NW1	2467787	726	581	4.40	0.04
Ogata & Kabeyasawa, 1985	K4	820892	547	438	2.57	0.08
Barda et al., 1977	B3-2	2479724	2603	2083	2.52	0.08
	B6-4	2816202	2957	2365	3.06	0.06
	B7-5	3085598	6479	5183	2.48	0.08
	B8-5	6704007	3519	2815	2.38	0.08
Oesterle et al., 1980	B1	1044792	229	183	3.41	0.06
	B2	2838904	621	497	3.40	0.06
	B3	1008773	221	177	3.40	0.06
	B5	3050217	667	534	3.36	0.06

Researcher	Specimen ID	Calculated monotonic shear capacity				
		V_{th} [kN]	V_{tv} [kN]	V_{cz} [kN]	V_a [kN]	V_n [kN]
Kabeyasawa & Hiraishi, 1998	NW1	590	131	142	68	931
Ogata & Kabeyasawa, 1985	K4	200	320	89	51	660
Barda et al., 1977	B3-2	128	513	186	39	866
	B6-4	123	234	172	35	564
	B7-5	62	1000	183	11	1256
	B8-5	246	248	177	44	716
Oesterle et al., 1980	B1	294	73	216	172	755
	B2	626	75	285	155	1140
	B3	270	67	208	159	704
	B5	590	71	269	135	1065

Researcher	Specimen ID	Shear degradation		
		χ (Eq. 8.17) [-]	1-η (Eq. 8.14) [-]	$V_{n,red}$ [kN]
Kabeyasawa & Hiraishi, 1998	NW1	0.52	0.00	374
Ogata & Kabeyasawa, 1985	K4	0.69	0.44	419
Barda et al., 1977	B3-2	0.93	0.56	718
	B6-4	0.92	0.16	363
	B7-5	0.90	0.34	1019
	B8-5	0.92	0.60	589
Oesterle et al., 1980	B1	0.80	0.00	293
	B2	0.83	0.00	584
	B3	0.74	0.00	250
	B5	0.80	0.00	528

(Barda et al. 1977; Kabeyasawa and Hiraishi 1998; Oesterle et al. 1980; Oesterle et al. 1976; Ogata and Kabeyasawa 1985)